NASA SP-167

CAS
COPY

Significant Achievements in

CASE FILE
COPY

Space Science 1967



NATIONAL AERONAUTICS AND SPACE ADMINISTRATION

NASA SP-167

Significant Achievements in

Space Science 1967

Scientific and Technical Information Division
OFFICE OF TECHNOLOGY UTILIZATION 1968
NATIONAL AERONAUTICS AND SPACE ADMINISTRATION
Washington, D.C.

For sale by the Superintendent of Documents
U.S. Government Printing Office, Washington, D.C. 20402
Price $2.50
Library of Congress Catalog Card Number 73-600960

Foreword

This volume is one of a series which summarizes the achievements made in the scientific and technical disciplines involving the Space Science and Applications Program of the United States. The contribution made by the National Aeronautics and Space Administration is highlighted against the background of the overall progress in these disciplines.

The achievements during the period 1958 to 1964 in the following areas were reported in NASA Special Publications 91 to 100: Astronomy, Bioscience, Communications and Navigation, Geodesy, Ionospheres and Radio Physics, Meteorology, Particles and Fields, Planetary Atmospheres Planetology, and Solar Physics.

The achievements in 1965 in space science and applications were printed in two volumes, SP–136 and SP–137, respectively. The first summarized the significant progress made in Astronomy, Ionospheres and Radio Physics, Particles and Fields, Planetary Atmospheres, Planetology, and Solar Physics; the second summarized the significant progress made in Communications, Geodesy, and Meteorology.

The achievements in 1966 in the following areas, Astronomy, Bioscience, Ionospheres and Radio Physics, Particles and Fields, Planetary Atmospheres, Planetology, and Solar Physics were described in SP–155. A companion volume (SP–156) summarized the progress in space applications in 1966 in the following areas: Applications Technology Satellites, Communications Satellites, Satellite Geodesy, the Meteorological Program, and the Navigation and Traffic Control Satellite Program.

Although we do not here attempt to name all those who have contributed to the NASA program during 1967, both in the experimental and theoretical research and in the analysis, compilation, and reporting to these results, nevertheless we wish to acknowledge all the contributions to a very fruitful program in which this country may take justifiable pride.

JOHN E. NAUGLE
Associate Administrator for
Space Science and Applications,
NASA

Page Intentionally Left Blank

Contents

	Page
STELLAR ASTRONOMY	1
L. W. Fredrick, D. D. Meizel, and A. C. Miller	
Introduction	3
X-Rays (E $<$ 100 keV)	3
Gamma Rays	10
Digest of X-Ray Studies	11
Ultraviolet	17
Infrared	27
Conclusions	29
References	30
SPACE BIOSCIENCE	41
B. Berman and D. W. Jenkins, Editors	
Introduction	43
Chemical Evolution	44
Search for Extraterrestrial Life	50
Spacecraft Sterilization and Planetary Quarantine	62
Environmental Biology	74
Behavioral Biology	88
Biosatellite Program	96
Physical Biology	121
Applications	127
Conclusions	130
References	132
IONOSPHERES AND RADIO PHYSICS	139
E. R. Schmerling and S. J. Bauer	
Introduction	141
The Lower Ionosphere	141
The Middle Ionosphere	142
The Upper Ionosphere	148
Radio Propagation and Radio Physics	153
Planetary Ionospheres	156
Conclusions	157
References	159

Page

PARTICLES AND FIELDS 163
L. D. Kavanagh, Jr., E. C. Roelof, and A. W. Schardt
Introduction 165
The Solar Wind 172
Interaction of Solar Wind With the Moon, Planets, and Interstellar Medium 191
Interactions Between Solar Wind and Earth's Magnetosphere 206
Solar Cosmic Rays 220
Conclusions 245
Appendix 247
References 253

PLANETARY ATMOSPHERES 267
F. S. Johnson, F. D. Colegrove, W. B. Hanson, R. R. Hodges, Jr., J. E. Midgley, A. Palm, and B. A. Tinsley
Introduction 269
Earth 269
Moon 281
Venus 283
Mars 289
Mercury 291
Jupiter 291
Micrometeorites 292
Conclusions 294
References 296

PLANETOLOGY 303
L. S. Walker, B. M. French, and P. D. Lowman, Editors
Introduction 305
The Planets 306
The Earth 313
The Moon 326
Impact Cratering and Shock Metamorphism 373
Iron and Stony-Iron Meteorites 381
Stony Meteorites 396
Tektites 412
Summary 415
References 421

SOLAR PHYSICS 439
G. K. Oertel, R. G. Teske, and H. Glaser
Introduction 441
Orbiting Solar Observatory Program 445
Neutrino Observations 465
Solar Rotation 468
Photosphere and Chromosphere 471

Page

SOLAR PHYSICS—Continued

Model Atmospheres 472
Solar Abundances 477
Observations 479
Granulation 482
Spicules 483
Corona 483
The Solar Cycle 493
Sunspots 495
Prominences 497
Flares 502
Solar Neutron Flux 515
Solar X-Rays 516
Supporting Laboratory and Theoretical Research 529
Outlook 539
References 546

STELLAR ASTRONOMY

L. W. Frederick, D. D. Meizel, and A. C. Miller
Leander McCormick Observatory
University of Virginia

Page Intentionally Left Blank

Stellar Astronomy

INTRODUCTION

This report of significant scientific and technical progress in stellar astronomy is based on the results that have been obtained, reported, or published during 1967. A wide range of techniques and instruments have been used to study the X-ray, gamma-ray, ultraviolet, and infrared regions of the electromagnetic spectrum. Experiments have been conducted aboard satellites, sounding rockets, high-altitude airplanes, and balloons, and using ground-based telescopes.

Some of the most exciting results were obtained in the X-ray region, using rockets, balloons, and the Orbiting Solar Observatory. New discrete sources have been discovered, and there appears to be a definite concentration of them in the galactic plane. A diffuse X-ray component also has been observed and is found to be isotropic. The brighter discrete sources have been studied intensively, and some are found to be variable with time; therefore, observations over long periods are necessary. By ground observations of their optical counterparts, important additional information has been gathered about the nature of these sources.

With balloon-borne instruments, gamma rays have been detected for the first time from the Crab Nebula and Cyg X–1.

Significant progress in 1967 was made using rocket-borne instruments to acquire high (1 Å) resolution ultraviolet spectra. The more striking results of ultraviolet research include the development of an improved temperature scale for hot stars, the determination of mass loss by OB supergiants, and an indication that there is little or no H_2 in interstellar gas.

Using ground-based telescopes at the Mount Wilson and Mount Palomar Observatories, the most notable observation in the infrared region was the detection of radiation from the direction of the galactic center. Further work is needed before it can be determined whether this is the true galactic nucleus.

X-RAYS ($E < 100$ keV)

Considerable progress has been made in the field of X-ray astronomy. Rocket and balloon flights, both in the Northern and Southern Hemispheres, supplemented by ground observations, have led to the discovery of some 40

discrete celestial X-ray sources since 1963. About 20 percent of these sources have spectral information available and about 10 percent have been identified or tentatively identified with optical or radio sources. A table of known sources and a detailed summary of available data (up to April 1968) are included in "Digest of X-ray Studies" (see p. 11). Reviews of data prior to 1967 have been given by Morrison (ref. 1), Friedman (ref. 2), and Gould (ref. 3).

Distribution of X-Ray Sources

Gursky, Gorenstein, and Giacconi (ref. 4) and Johnson (ref. 5) have discussed the distribution of the brightest X-ray sources as derived from rocket flight data. They found, in agreement with previous results, a definite concentration of sources in the galactic plane, primarily in Cygnus, Sagittarius, Scorpius, Centaurus, Vela, and Carina (fig. 1). Cooke, Pounds, Stewardson, and Adams (ref. 6) have shown that the number density of X-ray sources is considerably lower in the region from Carina to Orion than in the Cygnus region. Probable distances to the sources for which optical identifications are available fall in the range from 10^2 to 10^3 parsecs from the Sun.

The Diffuse X-Ray Component

In addition to the discrete sources, a diffuse X-ray component first indicated by rocket observations (Giacconi, Gursky, Paolini, and Rossi, ref. 7) has been confirmed on a number of occasions. Recent observations have been carried out by Seward, Chodil, Mark, Swift, and Toor (ref. 8) in the 4- to 40-keV range. Their results indicate that for all areas studied in the galactic plane, as well as perpendicular to it, the diffuse component has a similar spectral index, $E \propto \nu^{-1.6}$ (4 to 40 keV), and is isotropic within 10 percent. Giacconi, Gorenstein, Gursky, and Kellogg (ref. 9) have reported results of a survey of the galactic anticenter at 1 to 10 keV and found similar results, as have Bowyer, Field, and Mack (ref. 10). Fritz, Meekins, Henry, Byram, and Friedman (ref. 11) have reported observations in the soft X-ray range ($E \approx 0.25$ keV) in the area of the north galactic pole, which cannot be explained by an extrapolation of the 10-keV observations. They have also reported observations of the same area in the 1.5- to 7-keV range. An interpretation of the derived spectral index with a sharp break at 12 keV cannot result if the background source is caused entirely by Compton scattering of cosmic blackbody photons, as postulated by Brecher and Morrison (ref. 12) and Felten and Morrison (ref. 13). Gould and Burbidge (ref. 14) had earlier suggested that unresolved extragalactic sources might be responsible for the diffuse X-ray component. Silk (ref. 15); Friedman, Byram, and Chubb (ref. 16); and Oda (ref. 17) continued to investigate this possibility. However, Fritz et al. (ref. 11) concluded that their results favor instead a hot, dense intergalactic gas compatible with either

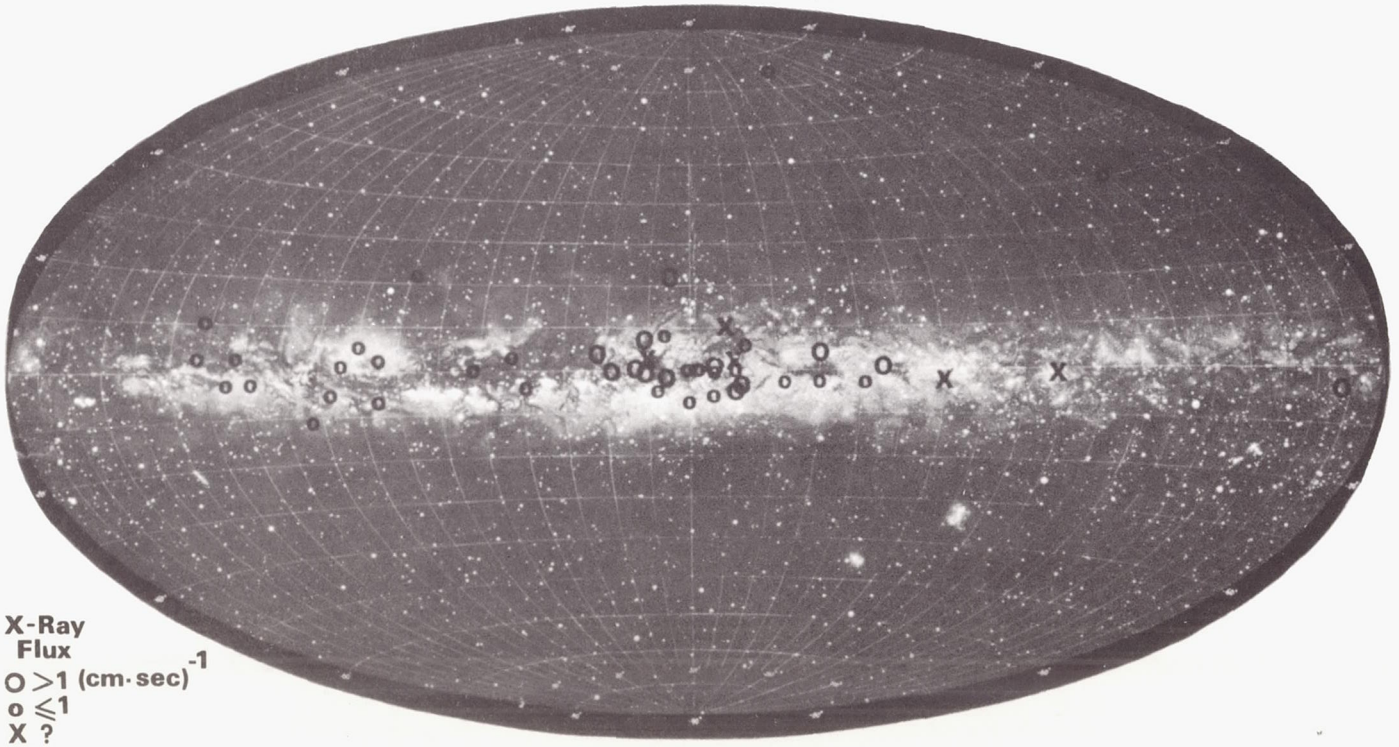


Figure 1.—Distribution of cosmic X-ray sources, the naked-eye stars, and the visual appearance of the Milky Way.

the model given by Field and Henry (ref. 18) for a universe with $T=4\times 10^6$ °K and $q_0=\frac{1}{2}$ or the model 3 universe investigated by Weymann (ref. 19).

It should be noted, however, that if the intensity of the diffuse X-rays is to be compatible with the observed upper limits of gamma rays, the hot intergalactic gas postulated by Fritz et al. (ref. 11) cannot be in equilibrium. A recent analysis of gamma rays produced by Compton scattering, assuming the observations of the diffuse X-ray source, has been given by Shen and Berkey (ref. 20). They tentatively conclude that a "disk" source distribution fits the available information on gamma ray upper limits and the X-ray data.

Variations in X-Ray Flux From Discrete Sources

Source variability has been summarized by Friedman, Byram, and Chubb (ref. 16). Secular changes, as well as irregular fluctuations, appear to occur for a number of sources, but experimental difficulties make quantitative comparisons difficult. X-ray variations in Cyg XR–1 (Overbeck and Tananbaum, ref. 21; Overbeck, Womack, and Tananbaum, ref. 22); Sco X–1 (Hill, Grader, and Seward, ref. 23); and Cen XR–2 (Chodil, Mark, Rodrigues, Seward, Swift, Hiltner, Wallerstein, and Mannery, ref. 24; Lewin, Clark, and Smith, ref. 25), have been reported recently, but satellite observations (Conner and Singer, ref. 26) show no variations larger than a factor of 2 in Sco X–1 over a 5-week period. Novalike behavior of Cen XR–2 has been suggested by Chodil, Mark, Rodrigues, and Swift (ref. 27). A hard (20- to 30-keV) X-ray flare from Sco X–1 was reported by Lewin, Clark, and Smith (ref. 28), while the source (Lup X–1) appeared to have decreased considerably in brightness within a 6-month period between balloon flights (Lewin, Clark, and Smith, ref. 25).

X-Ray Spectra of Discrete Sources

Surveys have been carried out over a fairly wide range of energies including both soft ($E>1$ keV) and hard ($E>10$ keV) X-rays and gamma rays. Instrument differences and possible time variations make it difficult to compare results from different observations. However, the data obtained by proportional counters flown on rockets are quite adequate to determine the spectral shape of the brighter X-ray sources. This is also true of balloon-borne observations of brighter sources.

A comparison of the spectrum of Crab Nebula (Tau X–1) with that of Sco X–1 has been made by Manley (ref. 29) and Tucker (ref. 30), who point out that these two appear to arise from different causes. The Crab Nebula spectrum was interpreted by Manley (ref. 29) as being caused by synchrotron emission. Meekins, Fritz, Henry, Byram, and Friedman (ref. 31) have obtained new spectra of Sco XR–1, Cyg XR–1, and Cyg XR–2.

The data indicate the following interpretations:

(1) Sco XR–1: bremsstrahlung at $T=(65\pm5)\times10^6$ °K

(2) Cyg XR–1: power law spectrum with energy $\propto \nu^{-0.4}$

(3) Cyg XR–2: bremsstrahlung at $T=(60\pm10)\times10^6$ °K

Hill, Grader, and Seward (ref. 23) reported a study of the soft X-rays in the 0.6- to 9-keV range from Sco X–1, but the results show no dropoff of the low-energy flux, which might be expected from interstellar absorption. These data, together with those of Meekins et al. (ref. 31), indicate the source may be nearer than previously thought. No conclusions concerning the type of spectrum were given.

High-energy surveys have been carried out with balloons by Peterson, Jacobson, and Pelling (ref. 32); Bleeker, Burger, Deerenberg, Scheepmaker, Swanenburg, and Tanaka (ref. 33); Brini, Ciriegi, Fuligni, Moretti, and Vespignani (ref. 34); Seward and Toor (ref. 35); and Clark, Lewin, and Smith (ref. 36). An extensive discussion of spectra (Gorenstein, Giacconi, and Gursky, ref. 37) indicates that several other sources show a spectrum in the 1- to 10-keV range, which is consistent with either self-absorption or interstellar absorption. Hard X-rays ($E>10$ keV) have been detected from Tau XR–1, Cyg XR–1, Cyg XR–3, Sco X–1, and from the general direction of Virgo XR–1. Most of the sources are so weak, however, that detailed spectra are not available over a sufficiently wide X-ray region to draw firm conclusions concerning the physics of the sources. There is also the possibility that the spectra of many X-ray sources are not constant but highly variable.

Optical Identifications

In 1966, Sco X–1 was identified with a 13th-magnitude stellar object. Since that time, Cyg X–2 (Giacconi, Gorenstein, Gursky, Usher, Waters, Sandage, Osmer, and Peach, ref. 38) and possibly Cen XR–2 (Blanco and Kunkel, ref. 39) have also been identified with optical stellar sources. X-ray sources near known supernovae remnants have been discussed by Friedman, Byram, and Chubb (ref. 16) and Poveda and Woltjer (ref. 40). The Crab Nebula was known to be an X-ray source in 1964. Rocket surveys of the Virgo Cluster (Bradt, Mayer, Naranan, Rappaport, and Spada, ref. 41) confirmed a source in the region of M 87 originally found by Friedman and Byram (ref. 42), but the suggested identification has been questioned (Argyle, ref. 43). A source in Leo may be extragalactic, but no optical identification has yet been made. Surveys of Southern Hemisphere objects have been carried out by Harries, McCracken, Francey, and Fenton (ref. 44); Seward and Toor (ref. 35); and Cooke et al. (ref. 6). Seward and Toor have established upper limits on the X-ray flux from the Magellanic Clouds; this measurement restricts the number of discrete sources, with intrinsic radiation as strong as the Crab Nebula, that might be present in the Large Cloud to less than 600.

Braes and Hovenier (ref. 45), as well as O'Dell (ref. 46), have argued that X-ray sources may be involved in O associations with thermal radio sources purely on the basis of positional correlations. Although direct confirmation of this view is lacking, it was recently suggested by Bless, Fischel, and Stecher (ref. 47) that the Vel XR–1 source may be associated with the stars ζ Pup (O*f* star) and/or γ^2 Vel (WR), rather than with the novae CP Pup or T Pyx as suggested by Chodil et al. (ref. 24). However, recent observations by Giacconi et al. (ref. 9) show that the Vela X-ray source is not associated with any of those stars. Wallerstein (ref. 48) has suggested that the source Lac XR–1 may be associated with the WR binary HD 211853, but the data are too incomplete to verify this. Other correlations have been suggested, but the X-ray positions are generally too poor to draw any firm conclusions.

Optical Characteristics of the Brighter Galactic X-Ray Sources

The discrete galactic X-ray sources that have optical identifications are of at least two types.

(1) Stellar blue objects: Sco X–1, Cyg X–2, and Cen X–2
(2) Diffuse sources: Tau X–1 (Crab Nebula)

Tau X–1

The optical properties of the Crab Nebula are well known (Minkowski, ref. 49). Although it has been argued that the observed X-rays are induced by synchrotron processes (Woltjer, ref. 50; Shklovsky, ref. 51), arguments in support of thermal emission from a hot plasma have also been presented (Sartori and Morrison, ref. 52). Recent comparisons between the dimensions of the Crab X-ray source and the visual image by Oda, Bradt, Garmire, Spada, Sreekantan, Gursky, Giacconi, Gorenstein, and Waters (ref. 53) indicate two principal results. First, the X-ray and visible light distributions agree in position to within 15 arc-secs. Second, the source has a finite angular extent. The data are consistent with a variety of X-ray emission models ranging from one having uniform emission over the central 2 minutes of arc to a distribution coinciding with that in visual wavelengths. It should be noted that the "off-center" features of the Crab do not appear to be simply related to the X-ray production.

Sco X–1

After identification and spectra of this source were obtained by Sandage, Osmer, Giacconi, Gorenstein, Gursky, Waters, Bradt, Garmine, Sreekantan, Oda, Osawa and Jugaku (ref. 54) and independently by Johnson and Stephenson (ref. 55) a rather intensive effort was made to study this interesting object. Interpretative discussions have been presented recently by Johnson (ref. 56), Shklovsky (ref. 57), Tucker (ref. 58), Prendergast and Burbidge (ref. 59), and Cameron and Mock (ref. 60).

Shklovsky (ref. 57), Cameron and Mock (ref. 60), and Prendergast and Burbidge (ref. 59) have followed an earlier suggestion by Hayakawa and Matsuoka (ref. 61) that the emission might arise from gaseous streams in close binary systems, while Manley (ref. 29), Tucker (refs. 30 and 58), and Johnson (ref. 56) have presented models requiring the coexistence of two or more ionized gases of different temperatures. Both types of models present inherent difficulties.

Although the optical emission lines in the spectrum of Sco X–1 do not show pronounced radial velocity variations, the continuum shows irregular and short-period changes. Both flares and flickering have been noted by a number of investigators (Hardie, ref. 62; Mook, ref. 63; Stepien, ref. 64; Mumford, ref. 65; Sandage et al., ref. 54). No evidence for periodicity has been found (Hiltner and Mook, refs. 66 and 67; Mook, ref. 63; Lawrence, Ostriker, and Hesser, ref. 68).

A study of the optical spectrum by photoelectric scanner techniques (Johnson, Spinrad, Taylor, and Peimbert, ref. 69) indicates possible composite features in the spectrum, but the question of binary nature remains unresolved at present. They concluded that continuum radiation was caused by a nonthermal source.

Cyg X–2

An X-ray survey by Giacconi, Gorenstein, Gursky, and Waters (ref. 70), followed by an optical search (ref. 38) in the complex of sources in Cygnus, indicated that Cyg X–2 might be identified with a stellar object. Usher (ref. 71) reported that the candidate showed secular brightness variations in a way similar to Sco X–1, but evidence is of marginal significance. Lynds (ref. 72) reported some similarity of the spectroscopic characteristics in the visual region between Cyg X–2 and Sco X–1. Burbidge, Lynds, and Stockton (ref. 73) found subsequent spectroscopic evidence that Cyg X–2 was really a binary star. Kristian, Sandage, and Westphal (ref. 74), on the basis of photoelectric photometry and spectroscopy, confirm both the existence of short-period (brightness) fluctuations and the radial velocity variations. Comparison of the profiles of $H\beta$ and $H\gamma$ shows a noticeable absence of damping wings. Kraft and Demoulin (ref. 75) have discussed other peculiarities of the Cyg X–2 candidate. In particular, they found evidence for a composite G-type spectrum in the source, possibly because of a subdwarf companion. Peculiar radial velocity variations, perhaps caused by gas streams, were also found. The situation is quite complicated, as they have pointed out.

While Kristian et al. (ref. 74) suggest that the optical flux is not primarily nonthermal in origin, Peimbert, Spinrad, Taylor, and Johnson (ref. 76) correct for the late-type companion and conclude that bremsstrahlung might be a major source of the optical spectrum and be responsible for its observed photometric behavior in a manner analogous to that of Sco X–1

333–240 O—69——2

(Johnson et al. ref. 69). In an investigation of the interstellar reddening, Cathey and Hayes (ref. 77) report additional evidence which supports the viewpoint that a major part of the optical spectrum is essentially "flat." However, a faint early-type companion (earlier than O9) cannot be entirely ruled out on the basis of present observations.

Visvanathan (ref. 78) has reported polarimetric observations of Cyg X–2 which probably represent only interstellar contributions.

Correlations With Radio Surveys

The correlations of X-ray source positions and known strong radio emitters are very weak. In particular, a pronounced absence of X-rays from the radio source Cygnus A was noted in the Cygnus survey carried out by Giacconi et al. (ref. 70). Cygnus X–3 appears, however, to be associated with the Cygnus X radio complex (Gursky et al., ref. 4). In addition to Tau X–1, the Virgo source appears to be associated with either M 87 or 3C 273, although both of these have been questioned by Argyle (ref. 43).

GAMMA RAYS

After the failure of others to detect, by satellite techniques, moderately hard gamma radiation from a number of celestial objects, a Rice University group (Haymes, Ellis, Fishman, Kurfess, and Tucker, ref. 79) using balloon techniques succeeded in detecting weak gamma radiation up to 560 keV from the Crab Nebula. The level found was relatively weak and required long integration times for obtaining satisfactory signal-to-noise ratios. Using very much the same equipment and techniques, Haymes et al. (ref. 80) succeeded in detecting gamma rays from the source Cyg X–1. Unlike the Crab, Cyg X–1 is not a radio source and so far has no optical identification. The Cygnus source is about 50 percent "brighter" (at this energy) than the Crab. Haymes, Ellis, Fishman, Glenn, and Kurfess (ref. 80) have commented that both gamma-ray sources may be the same type—with Cyg X–1 being observed at an earlier stage than the Crab.

Fichtel, Cline, Ehrmann, Kniffen, and Ross (ref. 81), using a balloon-borne digitized spark chamber (Ross, Ehrmann, Fichtel, and Kniffen, ref. 82), established upper limits of 3×10^{-5} $(cm^2sec)^{-1}$ for gamma rays above 30 MeV from a number of optical, radio, and X-ray sources. Similarly, Waddington, May, Long, Valdez, and Freier (ref. 83) found an upper limit for the Cas A radio source of 1.5×10^{-5} $(cm^2sec)^{-1}$ up to 250 MeV.

A number of papers on the observational, instrumental, and theoretical problems of gamma-ray astronomy were presented at the 10th International Conference on Cosmic Rays held in Calgary, Canada, on June 19–30, 1967. Some of the results presented have been used by Shen and Berkey (ref. 20) in a paper discussing gamma-ray production from Compton scattering. A common source for gamma rays and diffuse X-rays was assumed. The

mechanism of Compton scattering of thermal photons by cosmic-ray electrons investigated by Gould (ref. 84) and Fazio, Stecker, and Wright (ref. 85) has assumed new importance since the discovery of the 3° K background radio emission.

At extremely high proton energies ($E>6\times10^{12}$ eV), Stecker, Tsuruta, and Fazio (ref. 86) have indicated that the decay of nucleon isobars and hyperons may contribute significantly to the gamma ray flux. (The gamma rays at 100 MeV are affected strongly.)

It should be noted that the mechanism of gamma-ray production in the Crab and Cyg X–1 has not been examined in detail yet, but the synchrotron process was assumed in a preliminary way by Haymes et al. (refs. 79 and 80). However, because no gamma rays were observed from Virgo, although hard (40 to 107 keV) X-rays were found (Haymes, Ellis, Fishman, Glenn, and Kurfess, ref. 87), Felten (ref. 88) has argued against the synchrotron mechanism as being entirely responsible if M 87 is the X-ray source.

No stellar X-ray sources, except possibly Cyg X–1, have as yet (April 1968) been identified as gamma-ray sources.

DIGEST OF X-RAY STUDIES

This section deals with X-ray sources at low and high galactic latitudes. Table I lists X-ray sources with $b<20°$ and table II those with $b>20°$. The sources in tables I and II are listed in order as a function of galactic longitude, l, starting from $-180°$ through 0° to $+180°$. The several names or survey numbers (as designated for the same source by several observing groups) are given, together with their best positions. In four areas along the galactic plane the sources are so close together that it is not clear whether there are, in reality, several measured positions for the same source or two or perhaps three separate sources. In table I, these areas are blocked off from the sources with better determined positions. Equatorial coordinates (α, δ) and galactic coordinates (l, b) are referred to 1950. The errors in position are typically of the order of 1° and are generally smaller in one coordinate, l, than the other coordinate, b. However, because of blending of close sources and possible variability in intensity, the true errors could be larger than those listed.

Flux is given in counts per square centimeter per second and usually refers to the 1- to 10-keV energy range. Direct flux comparison between surveys is difficult because of such variable parameters as intensity, energy range, correction for detector efficiency, correction for absorption in the residual atmosphere, and angular resolution. Nevertheless, the listed values, in general, confirm the order of magnitude of the intensity of each source.

Approximately a dozen sources were observed on only one scan and are indicated by "*l*." For completeness, four possible sources with very weak flux in the Virgo region are also listed. All sources appear to be "point"

Table I.—*Sources at Low Galactic Latitudes*

Source	Equatorial coordinates			Galactic coordinates		Flux, counts/cm²/sec	Observing group [a]	Remarks [a]
	α		δ, deg	l, deg	b, deg			
	h	m						
Tau XR–1	05	31	22.1	−175.6	−5.8	2.7	NRL	B, H, ID, SP
Tau XR–1	.....	.....	.....	.....	.....	.6	LRL	.....
Tau XR–1	05	31.5	21.99	.....	.....	.....	ASE–MIT	.....
Tau XR–1	.....	.....	.....	.....	.....	.....	TU–ISAS	S
Vel XR–1	8	42	−44	−95.2	.4	.....	LRL	Weak
Cen XR–3	11	23	−59	−68.0	1.8	.....	LRL	.....
"CRUX"	13.5	.....	−66	−52.8	−3.5	1/3 Sco XR–1	AUS	.....
"CRUX"	13.7	.....	−62	−50.8	0	.....	AUS	.....
Cen XR–2	13	24	−62	−52.9	.3	5.4	LRL	.....
Cen X–2	13	20	−60±2°	−53.1	2.4	.....	UL	V
(Cen XR–2)	13	29.9	−65.71	Optical position				ID
Cen XR–1	14	28	−63	−46.0±1.5	−2.5±4.0	.17	NRL	1
Lup XR–1	15	02	−52	−37.1±1.5	5.4±1.5	.2	NRL	.....
Lup XR–1	14	59	−52	−37.6	5.7	1.8	LRL	.....
Nor XR–2	15	38	−57	−35.5±1.5	−1.6±4	.4	NRL	1
Nor XR–1	16	24	−51	−26.5±1.5	−1.6±1.5	.8	NRL	.....
Sco XR–4	16	25	−40	−18.5±1.5	6.0±1.5	.8	NRL	.....
Ara XR–1	17	05	−45.9	−18.2±1.5	−3.4±1.5	1.9	NRL	V

				Confused region				
Sco XR–3	17	23	−44.3	−15.0±1.5	−5.2±1.5	1.1	NRL	V
II–2	17	23	−44.2	−15.0	−5.1	.6	Lockheed survey II and I	.....
Sco X–2	16	50	—39.6	−14.9±1	2.6±3	.....	ASE–MIT	V
GX–14.1	.....	.....	.....	−14.1±.25	0±10°	.11	ASE	.....
GX–12.9	.....	.....	.....	−12.9±.3	>10°	.....	ASE	.....
				Confused region				
Sco XR–2	17	15	−38.4	−11.0±1.5	−.5±4	2.6	NRL	1
Sco XR–2	17	08	−36.4	−10.2±1.5	1.9±1.5	1.4	NRL	.....
II–3	17	08	−36.4	−10.2±1	1.9±3	1.5	Lockheed II and I SEES GX–10.7, –12.4 and –14.1 blended	.....
Sco XR–5	17	37	−40.4	−10.4±1.5	−5.2±4	.7	NRL	1
GX–10.7	.....	.....	.....	−10.7±0.1	0±5	.9	ASE	SD
GX–5.6	.....	.....	.....	−5.6±0.2	0±10	.11	ASE	.....

See footnotes at end of table.

Table I.—*Sources at Low Galactic Latitudes*—Continued

Source	Equatorial coordinates			Galactic coordinates		Flux, counts/cm²/sec	Observing group [a]	Remarks [a]
	α		δ, deg	*l*, deg	*b*, deg			
	h	*m*						
Confused region								
Sco XR–6	18	07	−35.6	−3.2±1.5	−7.8±4	0.3	NRL	1
GX–2.5	.....	.....	.....	−2.5±.15	0±10	.4	ASE	.....
Sgr XR–1	17	48	−30	−.3±1.5	−1.6±1.5	1.6	NRL	1
Sgr XR–1	17	55	−29.2	1.2±1.5	−2.5±1.5	1.6	NRL	.....
I–5	.....	.....	.....	.....	.....	.9	Lockheed I	.....
Oph XR–2	17	14	−23.5	1.1±1.5	8.3±4	.5	NRL	.....
Sgr XR–4	18	26	−31	2.8±1.5	−9.3±4	.6	NRL	1
GX +2.6	.....	.....	.....	2.6±.1	0±5	.68	ASE	1
Confused region								
GX +5.2	.....	.....	.....	5.2±.1	−1±4	1.24	ASE	S
II–4	18	02	−24.9	5.7±1	−1.8±3	.....	Lockheed II and I SEES GX +2.6 and +5.2 blended	.....
Sgr X–1	17	44	−23.2	5.5±1	2.9±3	.....	ASE–MIT	V

Oph XR–1	17	32	−20.7	5.7±1.5	6.5±1.5	1.3	NRL	V
Sgr XR–3	17	56	−21.6	7.9±1.5	1.1±1.5	2.8	NRL	V
GX +9.1				9.1±.1	2.5±4	.84	ASE	SD
II–5	18	03	−20.7	9.5±1	.1±3	1.0	Lockheed II and I	
Sgr XR–2	18	10	−17.1	13.4±1.5	0.5±1.5	1.5	NRL	V
II–6	18	11	−17.2	13.3±1	0.5±3	.6	Lockheed II	
GX +13.5				13.5±.1	−4±8	.37	ASE	B, SD
Ser XR–1	18	10	−12.9	17.1±1.5	2.5±1.5	2.0	NRL	V
GX +16.7				16.7±.1	4±3		ASE	SD
II–7	18	14	−14.3	16.3±1	1.0±3	.9	Lockheed II and I	
Aql XR–1	19	12	0	35.7±1.5	−5.1+2	.13	NRL	1
Ser XR–1	18	45	5.3	37.3±1.5	3.4±1.5	.7	NRL	
Ser XR–1	18	45	5.3			.7	NRL	
GX +36.1				36.3±.2	9±8	.15	ASE	
S							SGR	
GX +48.7				48.7±.2	0±15	.19	ASE	S, H
Vul XR–1	20	38	29	71.3±1.5	−7.6±1.5	.15	NRL	
Cyg XR–1	19	53	34.5	70.5±1.5	3.4±1.5	3.6	NRL	H, V
Cyg XR–1	19	57	34.5	70.9±1.5	2.8±1.5	.9	NRL	
Cyg X–1	19	56.57	35.1	71.4±.1	3.1±.1	.4	ASE	S
Cyg XR–1						.6	LRL	
Cl							SRG	S, H
"Region"							LDN	S, H
"Region"							TU–ISAS	S
Cyg XR–3	19	58	40.4	76.1±1.5	5.6±1.5	0.4	NRL, AUS	H, V
Cyg X–3	20	30.87	40.93	80.0±0.2	0.7±0.2	.13	ASE	SD
Cyg XR–4	21	2	42	84.5±1.5	−3.1±4	.3	NRL	1
Cyg X–4	21	9.18	38.55	82.9±0.1	−6.4±0.1	.05	ASE	

See footnotes at end of table.

Table I.—*Sources at Low Galactic Latitudes*—Concluded

Source	Equatorial coordinates			Galactic coordinates		Flux, counts/cm²/sec	Observing group [a]	Remarks [a]
	α		δ, deg	l, deg	b, deg			
	h	m						
Cyg XR–2	21	43	38. 8	87. 9±1. 5	−10. 8±1. 5	. 8	NRL	V
Cyg XR–2	21	42	38. 8	87. 8±1. 5	−10. 7±1. 5	1. 0	NRL	
Cyg X–2	21	42. 80	38. 18	87. 4±0. 1	−11. 3±0. 1	. 36	ASE	S
Cyg XR–2						. 87	LRL	(3.9–18.2 keV)
(Cyg XR–2)	21	42. 62	38. 09	Optical position				ID
C2							SRG	S, H
Lac XR–1	22	34	53. 8	103. 8±1. 5	−3. 7±1. 5	. 17	NRL	1
Cep XR–2	22	42	62	108. 7±1. 5	3. 0±1. 5	. 18	NRL	1
Cas XR–1	23	21	58. 5	111. 7±1. 5	−2. 2±1. 5	. 3	NRL	
Cep XR–3	23	54	72. 9	119. 0±1. 5	10. 7±4	. 15	NRL	1
Cep XR–1	0	15	66	119. 6±1. 5	3. 6±1. 5	. 3	NRL	

[a] For an explanation of the notation used in these columns, refer to "Notes" at the end of table II.

sources (certainly $<0°.1$), except for three which are indicated by B. Several sources appear to be variable and are indicated by V. Extensive spectral measurements have been made on a few sources which are indicated by S, SE, SP, SD, or SS. SE and SP indicate that data were sufficient to distinguish between exponential or power law relationship. SD represents sources for which there is a deficiency of photons near 1 keV, and SS indicates sources with high-intensity soft X-rays (energy <1 keV). Hard X-rays (energy >10 keV) have been detected from a few sources and are indicated by H. ID indicates source identifications that are fairly certain, and the coordinates of the optical or radio counterparts are also given. Figure 1 is a map of the location of these X-ray sources.

ULTRAVIOLET

Ultraviolet studies of the brightest (apparent magnitude) stars and planets (fig. 2) have continued, using sounding rockets, satellites (1964–83c), and manned vehicles (X–15 and Gemini XI and XII). Filter photometry and spectroscopic observations have led to a number of valuable results for studies of both the stellar atmosphere and the interstellar medium. Reports relating to the objects and instrumentation used in the photometric and spectroscopic observations are listed in tables III and IV, respectively. The number of observations, objects surveyed, and successful flights increased substantially during 1967 over previous years' efforts.

Photometry

Bless, Code, and Houck (ref. 141) reviewed the present status of ultraviolet filter photometry of early-type stars by comparing observations made by various workers including themselves. Flux agreement with photographic spectrophotometry by Boggess and Kondo (ref. 142) is $\pm 0^{m}.3$ for 10 stars in common. Using the temperature scale derived by Morton and Adams (ref. 143), agreement of $\pm 0^{m}.5$ or better can be obtained between observations and model calculations, provided line blanketing has been taken into account shortward of λ 2000. Morton and Adams (ref. 143) have derived new temperatures and bolometric corrections for early-type stars, permitting the transformation of observational data into zero-age main-sequence and mass luminosity relations. Some justification for using He/H of 0.10 or less (by number) to fit the mass-luminosity law was indicated (Morton, ref. 144). The spectrophotometry obtained by Stecher (ref. 145) using rocket-borne scanner techniques has shown satisfactory agreement with the line-blanketed models above 2100 Å. When completed, this spectrophotometry will enable calculation of bolometric corrections directly from observations. An example is shown in figure 3.

Table II.—*Sources at High Galactic Latitude*

Source	Equatorial coordinates			Galactic coordinates		Flux, counts/cm²/sec	Observing group	Remarks
	α		δ, deg	l, deg	b, deg			
	h	m						
Leo XR–1	9	35±16	8.6±1.5	−134.0	40.6	0.2	NRL	1
Virgo XR–1	12	28±16	12.7±1.5			.2	NRL	
M 87	12	30±16	12.6±1			.13	NRL May 1967	ID
M 87	12	30.7	12°30′	−74.7±3	75.1±3		MIT (rocket)	
Discrete source of hard X-rays in Virgo region							Rice	H
(M87)	12	28.3	12.7	−76.2	74.5		Radio position	
Other possible sources in Virgo region with flux <0.1							NRL May 1967 survey	
	ΔRA	±16ᵐ	Δδ±1°					
	12	30	10.3					
	12	30	7.0	−71.3	69.1			
	12	30	4.7					
	12	30	2.4					
3C 273	12	26.6	2.3				Radio position	
(Sco X–1)	16	17.01	−15.53	−.9	23.8		Optical position	H, ID, SE, SS, V
Sco XR–1	16	15	−15.2			18.7	NRL	
Sco XR–1	16	15	−15.0			21	NRL	
Sco XR–1	16.2		−15				AUS	
Sco XR–1	16.3		−16				AUS	

Sco XR–1	16	14±1	−15.6±.02				Lockheed survey I	
Sco X–1	16	17.12±.07	−15.515±.005				ASE–MIT	
Sco X–1	16	17.31±.07	−15.588±.005				ASE–MIT	
Sco XR–1						19	LRL (4.3 to 22.8 keV)	
Lyr XR–1	18	18±16	36±1.5	63.5	21.6	.17	NRL	1
Coma cluster							NASA	B, H

l= Source observed on only one scan in the 1- to 10-Å range during April 1965 survey (ref. 89).

B= Broadened sources: Tau XR–1 (refs. 90 and 91) and perhaps GX +13.5 (ref. 92) and Coma cluster (ref. 93).

Flux= NRL from 1.2 to 12 keV, ASE from 1.5 to 10 keV, Lockheed from 4 to 8 keV, UL from 2 to 5 keV, MIT (rocket) from 1.5 to 6 keV, LRL from 4.3 to 9.4 keV.

H= Hard X-rays detected (energy >10 keV) as described in review paper by Peterson, Jerde, and Jacobson (ref. 94) and more recent publications (refs. 95 to 106).

V= Variability summarized by Friedman, Byram, and Chubb (ref. 89) and more recent publications (refs. 107 to 109).

ID= Sources identified: Cen XR–2—stellar image (ref. 110), Cyg X–2—stellar image (ref. 111), Sco XR–1—stellar image (ref. 112), Tau XR–1—Crab Nebula (ref. 90), Virgo XR–1—external galaxy (refs. 113 and 114) and X-ray sources near known supernovae remnants (refs. 89 and 115).

S= Spectrum studied, SE—exponential spectrum, SP—power law spectrum, SD—deficiency of photons near 1 keV, SS—X-rays less than 1 keV detected. Spectral studies summarized in review article by Gould (ref. 116) and more recent publications (refs. 96, 98, 103, 104, 117 to 121).

ASE= The X-ray group of American Science and Engineering, Cambridge, Mass., is sponsored by the National Aeronautics and Space Administration (refs. 92, 119, 122).

ASE–MIT= The joint X-ray group of American Science and Engineering and Massachusetts Institute of Technology is sponsored by the National Aeronautics and Space Administration and by the U.S. Atomic Energy Commission (refs. 91, 123 to 125).

AUS= The X-ray group from the University of Adelaide and University of Tasmania in Australia is sponsored by the National Aeronautics and Space Administration and the Science Research Council of the United Kingdom (ref 126).

Lockheed= The X-ray group of the Lockheed Missiles & Space Co. is sponsored by the National Aeronautics and

Space Administration and Lockheed Independent Research Program (refs. 117, 127 to 129).

LRL= The X-ray group at the Lawrence Radiation Laboratory is sponsored by the U.S. Atomic Energy Commission (refs. 96, 97, 103, 105, 107, 130).

MIT (balloon)= The X-ray group of the Laboratory for Nuclear Science and the Department of Physics of the Massachusetts Institute of Technology is sponsored in part by National Aeronautics and Space Administration and in part by the U.S. Atomic Energy Commission (refs. 98, 102, 103, 106, 108).

MIT (rocket)= The X-ray group of the Department of Physics and Center for Space Research of the Massachusetts Institute of Technology is sponsored by National Aeronautics and Space Administration and U.S. Atomic Energy Commission (ref. 131).

NASA= The X-ray group at the Goddard Space Flight Center of the National Aeronautics and Space Administration (ref. 93).

NRL= The X-ray group of the E. O. Hulburt Center for Space Research is sponsored by the U.S. Office of Naval Research and the U.S. National Science Foundation (refs. 89, 90, 113, 114, 132 to 134).

Rice= The X-ray group of the Department of Space Science of Rice University is sponsored by the Air Force Office of Scientific Research (refs. 99 to 101).

UL= The X-ray group of the University of Leicester, England (ref. 135).

LDN (balloon)= Cosmic Ray Working Group—the Royal Dutch Academy of Sciences; Kamerlingh onnes Laboratorium, Leiden, Netherlands (ref. 136).

SRG (balloon)= Space Research Group of the GIFCO—C.N.R., Physics Institute, University of Bologna, Italy (ref. 137).

TU–ISAS= Tokyo University, Institute of Space and Aeronautical Science (refs. 138 to 140).

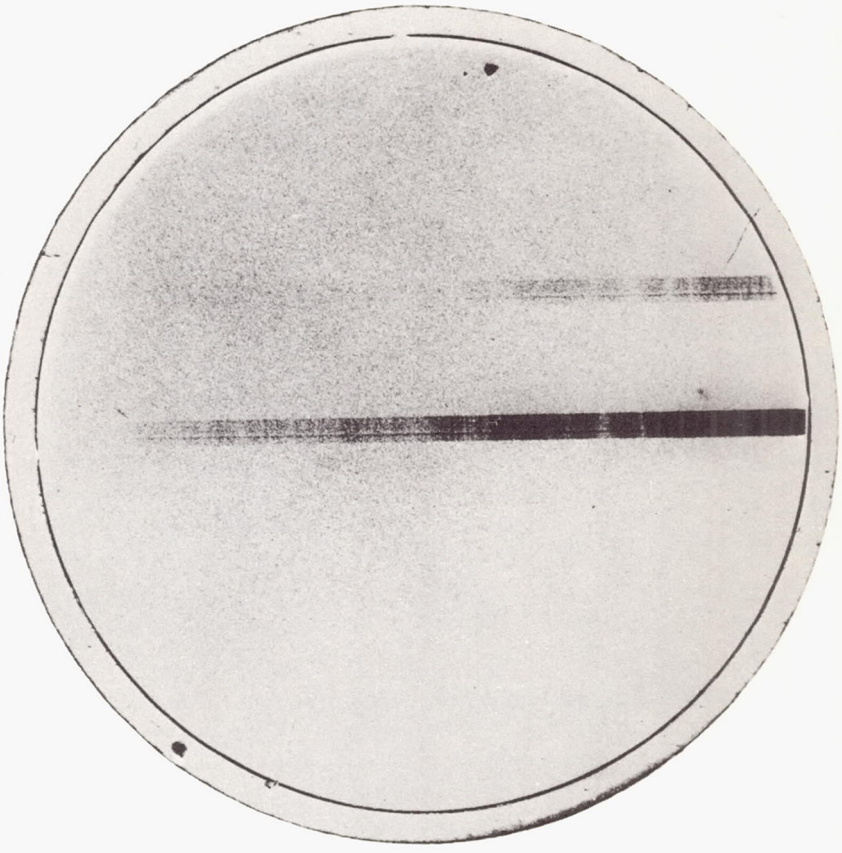


Figure 2.—**Ultraviolet spectra of Jupiter and Venus obtained on Aerobee flight KP 3.21, June 9, 1967, by Jenkins and Morton. Venus has the darker spectrum and covers the range 2100 to 3070 Å. Wavelengths increase toward the right. The features in both spectra are caused entirely by solar Fraunhofer structure.**

Spectroscopy

Objective-prism spectrograms obtained during the Gemini XI flight have been analyzed by Henize and Wray (ref. 146), who indicate that colors relative to 3600 Å can be obtained to within probable errors of $\pm \overset{m}{\odot} 1$ for early-type stars fainter than 5th magnitude. A Gemini XI photograph of the Orion region showed the Barnard Loop Nebula to have an unusual ultraviolet configuration (fig. 4). As analyzed by O'Dell, York, and Henize (ref. 147), the photograph in figure 4*b* appears to indicate that the material density of the nebula increases as the distance from the center of the nebula increases. Radiation pressure of starlight acting on a dust-gas mixture was a suggested mechanism for this interpretation.

Recently, Viton (ref. 148) has described a very low dispersion ultraviolet spectrogram that shows an ultraviolet "glow" in the general areas of Auriga, Orion, and Canis Major. No immediate confirmation has been found for this, although Witt (ref. 149) found evidence for a diffuse glow at optical wavelengths in Cygnus and Taurus-Auriga.

Table III.—*References to Ultraviolet Photometry*

Investigator(s)	Instrumentation	Objects (studied, surveyed)	Reference
Bless, Code, Houck, McNall, and Taylor	Rocket	~100 stars O,B and later types	141
Smith	Satellite	~96 stars	168
Bless, Code, and Houck	Rocket	BO–A7 stars	169
Carruthers	Rocket	γ Vel, ζ Pup, α CMa, κ Ori, γ Ori, λ Ori, ϕ^1 Ori, "Sword," "Belt"	155
Dougherty	X–15	α Aur	(To be published)

Table IV.—*References to Ultraviolet Spectroscopic Observations*

Investigator(s)	Instrumentation	Objects (studied, surveyed)	Reference
Morton and Spitzer	Objective grating	δ, π Sco	150
Stone and Morton	Objective grating		151
Morton	Objective grating	δ, ϵ, ζ, ι, κ Ori	153
Henize, Wackerling, and O'Callaghan	Objective prism	Vela-Carina	170
Henize and Wray	Objective prism	130 stars down to $M_v = 5$ or 6 incl. α Sco, 48 Lib	146
Stecher	Photoelectric scanner	Various O-, B-, A-type stars including α Lyr, λ Sco, ζ Oph	145
Carruthers	Image-converter spectrograph	κ, ι, ζ, λ, δ+E, γ, ι Ori, ζ Pup, γ Vel.	155
O'Dell, York, and Henize	Objective prism	Barnard's loop nebula	147
Boggess and Kondo	Objective grating	β, γ, κ, η, ϵ, ν, ζ, δ Ori, α, ζ, β, ξ CMa	142
Viton	Objective prisms	Auriga-Taurus-Orion	148
Morton and Jenkins	Objective grating	ζ Pup	158
Morton, Jenkins, and Bohlin	All-reflective spectrograph	γ, δ, ϵ, ζ, η, ι, σ, $\theta^1+\theta^2$ Ori	166

Interstellar lines in the ultraviolet have also been studied. Using the spectrum of δ and π Sco previously obtained by Morton and Spitzer (ref. 150), Stone and Morton (ref. 151) found lines caused by O I, C II, Si II, and Al II that were interpreted as being interstellar. Although the equivalent widths indicated roughly the solar proportion of these elements, the derived hydrogen abundance was too high by a factor of 30, if we adopt a recent measurement of the O I transition probability by Gaillard and Hesser (ref. 152). However, because Lyman-α was not observed for these stars, the hydrogen could not be estimated directly.

Interstellar Lyman-α equivalent widths for a number of stars have been reported by Morton (ref. 153), Jenkins (ref. 154), Stecher (ref. 145), and Carruthers (ref. 155). For ζ Ori, rough agreement in the equivalent widths of Lyman-α were obtained. Morton and Jenkins concluded that the mean H I density in the direction of Orion is 0.1 atom/cc. In contrast, the 21-cm radio observations give about 1 atom/cc. Fischel and Stecher (ref. 156) suggested that the radio estimates are in error because "optical pumping" (laser action) overpopulates the upper hyperfine state by about 10 percent.

An upper limit to the amount of interstellar molecular hydrogen (H_2)

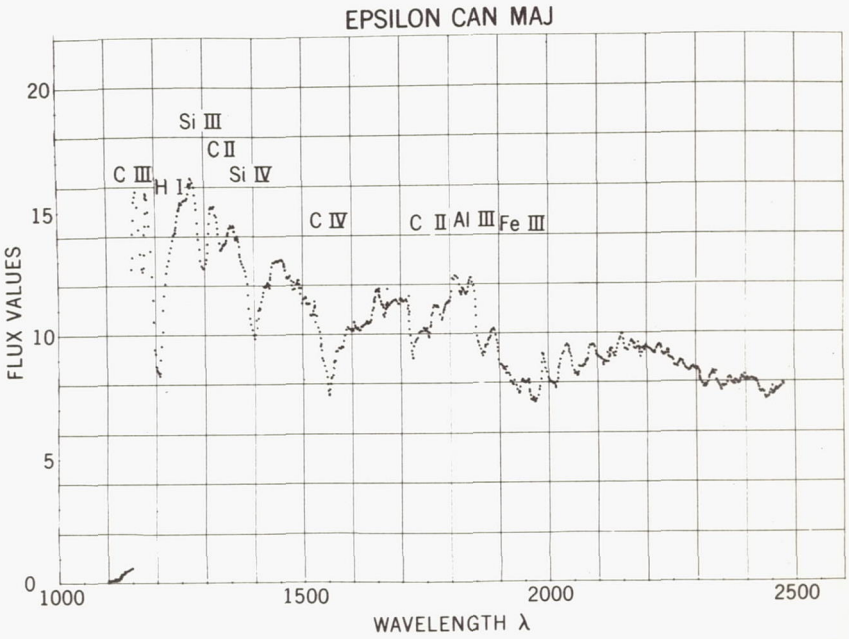


Figure 3.—Spectrophotometry (Stecher). Energy distribution of ϵ Can Maj., B_2 II, in ergs cm^{-2} s^{-1} $Å^{-1} \times 10^9$, showing the strong resonant line absorption in the ultraviolet. The resolution is 10 Å. Obtained on an Aerobee flight with 12-inch telescope and spectrometer.

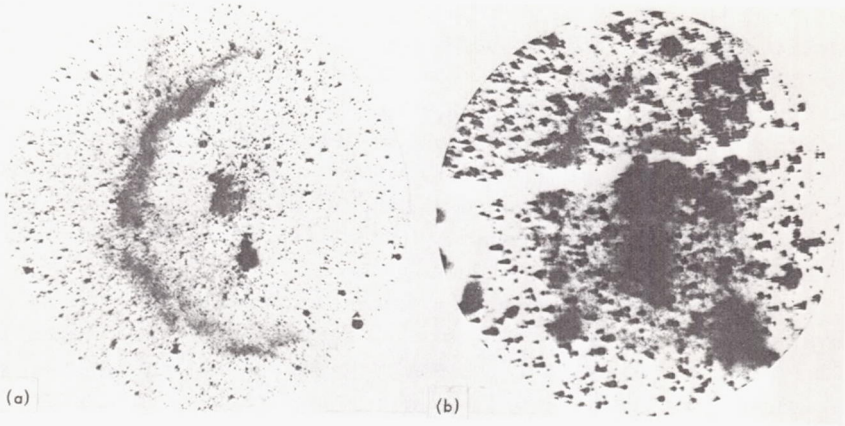


Figure 4.—Orion. (*a*) A negative print of Orion, photographed by Courtes with an interference filter isolating Hα and [N II] emission. The scale is the same as in figure 4 (*b*); the very different appearance in the two spectral regions is to be noted. (*b*) A negative, high-contrast print of Orion in the ultraviolet showing the low surface brightness Barnard loop Nebula throughout the inner Orion configuration.

of 10 percent of the atomic hydrogen density was derived by Carruthers (ref. 157) on the basis of an unsuccessful search for the Lyman bands ($B'\Sigma u^+ \leftarrow X'\Sigma g^+$) occurring shortward of 1108 Å in γ^2 Vel and ζ Pup. For ζPup, Carruthers (refs. 155 and 157) and Morton and Jenkins (ref. 158) found hydrogen densities somewhat lower than for Orion, although the observations were not corrected for the effect of the H II region surrounding ζPup (fig. 5).

Stecher and Williams (ref. 159), Wentzel (ref. 160), and Williams (ref. 161) have studied the formation of H_2 and other molecules formed on the basis of chemical-exchange reactions. Wentzel considered cloud-cloud collision effects and found an upper limit of 3 percent for regions which are optically thick to radiation with $\lambda < 1000$ Å. Stecher and Williams (ref. 162), however, have considered the photodestruction of H_2 and found that H_2 densities of 10^{-7} cm^{-3} are likely for the general interstellar region. However, since Heiles (ref. 163) has detected OH emission from a number of optically thick dust clouds, these observations imply the existence of H_2.

Another quite unexpected result obtained by Morton (ref. 164) is an indication of observable mass loss from three OB supergiants (δ, ϵ, and ζ Orionis). Rates of 10^{-6} $M_\odot$ yr^{-1} are indicated. Subsequently, Stecher (ref .145), Carruthers (ref. 155), and Morton and Jenkins (ref. 158) have obtained evidence for mass loss from other OB stars including the Of star ζPup. Lucy and Solomon (ref. 165) have suggested that the outer layers of

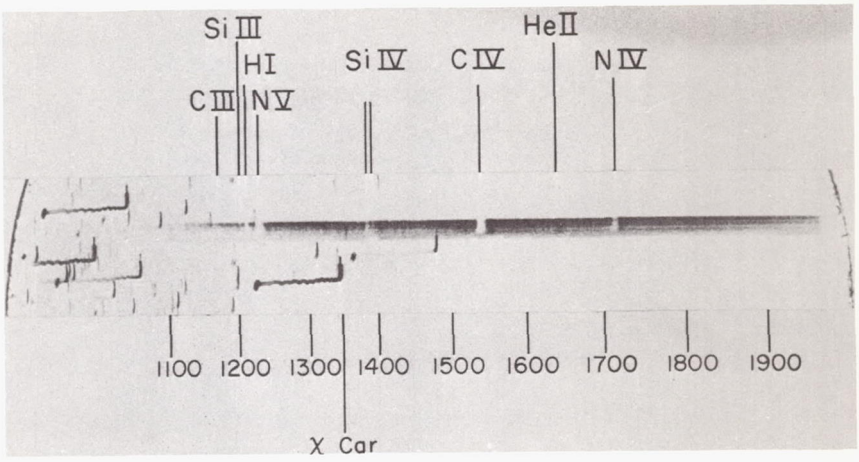


Figure 5.—**Ultraviolet spectrum of ζPup (05f) in the wavelength range from λλ1100 to 1965 obtained by Morton and Jenkins with a NASA Aerobee rocket November 1, 1967.**

a hot supergiant can be accelerated by the radiation pressure exerted on the matter by absorption in the strong ultraviolet resonance lines.

Using an all-reflecting spectrograph, Morton, Jenkins, and Bohlin (ref. 166) have measured 283 lines in 10 OB stars near ε Ori. The presence of circumstellar and interstellar lines was confirmed. Over 100 lines remain unidentified (fig. 6).

Courtes (ref. 167) has discussed multiple bandpass techniques applied to space telescopes and suggested a means of dispersing the image that makes the guiding errors less significant than for conventional instrumentation.

In summary, ultraviolet studies have produced the following important results. An improved temperature scale has been developed for hot stars. These stars are cooler and emit less energy than previously thought. OB supergiants are losing mass rapidly to the interstellar medium. As a consequence, these two items may require an adjustment of the evolutionary rates and times scales. Observations of interstellar gas abundances observed in the ultraviolet indicate little or no H_2, and this may imply that more galactic mass is locked up in "unobservable" objects such as cold bodies and/or neutron stars. Other ultraviolet interstellar abundances are inconsistent with radio measurements. Finally, Gemini pictures of the Orion Nebula give an improved model of the large-scale nebular complex and help tie together radio and visible observations.

There still remain unanswered questions and much work is needed in ultraviolet research. For example, the ultraviolet region is important for learning about the atmospheres of rapidly evolving hot stars. In addition,

333-240 O—69——3

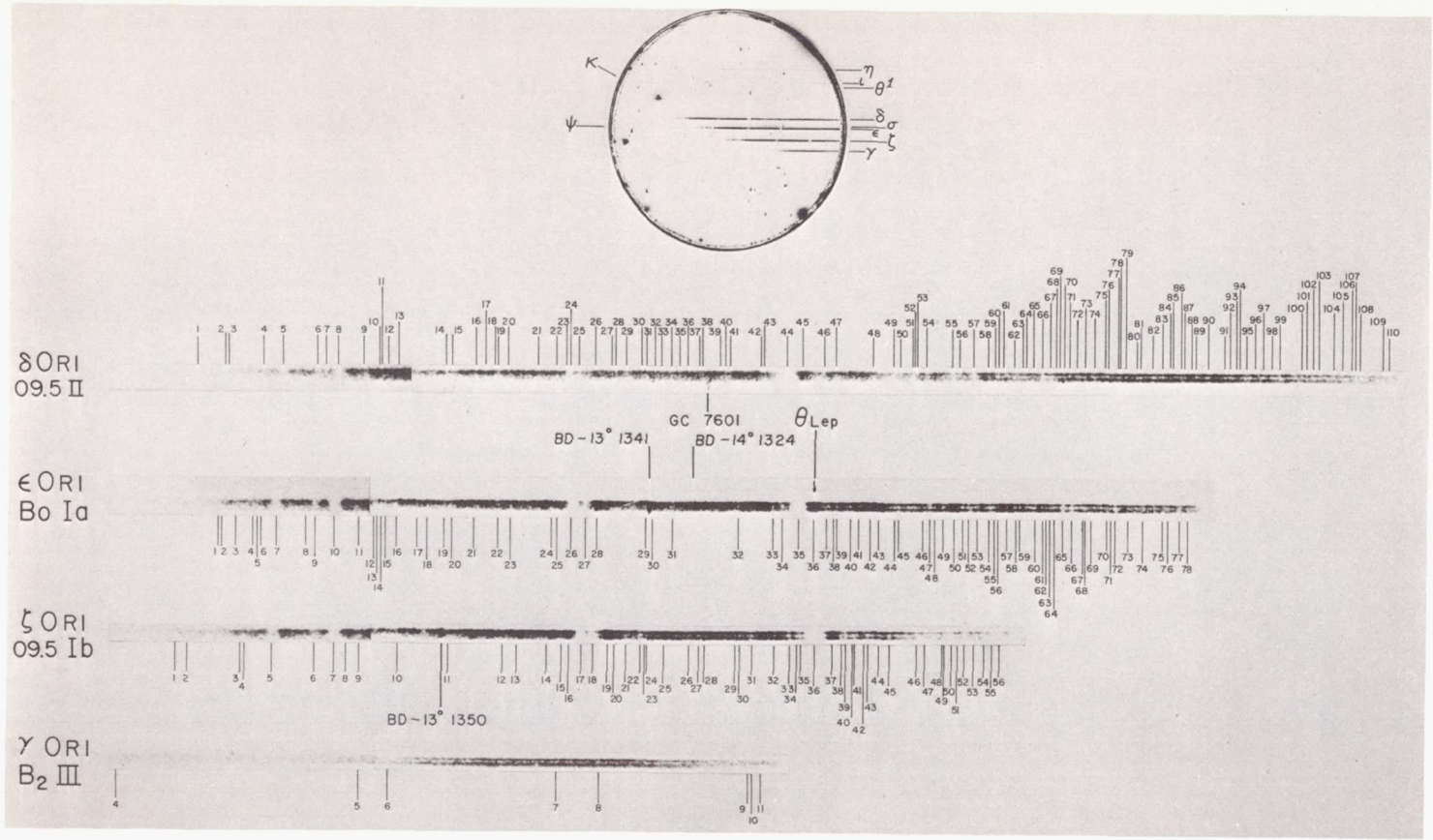


Figure 6.—Ultraviolet spectra of δOri, εOri, ζOri, γOri obtained by Morton, Jenkins, and Bohlin (ref. 166) from a rocket flight on September 20, 1966. The original film is reproduced at the top and enlargements of the four spectra are shown below. Wavelengths increase to the right and cover a range from 1100 to 2000 Å. The numbered markers indicate positions of absorption lines identified in the reference.

much more information is needed concerning abundances and excitation of interstellar gas. The discrepancies between the results found in the ultraviolet and radio regions are puzzling.

INFRARED

Hoffman and Woolf (ref. 171) have outlined the prospects for infrared astronomy for the next 20 years.

A balloon-borne, far-infrared bolometer was used for a sky survey by Hoffman et al. (ref. 172). Except for the Moon, no other source was observed. An upper limit to the flux from other sources was 2×10^{-23} W cm^{-2} Hz^{-1} or 10° K for a blackbody in the 300- to 360-μ range. The negative result suggests that either the interstellar grains do not radiate efficiently at these wavelengths or that their visual albedo is very high.

Ground-based observations of low-temperature objects continue to be made. Becklin and Neugebauer (ref. 173) discovered an infrared point source of low temperature in the Orion Nebula. Nearby, Kleinmann and Low (ref. 174) found an extended source at 22 μ of even lower temperature. In order to interpret the observations, both Cameron (ref. 175) and Hartmann (ref. 176) have considered models that include star formation. Previous to the discovery of the Orion sources, Davidson and Harwit (ref. 177) had considered a thermal dust cloud around "cocoon" stars with the prediction that both infrared and radio emissions might be detectable from such objects. Raimond and Eliasson (ref. 178) have suggested a possible connection between an Orion OH source and the Becklin and Neugebauer object.

Infrared photometry by Mendoza (refs. 179 and 180) indicated large infrared excesses and other peculiarities for T Tauri stars, while Low and Smith (ref. 181) interpreted observations of R Mon at 22 μ as being caused by circumstellar dust. However, Comella (ref. 182) failed to find any radio emission from R Mon and several other objects having large infrared excesses. Comella referred to an unpublished result obtained by Hogg in 1966 at 15.3 GHz for R Mon which indicated an upper limit of 0.03 flux units.

Infrared excesses for early-type stars have also been observed by Johnson (ref. 183). In addition, infrared observations by Lee and Nariai (ref. 184) indicate that υ Sgr has a stronger IR excess than any of the sources studied by Johnson. This star, an eclipsing binary with tidally distorted components, is primarily noted for its very low hydrogen abundance.

It should be noted that infrared excesses, particularly in the absence of detectable radio emissions, do not necessarily imply the presence of dust. Pottasch (ref. 185) has suggested discrete emission by Si at 64 μ, S at 25 μ, Fe at 24 μ, and O at 63 μ may be present in the nebula discovered by Kleinmann and Low (ref. 174).

Infrared (Gillett, Low, and Stein, ref. 186) and radio observations (Thompson, Colvin, and Stanley, ref. 187) of the planetary nebula NGC

7027 indicate that at least one object shows both infrared and radio emissions. Swamy and O'Dell (ref. 188) have interpreted this as thermal emission. If this is so, it is difficult to understand why R Mon and other objects with large IR excesses do not show a similar effect. Either (1) the emission is nonthermal, (2) the grains do not radiate as blackbodies, or (3) the radius of the emitting area is too small. The matter is still unresolved.

Infrared observations of the Crab Nebula by Ney and Stein (ref. 189), Becklin and Kleinmann (ref. 190) infer a possible break or steepening of the electromagnetic spectrum at about 50 μ. Becklin and Kleinmann find that 23 percent of the total energy is in the IR, 63 percent at <0.3 μ, 14 percent in the optical, and less than 0.5 percent in the radio regions. The luminosity is estimated as 7×10^{37} ergs sec $^{-1}$.

The infrared emission caused by a shock wave passing through an HI region has been investigated by Field, Rather, Aannestad, and Orszag (ref. 191). They predict that 8-μ and 12-μ emission of H_2 might be detectable under favorable circumstances using ground-based equipment. Werner and Harwit (ref. 192) have identified lines in the 8-μ region in the Orion Nebula using a pressure scanning Fabry-Perot interferometer attributed to H_2, but quantitative interpretation is very difficult.

Becklin and Neugebauer (ref. 193) have succeeded in detecting the galactic center in the infrared. They found a maximum coincident with the Sgr A radio source. Several secondary sources also were found. In addition to the extended sources, they discovered a "point" source. Several possibilities, including the true galactic nucleus, a bright IR star, or a close nearby star having an appropriate apparent position, were considered to be the source, but further observations are required.

The Taurus object identified by Neugebauer, Martz, and Leighton (ref. 194) was observed polarimetrically in the infrared by Forbes (ref. 195). He found a lack of appreciable polarization at 1.25, 1.62, and 2.2 μ. In the visual region, Appenzeller and O'Dell (ref. 196) found quite large polarization. They interpret this to mean that most polarization, if not all, is produced by grains quite near to the star. Observational results of the infrared photometry for this object and several other "infrared stars" have been published by Wisniewski, Wing, Spinrad, and Johnson (ref. 197).

Three infrared stars identified by Neugebauer, Martz, and Leighton (ref. 194), the Taurus object, the Cygnus object, and TX Cam, were investigated in detail by Wing, Spinrad, and Kuhi (ref. 198). They concluded that all were intrinsically red stars, the majority of which were Mira variables with periods longer than 1 year. The Cygnus object was an exception since no definite variations in color, magnitude, or spectrum were found.

McCammon, Münch, and Neugebauer (ref. 199) have reported on infrared spectroscopy of low-temperature stars, including those identified by

Neugebauer, Martz, and Leighton (ref. 194). In particular, several stellar water-vapor bands have been detected and studied using ground-based equipment.

CONCLUSIONS

One of the most striking results of space research has been the discovery of strong X-ray emitting objects. Some discrete sources have been positively associated with known radio or optical objects; most are still unidentified. A few of the sources have been tentatively associated with galaxies. Various interpretations of the physical processes involved have been studied, but it is difficult to determine specific mechanisms on the basis of the scanty spectral and temporal data available. X-ray astronomy from rockets is still limited by size of instrumentation and the duration of observation. However, techniques are developing rapidly in this field and progress is being made for obtaining more accurate X-ray positions and more sensitive detectors. There is a real need to study strong X-ray sources over long periods of time to understand the flares and flickering that have been observed.

In 1967, for the first time, techniques of data collection have developed in ultraviolet astronomy to the point where primary emphasis could be placed on interpretation. Improved resolution of ultraviolet spectra has resulted in observations of the stronger absorption line structure and additional knowledge of stellar atmospheric conditions. Ultraviolet photometry has provided an improved temperature scale for B and A stars. These stars are cooler and emit less energy than previously thought. The O and B supergiants are found to be losing mass rapidly to the interstellar medium. Theories concerning the evolutionary rates and time scales of early-type stars may require some adjustment as a result of these discoveries. The ultraviolet observations of interstellar gas abundances indicate there is much less H_2 than had been anticipated. As a result, it may be necessary to postulate that more of the galactic mass is locked up in unobservable objects such as cold bodies and/or neutron stars. Abundances of other elements in the ultraviolet do not agree well with those found by radio techniques, and more observations are required to resolve this problem. The Gemini pictures of the Orion Nebula are the first use of American man in space for stellar astronomical research. The pictures have resulted in an improved model of the large nebular complex in Orion and help tie together the radio and visible observations of this region.

An exciting beginning has been made in infrared astronomy with observations of low-temperature objects, presumably in a prestellar state of contraction, and with observations of sources toward the galactic center. Unfortunately, researchers working in this part of the spectrum are severely energy limited, and more sensitive detectors must be developed before the number of detectable infrared objects can be increased significantly.

REFERENCES

1. MORRISON, P.: Extrasolar X-Ray Sources. Ann. Rev. Astron. Ap. Goldberg, Layzer, and Phillips, eds. (Palo Alto: Annual Reviews, Inc.), vol. 5, 1967, pp. 325–350.
2. FRIEDMAN, H.: Discrete X-Ray Sources. Vol. 7, Nebulae and Interstellar Matter. Stars and Stellar Systems. B. Middlehurst and L. H. Aller, eds., Univ. of Chicago Press, Chicago, 1968, pp. 685–706.
3. GOULD, R. J.: Origin of Cosmic X-Rays. Am. J. Physics, vol. 35, 1967, pp. 376–393.
4. GURSKY, H.; GORENSTEIN, P.; AND GIACCONI, R.: The Distribution of Galactic X-Ray Sources From Scorpio to Cygnus. Astrophys. J., vol. 150, 1967, pp. L75–L84.
5. JOHNSON, H. M.: Galactic X-Ray Statistics (abstract). Astron. J., vol. 72, 1967, p. 806.
6. COOKE, B. A.; POUNDS, K. A.; STEWARDSON, E. A.; AND ADAMS, D. J.: A Cosmic X-Ray Survey in the Southern Hemisphere. Astrophys. J., vol. 150, 1967, pp. L189–L191.
7. GIACCONI, R.; GURSKY, H.; PAOLINI, F. R.; AND ROSSI, B. B.: Evidence for X-Rays From Sources Outside the Solar System. Phys. Rev. Letters, vol. 9, 1962, pp. 439–443.
8. SEWARD, F.; CHODIL, G.; MARK, H.; SWIFT, C.; AND TOOR, A.: Diffuse Cosmic X-Ray Background Between 4 and 40 keV. Astrophys. J., vol. 150, 1967, pp. 845–850.
9. GIACCONI, R.; GORENSTEIN, P.; GURSKY, H.; AND KELLOGG, E. M.: Observation of Cosmic X-Rays in the Region of the Galactic Anti-Center (abstract). Astron. J., vol. 73, 1968, pp. S94–S95.
10. BOWYER, C. S.; FIELD, G. B.; AND MACK, J. E.: Detection of an Anisotropic Soft X-ray Background Flux. Nature, vol. 217, 1968, pp. 32–34.
11. FRITZ, G.; MEEKINS, J. F.; HENRY, R. C.; BYRAM, E. T.; AND FRIEDMAN, H.: Possible Detection of a Dense Hot Intergalactic Medium. 126th Meeting Am. Astron. Soc. (Charlottesville, Va.), Apr. 1–4, 1968.
12. BRECHER, K.; AND MORRISON, P.: Cosmology, Black-Body Radiation, and the Diffuse X-Ray Background. Astrophys. J., vol. 150, 1967, pp. L61–L64.
13. FELTEN, J. R.; AND MORRISON, P.: Omnidirectional Inverse Compton and Synchrotron Radiation From Cosmic Distributions of Fast Electrons and Thermal Protons. Astrophys. J., vol. 146, 1966, pp. 686–708.
14. GOULD, R. J.; AND BURBIDGE, G. R.: X-Rays From the Galactic Center, External Galaxies, and the Intergalactic Medium. Astrophys., J., vol. 138, 1963, pp. 969–977.
15. SILK, J.: The Diffuse X-Ray Background. Astrophys. J., vol. 151, 1968, pp. L19–L22.
16. FRIEDMAN, H.; BYRAM, E. T.; AND CHUBB, T. A.: Distribution and Variability of Cosmic X-Ray Sources. Science, vol. 156, 1967, pp. 374–378.
17. ODA, M.: X-Ray and γ-Ray Astronomy. Proc. 9th Int. Conf. Cosmic Rays, Sept. 1965 (London, England), vol. 1, pp. 68–80 (publ. the Institute of Physics and the Physical Soc. London).
18. FIELD, G. B.; AND HENRY, R. C.: Free-free Emission by Intergalactic Hydrogen. Astrophys. J., vol. 140, 1964, pp. 1002–1012.
19. WEYMANN, R.: Possible Thermal Histories of Intergalactic Gas. Astrophys. J., vol. 147, 1967, pp. 887–900.
20. SHEN, C. S.; AND BERKEY, G.: Cosmic Gamma Rays From Inverse Compton Scattering. Astrophys. J., vol. 151, 1968, pp. 895–900.

21. Overbeck, J. W.; and Tananbaum, H. D.: Twofold Increase of the High-Energy X-Ray Flux From Cygnus XR–1. Phys. Rev. Letters, vol. 20, 1968, pp. 24–27.
22. Overbeck, J. W.; Womack, E. A.; and Tananbaum, H. D.: High-Energy X-Rays From Cygnus XR–1. Astrophys. J., vol. 150, 1967, pp. 47–56.
23. Hill, R. W.; Grader, R. G.; and Seward, F. D.: The Soft X-Ray Spectrum of Scorpius X–1 (abstract). Astron. J., vol. 73, 1968, pp. S97–S98.
24. Chodil, G.; Mark, H.; Rodrigues, R.; Seward, F.; Swift, C. D.; Hiltner, W. A.; Wallerstein, G.; and Mannery, E. J.: Spectral and Location Measurements of Several Cosmic X-Ray Sources Including a Variable Source in Centaurus. Phys. Rev. Letters, vol. 19, 1967, pp. 681–683.
25. Lewin, W. H. G.; Clark, G. W.; and Smith, W. B.: Observation of Cen XR–2 and Other High-Energy X-Ray Sources in the Southern Sky. Astrophys. J., vol. 152, 1968, pp. L49–L53.
26. Conner, J. P.; and Singer, S.: Satellite Observations of Galactic X-Ray Sources. 126th Meeting Am. Astron. Soc. (Charlottesville, Va.), Apr. 1–4, 1968.
27. Chodil, G.; Mark, H.; Rodrigues, R.; and Swift, C. D.: Nova-Like Behavior of the X-Ray Source Centaurus XR–2. Astrophys. J., vol. 152, 1968, pp. L45–L48.
28. Lewin, W. H. G.; Clark, G. W.; and Smith, W. B.: Observation of an X-Ray Flare From Sco X–1. Astrophys. J., vol. 152, 1968, pp. L55–L61.
29. Manley, O. P.: X-Ray Emission From Sco X–1. Astrophys. J., vol. 144, 1966, pp. 1253–1257.
30. Tucker, W. H.: Cosmic X–Ray Sources. Astrophys. J., vol. 148, 1967, pp. 745–765.
31. Meekins, J. F.; Fritz, G.; Henry, R. C.; Byram, E. T.; and Friedman, H.: New X-Ray Spectra of Sco XR–1, Cyg XR–1 and Cyg XR–2 (abstract). Astron. J., vol. 73, 1968, pp. S106–S107.
32. Peterson, L. E.; Jacobson, A. S.; and Pelling, R. M.: Spectrum of Crab Nebula X-Rays to 120 keV. Phys. Rev. Letters, vol. 16, 1966, pp. 142–144.
33. Bleeker, J. A. M.; Burger, J. J.; Deerenberg, A. J. M.; Scheepmaker, A.; Swanenburg, B. N.; and Tanaka, Y.: Balloon Observations of the X-Ray Sources in the Cygnus Region in the Energy Range 20–130 keV. Astrophys. J., vol. 147, 1967, pp. 391–394.
34. Brini, D.; Ciriegi, V.; Fuligni, F.; Moretti, E.; and Vespignani, G.: Cosmic X-Ray Sources in the 20–180 keV Energy Range. Astrophys. J., vol. 149, 1967, pp. 429–433.
35. Seward, F. D.; and Toor, A.: Search for 8–80 keV X-Rays From the Large Magellanic Cloud and the Crab Nebula. Astrophys. J., vol. 150, 1967, pp. 405–411.
36. Clark, G. W.; Lewin, W. H. G.; and Smith, W. B.: Sky Survey of High-Energy Cosmic X-Rays and Spectra of the Sources in the Crab Nebula and Cygnus. Astrophys. J., vol. 151, 1968, pp. 21–32.
37. Gorenstein, P.; Giacconi, R.; and Gursky, H.: The Spectra of Several X-Ray Sources in Cygnus and Scorpio. Astrophys. J., vol. 150, 1967, pp. L85–L94.
38. Giacconi, R.; Gorenstein, P.; Gursky, H.; Usher, P. D.; Waters, J. R.; Sandage, A.; Osmer, P.; and Peach, J. V.: On the Optical Search for the X-Ray Sources Cyg X–1 and Cyg X–2. Astrophys. J., vol. 148, 1967, pp. L129–L132.
39. Blanco, V. M.; and Kunkel, W. E.: Cen XR2 and NGC 5189 (abstract). Astron. J., vol. 73, 1968, p. S5.

40. POVEDA, A.; AND WOLTJER, L.: Supernovae and Supernova Remnants. Astron. J., vol. 73, 1968, pp. 65–74.
41. BRADT, H.; MAYER, W.; NARANAN, S.; RAPPAPORT, S.; AND SPADA, G.: Evidence for X-Radiation From the Radio Galaxy M87. Astrophys. J., vol. 150, 1967, pp. L199–L206.
42. FRIEDMAN, H.; AND BYRAM, E. T.: X-Rays From the Coma Cluster of Galaxies. Astrophys. J., vol. 147, 1967, pp. 389–401.
43. ARGYLE, E.: X-Rays From Source 3C 273. Science, vol. 159, 1968, p. 747.
44. HARRIES, J. R.; MCCRACKEN, K. G.; FRANCEY, R. J.; AND FENTON, A. G.: A Strong X-Ray Source in the Vicinity of the Constellation Crux. Nature, vol. 215, 1967, pp. 38–40.
45. BRAES, L. L. E.; AND HOVENIER, J. W.: Supernova Phenomena in OB Associations and Cosmic X-Ray Sources. Nature, vol. 209, 1966, pp. 360–361.
46. O'DELL, C. R.: Positional Correlations of Galactic Objects and X-Ray Sources. Astrophys. J., vol. 147, 1967, pp. 855–857.
47. BLESS, R. C.; FISCHEL, D.; AND STECHER, T. P.: Of and Wolf-Rayet Stars as X-Ray Sources. Astrophys. J., vol. 151, 1968, pp. L117–L119.
48. WALLERSTEIN, G.: A Possible Identification of Lac XR–1 With the Wolf-Rayet Binary HD 211853. Astrophys. J., vol. 151, 1968, pp. L121–L124.
49. MINKOWSKI, R.: Nonthermal Galactic Radio Sources. Vol. 7, Nebulae and Interstellar Matter. Stars and Stellar Systems. B. Middlehurst and L. H. Aller, eds., Univ. of Chicago Press, Chicago, 1968, pp. 623–666.
50. WOLTJER, L.: X-Rays and Type I Supernova Remnants. Astrophys. J., vol. 140, 1964, pp. 1309–1313.
51. SHKLOVSKY, I. S.: Remarks on the Synchrotron-Radiation Spectrum of the Crab Nebula. Sov. Astron.—AJ, vol. 10, 1966, pp. 6–7. (Astronomicheskii Zhurnal, vol. 43, 1966, pp. 10–12.)
52. SARTORI, L.; AND MORRISON, P.: Thermal X-Rays From Non-thermal Radio Sources. Astrophys. J., vol. 150, 1967, pp. 385–403.
53. ODA, M.; BRADT, H.; GARMIRE, G.; SPADA, G.; SREEKANTAN, B. V.; GURSKY, H.; GIACCONI, R.; GORENSTEIN, P.; AND WATERS, J. R.: The Size and Position of the X-ray Source in the Crab Nebula. Astrophys. J., vol. 148, 1967, pp. L5–L11.
54. SANDAGE, A. R.; OSMER, P.; GIACCONI, R.; GORENSTEIN, P.; GURSKY, H.; WATERS, J.; BRADT, H.; GARMIRE, G.; SREEKANTAN, B. V.; ODA, M.; OSAWA, K.; AND JUGAKU, J.: On the Optical Identification of Sco X–1. Astrophys. J., vol. 146, 1966, pp. 316–322.
55. JOHNSON, H. M.; AND STEPHENSON, C. B.: A Possible Old Nova Near Sco X–1. Astrophys. J., vol. 146, 1966, pp. 602–605.
56. JOHNSON, H. M.: Physical Characteristics of Sco X–1 II. Astrophys. J., vol. 147, 1967, pp. 1213–1218.
57. SHKLOVSKY, I. S.: On the Nature of the Source of X-Ray Emission of Sco XR–1. Astrophys. J., vol. 148, 1967, pp. L1–L3.
58. TUCKER, W. H.: Physical Conditions in Sco X–1. Astrophys. J., vol. 149, 1967, pp. L105–L109.
59. PRENDERGAST, K. H.; AND BURBIDGE, G. R.: On the Nature of Some Galactic X-Ray Sources. Astrophys. J., vol. 151, 1968, pp. L83–L88.
60. CAMERON, A. G. W.; AND MOCK, M.: Stellar Accretion and X-Ray Emission. Nature, vol. 215, 1967, pp. 464–466.
61. HAYAKAWA, S.; AND MATSUOKA, M.: Part V. Origin of Cosmic X-Rays. Progr. Theoret. Phys. Suppl. no. 30, 1964, pp. 204–228.
62. HARDIE, R. H.: Additional Photometry of Stars Near Sco-X–1. Publications Astron. Soc. Pacific, vol. 79, 1967, pp. 173–175.

63. Mook, D. E.: UBV Photometry of Sco XR–1. Astrophys. J., vol. 150, 1967, pp. L25–L30.
64. Stepien, K.: Photoelectric Observations of Sco X–1. Astrophys. J., vol. 151, 1968, pp. L15–L17.
65. Mumford, G. S.: Three-color Observations of Scorpius X–1, Nova Herculis 1963, Nova GK Persei 1901, and MHα 328–116. Astrophys. J., vol. 146, 1966, pp. 962–964.
66. Hiltner, W. A.; and Mook, D. E.: Photometric Monitoring of Sco XR–1. Astrophys. J., vol. 150, 1967, pp. L23–L30.
67. Hiltner, W. A.; and Mook, D. E.: Photometric Monitoring of Sco XR–1. Astrophys. J., vol. 150, 1967, pp. 851–869.
68. Lawrence, G. M.; Ostriker, J. P.; and Hesser, J. E.: Ultrashort-Period Stellar Oscillation I. Astrophys. J., vol. 148, 1967, pp. L161–L163.
69. Johnson, H. M.; Spinrad, H.; Taylor, B. J.; and Peimbert, M.: Photoelectric Scanner Spectrophotometry of Sco X–1 (abstract). Astrophys. J., vol. 149, 1967, pp. L45–L50.
70. Giacconi, R.; Gorenstein, P.; Gursky, H.; and Waters, J. R.: An X-Ray Survey of the Cygnus Region. Astrophys. J., vol. 148, 1967, pp. L119–L127.
71. Usher, P. D.: Secular Behavior of a Blue Object Near Cygnus X–2. Astrophys. J., vol. 149, 1967, pp. L19–L20.
72. Lynds, C. R.: Spectroscopic Observations of Cyg X–2. Astrophys. J., vol. 149, 1967, pp. L41–L43.
73. Burbidge, E. M.; Lynds, C. R.; and Stockton, A. N.: On the Binary Nature of Cyg X–2. Astrophys. J., vol. 150, 1967, pp. L95–L97.
74. Kristian, J.; Sandage, A.; and Westphal, J. A.: Rapid Photometric and Spectroscopic Variations of the X-Ray Source Cyg X–2. Astrophys. J., vol. 150, 1967, pp. L99–L105.
75. Kraft, R. P.; and Demoulin, M. H.: On the Remarkable Spectroscopic Complexities of Cyg X–2. Astrophys. J., vol. 150, 1967, pp. L183–L188.
76. Peimbert, M.; Spinrad, H.; Taylor, B. J.; and Johnson, H. M.: Photoelectric Scanner Spectrophotometry of Cyg X–2. Astrophys. J., vol. 151, 1968, pp. L93–L97.
77. Cathey, L. R.; and Hayes, J. E.: Interstellar Reddening in the Field of Cyg. X–2. Astrophys. J., vol. 151, 1968, pp. L89–L92.
78 Visvanathan, N.: Polarization Observations in the Radio Galaxy 3C 371 and the X-Ray Source Cyg X–2. Astrophys. J., vol. 150, 1967, pp. L149–L151.
79. Haymes, R. C.; Ellis, D. V.; Fishman, G J.; Kurfess, J. D.; and Tucker, W. H.: Observation of Gamma Radiation From the Crab Nebula. Astrophys. J., vol. 151, 1968, pp. L9–L14.
80. Haymes, R. C.; Ellis, D. V.; Fishman, G. J.; Glenn, S. W.; and Kurfess, J. D.: Detection of Hard X-Radiation From the Cygnus Region. Astrophys. J., vol. 151, 1968, pp. L125–L129.
81. Fichtel, C. E.; Cline, T. L.; Ehrmann, C. H.; Kniffen, D. A.; and Ross, R. W.: Search for Point Sources of Gamma Rays With a Digitized Spark Chamber (abstract). Astron. J., vol. 72, 1967, p. 797.
82. Ross, R. W.; Ehrmann, C. H.; Fichtel, C. E.; and Kniffen, D. A.: Digitized Spark Chamber for Space Science Experiments. I.E.E.E. Trans. Nuc. Sci., vol. NS–14, 1967, pp. 78–82.
83. Waddington, C. J.; May, T. C.; Long, C. D.; Valdez, J. V.; and Freier, P. S.: A New Limit on the Flux of Energetic γ-Rays From the Radio Source Cassiopeia A (abstract). Astron. J., vol. 73, 1968, p. S39.
84. Gould, R. J.: Origin of Cosmic X-Rays. Phys. Rev. Letters, vol. 15, 1965, pp. 511–512.

85. Fazio, G. G.; Stecker, F. W.; and Wright, J. P.: Cosmic Black-Body Radiation, High Energy Electrons, and the Origin of Isotropic X-Ray and Gamma Radiation. Astrophys. J., vol. 144, 1966, pp. 611–614.
86. Stecker, F. W.; Tsuruta, S.; and Fazio, G. G.: The Effects of the Decay of Nucleon Isobars and Hyperons on the Cosmic Gamma-Ray Spectrum. Astrophys. J., vol. 151, 1968, pp. 881–893.
87. Haymes, R. C.; Ellis, D. V.; Fishman, G. J.; Glenn, S. W.; and Kurfess, J. D.: Detection of Hard X-Radiation From Virgo. Astrophys. J., vol. 151, 1968, pp. L131–L134.
88. Felten, J. R.: The Radiation and Physical Properties of the M87 Jet. Astrophys. J., vol. 151, 1968, pp. 861–879.
89. Friedman, H.; Byram, E. T.; and Chubb, T. A.: Distribution and Variability of Cosmic X-Ray Sources. Science, vol. 156, 1967, pp. 374–378.
90. Bowyer, S.; Byram, E. T.; Chubb, T. A.; and Friedman, H.: Lunar Occultation of X-Ray Emission From the Crab Nebula. Science, vol. 146, 1964, pp. 912–917.
91. Oda, M.; Bradt, H.; Garmire, G.; Spada, G.; Sreekantan, B. V.; Gursky, H.; Giacconi, R.; Gorenstein, P.; and Waters, J. R.: The Size and Position of the X-Ray Source in the Crab Nebula. Astrophys. J., vol. 148, 1967, pp. L5–L11.
92. Gursky, H.; Gorenstein, P.; and Giacconi, R.: The Distribution of Galactic X-Ray Sources From Scorpio to Cygnus. Astrophys. J., vol. 150, 1967, pp. L75–L84.
93. Boldt, E.; McDonald, F. B.; Riegler, G.; and Serlemitsos, P.: Extended Source of Energetic Cosmic X-Rays. Phys. Rev. Letters, vol. 17, 1966, pp. 447–450.
94. Peterson, L. E.; Jerde, R. L.; and Jacobson, A. S.: Balloon X-Ray Astronomy. AIAA J., vol. 5, 1967, pp. 1921–1927.
95. Boldt, E.; Doong, H.; Serlemitsos, P.; and Riegler, G.: A Balloon-Borne X-Ray Survey of the Central Region of the Galaxy. Can. J. Phys., vol. 46, 1968, pp. S444–S447.
96. Chodil, G.; Mark, H.; Rodrigues, R.; Seward, F. D.; and Swift, C. D.: X-Ray Intensities and Spectra From Several Cosmic Sources. Astrophys. J., vol. 150, 1967, pp. 57–65.
97. Chodil, G.; Mark, H.; Rodrigues, R.; and Swift, C. D.: Observation of the Cygnus Region With a Balloon-Borne X-Ray Detector. Astrophys. J., vol. 151, 1968, pp. L1–L3.
98. Clark, G. W.; Lewin, W. H. G.; and Smith, W. B.: Sky Survey of High-Energy Cosmic X-Rays and Spectra of the Sources in the Crab Nebula and Cygnus. Astrophys. J., vol. 151, 1968, pp. 21–32.
99. Haymes, R. C.; Ellis, D. V.; Fishman, G. J.; Kurfess, J. D.; and Tucker, W. H.: Observation of Gamma Radiation From the Crab Nebula. Astrophys. J., vol. 151, 1968, pp. L9–L14.
100. Haymes, R. C.; Ellis, D. V.; Fishman, G. J.; Glenn, S. W.; and Kurfess, J. D.: Detection of Hard X-Radiation From the Cygnus Region. Astrophys. J., vol. 151, 1968, pp. L125–L129.
101. Haymes, R. C.; Ellis, D. V.; Fishman, G. J.; Glenn, S. W.; and Kurfess, J. D.: Detection of Hard X-Radiation From Virgo. Astrophys. J., vol. 151, 1968, pp. L131–L134.
102. Lewin, W. H. G.; Clark, G. W.; and Smith, W. B.: Spectral Data on Sco X–1 in the Energy Range From 20 to 100 keV. Astrophys. J., vol. 150, 1967, pp. L153–L155.

103. Overbeck, J. W.; Womack, E. A.; and Tananbaum, H. D.: High-Energy X-Rays From Cygnus XR–1. Astrophys. J., vol. 150, 1967, pp. 47–56.
104. Seward, F. D.; and Toor, A.: Search for 8–80 keV X–Rays from the Large Magellanic Cloud and the Crab Nebula. Astrophys. J., vol. 150, 1967, pp. 405–411.
105. Seward, F.; Chodil, G.; Mark, H.; Swift, C.; and Toor, A.: Diffuse Cosmic X-Ray Background Between 4 and 40 keV. Astrophys. J., vol. 150, 1967, pp. 845–850.
106. Lewin, W. H. G.; Clark, G. W.; and Smith, W. B.: Observation of Cen XR–2 and Other High-Energy X-Ray Sources in the Southern Sky. Astrophys. J., vol. 152, 1968, pp. L49–L53.
107. Chodil, G.; Mark, H.; Rodrigues, R.; and Swift, C. D.: Nova-Like Behavior of the X-Ray Source Centaurus XR–2. Astrophys. J., vol. 152, 1968, pp. L45–L48.
108. Lewin, W. H. G.; Clark, G. W.; and Smith, W. B.: Observation of an X-Ray Flare From Sco X–1. Astrophys. J., vol. 152, 1968, pp. L55–L61.
109. Hill, R. W.; Grader, R. G.; and Seward, F. D.: The Soft X-Ray Spectrum of Scorpius X–1 (abstract). Astron. J., vol. 73, 1968, pp. S97–S98.
110. Blanco, V. M.; and Kunkel, W. E.: Cen XR2 and NGC 5189 (abstract). Astron. J., vol. 73, 1968, p. S5.
111. Giacconi, R.; Gorenstein, P.; Gursky, H.; Usher, P. D.; Waters, J. R.; Sandage, A.; Osmer, P.; and Peach, J. V.: On the Optical Search for the X-Ray Sources Cyg X–1 and Cyg X–2. Astrophys. J., vol. 148, 1967, pp. L129–L132.
112. Sandage, A. R.; Osmer, P.; Giacconi, R.; Gorenstein, P.; Gursky, H.; Waters, J.; Bradt, H.; Garmire, G.; Sreekantan, B. V.; Oda, M.; Osawa, K.; and Jugaku, J.: On the Optical Identification of Sco X–1. Astrophys. J., vol. 146, 1966, pp. 316–322.
113. Friedman, H.; and Byram, E. T.: X-Rays From Sources 3C 273 and M 87. Science, vol. 158, 1967, pp. 257–259.
114. Friedman, H.; Byram, E. T.; and Chubb, T. A.: X-Rays From Source 3C 273. Science, vol. 159, 1968, pp. 747–748.
115. Poveda, A.; and Woltjer, L.: Supernovae and Supernova Remnants. Astron. J., vol. 73, 1968, pp. 65–74.
116. Gould, R. J.: Origin of Cosmic X-Rays. Am. J. Phys., vol. 35, 1967, pp. 376–393.
117. Fisher, P. C.; Jordan, W. C.; Meyerott, A. J.; Acton, L. W.; and Roethig, D. T.: X-Ray Spectra of Several Cosmic Sources. Astrophys. J., vol. 147, 1967, pp. 1209–1213.
118. Giacconi, R.; Gorenstein, P.; Gursky, H.; and Kellogg, E. M.: Observation of Cosmic X-Rays in the Region of the Galactic Anti-Center (abstract). Astron. J., vol. 73, 1968, pp. S94–S95.
119. Gorenstein, P.; Giacconi, R.; and Gursky, H.: The Spectra of Several X-Ray Sources in Cygnus and Scorpio. Astrophys. J., vol. 150, 1967, pp. L85–L94.
120. Meekins, J. F.; Fritz, G.; Henry, R. C.; Byram, E. T.; and Friedman, H.: New X-Ray Spectra of Sco XR–1, Cyg XR–1 and Cyg XR–2 (abstract). Astron. J., vol. 73, 1968, pp. S106–S107.
121. Metzger, A. E.; and Dolan, J. F.: X-Ray Emission From Cygnus XR–1 (abstract). Astron. J., vol. 73, 1968, p. S107.
122. Giacconi, R.; Gorenstein, P.; Gursky, H.; and Waters, J. R.: An X-Ray Survey of the Cygnus Region. Astrophys. J., vol. 148, 1967, pp. L119–L127.

123. CLARK, G.; GARMIRE, G.; ODA, M.; WADA, M.; GIACCONI, R.; GURSKY, H.; AND WATERS, J. R.: Positions of Three Cosmic X-Ray Sources in Scorpio and Sagittarius. Nature, vol. 207, 1965, pp. 584–587.

124. GURSKY, H.; GIACCONI, R.; GORENSTEIN, P.; WATERS, J. R.; ODA, M.; BRADT, H.; GARMIRE, G.; AND SREEKANTAN, B. V.: A Measurement of the Angular Size of the X-Ray Source Sco X–1. Astrophys. J., vol. 144, 1966, pp. 1249–1252.

125. GURSKY, H.; GIACCONI, R.; GORENSTEIN, P.; WATERS, J. R.; ODA, M.; BRADT, H.; GARMIRE, G.; AND SREEKANTAN, B. V.: A Measurement of the Location of the X-Ray Source Sco X–1. Astrophys. J., vol. 146, 1966, pp. 310–316.

126. HARRIES, J. R.; MCCRACKEN, K. G.; FRANCEY, R. J.; AND FENTON, A. G.: A Strong X-Ray Source in the Vicinity of the Constellation Crux. Nature, vol. 215, 1967, pp. 38–40.

127. FISHER, P. C.; JOHNSON, H. M.; JORDAN, W. C.; MEYEROTT, A. J.; AND ACTON, L. W.: Observations of Cosmic X-Rays. Astrophys. J., vol. 143, 1966, pp. 203–217.

128. FISHER, P. C.; JORDAN, W. C.; MEYEROTT, A. J.; ACTON, L. W.; AND ROETHIG, D. T.: Resolution of X-Ray Sources at Low Galactic Longitude. Nature, vol. 211, 1966, pp. 920–923.

129. FISHER, P. C.; JORDAN, W. C.; MEYEROTT, A. J.; ACTON, L. W.; AND ROETHIG, D. T.: Observations of Galactic X-Ray Sources. Astrophys. J., vol. 151, 1968, pp. 1–19.

130. CHODIL, G.; MARK, H.; RODRIGUES, R.; SEWARD, F.; SWIFT, C. D.; HILTNER, W. A.; WALLERSTEIN, G.; AND MANNERY, E. J.: Spectral and Location Measurements of Several Cosmic X-Ray Sources Including a Variable Source in Centaurus. Phys. Rev. Letters, vol. 19, 1967, pp. 681–683.

131. BRADT, H.; MAYER, W.; NARANAN, S.; RAPPAPORT, S.; AND SPADA, G.: Evidence for X-Radiation From the Radio Galaxy M87. Astrophys. J., vol. 150, 1967, L199–L206.

132. BOWYER, S.; BYRAM, E. T.; CHUBB, T. A.; AND FRIEDMAN, H.: Cosmic X-Ray Sources. Science, vol. 147, 1965, pp. 394–398.

133. BYRAM, E. T.; CHUBB, T. A.; AND FRIEDMAN, H.: Cosmic X-Ray Sources, Galactic and Extragalactic. Science, vol. 152, 1966, pp. 66–71.

134. FRIEDMAN, H.; AND BYRAM, E. T.: X-Rays From the Coma Cluster of Galaxies. Astrophys. J., vol. 147, 1967, pp. 389–401.

135. COOKE, B. A.; POUNDS, K. A.; STEWARDSON, E. A.; AND ADAMS, D. J.: A Cosmic X-Ray Survey in the Southern Hemisphere. Astrophys. J., vol. 150, 1967, pp. L189–L191.

136. BLEEKER, J. A. M.; BURGER, J. J.; DEERENBERG, A. J. M.; SCHEEPMAKER, A.; SWANENBURG, B. N.; AND TANAKA, Y.: Balloon Observations of the X-Ray Sources in the Cygnus Region in the Energy Range 20–130 keV. Astrophys. J., vol. 147, 1967, pp. 391–394.

137. BRINI, D.; CIRIEGI, U.; FULIGNI, F.; MORETTI, E.; AND VESPIGNANI, G.: Cosmic X-Ray Sources in the 20–180 keV Energy Range. Astrophys. J., vol. 149, 1967, pp. 429–433.

138. HAYAKAWA, S.; MATSUOKA, M.; AND SUGIMOTO, D.: Galactic X–Rays. Space Sci. Rev., vol. 5, 1966, pp. 109–163.

139. HAYAKAWA, S.; MATSUOKA, M.; AND YAMASHITA, K.: Observations of Energy Spectra of Galactic X–Rays. Rept. Ion. Space Res., vol. 20, 1966, pp. 480–500.

140. HAYAKAWA, S.; MATSUOKA, M.; OGAWA, H.; AND YAMASHITA, K.: Energy Spectra of Galactic X–Rays. R. L. Smith-Rose, ed., 1967, pp. 1306–1310.

141. Bless, R. C.; Code, A. D.; Houck, T. E.; McNall, J. F.; and Taylor, D. L.: Ultraviolet Observations of Stars (abstract). Astron. J., vol. 70, 1965, p. 667.
142. Boggess, A., III; and Kondo, Yoji: Rocket Ultraviolet Spectrophotometry in the Orion Region. Astrophys. J., vol. 151, 1968, pp. L5–L7.
143. Morton, D. C.; and Adams, T. F.: Effective Temperatures and Bolometric Corrections of Early-Type Stars. Astrophys. J., vol. 151, 1968, pp. 611–621.
144. Morton, D. C.: The Abundance of Helium in A- and B-type Stars. Astrophys. J., vol. 151, 1968, pp. 285–290.
145. Stecher, T. P.: Stellar Spectrophotometry From a Pointed Rocket (abstract). Astron. J., vol. 72, 1967, p. 831.
146. Henize, K. G.; and Wray, J. P.: Observations of Ultraviolet-Stellar Continua From Gemini XI Photographs. Paper presented at 126th Meeting Am. Astron. Soc. (Charlottesville, Va.), Apr. 1–4, 1968.
147. O'Dell, C. R.; York, D. G.; and Henize, K. G.: Structure of the Barnard Loop Nebula as Determined From Gemini XI Photographs. Astrophys. J., vol. 150, 1967, pp. 835–844.
148. Viton, M.: Astronomie-observations extra-atmospheriques du rayonnement ultraviolet dans la Voie lactee d'hiver. Compt. Rend. Acad. Sci. Paris, vol. 264, 1967, series B, pp. 1761–1764.
149. Witt, A. N.: Diffuse Galactic Radiation (abstract). Astron. J., vol. 72, 1967, p. 838.
150. Morton, D. C.; and Spitzer, L., Jr.: Line Spectra of Delta and Pi Scorpii in the Far-Ultraviolet. Astrophys. J., vol. 144, 1966, pp. 1–12.
151. Stone, M. E.; and Morton, D. C.: Far-Ultraviolet Interstellar Absorption Lines in Delta and Pi Scorpii. Astrophys. J., vol. 149, 1967, pp. 29–34.
152. Gaillard, M.; and Hesser, J. E: Experimental Oscillator Strengths for the O I Lines 1302–1306 and 1152 A. Astrophys. J., vol. 152, 1968, p. 695.
153. Morton, D. C.: The Far Ultraviolet Spectra of Six Stars in Orion. Astrophys. J., vol. 147, 1967, pp. 1017–1048.
154. Jenkins, E. B.: An Observation of the Interstellar Lyman-α Absorption Profile for Several Orion Stars (abstract). Astron. J., vol. 72, 1967, p. 304.
155. Carruthers, G. R.: Far-Ultraviolet Spectroscopy and Photometry of Some Early-type Stars. Astrophys. J., vol. 151, 1968, pp. 269–284.
156. Fischel, D.; and Stecher, T. P.: On the Interstellar Hydrogen Density Astrophys. J., vol. 150, 1967, pp. L51–L52.
157. Carruthers, G. R.: An Upper Limit on the Concentration of Molecular Hydrogen in Interstellar Space. Astrophys. J., vol. 148, 1967, pp. L141–L142.
158. Morton, D. C.; and Jenkins, Edward B.: Rocket Ultraviolet Spectra of Venus and Jupiter (abstract). Paper presented at 126th Meeting Am. Astron. Soc. (Charlottesville, Va.), Apr. 1–4, 1968.
159. Stecher, T. P.; and Williams, D. A.: Interstellar Molecule Formation. Astrophys. J., vol. 146, 1966, pp. 88–103.
160. Wentzel, D. G.: An Upper Limit on the Abundance of H_2 Formed by Chemical-Exchange Reactions. Astrophys. J., vol. 150, 1967, pp. 453–460.
161. Williams, D. A.: Physical Adsorption Processes on Interstellar Graphite Grains. Astrophys. J., vol. 151, 1968, pp. 935–944.
162. Stecher, T. P.; and Williams, D. A.: Photodestruction of Hydrogen Molecules in HI Regions. Astrophys. J., vol. 149, 1967, pp. L29–L30.
163. Heiles, C. E.: Normal OH Emission and Interstellar Dust Clouds. Astrophys. J., vol. 151, 1968, pp. 919–934.
164. Morton, D. C.: Mass Loss From Three OB Supergiants in Orion. Astrophys. J., vol. 150, 1967, pp. 535–542.

165. Lucy, L. B.; and Solomon, P. M.: Mass Loss from O and B Supergiants (abstract). Astron. J., vol. 72, 1967, p. 310.
166. Morton, D. C.; Jenkins, E. B.; and Bohlin, J. D.: Rocket Observations of Orion With All Reflective Ultraviolet Spectrograph. Princeton Univ. preprint, 1968.
167. Courtes, G.: Astronomie instrumentale—amelioration de la detection photographique des telescopes du sol et dans l'espace. Compt. Rend. Sci. Paris, vol. 264, series B, 1967, pp. 1757–1760.
168. Smith, A. M.: Stellar Photometry From a Satellite Vehicle. Astrophys. J., vol. 147, 1967, pp. 158–171.
169. Bless, R. C.; Code, A. D.; and Houck, T. E.: Stellar Ultraviolet Photometry (abstract). Astron. J., vol. 73, 1968, p. 55.
170. Henize, K. G.; Wackerling, L. R.; and O'Callaghan, F. G.: Ultraviolet Stellar Spectroscopy on Gemini XI. Science, vol. 155, 1966, pp. 1407–1408.
171. Hoffman, W. F.; and Woolf, N. J.: Infrared Astronomy—a 20 Year Projection—Instrumentation and Ground-Based and Space-Borne Projects in Infrared Astronomy, Research and Need Over 20-Year Period. Goddard Institute for Space Studies, New York, 1967.
172. Hoffman, W. F.; Woolf, N. J.; Frederick, C. L.; and Low, F. J.: A Far-Infrared Sky Survey (abstract). Astron. J., vol. 72, 1967, p. 804.
173. Becklin, E. E.; and Neugebauer, G.: Observations of an Infrared Star in the Orion Nebula. Astrophys. J., vol. 147, 1967, pp. 799–802.
174. Kleinmann, D. E.; and Low, F. J.: Discovery of an Infrared Nebula in Orion. Astrophys. J., vol. 149, 1967, pp. L1–L5.
175. Cameron, A. G. W.: Discussion on Infrared Astronomy. Royal Society of London, 1967.
176. Hartmann, W. K.: On the Nature of the Infrared Nebula in Orion. Astrophys. J., vol. 149, 1967, pp. L87–L90.
177. Davidson, K.; and Harwit, M.; Infrared and Radio Appearance of Cocoon Stars. Astrophys. J., vol. 148, 1967, pp. 443–448.
178. Raimond, E.; and Eliasson, B.: Possible Relation Between an OH Source and an Infrared Object in the Orion Nebula. Astrophys. J., vol. 150, 1967, pp. L171–L172.
179. Mendoza, V. E. E.: Infrared Photometry of T Tauri Stars and Related Objects. Astrophys. J., vol. 143, 1966, pp. 1010–1014.
180. Mendoza, V. E. E.: Infrared Excesses in T Tauri Stars and Related Objects. Astrophys. J., vol. 151, 1968, pp. 977–989.
181. Low, F. J.; and Smith, B. J.: Infra-red Observations of a Preplanetary System. Nature, vol. 212, 1966, pp. 675–676.
182. Comella, J.: Negative Results in a Search for Radio Emission From Infrared and T Tauri Stars. Astrophys. J., vol. 149, 1967, pp. L91–L92.
183. Johnson, H. L.: Infrared Emission From Circumstellar Shells. Astrophys. J., vol. 150, 1967, pp. L39–L43.
184. Lee, T. A.; and Nariai, K.: Infrared Observations of the Planetary Nebula NGC 7027. Astrophys. J., vol. 149, 1967, pp. L93–L95.
185. Pottasch, S. R.: On the Infrared Measurements From a Nebula in Orion. Astrophys. J., vol. 151, 1968, pp. L67–L68.
186. Gillett, F. C.; Low, F. J.; and Stein, W. A.: Infrared Observations of the Planetary Nebula NGC 7027. Astrophys. J., vol. 149, 1967, pp. L97–L100.
187. Thompson, A. R.; Colvin, R. S.; and Stanley, G. J.: Measurements of the Flux Densities, Positions and Angular Widths of Planetary Nebulae at 10- and 21-cm Wavelengths. Astrophys. J., vol. 148, 1967, pp. 429–442.

188. SWAMY, K. S. K.; AND O'DELL, C. R.: Thermal Emission by Particles in NGC 7027. Astrophys. J., vol. 151, 1968, pp. L61–L68.

189. NEY, E. P.; AND STEIN, W. A.: Observations of the Crab Nebula of λ=5800 Å, 2.2μ, and 3.5μ. With a 4-Minute Beam. Astrophys. J., vol. 152, 1968, pp. L21–L24.

190. BECKLIN, E. E.; AND KLEINMANN, D. E.: Infrared Observations of the Crab Nebula. Astrophys. J., vol. 152, 1968, pp. L25–L30.

191. FIELD, G. B.; RATHER, J. D. G.; AANNESTAD, P. A.; AND ORSZAG, S. A.: Hydromagnetic Shock Waves and Their Infrared Emission in HI Regions. Astrophys. J., vol. 151, 1968, pp. 953–975.

192. WERNER, M. W.; AND HARWIT, M.: A Search for Molecular Hydrogen in the Orion Nebula. 126th Meeting Am. Astron. Soc. (Charlottesville, Va.), Apr. 1–4, 1968.

193. BECKLIN, E. E.; AND NEUGEBAUER, G.: Infrared Observations of the Galactic Center. Astrophys. J., vol. 151, 1968, pp. 145–161.

194. NEUGEBAUER, G.; MARTZ, D. E.; AND LEIGHTON, R. B.: Observations of Extremely Cool Stars. Astrophys. J., vol. 142, 1965, pp. 399–401.

195. FORBES, F. F.: The Infrared Polarization of the Infrared Star in Cygnus. Astrophys. J., vol. 147, 1967, pp. 1226–1229.

196. APPENZELLER, I.; AND O'DELL, C. R.: Polarization of the Taurus Infrared Source. Astrophys. J., vol. 149, 1967, pp. L5–L6.

197. WISNIEWSKI, W. Z.; WING, R. F.; SPINRAD, H.; AND JOHNSON, H. L.: Additional Observations of "Infrared Stars." Astrophys. J., vol. 148, 1967, pp. L29–L32.

198. WING, R. F.; SPINRAD, H.; AND KUHI, L. V.: Infrared Stars. Astrophys. J., vol. 147, 1967, pp. 117–147.

199. MCCAMMON, D.; MÜNCH, G.; AND NEUGEBAUER, G.: Infrared Spectra of Low-Temperature Stars. Astrophys. J., vol. 147, 1967, pp. 575–586.

Page Intentionally Left Blank

SPACE BIOSCIENCE

Edited by

Bruce Berman
George Washington University

Dale W. Jenkins
Office of Space Science and Applications, NASA

333-240 O—69——4

Page Intentionally Left Blank

Space Bioscience

INTRODUCTION

NASA bioscience activities utilize the findings and expertise of space and planetary biology to examine the characteristics of the space environment and their effects on biologic organisms, and search for evidence of extraterrestrial life, study its origin and nature, and formulate basic theories and models of the origin of life.

This report presents NASA bioscience achievements for calendar year 1967. The goals and dimensions of this activity have been presented in previous research summaries in this series (refs. 1 and 2). The interest of the scientific community in the search for extraterrestrial life remains at a high level. Researchers in many disciplines continue to contribute to overcoming the biologic and engineering problems that must be solved before man can safely venture on long space journeys. To provide a basis for protection against the hazards of weightlessness and radiation in space, plant and animal experiments are being conducted in space on physiologic changes, metabolic disturbances, biorhythmic derangements, and systemic disruptions. The space biologist is cognizant of his opportunities to extend the frontiers of biology by comparisons of Earth life with other life forms in space. To this end, he is devoting himself to vigorous enterprise and rigorous development and refinement of theory.

The outstanding achievement in 1967 was the successful flight and recovery of Biosatellite II which carried 13 scientific experiments. The preliminary results are presented in this report. A Biosatellite II symposium was held in February 1968 and the results have been published in reference 3.

This report was written and compiled by the staff of Bioscience Programs, Office of Space Science and Applications. Exobiology was reported by Richard S. Young; environmental biology and the Biosatellite, by Joseph F. Saunders; behavioral biology, by Norman W. Weissman; physical biology, by George J. Jacobs; and sterilization and planetary quarantine, by Lawrence B. Hall. The report was edited by Dale W. Jenkins, Assistant Director (Science), Bioscience Programs, NASA, and by Bruce Berman, Biological Sciences Communication Project, George Washington University.

Although directed primarily at enlarging our comprehension of biologic fundamentals, NASA Bioscience Programs Division sponsors means for application of bioengineering to solving problems of life support and space hazards for astronauts. Bioengineering developments and technologic devices yielded by this aspect of the program are already receiving wide application in fields unrelated to the primary goals of space science.

The magnitude and depth the space biology effort has attained since its inception are reflected in some 250 active research projects in various phases of biology that have relevance to space flight. The additions to biologic knowledge coming from these projects may be found in the more than 2000 papers in nearly 300 scientific journals.

CHEMICAL EVOLUTION

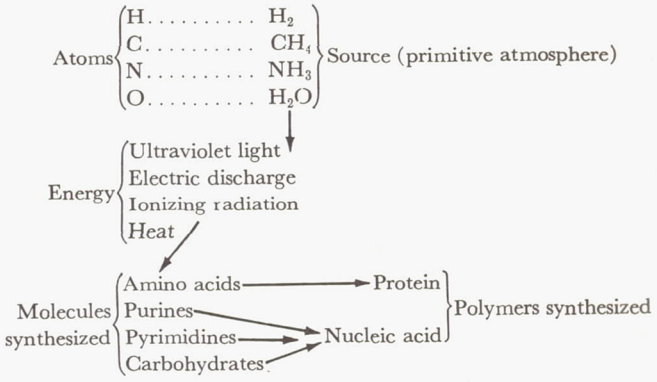
What are the controlling factors in the origin of life? What gives uniqueness to life on Earth? What conditions prevailed on the primitive Earth that were a necessary prelude to such life? These are some of the questions to which exobiologic investigations seek answers.

Central to exobiology is chemical evolution, which encompasses the chemical events on the primitive Earth (or on any primitive planet) that led to living matter. This embraces abiogenesis—the synthesis of biologically significant organic molecules by application of energy (electrical discharge, ultraviolet radiation, heat) to the simple components (hydrogen, methane, ammonia, and water) of the primitive atmosphere—and organic geochemistry—the analysis of ancient rocks and sediments of the Earth, Moon, and other planets, and of fossils that record the happenings when life began.

The effort to reconstruct the elements that induced primitive life on Earth encounters the obligation to define life. This question of definition has been a lively one ever since the isolation of viruses and the subsequent crystallization of tobacco mosaic virus; it has gained additional urgency as technology has made experimental exobiology a real possibility.

Research into the nature of life has sought to define the qualities of molecular and biologic self-replicating entities (Morowitz, ref. 4). All biologic systems utilize a universal type of membrane, and all populations of replicating biologic systems give rise to mutant phenotypes. Other important features are that all growing cells have ribosomes, which are the sites of protein synthesis, and that translations of information from nucleotide information to amino-acid language take place through specific activating enzymes and transfer RNA. The mechanism of protein synthesis has been found similar in all systems studied.

Many experiments have defined the presumed pathway of early abiogenesis: an atmosphere of methane, ammonia, and water; a variety of potential energy sources; and the synthesis of a variety of organic molecules.



It has been shown that many biologically significant molecules can be thus synthesized, suggesting they may have played an essential part in the origin of life.

Research has also demonstrated the synthesis, under primitive conditions, of purines and pyrimidines. These are joined with the sugars ribose and deoxyribose to produce nucleosides which, in the presence of phosphate in the primitive oceans, may well have reacted further to produce nucleic acids, the hereditary material of contemporary cells.

Gehrke, Stalling, and Ruyle (ref. 5) have been applying gas chromatography to the separation of nucleosides (fig. 1), which will provide a powerful tool for analysis of returned lunar samples. Use of bis(trimethylsilyl)-acetamide (BSA) has enabled these researchers to quantitatively prepare volatile derivatives of the bases, nucleosides, and nucleotides. These developments will permit gas chromatography of these substances to be routinely performed in the laboratory.

Since we are beginning to understand the essential biochemical constituents of life and the mechanism of replication, the synthesis of living matter by abiogenic experimental techniques has become a major goal. Investigations into the possible ways in which the primordial cell might have been formed have focused considerable attention on the catalytic activity of thermal polyanhydro-alpha-amino acids. The first substrate for which such activity was reported was the unnatural ester, *p*-nitrophenyl acetate (NPA) (Fox, Harada, and Rohlfing, ref. 6). Rohlfing and Fox (ref. 7) found that thermally prepared polyanhydro-alpha-amino acids common to protein accelerate the hydrolysis of NPA—an action that is catalytic, rather that stoichiometric. This truly catalytic action of thermal polyanhydro-alpha-amino acids in NPA and the ease of varying the amino-acid composition of the thermal polymers (resulting in different activity levels) suggest the use of these polymers as an alternate model compound in studies of the kinds of amino acids involved in the active sites of enzymes. In addition, thermal polymers (both proteinoids and copolymers of aspartic

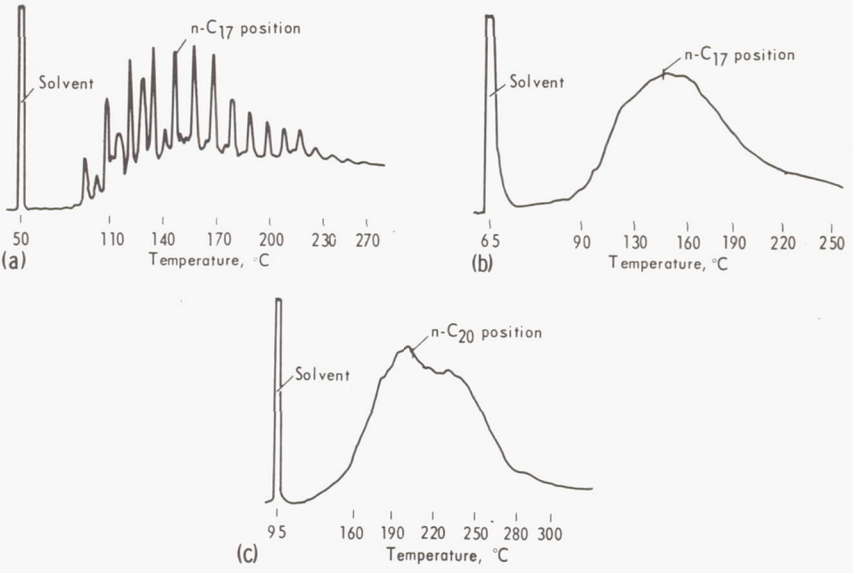


Figure 1.—**Determination of biological or nonbiological origin by gas chromatography. (*a*) Rock organic extract, biological origin. (*b*) Methane-electric-discharge extract, nonbiological origin. (*c*) Rock organic extract, probable nonbiological origin.**

acid and histidine) are inactivated by heating their buffered solutions. Since proteinoids are formed under geologic conditions, the above findings point to one way in which macromolecular catalysts could have been formed abiotically from amino acids, thence to become attributes of the primordial cell.

Amino acids, monosaccharides, pyrimidines and purines, porphyrine, and ATP have been produced under conditions which have been interpreted in a context of spontaneous synthetic organic chemistry on the primitive Earth. The necessary geophysical conditions for the model of a spontaneous sequence converting primordial gases through amino acids and preproteins to protocells, which participate in the reproduction of their own likenesses, are temperatures above the boiling point of water and sporadic rain or other sources of hydration. Such conditions are, of course, found on the contemporary Earth and are inferable for the primitive Earth (Fox, ref. 8).

Armstrong, Furukawa, and Reilly (ref. 9) have sought to define the thermodynamic properties of substances important in the possible spontaneous origin of life. To comprehend the molecular processes of living systems, it is necessary to know the energy relationships among them—an understanding second only in importance to knowledge of their structural relationships. After surveying the ubiquitous compounds (those which

available evidence indicates are present in every living thing, and which, with reasonable probability, would have been required when primitive life was formed), Armstrong et al. generalized that metabolic and other life processes are characterized by an economy of agents and by cyclic processes: economy, in that some few substances are found over and over again in various processes (e.g., amino acids, fatty acids, and sugars are all metabolized by many identical steps); cyclic, in that some agents necessary for continuing a process are generated during its course (e.g., the Krebs tricarboxylic degradation of sugar).

It is well known that proteins consist of alpha-amino acids. Less well known, perhaps, is that individual proteins are molecules of definite configuration, with a fixed order and number of amino acids. This is the protein primary structure, which is further defined by disulfide bridges linking sulfur-containing amino acids. Secondary protein structure is the configuration of the polypeptide chain resulting from the satisfaction of hydrogen bonding between the peptide N—H and C=O groups. Little is known about the last pattern, but there are one or two proteins for which tertiary structure is completely known (Armstrong et al., ref. 9).

Significant support for the theory of prebiologic chemical formation of amino acids and protein has come from successful phosphorylation (with polyphosphoric acid at temperatures of 0° to 22° C) of adenosine, cytidine, guanosine, uridine, deoxycytidine, and thermidine in yields of identified phosphates ranging from 25 to 45 percent. Polyphosphoric acid has been found useful also for phosphorylation of the four ribonucleosides and for the pyrimidine deoxyribonucleosides at low temperatures. The latter reactions yield substantial amounts of biologically significant mononucleotides (Waehneldt and Fox, ref. 10).

Phosphoric acid and its salts have been useful with calcium phosphates and sodium phosphates in the polymerization condensation of alpha-amino acids. This, along with the formation of the four ribonucleoside phosphates and the pyrimidine deoxyribonucleoside phosphates and with the known biochemical importance of phosphates, points increasingly to the significance of a primordial phosphoric medium (Waehneldt and Fox, ref. 10).

A generalized explanation for phosphorylation under primitive conditions has stemmed from a demonstration that a variety of phosphates can give rise to monophosphates, diphosphates, and di-, tri-, and tetranucleotides under simulated prebiotic conditions. Further explanation of these inorganic reactants has shown that the phosphorylation is via the P—O—P bonds (Ponnamperuma and Gabel, ref. 11).

The most meaningful simulation of primitive Earth conditions is the exposure of methane, ammonia, and water to high-intensity ultraviolet radiation. Ponnamperuma, Woeller, Flores, Romiez, and Allen (ref. 12) have designed an apparatus that does this by using a vacuum ultraviolet source having an output of 10^{19} photons/sec/cm^2. Ponnamperuma et al. have

hydrolyzed what seemed to be a polypeptide formed under simulated primitive conditions and obtained five amino acids: glycine, alanine, glutamic, aspartic, and serine. Further studies with radioactive glycine and alanine indicated these amino acids were being incorporated fully into the polymer. When the polymer was subjected to hydrolysis with the enzyme pronase, glycine and alanine were quantitatively released, indicating they were linked in the polymer by a peptide bond.

A careful examination of the "primordial soup" generated by electrical discharges through methane, ammonia, and water has revealed the presence of porphines, the first identification of a porphyrin molecule in such an experiment (ref. 11).

Studies have been made to determine the contribution of various portions of an enzyme molecule to its activity and specificity and to determine how these portions may have been formed on the primitive Earth. It has been shown that the solvent dimethyl sulfoxide (DMSO) increases the heat resistance of the enzyme trypsin, and that DMSO stimulates trypsin to as much as four times its activity in aqueous solution; this activity varies with the solvent, with the substrate used, and with the pH of the medium. Similar studies with other enzymes have shown the activity of some enzymes can be increased over that found in the native state (Henrich and Bugna, ref. 13).

Recent work has been concerned with synthesis of mitochondrial membranes and the association of acetyl-CoA synthetase with the developing mitochondria and with mechanisms controlling the desaturation of long-chain fatty acids. To determine if the acetyl-CoA synthetase might be associated with the mitochondria, Klein, Volkman, and Weibel (ref. 14) studied the activities of two other enzymes which are known indicators of mitochondrial membranes, namely, succinic dehydrogenase and cytochrome oxidase. They found that cells grown under anaerobic conditions and subsequently aerated for varying times showed no fractional changes when succinic dehydrogenase and cytochrome oxidase were assayed, but the characteristic change of the synthetase from small to large particles was seen. Similarly, when cells were grown aerobically a drastic change in the fractions was seen for acetyl-CoA synthetase, but not for the other two enzymes.

The exobiologist, as has been pointed out, seeks chemical evidence for evolution of organic compounds during geologic times and for earlier life on Earth. In this search, he studies the characterization of hydrocarbons from unusual geologic localities in order to develop criteria for differentiating biotic and abiotic organic compounds (fig. 1). In recent years, scientists have gathered a steadily growing collection of unusual hydrocarbon occurrences. Two recent additions came from Rainbow Springs in Yellowstone National Park: an oily material, which has a hydrocarbon mixture with characteristics associated with biologic activity, and a black oil associated with a fumarole, with hydrocarbons not definitely attributed to biologic processes (Ponnamperuma and Pering, ref. 15).

The oldest amino acids found have been detected in 3-billion-year-old sediments (fig. 2). Identification was made by ion-exchange chromatography (amino acid analyzer) and gas-liquid chromatography. This is the first time that amino acids have been confirmed in any geochemical sample by the latter method. Investigators are determining whether these ancient amino acids still possess properties which make them optically active (Schopf, Kvenvolden, and Barghoorn, ref. 16).

The search for fatty acids in ancient sediments has been hitherto hindered by potassium hydroxide contamination. New procedures to exclude this reagent have been applied to 32 samples of Green River oil shale, and it is anticipated that these may yield the diagenetic history of fatty acids over a 6-million-year span (Kvenvolden, refs. 17 and 18).

The role of hydrogen cyanide in prebiologic chemistry is being increasingly stressed. Various simple inorganic compounds yield HCN on application of such energy sources as heat, electric discharge, ionizing radiation, and

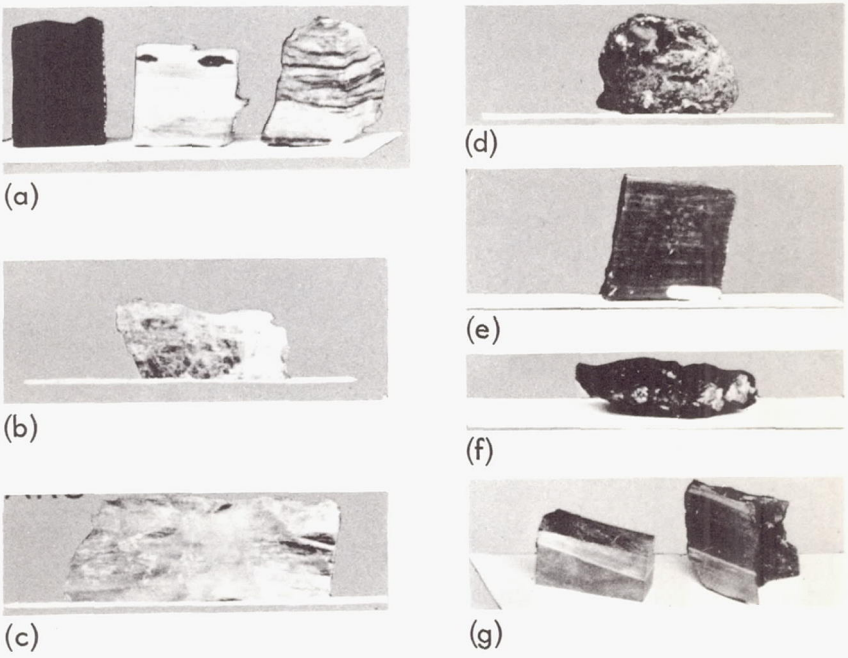


Figure 2.—Sediments containing clues to chemical evolution and the origin of life. (*a*) Green River oil shale, Colorado, 60 million years. (*b*) Bitter Springs limestone, Australia, 1.0 billion years. (*c*) Nonesuch shale, Michigan, 1.0 billion years. (*d*) Gunflint iron formation, Ontario, 1.9 billion years. (*e*) Gowganda formation, Ontario, 2.1 billion years. (*f*) Soudan iron formation, Minnesota, 2.7 billion years. (*g*) Fig tree shale, South Africa, 3.1 billion years.

short electromagnetic waves (gamma ray, X-ray, or ultraviolet). Since all these sources were primordially available both before and after formation of the Earth, HCN reactions would be important in chemical evolution. HCN is a product of the pyrolysis of ammonium formate and formamide; hydrolysis of the pyrolytic product has revealed several ninhydrin positive compounds, of which glycine, alanine, and aspartic acid have been confirmed. This suggests one pathway of amino acid formation by oligomerization of HCN (Harada, ref. 19).

Protobiochemistry has only recently begun to emphasize the role of sulfur in the chemical evolution of life. Sulfur's most important contemporary biochemical function is in the structure and reactivity of proteins, particularly enzymes and morphological proteins such as keratin and collagen. The forms of sulfur available on the primitive Earth have received far less attention than have other biologically essential elements. However, various sulfide minerals have been found in meteorites, and the recently reported niningerite (Keil and Snetsinger, ref. 20) is a mixed Fe-Mg-Mn-Ca-Cr sulfide. Although several experiments performed under the hypothetical conditions of primitive Earth have now accounted for the primordial appearance of nearly all classes of biomonomers, this very important group—the naturally occurring sulfur-containing amino acids—has persistently resisted synthesis. Steinman, Smith, and Silver (ref. 21), by ultraviolet irradiation of an aqueous solution of ammonium thiocyanate, have now succeeded in producing methionine, a sulfur-containing amino acid, thus filling another gap in the story of prebiologic chemical evolution on the primitive Earth. Although the yield was low (less than 1 percent), the detection procedures (paper chromatography and autoradiography) proved sufficiently sensitive to identify the amino acid.

SEARCH FOR EXTRATERRESTRIAL LIFE

Rationale and Techniques

Investigations into the occurrence of extraterrestrial life in the solar system continue to yield important data. Overall support for this activity occurs in a Space Science Board recommendation (ref. 22) that—

> a flexible, vigorous, and systematic program of planetary, solar, and interplanetary exploration can and should be mounted so as to take advantage of every available Venus and Mars opportunity over the next 5 years (1967 through 1971), using hardware which is either in existence or within the current state of the art.

In general, detection of life has taken two approaches: one recognizes manifestations of the process defined on Earth as life, such as growth, metabolism, or enzyme activity; the other detects recognizable nonliving by-products of life, that is, organic chemicals (Biemann, ref. 23).

The question of whether life exists, did exist, or could exist outside the Earth requires thorough examination of the organic compounds in extra-

terrestrial bodies. A continuing objective in life detection is the development of automated techniques to resolve this question. The key to the problem is the search for fundamental characteristics of life, and a number of devices have been developed (such as Wolf Trap, Gulliver, Multivator), each designed to look for a specific biologic manifestation, such as metabolism, growth, or chemical composition.

A highly effective technique for examining the organic compounds in extraterrestrial bodies is a system combining mass spectroscopy and gas chromatography. With its sensitivity, general applicability, and independence from known analogies, this method is very effective, and a sample weighing only fractions of a microgram will suffice for testing. This is the most generally applicable method, and interpretation of data does not depend on comparison with any system because any molecule has a specific mass (ref. 23). These considerations are very important if we are to detect minute quantities of a substance, as well as any substance different from anything known on Earth.

High-resolution mass spectrometry, a recent variant, employs magnetic deflection to interpret with much greater certainty the spectra of mixtures and thus identify the element present. It now permits routine determinations of molecular structure by computer-aided interpretation of high-resolution, mass-spectral fragmentation patterns. This approach allows minute, noncrystalline samples to be used and is not impeded by impurities from chemical isolation and separation procedures (Burlingame, ref. 24).

Updegrove, Oro, and Zlatkis (ref. 25) have devised a sophisticated combination of the two techniques that obtains, from samples of a few micrograms, mass spectra of individual components without using molecular separators. These investigators are applying this system to analytical determination of hydrocarbons and other molecules of presumed biologic origin (e.g., phytane, pristane, and farnesane); organic compounds resulting from thermal outgassing of terrestrial and extraterrestrial samples; and pyrolyzates of bacteria and other micro-organisms.

Gas chromatography-mass spectrometry has been especially productive in connection with the recent upsurge of interest in high-temperature synthesis of aromatic hydrocarbons as an approach to various space chemistry problems. A large number of such hydrocarbons, ranging from benzene to pyrene, have been separated and identified by applying gas chromatography and combined gas chromatography-mass spectrometry to the analysis of the pyrolysis products of methane at 1000° C. Using molecular separators to combine capillary gas chromatography with mass spectrometry, Oro and Han (ref. 26) have identified, from products of methane pyrolysis, 23 hydrocarbons on one to four rings, including benzene, toluene, styrene, indene, naphthalene, biphenyl, acenaphthylene, fluorene, phenathrene, anthracene, fluoranthene, and pyrene. Extension of the analytic technique to pyrolysis (300° to 1000° C) products of isoprene has demonstrated that isoprene

pyrolysis synthesizes many aliphatic and aromatic hydrocarbons (Oro, Han, and Zlatkis, ref. 27).

A possible life-detection technique is the collection and analysis of volatile organic materials in the atmosphere which may prove good indicators of biologic activity on the surface below. This approach, which is being explored on the Earth, uses samples collected by aircraft and the gas chromatograph and mass spectrometer as detectors.

Also receiving attention are problems of collecting and concentrating organic volatiles for analysis and the relationship of soil micro-organisms, the soil, and macroscopic vegetation forms. What is needed is an understanding of how the absence of higher forms of life affects both the kinds and numbers of micro-organisms in the soil and the production of organic volatiles by such organisms.

Chemical analysis of organic compounds can be an essential adjunct to other tests for biologic activity; such analyses look for specific molecular properties which should be applicable under any conditions. All of these tests for biologic activity and organic molecules can be applied on either returned samples or *in situ* on the planetary or lunar surface.

Planetary and Lunar Life

In the past, almost all investigations of extraterrestrial life have had an essentially biologic orientation and have sought to recognize such life in terms of well-known laboratory procedures of microbiology and biochemistry. This approach reflects geocentric bias and poses overwhelming problems of biochemical laboratory transport to another planet. It has now been suggested that planetary life may be perceived through relatively simple measurements of physical environment and superficial chemical composition.

Hitchock and Lovelock (ref. 28) have shown that on Earth, even without knowledge of the nature and extent of the dominant life forms, existence of life can be inferred from knowledge of the major and trace components of the atmosphere. Thus, any significant disequilibrium produced in an atmosphere (whose components are known) with which any planetary biota interacts could be evidence of life. Common to all life in the solar system is its maintenance in a state of relatively low entropy at the expense of the nonliving environment. After death, the free energy stored in a living system is gradually dissipated into the surrounding environment. Thus, a large chemical free-energy gradient between surface matter and contacting environment—not accountable in abiological terms—could be evidence of life. An example of this would be the simultaneous presence of two gases which, like hydrogen and oxygen, are chemically incompatible. This approach entails identification of the constituents of planetary atmospheres and the detection of any element that cannot be explained on abiological grounds.

There is now general agreement that quantitative results of this chemical equilibrium approach would facilitate understanding the origin of life on

Earth and on other planets. The gross chemical composition of planetary atmospheres can be approximated to some degree as the thermodynamic equilibrium distribution of the constituent atoms. The thermodynamic equilibrium composition of all possible combinations of the elements carbon, hydrogen, oxygen, and nitrogen at average pressures and temperatures has been calculated for the atmospheres of Earth, Venus, Mars, and Jupiter (Dayhoff, Lippincott, and Nagarajan, ref. 29). Under some circumstances, the presence of atmospheric organic molecules far in excess of their thermodynamic equilibrium proportions can be an indication of indigenous biologic activity. Since the equilibrium state is independent of particular reaction mechanisms and reaction rates, and since the computations of equilibrium states are quite straightforward, studies of thermodynamic equilibrium chemistry would appear prerequisite to considerations of nonequilibrium processes (Lippincott, Eck, Dayhoff, and Sagan, ref. 30).

Mars

Study of life on Mars has emphasized the question of biologic contamination—the possibility of release, survival, dissemination, and growth of terrestrial microbial contaminants on the Martian surface. Much work has been done on environments simulating that of Mars. The latest version of a Martian simulator (fig. 3) uses an airlock with a manipulator permitting introduction and removal of samples without impairing the integrity of the environment. Studies of the day-night, freeze-thaw Martian cycle—probing the likelihood of survival and growth of terrestrial bacteria—have shown that, although freeze-thaw conditions do kill to some extent, cultures can adapt and grow.

Sagan (ref. 31) has studied the possibility of liquid water on Mars' surface. Although the average partial pressure of water in the Martian atmosphere is far below the equilibrium vapor pressure, there are several possible ways in which liquid water could be present in isolated times and places. On Earth there are organisms capable of surviving in an environment where water availability would be as limited as on Mars. One such environment is the halophilic environment—the saturated salt solution found in some lakes or salt evaporation ponds, where water is extremely limited since it is bound to the salts and not easily available for biologic activity. Bacteria found in these ponds probably expend as much energy extracting water from the salt as they would from the Martian atmosphere.

Venus

Recent probes to Venus have provided new data which allow further speculation about the possibility of life and/or life-related molecules on that planet. Much work has gone into defining more precisely the nongray greenhouse models of Venus' atmosphere, using a wide variety of carbon dioxide and water-vapor-mixing ratios (Sagan, ref. 31). Although analyzed data do not indicate the presence or absence of biologic activity, the follow-

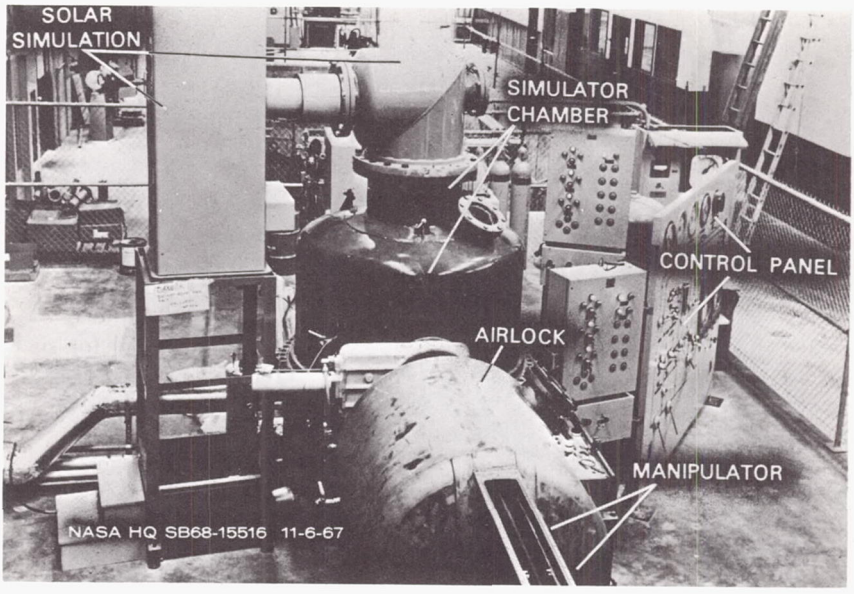


Figure 3.—Mars simulator.

ing inferences can be drawn: Venus most probably has carbon, hydrogen, nitrogen, oxygen, water, and light, the essential ingredients for chemical evolution, and is thus of direct interest in considering the origin of life. In addition, there are probably regions in the atmosphere of Venus compatible with terrestrial types of biologic activity. It is possible that the surface is compatible with organic chemistry not common on Earth. If the Soviet estimate of surface temperature is correct, the polar temperatures may be suitable for biologic activity. There remains, however, the problem of how life would arise in a completely atmospheric ecology since there is no terrestrial counterpart.

Surface.—The surface temperature and pressure of Venus, although not precisely known, are almost certainly too high to permit terrestrial-type biologic activity. The composition of the surface is unknown, but ground-based data are consistent with pulverized rocks (such as silicates and carbonates). The surface pressure is probably between 20 and 60 atmospheres; the temperature is between 540° and 870° F. This makes the presence of liquid water extremely unlikely, although a combination of the lower estimates of temperature and high estimates of pressure do not preclude the possibility of liquid water. Terrestrial organic compounds of biologic origin would be unstable under most combinations of this temperature-pressure regime. Even the polar temperatures are likely to be approximately 420° F.

Atmosphere.—The atmospheric composition at the surface should be very much like that of the lower atmosphere because of mixing. Soviet data

indicate 90 to 95 percent CO_2, 0.1 to 0.7 percent H_2O, and 0.4 to 0.8 percent O_2. In addition, U.S. Earth-based spectroscopic measurements indicate carbon monoxide, hydrochloric acid, and hydrofluoric acid in parts-per-million quantities. A critical atom, nitrogen, has not been detected. Soviet data, however, indicate that nitrogen could be present in amounts of less than 7 percent. The temperature at an altitude of 15.5 miles is about 104° F (U.S.S.R.), and the pressure about 7 atmospheres. The Soviet gas analysis was done in the 15.5-mile region, which should be in the lower cloud layer. It is felt that a region at least 6 miles above the surface provides a reasonable environment, in terms of temperature, pressure, light, and atmospheric composition, for biologic activity. We have no terrestrial model for such an airborne life cycle, however, and it is difficult to see how life could arise in such circumstances. This is certainly a region requiring further exploration.

Thermodynamic equilibria.—The most suggestive data are those measurements in the atmosphere indicating a disequilibrium in certain molecular constituents. First, there is a surprising amount of O_2 in the atmosphere, as measured by Venera 4. Our Earth-based spectroscopic data also indicate small amounts of CO, HCl, and HF. CO and HCl will combine readily with O_2; therefore, the excess of O_2 detected in the Venus atmosphere should have converted the CO to CO_2. Since CO is present, a source of renewal must be postulated. On Earth, biologic activity is the primary responsible agent (refs. 29 and 30).

In addition, Mariner V indicates the presence of large amounts of atomic hydrogen in the upper atmosphere of Venus, which may also suggest a disequilibrium. One of several possible explanations is biologic activity. (See table I.)

Jupiter

The visible surface of Jupiter reveals regions of contrasting and variegated colors, which are most plausibly explained by the presence of organic matter at the planet's cloud level. The bright and contrasting colors of the bands, belts, and spots, particularly the Great Red Spot, probably reflect differences in molecular composition (Lippincott et al., ref. 30). Known constituents of the Jovian atmosphere include hydrogen, methane, and ammonia. It is expected that water is also a major constituent, since oxygen, cosmically abundant, cannot escape in atomic form from contemporary Jupiter (fig. 4). In a theoretical calculation of Jovian atmospheric conditions, a mixture of hydrogen, methane, and ammonia, supplied with energy from a corona discharge, produced simple organic molecules such as hydrogen cyanide, methyl cyanide, acetylene, ethylene, and ethane (Sagan, Lippincott, Dayhoff, and Eck, ref. 32).

Studies of Jupiter's chemical phenomena have demonstrated the formation, by electric discharge in a simulated Jovian atmosphere (fig. 5), of

Table I.—*Thermodynamic Equilibria in Venus' Atmosphere*

Parameter	Mariner V	Venera 4	Ground-based and near-Earth observations	Summary
Temperature	Lower atmosphere, 275° F; surface, 870° F, by extrapolation; cloud temperature, −40° F or less.[a]	Surface, 540° F; 15.5 mi, 104° F.	Surface, 830° F; poles, 420° F; clouds, −40° F.	There is a zone in the atmosphere at least 6 mi thick in which the temperature-pressure conditions are compatible with life. This is likely near the lower clouds.
Pressure	Lower atmosphere, about 7 atm; surface, 60 atm, by extrapolation.[a]	Surface, 20 atm; 15.5 mi, 7 atm.	Near cloudtops, 0.1 atm; several 10's of atmosphere near surface.	Surface pressure, 20 atm.
Ultraviolet flux	No information	No information	Some evidence for UV opacity above clouds.	Probable atmospheric shielding of solar UV.
Surface composition	No information	No information	Data are consistent with pulverized rocks.	Data consistent with pulverized rocks.
Water	Some information possible from occultation experiment on water vapor or condensed H_2O; not yet available.	0.1–0.7 percent	Data ambiguous	Reasonable likelihood of water.
Oxygen	No information for lower atmosphere.	0.4–0.8 percent	Data ambiguous	Reasonable likelihood of oxygen.

Hydrogen	Large amounts of atomic hydrogen in upper atmosphere, at least as much as Earth.	Weak hydrogen corona on night side.	No information	No information for lower atmosphere.
Nitrogen	No information	Less than 7 percent	Data ambiguous	No information.
Chemical compounds with C, H, N, and O.	No information	90–95 percent CO_2	CO, HCl, HF in ppm quantities.	CO_2, CO, HCl, HF, H_2O, O_2 present.
Thermodynamic disequilibrium.[b]	The atomic hydrogen in upper atmosphere may imply disequilibrium.	The surprising amount of O_2 suggests a disequilibrium. One source of such a disequilibrium is biologic activity.	The amounts of CO and HCl detected represent a large disequilibrium in the presence of O_2.	Various chemical disequilibria present. One of several possible explanations is biologic activity.

[a] These extrapolations are for constant lapse rate as found by Mariner V, extending down to a surface at the radar diameter of 6056 ± 1 km. Note inconsistency with Venera 4 results.

[b] Thermodynamic disequilibrium is molecular imbalance; e.g., CO will combine readily with O_2. Therefore, the excess of O_2 detected in the Venus atmosphere should have converted almost all the CO to CO_2. Thus, a source of CO renewal must be postulated. On Earth, biologic activity is responsible.

333–240 O—69—5

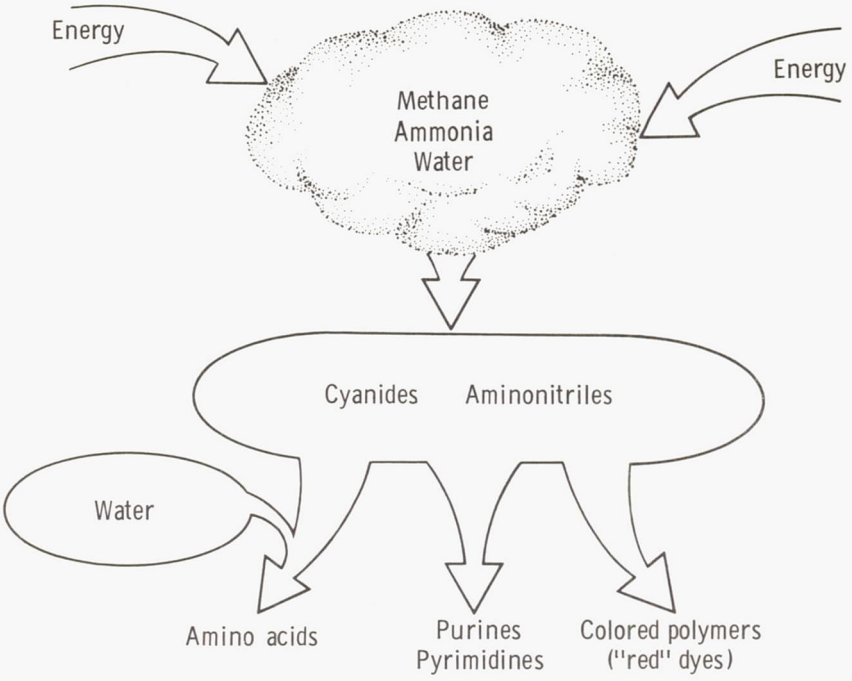


Figure 4.—**Possible chemical reactions in the atmosphere of Jupiter.**

several nitriles: methylcyanide, ethylcyanide, glycinonitrile and its C- and N-methyl derivatives (Ponnamperuma et al., ref. 12).

The same investigations are seeking a chemical explanation of the planet's color phenomena. Difficulties in using spectrometry to study chromophores of red polymers formed in the course of the investigation stem from the fact that the degree of polymerization changes when the material stands around even at low temperatures (ref. 12).

Moon

Advisory groups have recommended a deep commitment to lunar exploration and the return of samples for analysis. Biologic interest centers on detecting viable life forms, whether organisms or dormant spores; organic analyses; evidence of mircofossils; and back contamination, viable or dormat life forms existing on the Moon that might be hazardous to Earth life (Hess, ref. 33).

Scientists are agreed that *in situ* organic analyses on the lunar surface are feasible with a gas chromatograph-mass spectrometer combination. Updegrove and Oro (ref. 34) have developed such an apparatus that consists of two compact mass spectrometers, a quadrupole and a monopole, mounted in parallel on a space-simulation chamber which is evacuated to cislunar pressures with a combination of diffusion, sputter ion, sublimation, and

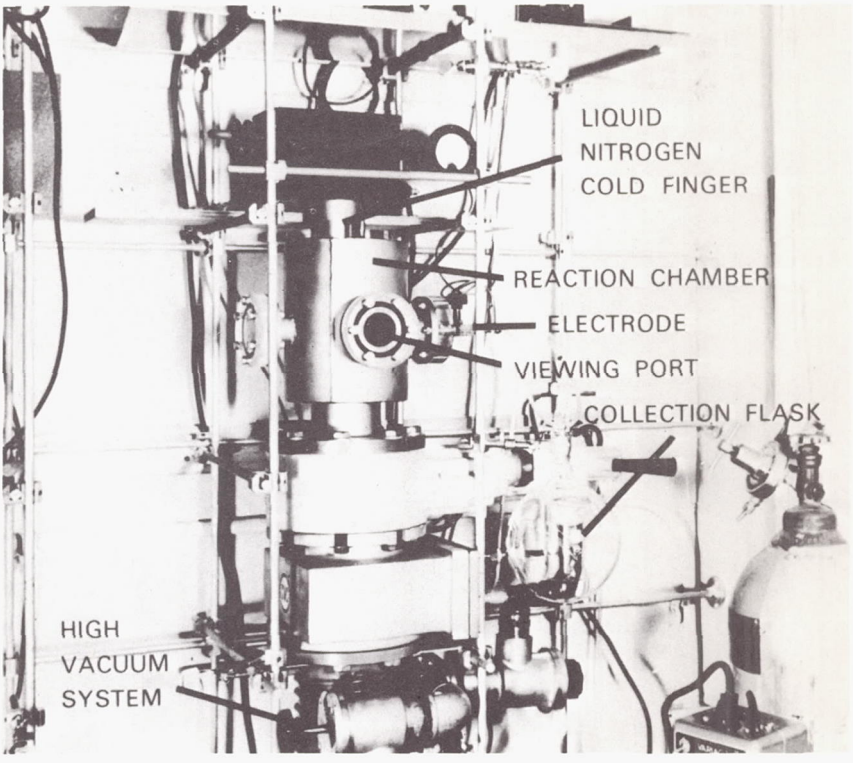


Figure 5.—Apparatus for studying electrical discharge in simulated Jovian atmosphere.

cryogenic pumping. Preliminary analyses on the Moon with such a device might allow distinction to be made between meteoritic and indigenous materials and between samples of high and low organic content. On the basis of information gathered by this apparatus, steps could be taken to reduce the risk of terrestrial contamination.

Volcanic Samples and Meteorites

Volcanic Samples

Samples from many volcanic zones, aseptically crushed and hydrolyzed to diminish possible microbial contamination, have been analyzed for evidence of amino acids. Typically, such analyses have revealed all the amino acids of bacteria except methionine and cystine, and deficiencies in proline, phenylalanine, and tyrosine. Results suggest that bacteria may have fallen on the lava and been partially decomposed (ref. 35).

Investigations are being made of the elemental and molecular composition of natural volcanic gases, with special search for trace quantities of biologically important compounds (fig. 6). Prebiotic components are being sought also in pockets or vesicles of gas in newly erupted lavas or in gaseous or fluid inclusions in ultrasonic nodules found in lava (J. J. Naughton, unpublished data).

Meteorites

Space-flight and celestial exploration have revived interest in chemical analyses of organic substances found in meteorites, especially in searching for evidence of extraterrestrial life. It has now been shown that significant amounts of extractable organic material may be expected, not only in the carbonaceous chondrites but also in the unequilibrated ordinary chondrites and in the ureilites (Hayes, ref. 36).

Firm conclusions on the biogenic or abiogenic origins of organic compounds in meteorites are not yet possible. Abiogenic support derives from the fact that every compound found in meteorites, with the exception of pristane and phytane, has been synthesized in some type of abiogenic synthesis. Evidence for optical activity or recognizable microfossils is still inconclusive. Apparently, the compounds contain no amino acids, and only

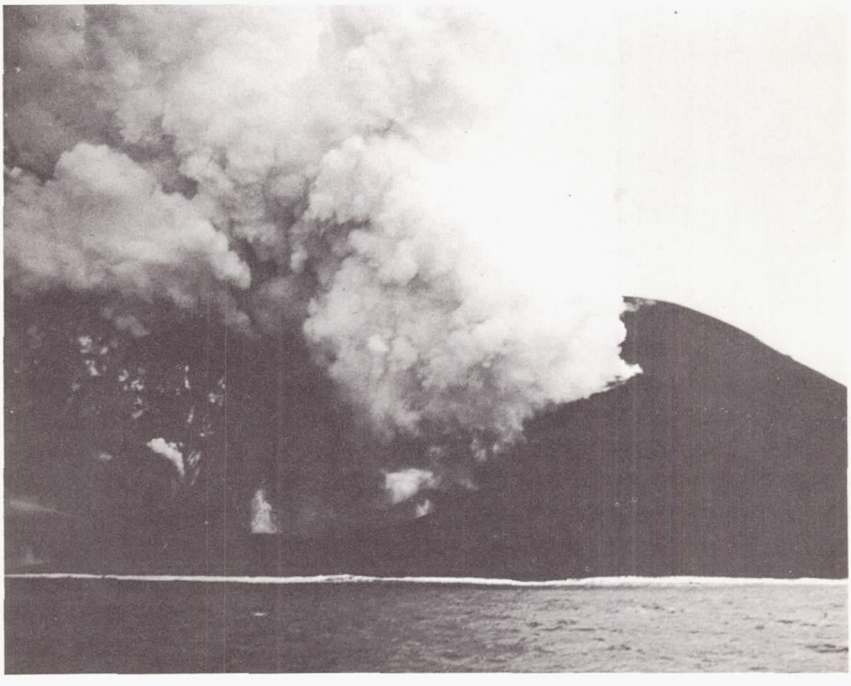
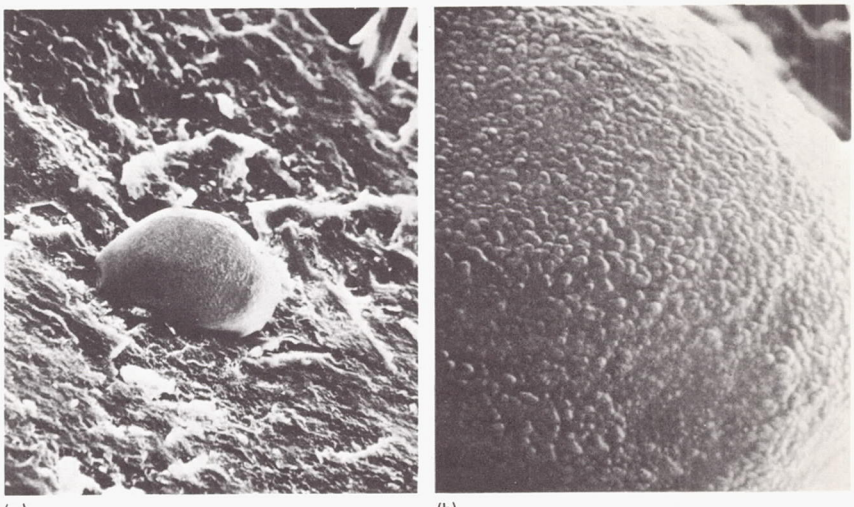


Figure 6.—Volcano eruption, Surtsey, Iceland.



(a) (b)

Figure 7.—**Electron photomicrographs of a particle in the Orgeuil meteorite, magnified (*a*) 1000 times and (*b*) 10 000 times.**

very small amounts of porphyrins. On the other hand, isoprenoid hydrocarbons (pristane and phytane) have been confirmed by Nooner and Oro (ref. 37), and a close correlation has been observed between meteoritic and terrestrial sedimentary hydrocarbons.

An analysis of hydrocarbons in the Orgeuil meteorite (fig. 7), a carbonaceous chondrite, suggested the extraterrestrial origin of these compounds and the probability is that these organic substances predate terrestrial life. Oro and Nooner (ref. 38) have now, through detailed gas chromatographic and mass spectrometric analysis, shown that most carbonaceous chondrites contain significant amounts of aliphatic hydrocarbons which could be presumed indigenous. However, similar quantities and distributions of alkanes found in iron meteorites suggest possible terrestrial contamination by fossil hydrocarbons of biologic origin. More work is needed to determine whether these meteoritic hydrocarbons are the result of terrestrial contamination, early biologic processes on the Earth-Moon system, or extraterrestrial abiotic or biotic synthesis.

All the nitrogen compounds seen in meteorites (adenine, guanine, melamine, ammeline, guanylurea) form spontaneously, in yields of 0.1 to 0.5 percent, when CO, H_2, and NH_3 are allowed to react in the presence of iron meteorite powder. Cytosine, cyanuric acid, biuret, and urea also form, along with a variety of hydrocarbons strongly resembling those in meteorites. This supports the theory that the organic compounds in meteorites formed in the solar nebula by spontaneous reactions on CO_2, H_2, and NH_3. Hayatsu (ref. 39) has suggested a large part of the prebiotic organic matter on the Earth may have originated in a similar manner.

SPACECRAFT STERILIZATION AND PLANETARY QUARANTINE

Background

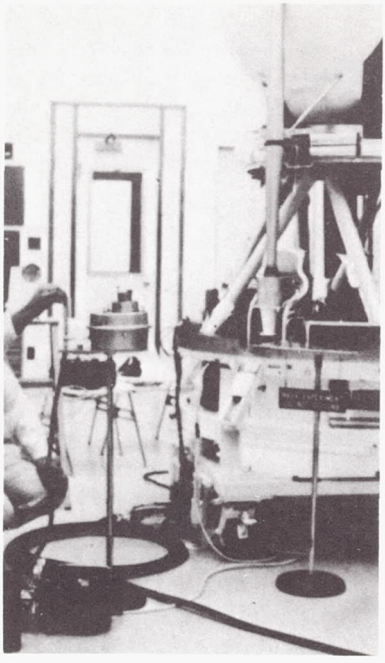
From the beginning of the space program the search for extraterrestrial life has been regarded as being of prime importance. Many investigators believe that if life does exist elsewhere in our solar system, it may be found on Mars, Venus, Jupiter, or the Moon. It has been recognized, also, that such search could be hopelessly compromised by contamination of the Moon and planets with Earth organisms transported by spacecraft or astronauts (Craven, ref. 40).

It is possible to build planetary exploratory spacecraft to fly by a planet and scoop out atmospheric samples or carry and eject hard-landing surface probes. They may also be constructed to eject automated soft-landing surface laboratories or to carry out surface observations while orbiting a planet for an extended period. An unsterilized probe could deposit on a planet micro-organisms which could multiply and irretrievably destroy any possibility of determining whether life was present or had ever developed on that planet. NASA attaches the highest importance to prevention of such contamination and subscribes to the National Academy of Sciences-National Research Council (NAS–NRC) statements that—

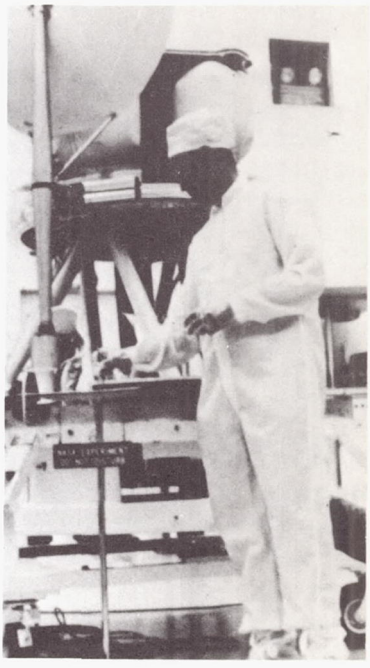
> the biological exploration of Mars is a scientific undertaking of the greatest validity and significance. . . . Its consequences for biology justify the highest priority among scientific objectives in space. . . . It is possible that Mars may provide our only chance to study life forms of entirely separate descent. . . . Contamination of the Martian surface with terrestrial microbes could irrevocably destroy a truly unique opportunity for mankind to pursue a study of extraterrestrial life.

As a participating member of the International Council of Scientific Unions, NASA subscribes also to the recommendation of the Council's Committee on Space Research (COSPAR) that seek to ensure that the probability of contaminating a planet during the period of biologic exploration be no greater than one chance in a thousand.

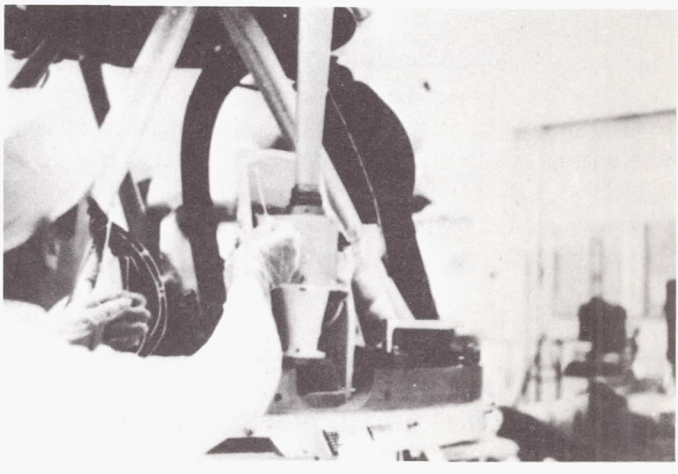
Planetary quarantine research has sought means for sterilizing spacecraft with maximum efficiency and minimum lowering of flight reliability. Sterilization activities are concerned primarily with bacterial spores, which, for space exploration, are the organism group considered an index of microbial contamination (Craven, ref. 40). One family of bacteria (*Bacillaceae,* which contains two genera—*Bacillus,* aerobic micro-organisms, and *Clostridium,* anaerobic micro-organisms) has the ability to form spores. The bacterial spore is a refractile body formed within the bacterial cell and it is extremely resistant to sterilization treatments. In fact, it is more resistant than any other known micro-organism. The spore thus becomes a major problem in controlling contamination, and sterilization procedures must be directed to its removal or destruction (fig. 8).



(a)



(b)



(c)

Figure 8.—Bioassay of spacecraft, showing (*a*) sampling of airborne bacteria, (*b*) collecting bacteria on metal settling coupons, and (*c*) removing bacteria by swab.

In general, the microbial contamination level within a given environment depends largely on the relative resistance of the individual micro-organisms to the conditions of the environment. External surfaces of a space vehicle are highly susceptible to the deposit of microbial contamination, or bioload. Gross surface contamination during manufacture results in gross internal contamination of the finished spacecraft and presents a very difficult sterilization problem. The most likely methods for sterilizing space hardware are exposure to heat, gaseous sterilants, and gamma radiation. Of these, heat is the most universally accepted because it may be used effectively on both external and internal surfaces and is generally less damaging to materials than gamma radiation (Craven, ref. 40). In 1964, the Space Science Board recommended dry heat for sterilizing spacecraft and their components, and dry heat is now specified as the sterilization method satisfying planetary quarantine requirements, although other methods may be used to meet special problems (Stern, ref. 41).

Planetary quarantine activities have made rapid technological progress by applying relevant findings of the Atomic Energy Commission and the Defense Department, and information supplied by the pharmaceutical and food-processing industries.

Examination of Planetary Quarantine Requirements

Standardized Mathematical Model

The probability of contamination of Mars can be analyzed by any number of mathematical models, each resulting in somewhat divergent values. A mathematical model is ultimately the instrument through which the information gleaned from the various tasks is assimilated logically into a probabilistic determination of the vehicle's sterility at launch. One such model was developed for determining dry-heat requirements to sterilize spacecraft. This sterilization process mathematical model will determine duration and level of dry-heat exposure needed for terminal sterilization immediately preceding launch of the spacecraft.

Basic inputs for the mathematical model will include elements constituting the dry-heat process: thermal design of the capsule (that part of a spacecraft which will land on a planet), microbial loading, the heating media, and thermal resistance of the micro-organisms. This total program will predict the physical distribution of the microbial load, will allow for the different resistance of buried and surface organisms, and will compute the transient lethality during heatup and cooldown. A microbial-burden model is being constructed by Stern to predict the burden by numbers and types at various capsule locations, as well as the total burden on the capsule. The outputs will be time/temperature parameters (fig. 9) for the terminal sterilization process; that is, the time when the oven is turned on, the length of time the capsule is held at temperature, the time the heating system is turned off, and the time the capsule in its canister is removed (ref. 41).

To provide input to the microbial load estimation subprogram of the terminal sterilization-process mathematical model, it is necessary to approximate the contribution of various piece parts. Therefore, data are being obtained on number and kinds of micro-organisms on and in electronic piece parts, typical of those to be found in a Mars capsule. By the end of 1967, more than 3000 piece parts had been evaluated. Continuing study will seek to determine possible modification of processes to reduce microbial surface contamination and to define the microbial distribution on and in such parts. All results will contribute to specifications for flight hardware and to the terminal sterlization mathematical model (Goddard, ref. 42).

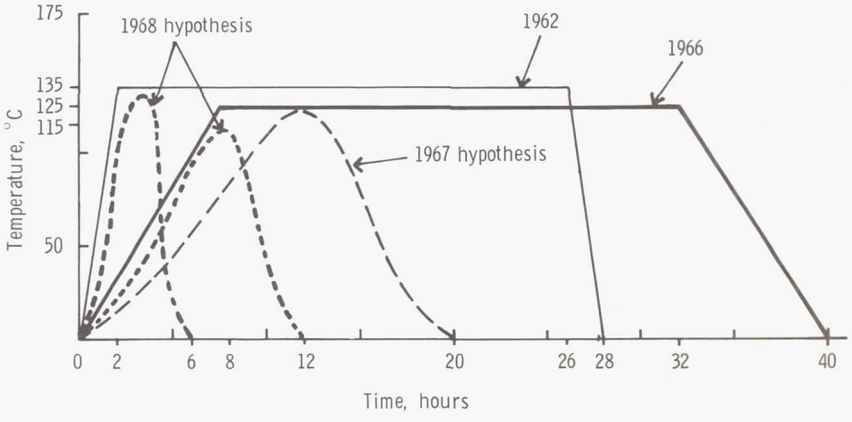


Figure 9.—**Conceptual development of sterilization time-temperature relationship.**

Probability of Release and Growth of Micro-organisms

The problem of contamination of lunar and planetary surfaces must deal with the probability of release of micro-organisms and of their survival, dissemination, and growth. The sources of contamination which affect this probability are as follows:

1. Spacecraft capsule not sterile.
2. Sterile capsule becomes recontaminated.
3. Launch vehicle impact.
4. Flight spacecraft impact.
5. Flight spacecraft ejecta/efflux impact.

To minimize the probability of contaminating planets with Earth organisms, a policy directive—aimed at all space-flight missions—calls for a basic probability of 1 in 1000 (1×10^{-3}) as a guide during the period of biologic explorations of Mars, Venus, Mercury, and Jupiter (Seamans, ref. 43). The directive stipulates that each planetary exploration flight, before launch, must meet requirements necessary to achieve policy objectives. Spacecraft will not "transport terrestrial life to the planets until it is determined that

life does or does not exist on the planet and the character of existing life is explored."

At the National Communicable Disease Center, one study of the probability of release of spores from fractured plastic demonstrated the interrelationship of spore concentration, fractured surface area exposed, and probability of release (Bond and Marshall, ref. 44). Another study, by Exotech, Inc., evaluated probabilities of release of viable organisms from three spacecraft locations: exterior surfaces, mated surfaces, and interiors of components and materials. A binomial model was developed to describe the conditional probability of release from component interiors as a function of the component's fracturing characteristic and the number of organisms present (Lyle, ref. 45). This model was found to compare favorably with experimental results provided by the National Communicable Disease Center.

In evaluating the probability of planetary contamination by interior contaminants released by accidental impact, some arguments have been made for relaxing COSPAR's sterilization standards. COSPAR recommended that the probability of a single viable organism aboard any spacecraft intended for Mars landing be less than 1×10^{-4}, and that the probability of accidental impact over a period of decades by each unsterilized flyby or orbiter be 3×10^{-5} or less (Sagan, Levinthal, and Lederberg, ref. 46). However, Horowitz, Sharp, and Davies (ref. 47) stated there is a small probability of release of entrapped organisms from inside a spacecraft and only a negligible probability of a terrestrial microbial contaminant reproducing on the surface of Mars. Surface sterilization should be sufficient. Murray, Davies, and Eckman (ref. 48), also in favor of relaxing standards, argue that, in any case, Mars and Venus may already have been contaminated by Soviet spacecraft.

Sagan et al. (ref. 46) maintain that it is too risky to relax sterilization standards. One serious possibility of contaminant release is a high-velocity impact of a capsule on a planet. Impact could result from failure of the spacecraft's braking mechanism or accidental failure of the craft's maneuvering devices. Bacteriologic warfare experience with shells and grenades suggests contained micro-organisms will survive such impacts. Spacecraft fragments spreading over a wide area would result in a loading density of roughly one micro-organism for every 10 square kilometers on Mars. Even higher loading densities could result from other failures; for example, inflight rupture of nutrient broth containers carried for bioassays on Mars. Investigators believe spacecraft should be designed to minimize such risks.

There are other possibilities of organism release, even if a spacecraft lands successfully. According to Sagan et al. (ref. 46), wind velocity is a factor, since large fluctuations of Martian temperature create dust devils with large vortex velocities. Mariner IV photographs show Martian craters considerably filled, probably by dust. Aeolian erosion of exterior spacecraft com-

ponents could also result in release of contaminants. Sterilization procedures (including probably heat soaking at lower temperatures or for shorter times) should discourage such occurrences.

Research over a period of decades has demonstrated strong possibilities for growth and replication of terrestrial micro-organisms on Mars. Laboratory studies under simulated Martian pressures and temperature cycling, in addition to a variety of wind velocities, support the conclusion that thin layers of liquid water develop each morning at tropical latitudes under limited diffusion. There is experimental evidence that, even if liquid water is available for only 15 minutes each day, in otherwise subzero conditions, many terrestrial micro-organisms will grow. They will grow even in soil microenvironments where liquid water results from freeze-thaw cycling. There remains existing evidence that suggests many micro-organisms can grow at slow rates at temperatures near 0° C (ref. 46).

Examination of Sterilization Parameters

Heat

Research results suggest the amount of heat applied to the spacecraft for sterilization may be reduced drastically, thus resulting in a reduction of costs. Outer space's deep vacuum appears to reduce some spore resistance, and exposure for 1 week at approximately 120° F will kill a full decade of the remaining population. The full effects of these conditions cannot be well defined until certain application problems are solved.

Effective thermal processes require realistic predictions of microbial levels, necessitating reliable means of microbiologic monitoring and sampling assembly operations (fig. 10). At Cape Kennedy, lunar spacecraft sampling is being conducted by the U.S. Public Health Service under NASA direction. During 1967, the Jet Propulsion Laboratory monitored and sampled the entire assembly of Mariner 1967 (fig. 11). Background data were made available for airborne particulate and microbial contamination levels for various areas of the spacecraft assembly (ref. 42).

Decontamination by heat has had the problem of dry-heat resistance of micro-organisms on both exposed and mated surfaces. Combined efforts of the NASA–AIBS Spacecraft Sterilization Advisory Committee, and of researchers, have developed a reliable, sensitive, and reproducible method for evaluating the dry-heat resistance of bacterial spores (fig. 11). Sterilization process-time derivations, such as the lethal effects of heatup and cooldown periods, are important areas for further studies. Investigations are now in progress to determine how process time is affected by various distributions of micro-organisms in and upon the space hardware. The dry-heat resistance and process-variables activities will contribute to the mathematical-model terminal process under development (Goddard, ref. 42).

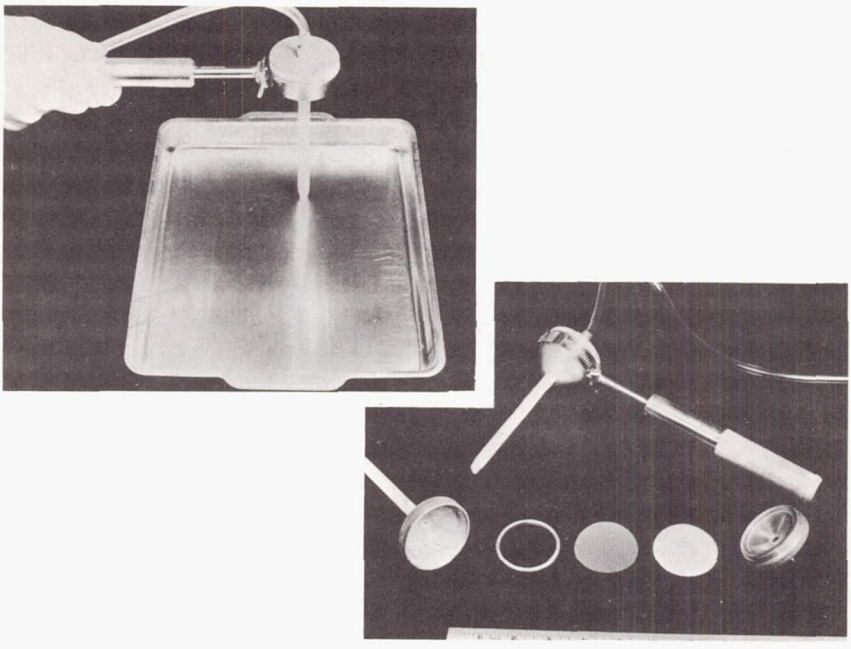


Figure 10.—Vacuum sampler for bioassay of spacecraft.

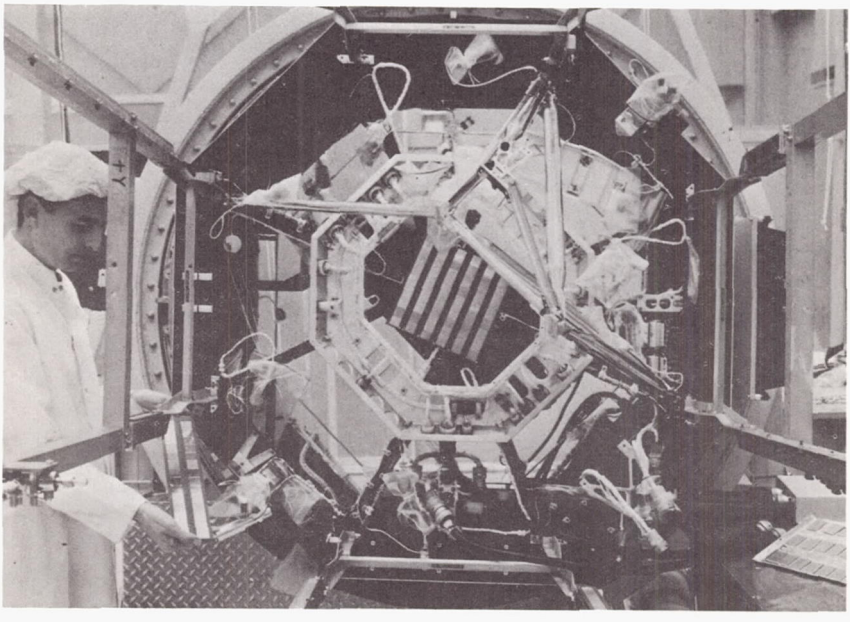


Figure 11.—Microbial sampling using stainless strips on Mariner 1967.

Time/temperature effects on the reliability of spacecraft components and assemblies require adequate terminal heat sterilization (Stern and Hoffman, ref. 49). A simple geometric and thermal conceptual model was so constructed that all effects of terminal sterilization and the relationship between the spacecraft's thermal characteristics and microbial contamination were defined. Various distributions of microbial load were postulated, and processes necessary to achieve sterility were determined. Results indicated that these variables and the microbial heat-resistance parameters significantly affected the derived process time at any temperature. Since lethality occurs during the heating and cooling phases of the sterilization cycle, the relationship between process time and spacecraft thermal behavior is complex. In general, as thermal conductivity increases, the required sterilizing process time decreases. Inclusion of transient-phase lethalities significantly influences the calculated process time, but neglect of these lethalities in the calculations will result in excessively conservative processes (Hoffman and Stern, ref. 50).

Water Activity

The resistance of spores of *Bacillus subtilis* to dry heat is increased by intermediate water activity. Strips of stainless steel inoculated with spores and contained in sealed tubes were placed in a heated environment at a specified water activity. Since condensation interfered with measurements of water effects, glass was substituted for steel as the test surface, and water-activity effects on thermal resistance were measured under conditions that either permitted or prevented water loss by the spores during heating (Angelotti, ref. 51).

In these experiments, the spores were adjusted to different water activities at the beginning of each heating exposure. During heating, moisture probably left the spores, entered the atmosphere within the sealed tube, and a new, much lower equilibrium relative humidity was observed. It was decided to determine the water-activity effect on spores under conditions that prevented water loss during heating. Spores were dried on glass strips, exposed to a measured water activity for 48 hours, then embedded in enough epoxy resin to prevent escape of water. Such spores showed much greater heat resistance than did naked spores adjusted to the same water activity, but exposed on glass alone.

Dieoff

Investigations have sought information on dieoff (viable-count reduction) of contaminants expected on space hardware under given conditions. In one study, at the University of Minnesota, using NASA standard assay procedures, the effects of 12 weeks' storage in a laminar-downflow facility on dieoff of contaminants on stainless-steel and epoxy strips were determined (Vesley and Smith, ref. 52). It was found that aerobic nonsporeforming organisms do die off relatively rapidly on stainless steel under laminar-flow

conditions, but much less so on the epoxy. It appeared that the dieoff of heat-resistant organisms (spores) is much less than that of species readily destroyed by heat.

Environmental Microbiology

Discovery and Quantification of Micro-Organisms

The total contamination load must be known before sterilization of spacecraft can be undertaken. Interior organisms may be grouped conveniently into three contamination categories, each with its own requirements of assay and sterilization: internal contamination of piece parts; occluded contamination in potting compounds, adhesives, and encapsulating plastics; and inaccessible contamination on intimately mated surfaces.

No simple assay method is available for measuring interior contamination of all potentially contaminated materials. The preferred technique for liberating embedded organisms is the use of a nontoxic solvent or nonlethal fine grinding or pulverization (Greene, Walker, and Anderson, ref. 53). In general, the accuracy and reliability of viable contamination will depend on the following: the specific material in which the organisms are embedded, the means of liberating viable spores, the nature of the inoculum employed, elapsed time between contamination and assay, temperature at which the material was stored, and interactions of all these elements.

A basic reference laboratory with established microbial standards and sampling techniques is essential for identifying and qualifying contamination in planetary and lunar missions. NASA has established such laboratories at the National Communicable Disease Center in Phoenix, Ariz. Spacecraft contamination is sampled and analyzed before launch (fig. 12) and accumulated data are processed in a computer to yield the total biologic load. These operations have provided estimates on the amount of biologic contamination U.S. activities have already transported to the Moon (fig. 13). In all planned space flights, similar calculations for future Apollo missions and returned lunar samples will facilitate budgeting, sterilization, and astronaut quarantining. Mission-recovery techniques and the Lunar Receiving Laboratory have been devised so that returned lunar samples and astronauts will not spread hazardous agents on Earth (ref. 53).

Recovery of viable micro-organisms trapped in solids is influenced by bacteriostatic and bactericidal effects of the solids in the recovery medium, mutilation by the physical technique employed, and nutritional efficacy of the recovery-growth media. Efforts have been directed to developing, testing, and evaluating procedures involving the following: dissolution, sawing, grinding, and pulverization of solids; neutralization of toxic substances contained in the solids; improving culturing techniques; and determination of maximum numbers of organisms which may be recovered from solids. A new approach is to determine whether the parts have been subjected to

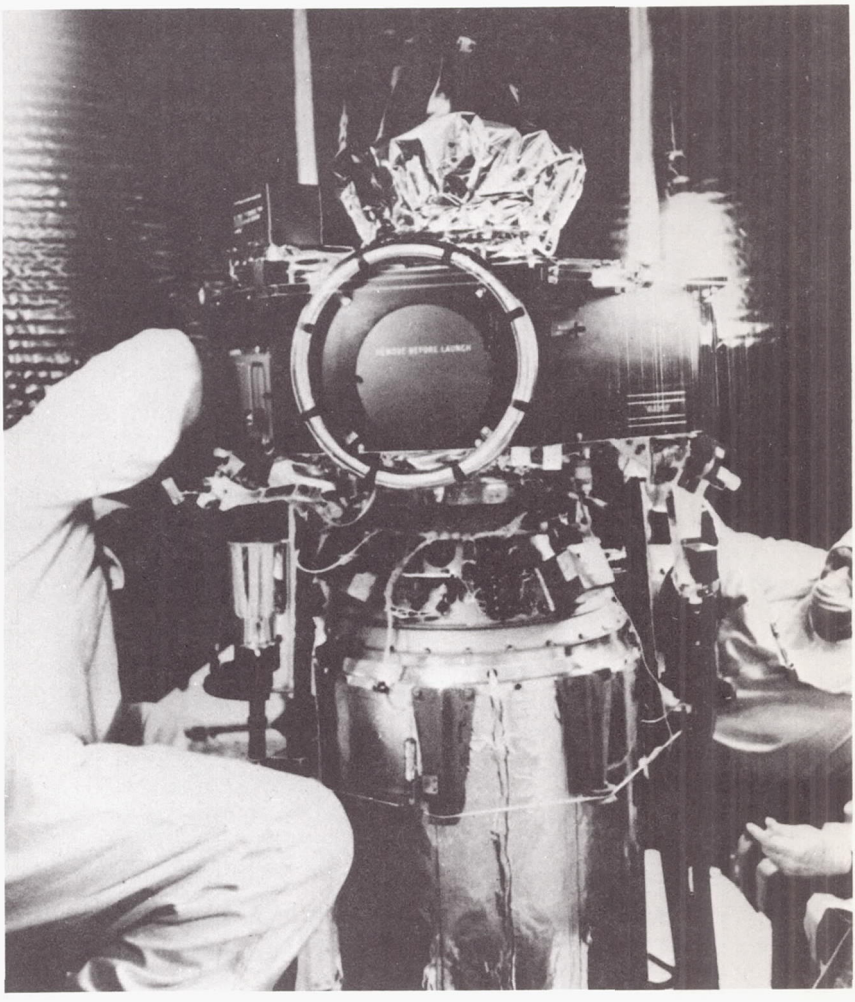


Figure 12.—**Final decontamination of AIMP-E spacecraft just before launch.**

sterilizing conditions (fig. 14) during manufacture, acceptance testing, or screening (Goddard, ref. 42).

Research in sterilization of occluded contaminants in polymerizable plastics has produced a variety of useful information (ref. 53). Different organic solvents have varying toxic effects on spores, but acetone, benzene, and ether had no deleterious effects. Embedded spores survived best under near freezing conditions, and showed significant and consistent diminution of viability (and/or recovery) at warmer temperatures. Dry heat at 135° C required more than 7 hours to lower the embedded spore concentration in

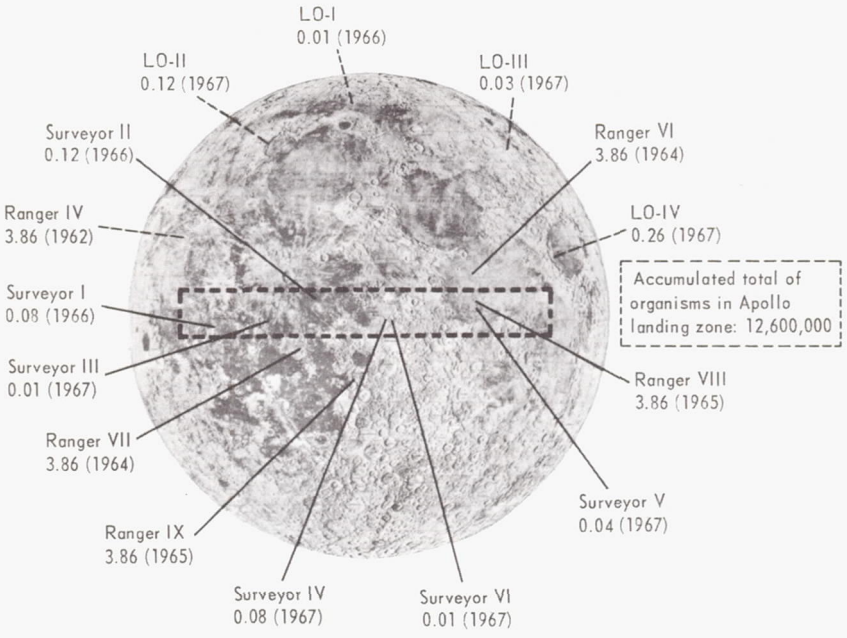


***Figure 13.*—Biological contamination of the Moon. Assuming contamination from each landing is confined to 1 square mile, figures are numbers of organisms per square meter.**

epoxy by one logarithmic cycle. Ethylene oxide did not penetrate beyond the surface of hardened epoxy. However, it did penetrate the interior of other plastics and exerted some sporicidal effects, depending on density and degree of polymerization.

Development of industrial "clean rooms" (any enclosed area where there is control over particulates in the air) for assembly and testing of spacecraft components demanded totally new standards of microbial detection. These clean rooms have sharply reduced the number of contaminants which accumulate on surfaces (Puleo, Favero, and Petersen, ref. 54). One approach has been use of ultrasonic energy (insonation), the application of a method used in physiologic studies of bacterial cells, in physical medicine, and in the dairy industry. Puleo, Favero, and Tritz (ref. 55) used an ultrasonic probe and showed that insonation could efficiently and precisely quantify micro-organisms on surfaces. Since a probe permitted only one sample at a time, ultrasonic tanks were evaluated for their ability to remove viable micro-organisms from various test surfaces (for example, polished stainless steel, frosted glass, smooth glass, electronic components) for subsequent enumeration. Ultrasonic energy proved more reliable and efficient than mechanical agitation in recovering surface contaminants.

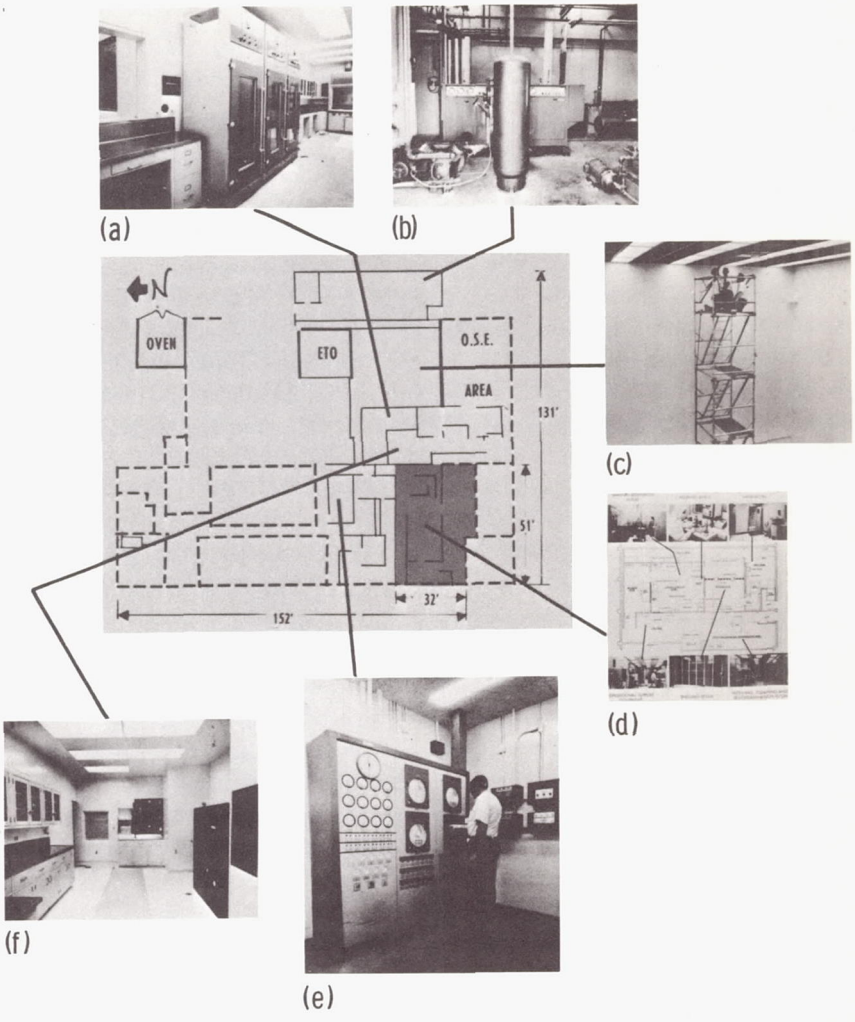


Figure 14.—Sterilization assembly development laboratory. (*a*) Biological area. (*b*) Mechanical equipment room. (*c*) High bay. (*d*) Experimental assembly sterilization laboratory. (*e*) FAC control center. (*f*) Media preparation area.

Further research has shown that ultrasonics not only enhances physical removal of micro-organisms from surfaces but also breaks up clumps of organisms (Bond and Marshall, ref. 44). A new ultrasonic method, developed by the Sandia Corp., employs a contaminated stainless-steel strip in a 250-milliliter beaker flat against the contaminated surface facing the bottom of the beaker; and a single beaker suspended in the middle of a full ultrasonic tank and insonated for 2 minutes. The current NASA standard

333-240 O—69——6

procedure employs sample bottles, each containing a strip set at a 40° angle to the bottom, resting on the bottom of an ultrasonic tank. A comparison of the Sandia and NASA procedures revealed that thickness of the glass container appeared to influence recovery of contaminants, but that the most important factor was the positioning of strips parallel to the tank bottom with the contaminated surface facing the transducers.

Sterile Insertion Techniques

Maintenance of sterility involves poststerilization monitoring (automated microbial or visual) of the capsule, and problems of sterile insertion of heat-labile components unable to withstand the terminal sterilization process. The Jet Propulsion Laboratory has already demonstrated that sterile assembly is accomplished with ethylene oxide, sterile air, or sterile nitrogen (using glove-box techniques), if the assembly parts are previously sterilized (ref. 42).

ENVIRONMENTAL BIOLOGY

Introduction

To understand and meet the problems man may face in ventures into space, environmental biology studies cover the whole range of biologic entities from micro-organisms to man at all development levels: molecular, cellular, systemic, and organismic. Living organisms are multicomponent systems combining remarkable stability with versatile adaptability to change. In environmental biology the discrete elements of space are identified, then defined as to how they influence biological organisms. It is important to determine what the stresses and adaptations of acceleration, radiation, and weightlessness impose upon the organism either in space or when readapting to return to Earth environs.

Altered Gravitational Force

One of the important scientific challenges today is determining the role of gravity in the origin, nature, and function of organized life. Receiving little attention from biologists in the past, gravitational influence, with the coming of space flight, has emerged as a subject of considerable and varied investigations. University of California (Davis) studies equate altered gravitational force with other environmental factors: if the alteration is sufficiently great, there is a toxic effect or region of debilitated survival (fig. 15). Physiologic adaptation, however, eventually dissipates the stressful condition.

In general, it appears that a spectrum of physiologic conditions accompanies the stress and adaptation of chronic acceleration. Thus, changes in ambient accelerative force, like the effects of exercise, lead to changes in muscle size. In birds living at 2 g for 3 months, the flexor and extensor hip muscle were hypertrophied; in birds exposed to 3 g for 3 months, the hip flexor was greatly reduced in absolute size, while the extensor was hyper-

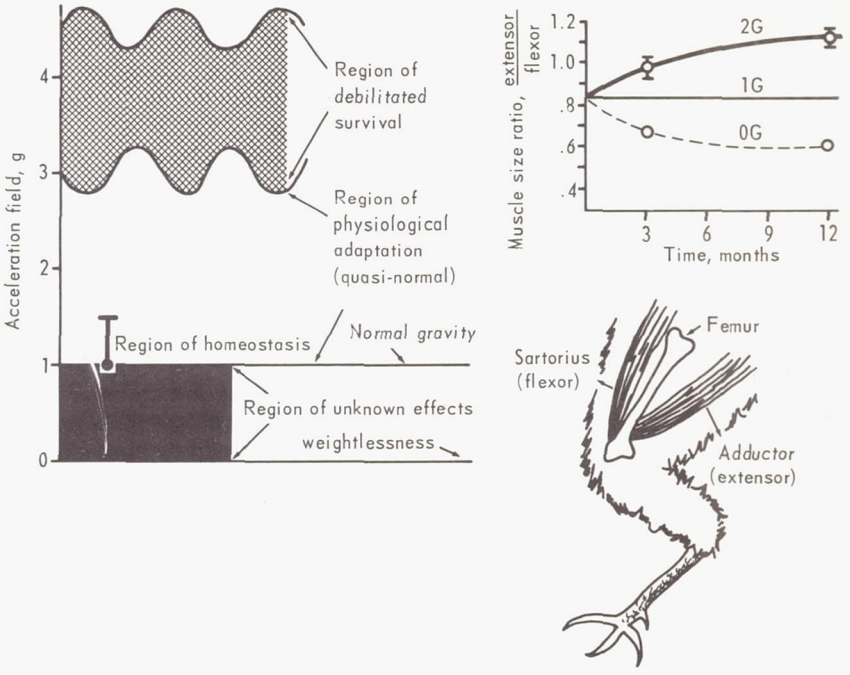


Figure 15.—**Animal response to chronic acceleration.**

trophied to about the same degree as in the 2-g birds (20 percent increase over controls). Increased acceleration for 1 year at the 1.5- and 2.0-g levels resulted in a consistent reduction in the flexors and a hypertrophy in the extensors (Burton, Besch, Sluka, and Smith, ref. 56). Under normal gravity, there is a definite ratio of the size of the extensor and flexor muscles. The direct effect of the accelerative force is an increase in the specific weight; weight, not mass, determines work for locomotion, maintenance of tonus, etc. The work occasioned by increased weight is borne by the extensor—the antigravity muscle—and this muscle increases in size systematically with the ambient accelerative force. The decrease in flexor size is less obvious. Perhaps this is a reciprocal inhibition induced by increased work of the antagonistic extensor muscles.

How does man perform under reduced gravity? Will he find working difficult? In 1953, it was first demonstrated that animals that adapt to increased chronic acceleration have been reported to develop anatomic and physiologic differences that presumably facilitate survival under this condition (C. F. Kelly and A. H. Smith, unpublished data). Birds returned to a reduced-gravity environment have outperformed animals resident at that environment, although some psychophysiologic adjustments appeared necessary.

Differential alterations found in the skeletal muscles of bipeds (chickens) exposed to low-order increases in acceleration led to speculation that the difficulty has a physiologic basis. Research has now shown that animals adapted to a hyperdynamic environment of 1.75 to 2.5 g, then returned to a normal 1-g environment (this simulated a reduced-gravity milieu), rapidly adjust to work in this "new" environment with no alteration in energy and fluid-balance kinetics heretofore associated with exercise and reduced gravity (Burton and Smith, ref. 57).

Since fat appears to be a major energy source for these skeletal muscles, and since evidence points to increased fat turnover in hyperdynamic environments, an increase in fat concentration, during weightlessness, may be expected. Energy reserves may limit muscular activity in these environments, and reduction in physical movement, consequently, would enhance survival. There is some evidence that metabolic shifts in weightlessness may make carbohydrates a more important energy source than fat. However, the principal muscle carbohydrate, glycogen, did not appear affected by changes in ambient accelerative force (Burton et al., ref. 56).

The most constant of environmental influences on life, because of the uniformity of gravity at the Earth's surface, is the weight-to-mass ratio. Little is known about the biologic response to chronic changes in the weight-to-mass ratio. Casey, Cordy, Goldman, and Smith (ref. 58) studied the effects of variation in the weight-to-mass ratio (above that of normal gravity). Using centrifugation, they produced artificial changes in weight by changing the ambient accelerative force, thus simulating an increase in gravity. To observe radiation effects in animals exposed to continued alterations in weight-to-mass ratio, whole-body irradiation permitted evaluation of the interaction of ionizing radiation and ambient accelerative force—a matter of importance for determining the effects of interaction of dynamic space-flight factors.

Results showed that acceleration per se does not produce deleterious results, since, by the 7th to 14th day, there was apparent physiologic adaptation. Accelerated animals, compared with controls, showed only a depletion of body fat deposits and a reduction in body mass. Continuous acceleration, immediately after irradiation, increased radiation mortality (lesions were typical of those produced by radiation), with mortality increasing progressively with accelerative increase. Results show that the biologic response to whole-body irradiation is altered by changing the weight-to-mass ratio with accelerative forces above normal gravity.

Burton and Smith (ref. 59), seeking criteria for physiologic condition relative to stress and adaptation, correlated hematologic indices with exercise capacity, sexual development, and survival in animals exposed to increased chronic acceleration. Lymphocyte (white blood cells, whose frequency is highly correlated with survival) counts and hematocrits strongly suggest that an individual's physiologic status under stress can be

estimated hematologically. Other physiologic effects of increased acceleration include a noticeable decrease in lymphocytes (fig. 16), changes in water and electrolyte balances, and a reduction in body size accompanied by greatly increased feed requirements (fig. 17).

Wunder (ref. 60) has established that chronic centrifugation influences the growth rate of animals, progressively decreasing the rate at sufficiently high fields, but sometimes stimulating growth at moderate intensities in a manner which is dependent upon temperature and size, but largely independent of the nongravitational (i.e., rotational) artifacts of centrifugation. It can sometimes provoke a temporary reduction in food intake, which is a partial cause of the initial decrement in growth observed with mammals. It results in eventual adjustments—which can include enhanced caloric intake, increased efficiency of oxygen metabolism, relatively larger supporting bones and muscles, enhanced circulatory pressure reflexes, together with

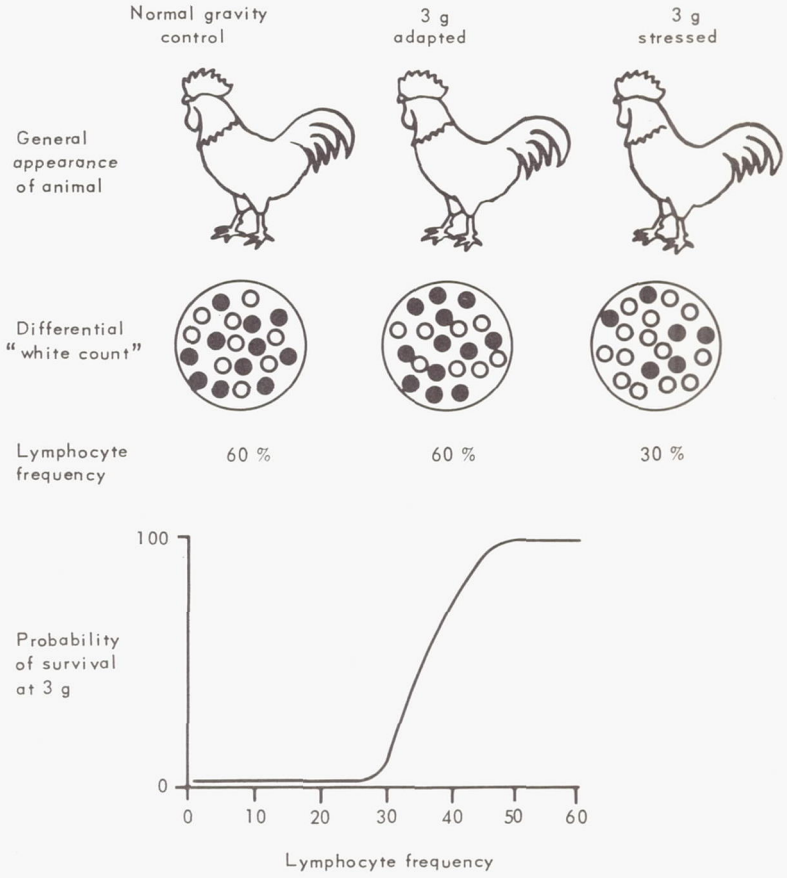


Figure 16.—White blood cell changes in response to chronic acceleration.

altered circulatory resistance and fluid balance—and influences life expectancy in a manner dependent upon field intensity.

Investigators have concentrated on developing physiologic procedures and automated instrumentation needed for measuring hemodynamic and metabolic parameters during prolonged weightlessness. Pace (unpublished data), working with a colony of subhuman primates, has developed relevant information on cardiac output, renal blood flow, arteriovenous pressure drop across the kidney, and respiratory physiology. The varieties of new bioinstrumentation contrived for this work include oxygen electrodes for chronic implantation in the great blood vessels, hard-wire thermistor probes also for vascular implantation, an automated hemodynamic blood-withdrawal unit, and an animal centrifuge. Unanesthetized monkeys, subjected to varying acceleration for different periods in a centrifuge and monitored for arterial, cardiac, and EKG data, are helping to define alterations in major body fluids and establish physiologic tolerance levels under conditions of weightlessness.

Bernstein, Gilfillan, and Rahlmann (ref. 61) have developed from the studies a transthoracic technique for implanting and maintaining patent

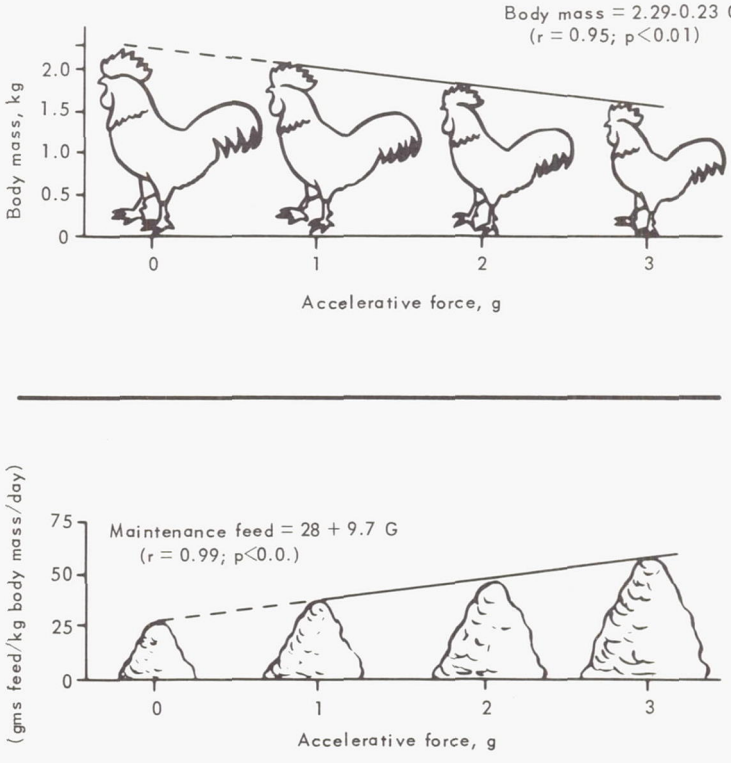


Figure 17.—**Changes in body size and food intake in response to chronic acceleration.**

polyvinyl catheters for more than a year at four separate sites in the vascular system of the monkey. These sites include the superior vena cava via the azygos vein, the thoracic aorta via the left subclavian artery, the left pulmonary artery, and the left atrium. Weekly flushing of the catheters has been found to suffice for insuring continued potency.

Work has proceeded in developing and adapting techniques for long-term cardiovascular studies during extended weightlessness (V. P. Popovic, unpublished data). Standard tests have been developed for evaluating cardiovascular parameters (arterial blood pressure, heart rate, EKG, arterial and venous oxygen contents, and cardiac output) in unrestrained monkeys during weightlessness.

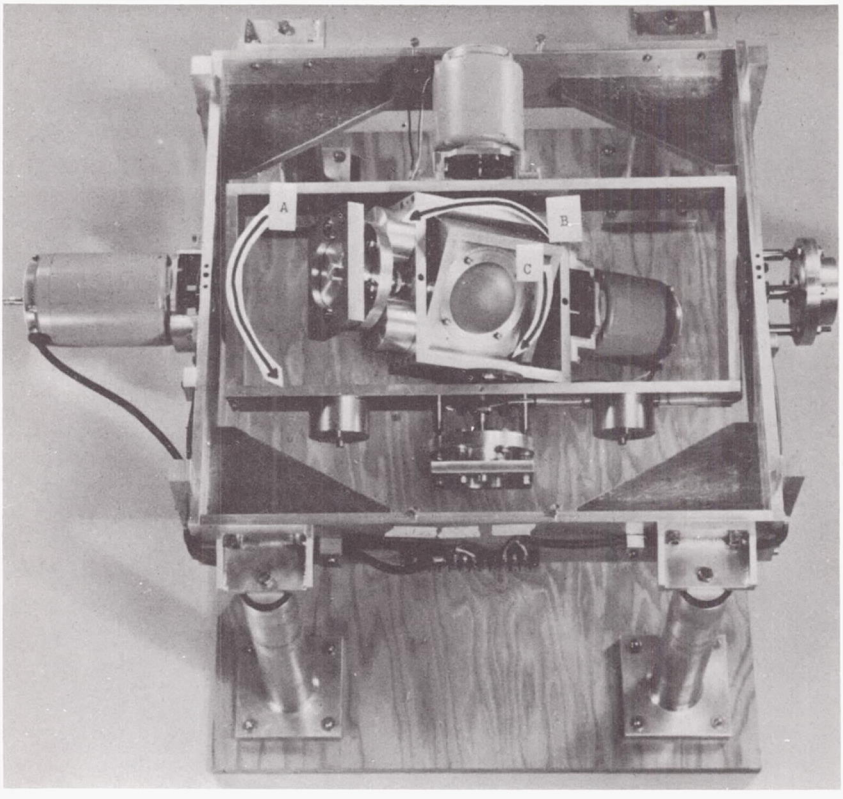
In experiments lasting 120 hours, Popovic and Addlestone (ref. 62) continuously recorded mean arterial pressure of 24 unanesthetized and unrestrained adult white rats. The blood pressure was recorded through polyethylene cannulas implanted in the aorta 1 month earlier. During recording, each rat was placed in a soundproof chamber with a 12/12-hour, light-dark cycle. The activity of the animal was monitored by a high-frequency transmitter and a receiver located in the chamber. During the activity periods the arterial blood pressure of rats was appreciably higher, 95 to 120 millimeters of mercury. However, these patterns were observed only after an initial "adaptation period" lasting between 12 and 72 hours during which time the arterial blood pressure as well as the activity of the animals fluctuated without any regularity.

To ascertain the still unknown mechanisms by which an organism senses accelerative force, scientists have devised the clinostat, a mechanical system that compensates for, or nullifies, the effects of gravity. Scientists at Argonne National Laboratory, dealing with the question of threshold of graviperception, have devised the four-π compensator (fig. 18), a device that, rotating simultaneously in three-dimensional coordinates, achieves nullification in the directional components of the Earth's field (Gordon and Shen, ref. 63).

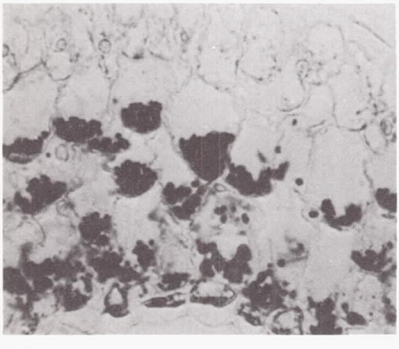
Cabin Environments

Atmospheres

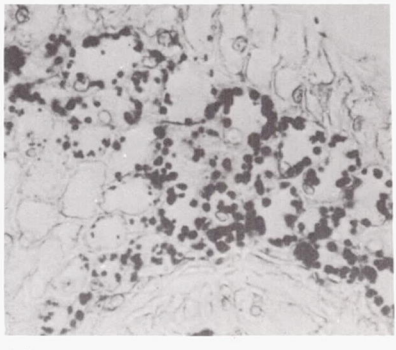
Increased use of sealed environments and artificial atmospheres for space flight has prompted study of eliminating or replacing nitrogen (N_2) in the respired gas. Nitrogen-free environments are being created experimentally to determine effects of nitrogen absence or decrease in the breathing atmosphere. The most frequent substitute for nitrogen has been an inert gas such as helium (He), thus establishing an oxygen-inert-gas atmosphere. Metabolic disturbances, however, have been frequently associated with helium-oxygen mixtures. Rhoades, Wright, Hiatt, and Weiss (ref. 64) exposed rats to a 79-percent-helium–21-percent-oxygen mixture at ambient temperatures between 23° and 33° C. Major effects of this exposure at 1



(a)



(b)



(c)

Figure 18.—Simulation of weightlessness by compensation for gravity. (*a*) 4π compensator (clinostat) with three-dimensional coordinates. (*b*) Distribution of particles in shoot tip cells erect to 1 g. (*c*) Distribution of particles in shoot tip cells on 4π compensator.

atmosphere were increases in food intake, oxygen consumption, urine osmolarity, heart rate, and respiratory rate, and a decrease in body temperature, particularly the subcutaneous temperature. These changes were influenced by environmental temperatures: they were most pronounced at 23° to 28° C; they were almost absent at 33° C. The results favor the explanation that the helium effect is an indirect function of its higher heat conductivity rather than a direct stimulation of oxidative processes at the cellular level.

Other studies have shown that in man, in a comfortable thermal environment, helium does not induce metabolic alterations at the cellular level, nor does the accelerated heat loss stimulate heat production measurably in brief exposures (Bower and Fox, ref. 65). At Ohio State University, researchers (who substituted helium for nitrogen in an apparatus in which the subject breathed an atmosphere not in contact with the skin) demonstrated conclusively that the fall in body temperatures—particularly skin temperature—is caused by the helium in contact with the skin rather than the breathed helium (fig. 19). Under normal conditions, the investigators found, the body-temperature decrease did not elicit an increase in metabolism, as it does in small animals.

Both Mercury and Gemini spacecraft used pure oxygen at a pressure of 258 millimeters of mercury. There is considerable evidence that exposure of animals to high-oxygen atmospheres adversely affects certain metabolic pathways, particularly those involving oxidation reduction, with toxic effects of coenzyme A and related compounds (Bond, Jordon, and Allred, ref. 66). Rats maintained in an oxygen atmosphere at 259 millimeters of mercury for periods up to 90 days, showed an 8-percent decrease in hematocrit. Coenzyme A in the rats' brains decreased during the first 4 to 5 weeks to about 50 percent of control values; this trend, however, did not continue after long exposure to the experimental environment. Animals exposed for 4 weeks to a continuous 100-percent-oxygen–5-psia environment metabolized 25 percent more sugar through an alternate pathway, thus diminishing biosynthesis of important body constituents—such as amino acids, proteins, and fatty acids—and increasing output of adrenal corticoids, reflecting a response to stress.

Depressed Metabolism

Depression of metabolism is a possible means of facilitating survival of living systems on prolonged space flights, perhaps using lowered body temperature to reduce energy expenditure. An effective method of depressing metabolism in certain animals is hypothermia (lowering body temperature by direct application of cold to a point where desired metabolic depression occurs), which is receiving wide study. Previous research has already shown the ease and speed of inducing hypothermia in animals in an ambient atmosphere of 80-percent helium–20-percent oxygen at a 5° C ambient tem-

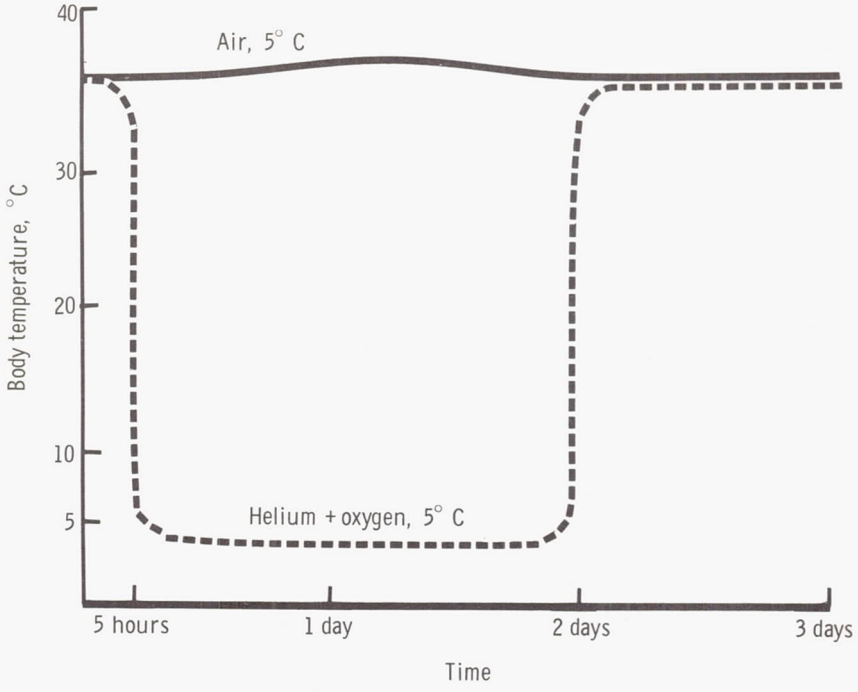


Figure 19.—**Depression of metabolism with helium.**

perature. Depending upon body size and ambient temperature, it takes from 6 to 12 hours for body temperature to approximate the ambient level. It has again been demonstrated that revival from hypothermia thus induced occurs upon exposure to room temperature, and that, in hypothermia, animals manifest greater radioprotection than do active animals (fig. 20).

Animals maintained in a 79-percent-helium–21-percent-oxygen environment for 10 to 22 days showed a higher metabolism than controls in air. When both groups were transferred to 100-percent oxygen, metabolism of controls remained unchanged, but that of experimentals fell to control levels. On first exposure to air, the experimentals showed a significant 7- to 11-percent depression in oxygen consumption below controls. Since the experimentals had undergone denitrogenation before the measurements, it was thought this may have sensitized them to the depressant properties of nitrogen (Rhoades, Wright, and Weiss, ref. 67). (Fig. 21 shows metabolic changes occurring in man on exposure to a 21-percent-oxygen–79-percent-helium environment.)

Another method of reducing metabolism is hibernation—a cyclic, stress-free physiologic state, usually seasonally linked, and characterized by reduction to minimal levels of many body processes. Hibernating squirrels receiving whole-body irradiation (900 to 20 000 roentgens) had a higher percentage of survival and longer mean survival time. Time of year and body

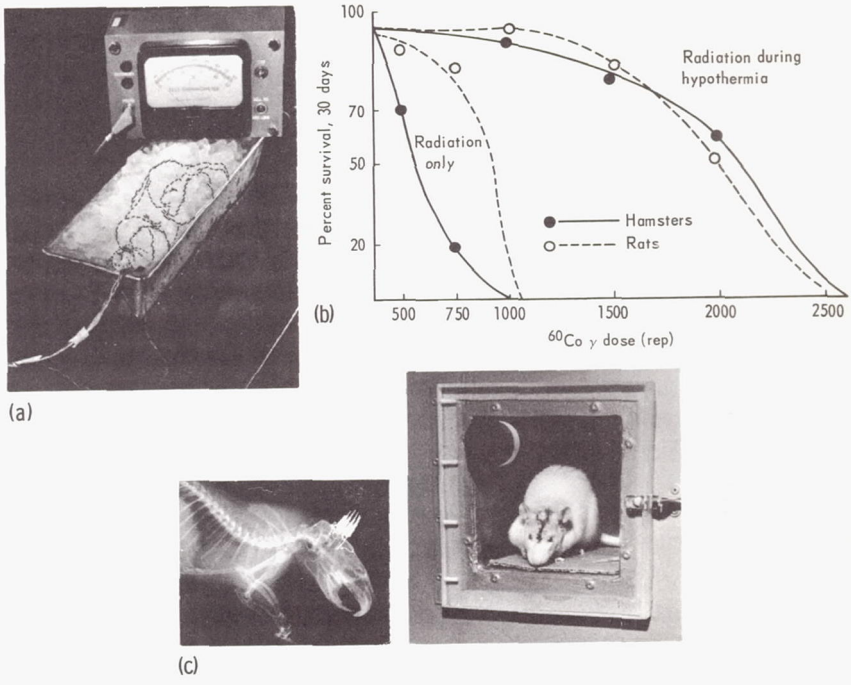


Figure 20.—**Radiation protection during hypothermia. (*a*) A method used to achieve body temperature reduction. (*b*) Graph demonstrating protective effect of hypothermia. (*c*) Electrode implantation for monitoring nerve function during hypothermia.**

temperature were directly related to degree of radioprotection (Barr, Musacchia, and Westhoff, ref. 68). Contrary to widespread opinion, radioprotection occurs not only during hibernation, but persists after arousal (Musacchia, Barr, and Westhoff, ref. 69). Hamsters, within 5 to 8 hours, became hypothermic in an atmosphere of 80-percent helium and 20-percent oxygen at 5° C ambient temperature, remained that way for 24 to 72 hours, and then regained normal body function within several hours after arousal. When exposed to 1000 roentgens of gamma radiation, these hypothermic animals survived, without apparent radiation damage, for periods longer than 90 days.

Study of metabolism in closed-circuit systems has been hindered by difficulties involving volumetric calibration, leak detection, temperature changes, and improper carbon dioxide absorption. These problems have been reduced by development of a metabolimeter, a simplified system that measures oxygen consumption simultaneously and continuously in 10 or more small animals exposed to different gaseous environments (Rhoades, Weiss, and Wright, ref. 70).

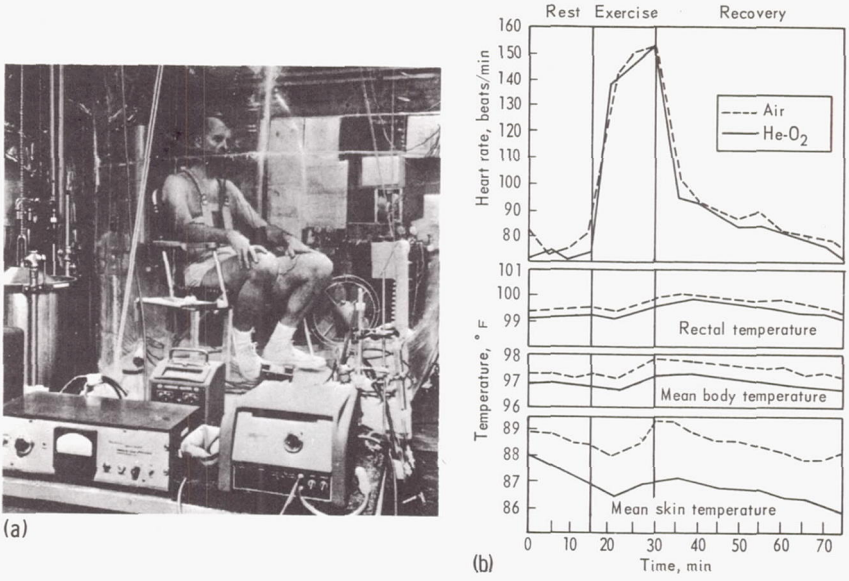


Figure 21.—**Effects of 21-percent-oxygen–79-percent-helium environment on man. (*a*) Environmental control chambers. (*b*) Metabolic changes.**

Radiation

To evaluate possible genetic effects of radiation on space travelers, scientists at the Lawrence Radiation Laboratory have exposed mice to the kind of radiation to be encountered on long voyages or during sudden solar flares. Using particle beams to simulate the radiation, the investigators have found, by accelerating the nuclei of heavy elements such as argon, that these "heavies" are more destructive than electrons and protons. Heavy irradiations (545 roentgens) of male mice every generation for seven generations have produced lethal mutations that reduced litter size by approximately 10 percent. However, except for weight gains by irradiated mice, there has been little evidence of any cumulative effect. If anything, irradiated mice appeared better able to resist the genetic effects of further irradiation.

In related experiments, electron irradiation, X-ray irradiation, and ultraviolet irradiation, applied to selected parts of the living cell (the nucleolus and the nucleus with exclusion of the nucleolus), produced a characteristic nucleolar rearrangement in the presence of chemical carcinogen. This response, designated a "nucleolar cap," was elicited only when the nucleus, but not the nucleolus, was subjected to ultraviolet radiation (P. O'B. Montgomery, unpublished data).

Effects on intestinal absorption of glucose were measured for 5 days in hamsters given whole-body irradiation of 1000 roentgens. Glucose ab-

sorption was elevated 25 to 30 percent in the second and third days after irradiation. On the fourth and fifth days, absorption was decreased and approached the control values (Musacchia and Barr, ref. 71).

Extreme Environments

Since adaptive mechanisms suitable under given terrestrial conditions may not suffice in the spatial and planetary milieux, investigations of life outside Earth must necessarily be preceded by studies of Earth organisms—preferably species found in environments matching approximately those of other planets—to provide baseline data. Of all life forms, micro-organisms seem best suited to survive the extreme physical conditions on other planets. Studies of adaptive potential of various mammals for withstanding environmental stresses have measured various biochemical reactions (plasma glycerol, serum lipase activity, tissue energy substrates, blood sugar, liver and muscle glycogen concentrations) under stress, and have produced sensitive recording devices, such as a temperature telemetry system that uses implanted transmitters (P. Morrisson, unpublished data). Investigators at Florida State University, studying biochemical and physiologic changes induced in micro-organisms under severe conditions of temperature and water and nutrient availability, have shown that certain bacteria and yeasts grow normally in a pure oil or hydrocarbon environment practically devoid of water (W. Schwartz, unpublished data) (fig. 22).

Study of heat-resistant halophiles has sought the upper temperature survival limit of several *Chromatium* isolates. Complete inactivation occurs for all strains of this bacterium on heating in brine at 80° C for 60 minutes. There is evidence that the rate-limiting process in growth is enzyme controlled rather than water diffusion limited (Witz, ref. 72).

Enzymes obtained from extreme halophiles not only function at high solute concentrations, but in many instances require a relatively high cation concentration for maximal activity. Potassium chloride is generally most effective in activating various enzymes isolated from extreme halophiles. During studies on a salt-dependent, reduced nicotinamide adenine dinucleotide ($NADH_2$) oxidase prepared from an extreme halophilic bacterium, Hochstein and Dalton (ref. 73) observed certain anomalies concerning the cation requirement for $NADH_2$ oxidation. In the course of experiments, he found that the cation requirement was nonspecific, since KCl, RbCl, and CaCl replaced NaCl with little or no loss of activity. NH_4Cl was only partially effective and LiCl failed to replace NaCl.

Fortunately, there are organisms on Earth that lead an existence similar to one that might be expected of a Martian organism, and whose study may yield insight into growth mechanisms on cold planets. Algid plants in mountainous regions actually grow at temperatures which never go above freezing. The cryophilic "snow alga," in winter, experiences long periods of freezing with no water available. As the weather warms, it is subjected

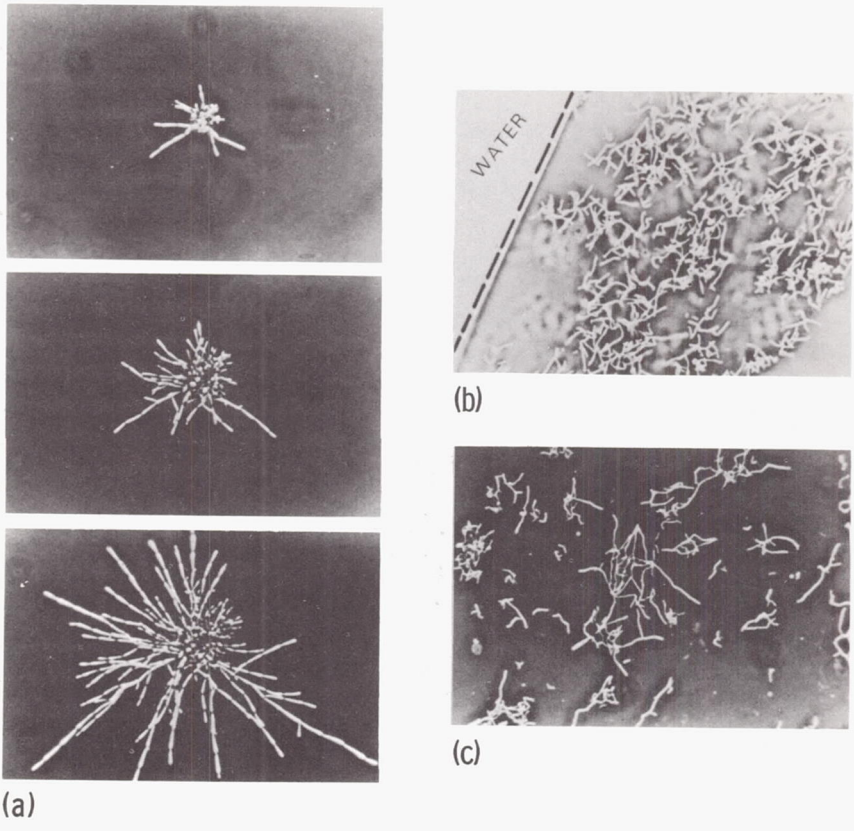


Figure 22.—Microbial growth in the absence of water. (*a*) Yeast growing in mineral oil. The middle photograph was taken 12 hours after the top one, and the bottom photograph was taken 24 hours after the top one. (*b*) *Mycobacterium phlei* growing in mineral oil. (*c*) *Nocardia asteroides,* oil-positive, growing in mineral oil.

to alternate freezing, thawing, and desiccation (Curl and Sutton, ref. 74). At the University of Colorado's Institute of Arctic and Alpine Research, an ecologic study of snowbanks was made and they were classified by the amount of daytime sunlight exposure received (Stein and Amundsen, ref. 75). A fungus, *Herpotrichia nigra,* commonly referred to as brown felt blight or snow mold, proliferated under snow cover, enveloping the needles of the host conifer tree and plugging the vestibules of the stomata (Simms, ref. 76). Snow algae reproduce to such an extent they color the snow red in many alpine and polar regions. Algae also grow in soil in the Antarctic dry valleys—one of the harshest environments on Earth, not varying greatly from Mars in temperature range.

Siegel, Roberts, Nathan, and Daly (ref. 77), investigating biologic behavior in exotic and harsh environments, studied ammonia-tolerant microflora in soils of different origins. A living, ammonia-obligate, umbellate form, similar to the Precambrian microfossil, *Kakabekia umbellata* (Barghoorn), has been isolated from two soil specimens collected at Harlech, Wales. These forms have been grown in glucose-ammonia, with the latter as the sole source of nitrogen. Ammonia is necessary, and growth is always slow without glucose.

Success in space ventures will depend on man's adaptability to environmental extremes he does not normally encounter on Earth. The magnetosphere is an intrinsic component of terrestrial environment, but is almost totally absent in space. This might lead one to expect certain kinds of hazards in extraterrestrial travel: an increase in mutation rate caused by cosmic radiation unimpeded by a magnetic field; alterations in physiology that is normally in a particular kind of balance in a magnetic field; and psychologic impairments (intellectual, emotional, perceptual, and motor). Beischer, Miller, and Knepton (ref. 78) exposed subjects to a condition free of a magnetic field (a specially contrived coil system created a field strength below 100 gamma) and, with one exception, could detect no significant physiologic or psychologic impairments. None of their subjects seemed to notice any difference between the geomagnetic field and the field-free environment. The exception was a phenomenon previously recorded: in all subjects the critical flicker-fusion frequency diminished gradually during the exposure period and recovered rapidly to pre-exposure levels following return to a normal environment.

Photosynthesis

Photosynthesis establishes a closed ecosystem by applying single-celled algae in an interaction of light energy with carbon dioxide (CO_2) and water (H_2O) to yield oxygen (O_2) and plant cells. Chlorophyll (contained in all green plants) picks up the light energy that thermodynamically converts CO_2 and H_2O into a carbohydrate that is later reconverted into other substances, such as protein and fat. In this process, CO_2 is consumed and an approximately equal amount of O_2 is liberated.

Research in physical biochemistry has demonstrated that photosynthesis is the result of two cooperating light reactions which have been designated photoacts I and II (Kok, Rurainski, and Owens, ref. 79; and Kok and Datko, ref. 80). The concept assumes that light absorption, in each system, is followed by formation of a primary oxidant and reductant. System I generates a strong reductant and a weak photo-oxidant; system II, a strong oxidant (yielding O_2) and a weak reductant. Perhaps the least understood aspects of photosynthesis are the reactions within photosystem II which result in evolution of oxygen.

Photosynthesis research, in this period, showed a general interest in conversion of light energy into cellular reducing power, such as reduced pyridine nucleotide and ATP. Biochemical studies with isolated chloroplasts suggest the intimate connection of ATP formation with photosystem I (Joliot and Kok, ref. 81).

A peculiarity of photosynthesis is its limited capacity to convert high intensities of light; indeed, algae cultures in sunlight or artificial light frequently show the deleterious effects (there is a considerable amount of irreversible destruction) of such intensities. Recent work in localizing the "rate-limiting reaction" attests to the complexity of this response to high intensity and the difficulty of pinpointing a specific site. Analysis of high-intensity inhibiting effects has suggested three different processes—one, a direct effect of ultraviolet light, and two others, a result of photosynthetically active wavelengths which inactivate the trapping centers of the two photosystems (Kok and Jones, ref. 82).

BEHAVIORAL BIOLOGY

Space bioscience continues to look to behavioral biology for research into how organisms react under space-flight conditions, and for utilizing the special qualities of space to derive new insights into behavior. The behavioral biologist examines and interprets all behavioral (biological and psychological) responses to variations in gravitational force, unusual sensory stimulation, alterations in the day-night cycle, and long-term social isolation. He seeks out the biological basis for all observed reactions and, equipped with facts, defines conditions for survival in space flight and contributes to the fuller understanding of man in his universe.

Effects of Space Environment

Artificial Gravity Selection

How will man perform in the weightless conditions of space during prolonged celestial flight? This is the overriding concern in planning and designing the craft that will carry astronauts on their extended journey. Largely unknown, yet, is man's response, over a period of time, to gravity levels between the 1 g of Earth and the zero of space. Still to be determined is the gravity level that will assure steady, efficacious biological functioning in space.

To develop this kind of information, and to determine the feasibility of conducting longer term gravity-level-preference studies in space, University of Kentucky scientists have designed and launched the first of four Aerobee rockets (fig. 23) equipped to examine the responses of animals in an artificial-gravity field. Chief feature of the Aerobee is its ability to create artificial gravity through centrifugal action. Since Earth-orbiting spacecraft operate under weightless conditions, rotating the vehicle like a centrifuge will produce artificial gravity. Extending the two arms of the spinning

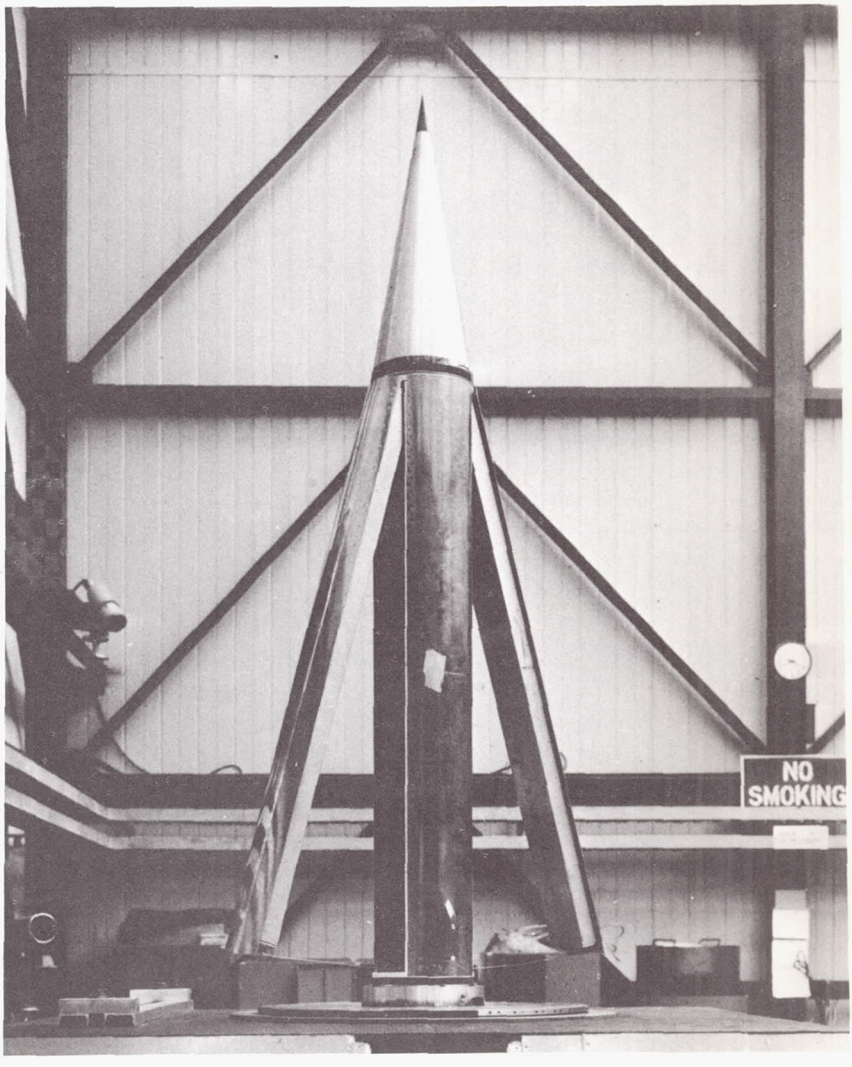


Figure 23.—**Aerobee payload for gravity-level selection.**

payload during flight produces a variable-radius centrifuge with artificial gravity levels ranging between 0.35 g and well above 1 g. Subject animals are allowed to walk along a tunnel runway in the extended arms, where they select their own gravity level. Low gravity is experienced at the end of the runway nearest the axis or center of rotation; higher gravity is encountered at the end farthest from the rotation center, where the longer radius occurs. Displaying its normal adaptive response, the animal selects its most comfortable position along the runway (K. O. Lange, unpublished data).

333–240 O—69——7

Ground-based tests at the University of Kentucky's Wenner-Gren Aeronautical Research Laboratory have been devised to permit a monkey in the cab of a large centrifuge (fig. 24) to control the gravity level by pressing a lever which changes the rotation rate. These tests, and others with trained rats, have demonstrated a decided preference for Earth's gravity when exposed to levels of 1 g and above.

Environmental Sensing

There is a considerable body of work showing the effects of environmental stimuli on physiology and behavior. The increase in systolic pressure with age, observable in many human populations, is regarded as a response to repeated symbolic stimuli inherent in the social environment (Henry, Meehan, and Stephens, ref. 83). Early experience or conditioning can influence later vascular responses to environmental elements. The behavior of sibling mice in a standard box (absence of fighting and persistent normotension) was contrasted with the repeated outbursts of threat and other competitive activities between mixed males in a box of the same size. The investigators believe the striking behavioral difference is attributable to the animal's early experience, which controls subsequent responses to a social situation.

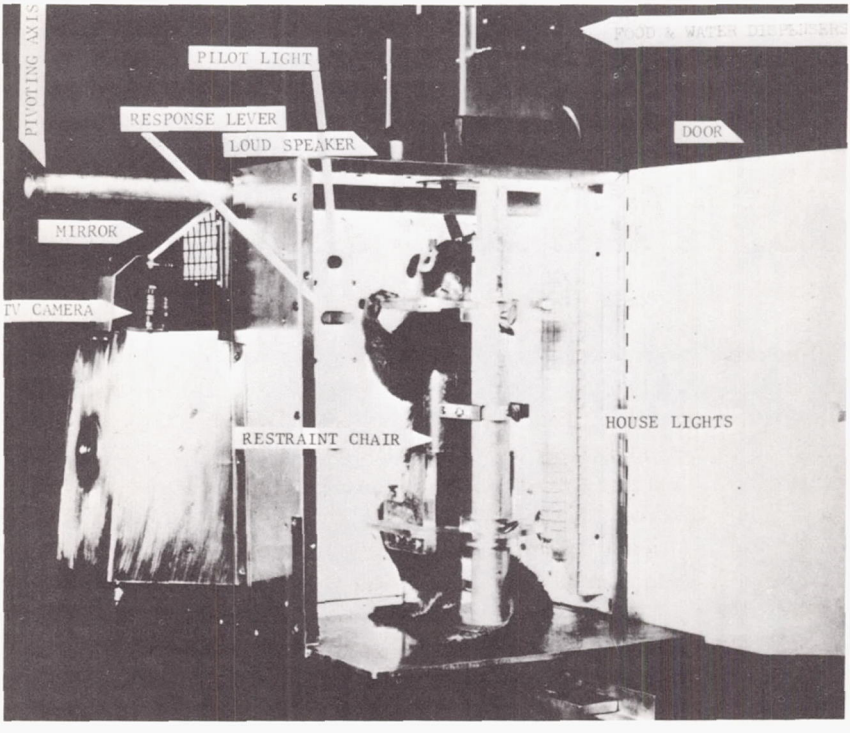


Figure 24.—Control of artificial gravity level by monkey in centrifuge.

Biological Bases of Behavior

Brain Stimulation

Various kinds of techniques have been developed for studying brain behavior connections. A brain stimulation-monitor system under development at Emory University transmits radio signals to stimulate an animal's brain and then verifies receipt of the signal (fig. 25) (B. W. Robinson, unpublished data). Telemetering heart, respiratory, and brain-activity records, and permitting transmission to and from the animal without restriction of activity, the instrumentation is being tried in exploratory manipulations of survival behavior.

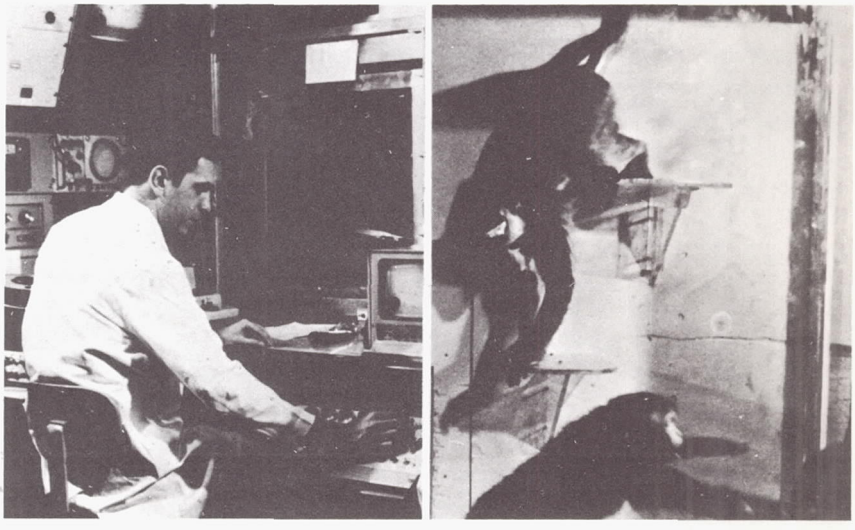


Figure 25.—**Aggressive behavior in monkeys induced by telestimulation.**

Exploring the brain's intricacies and defining areas related to specific behavioral patterns has been facilitated by a technique for remote-control brain stimulation by implanted electrodes (Robinson and Warren, ref. 84). Used on monkeys, the method identifies intracerebral structures directly by identifying the myelination pattern an electrode encounters as it moves through the brain. It is considerably more accurate than stereotaxis, which is based on skull or ventricular landmarks and the brain itself. Technically labeled the "impedance method," since it measures voltage generated between the moving electrode and a fixed electrode, the technique is being studied for application to the human brain. Early results with human brains removed at autopsy indicate the method's utility with both animals and humans.

Extended observations of brain cells and organelles in living vertebrates have been made possible by a new type of light microscope. The new micro-

scope—designed to scan the optical field in order to eliminate much of the unwanted reflected light that degrades the quality of the image in conventional microscopy—takes advantage of the contrast-enhancing properties of an illuminated field of small diameter (Egger and Petran, ref. 85).

Attention and Alertness

Many investigators believe that physiological monitoring of pilot or astronaut status, based on such considerations as the electrocardiogram or respiration, is not especially responsive to transient shifts in alertness and focused attention associated with drowsiness and fatigue (Adey, Kado, and Walter, ref. 86). For some time, there has been a need for a reliable, noninterfering monitoring system for a passive subject. Since exposure of the mammalian organism to ever-increasing periods of weightlessness has raised important questions about effects on basic brain mechanisms, it has seemed reasonable to seek evidence for altered cycling in brain-wave patterns.

New studies of alertness in pilots and astronauts have now begun to employ continuous monitoring of electroencephalographic (EEG) data as relevant indices (Walter, Kado, Rhodes, and Adey, ref. 87). Investigators at the MIT Research Laboratory of Electronics, using signals that can be recorded from the intact human scalp in various stages of alertness, have studied the temporal structure of EEG data in man. Special emphasis has been placed on instrumentation techniques, data-reduction application, and the use of three-dimensional, continuous displays showing changes in physiologic condition. Such a display, imperative when immediate response must be made to a perilous physiologic state, provides a synthesis of data and perspective in assessing an individual's condition.

Electroencephalographic complexities require analytical methods that compress primary records into an overview of long-term data, without losing sight of individual subtleties. However, the usefulness of the most elegant display of data depends upon the reliability with which the observed pattern can be equated with norms already determined for a comparable population.

Sleep and Wakefulness

Largely unexplored, the interconnections of sleep, fatigue, and gravitational effects are being unraveled by EEG techniques that, at the same time, are explicating associated behavioral aspects and hitherto little-understood workings of the brain.

Research has now defined three distinct "states of existence": wakefulness, sleep, and rapid eye movement (REM) sleep (a condition of frenzied internal activities in many ways similar to alert wakefulness). Especially relevant to man in space is the new knowledge beginning to emerge from studies of the neurophysiologic and biochemical changes during REM sleep.

A Stanford University study is underscoring the great importance of REM sleep in normal organism function, and the effects of REM sleep deprivation

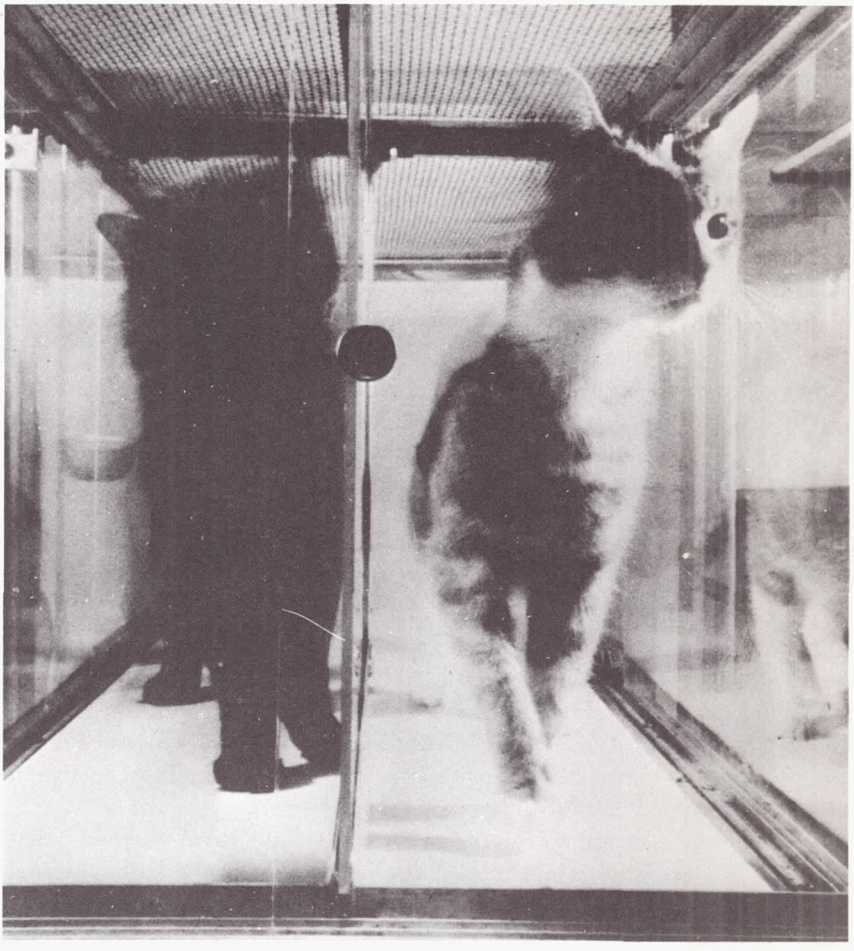


Figure 26.—**Study of sleep deprivation using cats on treadmill.**

on animal and man. Placing animals on a slow-moving treadmill (fig. 26) or on a small flower pot surrounded with water (fig. 27) permits some sleep, but not REM sleep, in which there is complete muscle relaxation. Deprived of REM sleep, animals display decided increases in aggressiveness, sexuality, and susceptibility to seizures. In addition, changes in other body systems (heart rate, blood pressure, etc.) reflect the enormous influence of REM sleep on drive behavior and physiological function. All modifications apparently persist until the sleep indebtedness is fully paid.

A number of drugs affect REM sleep in one way or another. Alcohol and pep pills, for example, interfere with REM sleep (delirium tremens may be a result of REM-sleep deprivation). There is much evidence that this sleep is biochemically controlled (the fact that it must be made up over

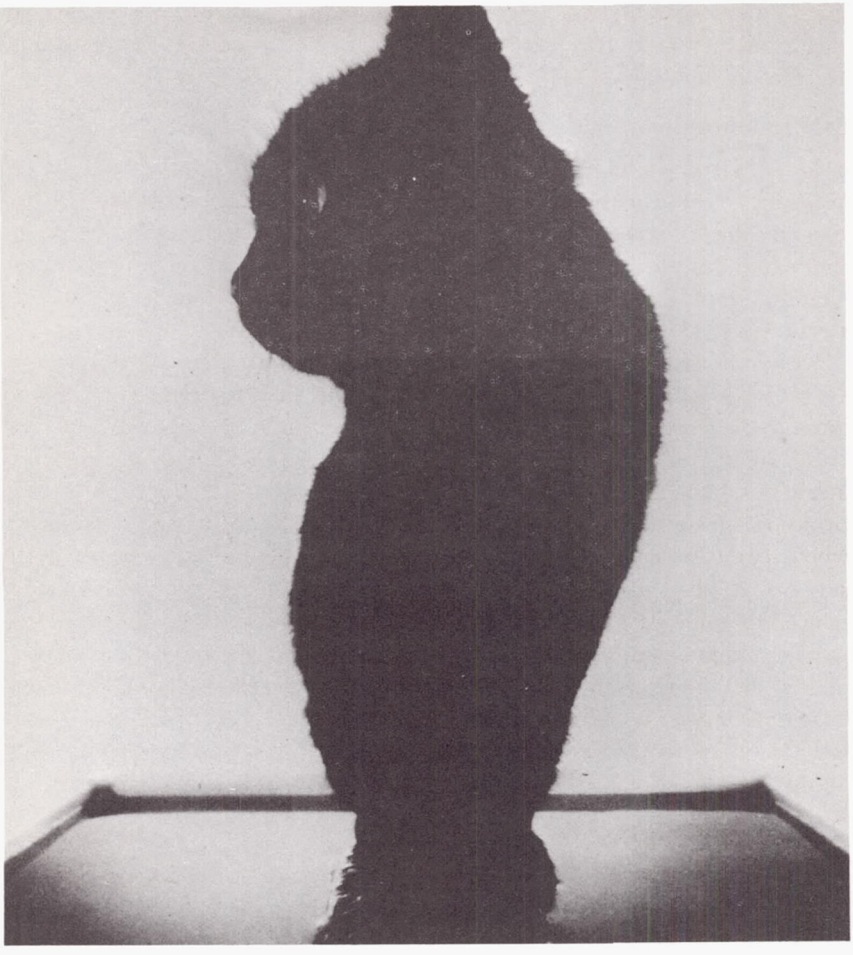


Figure 27.—**Rapid-eye-movement sleep deprivation using island in water tank.**

many days and weeks suggests an accumulation of a chemical compound), and drugs known to stop specific biochemical processes are being studied for their effects on REM sleep. Similar investigations are being made of those chemical compounds (neuroregulatory agents) in the brain that might influence REM sleep.

The relation of REM sleep to long-term behavior and performance, such as would be required in space flight, requires special research efforts. What needs to be made clear is how REM sleep is involved in control of drive states, in moderating cognitive activity and social interaction, in triggering certain illness. The potential value of this research for biomedicine is considerable,

as investigation establishes a connection between the REM sleep process and nocturnal angina attacks, cardiovascular and cerebrovascular accidents, and certain psychotic manifestations.

Sensorimotor Coordination

Man in space will be subject to new and unexpected demands on his capacity to coordinate sensorimotor events. Analyses of visually guided reaching have been carried out as part of an extensive investigation of the limits and varieties of sensorimotor coordination, particularly in relation to changes in gravitational force and consequent alterations in feedback from the muscles (Held and Bauer, ref. 88).

Research with monkeys and men has shown that the act of reaching for a visible target is dependent upon capability, first, to orient the eyes and head to the target, and, second, to match the direction of hand reaching with orientation of the head to the target. This matching is altered when adults adapt to displaced vision of the arm, and this change shows little or no transfer to the unexposed hand (ref. 88). Infant macaque monkeys, when reared to a point where visual and motor capabilities were ready to support visually guided reaching, were unable to carry out such behavior when the relevant visual-motor interaction was experimentally interfered with. Although allowed a wide range of normal exploratory and manipulatory activities, such monkeys were reared with their limbs concealed from the monkeys' view by a circular plywood body shield with an opening in the center through which the animal's head protruded (fig. 28). Within 12 hours of birth, the infant monkey was placed in the apparatus and, for the next 34 days, was not allowed to view any part of its body.

An animal reared under normal conditions will accurately reach for and manipulate visible objects before 1 month of age. These monkeys were allowed, on the 35th day, to view one hand for the first time. With intense visual curiosity, each monkey gazed at its hand as if it were a foreign object. Sight of a bottle elicited arm extension, but, as long as a light was on, the action was uncoordinated and stopped when the hand entered the monkey's field of vision. When vision was excluded, the monkey used its arm in a perfectly normal fashion. The entire cycle was repeated for the other hand, taking just as long to map into the visual field as it did the first.

Held and Bauer (ref. 88) believe that the necessary information for matching and integrating orientations of head to target and directions of arm reaching comes from the earliest experience of watching the moving limb. Confirmatory evidence for these conclusions was provided by Hein and Held (ref. 89) who reared kittens that were not permitted sight of their limbs. They discovered the animals extended their forelimbs when carried toward the end of a horizontal surface but, unlike normally reared kittens, were unable to guide their paws accurately. The investigators concluded that elicited extension in the kittens develops without sight of

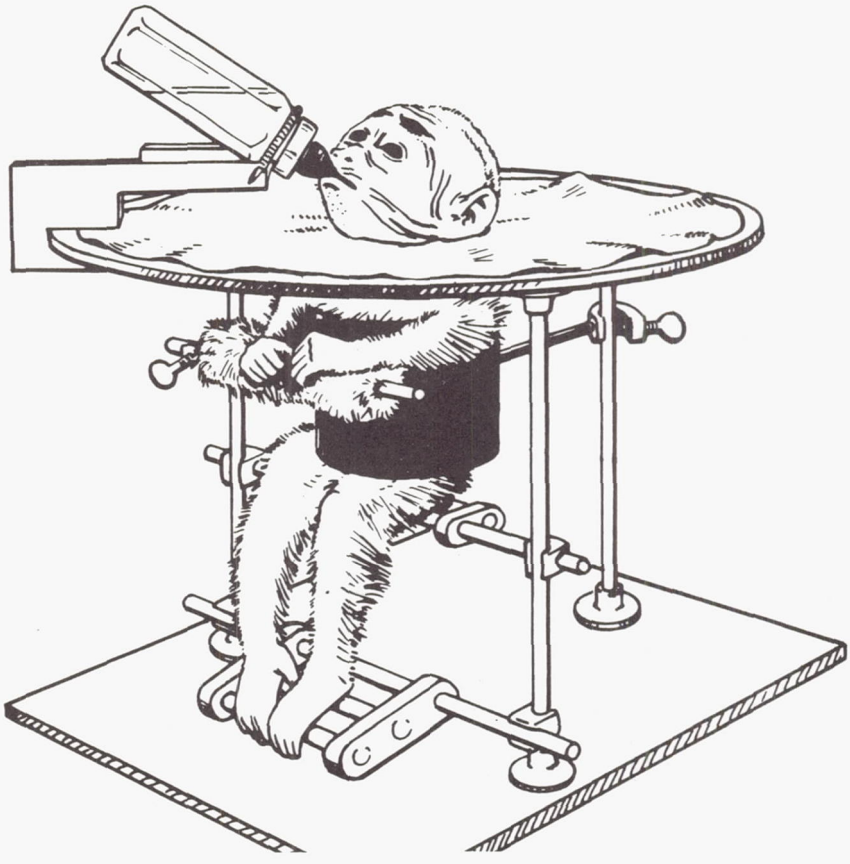


Figure 28.—**Visual-motor coordination studies on baby monkey deprived of seeing its own limbs.**

the forelimbs, but guided placing seems to require an integration of sensorimotor systems provided by prolonged viewing of the limbs. The investigators have developed a test that allows more precise assessment of visuomotor capability.

BIOSATELLITE PROGRAM

The successful aerial recovery of Biosatellite II after 2 days in space, and the delivery of the experiments to the bioscientists for analysis, culminated 4 years of intensive research and development in space biology.

The Biosatellites are Earth orbiting, and they contain biologic experiments (table II) to study the effects of space environment on living organisms: specifically, the effects of weightlessness, weightlessness combined with a known source of gamma radiation, and removal from the Earth's 24-hour periodicity. There are three missions, each with two flights: a 3-day mission (flights I and II), a 30-day mission (flights D and F), and a 21-day

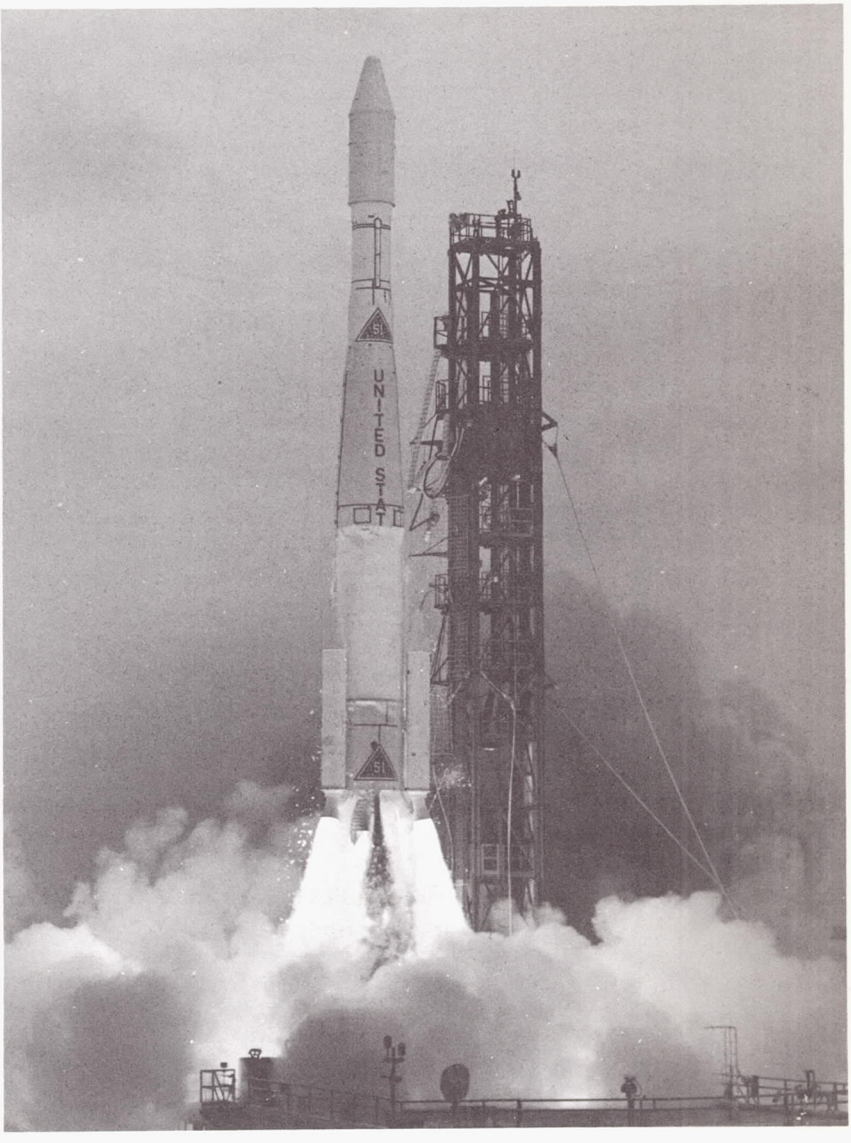


Figure 29.—**Two-stage, thrust-augmented, improved Delta used to orbit the Biosatellites.**

mission (flights C and E).* Both 3-day flights have been accomplished.

The Biosatellites are launched from Cape Kennedy by the two-stage, thrust-augmented, improved Delta (fig. 29) into a circular orbit of approxi-

*The 21-day Biosatellite mission has been cancelled as of the date of publication of this document. NASA, however, is investigating other ways of conducting the mission's experiments.

Table II.—*The Biosatellite II Experiments*

Experiment no.	Investigators	Institution	Experiment
P–1017	S. P. Johnson	North American Aviation	Weightlessness effects on the pepper plant.
	T. W. Tibbitts	University of Wisconsin	
P–1020	S. W. Gray	Emory University	Weightlessness effects on wheat-seed anatomy.
	B. F. Edwards		
P–1138	H. M. Conrad	Resources Planning & Control Corp	Weightlessness effects on wheat-seed biochemistry.
	S. P. Johnson	North American Aviation	
P–1096	C. J. Lyon	Dartmouth College	Weightlessness effects on wheat-seed physiology.
P–1035	R. W. Price	Colorado State University	Weightlessness effects on the ameba.
	D. E. Ekberg	General Electric Co.	
P–1047	R. S. Young	Ames Research Center	Weightlessness effects on the frog egg.
	J. W. Tremor		
P–1037	F. J. Deserres	Oak Ridge National Laboratory	Radiation-weightlessness effects on bread mold.
	B. B. Webber		
P–1039	J. V. Slater	University of California, Berkeley	Radiation-weightlessness effects on flour beetle.
	B. Buckhold		
P–1079	R. C. Von Borstel	Oak Ridge National Laboratory	Radiation-weightlessness effects on parasitic wasp.
	A. R. Whiting		
	R. H. Smith		
	R. L. Amy	Southwestern University, Memphis	
	D. S. Grosch	North Carolina State University, Raleigh	

P–1123	A. H. Sparrow	Brookhaven National Laboratory	Radiation-weightlessness effects on blue flower (spiderwort).
	L. A. Schairer		
P–1135	R. H. Mattoni	NUS Corp	Radiation-weightlessness effects on bacteria.
	E. C. Keller		
	W. T. Ebersold	University of California, Los Angeles	
	W. T. Romig		
	F. Eiserling		
P–1159	E. Altenburg*	Rice University	Radiation-weightlessness effects on vinegar gnat adults.
	L. Browning		
P–1160	I. I. Oster	Bowling Green State University	Radiation-weightlessness effects on vinegar gnat larvae.

*Deceased.

mately 200 kilometers altitude and 33.5° inclination from the Equator, which permits telemetry reception during each orbit at one of the five or more tracking stations assigned to a given flight.

The 3-day Biosatellites used bottled air; the 30-day and 21-day satellites will use a two-gas (80-percent nitrogen–20-percent oxygen) environment with a pressure of one atmosphere (sea level pressure). Temperature and humidity are very closely controlled to specifications. A major requirement is that accelerations during orbit should not exceed one ten-thousandth (10^{-4}) g and should maintain 10^{-5} g for 95 percent of the mission.

Three-Day Biosatellite Mission

Biosatellite I was launched from Cape Kennedy's Eastern Test Range on December 14, 1966, but, after 72 hours, failed to deorbit because of retrorocket malfunction and was not recovered. Although valuable engineering and spacecraft performance data were obtained by telemetry, and all experiment requirements were met on orbit, no scientific data were obtained.

Biosatellite II was launched on September 7, 1967, into an orbit of 176 nautical miles at apogee and 159 nautical miles at perigee. The target was a 170-nautical-mile circular orbit. All the experimental events planned during orbital flight occurred as scheduled.

The overall Biosatellite flight was a success during the 45 hours of space flight, but the weather satellite, ATS–I, indicated a severe storm in the recovery area on the recovery day, and Biosatellite II was commanded to reenter 1 day earlier than planned.

The Biosatellite II capsule was recovered near Hawaii in midair by a U.S. Air Force recovery plane at 3:25p.m., EDT, on September 9, 1967 (fig. 30). Three hours and 20 minutes later, the Air Force delivered the capsule to Hickam Air Force Base. Seven minutes later, it was disassembled in the air-conditioned laboratory complex and the experiments were turned over to the investigators (figs. 31 and 32).

Biosatellite II Experiments

Thirteen biological experiments were flown aboard Biosatellite II to study the effects of weightlessness and the effects of weightlessness combined with gamma radiation on fundamental biochemical processes in cells, the development and growth of plants and animals, the structure of living tissues, and changes in the transmission of hereditary characteristics.

The payload was divided into two groups. In the experiments concerned with the effects of the combination of weightlessness and radiation, bacteria, mold, insects, and plants were exposed to precise doses of gamma radiation from a strontium-85 source. The forward group of seven radiation experiments was mounted on a tungsten backscatter shield and each experiment was placed around the radiation source in a position to receive radiation dose levels from 200 to 5000 roentgens during the flight (fig. 33). The

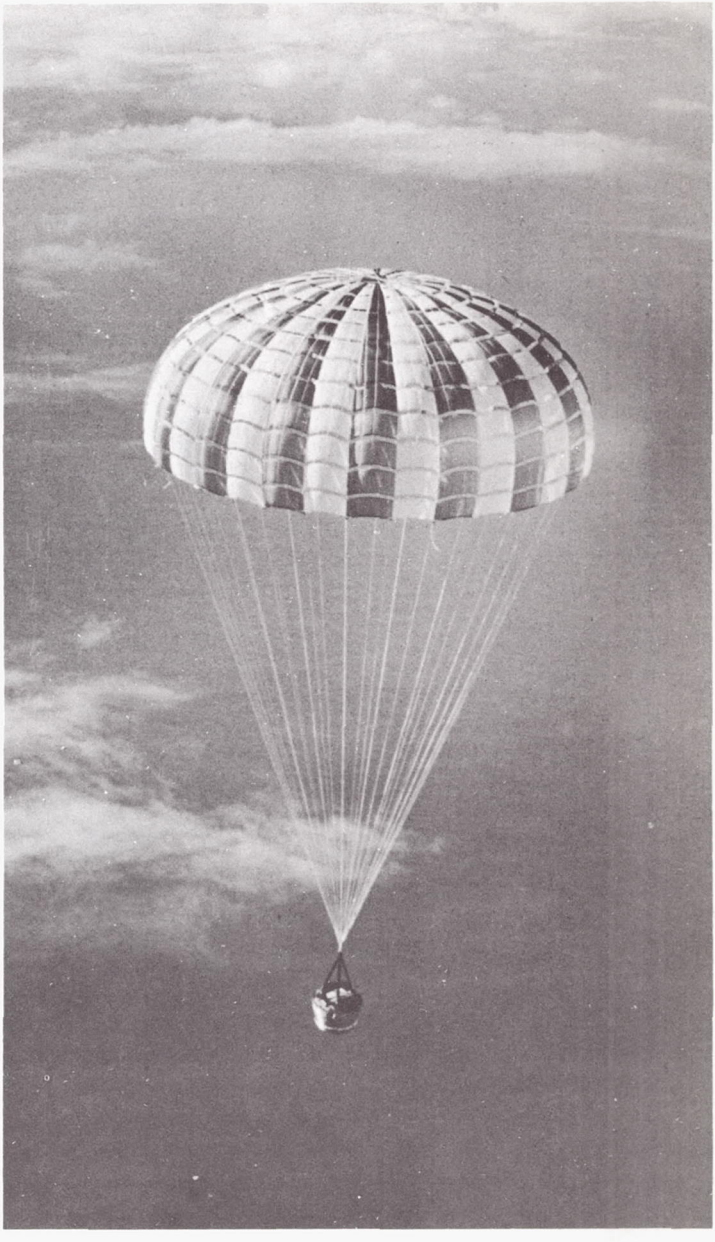


Figure 30.—Biosatellite II descends on its parachute just prior to recovery by a U.S. Air Force airplane at 3:25 p.m., EDT, September 9, 1967.

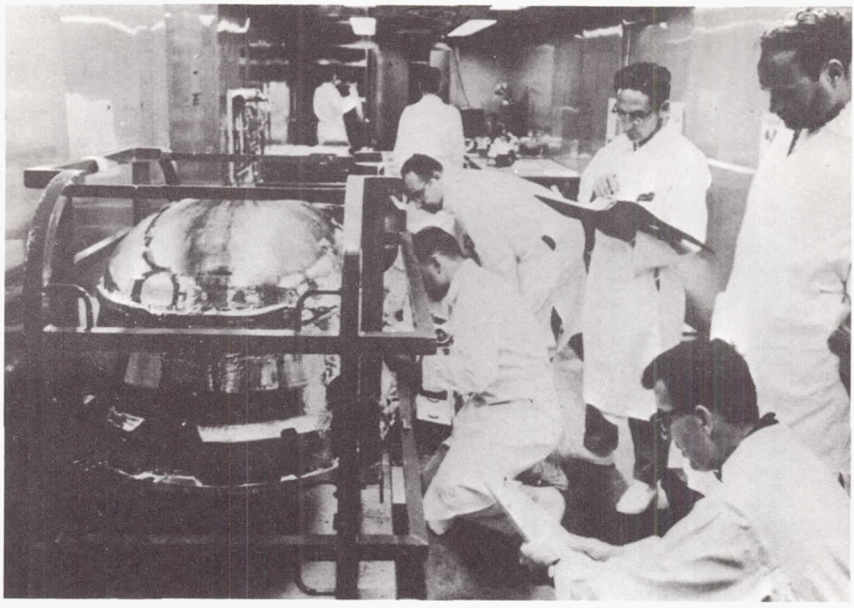


Figure 31.—Inspection of Biosatellite II capsule in Hawaii following recovery.

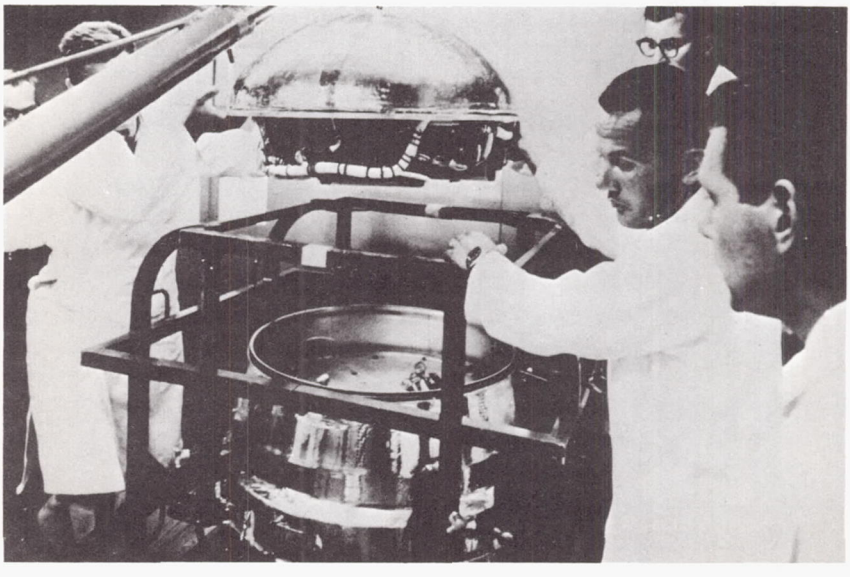


Figure 32.—Disassembly of Biosatellite II capsule in Hawaii following recovery.

radiation source was contained in a tungsten-nickel-copper sphere which, on command, was opened on orbit by a spring mechanism and closed, by command, prior to reentry. Experiments on the interaction of living systems with weightlessness involved wheat-seedling anatomy, biochemistry, and physiology; pepper-plant behavior; metabolic function of the ameba; and frog-egg development. The six weightlessness experiments and the nonirradiated weightlessness controls for the radiation experiments were in the back, or aft, section of the capsule, walled off from the forward radiation experiments. All 13 of the experiments were duplicated in laboratories on Earth during the flights. Two Earth controls for each experiment repeated all of the environments and events, except that of weightlessness.

Earth control experiments were simultaneously operative at Cape Kennedy and in the recovery area at Hickam Air Force Base. In addition, another group of control experiments was begun 4 hours after initiation of the flight. These experiments were continually adjusted for the 45 hours of orbital flight according to actual environmental control-system data as received, through telemetry, from Biosatellite II.

The capsule life-support system consisted of a high-pressure sphere containing normal air, delivered at Earth's atmospheric pressure of 14.7 psia. The temperature was maintained at an average of 68° F during the flight, while the relative humidity averaged 59 percent. Temperatures and humid-

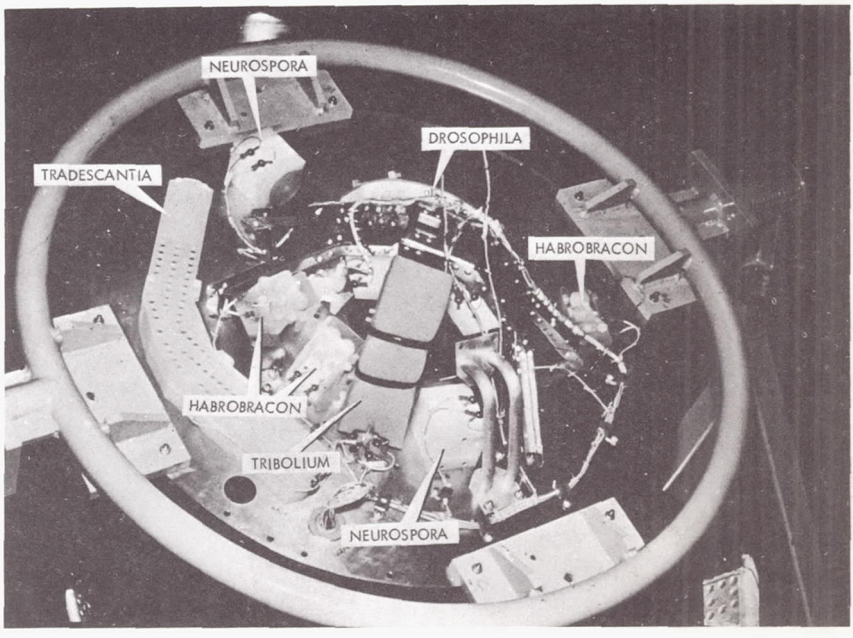


Figure 33.—Biosatellite experiments payload assembly located around radiation source.

ity in individual experiment packages such as those of the wheat seed and flour beetle (85° F) were consistent with specifications.

Fifty days after recovery of Biosatellite II, all the experimenters reported their experiments had produced valuable data and results. The greatest effects of weightlessness were seen in young and actively growing cells and tissues. Rapidly dividing cells with high metabolic activity were more affected than were mature cells which divided more slowly. These effects were modified in some organisms by irradiation during weightlessness.

In the weightless environment of the orbiting Biosatellite II, the radiation effects observed depended on the nature of the organism. In some cases the effects of radiation combined with weightlessness were greater than those observed in Earth-based controls; in other cases, the effects were less.

The effects studied by the experimenters included cell division and differentiation, development and growth, chromosome damage and chromosome mechanics, genetic mutations, and biochemical regulation of cell nutrition and metabolism. The preliminary observations in each experiment are presented below.

Pepper Plant—*Capsicum annuum*

Films were taken of pepper plants in the satellite and also of control pepper plants on Earth. Some controls were growing erect to gravity, and some were on a clinostat. (The clinostat is a mechanical device which rotates plants horizontally with respect to Earth, thereby nullifying the effects of Earth's gravitational field.) Three frames from each film are shown in figure 34. A visual comparison shows that curvature (epinasty) of the pepper-plant leaves and stems in response to weightlessness is similar to that of the plants on the rotating clinostat.

A frame-by-frame comparison of each film (each contained 265 frames) showed that the flight plants were more immobile than those on the clinostat in that the experimental group showed less leaf movement. There was a delay of approximately 3 hours in initiation of leaf curvature in the flight plants. Final results on biochemical and physiologic changes are being subjected to statistical treatment and computer analysis.

Wheat-Seedling Anatomy—*Triticum vulgare*

Structural changes occurred in the developing wheat seed as a result of weightlessness. The coleoptiles, or shoots, of the flight seedlings are 14 percent taller than those of erect Earth-control seedlings. The ratio of the shoot height to total root length is shifted so that flight seedlings have coleoptiles longer in proportion to their roots than do erect Earth-control seedlings. Where specific growth patterns of the flight seedlings differed from those of ground-control seedlings, it was usually the result of accelerated, rather than retarded, growth in the plants recovered from orbit.

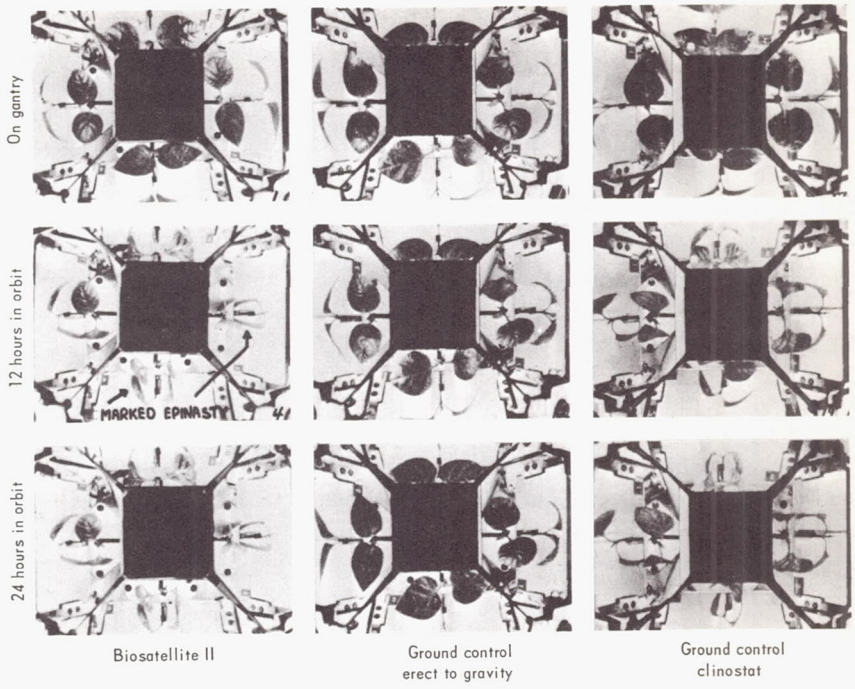


Figure 34.—**Effect of weightlessness on pepper plant.**

The flight seedlings showed a distribution of plastids (specialized structures in the cell, such as starch granules) very different from that of the erect Earth controls, and similar to that of the Earth clinostat controls (fig. 35).

Wheat-Seedling Physiology

Wheat seeds germinated well, and healthy plants with normal seedling organs developed under conditions of weightlessness. As shown in figure 36, the orientation of the flight seedling roots was unlike that of seedlings grown erect to gravity on Earth. The roots of the orbiting plants curved upward toward the shoots and out to the side. Such displacement from normal positions of roots and shoots was expected.

The good germination (approximately 96 percent) of the seeds and the growth of healthy seedlings is a significant point in the results of the Biosatellite II experiment. The absence of a gravitational force on the contents of the embryonic cells does not seem to disrupt the principal physiologic processes which provide energy and materials for the growth of seedling tissues.

333-240 O—69——8

Wheat-Seedling Biochemistry

Preliminary results indicate that less scutella tissue (the site of rapid cell division) was formed during weightlessness than when grown on a horizontal clinostat or in the stationary vertical conditions of Earth.

The results of enzyme studies performed to date indicate a possible alteration in carbohydrate metabolism in the shoots grown in space (fig. 37). Both the aerobic and anaerobic pathways of sugar utilization appear to be affected as indicated through the analysis of the activities of the key enzymes, glyceraldehyde-3-phosphate dehydrogenase and glucose-6-phosphate dehydrogenase as well as peroxidase. It appears that tissues grown in space exhibit greater activities of these enzymes than do their corresponding Earth-based controls.

Ameba—*Pelomyxa carolinensis*

This experiment was designed to determine the effects of weightlessness on nutrition, nuclear division, and growth of both starved and fed amebas. Growth-rate data indicate little difference between the flight organisms and the Earth controls. The organisms starved during the flight appear to have divided less frequently than those fed during the flight. Initial study

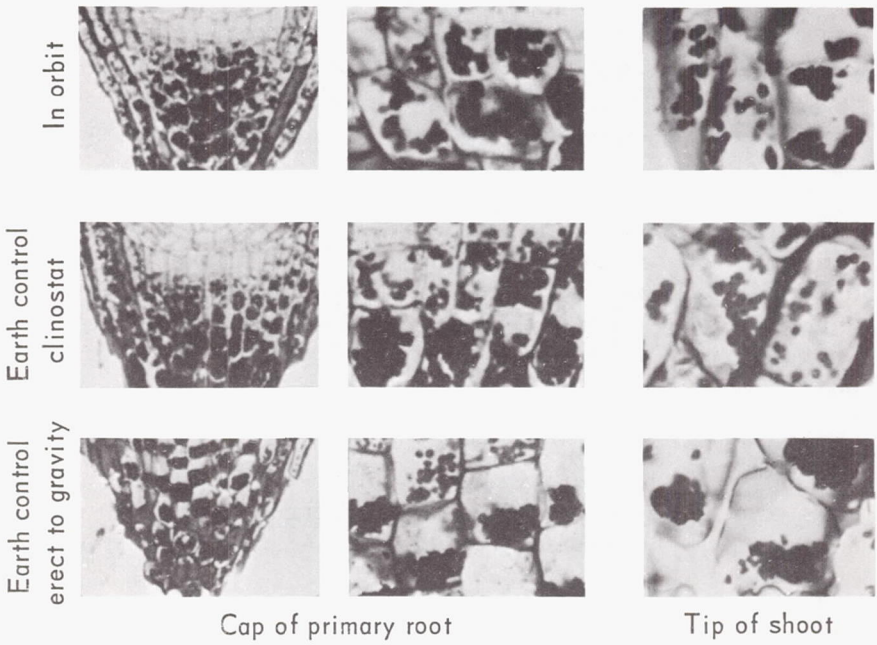


Figure 35.—Effect of weightlessness on wheat seedling: particle distribution in cells.

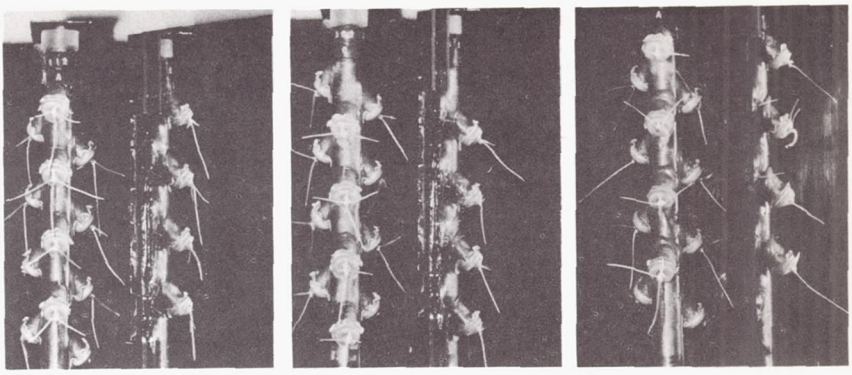


Figure 36.—Effect of weightlessness on developing wheat seeds. (*a*) Ground control normal. (*b*) Ground control clinostat. (*c*) Biosatellite II, after 45 hours on orbit.

of the data on food vacuole formation (fig. 38) indicates a significant difference between flight and Earth-control experiments.

Frog Eggs—*Rana pipiens*

This experiment was carried out to determine whether weightlessness would affect the ability of the fertilized frog egg to divide, differentiate, and develop normally. The basis for the hypothesis is that this gravity-sensitive embryonic system has long been known to respond to disorientation with respect to the force of gravity.

Unfortunately, the 3-hour hold beyond planned launch time was sufficient to allow, on the pad, the beginning of cell cleavage, the experimentally proved gravity-sensitive phase of development immediately following fertilization. Nevertheless, the Biosatellite II flight did permit a valid study on the normality and rate of development of the frog egg from first-cell cleavage through neural fold stages.

Figure 39 indicates no significant difference between rates of development in space compared to Earth controls.

Orange Bread Mold—*Neurospora crassa*

No differences have been found between the flight and Earth-control organisms with regard to the radiation-dose-effect curves for either survival or the overall forward-mutation frequencies. Assays to characterize the specific locus mutants (fig. 40) are in progress.

Flour Beetle—*Tribolium confusum*

Young pupae irradiated with X-rays or gamma rays (1500 roentgens) develop into adults having a wing abnormality of a median wing-cover

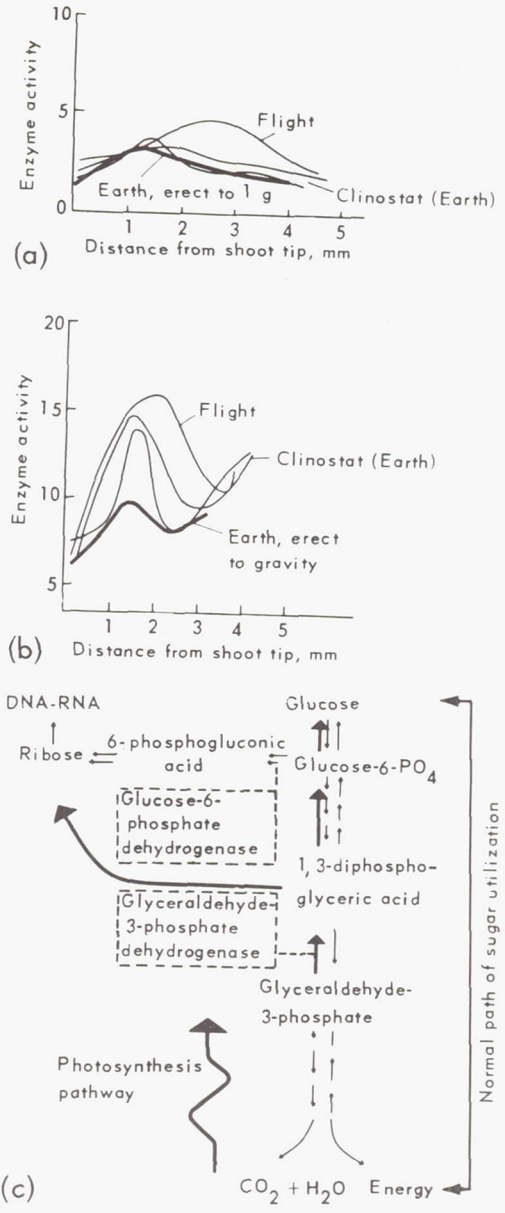


Figure 37.—Effect of weightlessness on wheat seedling: biochemical changes. (*a*) Glyceraldehyde-3-phosphate dehydrogenase activity in coleoptile. (*b*) Glucose-6-phosphate dehydrogenase activity in coleoptile. (*c*) Biochemical adaptation due to weightlessness or accumulation of photosynthesis enzymes in the absence of light.

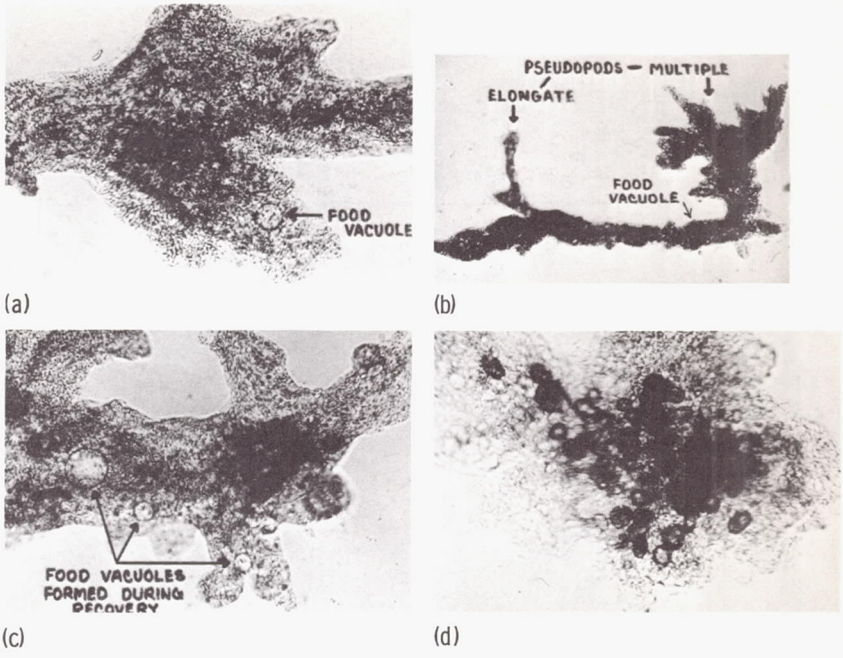


Figure 38.—Effect of weightlessness on the ameba. (*a*) Nonstarved Earth control. (*b*) Starved flight ameba. (*c*) Nonstarved flight ameba. (*d*) Ameba fixed in flight after 24 hours.

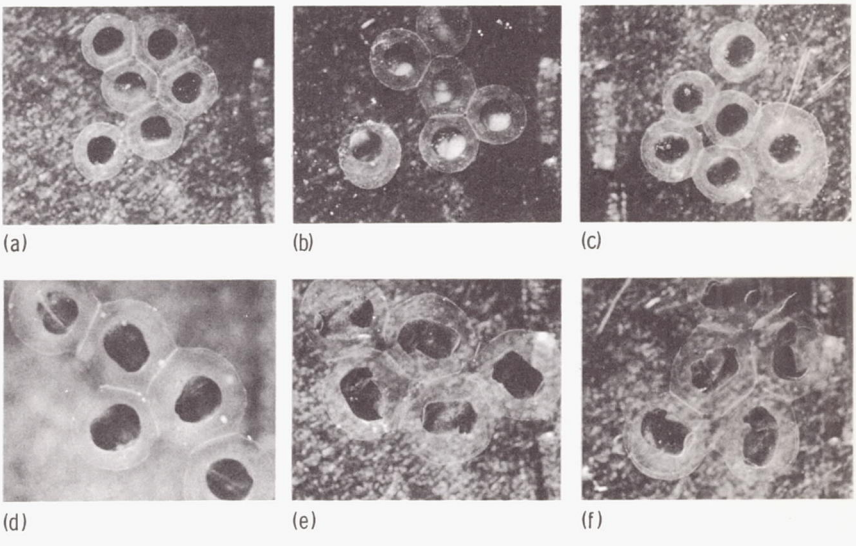
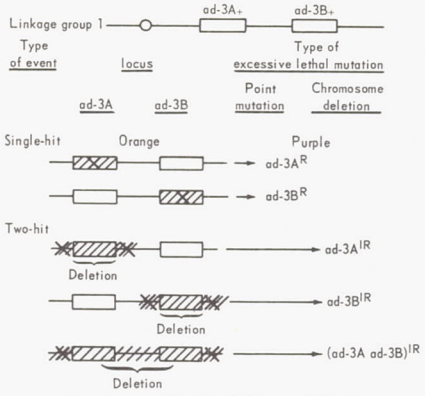
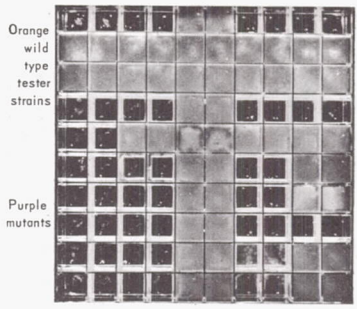


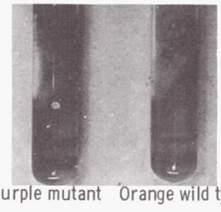
Figure 39.—Effect of weightlessness on developing frog egg. (*a*) Fixed at T−57 seconds, on pad. (*b*) Fixed at T+2 hours, on orbit. (*c*) Fixed at T+3 hours, on orbit. (*d*) Alive at T+51 hours, recovery. (*e*) Flight alive, on Earth. (*f*) Earth control.



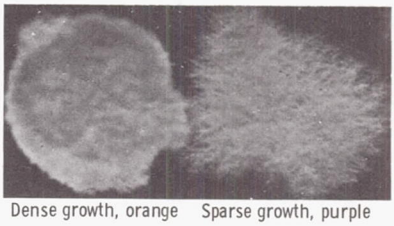
Events resulting in lethal mutations giving rise to purple mutants



Characterization of mutants



Purple mutant Orange wild type



Dense growth, orange Sparse growth, purple

Figure 40.—**Effect of weightlessness and radiation on *Neurospora.***

(angle at the base of the wing) split, wing-cover blistering, and protrusion of the underlying membranous wings (fig. 41).

Seven hundred and twenty pupae, between 17 and 27 hours old, were orbited in Biosatellite II, half in the presence of the strontium-85 gamma-radiation source and half shielded from it. Two-thirds of the pupae in each section of the Biosatellite II capsule had been preirradiated on Earth prior to flight with 1350 roentgens of 180-keV X-rays to bring them to a highly sensitive stage. In flight, pupae in the forward section received an additional 100 roentgens of gamma radiation.

A significant difference occurred in that 44.8 percent of the pupae irradiated in flight developed into adults with wing abnormalities compared with the flight nonirradiated (30 percent) and the Earth-control irradiated adults with 29.9 percent abnormalities. Figure 42 illustrates a normal pupa, a normal adult, and wing abnormalities in adults developed from pupae irradiated in flight.

There is an increase in dominant lethality in the offspring of females irradiated in space: 78 ± 6 percent for flight versus 27 ± 5 percent for Earth controls. There were no significant differences between the flight nonirradiated and the Earth-control organisms.

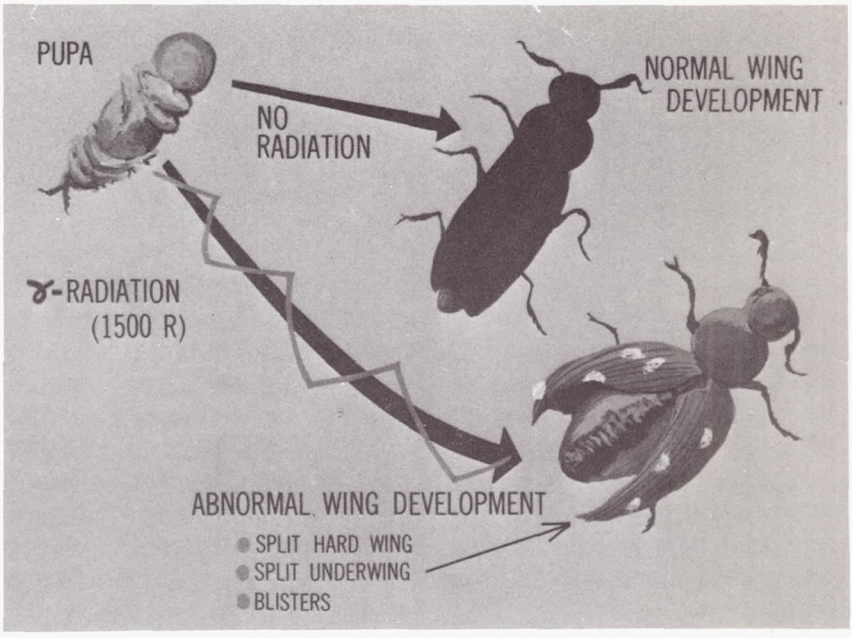


Figure 41.—Effect of weightlessness and radiation on *Tribolium* (flour beetle). Irradiation of ground control produced 30 percent abnormality, weightlessness alone caused 30 percent abnormality, and radiation and weightlessness combined produced 45 percent abnormality.

Parasitic Wasp—*Habrobracon junglandis*

No significant difference from Earth controls was found in spontaneous recessive lethal mutation frequencies in the female offspring of normal females mated to normal males during weightlessness in Biosatellite II.

The hatchability of eggs laid in Biosatellite II and irradiated during metaphase I (very sensitive stage of cell division) shows that a marked sensitivity difference exists between those irradiated in flight and the irradiated Earth controls. Earth-control eggs exposed to 2000 roentgens showed 0 percent hatchability compared to 95 percent hatchability in nonirradiated Earth controls. Preirradiated flight eggs showed 75 percent hatchability, indicating that there must have been recovery from radiation damage during the flight due to some protective mechanism operative during metaphase I.

Figure 43 shows that egg production during exposure to the combination of radiation and weightlessness is greater than it is for irradiated and nonirradiated Earth controls. Figure 44 illustrates some of the somatic defects or abnormalities in the offspring males exposed to the combination of radiation and weightlessness in Biosatellite II.

Blue-Flowering Spiderwort—*Tradescantia sp.* (Clone 02)

The condition of the flower cuttings was good at recovery but did show some bud blasting 6 days later. The bud blasting was more severe in the flight material than in the Earth controls. The loss of buds is reflected in the flower production and in the loss of early mutation data for the flight material.

Scoring is underway for the frequencies of somatic mutations and various abnormalities in stamen hairs. Without irradiation the Earth and flight samples had a consistently low mutation rate; that is, from blue to pink and blue to colorless cell mutations (fig. 45). The Earth flight radiation treatments exhibited the expected mutation response with a suggestion of a delayed and slightly higher mutation rate in the Earth-irradiated controls. This difference is probably not significant. The occurrence of colorless

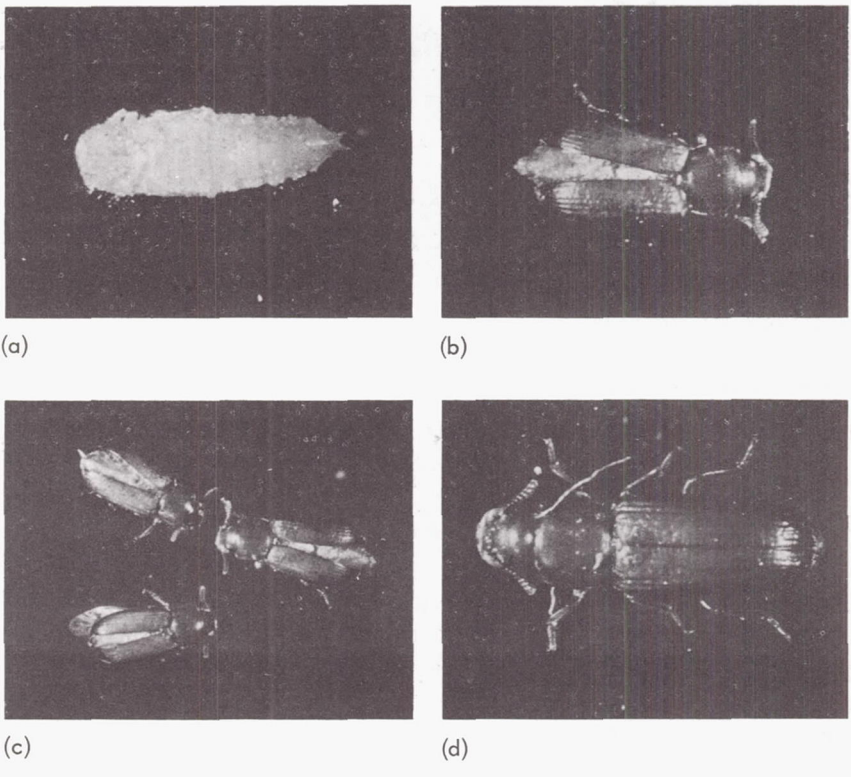


Figure 42.—Effect of weightlessness and radiation on *Tribolium.* (*a*) Preirradiated pupa flown in Biosatellite II. (*b*) Adult with split wing from Biosatellite irradiated pupa. (*c*) Split wings and protrusion of membranous wing. (*d*) Normal Earth control adult.

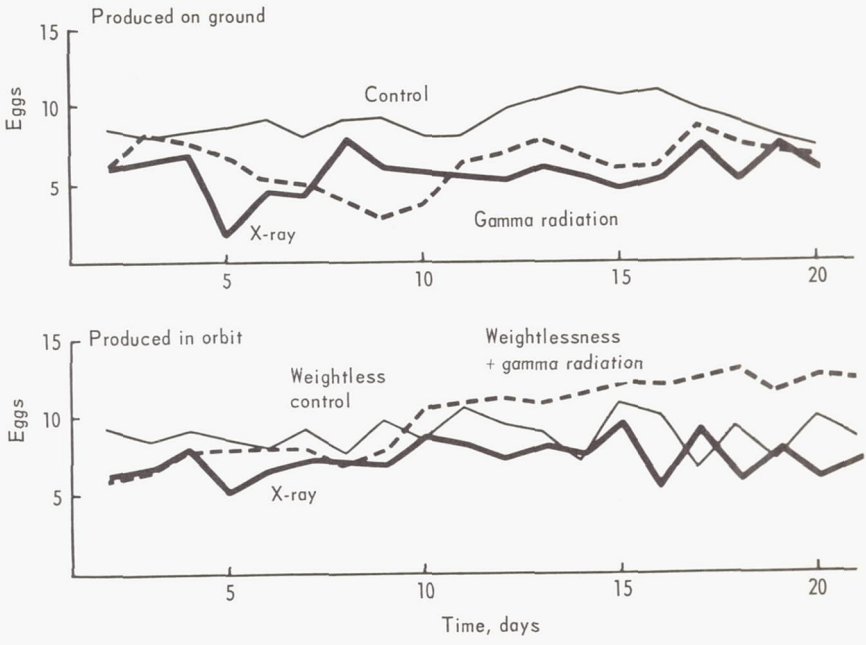


***Figure 43.*—Effect of weightlessness and radiation on egg production in *Habrobracon.* (Note increased egg production due to antagonism of radiation by weightlessness.)**

mutations appears to be nearly the same for both flight and Earth samples. Stamen scoring for irregular and bent cells, giant and dwarf cell formation, and loss of reproductive integrity is still in process.

Lysogenic Bacteria—*Escherichia coli* and *Salmonella typhimurium*

Preliminary results of the effect of space environmental factors on lysogenic bacteria (fig. 46) indicate definite effects on bacterial growth and virus formation. In the strains of *Escherichia coli* and *Salmonella typhimurium* used, there was an increase in cell number during weightlessness without radiation as compared with Earth controls (fig. 47). In the *E. coli* there was an increased cell number with increasing radiation during space flight compared to a decreasing number of cells with increasing radiation in the Earth controls. In the *S. typhimurium* there was a decrease in cell number with increasing radiation, both in space-flight samples and in Earth controls, but with high and parallel numbers in the population grown in the space environment.

Adult Vinegar Gnats—*Drosophila melanogaster*

Among the flies hatching during the first 5 days from the eggs laid in space by the irradiated, inseminated females, there were a number of flies (44

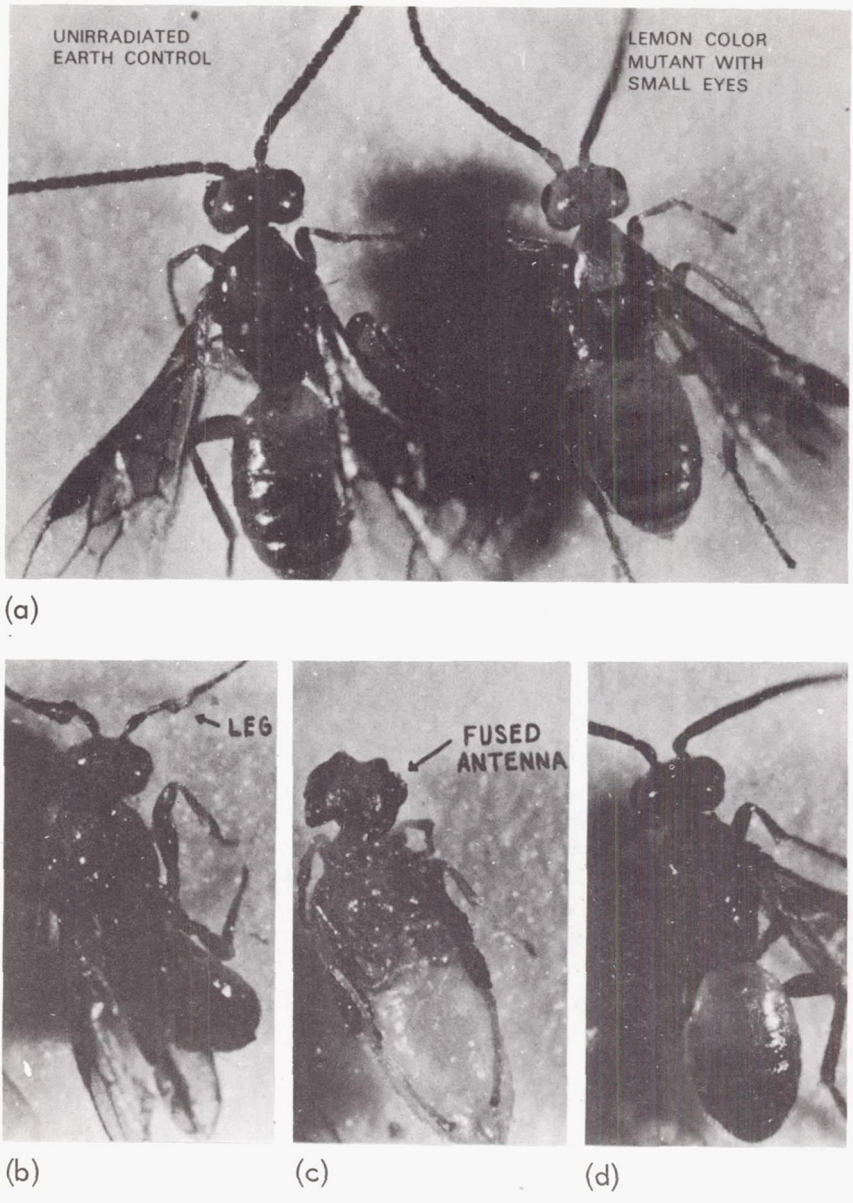


Figure 44.—Effect of weightlessness and radiation on *Habrobracon.* (*a*) Second-generation male offspring of flight-irradiated males—609 roentgens. (*b*) Antennopedial mutant legs instead of antenna—609 roentgens. (*c*) Pupal lethal mutant—523 roentgens. (*d*) Black color body—1200 roentgens.

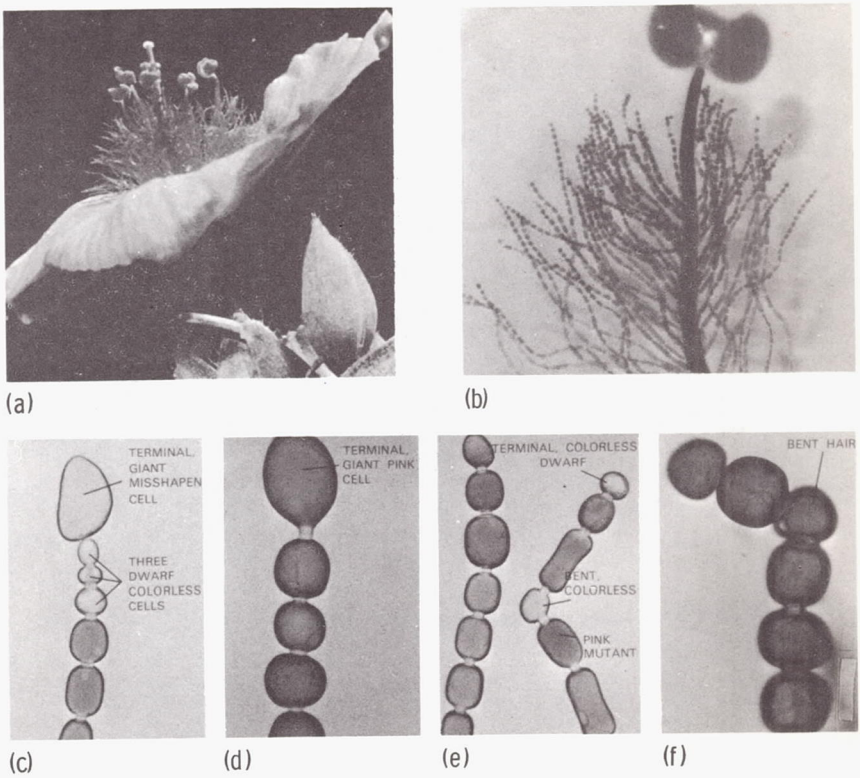


Figure 45.—Effect of weightlessness and radiation on *Tradescantia.* (*a*) Pinkish coloration in normally blue flower. (*b*) Stamen hairs. (*c*) Multiple mutant in single stamen hair. (*d*) Single mutant. (*e*) Multiple mutant. (*f*) Single mutant.

in 943, or 4.7±0.7 percent) with a deformed thorax and a missing wing on the same side of the body. In the irradiated Earth controls, 33 of 983, or 3.4±0.6 percent, of the eggs hatched into abnormal flies (fig. 48). The difference is not considered significant. This abnormality occurs rarely in nonirradiated populations (1 in 10 000).

The offspring of males irradiated on Earth and then mated in flight with nonirradiated females showed a mutation rate (losses of fragments of the Y or male sex chromosome) of 5.7±1.0 percent, while those of the Earth controls showed a rate of 2.9±0.9 percent. This is considered a significant effect.

Vinegar Gnat Larvae—*Drosophila melanogaster*

Adults from irradiated (1500 to 3500 roentgens) *Drosophila* larvae develop into weak individuals with a decreased lifespan. Such premature aging may have a genetic basis because males are affected by radiation more than females.

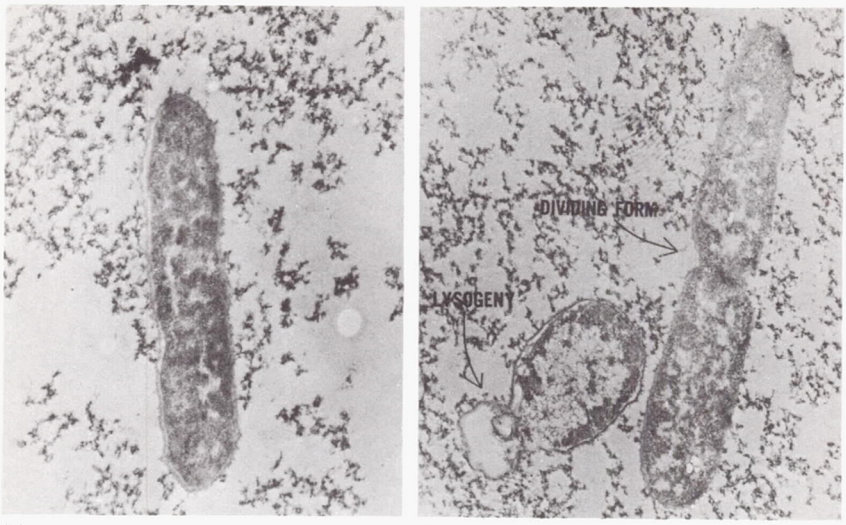


Figure 46.—Lysogenic bacteria, *Salmonella typhimurium.* (*a*) Non-irradiated normal nucleus. (*b*) Irradiated.

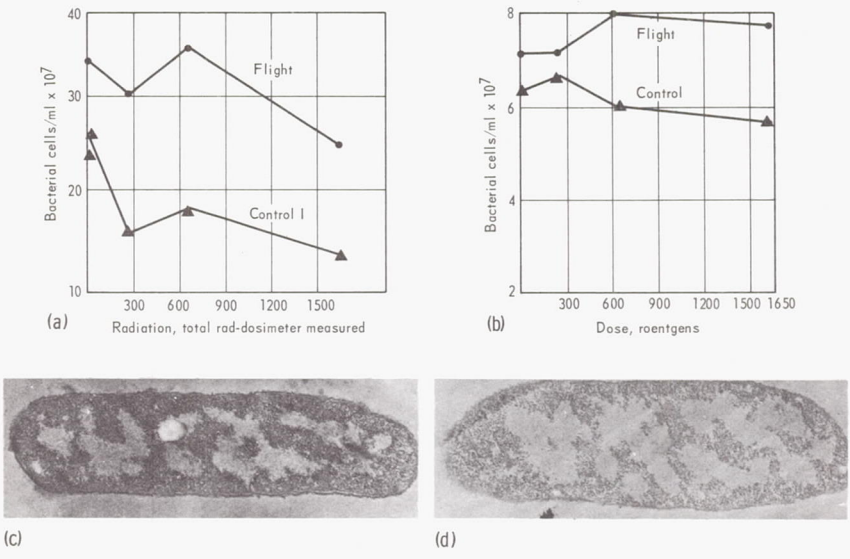


Figure 47.—Effect of weightlessness and radiation on bacteria. (*a*) Growth of *Salmonella typhimurium.* (*b*) Growth of *Escherichia coli.* Note no significant structural differences between (*c*) flight *E. coli* and (*d*) Earth control *E. coli.*

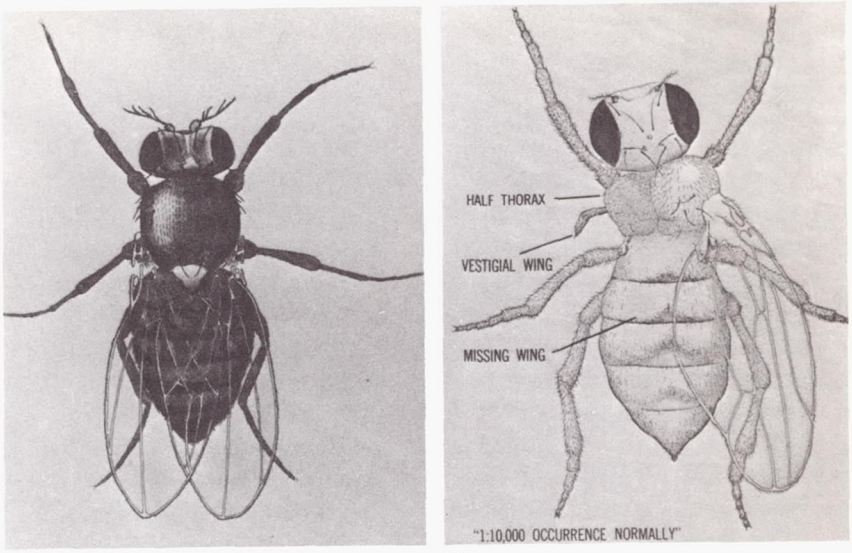


Figure 48.—**Effect of weightlessness and radiation on *Drosophila*. (*a*) Adult from normal egg (ground). (*b*) Adult from egg laid in Biosatellite II. There was 50 percent more abnormality in Biosatellite eggs.**

In *Drosophila* larvae on Biosatellite II, in both the forward and back sections, abnormal chromosome pairing occurred, presumably a result of improper chromosome separation. This has never been seen before by the experimenter, who believes genetic characteristics will thus be transmitted differently, as by two Y chromosomes in the daughter cell (fig. 49). Some cells exhibited missing or extra chromosomes such as would result from nondisjunction or improper separation. These differences were observed only in the flight specimens.

Numerous chromosome breaks occurred in flight-irradiated larvae compared to only some in the flight nonirradiated larvae. These observations were significantly different from the Earth controls.

Summary

The preliminary findings of the Biosatellite II experiments are summarized in table III.

As anticipated from Earth-based clinostat data during the past 100 years, plants are sensitive to changes in gravity. The Biosatellite II plant experiments exhibited dramatic changes in orientation in the space environment.

In the radiation-weightlessness experiments there are indications of null, increased, and decreased effects, as compared to the effects of either radia-

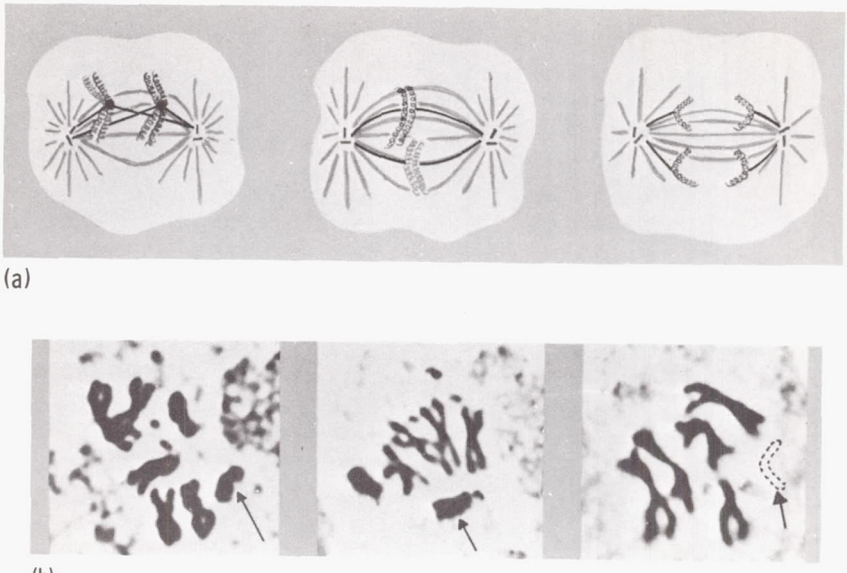


Figure 49.—**Weightlessness and cell division. (*a*) Normal chromosome pairing and separation at 1 g. (*b*) Improper chromosome separation as a result of weightlessness showing (left to right) extra Y-chromosome, extra fourth chromosome, and missing Y-chromosome.**

tion or weightlessness individually. In flour beetles, these two forces worked together to produce a greater effect than either one produced alone. Similar actions occurred in the production of virus, defects in males hatched from flight-laid eggs by parasitic wasps, and in chromosome abnormalities in vinegar gnat larvae.

Modification or reduction of radiation damage by weightlessness is assumed in the experiments concerned with the spiderwort plant, the growth of bacteria, and egg production in the wasps.

It will be some time before the implications of the Biosatellite II results will be fully understood, and their impact on our fundamental knowledge of biologic processes or on the biologic effects of the space environment are assessed. However, the largely unexpected nature of the results themselves makes it clear at this time that further bioscience experimentation in space will be both necessary and fruitful.

Biosatellite Primate Mission (30 Days)

The pigtailed monkey, *Macaca nemestrina,* will be instrumented to detect changes in the central nervous system (decisionmaking and performance, alertness, fatigue, and sleep-wakefulness); the cardiovascular system (heart activity, blood pressure, and circulatory dynamics); and general metabolism

Table III.—*Summary of Preliminary Results of Biosatellite II Experiments (Oct. 30, 1967)*

Experiment	Environment	Reaction	Preliminary observations
Pepper plant—*Capsicum annuum*	W	Positive	Disorientation (marked bending) of leaves and stems.
Wheat-seed anatomy	W	Positive	Increased shoot growth; symmetric distribution of cell particles (plastids).
Wheat-seed biochemistry	W	Positive	Increased activity of enzymes for sugar synthesis.
Wheat-seed physiology	W	Positive	Disorientation (upward and to the side) of roots.
Frog egg—*Rana pipiens*	W	Negative [a]	No difference in development from first-cell cleavage.
Ameba—*Pelomyxa carolinesis*	W	Positive	Less cell division; slightly lower growth rate; increased feeding in flight.
Orange bread mold—*Neurospora*	W+R	Indeterminate	No immediate differences in survival and spore development.
Spiderwort—*Tradescantia*	W+R	Indeterminate	Lower mutation in flight and Earth-nonirradiated flower buds.
Vinegar gnat adults—*Drosophila*	W+R	Positive	Deformities in chest wall and absence of wings more frequent in flight; male infertility.
Vinegar gnat larvae—*Drosophila*	W+R	Positive	Improper chromosome separation; missing and extra chromosomes; increased chromosome breaks.
Flour beetle—*Tribolium*	W+R	Positive	Wing deformities; decreased egg production.
Bacteria—*E. coli* and *Salmonella*	W+R	Positive	Increased growth; increased virus production.
Wasps—*Habrobracon*	W+R	Positive	Greater egg production; body deformities in second-generation males.

W = Weightlessness.

W+R = Weightlessness and radiation.

[a] Gravity-sensitive cell-development stage between fertilization and first-cell cleavage was under 1-g influence and did not experience weightlessness due to launch delay.

(dietary utilization, energy, and biochemical changes in tissue, such as muscle, bone, and kidney).

During the flights, planned in the second and fourth quarters of 1969, the monkeys will be comfortably restrained in a special couch. Experiment instrumentation is designed to enable the scientists to monitor central-nervous-system function by surface and deeply implanted electrodes in specific areas of the brain. Performance, behavior, and decisionmaking will be measured by a variety of these special-purpose devices, providing a combination of preprogramed visual-motor coordination and visual-discrimination tasks. Each time the monkey accomplishes a task satisfactorily, he is rewarded with a pellet of food. Implanted sensors are used to measure blood pressure and respiratory rate for correlation with the central-nervous-system data. The instrumented monkey has been maintained in the spacecraft for an integrated primate spacecraft development test at the University of California, Los Angeles.

Unique instrumentation will permit "wet" chemical analysis of the monkey's urine every 6 hours on orbit. This automatic urine analyzer, developed by the Jet Propulsion Laboratory, California Institute of Technology, will measure the urinary excretion of creatine, creatinine, and calcium by the primate. Reliable estimates will thus be obtained of the animal's general metabolism, especially muscle, bone, kidney, heart, and, perhaps, stress responses. The urine analyzer is contained in a volume of 330 cubic inches, weighs about 13 pounds, and has a potential application to manned missions.

A major accomplishment of the 30-day Biosatellite project is the development of a gas-management system for a two-gas atmosphere. This will be the first time that such a system will be flown in a U.S. satellite. The spacecraft for the 30-day Biosatellites, flights D and F, are now being fabricated and assembled. The developmental model, including the fuel cell, has passed a complete subsystem test.

Biosatellite Advanced Experimental Biology Mission (21 Days)

The 21-day mission, Biosatellites C and E, will contain general biology experiments to determine the effects of weightlessness on development, structure, and function of plants, and its effect on growth of isolated human liver cells in tissue culture. Rats will be used to study changes in composition and function of vital body organs and systems. Circadian (near 24-hour) rhythms will be studied primarily by changes in body temperature, body activity, and food consumption. Eight rats will be housed in individual chambers arranged in a cylindrical pattern around a central life-support system, which includes the food supply, waste disposal, and air-circulation equipment.

The effects of weightlessness will be determined on the development and function of the *Arabidopsis* plant (with a 21-day life cycle). The growth of

liver cells will be recorded on 16-millimeter film by time-lapse photography for postflight analysis.

The 21-day Biosatellite will use many components common to the 30-day craft (such as the fuel cells and tanks) and development of these components is proceeding in accordance with the 30-day mission schedule.

The 21-day developmental test, conducted in a spacecraft mockup, has been completed. Interface definition and studies applicable to the integration of the experiment modules with the spacecraft are underway. Problems need to be resolved concerning the control of temperature and lighting for *Arabidopsis* and the food-dispensing system for the rats. The fabrication of flight hardware for the 21-day Biosatellite is scheduled for 1969 with flights planned in calendar years 1970 and 1971.

Summary

The biology experiments in the Biosatellite program are carefully designed and have required several years of development. They are substantiated by an accumulation of considerable baseline data obtained in prior years. Such data are still being compiled for postflight ground-control tests.

The Biosatellite investigations provide opportunities for controlled, quantitative testing of hypotheses concerning genetics, physiology, and biochemical regulation of cellular and body activities. Information obtained should be of exceptional value in solving problems associated with prolonged space flights. The experiments will be important in advancing knowledge of basic biology. Some of the theoretical and technical sequelae can be expected to contribute to solving many biologic and medical problems unrelated to space flight.

PHYSICAL BIOLOGY

Comparative Physiology

Living systems exhibit various periodic rhythms (biological clocks) that are persistent throughout their lifetimes. The extent and nature of these rhythms are poorly understood despite an upsurge in research deriving from their importance for manned space flight and the possible deleterious consequences of their disruption. Because organisms placed in Earth orbit have exhibited some abnormal responses during and after flight, clarification of the long-term effects of biorhythmic interruption has become a necessity, especially in anticipation of longer missions in space by man.

Studies of the physical-chemical dynamics of various physiological systems in man and other mammals by Iberall and Cardon (ref. 90) have demonstrated not only biological rhythms but also that living systems exhibit smaller and more subtle cyclic oscillations—apparently a function of biological regulatory processes. Intermittent operation of this type is seen in many vital functions, such as heartbeat, respiration, temperature regulation, blood

333-240 O—69——9

flow, water balance, weight control, and behavioral responses, as well as in the nervous system and in the outpouring of the endocrine system. It is highly likely that all life processes are a combination of rhythms, pulses, beats, and oscillations occurring within specific time domains, and varying in response to different stimuli.

Bioinstrumentation

Progress in instrumentation has preceded nearly every advance in the knowledge and techniques of the life sciences. Instrumentation allows the life scientist and technician to increase and extend his technical abilities to observe and measure all levels of biological phenomena. The bioinstrumentation program seeks optimum utilization of instrumentation, as well as new and modified devices and techniques for measuring and analyzing the broad array of biological and behavioral phenomena.

A prime need in space biology is more sophisticated biotelemetry for experimentation in space, under diverse conditions, and in strange environments. Equally important are the acquisition, analysis, and storage of data resulting from space biology endeavors. However, one large obstacle to using biological instrumentation has been poor communication between the biological scientists and the physicist-engineer. This obstacle stems from lack of interdisciplinary understanding regarding vocabularies and basic knowledge. The result is inhibition of the full impact of present instrumentation developments in the life sciences.

The Bio-Instrumentation Advisory Council (BIAC) of the American Institute of Biological Sciences, supported by NASA, seeks to remedy these problems. To achieve this end, it has the following functions: to facilitate directed information flow between biological and physical scientists when appropriate in the interest of improving experimental biology; to evaluate the current status of the application of the physical sciences to biological problems and to initiate and support the extension and/or development of widely applicable new techniques; and to prepare surveys and/or summaries of the contemporary status of instrumentation for biologists.

During 1967, BIAC has communicated directly with over 180 individual biologists and aided them in the solution of problems in bioinstrumentation. It reported on specific instrumentation, pertinent techniques, or on the state of the art in a particular area of instrumentation to satisfy about 2000 requests (the mailing list for this service has increased from 260 at the end of 1966, to over 2000 for 1967). BIAC evaluated bioscience proposals involving instrumentation and sent a team of troubleshooters to solve a problem arising during the integration of experiments on the Biosatellite.

Biotelemetric instrument development for use in space flight has resulted in remarkably stable, accurate, long-lived implantable telemetric devices for recording temperature changes indicative of cyclic (circadian) biological

clock phenomena. Such devices have been applied to the design of Biosatellite experiments and by NASA-supported researchers studying biological rhythms. Work by Goodman (ref. 91) is continuing on development of low-cost multichannel implantable transmitting devices capable of efficient operation over a long period of time (perhaps 2 years), weighing no more than 3.5 grams, and not exceeding 2 cubic centimeters in volume. This type of sensor detects temperature changes of 1° C per minute from two different areas or two different organs of the body (fig. 50).

Another telemetric device being developed is a sterile, thermal, deep-brain probe for mammals. This probe (fig. 51) is a sensor with a maximum diameter of 1.0 millimeter. It is attached to the skull and is capable of sensing temperatures in various areas of the brain over a range of 18° to 40° C.

Biophysics and Theoretical Biology

In order to understand that which could be found on another planet (and to know its stage of evolution), it is vital to have an understanding of the origin, evolution, and mechanisms of living cells on Earth. Both biophysics and theoretical biology are intimately concerned with the search for extraterrestrial life. Knowledge attained concerning cellular physiology and behavior, origin of life, and evolutionary phenomena can be extended to predict whether life can be found (and indicate what should be searched for) on other planets.

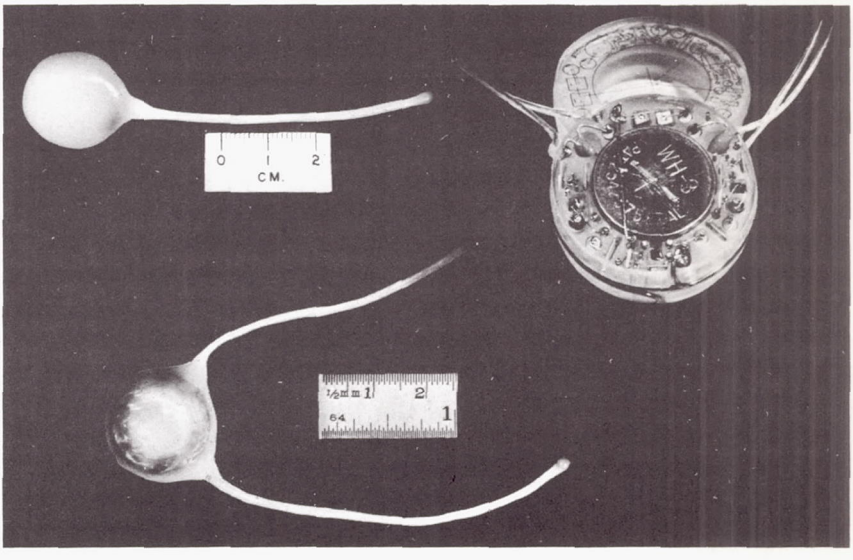


Figure 50.—**Implantable telemeters for transmitting physiological data from small animals.**

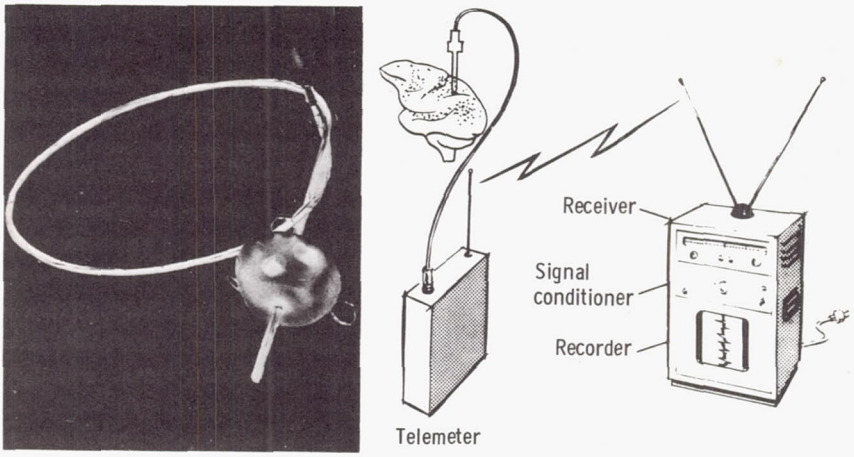


Figure 51.—**Deep brain probe for telemetry of temperature in primates.**

Pollard and Weller (ref. 92) are studying the function and mode of operation of cells and their parts, especially the relationship of cellular inclusions and membranes, and their reactions to stress situations such as pressure, radiation, and gravitational fields.

Relatively low pressure affects bacteria and the components, especially protein synthesis mechanisms of the cell. Colony-forming ability of bacteria is little affected by pressures as high as 14 500 psi for 2-hour periods.

Irradiating bacterial cells has resulted in the leakage of cellular inclusions. Examination of leakage products indicates that the initial site of radiation damage is the cell membrane. It appears that the primary lesion on the membrane is the result of the radiation, changing one of the membrane components, lecithin, which is insoluble, to a soluble component, lycolecithin. The tightly coiled DNA inside the cell, because of the lesion on the membrane, is immediately allowed to push outward at the site of damage and the whole cellular structure becomes disorganized at the site of the damage. Further work is being conducted to examine this hypothesis of the mechanism of X-ray irradiation on cells (Grady and Pollard, ref. 93).

Varying gravitational fields on bacterial cells has shown that centrifugal forces as high as 50 000 g have no effect on DNA and RNA synthesis and very little effect on protein synthesis. Additional study is being conducted on the effects of various stresses on cells, involving larger cells and higher pressure fields, higher levels of centrifugation, and heavier radiation doses.

Research is being directed to basic molecular biochemical problems concerning proteins and nucleic acids of cell mechanisms in order to find a common molecular basis for all forms of living plants and animals (Jukes, ref. 94; and Matsubara, Sasaki, and Chain, ref. 95). All known life on Earth is based on the DNA–RNA-protein system. Inherited characteristics

are carried from one generation to another by genes made up of the DNA molecule. The DNA transmits its information to a second class of molecules made up of RNA, and this information is used to make proteins. Some of these proteins are enzymatic; that is, they act as catalysts for various reactions necessary for the activity of RNA and the production of proteins. The total DNA–RNA-protein system is responsible for all attributes of living systems.

In order to investigate the evolutionary significance of various biological molecules, comparisons are being made between proteins of primitive organisms and advanced organisms. One such class of protein molecules, ferredoxins, is found in many plants and animals. (Ferredoxin is an iron-containing protein.) The idea that bacterial and plant ferredoxins have evolved from a common archetype has received strong support from determination of the complete amino acid sequence of spinach ferredoxin. Although the structure of spinach ferredoxin differs in detail from that of bacterial ferredoxins, it also significantly resembles the bacterial protein.

There are two types of ferredoxins: bacterial ferredoxins that occur in nonphotosynthetic and photosynthetic bacteria, and plant ferredoxins that are present in green leaves and algae. The similarity in properties between the two types and their partial interchangeability in photosynthetic reactions suggests that the bacterial and plant ferredoxins may have some evolutionary relationship (fig. 52). Evidence for this now comes from a comparison of the amino acid composition of the bacterial and plant proteins.

Cytochrome contains 104 amino acids in a single sequence and has been found in animals and some plant groups. The similarities of the cytochromes in all these living organisms is one of the best pieces of evidence, indicating that all living forms on Earth are descended from a single ancestor which lived at least 1 billion years ago. By comparing the cyto-

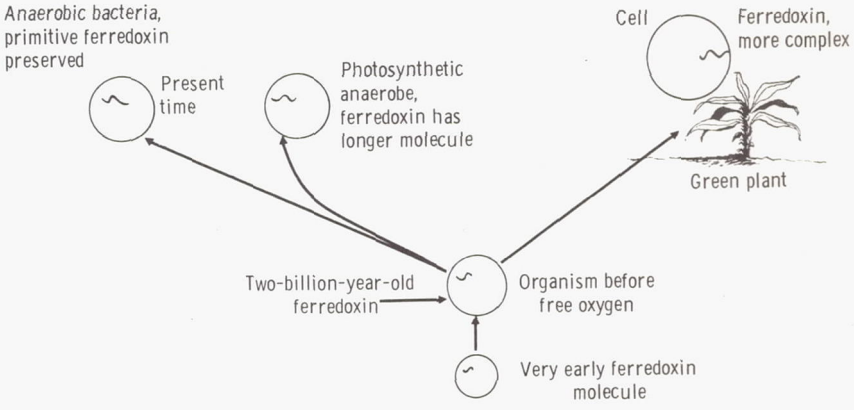


Figure 52.—**Persistence of a molecule during 3 billion years of biological evolution.**

chromes in human heart muscle and in common bread mold, we can see clear evidence of the same ancestor, because approximately 60 percent of the structure of our heart cytochrome is identical with the structure of mold cytochrome. The statistical chances are many billions to one in favor of this being the result of divergent evolution from a common ancestor.

Of further interest in understanding cellular processes is the study of the energy exchange which must function in order for all chemical reactions to proceed. All the organic energy (calories) ever consumed in animal nutrition (or stored in the fossil deposits of oil or coal on our planet) originated—and continues to originate—from energy of inorganic sources. A cycling sequence of biochemical reactions in which this "assimilation" is performed was discovered by Kiesow (ref. 96). The micro-organism *Nitrobacter winogradskyi* revealed in this work why primitive "chemo-autotrophic" organisms can live and propagate without supply of food or light. *Nitrobacter* can repeat—in reversed thermodynamic direction and sequence—for buildup purposes, the major breakdown steps of human and mammalian metabolism. These biochemical reaction steps are linked to disphosphopyridinenucleotide (DPN) and adenosine triphosphate (ATP).

The cycling operation of the crucial biochemical reactions represents, presumably, the essential mechanism of photosynthesis, also. The cycle and the organism depend only on energy supply from an inorganic salt of nitrous acid in soil or water, oxygen at low partial pressure, and carbon dioxide from a dense, dark atmosphere. Inorganic phosphate, iron, copper, and molybdenum are required in small amounts for the culture. The cycle could nevertheless conceptually provide adequate food for a world of animals.

Studies by Stryer and Haugland (ref. 97) on RNA and DNA polymerase molecules are utilizing optical methods to elucidate the physical properties and structure of biological macromolecules. A protein crystal is made fluorescent by attaching it to a specific dye. The fluorescent dye is located at the most important part of the protein, its active site. An ultrafast light-pulse measuring device, a nanosecond fluorimeter developed by these researchers, which allows the light pulse to last a billionth of a second, makes it possible to look at very rapid events on the protein. Using this technique it has been found that a number of proteins have defined rigid three-dimensional structures. This technique has also enabled the researchers to measure distance in the 10- to 60-angstrom range on proteins and nucleic acids. These studies on the relationship between structure and function at the atomic and molecular level will help provide insight into evolutionary processes and constraints. Further, the sensitivity of fluorescence techniques makes the method a potentially choice one in the search for extraterrestrial life.

APPLICATIONS

An important aspect of the space program is the transfer to medical, industrial, commercial, and general public use of all relevant findings deriving from space research. Indeed, a major justification of a space program is found in the immediate or eventual benefits to mankind of space research and penetration. It has already become apparent that flight missions in space provide direct and indirect benefits to all our people. In the years since the space program's inception, the beneficiaries of this research have been constantly growing in number. The space program has become, and will become even more firmly, an integral part of the Nation's economy.

That portion of space research which is biologically oriented is concerned, firstly, with additions to the pool of biological knowledge, which, alone, can extend man's awareness of himself and his place in the universal scheme of things. Secondarily, but with ever growing utility to mankind's material and spiritual well-being, are the theoretical and practical developments in space biology, concerned, not directly with increasing scientific comprehension, but with solving problems of life support and space hazards for astronauts. Developments in this phase have already yielded various engineering constructs, methods, and instruments applicable outside the space context, and have been beneficial in medicine, agriculture, industry, and elsewhere.

Health and Medicine

For the wide area of biomedicine and pathology, space bioscience activities provide hitherto unavailable occasions for testing human response to chronic acceleration, to weightlessness, to removal from the 24-hour Earth rotational period, and to other factors of outer space. What human ailments derive from these conditions? Which existing ones are exacerbated or ameliorated? All life on Earth evolved in a 1-g environment. Now, for the first time, medical scientists can study morphogenesis, physiologic responses, and psychological behavior of gravity-dependent organisms in a weightlessness environment.

Research in chronic acceleration has demonstrated the considerable influence of altered gravity on metabolism. For example, since gravity affects the hydrostatic component of blood pressure, which is involved in degenerative cardiovascular disease, gravity may turn out to be the yet unidentified element in the Earth environment that affects this and other degenerative events that occur late in life. Perhaps such deterioration has a long induction period under the influence of gravity.

It seems highly probable that gravity plays a part not only in gerontological diseases but also in various pathologies that occur throughout life. The fetus, which develops in a phenomenologically weightless environment, is abruptly subjected, at birth, to the stress of terrestrial gravity. Many perinatal conditions may well reflect the influence of gravity. It has been

generally noted that in chronic acceleration there is a noticeable limitation of fat deposition, suggesting the existence of a fat-regulating mechanism whose identification would have wide medical and sociologic importance.

Gravity strongly influences the distribution of blood and gas within the lungs, and space flight furnishes optimal conditions for studying basic pulmonary physiology and pathology under weightlessness. The same considerations apply to various fundamental metabolic anomalies associated with the physiologic alterations induced by oxygen toxicity—such as retrolental fibroplasia in infants or retinal detachment.

The medical benefits from biospace research are every day becoming manifest. Research in astronaut life support, by demonstrating that chronic exposure to high levels of oxygen partial pressure leads to cardiac synthesis of cholesterol and other lipids, has given insight into predispositions to heart disease (Bond, ref. 98). Hibernation research has led to improved therapy for radiation injury, improvements in hypothermic surgery, and new techniques for perserving tissues for grafting (South, ref. 99). Studies of mutations in bacterial cells have made it possible to alter organisms in order to increase the yield of a specific enzyme. This is being applied to the production of the bacterial enzyme, asparagenase, which has shown promise in leukemia therapy.

Research into neural networks and sensory communication—important for astronaut performance—has sought to define information processing in the visual pathway, the processing of biological information, and the nature of the central nervous system (CNS) code. Such understanding will help deal with CNS, psychic, and emotional disturbances.

Biological telemetry, used in Biosatellites and other space vehicles, has applicability to large-scale animal colonies in studies of drug efficacy and toxicology-pharmacology.

The following examples of new apparatus illustrate the wide range of biomedical applicability achieved by technological developments in space bioscience.

Nanosecond Fluorimeter.—Developed at Stanford University for detecting activity at specific sites in proteins, this instrument makes it possible to study processes that last for only a few billionths of a second. The techniques used for control of this device are generally applicable to biomedical research.

Tympanic Thermometer.—This instrument was developed in NASA-supported microcalorimetry studies, and is now used by the Navy to get accurate temperatures of deep-sea divers. Related research has formulated quantitative mechanisms of human thermoregulation, which depend on various "thermostat" centers in the brain. These findings are pertinent to many life sciences, such as clinical medicine and stress physiology (ref. 100).

Laminar Clean Rooms for Surgery and Recovery Rooms.—As a result of a need to provide germ-free environments for the housing of planetary

landing craft prior to sterilization, the biological characteristics of clean rooms were investigated in 1963. Particular attention was directed to the biological characteristics of the downward laminar-flow clean rooms developed by the Atomic Energy Commission for control of physical contaminants. Planetary quarantine personnel requested a biological evaluation of the experimental clean rooms of the Sandia Corp. and suggested a research protocol. To provide a broader base for these studies, support was given to research at Sandia and the construction and operation of a major laminar-flow clean room know as the Experimental Assembly and Sterilization Laboratory (EASL) at the Jet Propulsion Laboratory. The capability of attaining a biologically clean environment was demonstrated in this facility (McDade, ref. 101).

NASA's successful experience with the application of the laminar-flow principle to the control of biological contaminants received favorable attention from leading medical and hospital authorities, both during the period of the EASL studies and following publication of the results (Phillips, ref. 102). The first known medical application was in a surgical suite at the Albuquerque Memorial Hospital. Since that time at least 10 laminar-flow-equipped surgeries have been installed in hospitals throughout the country (McDade and Rypka, ref. 103). Facilities of a similar nature are being widely used to protect burn patients from infection, and recoveries are reported in about half the normal time. The U.S. forces in Vietnam are using laminar-flow devices regularly for burn patients and for handling sick and wounded who must be kept in isolation. The Guthrie Clinic in Sayre, Pa., is investigating the potential of laminar-flow facilities for treating allergy patients.

Silicone Rubber Urinary Catheters.—The primate experiment for the 30-day Biosatellite mission presented new and unique problems, notably that of finding a method for continuous collection of urine. Solution of that problem came with development of a catheter of silicone rubber. This material proved ideal as it is not reactive with living tissue, and it permits a comparatively large bore in a small overall diameter while retaining sufficient strength to prevent breakage or kinking. These catheters have functioned successfully in the ureters (small duct carrying urine from the kidney to the bladder) of experimental animals (ref. 104).

Silicone-rubber catheters are now being used routinely at Harbor General Hospital in treating children with urinary-tract disorders requiring long catheterizations. The nonreactive quality of the catheter, together with better drainage provided by the large bore, have significantly improved such treatment. In other hospitals, surgeons have used small sections of silicone-rubber tubing to "splint" ureters weakened by infection. The tubing is accepted by the body and a "patch" grows over the weakened area bridged by the catheter tubing. It has been observed in dogs that the severed ends of the ureter, when connected by a silicone-rubber catheter section, will

grow over the catheter surface and rejoin. An operation of this type was performed on a monkey on December 21, 1967, and will be used with human patients in the near future.

Other applications of this unique tubing include a kidney drain in adults requiring nephrostomy (an artificial fistula). Now under development is the incorporation of antibiotics into the catheter to forestall urinary-tract infection, an ever-present danger in catheterization (ref. 104).

Food, Agriculture, and Animal Husbandry

Knowledge derived from space research has wide applicability to improvement of food crops, to production of varied plant and animal foods, and to development of new forest products. Thus, the need to devise diets suitable for astronaut needs on long flights has resulted in better methods of preserving, processing, packaging, and storing foods. Stemming from research on the bioregenerative life-support system has come new technology applicable to production, by large-scale fermentation, of a new protein-rich food source (Waslien and Calloway, ref. 105).

A recently developed respirometer can be used for research with small plants and vegetables, fruits, and tissue cultures. The instrument has uses in studies of plant metabolism.

Techniques derived from NASA-sponsored research at the Franklin Institute are being used in devices implanted in ruminant animals for nutritional studies seeking to improve animal feeds and feeding methods, and benefit veterinary medical practice.

Industry

From investigations in plant metabolism have come a new design for a magnetically activated valve that can serve as an inexpensive pressure-release mechanism where high sensitivity to slight overpressure is needed (ref. 106).

An improved fuel cell developed for Gemini and Biosatellite power supplies is being applied to automotive and other types of locomotion.

CONCLUSIONS

The most notable accomplishment in space biology during 1967 was the controlled, quantitative testing of biological hypotheses provided by the successful flight and recovery of Biosatellite II. Thirteen carefully designed experiments, developed over a period of at least 4 years, examined vital assumptions in genetics, physiology, and biochemical regulation of cellular and body activities. Experimental results have given new insight into cell division and differentiation, development and growth, chromosome damage and differentiation, genetic mutations, and biochemical regulation of cell nutrition and metabolism. The greatest effects of weightlessness were seen in

young and actively growing cells and tissues. Rapidly dividing cells with high metabolic activity were more affected than were mature cells which divide more slowly. These effects were modified in some organisms by irradiation during weightlessness. Radiation effects depended on the nature of the organism. In some cases, effects of radiation combined with weightlessness were greater than those observed in Earth-based controls; in other cases, the effects were less. Data gleaned from these experiments should be valuable not only in solving prolonged space-flight problems but also in increasing the general wealth of biologic knowledge and solving many nonspace biological and medical problems.

Extraterrestrial life detection has been enhanced by continued development of automated techniques for detecting significant chemical activity and identifying organic compounds. A highly effective tool for examining such compounds in extraterrestrial bodies is mass spectroscopy combined with gas chromatography. Combining sensitivity, general applicability, and independence from known analogies, this method is very effective, and a sample weighing fractions of a microgram will suffice. These are indispensable qualities for detecting very minute quantities of a substance, particularly one different from anything known on Earth.

Research into the nature of life, which has sought to define the qualities of molecular and biologic entities, has now demonstrated the presence of a universal type of membrane in all biologic systems and the similarity of protein synthesis in all systems. Protein primary structure has been further defined by disulfide bridges linking sulfur-containing amino acids. Exobiologic research has, in addition, satisfactorily defined the presumed pathway of early abiogenesis: utilizing an atmosphere of methane, ammonia, and water and an assortment of potential energy sources, the synthesis of a variety of organic molecules has occurred. Demonstrations that, in this fashion, many biologically important molecules can be synthesized point to their having played a central role in the origin of life.

With the essential biochemical constituents and the mechanism of replication beginning to be understood, the synthesis of living matter by abiogenic experimental techniques has become a major goal. Amino acids, monosaccharides, pyrimidines and purines, porphyrine, and ATP have been produced under conditions which have been interpreted in a context of spontaneous synthetic organic chemistry on the primitive Earth.

Planetary quarantine research has sought means for sterilizing spacecraft with maximum efficiency and minimum lowering of reliability. Dry heat is generally considered the most effective spacecraft sterilant, and study has now shown that the quantity of such heat applied to a spacecraft can be drastically reduced, with consequent money savings. Good progress has been made in predicting the probability of contaminating the planet Mars through construction of various mathematical models. One such model is being constructed for determining the duration and level of dry-heat ex-

posure needed to sterilize spacecraft. In addition to operational and systems requirements, mathematical models must include compatibility with international programs. International agreement has established that a 1×10^{-3} probability of contaminating planets of biologic interest during the entire period of unmanned exploration is required.

The role of gravitational force in the origin, nature, and function of organized life has been further defined. Alterations in gravity are equated with other environmental factors: if the alteration is sufficiently great, a toxic effect or region of debilitated survival will result. Physiologic adaptation, however, eventually dissipates the stressful condition. Stress and adaptation of chronic acceleration are accompanied by a spectrum of physiologic conditions: changes in muscle size, a noticeable decrease in lymphocytes, and changes in water and electrolyte balances. Of crucial importance to long space flights have been the X-ray densitometry studies showing that weightlessness causes bone mineral loss.

Still largely unknown is man's response, over a period of time, to gravity levels between the 1 g of Earth and the 0 g of space. The launching of the first of four Aerobee rockets that create artificial gravity through centrifugal action has shown that animals tend to select a gravity level in accordance with their normal adaptive responses and personal comfort.

Since exposure to ever-increasing periods of weightlessness has raised questions about effects on brain mechanisms, researchers are looking for altered cycling in brain-wave patterns. New studies of alertness in astronauts are beginning to use continuous monitoring of electroencephalographic data as relevant indices. Special emphasis has been placed on instrumentation techniques, data-reduction applications, and three-dimensional, continuous displays showing changes in physiologic condition.

REFERENCES

1. Anon.: Significant Achievements in Space Bioscience, 1958–64. NASA SP–92, 1966.
2. Anon.: Significant Achievements in Space Science, 1966. NASA SP–155, 1967.
3. Anon.: The Biosatellite II Experiments, 1967, Preliminary Results. Bioscience, vol. 18, no. 6, 1967, pp. 537–661.
4. Morowitz, H. J.: Biological Self-Replication Systems. *In:* Progress in Theoretical Biology, vol. 1, Academic Press, 1967.
5. Gehrke, C.; Stalling, D.; and Ruyle, C.: Quantitative Gas-Liquid Chromatography of TMS Nucleic Acid Constituents. Biochem. Biophys. Res. Commun., vol. 28, 1967, pp. 869–874.
6. Fox, S. W.; Harada, K.; and Rohlfing, D. L.: Polyamine Acids, Polypeptides, and Proteins. Univ. of Wisconsin Press, 1962, p. 47.
7. Rohlfing, D. L.; and Fox, S. W.: Catalytic Activity of Thermal Polyanhydro-alpha-Amino Acids for the Hydrolysis of p-Nitrophenyl Acetate. Arch. Biochem. Biophys., vol. 118, 1967, p. 122.

8. Fox, S. W.: A Model of the Synthesis of a Primitive Cell. Inst. Mol. Evolution, Univ. of Miami. Presentation at Intl. Conv. Biochem. (Bangalore, India), Sept. 1967.
9. Armstrong, G. T.; Furukawa, G. T.; and Reilly, M. L.: A Survey of Thermodynamic Properties of the Compounds of the Elements, C, H, N, O, P, S. NBS Rept. no. 9553, Natl. Bur. Standards, U.S. Dept. of Com., Mar. 31, 1967.
10. Waehneldt, T. V.; and Fox, S. W.: Phosphorylation of Nucleosides With Polyphosphoric Acid. Biochem. Biophys. Acta, vol. 134, 1967, pp. 1–8.
11. Ponnamperuma, C.; and Gabel, N.: Current Status of Chemical Studies on the Origin of Life. Space Life Sci., May 1967.
12. Ponnamperuma, C.; Woeller, F.; Flores, J.; Romiez, M.; and Allen, W.: Synthesis of Organic Compounds by Action of Electric Discharges in Simulated Primitive Atmospheres. ACS Advan. Chem. Ser., Apr. 1967.
13. Heinrich, M. R.; and Bugna, E.: Determination of Basic Dinitrophenyl-Amino Acids by Ion-Exchange Chromatography. Proc. 7th Intern. Congr. Biochem., Abstr. A–138, Aug. 1967, p. 613.
14. Klein, H. P.; Volkman, C.; and Weibel, J.: Membranes of *Saccharomyces cerevisiae*. J. Bacteriol., vol. 84, 1967, pp. 475–481.
15. Ponnamperuma, C.; and Pering, K.: Aliphatic and Alicyclic Hydrocarbons Isolated from the Trinidad Lake Asphalt. Geochim. Cosmochim. Acta, vol. 31, no. 8, 1967, pp. 1350–1354.
16. Schopf, J. W.; Kvenvolden, K.; and Barghoorn, E. S.: Amino Acids in Pre-Cambrian Sediments: An Assay. Presentation at meeting of Group for Analysis of Carbonaceous Chondrites, Ames Res. Center (Moffett Field, Calif.), Oct. 25–27, 1967.
17. Kvenvolden, K.: Molecular Distributions of Fatty Acids of Various Geologic Ages. Presentation at annual meeting, Geol. Soc. Am. (New Orleans, La.), Nov. 20–22, 1967.
18. Kvenvolden, K.: Contamination Problem in the Analysis of Trace Organic Constituents of Sediment. Presentation at meeting of Group for Analysis of Carbonaceous Chondrites, Ames Res. Center (Moffett Field, Calif.), Oct. 25–27, 1967.
19. Harada, K.: Formation of Amino Acids by Thermal Decomposition of Formamide—Oligomerization of Hydrogen Cyanide. Nature, vol. 214, 1967, p. 479.
20. Keil, K.; and Snetsinger, K. G.: Prebiological Sulfur Compounds. Science, vol. 155, 1967, pp. 451–453.
21. Steinman, G.; Smith, A. E.; and Silver, J. J.: Synthesis of a Sulfur-Containing Amino Acid Under Simulated Prebiotic Conditions. Science, vol. 159, Jan. 15, 1968, pp. 1108–1109.
22. Anon.: Explorations in Space With Sub-Voyager Systems. Space Science Board, National Research Council—National Academy of Sciences, Natl. Acad. Engrs., Washington, D.C., Jan. 1967.
23. Biemann, K.: Potentialities of the GC/MS System for Detecting Organic Compounds in Extraterrestrial Materials. *In*: The Search for Extraterrestrial Life, Advan. Astronaut. Sci., vol. 22, 1967.
24. Burlingame, A. L.: Analytical Techniques for Identification and Study of Organic Matter in Returned Lunar Samples. Space Sci. Lab., Univ. of California, Berkeley, Mar. 31, 1967.
25. Updegrove, W. S.; Oro, J.: and Zlatkis, A.: Gas Chromatograph—A Quadruple Mass Spectrometric Analysis of Organic Compounds. J. Gas Chromatog., July 1967, pp. 359–361.

26. Oro, J.; and Han, J.: Application of Combined Chromatography-Mass Spectrometry to Analysis of Aromatic Hydrocarbons Formed by Pyrolysis of Methane. J. Gas Chromatog., Sept. 1967, pp. 480–485.
27. Oro, J.; Han, J.; and Zlatkis, A.: Application of High-Resolution Gas Chromatography-Mass Spectrometry to Analysis of the Pyrolysis Products of Isoprene. Anal. Chem., vol. 39, Jan. 1967, p. 27.
28. Hitchcock, D. R.; and Lovelock, J. E.: Life Detection by Atmospheric Analysis. Icarus, vol. 7, no. 2, Sept. 1967, pp. 149–159.
29. Dayhoff, M. O.; Lippincott, E. R.; and Nagarajan, G.: Thermodynamic Equilibrium in Prebiological Atmospheres of C, H, O, N, P, S, and Cl. NASA SP–3040, 1967.
30. Lippincott, E. R.; Eck, R. V.; Dayhoff, M. O.; and Sagan, R. V.: Thermodynamic Equilibrium in Planetary Atmospheres. Astrophys, J., vol. 147, no. 2, 1967, pp. 753–763.
31. Sagan, C.: Selected Studies in Exobiology, Planetary Environments, and Problems Related to Origin of Life. Smithsonian Inst., Astrophys. Obs., Cambridge, Mass., June 1966–May 1967.
32. Sagan, C. E.; Lippincott, E. R.; Dayhoff, M. O.; and Eck, R. V.: Organic Molecules and the Coloration of Jupiter. Nature, vol. 213, no. 5073, 1967, pp. 273–274.
33. Hess, W. N.: Lunar Science and Exploration. NASA SP–157, 1967.
34. Updegrove, W. S.; and Oro, J.: Analysis of Organic Matter by Gas Chromatography-Mass Spectrometry. Chem. Dept., Univ. of Houston, 1967.
35. Anon.: Institute of Molecular Evolution. Third Ann. Rept., Univ. of Miami, Sept. 30, 1967.
36. Hayes, J. M.: Organic Constituents of Meteorites—A Review. Geochim. Geophys. Acta, vol. 31, 1967, pp. 1395–1440.
37. Nooner, D. W.; and Oro, J.: Organic Compounds in Meteorites. Geochim. Geophys. Acta, vol. 31, 1967, pp. 1359–1394.
38. Oro, J.; and Nooner, D. W.: Aliphatic Hydrocarbons in Carbonaceous Chondrites. Nature, vol. 213, 1967, p. 1085.
39. Hayatsu, R.: Origin of Organic Matter in the Early Solar System. II. Nitrogen Compounds. Geochim. Cosmochim. Acta, vol. 32, 1968, pp. 175–190.
40. Craven, C. W.: Sterilization and Decontamination Techniques for Space Vehicles. Jet Propulsion Lab., California Inst. Tech., Tech. Mem. 33–370, Dec. 1, 1967.
41. Stern, J. A.: Sterilization Group. Jet Propulsion Lab., California Inst. Tech., Apr. 24, 1967.
42. Goddard, F. E.: The FY 1967 Bioscience Program at the Jet Propulsion Laboratory. Jet Propulsion Lab., California Inst. Tech., Mar. 15, 1967.
43. Seamans, R. C.: Outbound Planetary Biological Contamination Control: Policy and Responsibility. NASA NPD 8020.10, Sept. 6, 1967.
44. Bond, W.; and Marshall, J.: Support of Planetary Quarantine Requirements of NASA. Public Health Service, Communicable Disease Center, Phoenix, Ariz., Jan. 19, 1968.
45. Lyle, R. G.: Technical Manuals and Planning Study in Planetary Quarantine. Exotech, Inc., Feb. 9, 1968.
46. Sagan, C.; Levinthal, E. C.; and Lederberg, J.: Contamination of Mars. Science, vol. 159, no. 3820, Mar. 15, 1968, pp. 1191–1196.
47. Horowitz, N. H.; Sharp, R. P.; and Davies, R. W.: Planetary Contamination. Science, vol. 155, 1967, p. 1501.

48. MURRAY, B. C.; DAVIES, M. E.; AND ECKMAN, P. K.: Contamination of Mars and Venus. Science, vol. 155, 1967, p. 1505.
49. STERN, J. A.; AND HOFFMAN, A. R.: Determination of Terminal Sterilization Process Parameters. Tech. rept. no. 32–1191, Jet Propulsion Lab., California Inst. Tech., Oct. 1, 1967.
50. HOFFMAN, A. R.; AND STERN, J. A.: Terminal Sterilization Process Calculation for Spacecraft. Jet Propulsion Lab., California Inst. Tech., Tech. rept. no. 32–1209, Nov. 15, 1967.
51. ANGELOTTI, R.: Ecology and Thermal Inactivation of Microbes in and on Interplanetary Space Vehicle Components. Public Health Serv., Center for Urban and Industrial Health, Cincinnati, Ohio, Oct. 1967.
52. VESLEY, D.; AND SMITH, G.: Die-Off of Microbial Contamination. Department Environ. Health, Univ. of Minnesota, 1967.
53. GREENE, V. W.; WALKER, B.; AND ANDERSON, O. H.: Methodology of Measuring Internal Contamination in Spacecraft. Department Environ. Health, Univ. of Minnesota, Dec. 1967.
54. PULEO, J. R.; FAVERO, M. S.; AND PETERSEN, N. Y.: Use of Ultrasonic Energy in Assessing Microbial Contamination on Surfaces. Appl. Microbiol., vol. 15, no. 6, Nov. 1967, pp. 1345–1351.
55. PULEO, J. R.; FAVERO, M. S.; AND TRITZ, G. J.: Feasibility of Using Ultrasonics for Removing Micro-Organisms From Surfaces. Contamination Control, vol. 6, 1966, pp. 58–67.
56. BURTON, R. R.; BESCH, E. L.; SLUKA, S. J.; AND SMITH, A. H.: Differential Effects of Chronic Acceleration on Skeletal Muscles. J. Appl. Physiol., vol. 23, no. 1, July 1967, pp. 80–84.
57. BURTON, R. R.; AND SMITH, A. H.: Muscle Size, Gravity, and Work Capacity. XVI Intern. Cong. Aviation Space Med., Lisbon, Sept. 11–15, 1967.
58. CASEY, H. W.; CORDY, D. R.; GOLDMAN, M.; AND SMITH, A. H.: Influence of Chronic Acceleration on the Effects of Whole-Body Irradiation in Rats. Aerospace Med., May 1967, pp. 451–456.
59. BURTON, R. R.; AND SMITH, A. G.: Criteria for Physiological Stress and Adaptation. The Physiologist, vol. 10, no. 3, 1967, p. 137.
60. WUNDER, C. C.: A Discussion of the Effects of Chronic Acceleration on Animals. Symposium on Gravity and the Organism (New York, N.Y.) (in press).
61. BERNSTEIN, N. J.; GILFILLAN, R. P.; AND RAHLMANN, D. F.: Chronic Intravascular Catheterization. J. Surg. Res., vol. 6, no. 12, 1966, pp. 511–521.
62. POPOVIC, V. P.; AND ADDLESTONE, R. B.: Arterial Blood Pressure During Sleep. The Physiologist, vol. 10, 1967, p. 280.
63. GORDON, S. A.; AND SHEN, M. J.: On the Thresholds of Gravitational Force Perception by Plants. *In*: Life Sciences and Space Research, A. H. Brown and M. L. Florkin, eds., Spartan Books, 1966, pp. 22–34.
64. RHOADES, R. A.; WRIGHT, R. A.; HIATT, E. P.; AND WEISS, H. S.: Metabolic and Thermal Responses to a He-O_2 Environment. Am. J. Physiol., vol. 213, no. 4, Oct. 1967.
65. BOWER, R. W.; AND FOX, E. L.: Metabolic and Thermal Responses of Man in Various He-O_2 Environments. J. Appl. Physiol., vol. 23, no. 4, Oct. 1967, pp. 561–565.
66. BOND, A. D.; JORDON, J. P.; AND ALLRED, J. B.: Metabolic Changes in Rats Exposed to an Oxygen-Enriched Environment. Am. J. Physiol., vol. 212, 1967, pp. 526–529.
67. RHOADES, R. A.; WRIGHT, R. A.; AND WEISS, H. S.: Metabolic Depression

in Animals Exposed to Air After Living in a He-O_2 Environment. Proc. Soc. Exptl. Biol. Med., vol. 124, no. 1, Jan. 1967, pp. 176–180.

68. Barr, R. E.; Musacchia, X. J.; and Westhoff, D. D.: Radioprotection in the Hibernating Ground Squirrel; Seasonal and Body Temperature Variation. Radiation Res., vol. 31, no. 3, July 1967.
69. Musacchia, X. J.; Barr, R. E.; and Westhoff, D. D.: Radiation Protection in Hibernating Animals. Federal Proc., vol. 26, no. 2, Mar.–Apr. 1967, p. 336.
70. Rhoades, R. A.; Weiss, H. S.; and Wright, R. A.: A Multiplace Metabolimeter With a Servo-Driven Volume Meter for Use With Artificial Atmospheres. J. Lab. Clin. Med., vol. 69, no. 2, Feb. 1967, pp. 330–335.
71. Musacchia, X. J.; and Barr, R. E.: Intestinal Absorption in Irradiated Hamsters. Radiation Res., vol. 31, no. 3, July 1967.
72. Witz, S.: Studies of Photosynthetic Halophiles From Owens Lake. Space-General, Aerojet-General Corp., Sept. 15, 1967.
73. Hochstein, L. I.; and Dalton, B. P.: Salt Specificity of $NADH_2$ Oxidase Prepared From a Halophilic Bacterium. J. Bacteriol., vol. 95, no. 1, 1968, pp. 37–42.
74. Curl, H.; and Sutton, E.: Physiological Ecology of Cryophilic Algae. Dept. Oceanog., Oregon State Univ., Aug. 21, 1967.
75. Stein, J.; and Amundsen, C. C.: Studies on Snow Algae and Fungi From the Front Range of Colorado. Can. J. Botan., vol. 45, 1967, pp. 2033–2045.
76. Simms, H. R.: On the Ecology of *Herpotrichia nigra*. Mycologia, vol. 59, no. 5, Sept.–Oct. 1967.
77. Siegel, S. M.; Roberts, K.; Nathan, H.; and Daly, O.: Living Relative of the Microfossil Kakabekia. Science, vol. 156, no. 3779, 1967, pp. 1231–1234.
78. Beischer, D. E.; Miller, E. F.; and Knepton, J. C.: Exposure of Man to Low-Intensity Magnetic Fields in a Coil System. NASA Joint Rept., NAMI–1018, Naval Aerospace Med. Inst., Oct. 1967.
79. Kok, B.; Rurainski, H. J.; and Owens, O. V. H.: The Reducing Power Generated in Photoact I of Photosynthesis. Biochim. Biophys. Acta, vol. 109, 1965, pp. 347–356.
80. Kok, B.; and Datko, E. A.: Reducing Power Generated in the Second Photoact of Photosynthesis. Plant Physiol., vol. 40, no. 6, 1965, pp. 1171–1177.
81. Joliot, P.; and Kok, B.: Analysis of the Interaction Between the Two Photosystems of Photosynthesis. Res. Inst. Advanced Studies, 1967.
82. Kok, B.; and Jones, L. W.: Photoinhibition of Chloroplast Reactions. 1. Kinetics and Action Spectra. Plant Physiol., vol. 41, 1967, pp. 1037–1044.
83. Henry, S. P.; Meehan, J. P.; and Stephens, P. M.: Use of Psychosocial Stimuli To Induce Prolonged Systolic Hypertension in Mice. Psychosomat. Med., vol. 29, no. 5, Sept.–Oct. 1967, pp. 408–431.
84. Robinson, B. W.; and Warren, H.: Telestimulation of the Primate Brain. Arch. Phys. Med. Rehabil., vol. 48, Sept. 1967, pp. 468–473.
85. Egger, M. D.; and Petran, M.: New Reflected-Light Microscope for Viewing Unstained Brain and Ganglion Cells. Science, vol. 157, no. 3786, July 1967, pp. 305–307.
86. Adey, W. R.; Kado, R. T.; and Walter, D. O.: Analysis of Brain Wave Records From Gemini Flight GT–7. *In:* Life Sci. Space Res., A. H. Brown and F. G. Favorite, eds., North-Holland Publ. Co. (Amsterdam), 1967, pp. 65–93.
87. Walter, D. O.; Kado, R. T.; Rhodes, J. M.; and Adey, W. R.: Electroencephalographic Baselines in Astronaut Candidates Estimated by Computa-

tion and Pattern-Recognition Techniques. Aerospace Med., Apr. 1967, pp. 371–374.

88. HELD, R.; AND BAUER, J. A.: Visually Guided Reaching in Infant Monkeys After Restricted Rearing. Science, vol. 155, Feb. 10, 1967, pp. 718–720.
89. HEIN, A.; AND HELD, R.: Dissociation of the Visual Placing Response Into Elicited and Guided Components. Science, vol. 158, Oct. 20, 1967, pp. 390–392.
90. IBERALL, A. S.; AND CARDON, S. Z.: Metabolic Control in the Mammalian Microcirculation. Proc. 19th Ann. Conf. Eng. Med. Biol., 1966, p. 50.
91. GOODMAN, R. M.: Simultaneous, Multi-Parameter Data From Implantable Telemeters. Dig. Seventh Intern. Conf. Biol. Med. Eng., Stockholm, 1967, p. 87.
92. POLLARD, E. C.; AND WELLER, P. K.: The Effect of Hydrostatic Pressure on the Synthetic Processes in Bacteria. Biochim. Biophys. Acta, vol. 112, 1966, pp. 573–580.
93. GRADY, L. J.; AND POLLARD, E. C.: DNA Degradation by Ionizing Radiation in *Bacillus subtilis*. Synergistic Effect of Actino-mycin D. Biochim. Biophys. Acta, vol. 145, 1967, pp. 837–839.
94. JUKES, T. H.: Molecules and Evolution. Columbia Univ. Press, 1966.
95. MATSUBARA, H.; SASAKI, R. M.; AND CHAIN, R. K.: The Amino Acid Sequence of Spinach Ferredoxin. Proc. Nat. Acad. Sci., vol. 57, no. 2, Feb. 1967, pp. 439–445.
96. KIESOW, L. A.: Energy-Linked Reactions in Chemoautotrophic Organisms. Current Topics in Bioenergetics, vol. 2, 1967, pp. 195–223.
97. STRYER, L.; AND HAUGLAND, R. P.: Energy Transfer: A Spectroscopic Ruler. Proc. Nat. Acad. Sci., vol. 58, 1967, pp. 719–726.
98. BOND, A. D.: Metabolic Changes in Rats Exposed to an Oxygen-Enriched Environment. Am. J. Physiol., vol. 212, 1967, pp. 526–529.
99. SOUTH, P. E.: Radioprotection and Profound Hypothermia in Rats and Hamsters. Space Sci. Res. Center Rept., Univ. of Missouri, St. Louis, 1967.
100. ANON.: Medical Benefits From Space Research. U.S. Govt. Printing Off., 1967.
101. MCDADE, J.: Environmental Microbiology and the Control of Microbial Sterilization and Technology. NASA SP–108, 1966.
102. PHILLIPS, G. B.: Laminar Air Flow for Microbiological Contamination Control. Proc. 67th Ann. Meeting, Am. Soc. Microbiol., Apr. 1967, p. 7.
103. MCDADE, J. J.; AND RYPKA, E. W.: Laminar Air Flow in the Surgical Theater. Proc. 67th Ann. Meeting, Am. Soc. Microbiol., Apr. 1967.
104. ANON.: Antibiot. News, Nov. 15, 1967, p. 6.
105. WASLIEN, C. I.; AND CALLOWAY, D. H.: *Hydrogenomonas eutropha* as a Space Food Resource. Life Sci. Space Res. VI, North-Holland Publ. Co. (Amsterdam), 1968.
106. ANON.: Plant Respirometer Enables High Resolution of Oxygen Consumption Rates. NASA Tech. Brief 66–10406, Clearinghouse for Federal Scientific and Technical Information, Springfield, Va. 22151.

333-240 O—69——10

Page Intentionally Left Blank

IONOSPHERES AND RADIO PHYSICS

E. R. Schmerling
Office of Space Science and Applications, NASA

S. J. Bauer
Goddard Space Flight Center, NASA

Page Intentionally Left Blank

Ionospheres and Radio Physics

INTRODUCTION

In 1967 the following spacecraft were launched with ionospheric and radio physics experiments: OGO–IV, Ariel III, Mariner V, ATS–II and III, and Pioneer VIII. In addition, approximately 20 sounding rockets were launched.

This section deals with results in ionospheres and radio physics published in 1967. The most notable event was the occultation by Venus of Mariner V on October 19, 1967. This occultation was observed both on the S-band telemetry and on a two-frequency radio propagation experiment at a range of nearly 80 million kilometers. Together, these observations provided data on the atmosphere and day and night ionospheres of Venus. The striking difference between the day and night ionospheres provided evidence of a direct interaction between the solar wind and a planetary ionosphere that, unlike the Earth's, is not shielded by an intrinsic magnetic field. Radio signals originating from the telemetry transmitter on Lunar Orbiter I and reflected by the surface of the Moon were observed.

Progress has been reported in the difficult art of measuring electric fields in the ionosphere, using chemical releases from rockets and making whistler measurements of plasma motions. A beginning has been made in developing a consistent theory of dynamic effects, by starting with large-scale neutral winds computed from known atmospheric pressure variations.

Progress has also been reported in the development of theories whereby electrons can transfer energy to waves which are seen as very-low-frequency emissions. The ion wake behind Ariel I was partially mapped by examining the effects seen on two of its probes carried at different distances from the spacecraft.

Alouette I, the U.S.-Canadian topside sounder satellite, celebrated its fifth birthday on September 29, 1967, with all electronic units still working and a log of 1.77 million ionograms recorded.

THE LOWER IONOSPHERE

Progress in understanding the lower ionosphere is hampered by the difficulty of making *in situ* measurements, as a result of which the positive and negative ion composition is still uncertain. The need for better laboratory

determinations of the reaction rates of the processes which control the ionization has also hindered such progress.

Techniques for measuring electron concentration profiles are now fairly well developed. Kane and Troim (ref. 1) reported on radio propagation measurements made with Arcas rockets during the May 30, 1965, eclipse of the Sun. Their results indicated that the electron concentrations tended to follow the computed trends in Lyman-alpha flux. Mechtly, Bowhill, Smith, and Knoebel (ref. 2) show how the radio propagation technique can be combined with a Langmuir-probe determination to provide fine-structure data. Sonin (ref. 3) has examined the theory of ion collection by probes on supersonic rockets at altitudes below 70 kilometers. He concludes that it is practical to employ electric fields so high that the ion collection rate is independent of dynamic flow effects. Hoult and Kuo (ref. 4), on the other hand, consider the theory of a mobility spectrometer in the subsonic regime for the 40- to 70-kilometer region.

Further consideration has been given to the "winter anomaly" in the absorption of radio waves. This actually consists of two parts: the greater day-to-day variability in absorption in winter, so that some days have unusually high absorption; and the greater average absorption in winter (including all days in the average) than would be expected by extrapolating summer absorption values to the appropriate winter solar zenith angles. Maehlum (ref. 5) considers this to be the effect of precipitating electrons, based mostly on Injun III data. The summer absorption behavior is ascribed to the fact that the ionization production resulting from the precipitating electrons is swamped by solar ionization. Sechrist (ref. 6), on the other hand, refers to meteorological data and associates the anomaly with D-region temperature inversions which have the effect of increasing the nitric oxide concentration.

In the E-region the relationships between sporadic E and wind structure have been further elucidated by Wright, Murphy, and Bull (ref. 7). Furthermore, the possible role of ionization produced by micrometeorites has been revived by Fiocco (ref. 8), since there is evidence from ion composition data that meteoric matter may be present in ionized form.

New laboratory measurements have been made of chemical reaction rates thought to be of importance in the lower ionosphere. Fehsenfeld et al. (ref. 9) reported measuring negative ion reactions in a flowing afterglow system. Their measurements point to the importance of the negative ion chemistry of oxygen, and to the role of O_3^- as an intermediate in the production of CO_3^-, NO_2^-, and NO_3^-.

THE MIDDLE IONOSPHERE

A very important feature of the ionosphere is the temperature of the various constituents. Considerable effort has been put into the measurement of neutral, ion, and electron temperatures and the consequences of

thermal nonequilibrium between the species. Important contributions have been made using incoherent-backscatter (Thomson-scatter) sounders which can be used to obtain temperature measurements at a single location with high time resolution. These measurements are important in complementing the geographic coverage obtainable from satellites. Sounding rockets, on the other hand, have the unique capability of making other measurements at the same time. All these methods of investigation thus play an important role in studying the thermal balance and heat budget of the ionosphere.

Banks (ref. 10) and Dalgarno and Walker (ref. 11) have investigated theoretically the heat transfer among electrons, ions, and neutral constituents. Below about 250 kilometers the ion temperature is approximately equal to the neutral temperature. Above this altitude the ion temperature increases, remaining between the neutral and electron temperatures but tending to the electron temperature at high altitudes. In addition, some differences are noted between the temperatures of the ions; peak temperature differences of the order of 200° K are expected between H^+ and O^+, with H^+ being hotter. Although there is experimental evidence of these trends of electron, neutral, and ion temperatures, measurement techniques are not yet sufficiently sensitive to show the predicted variations between the different ionic species. Figures 1 and 2 show, respectively, the expected differences between H^+ and O^+, and between He^+ and O^+, according to Banks.

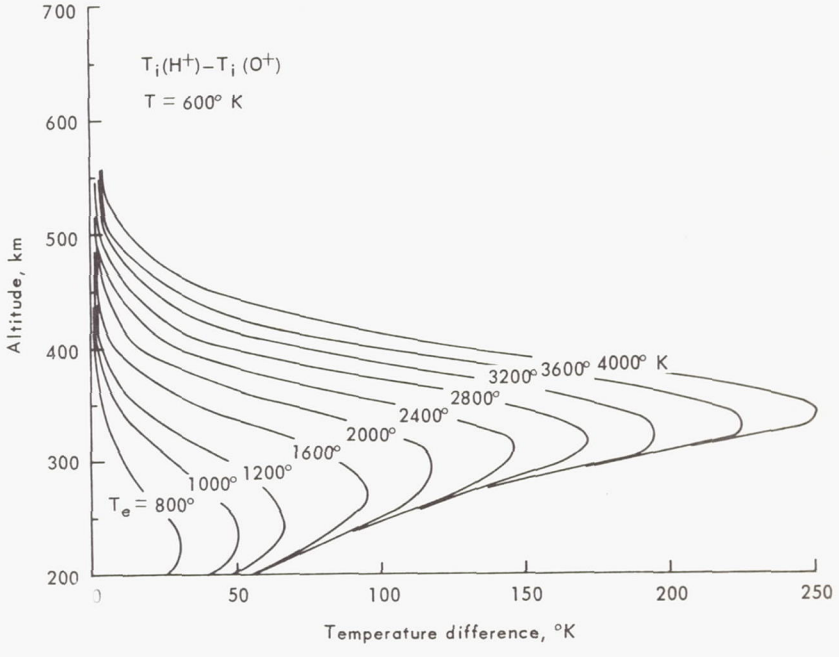


***Figure 1.*—Temperature difference between atomic hydrogen and oxygen ions for different electron temperatures and a neutral atmosphere temperature of 600° K.**

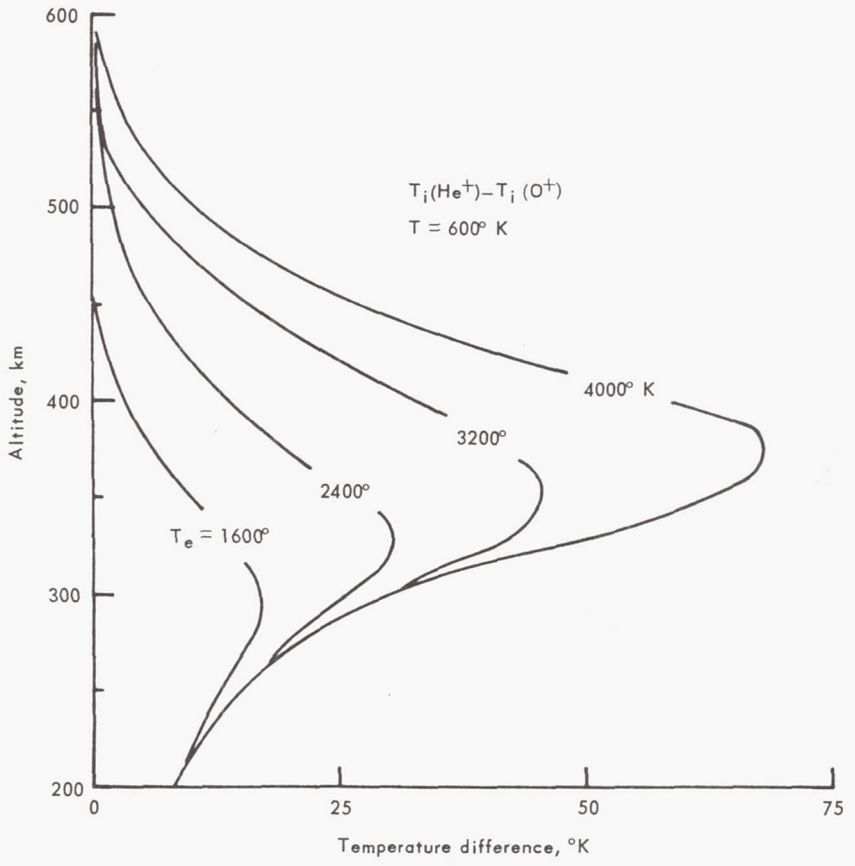


Figure 2.—**Temperature difference between helium and atomic oxygen ions for different electron temperatures and a neutral atmosphere temperature of 600° K.**

Nagy and Walker (ref. 12) described two simultaneous nighttime rocket measurements of electron temperature and concentration. Using a standard atmospheric model for the neutral temperature, it was found that the electron temperature was above the neutral temperature and consistent with a downward heat flux from the protonosphere. Although a local heat source proportional to the neutral density could be ruled out, a heat source proportional to the local electron concentration would also fit the data.

Further evidence shows that account must be taken not only of the heat flux from the protonosphere, but also of the escape of photoelectrons, which can travel along a line of magnetic force to the conjugate ionosphere. Carru, Petit, and Waldteufel (ref. 13), using the French Thomson-scatter installation, have shown that there is a consistently observable increase in elecron temperature in the ionosphere at about the time of sunrise at the

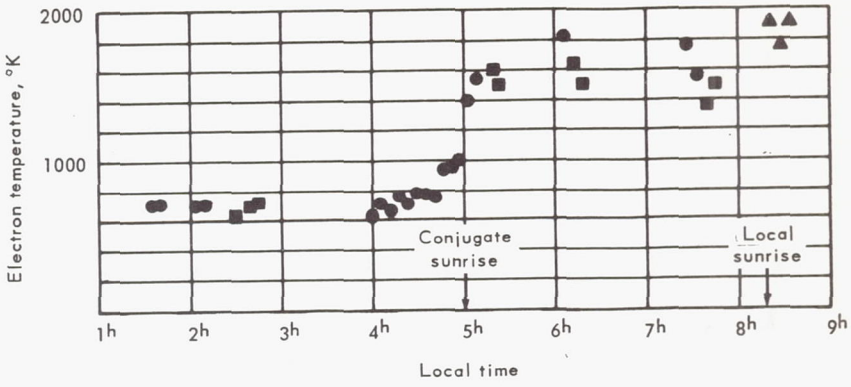


Figure 3.—The effect of sunrise at the conjugate point on electron temperature on January 25–26, 1966, at Nançay, France. (●, 300 km; ■, 275 km, Jan. 26, 1966; ▲, 275 km, Jan. 25, 1966.)

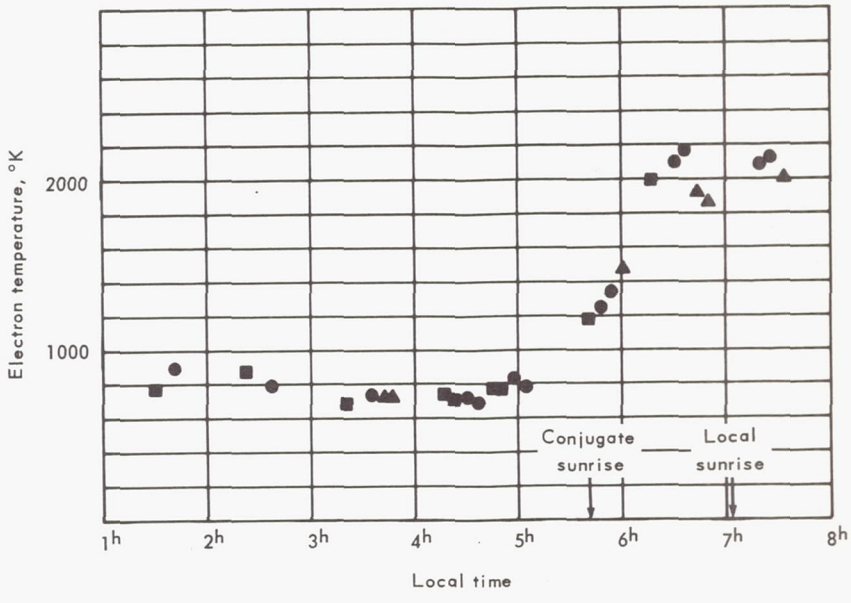


Figure 4.—The effect of sunrise at the conjugate point on electron temperature on March 15, 1966, at Nançay, France. (■, 350 km; ●, 300 km; ▲, 275 km.)

conjugate location, but well before local sunrise. Carlson at Arecibo had reported this effect previously (ref. 14). Figures 3 and 4 show data obtained by Carru et al. There is also evidence from the Arecibo Ionospheric Observatory that these fast photoelectrons have been detected by the enhancement of the plasma line (Yngvesson, private communication).

Evans (ref. 15) has studied the midlatitude F-region at sunspot minimum. The well-known seasonal anomaly is found, with peak F-region electron concentrations approximately twice as high on a winter day as on a summer day. Very important in this connection is Evans' finding that there are no significant seasonal temperature variations in the 200- to 400-kilometer range. This appears to rule out the possibility that the seasonal anomaly can be ascribed to changes in the electron loss rates as a result of temperature-dependent reaction rates. The daytime electron-temperature gradients lead to an estimated photoelectron flux of $5 \times 10^8/cm^2/sec$ in winter through the 500-kilometer level. While there are only small seasonal temperature changes during the day, there are marked changes at night. The high nighttime electron temperatures in winter are ascribed to high heat fluxes from the conjugate summer hemisphere.

The theoretical study of Thomas and Venables (ref. 16) examines the time-varying solution of the F2-region electron continuity equation in the presence of a diurnal temperature variation and includes the effects of an elevated electron temperature. Although sunspot maximum computations are in reasonable agreement with observations, sunspot minimum values are too small by a factor of approximately 2. In addition, changes of temperature alone would be unable to account for the seasonal anomaly.

Thomson-scatter measurements made at the magnetic equator by Farley, McClure, Sterling, and Green (ref. 17) differ significantly from those made at higher latitudes. In particular, ion and electron temperatures were found to be equal at night at all altitudes and during the day above approximately 300 kilometers. This is illustrated in figure 5.

Important progress was made with the difficult problem of measuring electric fields in the ionosphere. Notable is the ejection of a mixture of barium and strontium from a rocket at twilight. The electric field can be deduced by observing the separation between the neutral strontium and ionized barium clouds. The techniques, reactions, and yields are discussed by Föppl et al. (ref. 18). The theory, and some measurements, are described by Haerendel, Lüst, and Rieger (ref. 19). The motion of the ion cloud in a direction perpendicular to the Earth's magnetic field is caused by the electric field, but this motion is modified by the induced polarization, governed by a parameter λ, the ratio of the integrated Pederson conductivities inside and outside the ionized column. Since there is some uncertainty about λ, there is a corresponding uncertainty about the magnitude of the deduced electric field. Measurements have been made near altitudes of 200 and 2000 kilometers. In the auroral region, electric fields of 35 to

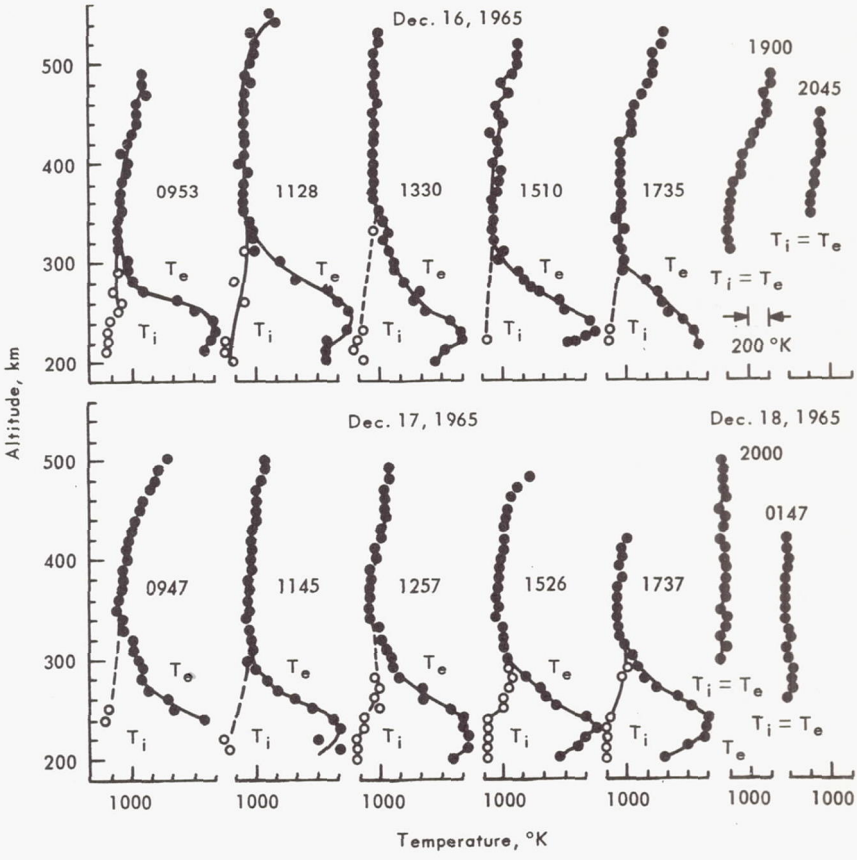


Figure 5.—**Electron and ion temperatures in summer, at Jicamarca, Peru.**

100 mV/m have been measured. At altitudes around 2000 kilometers in the ionosphere, electric fields in the range 1 to 3 mV/m have been observed.

Boyd (ref. 20) briefly discusses methods of measuring electric fields in space. In particular, he points out the advantages of making boom measurements on spacecraft at space potential rather than at floating potential.

Wright and Fedor (ref. 21) have compared the ionospheric drift velocities obtained by the "spaced receiver" radio method with simultaneously observed motions of luminous trails emitted from rockets. The rocket data provide neutral wind velocities, while the radio method measures the velocity of a diffraction pattern over the ground. The relationship between this diffraction pattern velocity and actual wind velocities in the ionosphere is open to question. Wright and Fedor concentrated on data at sporadic E-altitudes, where the altitude of the radio "wind" is unambiguous. They found that the neutral and radio wind directions always agreed well. The

magnitudes of the winds, however, showed more scatter. On roughly half the occasions examined, the magnitudes as well as directions were in good agreement. On other occasions, however, there was a factor of 2 discrepancy, which could be interpreted either as a motion of ionized irregularities with half the speed of the neutral wind, or in terms of a corrected diffraction theory which would require the velocity of the diffraction pattern on the ground to be equal to that of the irregularities (rather than twice as fast). Further work is clearly required here, not only to investigate the theoretical problems raised but also to determine whether the radio-wind determinations can be used to obtain meaningful motional data during the day when rocket chemical releases cannot be seen against the bright sky background.

Maynard (ref. 22) reported on the measurement of ionospheric currents off the coast of Peru, with a rocket-borne proton magnetometer. On the dip equator a single intense sheet of current was seen centered on 109 kilometers. North of this, however, two current layers were seen centered on 100 and 120 kilometers. On another occasion, a negative current was observed near 109 kilometers. The last two observations do not seem to fit our present theoretical models.

Further laboratory measurements of change-transfer and ion-atom interchange reactions involving oxygen and nitrogen have been made, and agreement is now being obtained by different workers using different techniques. Warneck (ref. 23) used a photoionization mass spectrometer and achieved temperatures of 400° to 800° K for N_2^+ and 700° to 1400° K for O^+. No significant temperature dependence was found for most of the reactions, with the possible exception of $O^+ + O_2 \rightarrow O_2^+ + O$, for which the data were not sufficiently conclusive. Schmeltekopf et al. (ref. 24), however, point out that the reaction $O^+ + N_2 \rightarrow NO^+ + N$ can have a greatly increased rate if N_2 is vibrationally excited. For vibration states with temperatures of about 4000° K, they report an increase in reaction rate by a factor of 20. This is likely to be of importance in explaining ionospheric changes during magnetic storms and under auroral conditions.

THE UPPER IONOSPHERE

The upper ionosphere, starting at the electron peak of the F-region, is particularly suited to exploration by satellites. During 1967 our knowledge concerning the global variations of the concentrations, temperatures, and species of the ionized constituents has been significantly extended. Further work has proceeded on the plasma properties of this region, as exemplified by measurements on very-low-frequency (VLF) radio waves, sounder resonances, spacecraft wake disturbances, and particle-field interactions. In addition, with our improved knowledge of the neutral atmosphere, work has begun on the large-scale dynamics of the ionosphere.

The data obtained by Brace, Reddy, and Mayr (ref. 25) on Explorer XXII show the global variation of electron concentration and temperature, albeit at a fixed altitude of 1000 kilometers. Particularly striking are the electron temperature minima over the magnetic equator, shallow during the day but deeper at night, and the characteristic variations of electron concentration, as shown in figures 6 to 9.

Satellite observations by Knudsen and Sharp (ref. 26) of ion temperatures in the altitude range from 210 to 516 kilometers at middle and low latitudes show low values representative of the neutral gas temperature and high values corresponding to the electron temperature. In the auroral zone, ion temperatures as high as 6000° K were observed.

Ion mass spectrometry observations have become more prevalent, both on sounding rockets and on satellites, leading to a better understanding of the structure of the upper ionosphere. Hoffman (ref. 27) reported the results of a rocket flight from Wallops Island on January 17, 1964; his data are shown in figure 10. Mayr, Brace, and Dunham (ref. 28) examined synoptic data and related these to solutions of the ion continuity equations. Based on these observations, it appears He^+ does not become a predominant ion in any altitude region, and the distribution of the light ions (He^+ and H^+) cannot, in general, be explained by simple equilibrium conditions.

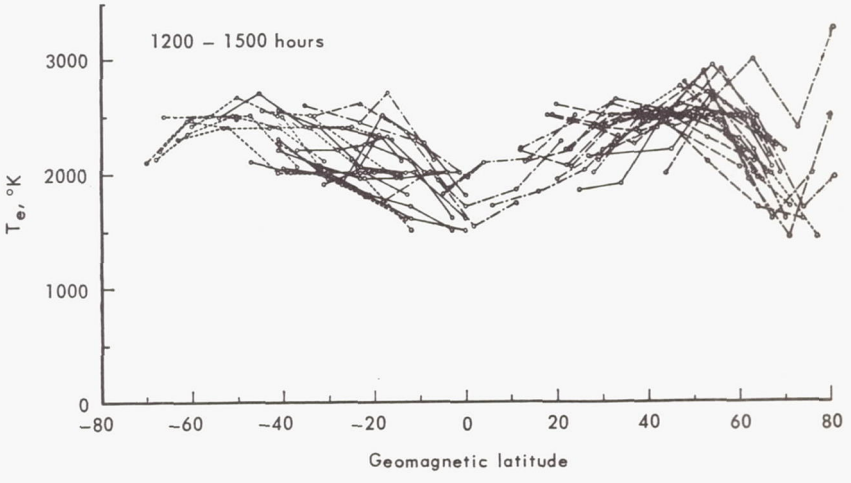


***Figure 6.*—Actual T_e data points derived from about 50 daytime satellite passes recorded in a 3-week period in February 1965. The points derived from a single pass are joined by lines to approximate the instantaneous latitudinal structure. The solid lines identify data from the longitude range 50° E–50° W; the long dashes, 100° W–130° W; the short dashes, 110° E–150° E; and the long and short dashes, 50° W–100° W.**

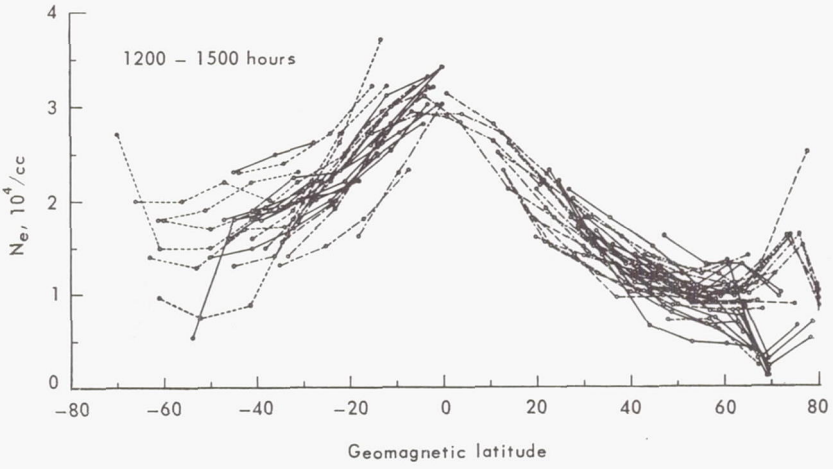


Figure 7.—Actual N_e data points derived from the same passes as discussed in figure 6.

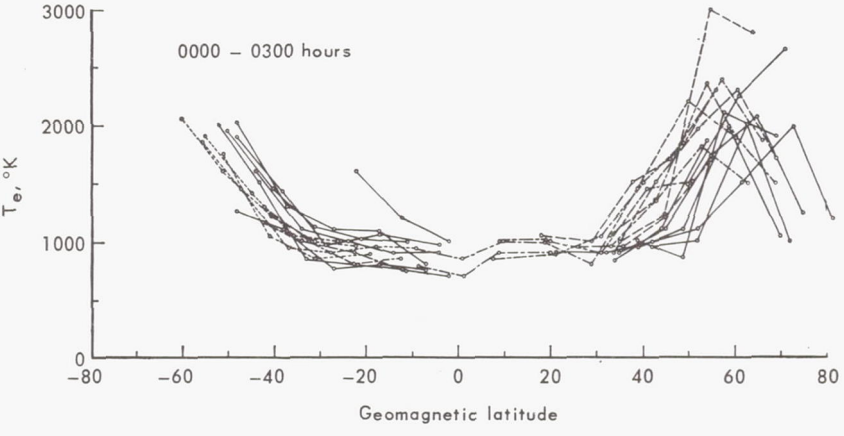


Figure 8.—Actual T_e data points from nighttime passes in the same 3-week period of figures 6 and 7.

Hoffman (ref. 29) has presented preliminary data from his ion mass spectrometer flown on Explorer XXXI. He notes that during the December 1965 through March 1966 period, He^+ was everywhere a minor constituent. He also noted a number of other minor constituents, tentatively identified as D^+, O^{2+} (or He^{2+}), and N^{2+}.

Nishida (ref. 30) has constructed a synoptic sunspot-minimum model of the topside ionosphere at latitudes above 40° N from Alouette I electron concentration profiles for the period 1962 through 1964. He notes characteristic maxima and minima in electron concentration and discusses their variation with magnetic activity.

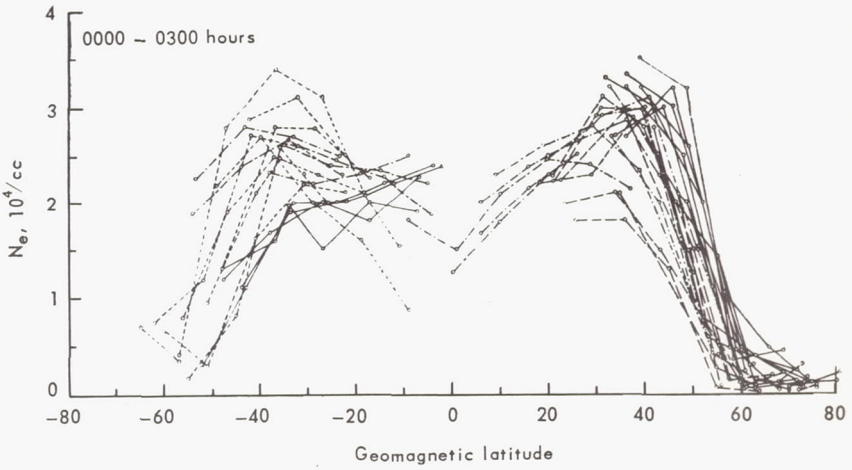


Figure 9.—Actual N_e data points corresponding to T_e data in figure 8.

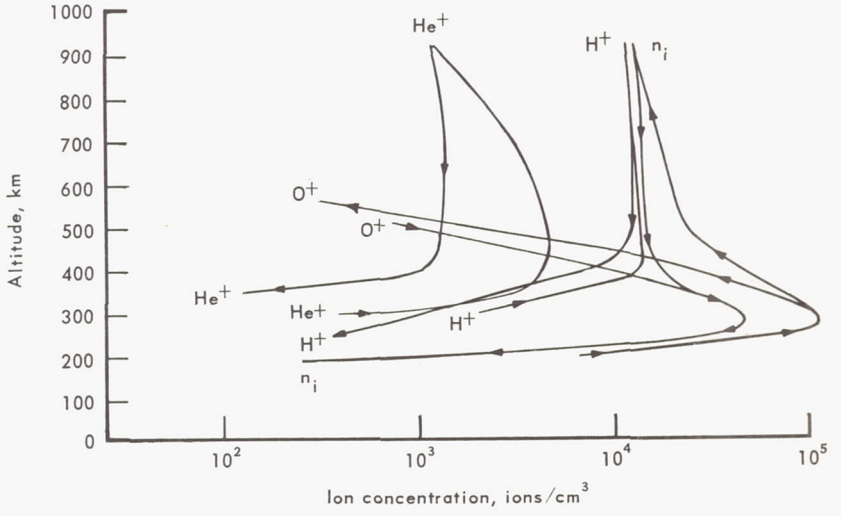


Figure 10.—Concentrations of H^+, He^+, and O^+ and total ion density as a function of altitude.

The relationship between the upper limit of the terrestrial ionosphere, i.e., the plasmapause, and magnetic activity has been further elucidated by whistler observations (Carpenter, ref. 31). In addition, *in situ* measurements with the MIT plasma probe on IMP-II have verified the general behavior of the plasmapause position as a function of time and magnetic activity (Binsack, ref. 32). The theoretical aspects of the plasmapause have been treated by Brice (ref. 33) in terms of dynamical features of the magnetosphere. It is currently believed that the plasmapause represents the

boundary between the dense terrestrial (ionospheric) plasma and the low-density plasma of solar-wind origin, and that it is in the form of a stagnation surface between convective inward motions in the magnetosphere and the co-rotating (ionospheric) plasma.

King, Legg, and Reed (ref. 34) studied the effects of three solar eclipses on the upper ionosphere using data from Alouette I. For the first two occasions, during magnetically quiet conditions, they observed a decrease of electron concentration by a factor of approximately 2 at all heights coincident with a downward movement of the F-region. During the third eclipse on June 10, 1964, no effect was observed which could be ascribed to the eclipse. This led to the conclusion that any such effect was masked by a concurrent magnetic storm. King et al. (ref. 35) also examined the behavior of the upper ionosphere during storm conditions on five occasions in the 1963 through 1966 period. They conclude that the effects of these storms were greater at lower altitudes and might be explained by vertical movements.

In an effort to investigate the dynamics of the ionosphere, Kohl and King (ref. 36) computed the wind systems which result from the pressure gradients shown on standard model atmospheres. Ion drag effects were included, and computed horizontal winds were of the order 100 m/sec for F2-peak electron concentrations of 3×10^5 cm^{-3}, and 35 m/sec for F2 peaks of 10^6 cm^{-3}. Electric fields were neglected, and ion velocities were obtained by projecting the neutral horizontal winds along lines of force of the Earth's magnetic field. At middle latitudes, this gave downward ion drifts during 08 to 20 local mean time (LMT) and upward drifts during 20 to 08 LMT. Observed perturbations in F2 layer critical frequencies were found to be in the direction that would be expected from such motions. King, Kohl, and Pratt (ref. 37) later showed how the height of the F2 electron peak, h_m F2, also follows the vertical ion drifts at high and middle latitude stations. An example is given in figure 11.

This work is important in showing how large ionospheric perturbations can be produced by large-scale motions computed from the observed behavior of the neutral atmosphere, rather than on ad hoc assumptions made about these motions.

Kimura (ref. 38) has surveyed the observations and theories of VLF emissions, with particular emphasis on the "chorus" and "hiss" types. He concludes that they can only be explained by a coherent interaction mechanism. Helliwell (ref. 39) discusses such a mechanism, where the spatial variations of the electron gyrofrequency and the Doppler-shifted wave frequency are matched. His mechanism involves the transfer of energy from kilovolt electrons with efficiencies of the order 0.1 percent, and it appears to account for the spectral shapes of some classes of VLF emission.

From ground-based whistler observations, the equatorial radius of the whistler path can be observed. Carpenter and Stone (ref. 40) observed

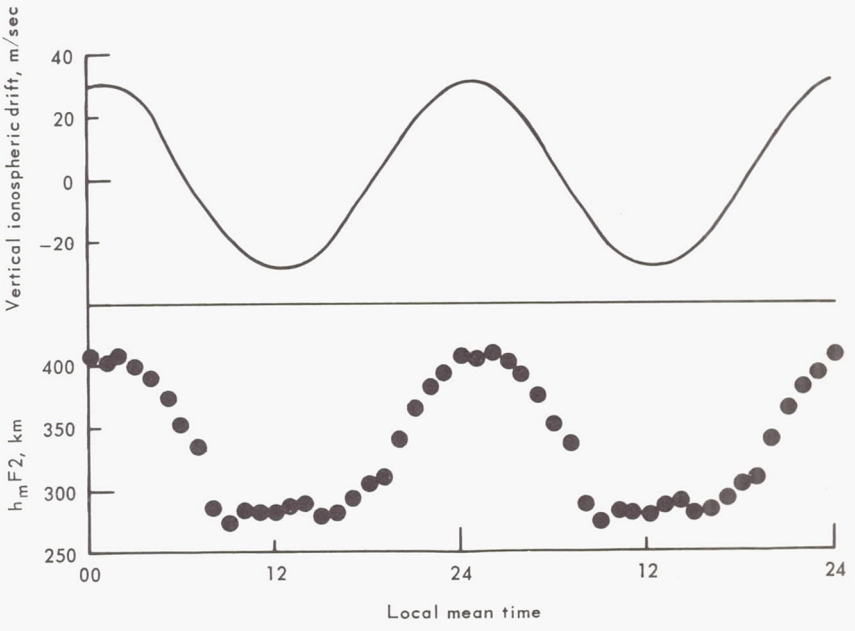


Figure 11.—**Diurnal variation of the vertical ionospheric drift at Slough (positive upward) and mean h_m F2 (quiet days, January 1950, after Schmerling and Thomas, 1955).**

fluctuations in this path during a polar substorm on July 15, 1965, and interpreted this in terms of a transient westward electric field of about 0.3 mV/m at 4 earth radii, driving the plasma inward at approximately 700 m/sec.

RADIO PROPAGATION AND RADIO PHYSICS

The study of radio emissions from satellites by observations of Doppler shifts and Faraday rotation from the ground continues to provide significant results. Observations of the total electron content of the ionosphere at high latitudes (60° to 75° N) show a secondary maximum near midnight, as illustrated in figure 12. Rai and Hook (ref. 41) ascribe this to the precipitation of low-energy electrons. Da Rosa and Smith (ref. 42) also conclude from an analysis of their electron-content observations that a downward flux of electrons at night is required to maintain the nighttime ionosphere at middle latitudes.

The variations in electron content during magnetic storms at middle latitudes were investigated by Hibberd and Ross (ref. 43). These studies indicate an initial increase, followed by a decrease below the quiet-day values and a recovery period of several days. Titheridge and Andrews (ref. 44) are in substantial agreement with these conclusions, but trace the effects of a

333-240 O—69——11

storm in winter at sunspot minimum, for 5 days. They show that the total electron content is a better indicator of the disturbed state of the ionosphere than the peak electron density.

The effect of solar flares was investigated by Garriott et al. (ref. 45) using radio signals from the geostationary satellite ATS–I, which permitted the study to be concentrated on the changes that occur with time over fixed portions of the ionosphere. For a flare on May 21, 1967, increases in electron content of about 5 percent were observed simultaneously at four stations, indicating that the effect was primarily a result of increases in ionizing radiation. These observations are shown in figure 13. The results can be explained by an increase in solar UV emission by a factor of 3 for about 100 seconds, together with some increase in the X-ray flux. Comparison with other observations showed that an X-ray enhancement alone would not account for the results.

Howard (ref. 46) has reanalyzed the data obtained by measurements of the group delay of lunar echoes from a ground-based radar. Measurements made of the electron content of the Earth's ionosphere from satellites are very important in this work, since subtraction of this contribution enables the electron content to be determined at greater distances. Howard concluded that the electron concentration in the geomagnetic tail was not markedly different from that of interplanetary space.

Farley (ref. 47) reported that the proton gyroresonance has been observed in the beam of the Jicamarca backscatter radar in Peru. This resonance was seen on the autocorrelation function of the echo when the beam was perpendicular to the magnetic field. Observations of this type enhance the capability of the installation to provide information on ion composition.

Further studies have been made of the phenomenon of resonance rectification, whereby resonances are observed at distinct frequencies when

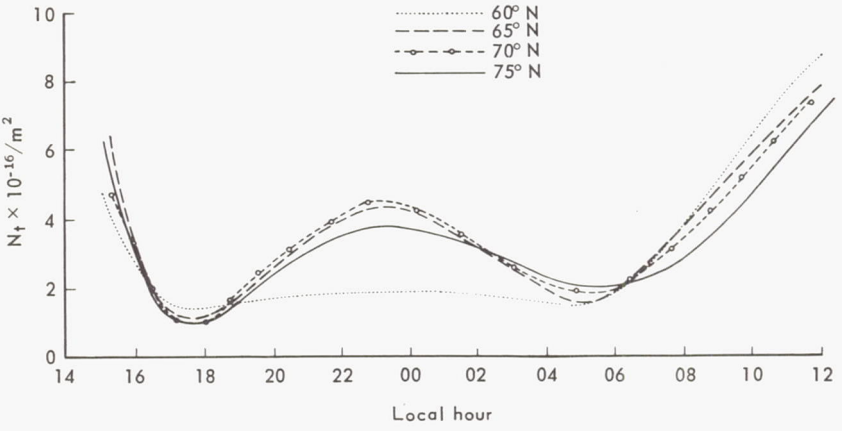


Figure 12.—**Diurnal variation of electron content during the winter period (1963–1964) at College, Alaska.**

a probe is immersed in a plasma. Crawford, Harp, and Mantei (ref. 48) presented the theory and laboratory observations of these resonances. Warm plasma theory was needed to explain the generation of two series of resonances, one at the cyclotron harmonics and another between these cyclotron harmonics.

Hagg (ref. 49) reports on another plasma phenomenon observed on the ionograms produced by Alouette II. This consists of a beat pattern between the electron gyroresonance and upper hybrid-resonance lines when the electron concentration near the satellite is low. Since the upper hybrid-resonance is always above the electron gyroresonance, this beat can be used to determine local electron concentrations in the range 8 to 100 electrons/cm^3. These resonances are thought to involve interactions with fairly large volumes of space; the electron concentration determinations are, therefore, considered to be insensitive to local disturbances from spacecraft wakes and photoemission.

Very few attempts have been made to investigate systematically the disturbed region around a spacecraft. Henderson and Samir (ref. 50) used a Langmuir probe on Ariel I and observed both the disturbance caused by the spacecraft and that caused by a spherical ion probe also on the satellite. No fluctuations of electron temperature were seen, but a region of enhanced electron concentration was observed in the center of the wake, where the electron concentration was above that observed nearby but below that in the ambient medium.

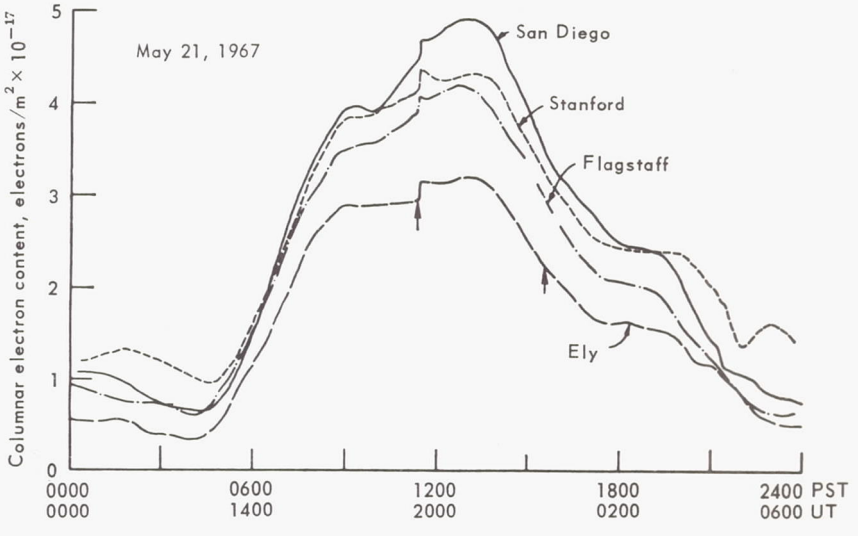


***Figure 13.*—The diurnal variation of electron content observed at Stanford University and San Diego, Calif., Flagstaff, Ariz., and Ely, Nev. The times of flare initiation are shown by arrows.**

The effect of the ion sheath around a satellite in "coupling" signals from one experiment to another has been noted on several occasions. Osborne et al. (ref. 51) describe such a phenomenon observed on Alouette I, whereby interference from a converter was seen on the VLF records in daylight, and exhibited characteristic spin modulation.

The power of radio techniques in providing information by "remote sensing" was demonstrated in a novel way on Lunar Orbiter I. Tyler et al. (ref. 52) report on their observation of the telemetry transmission from that spacecraft. Not only the direct component but also signals reflected from the Moon in the bistatic mode were observed. These components were separated by their different Doppler frequency shifts. Some correlation was seen between the amplitudes of the signal and observed lunar features. This technique has definite promise for providing surface details of Venus, which are hidden below a cloud layer too low for a photographic orbiter.

Further work was reported on the theory of the "remote resonance" by Muldrew (ref. 53). This is seen on Alouette II ionograms as a "spike" that ends on the ionogram trace rather than at the transmitter pulse. To generate these it is believed that ionospheric ducts must be present, as well as variations of electron concentration which lead to electric field strength fluctuations of about 7 percent within an electron cyclotron radius at the resonant region.

Weil and Walsh (ref. 54) have made further contributions to the difficult theory of antennas and radio field strengths in a magnetoplasma. Thermodynamic methods were used to derive general relations between conventional antenna parameters and properties of the medium. Deschamps and Kesler (ref. 55) also derived a formula for the radiation field of an arbitrary antenna in a compressible magnetoplasma.

PLANETARY IONOSPHERES

Following the success of Mariner IV in obtaining atmospheric and ionospheric data from Mars by a radio propagation experiment, a similar investigation was made of Venus by Mariner V on October 19, 1967, at a range of nearly 80 million kilometers. Two techniques were used. The occultation of the S-band telemetry (about 2000 MHz) was observed on the ground in a way similar to the Mariner IV mission (Kliore et al., ref. 56). In addition, Mariner V performed a two-frequency experiment, with phase-locked 49.8- and 423.3-MHz transmissions from the ground received on the spacecraft (Mariner Stanford Group, ref. 57). The former observations were more sensitive to the atmosphere; the latter were more sensitive to the upper ionosphere. It is interesting to note that it was necessary to correct for changes in the Earth's ionosphere (as measured from a NASA Applications Technology Satellite propagation experiment) during the occultation. Unlike the Mars observations made by Mariner IV, data were

not obtained down to the surface of the planet because of superrefraction in the dense atmosphere of Venus—an effect whose likelihood had been foreseen.

The day and night ionospheric profiles are shown in figure 14, which is taken from reference No. 57. Notable is a daytime peak electron concentration almost two orders of magnitude greater than at night and a sharp "plasmapause" during the day above 6500 kilometers (measured from the center of Venus). At night, however, the ionosphere was seen to extend to a radial distance of about 10 000 kilometers. These observations are indicative of a direct solar-wind interaction with the ionosphere of Venus, in contrast to conditions on Earth, where the ionosphere is shielded by the magnetic field and magnetosphere boundary.

CONCLUSIONS

One of the more striking trends that has emerged in recent years is the power of radio techniques to provide information by "remote sensing" and the increasing use of such techniques. Ground-based ionosondes have long

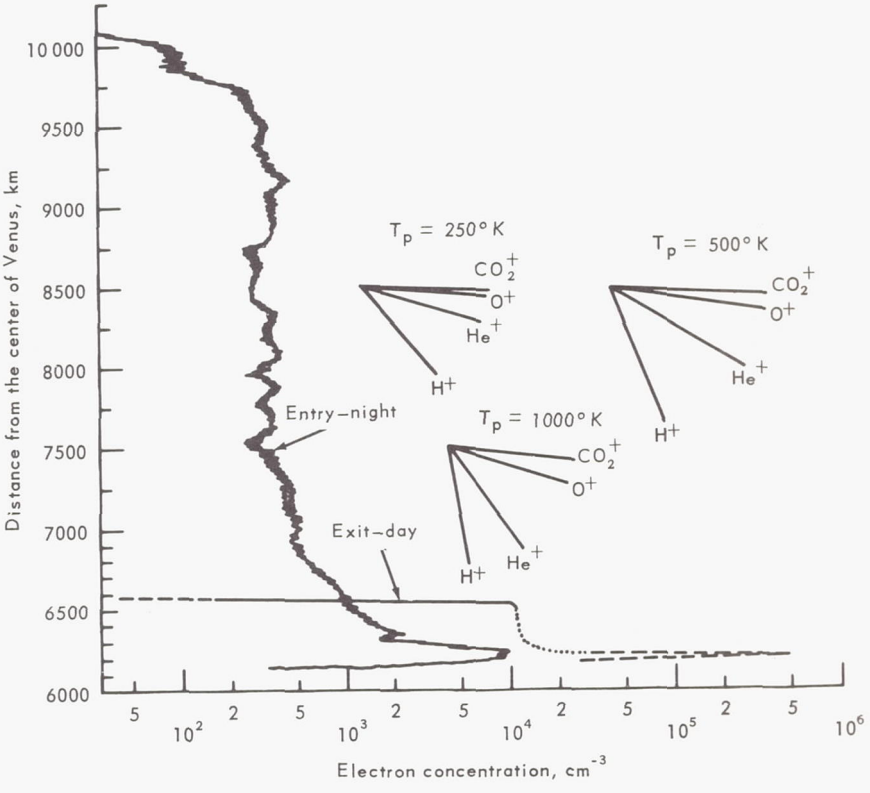


***Figure 14.*—Profiles of electron concentrations in the night and day ionospheres of Venus.**

been familiar in ionospheric work, and they provide data from the lower ionosphere *up* to the electron peak of the F-region. A logical extension of the technique was to place ionosondes on satellites, and Alouette I, Explorer XX, and Alouette II have thus provided a wealth of data from the altitude of the satellite *down* to the F-region electron peak. As a byproduct, plasma resonances have also resulted in local measurements—but less contaminated by near-surface effects on the spacecraft than from the more conventional direct measurement instruments. Radio propagation techniques have also been further developed: Total electron content measurements have been made from Earth-orbiting spacecraft, from geostationary satellites, and from interplanetary probes. Together, they provide knowledge of average electron concentrations in the ionosphere, the magnetosphere, and interplanetary space, as well as information on electron motions and irregularities. Propagation measurements from Mariner IV and V have provided enormously valuable data on the atmospheres and ionospheres of Mars and Venus. Considering the basic simplicity of the techniques used, this amounts to a veritable tour de force. Observations of very-low-frequency (VLF) waves have also been developed to the extent that ion composition, particle-wave interactions, and, under some circumstances, electric fields can also be measured. On the ground, the Thomson-scatter installations have shown their capabilities in observing electron concentration and temperature with high time resolution and have thus discovered the effects of downcoming photoelectrons. In addition, the observations of the plasma line and proton gyroresonance and the capability of observing movements of ionization have greatly enhanced the usefulness of the installations in providing data which complement, in important respects, those available from satellite-borne instrumentation.

The striking differences between the day and night ionospheres of Venus open up a new area of solar-wind/ionosphere investigation for a planet possessing essentially no magnetic field. Further study is likely to prove important in increasing our understanding of plasma interactions and will surely require a determination of the incoming solar wind and neutral atmosphere at the same time as the ionospheric measurements are being made.

Good progress has been made in investigating the thermal balance in the ionosphere. Once again, emphasis has been placed on the dynamic behavior. With continuous improvements in knowledge about the neutral atmosphere, a good beginning seems to have been made in estimating the motions caused by the subsolar pressure bulge and in estimating the resulting effect on the ionosphere. More work in this area is clearly indicated to put the theories of ionospheric drift on a firm basis and to incorporate the effects of the electric fields, which are just beginning to be reliably measured.

Further progress has been made with laboratory determinations of chemical reaction rates. Agreement is now being found in measurements of several key reaction rates by different techniques. This work has also underlined the importance of the negative ion chemistry of oxygen and its compounds at low altitudes. In the ionosphere, lack of detailed knowledge about the incoming ultraviolet flux is hampering progress in elucidating the *in situ* photochemistry. At low altitudes, further work is also needed to develop positive- and negative-ion mass spectrometers.

REFERENCES

1. KANE, J. A.; AND TROIM, J.: Rocket Measurements of D-Region Electron Number Densities. J. Geophys. Res., vol. 72, 1967, pp. 1118–1120.
2. MECHTLY, E. A.; BOWHILL, S. A.; SMITH, L. G.; AND KNOEBEL, H. W.: Lower Ionosphere Electron Concentration and Collision Frequency From Rocket Measurements of Faraday Rotation, Differential Absorption and Probe Current. J. Geophys. Res., vol. 72, 1967, pp. 5239–5246.
3. SONIN, A. A.: Theory of Ion Collection by a Supersonic Atmospheric Sounding Rocket. J. Geophys. Res., vol. 72, 1967, pp. 4547–4558.
4. HOULT, D. P.; AND KUO, T.: D-Region Mobility Spectrometer. J. Geophys. Res., vol. 72, 1967, pp. 4529–4532.
5. MAEHLUM, B.: On the "Winter Anomaly" in the Midlatitude D-Region. J. Geophys. Res., vol. 72, 1967, pp. 2287–2300.
6. SECHRIST, C. F.: A Theory of the Winter Absorption Anomaly at Middle Latitudes. J. Atmospheric Terrest. Phys., vol. 29, 1967, pp. 113–136.
7. WRIGHT, J. W.; MURPHY, C. H.; AND BULL, G. V.: Sporadic E and the Wind Structure of the E-Region. J. Geophys. Res., vol. 72, 1967, pp. 1443–1460.
8. FIOCCO, G.: On the Production of Ionization by Micrometeorites. J. Geophys. Res., vol. 72, 1967, pp. 3597–3602.
9. FEHSENFELD, A. L.; ET AL.: Laboratory Measurements of Negative Ion Reactions. Planet. Space Sci., vol. 15, 1967, 373–379.
10. BANKS, P. M.: The Temperature Coupling of Ions in the Ionosphere. Planet. Space Sci., vol. 15, 1967, pp. 77–93.
11. DALGARNO, A.; AND WALKER, J. C. G.: Ion Temperatures in the Topside Ionosphere. Planet. Space Sci., vol. 15, 1967, pp. 200–203.
12. NAGY, A. F.; AND WALKER, J. C. G.: Direct Measurements Bearing on the Question of the Nighttime Heating Mechanism in the Ionosphere. Planet. Space Sci., vol. 15, 1967, pp. 95–101.
13. CARRU, H.; PETIT, M.; AND WALDTEUFEL, P.: Mesures de Temperatures Electroniques et Ioniques par Diffusion Incoherente. J. Atmospheric Terrest. Phys., vol. 29, 1967, pp. 351–366.
14. CARLSON, H. C.: Ionospheric Heating by Magnetic Conjugate-Point Photoelectrons. J. Geophys. Res., vol. 71, 1966, pp. 195–199.
15. EVANS, J. V.: Midlatitude F-Region Densities and Temperatures at Sunspot Minimum. Planet. Space Sci., vol. 15, 1967, pp. 1387–1405.
16. THOMAS, G. R.; AND VENABLES, F. H.: The Effect of Diurnal Temperature Changes in the F2-Layer. J. Atmospheric Terrest. Phys., vol. 29, 1967, pp. 621–640.
17. FARLEY, D. T.; MCCLURE, J. P.; STERLING, D. L.; AND GREEN, J. L.: Temperature and Composition of the Equatorial Ionosphere. J. Geophys. Res., vol. 72, 1967, pp. 5837–5851.

18. Föppl, H.; et al.: Artificial Strontium and Barium Clouds in the Upper Atmosphere. Planet. Space Sci., vol. 15, 1967, pp. 357–372.
19. Haerendel, G.; Lüst, R.; and Rieger, E.: Motion of Artificial Ion Clouds in the Upper Atmosphere. Planet. Space Sci., vol. 15, 1967, pp. 1–18.
20. Boyd, R. L. F.: Measurement of Electric Fields in the Ionosphere and Magnetosphere. Space Sci. Rev., vol. 7, 1967, pp. 230–237.
21. Wright, J. W.; and Fedor, L. S.: Comparison of Ionospheric Drift Velocities by the Spaced Receiver Technique With Neutral Winds From Luminous Rocket Trails. Space Res., vol. 7, North-Holland Publ. Co. (Amsterdam), 1967, pp. 67–72.
22. Maynard, N. C.: Measurements of Ionospheric Currents off the Coast of Peru. J. Geophys. Res., vol. 72, 1967, pp. 1863–1876.
23. Warneck, P.: Studies of Ion-Neutral Reactions by a Photoionization-Mass Spectrometer Technique—III Several Ionospheric Reactions. Planet. Space Sci., vol. 15, 1967, pp. 1349–1359.
24. Schmeltekopf, A. L.; et al.: Reaction of Atomic Oxygen Ions With Vibrationally Excited Nitrogen Molecules. Planet. Space Sci., vol. 15, 1967, pp. 401–406.
25. Brace, L. H.; Reddy, B. M.; and Mayr, H. G.: Global Behavior of the Ionosphere at 1000 km Altitude. J. Geophys. Res., vol. 72, 1967, pp. 265–284.
26. Knudsen, W. C.; and Sharp, G. W.: Ion Temperatures Measured Around a Dawn-Dusk-Auroral Zone Satellite Orbit. J. Geophys. Res., vol. 72, 1967, pp. 1061–1072.
27. Hoffman, J. H.: A Mass Spectrometric Determination of the Composition of the Nighttime Topside Ionosphere. J. Geophys. Res., vol. 72, 1967, pp. 1883–1888.
28. Mayr, H. G.: Brace, L. H.; and Dunham, G. S.: Ion Composition and Temperature in the Topside Ionosphere. J. Geophys. Res., 1967, pp. 4391–4404.
29. Hoffman, J. H.: Composition Measurements of the Topside Ionosphere. Science, vol. 155, 1967, p. 322–324.
30. Nishida, A.: Average Structure and Storm-Time Change of the Polar Topside Ionosphere at Sunspot Minimum. J. Geophys. Res., vol. 72, 1967, pp. 6051–6061.
31. Carpenter, D. L.: Relations Between the Dawn Minimum in the Equatorial Radius of the Plasma-pause and Dst, Kp and Local K at Byrd Station. J. Geophys. Res., vol. 72, 1967, pp. 2969–2971.
32. Binsack, J. H.: Plasmapause Observations With the MIT Experiment on IMP II. J. Geophys. Res., vol. 72, 1967, pp. 5231–5238.
33. Brice, N. M.: Bulk Motion of the Magnetosphere. J. Geophys Res., vol. 72, 1967.
34. King, J. W.; Legg, A. J.; and Reed, K. C.: Observations of the Topside Ionosphere During Three Solar Eclipses. J. Atmospheric Terrest. Phys., vol. 29, 1967, pp. 1365–1371.
35. King, J. W.; et al.: The Behavior of the Topside Ionosphere During Storm Conditions. J. Atmospheric Terrest. Phys., vol. 29, 1967, pp. 1355–1363.
36. Kohl, H.; and King, J. W.: Atmospheric Winds Between 100 and 700 km and Their Effects on the Ionosphere. J. Atmospheric Terrest. Phys., vol. 29, 1967, pp. 1045–1062.
37. King, J. W.; Kohl, H.; and Pratt, R.: The Effect of Atmospheric Winds on the F2-Layer Peak at Middle and High Latitudes. J. Atmospheric Terrest. Phys., vol. 29, 1967, pp. 1529–1539.
38. Kimura, I.: On Observations and Theories of the VLF Emissions. Planet. Space Sci., vol. 15, 1967, pp. 1427–1462.

39. HELLIWELL, R. A.: A Theory of Discrete VLF Emissions From the Magnetosphere. J. Geophys. Res., vol. 72, 1967, pp. 4773–4790.
40. CARPENTER, D. L.; AND STONE, K.: Direct Detection by a Whistler Method of the Magnetospheric Electric Field Associated With a Polar Substorm. Planet. Space Sci., vol. 15, 1967, pp. 395–397.
41. RAI, D. B.; AND HOOK, J. L.: Total Electron Content and Its Variations in the Auroral-Zone Ionosphere During Winter. J. Geophys. Res., vol. 72, 1967, pp. 5319–5324.
42. DA ROSA, A. V.; AND SMITH, F. L., III: Behavior of the Nighttime Ionosphere. J. Geophys. Res., vol. 72, 1967, 1829–1836.
43. HIBBERD, F. H.; AND ROSS, W. J.: Variations in Total Electron Content and Other Ionospheric Parameters Associated With Magnetic Storms. J. Geophys. Res., vol. 72, 1967, pp. 5331–5337.
44. TITHERIDGE, J. E.; AND ANDREWS, M. K.: Changes in the Topside Ionosphere During a Large Magnetic Storm. Planet. Space Sci., vol. 15, 1967, pp. 1157–1167.
45. GARRIOTT, O. K.; ET AL.: Solar Flare Effects in the Ionosphere. J. Geophys. Res., vol. 72, 1967, pp. 6099–6103.
46. HOWARD, H. T.: Cislunar Electron Content as Determined by Radar Group Delay Measurements. J. Geophys. Res., vol. 72, 1967, pp. 2729–2735.
47. FARLEY, D. T., JR.: Proton Gyroresonance Observed in Incoherent Scattering From the Ionosphere. The Physics of Fluids, vol. 10, 1967, pp. 1584–1586.
48. CRAWFORD, F. W.; HARP, R. S.; AND MANTEI, T. D.: Resonance-Rectification Effects in Warm Magnetoplasmas. J. Appl. Phys., vol. 38, 1967, pp. 5077–5082.
49. HAGG, E. L.: Electron Densities of 8–100 Electrons CM^{-3} Deduced From Alouette II High-Latitude Ionograms. Can. J. Phys., vol. 45, 1967, pp. 27–36.
50. HENDERSON, C. L.; AND SAMIR, U.: Observations of the Disturbed Region Around an Ionospheric Spacecraft. Planet. Space Sci., vol. 15, 1967, pp. 1499–1513.
51. OSBORNE, F. J. F.; ET AL.: Plasma-Induced Interference in Satellite VLF Receivers. Can. J. Phys., vol. 45, 1967, pp. 47–56.
52. TYLER, G. L.; ET AL.: Bistatic-Radar Detection of Lunar Scattering Centers With Lunar Orbiter I. Science, vol. 157, 1967, pp. 193–195.
53. MULDREW, D. B.: Delayed Generation of an Electromagnetic Pulse in the Topside Ionosphere. J. Geophys. Res., vol. 72, 1967, pp. 3777–3794.
54. WEIL, H.; AND WALSH, D.: Thermal Radiation Fields and Antenna Parameters in Magnetoplasma. Radio Sci., vol. 2, 1967, pp. 225–239.
55. DESCHAMPS, G. A.; AND KESLER, O. B.: Radiation of an Antenna in a Compressible Magnetoplasma. Radio Sci., vol. 2, 1967, pp. 757–767.
56. KLIORE, A.; ET AL.: Atmosphere and Ionosphere of Venus From the Mariner V S-Band Radio Occultation Measurement. Science, vol. 158, 1967, pp. 1683–1688.
57. MARINER STANFORD GROUP: Venus: Ionosphere and Atmosphere as Measured by Dual-Frequency Radio Occultation of Mariner V. Science, vol. 158, 1967, pp. 1678–1683.

Page Intentionally Left Blank

PARTICLES AND FIELDS

L. D. Kavanagh, Jr., and A. W. Schardt
Office of Space Science and Applications, NASA

E. C. Roelof
Goddard Space Flight Center, NASA

Page Intentionally Left Blank

Particles and Fields

INTRODUCTION

In sharp contrast to the first few faltering steps that were being taken in 1957 to place a set of Geiger counters in minimal Earth orbit, this second decade of space exploration has started with sophisticated experiments in the area of particles and fields. Particle measurements in space with Geiger counters have been augmented by an array of other flight-qualified instruments, including solid-state devices, scintillation crystals, and plasma detectors. Charged particles of every energy from a fraction of an electron volt up to several hundred MeV have been measured in space, and their directions determined. Magnetic fields whose strength is more than four orders of magnitude smaller than the Earth's surface field have been measured accurately from as far away as the planets Venus and Mars; and substantial progress has been made toward developing detectors capable of measuring electric fields in a tenuous plasma. In the Earth's magnetosphere, random observations of particles and fields have given way to precise measurements conducted for the purpose of specific investigations. The plasma and magnetic fields near the Moon have been studied from lunar orbit. A small but highly informative body of data has been obtained in the vicinity of Venus and Mars, and a great deal of information is now available about the interplanetary medium in between. We have reached the point at which automated exploration as near to the Sun as Mercury and as far away as the asteroidal belt and Jupiter is practical.

This article, following the sequence of review papers begun in references 1 to 3, attempts to summarize the progress made since 1966 in the area of particles and fields. The major spacecraft accumulating data of interest to the particles and fields discipline during this time are listed in table I, along with salient features of their orbits and the times of active data transmission. Figures 1, 2, and 3 illustrate graphically the regions of space covered by these satellites and probes, and the appendix lists the operating scientific apparatus on board.

As can be seen from figures 1 and 2, virtually the entire volume of space from the upper atmosphere of the Earth out to the orbit of the Moon was monitored by a satellite during 1967. A variety of satellites in low- and high-inclination orbits not shown in the figures swept through the inner magneto-

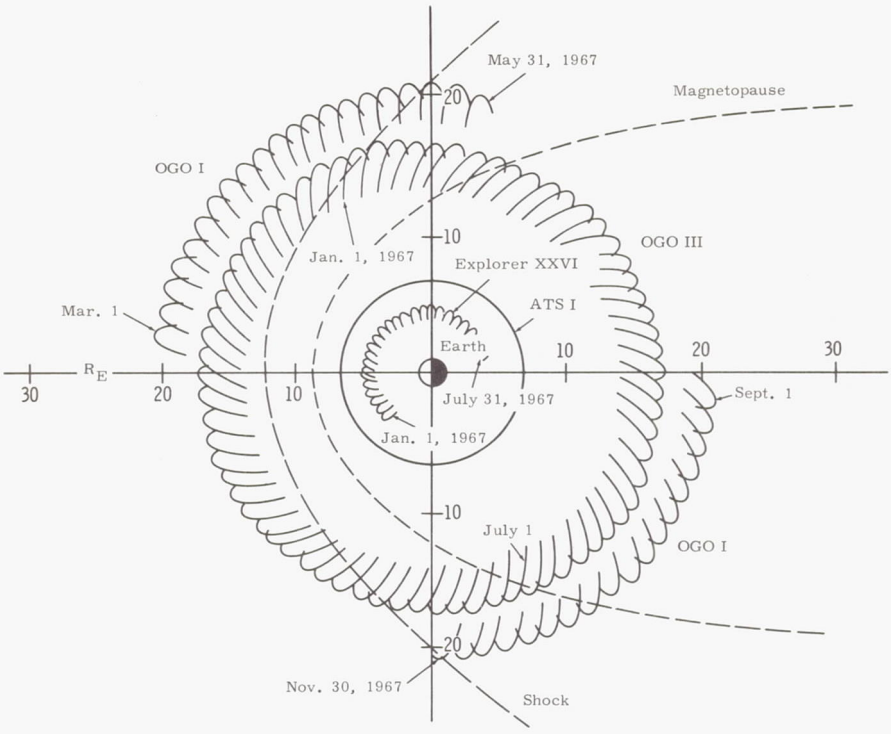


Figure 1.—**Apogee distance, in units of Earth radii R_E, and projection on the plane of the ecliptic of the Sun-Earth-probe (SEP) angle are shown for OGO-I, OGO-III, and Explorer XXVI. The inclination of the orbits (table I) is not illustrated. Also shown is the circular path traced out by ATS-I as it corotates with the Earth.**

sphere. In the outer magnetosphere and in the magnetopause and bow shock regions, many of the active satellites had orbits that were inclined to the equatorial plane, so that the coverage extended well above and below the equator. The Applications Technology Satellite (ATS–I) monitored the magnetosphere from a geostationary orbit above the Pacific Ocean. Four Orbiting Geophysical Observatory (OGO) satellites, six Air Force-launched Vela satellites with inclined circular orbits, the Explorer XXVI satellite, and the Environmental Radiation Satellite (ERS XVIII) all monitored various parts of the magnetosphere. Explorers XXVIII and XXXIV monitored the geomagnetic tail region and the region of interplanetary space just outside the Earth's bow shock. Explorer XXXIII, with an orbit near the ecliptic plane, investigated space out to the vicinity of lunar orbit. Explorer XXXV orbited the moon itself. As shown in figure 3, the interplanetary medium was examined by three Pioneer spacecraft, along with Mariner IV. Two probes reached Venus in 1967: the Russian Venera

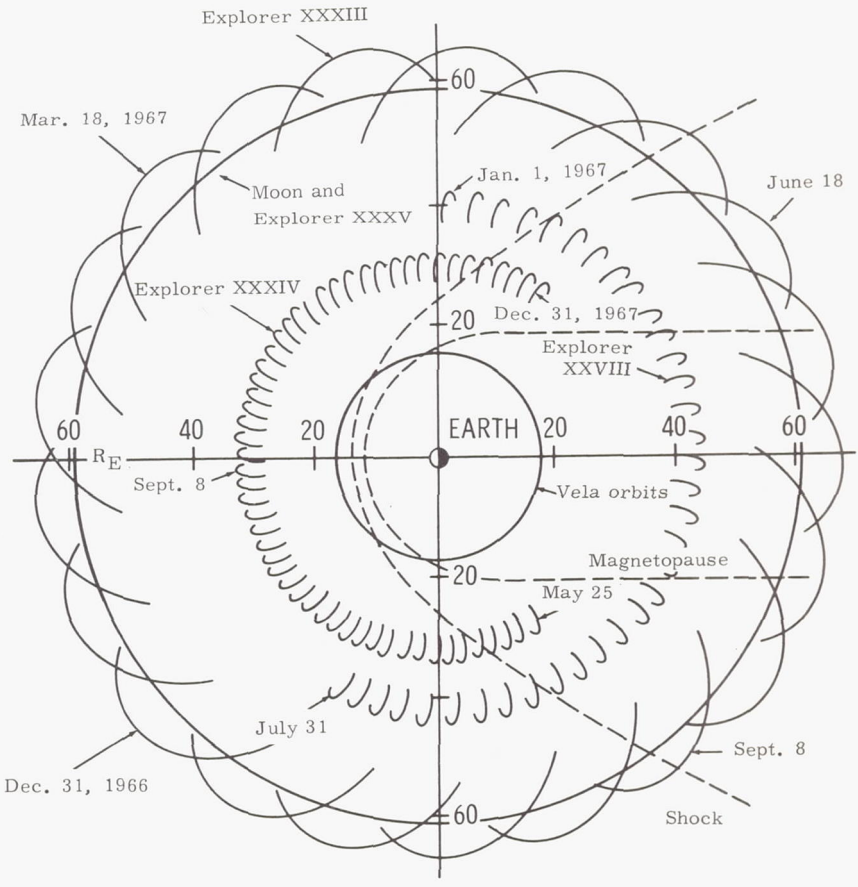


***Figure 2.*—Apogee distance, in units of R_E, and projection in the plane of the ecliptic of the SEP angle are shown for Explorers XXVIII, XXXIII, and XXXIV. The satellite orbits are inclined (table I) and do not cross the magnetopause and bow shock at the precise points indicated.**

4 craft, which landed on October 18, 1967, and Mariner V, which passed within about 4000 kilometers of the planetary surface on the following day.

The solar wind dominates interplanetary space at least out to the orbit of Jupiter (at 5.0 astronomical units (AU) from the Sun) and probably out to 50 or even 100 AU. Studies of the interaction of the solar wind with the geomagnetic field have divulged that the solar wind acts like a supersonic fluid on that scale size, even though collisions between the individual particles are unimportant. As yet poorly understood interactions between the ions, magnetic field, and waves in the solar wind have been called on to explain the magnetohydrodynamic behavior. Recently, we had the first

Table I.—*Major Particles and Fields Spacecraft Operating During 1967* [a]

Spacecraft	Launch	Perigee altitude, km	Apogee altitude, km	Inclination, deg	Period, hr	Months operated
						J F M A M J J A S O N D
Apogee Less Than 8 Earth Radii						
1963–38C	Sept. 28, 1963	1 074	1 136	90	1.8	
Relay II (1964–3A)	Jan. 21, 1964	2 070	7 428	46	3.3	
Explorer XXVI (EPE IV) (1964–86A)	Dec. 21, 1964	306	26 205	20	7.6	
OGO II (1965–81A)	Oct. 14, 1965	420	1 511	87	1.7	
OV3–1 (1966–34A)[b]	Apr. 22, 1966	358	5 657	82	2.5	
OV3–4 (1966–52A)[b]	June 10, 1966	643	4 727	41	2.4	
OV3–3 (1966–70A)[b]	Aug. 4, 1966	362	4 483	81	2.3	
OV3–2 (1966–97A)[b]	Oct. 28, 1966	305	1 597	82	1.7	
ATS I (1966–110A)	Dec. 6, 1966	35 557	35 576	0	23.9	
Aurora I (1967–65B)	June 29, 1967	3 797	3 949	90	2.9	
OGO IV (1967–73A)	July 28, 1967	409	866	86	1.6	
Apogee Greater Than 8 Earth Radii						
Vela IIA+B (1964–40A+B)[c]	July 17, 1964	102 754	103 875	38	100.4	
OGO I (1964–54A)	Sept. 5, 1964	4 930	144 824	41	64.0	
Explorer XXVIII (IMP III) (1966–58A)	May 29, 1965	196	264 247	34	143.2	
Vela IIIA+B (1965–58A+B)[c]	July 20, 1965	105 583	117 344	35	111.8	
OGO III (1966–49A)	June 7, 1966	715	121 688	39	48.5	
Explorer XXXIII (AIMP I) (1966–58A)	July 1, 1966	40 800	476 233	8	[d] 377.1	

Vela 4 A+B (1967–40A+B)[c]	Apr. 28, 1967	107 155	115 227	33	111.2
ERS XVIII (1967–40C)	Apr. 28, 1967	10 284	109 564	34	47.2
Explorer XXXIV (1967–51A)	May 24, 1967	242	214 382	67	106.0

Planetary and Interplanetary Probes

Spacecraft	Launch		Months operated
			J F M A M J J A S O N D
Mariner IV (1964–77A)	Nov. 28, 1964	Mars flyby, 1.11 AU perihelion, 1.57 AU aphelion. Mars encountered July 14, 1965.	
Pioneer VI (1965–105A)	Dec. 16, 1965	In interplanetary medium, 0.81 AU perihelion, 0.99 AU aphelion.	
Pioneer VII (1966–75A)	Aug. 17, 1966	In interplanetary medium, 1.01 AU perihelion, 1.13 AU aphelion.	
Venera IV (1967–58A)	June 12, 1967	Soft landed on Venus Oct. 18, 1967.	
Mariner V (1967–60A)	June 14, 1967	Venus flyby, 0.56 AU perihelion, 0.73 AU aphelion. Venus encountered Oct. 19, 1967.	
Explorer XXXV (1967–70A)	July 19, 1967	In lunar orbit, 805 km perilune, 7400 km apolune.	
Pioneer VIII (1967–123A)	Dec. 13, 1967	In interplanetary medium, 1.00 AU perihelion, 1.10 AU aphelion.	

[a] Except for Venera 4, U.S.S.R. spacecraft have not been included in this table, due to lack of definitive information on detector complements and data returned. As of Dec. 31, 1967, the U.S.S.R. has launched 198 Cosmos satellites, 13 lunar probes, and 7 interplanetary probes.

[b] The OV3 satellites are not monitored continuously.

[c] Vela satellites are placed into nearly identical circular orbits, with A and B payloads 180° out of phase. Orbital parameters quoted are for A payloads.

[d] This is a sample orbit. Because of perturbations, apogee varies about 60 000 km and inclination by about 18°.

333–240 O—69——12

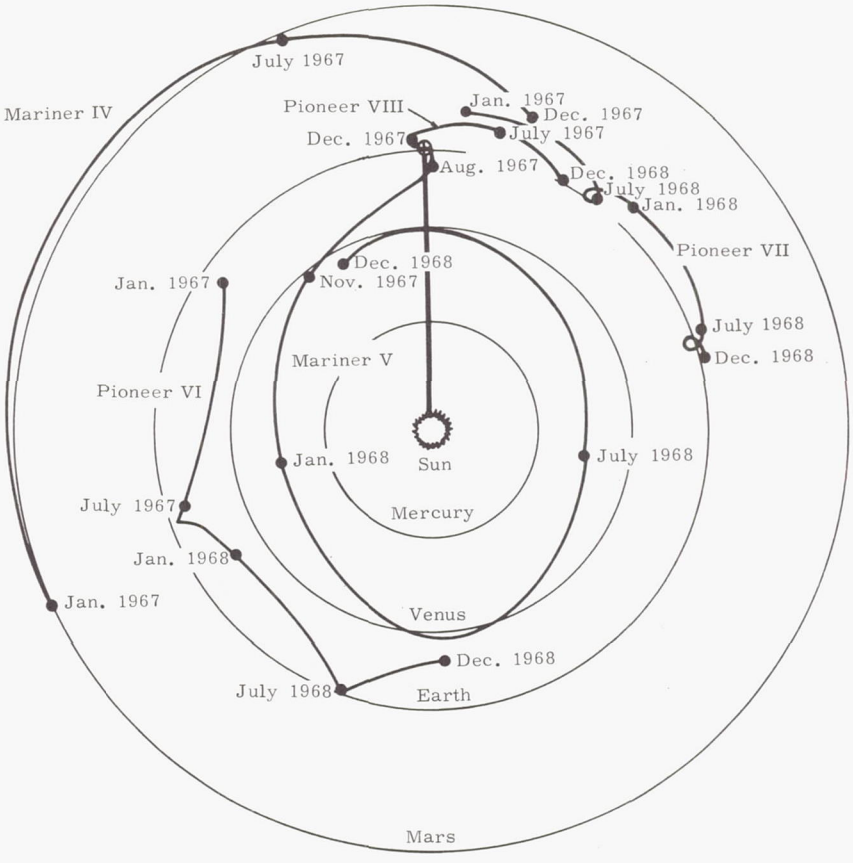


Figure 3.—**Trajectories of deep-space probes with respect to the Earth-Sun system, using rotating coordinates.**

opportunity to study solar-wind interactions with the Moon and to obtain an initial picture of solar-wind interaction with Venus and Mars.

Interactions with the Moon were studied in detail with a lunar-orbiting satellite, Explorer XXXV. Contrary to expectations, no bow shock was found around the Moon as had been the case for the Earth. A diamagnetic cavity was discovered behind the Moon in the wake left by the solar wind. In this plasma-free region in the lunar shadow, the magnetic-field strength is higher than in the interplanetary medium caused, at least partially, by electric currents set up in the adjacent plasma. It has been shown rather definitively that interplanetary magnetic-field fluctuations pass unimpeded and undiminished through the body of the Moon, and that there is no apparent pileup of magnetic field on the sunward side of the Moon, as had been predicted previously. The observed phenomenology has been ex-

plained quite well in terms of a single-particle description of the solar wind. Theoretical analysis is being continued to assess the role of collective or fluidlike behavior in interactions at this scale. Apparently, solar-wind particles strike the lunar surface, are neutralized, and can no longer interact with the magnetic field of the solar wind; thus, individual particles near the lunar surface are not coupled to the solar wind and collective behavior is minimal.

The interactions of the solar wind with Venus and Mars are intermediate between the extremes represented by the Earth and the Moon. A bow shock in the solar wind was discovered around Venus by Mariner V and Venera 4, and a weak shock around Mars has been tentatively identified from Mariner IV observations. In the case of Venus, the absence of a planetary magnetic field permits the solar wind to impinge directly on the Venusian ionosphere. An ionospheric current system is produced that is responsible for the formation of the shock. For Mars, the interaction could be with the ionosphere, as in the case of Venus, or alternately with a weak Martian magnetic field. In that case the dipole moment of Mars would be about 2×10^{-4} of that of the Earth.

The bow shock and magnetosphere of the Earth have been investigated in depth both experimentally and theoretically in efforts to determine their structure, stability, and response to solar-wind parameters. A rigorous model of a collisionless shock has been derived that can account for most of the experimental observations of plasma parameters at the Earth's bow shock (change in plasma density, magnetic field, and spectrum of magnetic fluctuations both upstream and downstream from the shock). This constitutes a major advance in our understanding of processes in collisionless plasmas, because previous descriptions were based only on a hydrodynamic analog. Further studies of nonthermal but low-energy plasma (10 eV to 50 keV) in the magnetosphere have led to new insight. Field-line merging in the geomagnetotail has been established, and a reason has been found for the absence of thermal plasma beyond about 4 Earth radii (R_E). Apparently, plasma is convected across the magnetosphere in the region between the plasmapause (at 4 to 5 R_E) and the magnetopause (at 8 to 10 R_E). This convection is driven by a large-scale electric field; various theories have been proposed to explain the existence of such a field. Substantial advances are being made in our understanding of many other magnetospheric processes, but they are not discussed here because they were summarized recently in reference 3.

Detailed investigations of the solar wind itself through the use of high-apogee satellites and interplanetary probes have disclosed the presence of frequent discontinuities in the plasma and magnetic-field properties, shock waves and hydromagnetic waves traveling through the interplanetary medium, and an overriding sector and filamentary structure in the interplanetary magnetic field. These properties have been found to correlate to

some extent with geomagnetic storm phenomena as seen on Earth. In addition, a temperature anisotropy has been found in the solar wind, in which particles traveling parallel to the local magnetic field have greater thermal energy than those traveling perpendicular to it. Some preliminary measurements of the heavy ion component of the solar wind have been made, and they should eventually yield information on the composition and temperature of the solar corona, as well as on atomic collisional and recombination processes occurring in the interplanetary medium.

The year 1967 was a period of increasing solar activity, and a number of solar flares associated with new active centers were observed. The distribution of satellites and space probes (figs. 1 and 3) permitted observations of the energetic particles produced by these flares at several points in the solar system. For the first time we were able to observe not only high-energy protons (>30 MeV) but also low-energy protons from 100 keV to 30 MeV and electrons from 40 keV to several MeV. In addition, the angular distribution of these particles could be measured relative to the local interplanetary magnetic field.

Substantial revisions have been made in our understanding of solar cosmic rays and of their propagation through the solar system. We no longer believe that all energetic particles are produced in one impulsive event during the flash phase of the flare. We have found proton precursors in some flares and have evidence that energetic particles continue to leave the sight of the flare for hours or even days. It may be concluded, therefore, that protons are either accelerated to a few MeV continuously or are magnetically confined near the active region and leak out slowly. Once they have left the vicinity of the Sun, the protons and electrons travel with little scattering along magnetic-field lines at least out to the orbit of Earth. The particle flux observed at any position around the Sun depends primarily on the intensity of particles injected at the feet of the field lines near the Sun and only to a minor degree on cross-field diffusion in interplanetary space.

Numerous correlations have been established between optical observations, the character of flare-associated radio and X-ray bursts, the position of the flare, and the energy spectrum and time history of observed particles. Particularly striking are the correlations between energetic electrons and type III radio bursts. Each solar flare, however, appears to be a special case, and as yet no consistent picture of a "typical flare event" has emerged. Thus, the wealth of processes provide a continuing challenge to the investigators who are trying to unravel the various plasma processes occurring in the solar "atmosphere."

THE SOLAR WIND

More than half a century ago, it was suggested that magnetic storms, aurorae, and the direction of comet tails could all be explained by the

existence of a steady stream of charged particles emanating radially from the Sun. However, these suggestions were not accepted by the general scientific community at the time, partly because of other errors in the theories and partly because of conflicting theories which were more popular or more vociferously professed. The charged particle picture gained more general acceptance from 1950 to 1960 and has now been verified in substantial detail by direct measurements in space. Dessler (ref. 4) has recently reviewed the accepted solar-wind theory and its historical development. In other review papers, Axford (ref. 5) placed the emphasis on observational results, and Wilcox (ref. 6) on the effect of solar photospheric fields on the structure of the solar wind.

It has been well established that the solar wind near the Earth consists primarily of protons and electrons, with a density of 3 to 10 protons per cm^3 that move with a velocity of 300 to 500 km/sec nearly radially away from the Sun. The temperature of this plasma falls generally into the range of 10^4 to 10^6 °K. A magnetic field of 3 to 10 γ ($1\ \gamma = 10^{-5}$ gauss) is embedded in it. The origin of this field has been traced back to the solar photosphere, and the general structure of the photospheric field organizes the solar wind into sectors of dominant magnetic-field direction. Recent research in this area has been concentrated on following changes of the average properties of the solar wind with the solar cycle and on studying more detailed plasma properties such as temperature anisotropy, plasma instabilities, and collisionless shocks. Some attention has also been given to the astrophysical implication of "stellar winds" on the formation and evolution of stars and planets.

Sector Structure and Filaments

Magnetic field from the surface of the Sun becomes frozen into the solar-wind plasma because of its high conductivity. As a result, the lines of magnetic force are stretched out along the radial path of the plasma. Under the combined action of solar rotation and the radial plasma velocity, the interplanetary magnetic field assumes the configuration of an Archimedes spiral, as illustrated in figure 4. This figure also demonstrates the sector structure of the field that was first noted by Wilcox and Ness (ref. 7); that is, the distinct, large regions in which the interplanetary magnetic field points predominantly toward the Sun or predominantly away. These sectors, which appear to be associated with large areas of directed magnetic field on the solar surface, rotate past the Earth with a regularity associated with the solar rotational period. A single sector requires 6 or 7 days to pass the Earth.

Sector structure is only a gross feature of the interplanetary magnetic field; variations in such quantities as solar-wind velocity tend to mar the regularity of appearance of the sector boundaries (ref. 8). However, in spite of these fluctuations the sectors display a definite structure. As shown

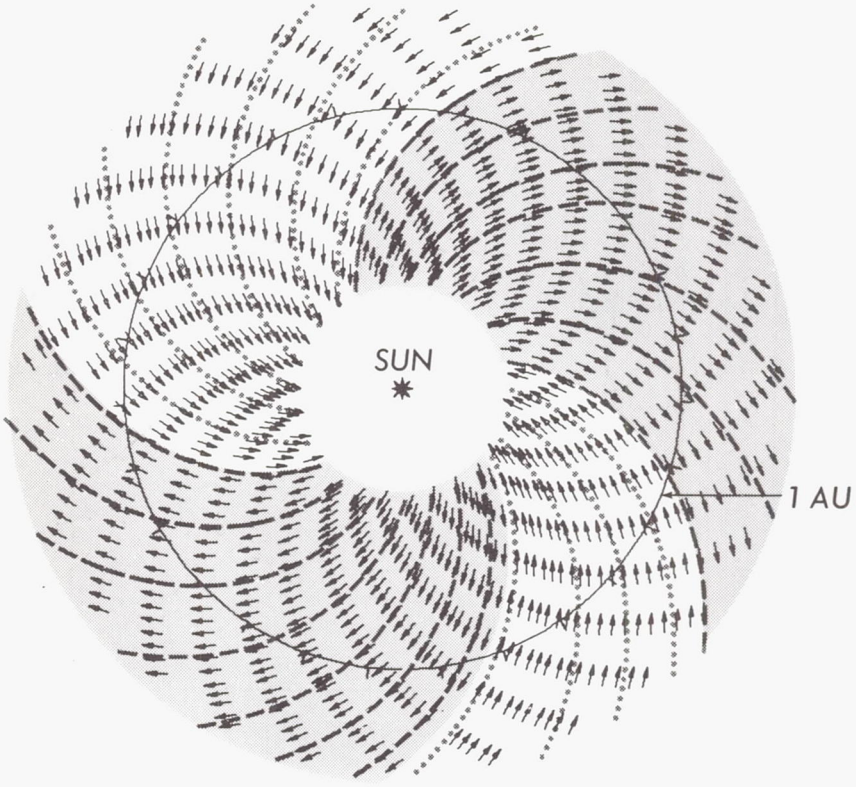


Figure 4.—Average sector pattern of interplanetary magnetic field (December 1963 to February 1964) extrapolated to either side of 1 AU. Each arrow represents an equivalent flux of magnetic field of 5 gammas for 6 hours. Dashed lines indicate fields away from the Sun; dotted lines represent fields pointed toward the Sun. The shaded regions represent away-from-the-Sun sectors (Schatten et al., ref. 11).

in figure 5, average properties observed during the last solar minimum (December 1963 to February 1964) display a regular pattern. The magnetic field is low at the sector boundary (3 to 4 γ) and peaks during the first and last 2 days of a sector. The solar-wind density peaks just after the sector boundary has passed, and the bulk velocity is highest when the center of the sector passes. Because these observations were made at 1 AU, these parameters do not necessarily correspond to conditions found close to the Sun. Thus the peak in plasma density observed after the passage of a sector boundary could be created by a faster plasma (400 km/sec) piling up behind the slower plasma flow (300 km/sec) characteristic of this sector boundary.

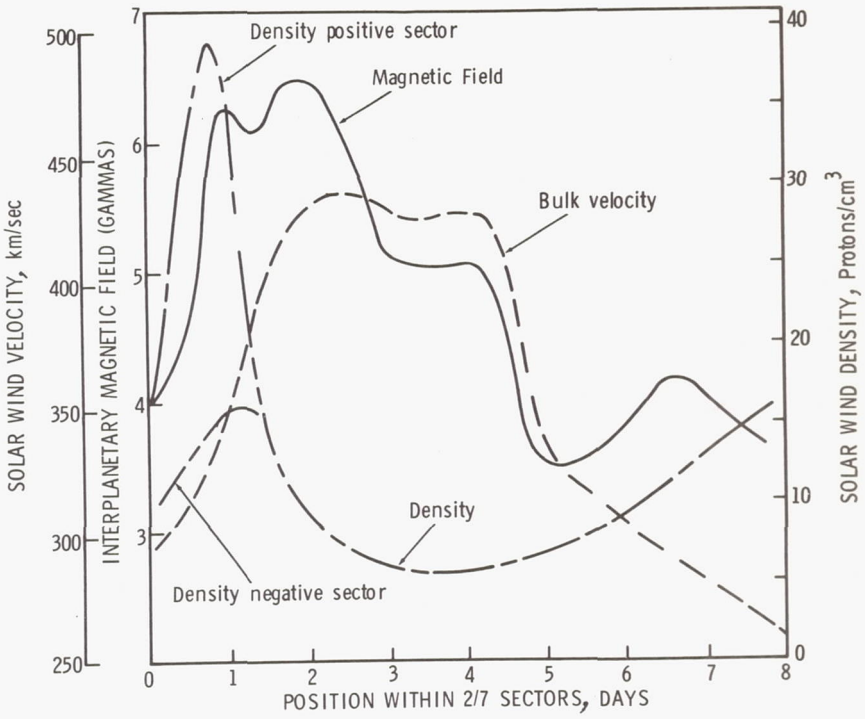


Figure 5.—**Superimposed epoch analysis of the average magnitudes of the interplanetary magnetic field, solar-wind velocity, and solar-wind density. The abscissa represents position within the 2/7 sectors shown in figure 4. The ordinate is the average magnitude at the same relative position within the sector (composite graph after Wilcox and Ness, ref. 7).**

Since the faster plasma in this case takes about 1½ days less to reach the earth, the observed time sequence is reasonable. This appears to be a general process because highest densities normally precede peak velocities by ½ to 2 days (refs. 9 and 10).

Based on these observations, Wilcox (ref. 6) has proposed the model of a sector boundary shown in figure 6. At the boundary itself, a bipolar region confines the corona and prevents the escape of solar wind. The field is weaker on either side and permits escape. Since the fields observed near Earth are characteristic of average coronal conditions, it is probable that the solar wind originates from a major part of the coronal area rather than from a few hot spots.

The sector structure of the interplanetary field goes through a process of evolution that reflects the evolution of gross features of the solar magnetic field (ref. 11). Figure 7 shows that major features of the sector structure

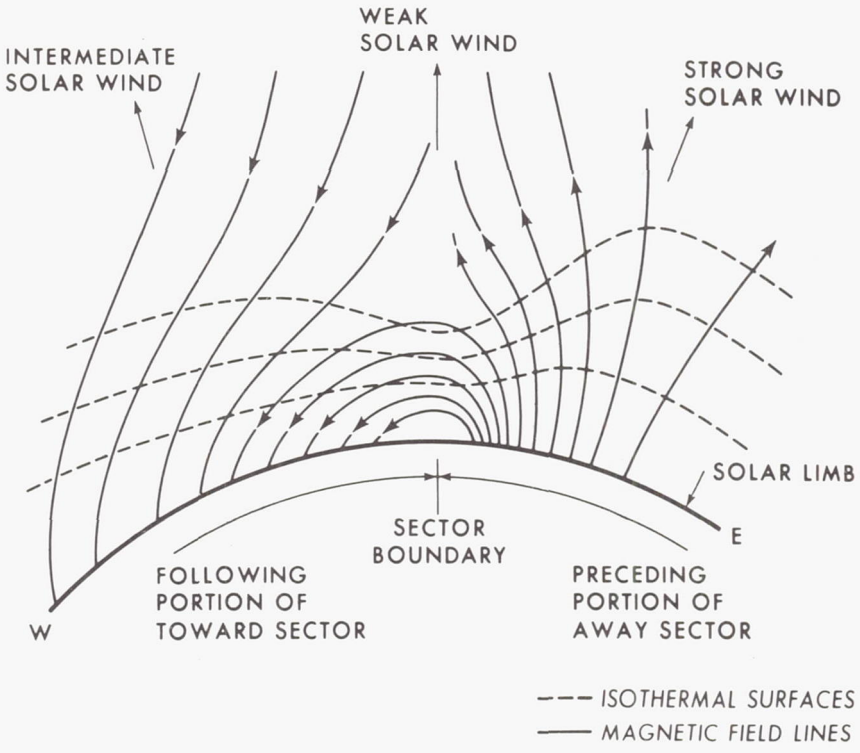


Figure 6.—**Plausible magnetic-field pattern and isothermal surfaces near a sector boundary (Wilcox, ref. 6).**

observed by Mariner II in 1962 persisted through solar minimum (ref. 12). As new activity centers developed, however, the sector structure underwent dramatic changes. New sectors evolved and the old ones either disappeared or were absorbed into the new structure. Thus, the new field configuration observed by Pioneer VI in December 1965, as shown in figure 8, displays little resemblance to that observed by IMP–I 3 years earlier (fig. 4).

Schatten et al. (ref. 11) have demonstrated that magnetic flux is transported away from the Sun during the evolution of a new sector. Since this type of process continues to go on, one has to postulate the existence of a mechanism that permits the field from the old sector to collapse. If no such mechanism existed, the amount of flux transported away from the Sun would soon equal the total flux available from the solar internal magnetic field (see ref. 4). One possible place for such field reconnection to occur is in or near the corona. Another logical place is at the sector boundaries. However, the rate of reconnection at the boundaries must be

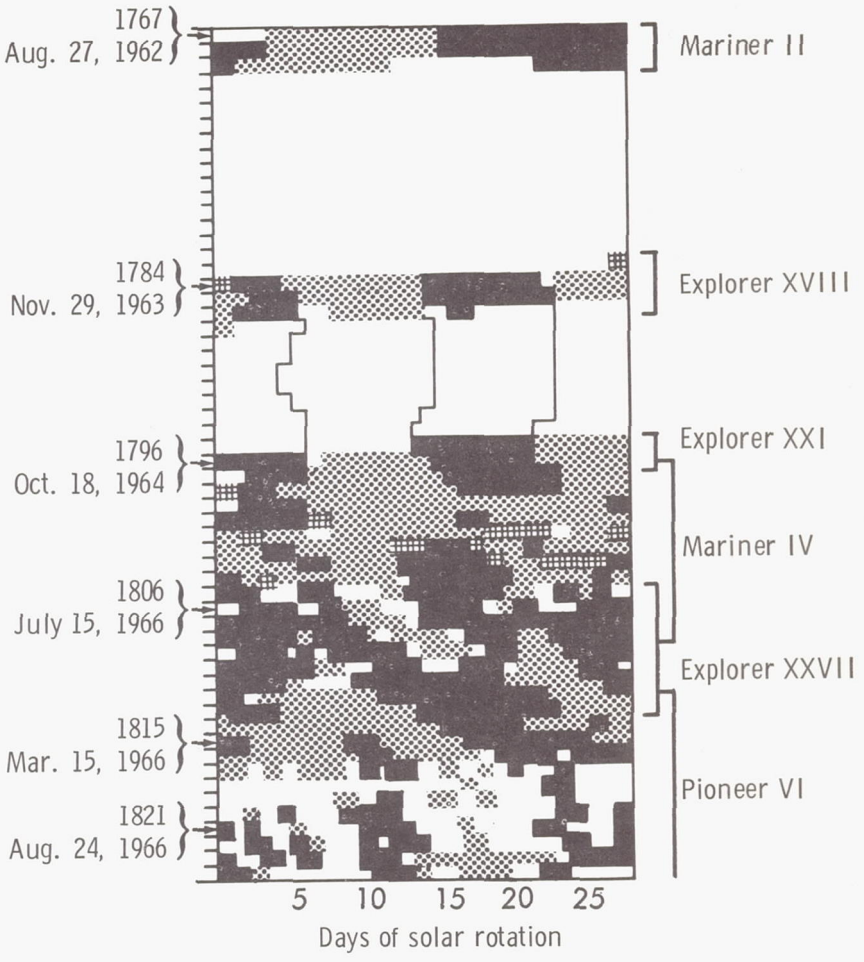


Figure 7.—**Development of sector structure in the interplanetary magnetic field from 1962 through 1966. Light shading indicates sectors with fields away from Sun, dark shading indicates those with fields toward the Sun, and diagonal bars indicate mixed polarity (Ness and Wilcox, ref. 12).**

slow because boundaries are convected essentially intact from the Sun to the Earth; the structure is thus preserved for at least 3 to 6 days. The higher plasma velocity at the beginning of a sector (fig. 5) will tend to preserve a sharp boundary. The occurrence of reconnection has not been experimentally verified. More detailed studies of sector boundaries will be required as well as explorations of sector structure and magnetic-field strength as a function of distance from the Sun.

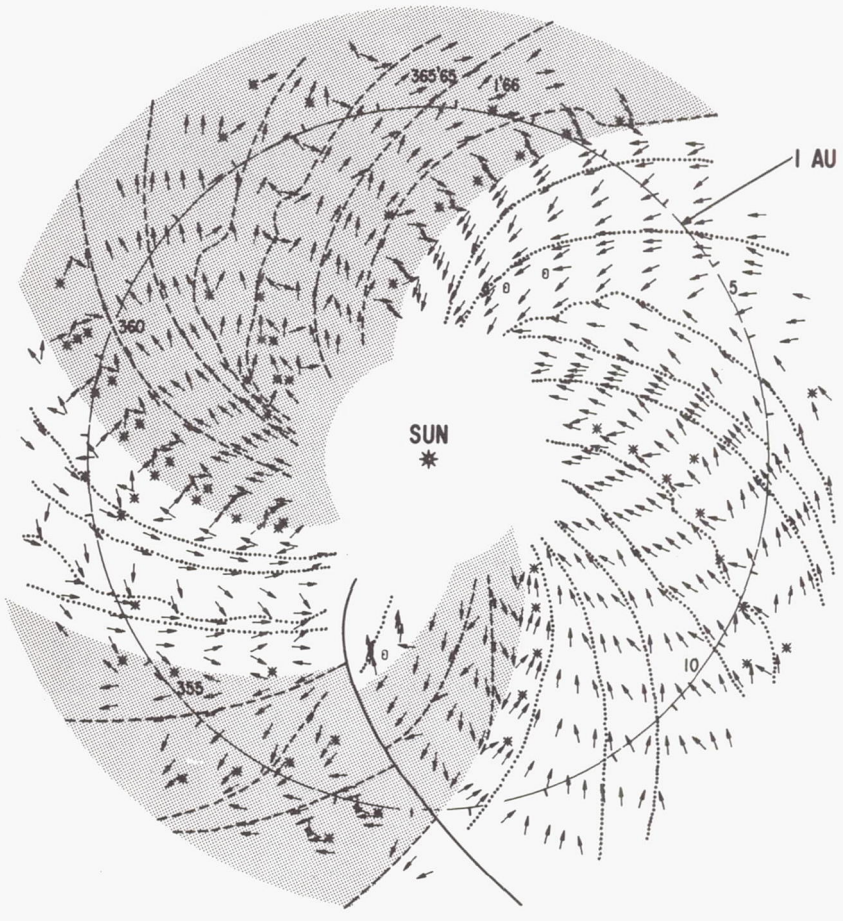


Figure 8.—Extrapolated ecliptic magnetic-field pattern during Carrington solar rotation 1502 (Dec. 18, 1965, to Jan. 14, 1966), prepared with Pioneer VI data. Each arrow represents an equivalent flux of magnetic field of 5 gammas for 6 hours. Dashed lines indicate fields away from the Sun; dotted lines represent fields pointed toward the Sun. The shaded regions represent away-from-the-Sun sectors. The asterisks and the oval-shaped symbols represent places where the magnetic field was fluctuating significantly or where it had a large component normal to the ecliptic plane (Schatten et al., ref. 11).

Within each sector there exists a smaller scaled, filamentary structure to the magnetic field, as illustrated in figure 9. This filamentary structure was described by McCracken and Ness (ref. 13) and by Bartley et al. (ref. 14), who observed from Pioneer VI measurements that anisotropies in

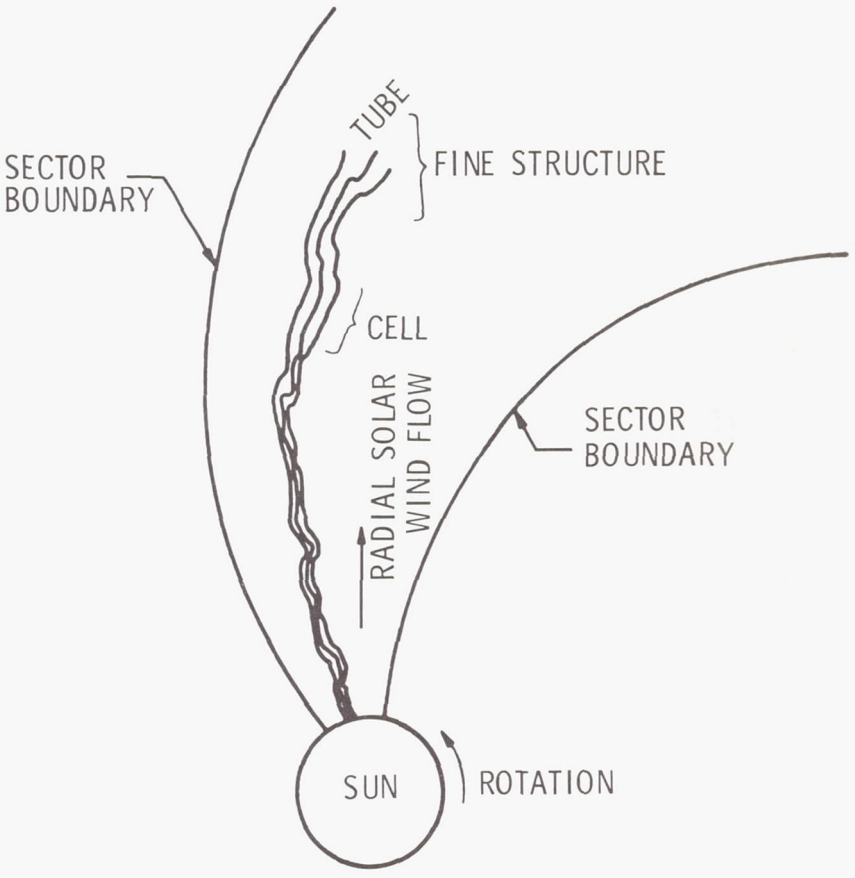


Figure 9.—**Schematic of structure within the solar wind illustrating filamentary structure of the interplanetary magnetic field. The field lines in a given filament lead to the site of origin of the filament (Michel, ref. 15).**

cosmic rays produced by solar flares tend to line up with the location direction of the interplanetary magnetic field. This implies that the magnetic field is uniform over at least the dimension of a cyclotron radius, which is about 10^5 km for the cosmic rays that were observed. A better estimate for the width of the filaments, based on the time required for a single filamentary structure to pass the spacecraft, is about 3×10^6 km. Individual filaments can slide along the contact surfaces between them and become intertwined because of variations in the velocity of plasma traveling within different filaments, and because of turbulence at the origin of the filaments,

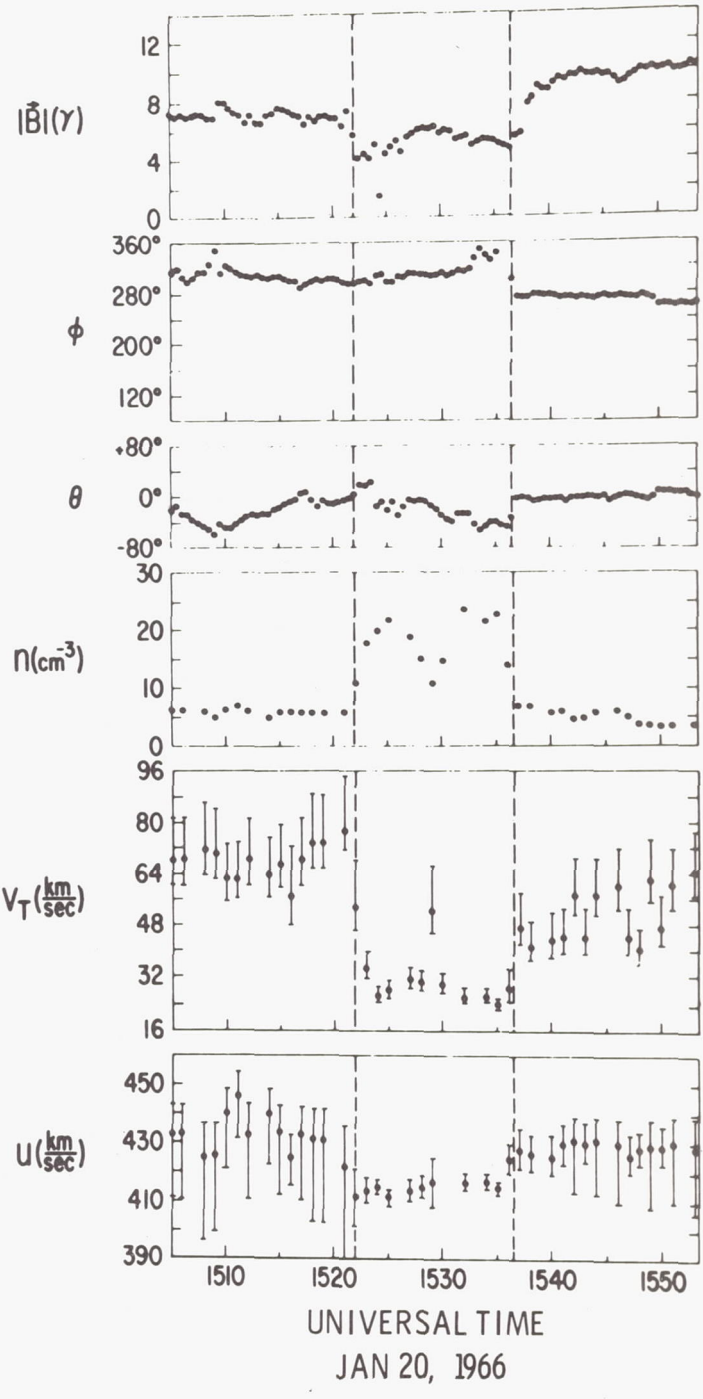
so that on a scale of about 3×10^6 km the interplanetary magnetic field may appear to be quite disordered. Michel (ref. 15) has suggested that the filamentary structure results from plasma streaming out of individual convective cells on the solar surface. These cells are in random motion at the photosphere, where their diameter is typically 3×10^3 km. When allowance is made for expansion as the cells travel out to 1 AU, the cells at the vicinity of the earth become roughly the same dimension as the filaments observed from Pioneer VI. Jokipii and Parker (ref. 16) have noted that the random motions of the convective cells (or photospheric granules and super granules) will create a significant bunching and twisting of the interplanetary filaments, since the feet of the filaments are tied to these structures. This process probably can account for as much of the large-scale randomness of the interplanetary field as can variations in the plasma velocity within each filament.

Different filaments of magnetized plasma cannot interpenetrate, and sharp boundaries are expected to exist between two regions in which plasma properties differ significantly (ref. 17). One would expect pressure equilibrium in the solar wind by the time it reaches the Earth; therefore, the sum of particle and magnetic-field pressures has to balance across the boundary. Such tangential discontinuities have been observed, and an analysis of both plasma and field data by Burlaga (ref. 18) demonstrated experimentally the existence of pressure balance across the boundaries. Figure 10 illustrates the passage over Pioneer VI of a filament of plasma characterized by a high-density (20 protons/cm^3), low-proton temperature, and lower magnetic-field strength.

Several experimenters have observed tangential discontinuities, including Siscoe et al. (ref. 19), Burlaga (ref. 18), Burlaga and Ness (ref. 20), Fairfield (ref. 21), and Ogilvie et al. (ref. 22). It has been found that the most commonly observed tangential discontinuity is characterized by no change in plasma properties; only the direction of the magnetic-field changes. Many discontinuities are quite thin, of the order of 1.3×10^4 km, and pass over the satellite in about 30 to 60 seconds (refs. 19 and 20). Other tangential discontinuities are characterized by a gradual decrease in field

---

Figure 10.—**Two tangential discontinuities, from Pioneer VI data. The figure shows the magnitude and direction angles of the interplanetary magnetic field, where ϕ indicates longitude in the ecliptic plane and θ indicates field direction above or below the ecliptic. Also shown are plasma density n, characteristic thermal velocity V_T, and bulk velocity u. The fact that the discontinuities are complementary indicates that the spacecraft passed into and out of a filament separating two distinct regions (Burlaga, ref. 18).**


|B|(γ)
12
8
4
0
φ
360°
280°
200°
120°
θ
+80°
0°
-80°
n(cm⁻³)
30
20
10
0
V_T(km/sec)
96
80
64
48
32
16
u(km/sec)
450
430
410
390
1510
1520
1530
1540
1550
UNIVERSAL TIME
JAN 20, 1966

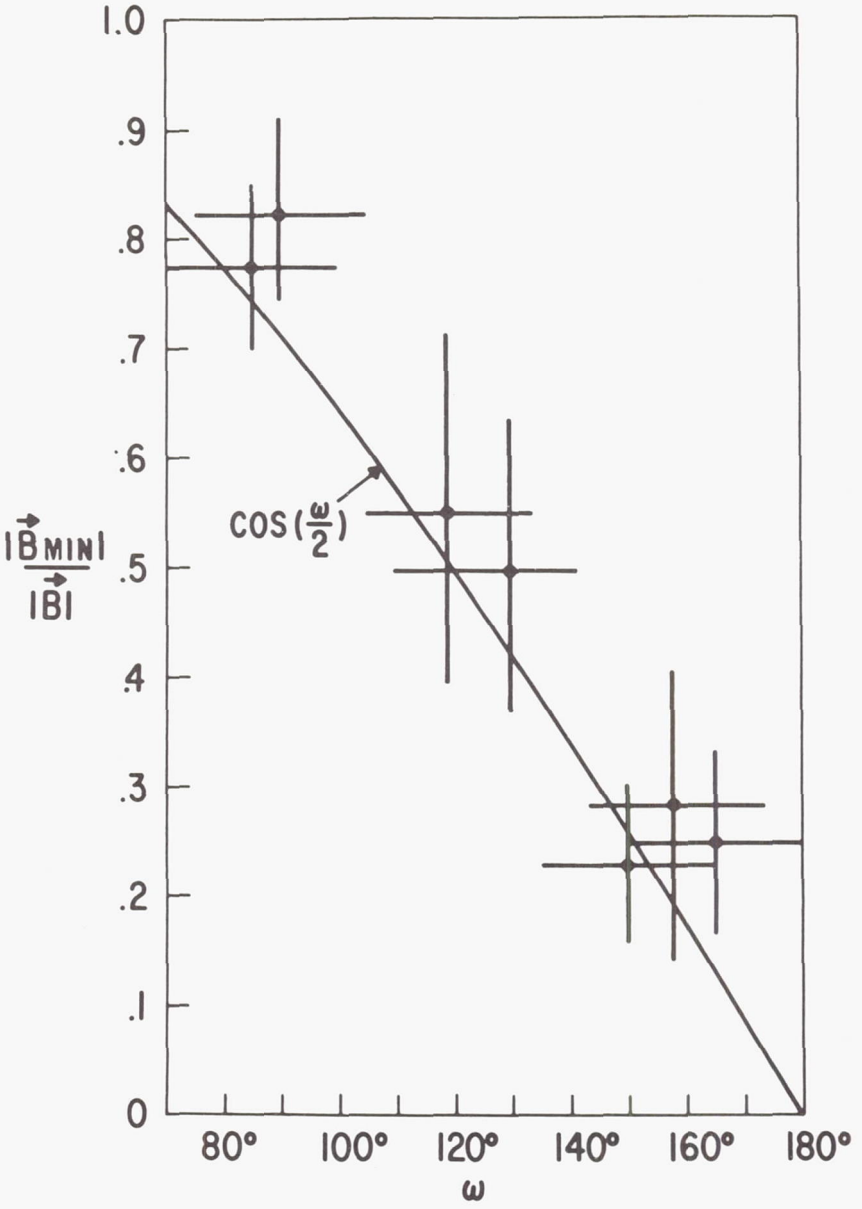


Figure 11.—The ratio of the minimum field strength $|B_{min}|$ at a discontinuity to the average field $|B|$ on either side, as a function of the angle ω between the two field directions. The solid curve is computed on the basis of field-line connection across the discontinuity (Burlaga and Ness, ref. 20).

strength lasting several minutes and an equally slow recovery to the former strength but in a different direction. Burlaga and Ness (ref. 20) have shown that the magnitude of the dip depends on the change of field direction (fig. 11) and is not inconsistent with what would be expected if the boundary is being eroded by field-line merging. This process would heat the plasma at the discontinuity, and such a rise in temperature was observed by Burlaga (ref. 18) in one case in which an exceptionally large amount of magnetic energy may have been "annihilated." The major questions to be answered are the rate of merging and whether other processes such as pressure gradients in the solar wind tend to maintain a sharp boundary in the face of merging. A study of the solar wind at several AU from the Sun should provide answers to many such questions.

The equilibrium conditions in the solar wind are disturbed at times by violent plasma ejections from the Sun associated with large solar flares. The expansion of this material is at super-Alfvén speed with respect to the surrounding plasma and the subsequent behavior can be described by the gas dynamic analog of a supersonic shock traveling in the solar-wind medium. The major physical feature distinguishing these events from the discontinuities discussed previously is a substantial pressure discontinuity across the shock front. The original observations of this phenomenon were made with Pioneer V in 1961 and Mariner II in 1962. Colburn and Sonett (ref. 17) showed that the Rankine-Hugoniot shock equations are satisfied within the accuracy of the measurements.

Observations of shocks from this solar cycle have been reported by Lazarus and Binsack (ref. 23), Ogilvie et al. (ref. 22), Gosling et al. (ref. 24), Van Allen and Ness (ref. 25), and Gringauz et al. (ref. 26), and were summarized by Wilcox (ref. 6). Near 1 AU from the Sun, these shock waves are characterized by a difference in plasma velocity of 50 to 200 km/sec and an approximate doubling in plasma density, temperature, and magnetic-field strength. The computed shock velocities are generally 500 to 800 km/sec and are somewhat lower than the average transit velocity from the Sun. Ogilvie et al. (ref. 22) have found that the shock wave itself is often accompanied by tangential discontinuities and by a change in the hydrogen/helium ratio of the solar wind.

Plasma Properties

A small volume element of solar wind is characterized by its composition, density, particle velocity, distribution or temperature, magnetic field, and the spectrum of electric- and magnetic-field fluctuations contained within it. Each one of these parameters has an important bearing on the properties of the solar wind and many of them are interrelated. For instance, there is some evidence that equipartition of energy may occur between the various degrees of freedom of particle motion. In a frame of reference

moving with the solar wind, one finds nearly equal energies in thermal motion, average magnetic-field strength, magnetic-field fluctuations, and velocity fluctuations. However, the processes leading to statistical equilibrium are not sufficiently dominant to prevent mildly unstable conditions; thus there is generally a small temperature anisotropy.

As would be expected from solar abundances, the solar wind contains primarily hydrogen. Since the solar wind is a magnetized plasma, ions of other elements have to move with the bulk speed of the solar wind. Ions that originally had other velocities would be accelerated to the bulk velocity by the motional electric field, $\mathbf{V}\times\mathbf{B}$. Energies are therefore proportional to the mass of the ions, and the potential needed to deflect them a given amount in an electrostatic analyzer is proportional to the mass-to-charge ratio, m/Z. Figure 12 shows a complete scan of the solar-wind spectrum, obtained with a high-resolution electrostatic analyzer. The width of the individual peaks depends, in this case, only on the ion temperature. Normally, the temperature is so high that only the $m/Z=1$ and $m/Z=2$ peaks can be resolved.

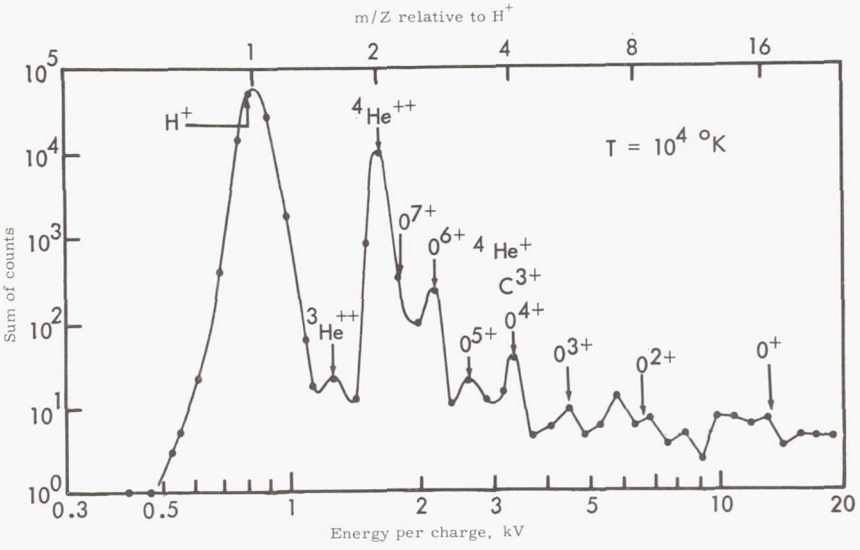


Figure 12.—**Energy per unit charge spectrum of the solar wind obtained on October 8, 1965, at 0338 to 0355 UT. Arrows indicate expected positions for various ion species. In general, O^{16}, N^{14}, and C^{12} ions with a similar mass-to-charge ratio cannot be separated (Bame et al., ref. 29).**

The interpretation of the second largest peak as resulting from $m/Z=2$ ions was confirmed by Ogilvie et al. (ref. 22). They flew an instrument on Explorer XXXIV (IMP–IV) that used a velocity filter after the electrostatic analyzer. Based on elemental abundances this peak must be caused primarily by $^4He^{++}$. The average He^{++}/H^+ ratio has been 4.5 percent during declining solar activity in 1962 (ref. 9) and during solar minimum (refs. 27 and 28). This ratio is quite variable, however, between limits of 0.5 and 15 percent. Plasma observed after solar flares tends toward the larger He^{++} content.

The other peaks shown in figure 12 can be observed only when the solar wind has an unusually low temperature (10^4 °K or less), and when it is sufficiently steady to permit integration of the measurement over an extended period of time. Even under these conditions, the intensity ratio of the various m/Z peaks varies by at least a factor of 2 (ref. 29). The identification of the peak label $^3He^{++}$ is unique and gives an $^3He^{++}/^4He^{++}$ ratio of about 10^{-3}. The peaks labeled O^{7+}, O^{6+}, and O^{5+} could also contain contributions from carbon and nitrogen, because the solar-abundance ratios are C:N:O=6:1.5:10 (ref. 30). However, the ionization potential of stripped carbon is lower than that of oxygen, and Hundhausen et al. (ref. 31) argued that carbon is nearly fully ionized in the region from which the solar wind originated. In that case, the C^{6+} contribution would appear at $m/Z=2$, and is masked by the He^{++} peak. Assuming carbon and nitrogen do not contribute significantly to the oxygen peaks, the He/O ratio from several observations was found to vary between 25 and 80.

Although our knowledge of solar-wind composition is still in a rudimentary state, it has been mentioned because of its important implications toward our understanding of the solar corona and the solar wind. According to present theories, three processes in the solar atmosphere can affect the composition of the solar wind. Diffusion of ions in a magnetized plasma occurs in the chromosphere under the influence of gravitation and temperature gradient. The net effect of this process is to enhance greatly the concentration of multiply charged ions above the chromosphere at the base of the corona (ref. 32, and M. P. Nakada, private communication). At higher altitudes the corona is thought to be nearly isothermal, and diffusion in only a gravitational field enhances the lighter nuclei in the solar wind. Superimposed on the two types of diffusion are mixing processes that tend to equalize elemental composition toward that found in the photosphere. The variability of the observed abundance ratios indicates that diffusion processes are important. Both types of diffusion must be involved because both hydrogen and oxygen are enhanced at times relative to the expected helium abundance. Still, on the average, mixing is likely to dominate because the average abundance ratios agree within about a factor of 2 with equivalent ratios observed optically or in solar cosmic rays (ref. 33).

333-240 O—69——13

The relative abundance of different charge states of one element such as $O^{7+}:O^{6+}:O^{5+}$ are very sensitive to the coronal temperature where the solar wind originates. Hundhausen et al. (refs. 31 and 34) carried out an analysis of this problem for two coronal models and concluded that the temperatures fall in the range of 1.5×10^6 to 3.5×10^6 °K. The accuracy of these numbers cannot be assessed easily because of possible contributions of C and N ions to the measurements of Bame et al. (ref. 29) as shown in figure 12. The lower temperature is close to values derived from intensities of coronal emission lines. If the coronal temperatures are indeed this high, one would not expect to observe measurable amounts of $^4He^+$, C^{3+}, and O^{5+}. If their existence is confirmed, it may be explainable in terms of charge-exchange collisions with neutral hydrogen in interplanetary space (ref. 34).

The solar-wind gas expands adiabatically and should cool from its million or so degrees kelvin at the corona as it travels to Earth. According to the two-fluid models of Sturrock and Hartel (ref. 35) for the solar wind, the proton temperature near Earth should be about 2800° K, and the electron temperature, about 4.6×10^5 °K. In the absence of plasma instabilities, the first adiabatic invariant of individual particles should be conserved ($mv_\perp^2/2B$=constant) in a frame of reference moving with the solar wind. Therefore as the magnetic field decreases, the average velocity perpendicular to the field decreases. This process should thus produce a substantial anisotropy in the velocity distribution of solar-wind ions.

These theoretical predictions are partially borne out. Figure 13 shows contours of proton flux in the V_1, V_2 plane, where V_1 is the radial velocity away from the Sun and V_2 is the perpendicular velocity. The small triangle indicates the bulk velocity of the solar wind. The predicted anisotropy is indicated by the large velocity component along the field line away from the Sun. The velocity distribution in any given direction can be translated into an equivalent temperature ($kT_\phi=\frac{1}{2}m<V_\phi^2>$, where the angle ϕ is measured relative to the satellite-Sun line, and $<V_\phi^2>$ is the mean square velocity in the moving frame of reference). Hundhausen et al. (ref. 36) have shown that the anisotropy is field-alined and tracks changes in field direction. It is therefore, in general, adequate to characterize the solar wind with a temperature perpendicular and parallel to the magnetic field. Both isotropic velocity distribution ($T_\parallel=T_\perp$) and values of $T_\parallel/T_\perp$ as large as 5 are rarely observed at 1 AU, the more usual situation being $T_\parallel/T_\perp\approx2$ (refs. 36 and 37).

The observed temperature anisotropy is much smaller than would be expected if the first adiabatic invariant were conserved. As a matter of fact, if the solar wind were characterized by $T_\parallel=T_\perp$ at 0.6 AU and were then allowed to expand adiabatically, the ratio $T_\parallel/T_\perp$ would be 5 at 1 AU. Various plasma instabilities that could redistribute the velocities have been

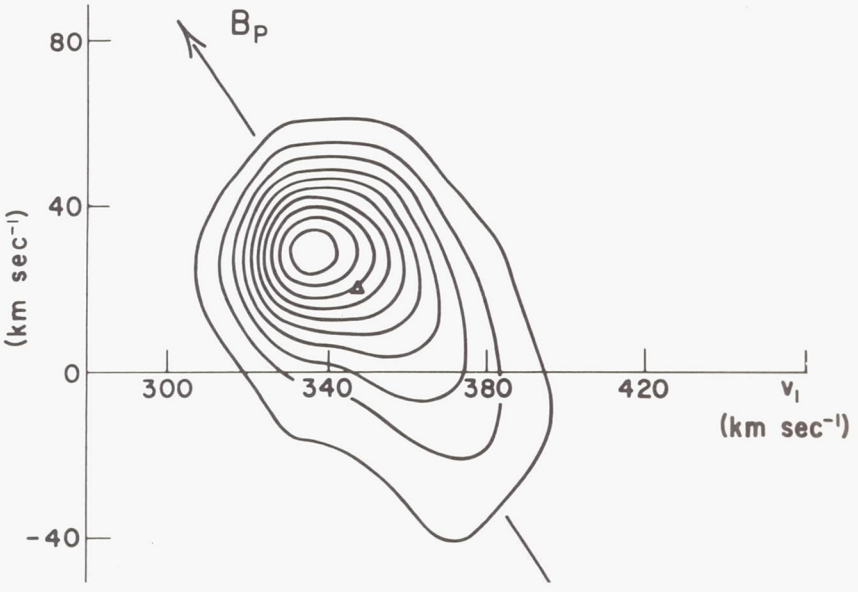


Figure 13.—A contour mapping in the plane of observation of a typical proton velocity distribution function derived from Vela III data on August 5, 1965. The small triangle indicates the bulk velocity; B_p indicates the 5.46-minute average magnetic field projected onto the plane of observation (Hundhausen et al., ref. 36).

investigated by Kennel and Scarf (ref. 38), and by Scarf et al. (ref. 37). These authors have shown that a cyclotron wave will interact to redistribute the parallel and perpendicular velocities whenever the anisotropy becomes too large. The growth rate of such a wave can be quite short. This or one of numerous other instabilities could be responsible for keeping the anisotropy small; it would thus appear that the observed anisotropy is generally near the stability limit and varies with plasma conditions.

The predictions about cooling of the solar wind caused by adiabatic expansion is also only partially correct. Sturrock and Hartel (ref. 35) predicted a decrease of average proton temperatures from 2×10^6 °K in the corona to 2800° K at 1 AU. Actual observations place the mean temperature in the range from 6×10^3 to 7×10^5 °K (refs. 27, 28, 36, and 39). This heating can be attributed to interactions of the protons with the spectrum of electric (refs. 40 and 41) and magnetic (refs. 42 to 45) field fluctuations. Both types of fluctuations can be observed at all times with sporadic increases in magnitude. Electric-field measurements are difficult to obtain and have been attempted only recently; in contrast, magnetic measurements are

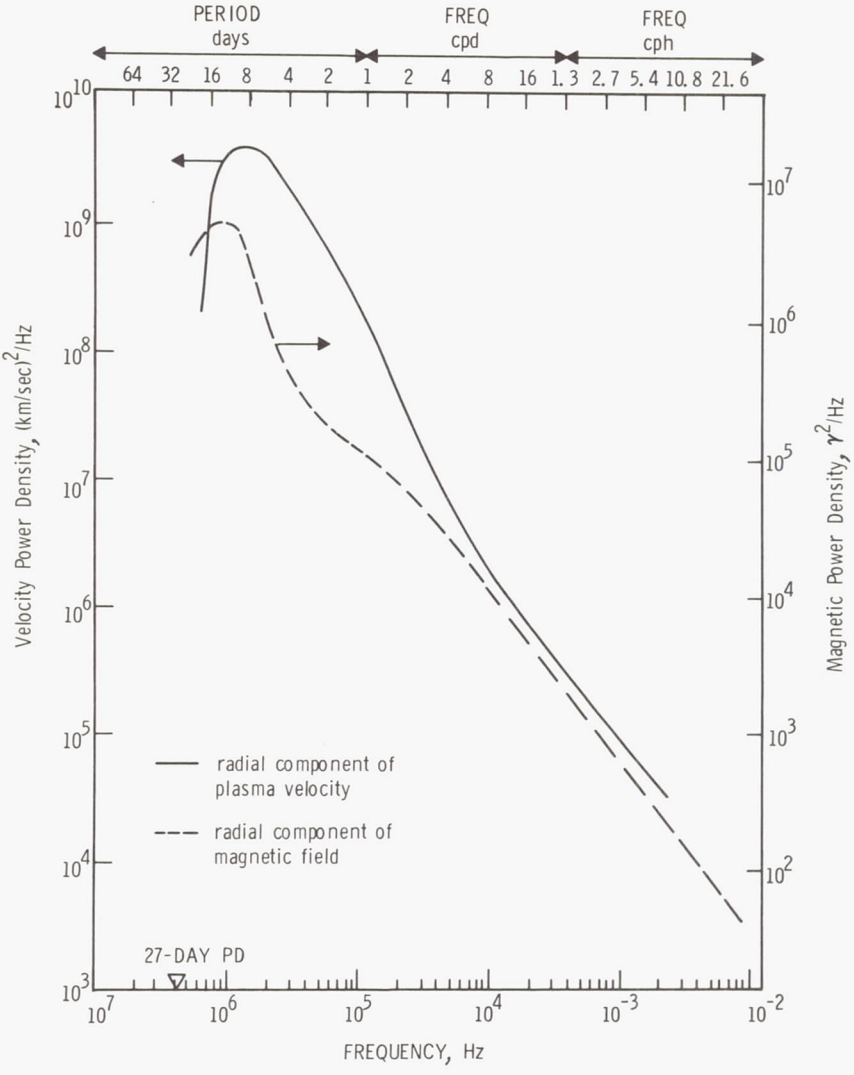


Figure 14.—Power spectra of V_r, the magnitude of the radial component of the solar-wind velocity, and of B_r, the magnitude of the radial component of the interplanetary magnetic field. These curves are based on Mariner II observations from August 29 to October 31, 1962 (Coleman, ref. 45).

available starting with Mariner II and have been analyzed in great detail. Coleman (ref. 45) finds that the power density varies proportionally to $f^{-1.2}$ between 2×10^{-5} and 10^{-2} hertz.

On the basis of an analysis of the fluctuation spectrum of the magnetic and plasma data from Mariner II shown in figure 14, Coleman (ref. 45) arrived at the following conclusions. Energy is available from the differential bulk velocities of different solar-wind segments. Through the operation of instabilities as yet unidentified, this energy is fed into fluctuations of $10^{-5}<f<10^{-4}$ Hz and then cascades through the frequency range of $10^{-4}<f<f_c$ (where f_c is the proton plasma frequency $\approx$0.2 hertz). In this spectrum equipartition occurs for frequencies above 10^{-4} hertz between fluctuations in kinetic and magnetic energy. Once the energy reaches the proton plasma frequency, it is dissipated and heats the proton population of the solar wind. The minimum heating between the Sun and Earth was estimated to be 3.6×10^{3} °K, with a potential for additional heating beyond the orbit of Earth of 8×10^{5} °K.

The temperatures of the doubly charged helium ions in the solar wind cannot be derived as easily as they can be for protons because of poorer statistics in the observations. Hundhausen et al. (ref. 27) found that for He^{++} the ratio of $T_{\parallel}/T_{\perp}$ is, on the average, the same as that for protons but variations do occur. The average temperature of He^{++} was found to be nearly four times the proton temperature. This implies that velocity rather than energy equipartition occurs between different species of ions.

The electron component of the solar wind is more difficult to observe than the ions because of spacecraft potential, the photoelectron cloud surrounding the spacecraft, and because the geometric aperture of the instrument is not necessarily the effective aperture. Montgomery et al. (ref. 46) minimized these effects by fitting a bi-Maxwellian distribution to electron measurements above 16.5 eV and extrapolating this distribution to lower energies. In agreement with the predictions by Sturrock and Hartel (ref. 35), the electron temperatures are always higher than the proton temperatures, not by the calculated factor of 160 but only by 1.5 to 5. During the period in May and June 1967 that was studied, the electron temperature was more steady than the proton temperature and fell into the range of 7×10^{4} to 2×10^{5} °K. Wolfe and McKibbin (ref. 47) observed a similar electron temperature. The temperature is also slightly anisotropic with respect to the magnetic-field direction but to a smaller extent than the ion temperature. Apparently, the Coulomb collision time for electrons with their high thermal velocity is sufficiently short to prevent substantial buildup of thermal anisotropy.

Astrophysical Implications

The study of the solar wind is of interest for developing the theory of collisionless plasmas. The role of the interstellar medium in the evolution of a galaxy or in processes leading to nonthermal emission of electromagnetic radiation (quasars, radio galaxies, and X-ray stars) has been attributed to plasma processes. In this area, proper extrapolation of our knowledge depends largely on our understanding of plasma instabilities. Since these instabilities are the most difficult to resolve, progress has been relatively slow. Of more immediate value is our understanding of the role the solar wind played in the evolution of the Sun and planets.

A major problem for the astrophysicist is that of finding a mechanism by which the Sun has lost its angular momentum. The solar wind does act as a brake on the Sun's rotation, because the magnetic field embedded in it can transmit a tangential stress back to the photosphere where the lines of force are anchored. According to a simple picture, the magnetic field out to 20 to 40 solar radii ($R\odot$) is primarily radial, corotates with the Sun, and can support the tangential stress required to maintain the expanding solar wind at the same angular velocity as the photosphere. A more rigorous model was derived by Weber and Davis (ref. 48) for the steady-state flow of solar wind in the equatorial plane of the Sun. They solved numerically the magnetohydrodynamic equations for a fluid of infinite conductivity and no viscosity in the gravitational and magnetic fields around the Sun.

A solution was obtained for typical solar-wind parameters at 1 AU, that is, for a bulk velocity of 400 km/sec, 7 protons/cm^3, proton temperature of 5×10^5 °K, and magnetic field of 5 gammas. The magnetic-field configuration was found to be almost identical to the Archimedes spiral field derived by Parker (ref. 49) on the basis of no tangential magnetic stress. The maximum tangential bulk velocity of 4 km/sec is reached at 11.5 $R_\odot$; it decreases to about 1 km/sec at 1 AU and continues to decrease somewhat slower than 1/r beyond the orbit of Earth. At the orbit of Earth, magnetic stress still accounts for a substantial fraction of the angular momentum lost by the Sun. If a similar solar-wind flow occurs over the whole surface of the Sun, the characteristic slowing-down time is 7×10^9 years, or equivalent to the age of the Sun.

The calculations of Weber and Davis (ref. 48) give a lower limit to the loss of angular momentum, because a steady-state model does not include momentum that may be carried by the fluctuations in the solar-wind plasma. Schubert and Coleman (ref. 50) have shown that fast-mode magnetosonic waves propagating through the solar wind near 1 AU exert an effective torque that is of the same order of magnitude as that produced by the mean solar wind. Direct observations of the small tangential velocity at 1 AU are relatively difficult. At times, however, the solar wind has relatively large tangential velocities, such as 15 km/sec, that appear to be inconsistent with these

models. Observations of the deflection of comet tails (ref. 51) indicate tangential velocities near 1 AU of 9 km/sec. Additional discussions of this problem are given by Alfonso-Faus (refs. 52 and 53), Modisette (ref. 54), and Brandt (ref. 55). In spite of differences in detail, the different analyses result in the same general slowing-down time for the Sun.

The substantial torque exerted by the solar wind on the Sun could have rather extreme effects on the internal structure of the Sun. One model has been described by Dicke and Goldberg (ref. 56) to explain their observations of solar oblateness. According to this model (ref. 57), the outer shell of the Sun has been slowed down by the action of the solar wind and is detached from the bulk of solar mass that continues to rotate with a period of 1 to 2 days. The value of the solar-wind torque derived by Weber and Davis is adequate for Dicke's model. As Dicke and Goldberg point out, a solar oblateness of the magnitude observed by them would have a profound effect on our understanding of general relativity.

The solar wind may also have played a role in the evolution of the planets. In particular, if a planet is not protected by a magnetic field, ions from the ionosphere may become attached to magnetic-field lines of the solar wind and be removed from the atmosphere of the planet. Such a process would be slow and may not have affected significantly a dense atmosphere, such as that found around Venus. In the case of the Moon, however, this process may have prevented the buildup of a tenuous atmosphere of heavy noble gases if such gases were released slowly by volcanism.

As yet we are unable to determine whether the present strength of the solar wind is typical of the solar evolution or whether the Sun could have evolved through a T-Tauri phase. This phase appears to occur primarily in young stars and is characterized by rather high-density plasma streaming away from the star. During such a phase, the stellar wind could easily be able to carry away a large amount of angular momentum. Such a wind could conceivably also produce eddy-current heating in planetary or other solid bodies in the vicinity of the star.

INTERACTION OF THE SOLAR WIND WITH THE MOON, PLANETS, AND INTERSTELLAR MEDIUM

The phenomena described in the previous section are observed when the solar wind is able to expand freely into space. If an obstacle is placed into the path of the solar wind, a new set of phenomena is produced. If the obstacle is comparable to or smaller than the proton gyroradius ($\sim$500 km for average conditions), one would expect that a single-particle theory could describe the phenomena. In contrast, if the object is large compared with the proton gyroradius, collective behavior would be expected to become important, in which case the solar wind would behave like a supersonic fluid.

The Earth with its magnetic field constitutes a large object, and its interaction with the solar wind has been studied extensively. The solar wind is stopped by the geomagnetic field when the pressure produced by the solar wind is balanced by the compressed geomagnetic field at 8 to 12 R_E. Upstream from this boundary (called the magnetopause) is a detached shock at 13 to 15 R_E. Between the shock and the magnetopause is a region in which the plasma has been heated as it passes through the shock. The solar wind does not close in again behind the Earth because, in its interactions with the geomagnetic field, it produces a long magnetic structure, the magnetotail, that excludes the solar wind for at least 80 R_E in the antisolar direction. Processes associated with this interaction appear to be responsible for the existence of most of the energetic electrons and protons found in the magnetosphere. They are found both as trapped particles in the Van Allen belts and as particles confined only temporarily, such as in aurora or in the magnetotail.

Further details about the Earth's environment are given in the next section. Of interest here are the interactions of the solar wind with the Moon, the planets, and the interstellar or galactic medium. The experimental results of Mariners IV and V for Mars and Venus, and of Explorer XXXV for the Moon, have provided most valuable information about solar-wind interactions that are distinctly different from those around the Earth.

Moon

Prior to the flight of the lunar-orbiting spacecraft Explorer XXXV, it was thought that there might be an enhanced magnetic field on the sunward side of the Moon, perhaps strong and extensive enough to create a lunar shock front. Three possible sources of such a field had been suggested. The first was an intrinsic dipole moment caused by magnetic materials on the lunar surface or in the interior. However, measurements taken on the lunar surface by the Surveyor V, VI, and VII spacecraft had made this possibility seem remote. Turkevich et al. (refs. 58 to 60) have concluded from an alpha-particle scattering experiment that the chemical composition of the surface is similar to that of basalt, which is a nonmagnetic substance; and surface magnetometer results by deWys (ref. 61) indicated the presence of only small amounts of magnetic iron material. Another suggested source of magnetic field near the Moon was eddy currents in the lunar interior resulting from fluctuations in the interplanetary magnetic field. These would be especially prominent if the Moon had a high electrical conductivity. Lunar magnetic fields associated with these currents have been discussed recently by Johnson and Midgley (ref. 62). A third possible source of lunar magnetic field, proposed by Gold (ref. 63)

and formulated somewhat differently by Sonett and Colburn (ref. 64), was the establishment of a lunar unipolar generator by the solar wind. The manner in which such a field would be produced is as follows: First, an electric field would be created in the frame of reference of the Moon by the solar wind and its associated magnetic field flowing past the lunar surface. This electric field would then induce a polarization charge in the conducting lunar material. Contact with the highly conducting solar-wind plasma would allow the polarization to discharge continuously, and the continual replenishment of this charge would create a current pattern in the lunar interior and in the solar wind. The current thus established would have many of the external characteristics of a dynamo and would produce a magnetic field near the Moon that enhances the interplanetary magnetic field on the sunward side and diminishes it on the night side. For a highly conducting lunar body, the magnitude of the unipolar current would be limited only by the solar-wind power flux on the surface area of the Moon; however, if a sufficiently thick layer of insulating material surrounds a conducting lunar core, the current could be greatly diminished by the electrical resistance involved.

Explorer XXXV was injected into a lunar orbit on July 21, 1967, during a time when the Moon was immersed in the geomagnetic tail. The satellite carried two separate triaxial fluxgate magnetometers with sensitivities of ± 0.1 γ and ± 0.2 γ. Initial results reported by Ness et al. (refs. 65 and 66) and Sonett et al. (ref. 67) indicated that there was apparently no measurable intrinsic magnetic field associated with the Moon. A later, more detailed study of paired orbital passes above and below the geomagnetic neutral sheet was made and reported by Behannon (ref. 68) in an effort to separate a permanent lunar magnetic field from any induced fields. As a result of Behannon's study, an upper limit on the intrinsic lunar magnetic moment of 1×10^{20} gauss-cm^3, or about 1.2×10^{-6} of the magnetic moment of Earth, was established.

A large body of magnetic-field information has been received for times at which the Explorer XXXV-Moon system was directly in the solar wind. After scanning the data from 150 lunar orbits, Ness (ref. 69) concluded there was no evidence of any crossing of a shock wave associated with the Moon. This same conclusion was also reached in studies by Colburn et al. (ref. 70) and by Taylor et al. (ref. 71). Thus the evidence to date has not given any support to the postulate that such a shock wave exists. Also, no apparent enhancement of the interplanetary magnetic field on the sunward side of the Moon has been observed. From this one may conclude that either the Moon has a low overall electric conductivity (less than 10^{-5} mho/m), or that the outer layers of the lunar body are of very low conductivity while the core might still be conducting. England et al. (ref. 72) have derived different conductivity profiles for the Moon on the basis of

various models for the internal lunar temperature. All models are consistent with observations, since they all predict that material in the outer 10 percent of the lunar radius has a low conductivity.

It is virtually impossible to establish from satellite measurements alone whether the Moon contains a highly conducting core. As pointed out by Sonett et al. (ref. 67), if a purely hypothetical cold metallic core of size 0.1 lunar radius were immersed in a magnetic field of 10 γ, it would produce an induced magnetic field at the lunar surface of only 0.01 γ; this is far below the sensitivity of present satellite magnetometers. However, if the Moon had a larger core, of size perhaps 0.8 lunar radius or greater, its magnetic effects should be observable. A desirable experiment would be a two-satellite observation, in which one satellite monitored the solar wind at a distance of many lunar radii while the other satellite orbited the Moon at close proximity. The convenient presence of Explorer XXXIII occasionally in the vicinity of the Moon has made such an experiment possible. Explorers XXXIII and XXXV carried identical magnetometer payloads, and thus valuable comparisons could be made at times at which Explorer XXXIII was in the solar wind and Explorer XXXV was near perilune.

Figure 15 shows one such comparison using data obtained on September 13, 1967, at which time Explorer XXXIII was slightly upstream from Explorer XXXV in the solar wind. A series of tangential discontinuities in the interplanetary field (marked by 180° changes in the direction angle ϕ) were recorded by Explorer XXXIII, and after a short transit time consistent with a nominal solar-wind velocity, these same reversals were also recorded by Explorer XXXV. At the time, Explorer XXXV was passing through the "shadow region" on the night side of the Moon, so these measurements were able to show that no noticeable induction fields from a conducting core had been seen. Detailed theoretical analysis of the response of the Moon to large magnetic discontinuities will be required to derive a conductivity profile. However, observations of discontinuities with Explorer XXXV have been interpreted by Ness (ref. 69) as showing that most of the lunar interior has a conductivity of less than 10^{-5} mho/m.

Whenever Explorer XXXV passed through the lunar-shadow region at low altitudes, the presence of a region void of plasma was clearly identified with a plasma probe (ref. 73) and affected the magnetometer readings (refs. 66, 70, and 74). This void is lined up with the aberration angle of the solar wind (that is, the direction of the solar wind as seen in the Moon's frame of reference) and is bounded by a region of gradually increasing particle density until the full solar-wind strength is reached beyond the geometric size of the Moon. The diamagnetic effects of the void region are strikingly evident from magnetometer readings. Figure 16 shows a weighted average of magnetometer readings for four passes through the lunar shadow between

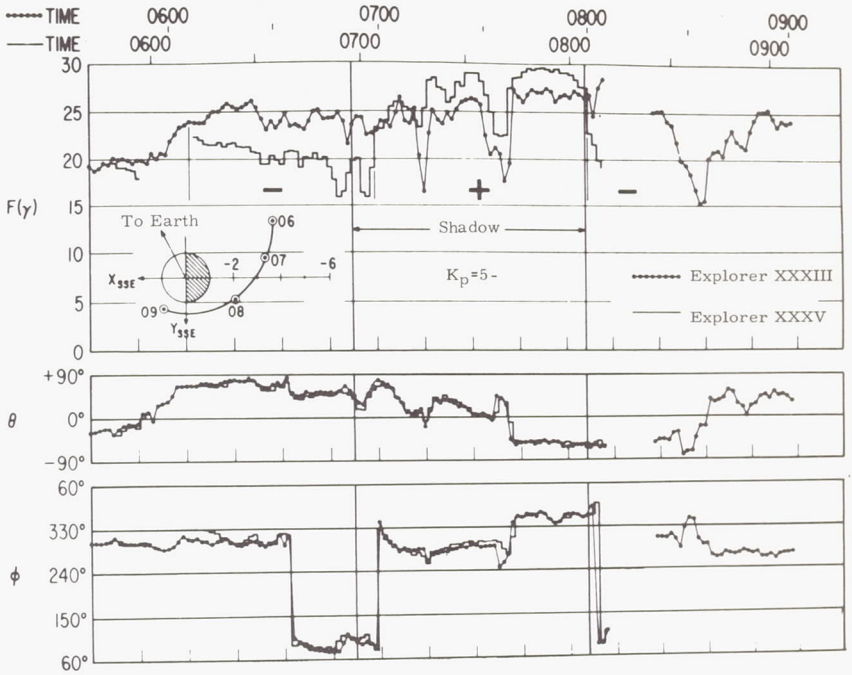


Figure 15.—Simultaneous magnetic-field measurements made by Explorers XXXIII and XXXV presented in solar ecliptic coordinates. F is the field magnitude in gammas; θ, its latitude angle (0° is the ecliptic plane and positive angles are northward); and ϕ, the azimuthal angle (0° is toward the Sun and 90° toward dusk). The position of Explorer XXXV relative to the Moon is shown in ecliptic plane projection in the upper left. The + and − signs indicate regions where the field magnitude measured by Explorer XXXV is greater than and less than that at Explorer XXXIII. This figure illustrates a traversal of the lunar wake during a magnetic storm on Earth (Taylor et al., ref. 71).

August 4 and 9, 1967 (ref. 75). This figure shows the typical result that the field magnitude is decreased during passage through the region just outside the Moon's optical shadow (the penubra) and increased within the shadow itself (the umbra). This same effect is visible also in figure 15, where we see that the field magnitude recorded by Explorer XXXV is lower than that recorded by Explorer XXXIII when in the penumbral region (indicated by the −), and is higher than the Explorer XXXIII value when in the umbra (indicated by the +).

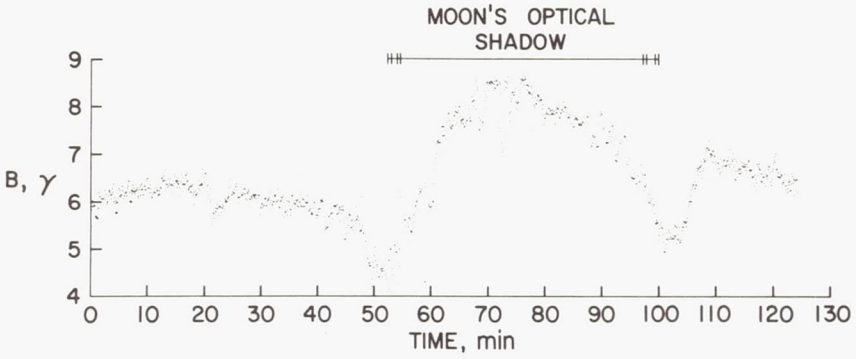


Figure 16.—**Measurements of typical magnetic field magnitude observed during four passes (Aug. 4 to 9, 1967) of Explorer XXXV through the lunar shadow. The satellite's distance behind the Moon in the shadow region ranged from about 0.5 to 1.0 lunar radius (Colburn et al., ref. 75).**

The diamagnetic effect of the plasma void region has been explained theoretically by two entirely separate approaches: the particle drift, or kinetic theory approximation; and the fluid-flow approximation. In the particle-drift approximation, as expressed in papers by Whang (refs. 76 and 77), the motion of individual particles is approximated by a guiding center velocity equal to the plasma bulk velocity, plus a one-dimensional thermal velocity in the direction parallel to the magnetic field. This thermal velocity is assumed to have a Maxwellian distribution centered at the parallel temperature. It is assumed that any particle striking the lunar surface is totally absorbed, and that the lunar body is entirely nonconducting. The void region on the dark side of the Moon is then filled in by particle thermal motion parallel to the field. (In a similar picture by Alfonso-Faus and Kellogg (ref. 78), the parallel velocity is provided by electron pressure rather than ion thermal velocity.) Because the proton gyroradius is large, about ½ lunar radius, collective plasma effects are assumed to play only a secondary role. Therefore, the assumptions that are made exclude the possibility of a shock wave in the region behind the Moon. From the particle velocity distributions, it is possible to calculate steady-state values of plasma density in all areas behind the Moon, for arbitrary orientations of the interplanetary field. Using typical values for the particle and field parameters, the field distribution and particle densities shown in figure 17 were calculated. The "plasma shadow" region consists of a conical-shaped umbra totally devoid of plasma and a penumbral region where plasma density is lower than in the solar wind. This figure is in essential agreement with the actual plasma densities reported in preliminary form by Lyon et al. (ref. 73).

A desirable next step is to calculate the currents associated with the particles in this plasma-shadow region (such as diamagnetism and various drift currents) in order to determine how these currents affect the local magnetic field. Results from such a calculation are presented in figure 18. This figure shows the total field predicted behind the Moon at 4.0 and 1.7 lunar radii, for three different choices of solar-wind parameters. This figure may be compared with the measured fields shown in figure 16. Higher order calculations of particle and field distributions leading to full self-consistency are also possible, although they become increasingly more difficult to perform.

The alternative way of treating the flow of plasma past the Moon, the fluid-flow approximation, has been employed by Michel (refs. 79 and 80) and Wolf (ref. 81). In this approach, collective interactions between particles are invoked, and the plasma is considered to be analogous to a hydrodynamic fluid striking a spherical object. Directly behind the object a rarefaction wave is generated which propagates into the unperturbed fluid, while the fluid begins collapsing into the vacuum behind the object. At the

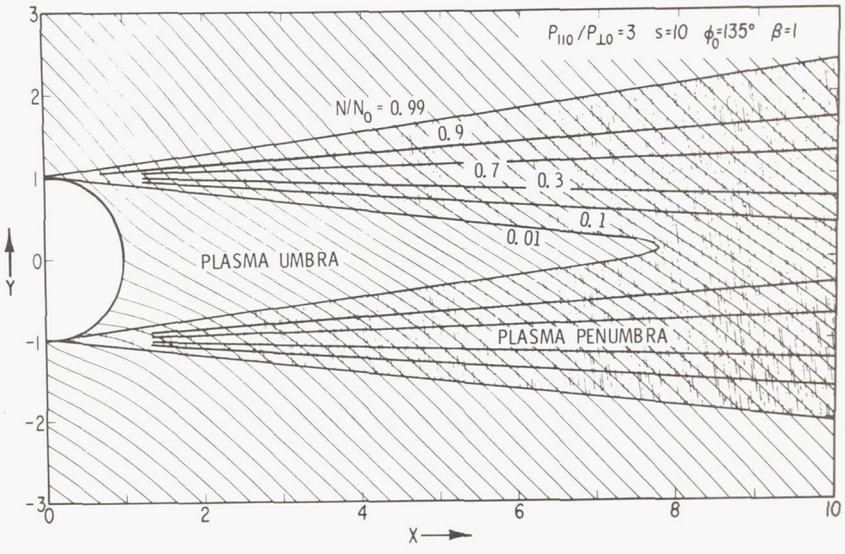


Figure 17.—Distribution of plasma in the shadow regions behind the Moon, from kinetic theory approximation. Contour lines of N/N_0 indicate plasma density in penumbral region relative to undisturbed solar wind. Magnetic-field lines show distortions from currents in the plasma. Calculations are appropriate for a ratio of $T_{\|}/T_{\perp}$ (equivalent to $P_{\|0}/P_{\perp 0}$) of 3, a ratio of bulk velocity to thermal velocity (s) of 10, β of 1, and angle between Moon-Sun line and interplanetary field (ϕ_0) of 135° (Whang, ref. 77).

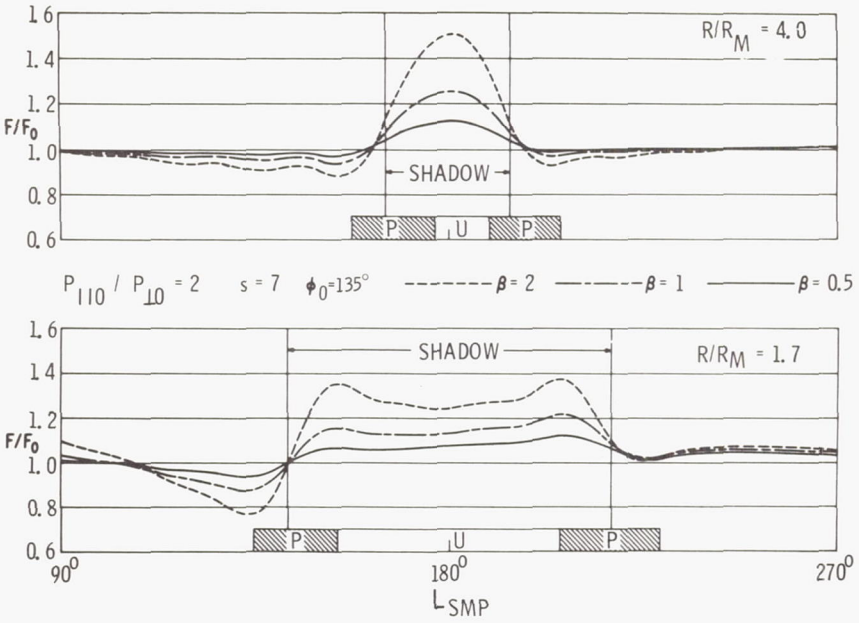


Figure 18.—**Theoretical values of perturbed interplanetary magnetic field F, relative to undisturbed value F_0, at distances behind the Moon of 4.0 and 1.7 lunar radii (R_M), from kinetic theory approximation. Field values are shown for $\beta = 0.5$, 1.0, and 2.0 (Ness et al., ref. 74).**

point where the collapsing fluid collides with itself (the apex of the conical-shaped void region), a shock wave is generated. In addition to this inner shock wave, there can be an outer shock wave, or at least a discontinuity, which forms when the recompression wave (trailing the rarefaction) becomes sufficiently steep. In the more realistic situation in which the fluid is the solar-wind plasma embedded in a magnetic field, additional account must be made of the magnetic-field pressure and of the fact that the fluid pressure is not isotropic but is strongest in the direction parallel to the field. Figure 19 shows the void region and shock configurations that would be expected in this model for two different orientations of the interplanetary field. The figure also shows the trajectory of Explorer XXXV during a typical pass in July 1967. The precession of the orbit of Explorer XXXV should have brought it into the predicted shock position by November 1967. According to Ness (ref. 69), no shock wave was seen by the spacecraft magnetometer when the satellite reached this position. However, the trailing shock wave predicted by Michel is a weak shock at best, and positive identification of it by a spacecraft magnetometer would be difficult in any case. From an assumption that magnetic flux is frozen into the solar-wind plasma during its

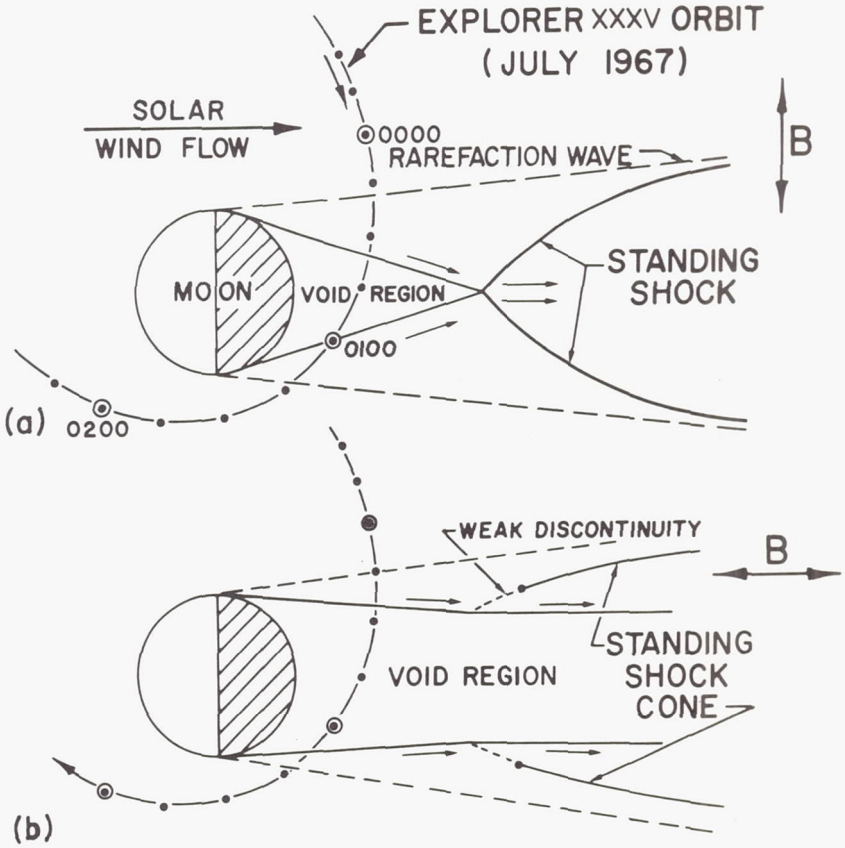


Figure 19.—The hydromagnetic flow structure behind the Moon, from the fluid-flow approximation, as seen looking southward at the plane of the ecliptic. Figure shows a projected orbit of Explorer XXXV in July 1967. (*a*) The structure which is appropriate for an interplanetary magnetic field perpendicular to the flow vector; (*b*) the structure if field lines are parallel to the flow (Michel, ref. 80).

expansion and recompression, Michel has shown qualitatively that the magnetic-field magnitude in the lunar wake region should vary in approximately the same fashion as that recorded by the satellite magnetometers.

Planets

It is of considerable interest to determine whether the planets have intrinsic magnetic fields, plasma shock fronts similar to the bow shock at Earth, or other features, such as radiation belts, which may be analogous to the Earth's magnetosphere. These features are all relevant to the question of

whether the planets have molten cores or similar interior composition, and are ultimately related to the origin of the planets themselves, the cause of planetary rotation, and other fundamental questions regarding the entire solar system. Because of their proximity to Earth, Mars and Venus have been the targets of several space probes during the last few years. As our technical capability expands, it is hoped that future investigations will extend inward to Mercury, and outward to the asteroid belt and Jupiter.

In the case of Venus, a wealth of information has recently become available to the scientific community, as a result of the success of Mariner V and the Russian interplanetary probe Venera 4. As reported by Bridge et al. (ref. 82) and Jastrow (ref. 83), the Mariner V magnetometer detected a bow shock about Venus. Plasma data reported by Gringauz et al. (ref. 83a) and the magnetic-field data of Dolginov et al. (ref. 84) from Venera 4 both serve to confirm this result. The trajectories of these two spacecraft near Venus, with a suggested bow shock sketched in to coincide with the three points of observations, are shown in figure 20. This figure also identifies five points of interest in the Mariner V trajectory which are keyed to the five points marked in the fields and particles data as displayed in figure 21. These points are: two crossings of the shock, (1) and (5); two crossings of the shock-associated rarefaction wave, (2) and (4); and entrance into a region void of plasma behind the rarefaction wave, (3).

It is well established that the bow shock around the Earth forms just in advance of the point where the Earth's magnetic field becomes strong enough to deflect further penetration of the solar plasma. However, Van Allen et al. (refs. 85 and 86), have concluded that the magnetic dipole moment of Venus must be less than 10^{-2}, and probably is less than 10^{-3}, of that of Earth, based on the absence of any measurable Venusian radiation belts. It is doubtful that such a small intrinsic magnetic field could alone deflect the solar plasma before it strikes the planetary surface. As to the question then of what on Venus can effectively deflect the solar plasma, one possible answer is that Venus has a dense ionosphere. Radio-occultation experiments from Mariner V, reported by Eshleman et al. (ref. 87) and by Kliore et al. (ref. 86), have established the fact that the density of the daytime Venusian ionosphere can be as high as 5×10^5 electrons/cm^3 at an altitude of about 100 kilometers, a density almost as high as the peak concentration in the Earth's ionosphere. The high conductivity of this dense ionospheric plasma would act as a shield against penetration by the interplanetary magnetic field and thus would be a suitable obstacle necessary for the formation of a shock front.

The Mariner IV probe to Mars also detected what might have been a shock, although it was considerably weaker than the Venus shock, and its presence could not be confirmed with confidence. Figure 22 (from ref.

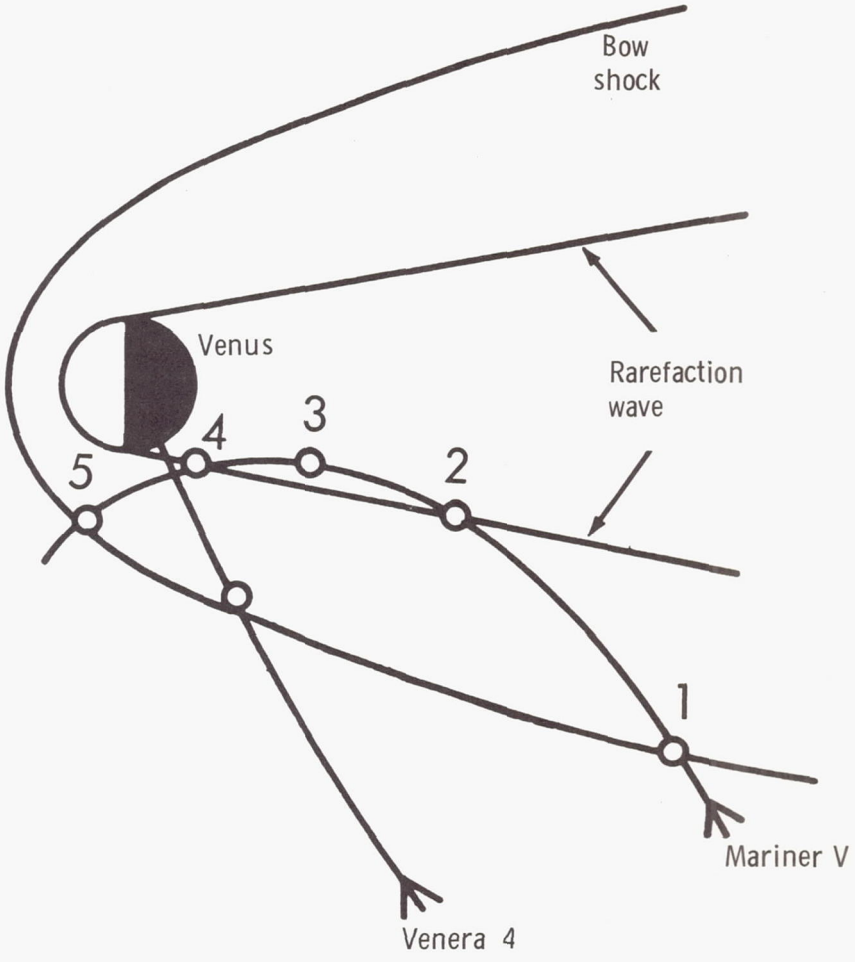


Figure 20.—Schematic representation of the solar-wind interaction with Venus. The Mariner V trajectory is sketched in with five noteworthy points of the orbit indicated. The Venera 4 orbit is also shown, and the circled point indicates the place where Venera 4 encountered the Venusian shock. Modified from a figure by Bridge et al. (ref. 82).

89) shows the Mariner IV trajectory as it swept by Mars, with a bow shock sketched in so that it intersects the trajectory at the two points where the magnetometer recorded sharp discontinuities in the total field. Smith et al. (ref. 90), who first reported the magnetometer data, have cautioned that the field disturbances seen while the spacecraft was near Mars possibly

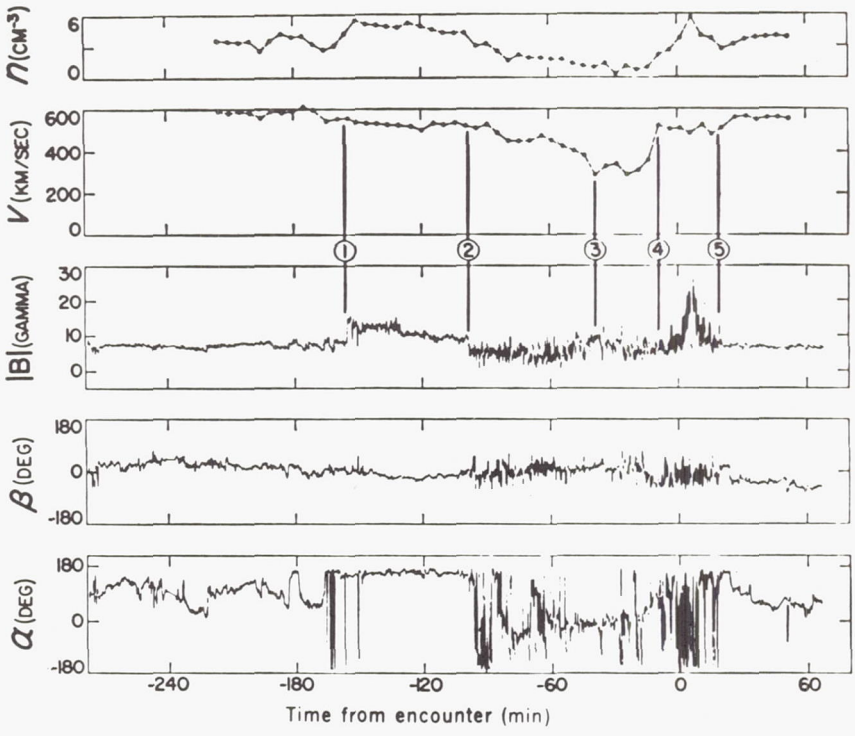


Figure 21.—Plasma and magnetic-field data near Venus obtained by Mariner V. Shown are solar-wind density n and bulk velocity V, along with the field magnitude and direction. Time indicated at zero corresponds to closest approach. Vertical lines and circled numbers correspond to the features noted in figure 20: (1) and (5) are interpreted as shock crossings; (2) and (4) as rarefaction wave crossings; and (3), as entrance into a region void of plasma behind the rarefaction wave (Bridge et al., ref. 82).

could have been an interplanetary field fluctuation bearing no relation at all to the planet. Plasma detector data taken while Mariner IV was inside the supposed Martian shock front, reported by Lazarus et al. (ref. 91), showed a slightly broader than average energy spectrum from about 300 to 1000 eV. Such broadening is characteristic of a magnetosheath observation; however, a failure in the instrument's high-voltage supply made the lower energy data unreliable. Assuming that the disturbance recorded by the magnetometer was, in fact, a Martian bow shock, Dryer and Heckman (ref. 92) concluded that this would imply a Martian dipole moment of about 2.1×10^{-4} of the dipole moment of Earth. (The smaller diameter of Mars and its greater solar distance would permit a shock to form with a

weaker dipole moment than in the case of Venus.) A Martian ionosphere would be an alternative source for production of the shock, in the same manner as the Venus ionosphere. As reported by Kliore et al. (ref. 93) from Martian radio-occultation measurements, a suitably dense Martian ionosphere does exist and could serve this purpose.

No spacecraft have as yet been sent to Jupiter, although this planet is of great interest. Strong radio signals in decimeter and decameter wavelengths have been observed to emanate from Jupiter, and the polarization of the decametric signals suggests that they are the result of synchrotron radiation. Synchrotron radiation at these wavelengths is most plausibly explained as the result of electrons of energy 10 to 100 MeV trapped in a Jovian magnetic field of about 1 gauss. With such a large trapping field, Jupiter must have a magnetic moment of perhaps 10^4 to 10^5 that of Earth.

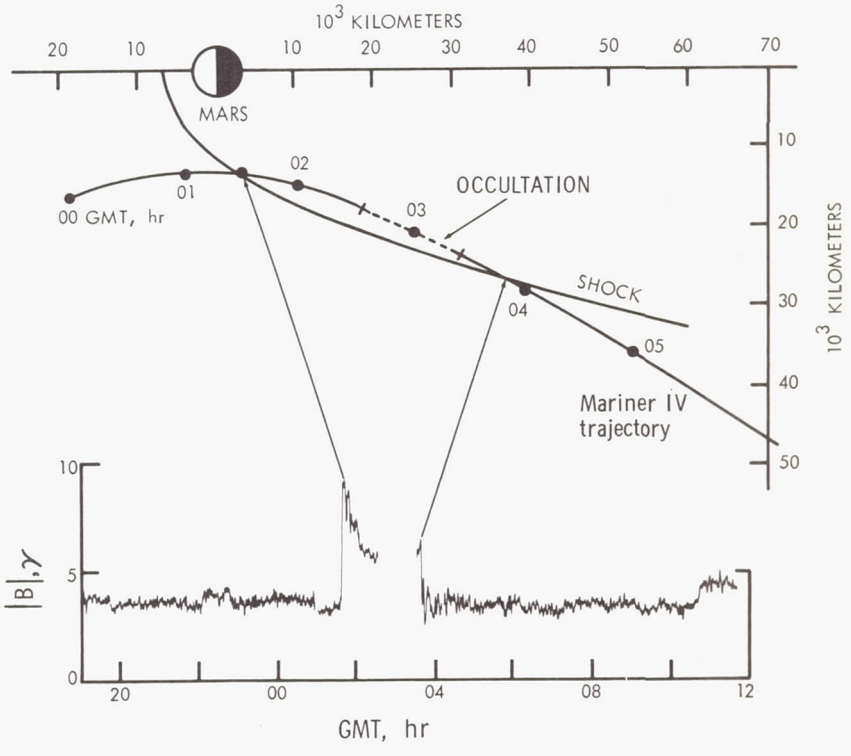


Figure 22.—Trajectory of Mariner IV during Mars encounter (July 14 and 15, 1965) showing probable penetration through shock front. Magnetic-field strength near Mars is shown in insert at bottom of figure. The arrows connect the magnetic-field measurements to corresponding points in the orbit (after Smith, ref. 89).

Because of its large magnetic field, Jupiter is expected to have intense radiation belts and a magnetospheric shock configuration which may be like that of Earth. For a review of radio observations of Jupiter, the reader is referred to recent articles by Warwick (ref. 94), Ellis (ref. 95), and Franklin (ref. 96). Synchrotron radiation from Jupiter has been discussed by Chang and Davis (ref. 97). On the basis of the strength of the synchrotron signals, the flux of 10-MeV electrons in the Jovian radiation belts at 2.5 Jupiter radii has been estimated to be about 10^5 electrons/cm^2-sec. Presumably, substantial fluxes of charged particles of other energies also exist in Jupiter's radiation belts. The Jovian magnetosphere, including a discussion on ring current belts of Jupiter, has been treated by Piddington (ref. 98).

The most striking recent observation relating to Jupiter has been the discovery that the probability of observing decametric radio signals depends strongly on the position of Io, the first Galilean satellite of Jupiter. This discovery, first announced by Bigg (ref. 99) and Duncan (ref. 100), has been made even more intriguing with a recent study by Tiainen (ref. 101), which reported that a weaker but measurable correlation exists between the probability of decametric emission and the position of Europa, the second Galilean satellite. Piddington and Drake (ref. 102) and Burns (ref. 103) have offered similar explanations for the control of Io over these radio bursts. The explanations require that either Io is permanently magnetized or, more likely, that Io has a high electrical conductivity and thus a magnetic flux tube from Jupiter is permanently anchored to it. In either case, a large number of energetic trapped electrons are constrained to move with lines of force that are anchored to the motion of Io rather than to a corotational motion with Jupiter. Particles moving with this "traveling flux tube" will experience the greatest energization when a magnetic pole of Jupiter is most inclined toward Io, and the most favorable position on Earth from which to observe the resultant enhanced synchrotron emission is along a line of sight perpendicular to the magnetic-field vector at the foot of this tube. The directions defined in this manner are, in fact, the same directions from which the Jovian decametric emission has been observed to be enhanced. Figure 23 illustrates a possible configuration of the magnetic field near Io and demonstrates the appearance of a tube of flux traveling with this satellite.

One of the intriguing features of the relationship between the solar wind and the planets is the possibility that the solar wind may be responsible for planetary rotation. In recent papers by Alfonso-Faus (ref. 104) and Burns and Alfonso-Faus (ref. 105), it has been pointed out that a torque will be exerted on a cloud of cosmic material as it orbits the Sun and condenses to form a planet. Since the solar-wind density decreases with radial distance, the strongest flux of solar-wind particles will be felt by that part of the cloud nearest the Sun, and the gradient in the flux will introduce a slight torque on the condensing matter. Calculations on the magnitude of

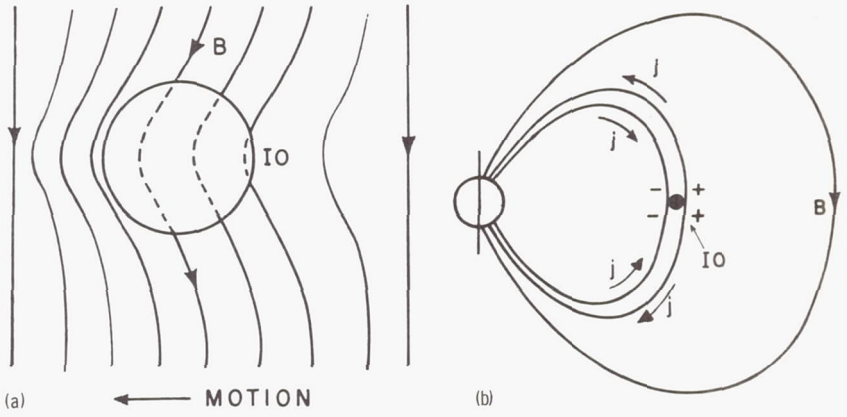


Figure 23.—**The passage of the satellite Io through the magnetic field of Jupiter, where Io is considered to be a highly conducting object. (*a*) Field lines (dashed) magnetize Io which otherwise causes no major distortion among the surrounding lines. (*b*) Io rotates relative to the planet carrying its frozen-in magnetic force tube westward. The whole force tube, from ionosphere to ionosphere, moves with Io but suffers considerable distortion (Piddington, ref. 98).**

this effect indicate that such a torque comes within better than an order of magnitude of accounting for the present rotational velocity of the Earth, and it does about as well in accounting for the rotations of Mars, Jupiter, and Saturn. This particular torque is such as to give a rotation in the prograde direction; that is, the same sense of rotation as the orbital motion. In contrast to this solar-wind-induced torque is the torque induced in a condensing cloud of particles through the differential in their orbital velocities around the Sun. As shown by Giuli (ref. 106), if a cloud of particles is in circular orbit about the Sun, neglecting effects from the solar wind, it would acquire rotation in the retrograde direction. However, if the same small particles are initially in elliptical orbits, the condensing cloud can acquire prograde rotation if the eccentricity of the ellipse is high enough. This latter result has been used by Alfvén (refs. 107 and 108) in support of his hypothesis that the initial material of the planets was a plasma which condensed in partial corotation about the Sun. One of the points on which the hypothesis rests is the fact that when corotating charged particles begin condensing into microscopic pieces of dust, their orbits become elliptical.

Interstellar Medium

Somewhere beyond Mars, at the point where the dynamic pressure of the solar wind is balanced by the background pressure of the interstellar medium, the supersonic solar-wind plasma flow is believed to terminate in a shock

transition and become subsonic. On the basis of a nominal 0.5 γ interstellar magnetic field, the radius of the region in which the dynamic pressure of the solar-wind flow exceeds the pressure of the galactic field is about 100 AU. This region is generally called the heliosphere. It is expected that a permanent shock structure exists in the solar wind somewhere inside the boundary of the heliosphere. In the region beyond this shock, the solar-wind protons may undergo considerable charge exchange with the ambient interstellar hydrogen atoms. This process is thought to produce a large source of hot hydrogen atoms with random velocities comparable to the flow velocity of the solar wind, and thus the atoms are capable of diffusing rapidly to the vicinity of Earth. Using night-sky observations of scattered ultraviolet radiation as the basis for estimating the density of neutral hydrogen near Earth, Patterson et al. (ref. 109) estimated that the charge-exchange region beyond the shock should be at about 20 AU rather than 50 or 100 AU. More recently, Hundhausen (ref. 110) has reviewed the problem and noted that the mean free path of postshock solar-wind protons against charge exchange should be very large, so that if a considerable amount of charge exchange is to occur within 20 AU, the shock must occur much closer in, perhaps as close as 5 AU, or roughly at the orbit of Jupiter. At present, it is not clear what physical mechanism could produce a shock this close, and an alternative may be to look for another source for the neutral hydrogen near the Sun. Nevertheless, Hundhausen's arguments serve to raise the interesting possibility that conceivably there might be another permanent shock feature near Jupiter in addition to the Jovian bow shock. Also, we have the interesting thought that solar-wind control over the interplanetary medium may terminate at about the position of Jupiter.

INTERACTIONS BETWEEN SOLAR WIND AND EARTH'S MAGNETOSPHERE

Bow Shock, Magnetosheath, and Magnetopause

When the supersonic solar wind reaches the vicinity of the Earth, the geomagnetic field forces the flow to be diverted. The familiar hydromagnetic shock wave forms at a standoff distance from the Earth of perhaps 10 to 15 R_E at the subsolar point. The thickness of the shock front at this point is no more than a few proton cyclotron radii (about 250 to 1000 km) and may be as small as 10 kilometers. Behind the shock is a disturbed region of plasma and fields which has been termed the magnetosheath; and behind the magnetosheath, at a subsolar distance of about 8 to 12 R_E, is the magnetopause, a boundary that delineates the highly disturbed region from the geomagnetic field that is associated with the trapped and quasi-trapped radiation.

On several occasions, when satellites have been in the interplanetary medium just outside the shock front, fluxes of energetic electrons and protons have been reported that appear to be of magnetosheath or magnetosphere origin (fig. 24). These particles are normally observed in relatively short bursts, and while their appearances are not as frequent as similar fluxes seen behind the shock in the magnetosheath, they are nevertheless common events. Examples of proton fluxes of this type from 0.2 to 20 keV have been reported by Asbridge et al. (ref. 111); electrons of this type greater than 40 keV have been reported recently by Anderson (ref. 112) and Oliven and Van Allen (ref. 113). One explanation for the appearance of these fluxes in the solar wind is that the particles originate in the magnetosheath as spikes (extremely short bursts) or islands and then move outward into the solar wind along interplanetary field lines. Figure 24 illustrates

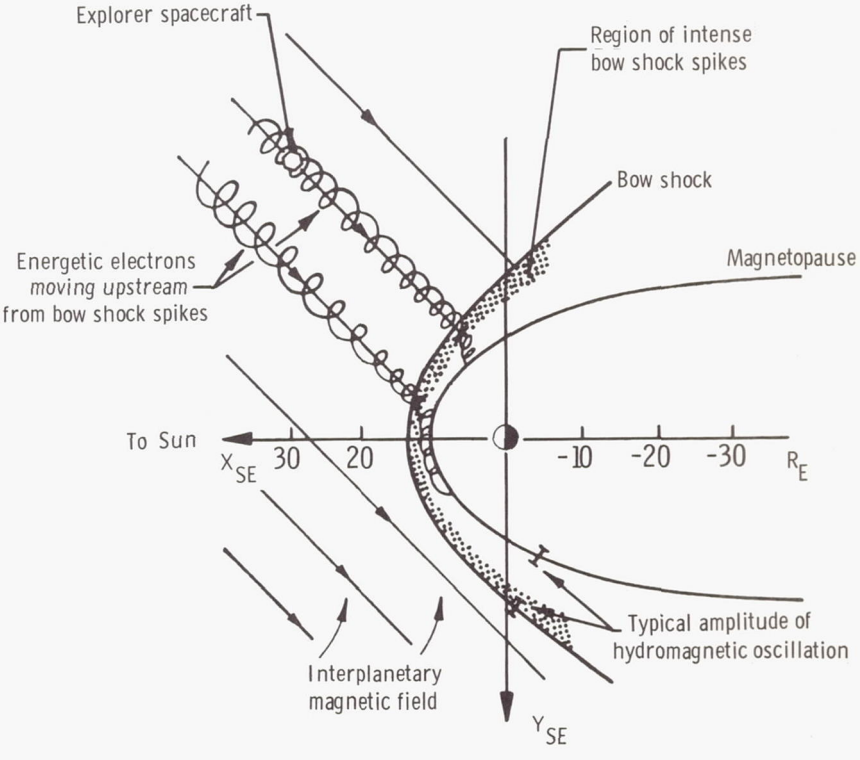


Figure 24.—**A model for the origin of energetic electrons upstream of the bow shock. Spikes of energetic electrons are known to be produced in the magnetosheath by action of the shock. These electrons might move through the shock toward the Sun on interplanetary magnetic-field lines and thus make their appearance in interplanetary space (Anderson, ref. 112).**

their paths and the positions relative to the bow shock where they can be observed.

Hydromagnetic waves, whistler waves, and magnetic noise bursts have all been reported near the shock front, in the magnetosheath, and near the magetopause. Heppner et al. (ref. 114), from OGO–I data, have observed wave trains of fairly coherent oscillations in the magnetic field near the shock, with frequencies in the range of 0.5 to 1.5 hertz. Smith et al. (ref. 115), with data from the same satellite, have observed and recorded a spectrum of fluctuations in the magnetosheath over the range of 3 to 300 hertz. Comparing their power spectrum at these frequencies to lower frequency observations from other satellites in the magnetosheath, Smith et al. obtained a composite power spectrum of disturbances in this region covering five decades of frequencies. This spectrum, reproduced in figure 25, has a break in the frequency dependence somewhere between 0.1 and 1.0 hertz. The break has been attributed to the disappearance of Alfvén waves at frequencies above about 0.1 hertz (the ion cyclotron frequency) and the disappearance of the omnidirectional mode of whistler waves above frequencies of about 3 to 10 hertz (the lower hybrid resonance frequency).

A theoretical model of the Earth's bow shock, in which the structure of the shock is determined by ion-wave instabilities of about 1 hertz in the shock transition region, has been presented by Tidman (ref. 116). In this model the wave instability is driven by the difference in streaming velocities of the supersonic plasma striking the shock on one side and the subsonic plasma leaving it on the other. The shock itself is filled with ion waves, and a spectrum of high-frequency noise continually emanates from either side of the shock, in the manner suggested in figure 26. A method for calculating the spectrum of plasma waves emitted upstream and downstream from the shock has been developed by Tidman and Northrop (ref. 117). Their theoretical model may be used to explain magnetic fluctations observed on OGO–I, if these fluctuations were in fact caused by ion waves rather than whistler-type waves.

The magnetopause has been observed to have occasionally a quasi-periodic motion, at frequencies much smaller than the above-mentioned magnetosheath disturbances. Freeman et al. (ref. 118) have reported cases of apparent 15- to 30-minute periodicities in magnetopause motion from Explorer XII data, and Anderson et al. (ref. 119) have noted 3- to 15-minute periodicities in this motion from Explorer XXI (Imp II) data. Freeman et al. have attributed this low-frequency boundary motion to quasi-periodic variations in the solar wind, the result of plasma from individual convective cells on the solar photosphere sweeping successively past the Earth.

The basic structure of the magnetopause has been studied in detail by Sonnerup and Cahill (refs. 120 and 121) by means of magnetometer data from 91 magnetopause crossings of Explorer XII. Two distinct types

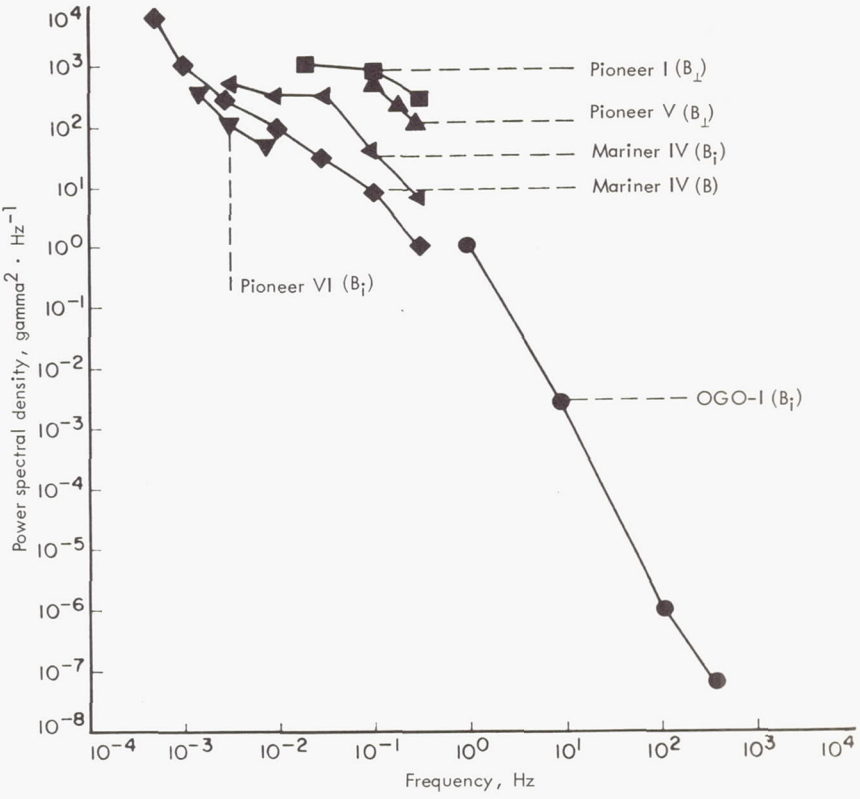


Figure 25.—Power spectral density estimates for fluctuations in the magnetosheath, based on data from five spacecraft. Some of the estimates are based on the field component perpendicular to the spin axis of the pertinent spacecraft ($B_\perp$), some on an individual component (B_t), and one on the total field magnitude (B). The single most significant feature of the spectrum is probably the change in frequency dependence that occurs somewhere between 0.1 and 1.0 Hz (Smith et al., ref. 115).

of boundary structure were observed: a rotational discontinuity, in which the magnitude of the field remains constant as the direction reverses from magnetosphere to magnetosheath; and a tangential discontinuity, in which the field magnitude goes through a minimum at the magnetopause current layer and is generally different on the two sides of it. In the latter case, the differences in magnetic pressure are presumably balanced by particle pressure. In the rotational discontinuity case, there may be a nonzero component of field normal to the boundary surface. When such a component exists, it is an indication of field-line connection between the mag-

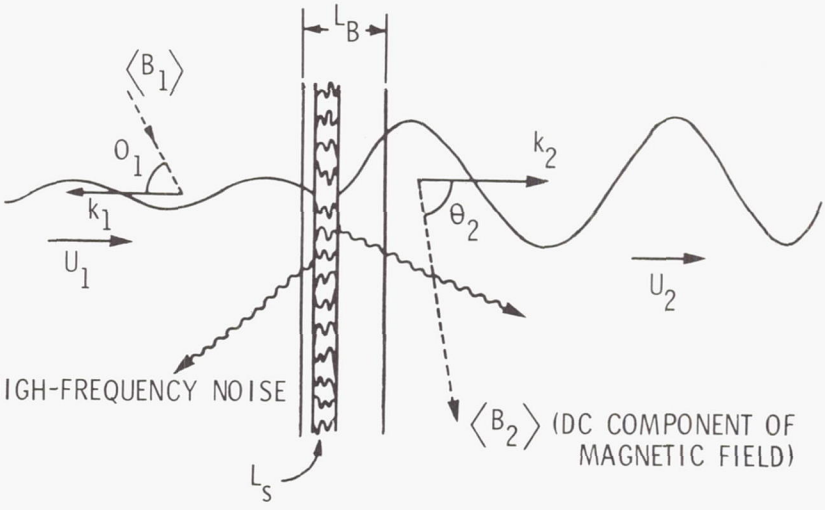


Figure 26.—**Schematic diagram of a theoretical shock structure produced by an ion-wave instability. The structure consists of a thin ion-wave shock (thickness L_s) over which the plasma density jumps discontinuously, a somewhat larger boundary (thickness L_B) over which the magnetic field jumps, and high-frequency noise emanating from the inner layer of ion waves (Tidman, ref. 116).**

netosphere and the magnetosheath. It is difficult to establish firmly the existence of a rotational discontinuity experimentally, because there is some uncertainty associated with establishing what is the plane of the boundary. Nevertheless, Sonnerup and Cahill estimated that about one-third of the 91 observed boundary crossings were of the rotational-discontinuity type and that the occurrence of this type of discontinuity seemed to be closely associated with magnetic storms.

It is to be expected that magnetic events occurring at the magnetopause are also reflected in ground-based magnetic observations. To find such a relation, various authors have correlated the fluctuations in the interplanetary magnetic field with the geomagnetic activity index K_p (refs. 122 to 125). A weak correlation exists between the 3-hour K_p index and the 3-hour-average magnitude of the total interplanetary field. However, there is a much closer correlation between K_p and the variance of the transverse interplanetary field (that is, that part of the field which is normal to the Earth-Sun line). Defining $\sigma\overline{B}_{T,N}$ to be the root-sum-of-squares of the variances of 1-minute samples of the two transverse components of the field, taken in 3-hour intervals, Ballif et al. (ref. 123) compared $\sigma\overline{B}_{T,N}$ with $\overline{K}_p$. The result is shown in figure 27, where $\overline{K}_p$, $\sigma\overline{B}_{T,N}$ and $\overline{B}/2$ ($\overline{B}$ is the average magnitude of the interplanetary field) are compared for the week of Jan-

uary 19 to 26, 1965, using Mariner IV data. The bars over the quantities indicate a smoothing by using 21-hour running means. It can be seen easily that the averaging process has brought $\sigma B_{T,N}$ into good correlation with $\overline{K_p}$, while for $\overline{B}/2$ the correlation is still poor. A more detailed comparison of the relation of $\overline{K_p}$ to fluctuations in each individual component of interplanetary field has shown that the correlation is weakest for the radial component $\overline{B_R}$ (that is, the component parallel to the Earth-Sun line), and the strongest correlation seems to vary from event to event between the two tangential components (north-south and east-west). Thus, these Mariner IV results only partially substantiate the theoretical arguments of Maguire and Carovillano (ref. 126) that fluctuations in the north-south component of the interplanetary field have a greater effect on geomagnetic disturbances than any other field fluctuations.

A large magnetic storm occurred on January 13 and 14, 1967. During this storm the magnetopause made its deepest penetration into the geomag-

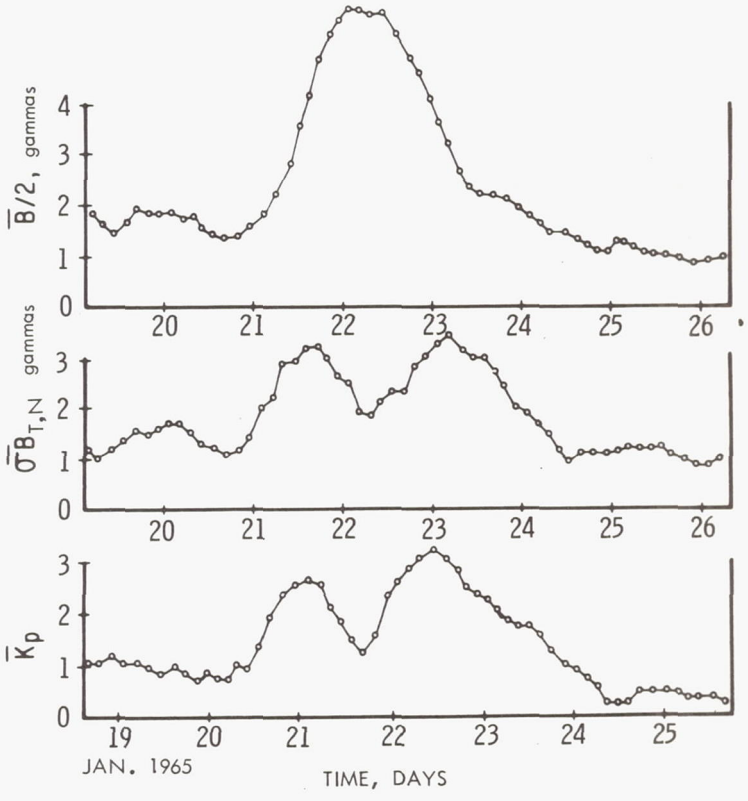


Figure 27.—**The mean interplanetary magnetic field $\overline{B}/_2$, transverse oscillations in the interplanetary field ($\overline{\sigma}\ B_{T,N}$), and the planetary magnetic index $\overline{K}_p$ observed from January 19 to 25, 1965 (Ballif et al., ref. 123).**

netic cavity ever recorded. The geostationary satellite ATS I, which is in circular orbit at 6.6 R_E, noted the passage of this boundary at about midnight UT on January 13 and 14, at which time the satellite was located in the early-afternoon part of the magnetosphere. For about an hour after this initial penetration, the magnetopause stayed within the proximity of 6.6R_E and made repeated crossings past the satellite. During this time, a number of significant observations were made by the complement of detectors on ATS–I, both confirming the fact that the boundary had actually crossed the satellite and investigating detailed particle behavior on both sides of the boundary.

The prime evidence confirming the boundary crossing is the magnetometer information which was reported by Cummings and Coleman (ref-127). Part of the data is displayed in figure 28. The figure shows, among

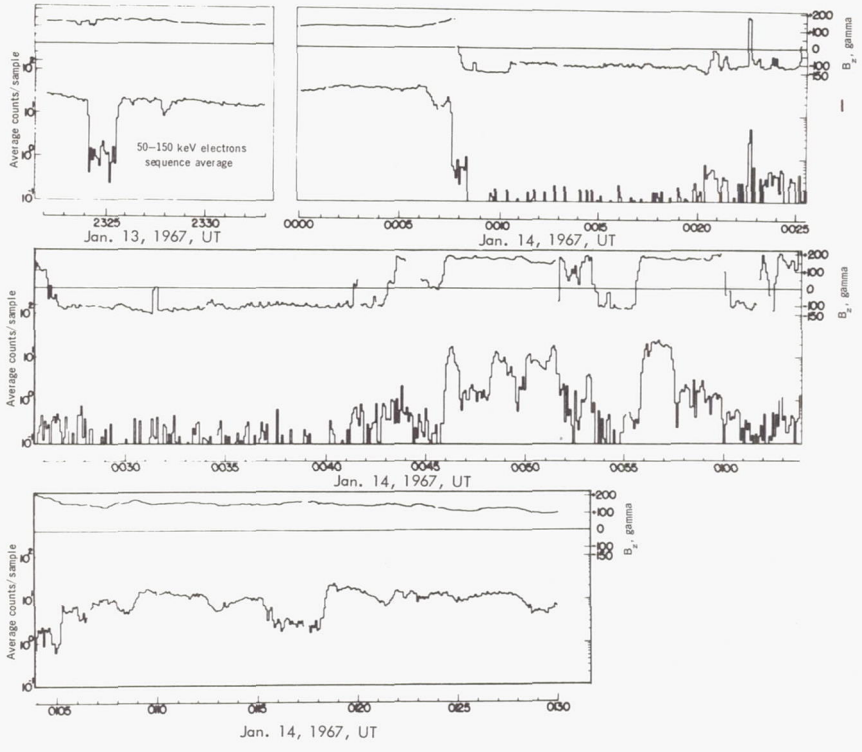


Figure 28.—**The magnetic field component B_Z along the satellite axis (approximately perpendicular to the geomagnetic equatorial plane) is plotted with 5.12-second averages of 50 to 150 keV electron counting rates during the ATS-I boundary-crossing event of January 13 and 14, 1967 (Lezniak and Winckler, ref. 128).**

other things, the B_Z component of magnetic field at the satellite (i.e., the component normal to the equatorial plane), which in this case is very nearly the same as the total field. The several changes of sign in B_Z are indications of the passage of the magnetopause current sheet past the satellite. Supplementary evidence of the boundary crossing is provided by the changes in flux of 50- to 150-keV electrons at ATS–I as reported by Lezniak and Winckler (ref. 128). A high-resolution time history of these fluxes compared with the magnetometer data is also shown in figure 28. Note that each time the B_Z component of the magnetic field became negative, the electron flux decreased by about two orders of magnitude down to background level. For 50- to 150-keV electrons, this is a phenomenon that can normally be associated with boundary crossings. Other data from ATS–I, including high-energy electron measurements reported by Lanzerotti et al. (ref. 129) and by Paulikas et al. (ref. 130), also correlate with the magnetometer observations. Independent evidence from other spacecraft in operation at the same time, such as that reported by Russell et al. (ref. 131) and by Bame et al. (ref. 132), has also been consistent with the observations of a deep boundary penetration.

In contrast with what might have been expected from the boundary-structure studies of Sonnerup and Cahill (refs. 120 and 121), a close study of the ATS–I vector magnetometer measurements by Cummings and Coleman (ref. 127) indicated that the nature of the boundary during the crossings at 6.6 R_E was that of tangential discontinuity and not a rotational discontinuity. Thus, even though a strong impulse at the front of the geomagnetic cavity had pushed the boundary far from its normal position, these authors concluded that there was still apparently little field-line connection between the magnetosphere and the magnetosheath.

During the time that the boundary was near ATS–I, a low-energy ion detector on the satellite recorded strong evidence of a directed flow of $>$50-eV ions on both sides of the boundary surface in the direction generally parallel with the boundary. This finding, reported by Freeman et al. (ref. 133), Freeman (ref. 134), and Warren (ref. 135), is illustrated in figure 29 by a somewhat idealized representation of the observed flow. This type of flow pattern may be evidence for an electric field normal to the boundary surface that emanates outward in both directions from the boundary. The observed ion flow is then interpreted as an electric-field drift motion near the boundary. The implications of this inferred electric field on models of convective plasma flow in the magnetosphere are discussed in a later section.

As a final point about the dramatic motion of the boundary on January 13 and 14, Schield (ref. 136) has noted the extent to which solar-wind pressure must increase in order to move the boundary into 6.6 R_E. Whereas under normal conditions the solar wind has a velocity of about 400 km/sec

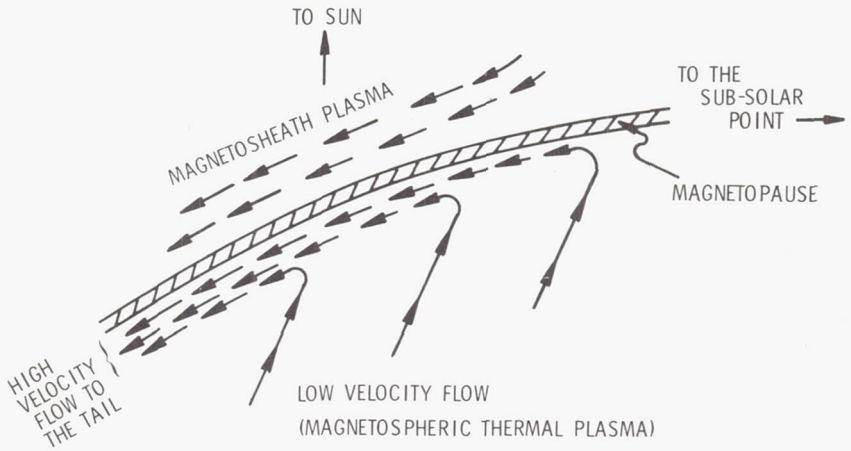


Figure 29.—**A diagrammatic representation of the plasma flow observed near the boundary by the low-energy ion detector on ATS–I. The drawing is somewhat idealized; actually there were a few short intervals in which the plasma flow appeared to have a component normal to the boundary. The description of the flow velocity as low inside the magnetosphere and high near the boundary is conjecture (Freeman et al., ref. 133).**

and a density of about 5 protons/cm^3, a boundary penetration into 6.6 R_E would require either an increase in solar-wind density to about 100 proton masses/cm^3, or an increase in velocity to about 1500 km/sec. According to Bame et al. (ref. 132), the Vela IIIA plasma detector indicated that the solar-wind speed was about 410 km/sec at the time of the boundary compression. Also at this time (0030 to 0130 UT on January 14) the solar-wind density rose to about 45 protons/cm^3 with about 9 alphas/cm^3. (The measured alpha/proton ratio of 18 percent at this time is exceptionally high; normally the alpha/proton ratio in the solar wind is about 5 percent.) Thus, there was a total density of about 81 proton masses/cm^3, which is reasonably close to the 100/cm^3 which was expected for this extreme boundary compression.

Neutral Sheet and Magnetotail

It is a well-established fact that geomagnetic field lines from high-latitude regions on the Earth are drawn back in the antisolar direction into an extended tail configuration. The general topology of the tail consists of field lines from the northern polar regions directed toward the Earth, and lines from the southern regions directed away from the Earth. These two volumes of oppositely directed fields are separated by a "neutral"

plane or sheet inside which the field has a low magnitude and frequently reverses. Although the existence of the tail is no longer in doubt, the length of the tail has been a point of substantial contention. This length depends on the rate at which magnetic merging can proceed; that is, the rate at which field lines from the northern latitudes can reconnect in the tail with field lines from southern latitudes. A simple indication of whether the merging is actually proceeding is the presence of a Z-component of magnetic field in the tail (that is, a component normal to the plane of the neutral sheet).

Detailed examinations of Explorer XIV magnetometer records by Laird (ref. 137) and of Explorer XXXIII records by Mihalov et al. (ref. 138) have found substantial evidence of field-line reconnection (that is, a substantial northward Z-component of field) at all distances in the neutral sheet for which measurements were available. Explorer XIV crossed the tail region at about 16 R_E; Explorer XXXIII made repeated crossings of the tail, from 35 R_E out to 82 R_E. At the farthest crossing of Explorer XXXIII, the neutral sheet still appeared to be present in the tail. A map of geomagnetic tail structure near the noon-midnight plane as seen by Explorer XXXIII has been compiled recently by Behannon (ref. 139), and is reproduced in figure 30. It is evident from the figure that the

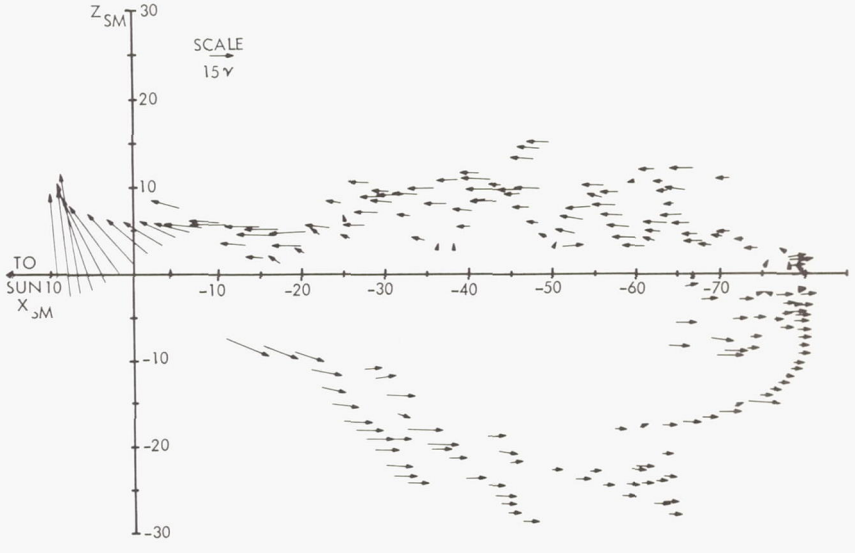


Figure 30.—**Average vector magnetic-field topology in the geomagnetic tail from July to November 1966, as typified by the projection of hourly average field vectors from Explorer XXXIII onto the plane perpendicular to the solar magnetospheric equatorial plane (Behannon, ref. 139).**

geomagnetic tail extends at least to 80 R_E (that is, past the lunar orbit) and that the field strength decreases with increasing distance from the Earth.

One evidence for field annihilation by particle currents at the neutral sheet would be the preferential occurrence of high-energy electrons there. Murayama and Simpson (ref. 140) have analyzed 20 neutral sheet crossings of Explorer XVIII (IMP–I) and have found fluxes of >160-keV electrons in all crossings. The flux generally peaks in the neutral sheet and has about twice the amplitude there as in adjacent regions. Even higher energy electrons were observed by Pioneer VII when it crossed the neutral sheet twice at about 20 and 40 R_E (Simpson, private communication). As shown in figure 31, the flux of >400-keV electrons seen by Pioneer VII peaked sharply at the exact position of the neutral sheet. This position is identified by the minimum in magnetic-field strength.

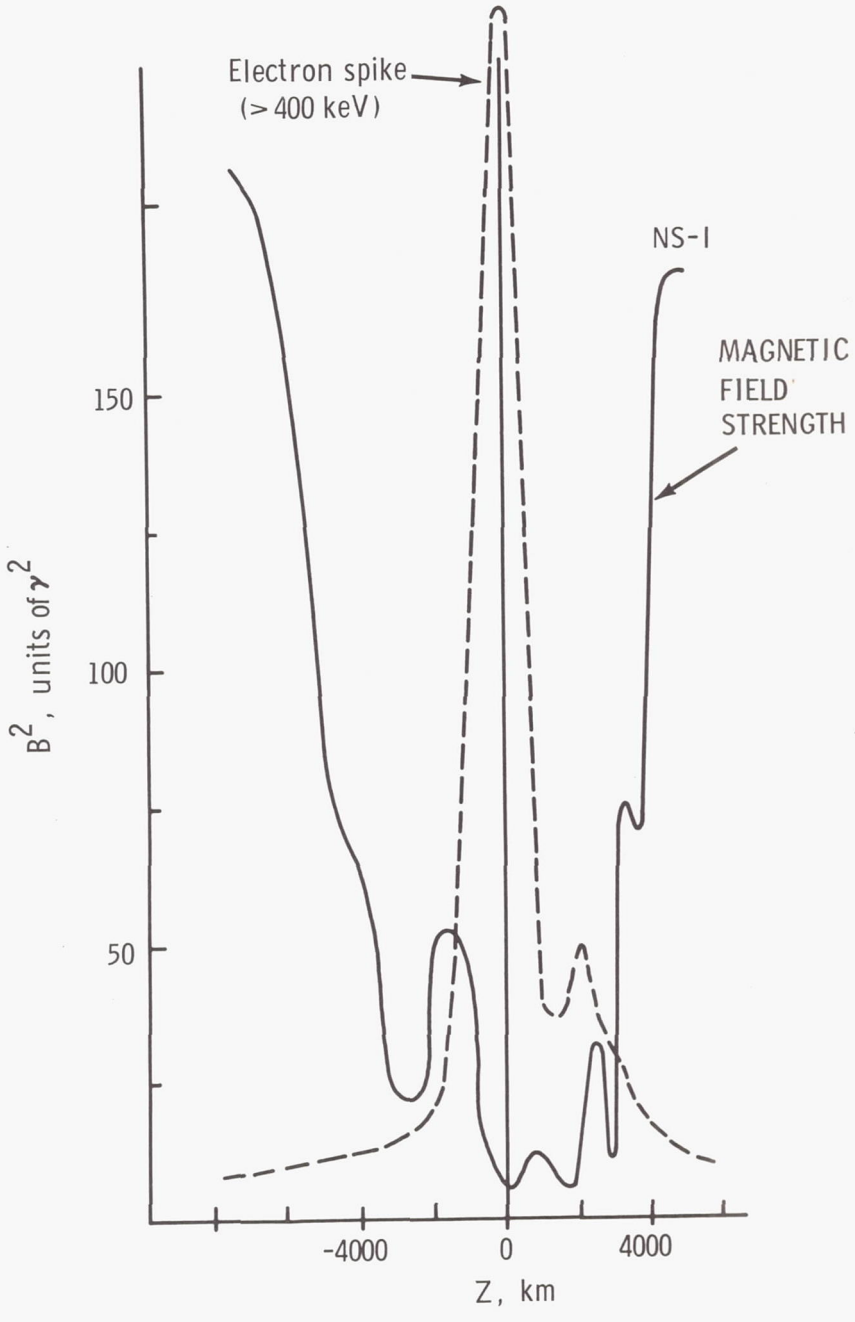
Particle-Trapping Region

While a substantial body of work related to the interior of the geomagnetic cavity has been performed since 1966, we shall confine our attention here to one topic that is perhaps critical to our understanding of the entire magnetospheric phenomenology: namely, the convective flow of plasma in the magnetosphere.

One of the most perplexing problems about the Van Allen radiation belts that surround the Earth is to find an explanation for why they should exist at all. During a lifelong study on aurorae that began in 1903, Störmer (ref. 141) worked out trajectories for charged particles fired from large distances toward a magnetic dipole. He found that for each particle there are certain "excluded" regions surrounding the dipole; that is, regions through which the particle trajectory cannot pass, no matter what its initial direction is. On the other hand, particles originating in the excluded region are trapped and cannot escape from the magnetic field. Applying Störmer's theory to the geomagnetic field, with cosmic rays and the solar wind as particle sources, one would conclude that these particles cannot enter or become trapped in the Van Allen belts. To explain the observed belts, another source, such as particles from the Earth's atmosphere, has to be invoked; however, observed particle densities and temperatures in the upper atmosphere and ionosphere make this assumption unlikely. Hess (ref. 142),

---

***Figure 31.*—First neutral sheet crossing (NS–I) with Pioneer VII (Aug. 18, 1966, 0110 UT). The magnetic-field configuration and the flux of electrons above 400 keV are shown. The sharp spike in the electron flux is suggestive of confinement to a magnetic gradient well (Simpson, private communication).** ◊



333-240 O—69——15

Freden and White (ref. 143), and others have investigated cosmic-ray neutron albedo as a source for the radiation belts; but this, too, is inadequate except possibly for high-energy particles at L-values less than about 2.5 (roughly, L is particle distance from the center of the Earth at the equatorial plane, measured in units of Earth radii).

The idea that particles which originate in the solar wind can enter the Störmer excluded region by means of a convective flow of plasma through the magnetosphere is perhaps one of the most plausible explanations for the origin of trapped radiation presently available, although the description of the flow is not yet completely satisfying. The idea of a convective plasma flow depends on a large-scale electric field perpendicular to the magnetic field to drive the plasma by means of the $\mathbf{E}=-\mathbf{V}\times\mathbf{B}$ drift motion. There is evidence that a suitable large-scale electric field probably does exist; however, there is considerable disagreement regarding certain aspects of the electric-field configuration and the mechanism which maintains it. At least three distinct sources have been proposed thus far to explain the origin of a gross magnetospheric electric field. They are: bulk motion of the solar-wind plasma and magnetic field past the magnetosphere, creating an induced electric field in the frame of reference of the Earth (discussed by Alfvén, ref. 144); a viscouslike interaction between the solar wind and the magnetospheric boundary, creating a polarization electric field (Axford, ref. 145); and magnetic merging in the tail, creating an electric field through motion of tail field lines of force (Dungey, ref. 146).

In a recent study, Brice (ref. 147) has examined the above theories of the gross magnetospheric electric field and has added an electric field arising from plasma corotation with the Earth, in order to find a "best estimate" for the flow patterns of plasma that might be expected in the magnetosphere. Kavanagh et al. (ref. 148), extending the work of Brice, have accounted additionally for the gradient drift motion of more energetic components of the plasma and for the effect on the overall field of the conductivity of the dense plasma inside about 4 R_E (that is, the plasmasphere). Figure 32 shows possible drift paths in the equatorial plane for energetic electrons traveling through the magnetosphere from the geomagnetic-tail region to the dayside magnetopause, under the action of a gross electric field of 0.3 mV/m. For protons, the drift paths are similar, except that they appear to be reflections of the electron drift paths about the noon-midnight line. The egg-shaped region enclosed by a solid line in the figure is the "forbidden" region; that is, a region which is excluded to particles drifting in from the tail, and which is a boundary between particles being swept through the magnetosphere and particles trapped in stable, closed-drift orbits. The size of the forbidden region is a function of both particle energy and the magnitude of the electric field. It expands as the particle energy increases or as the electric field decreases.

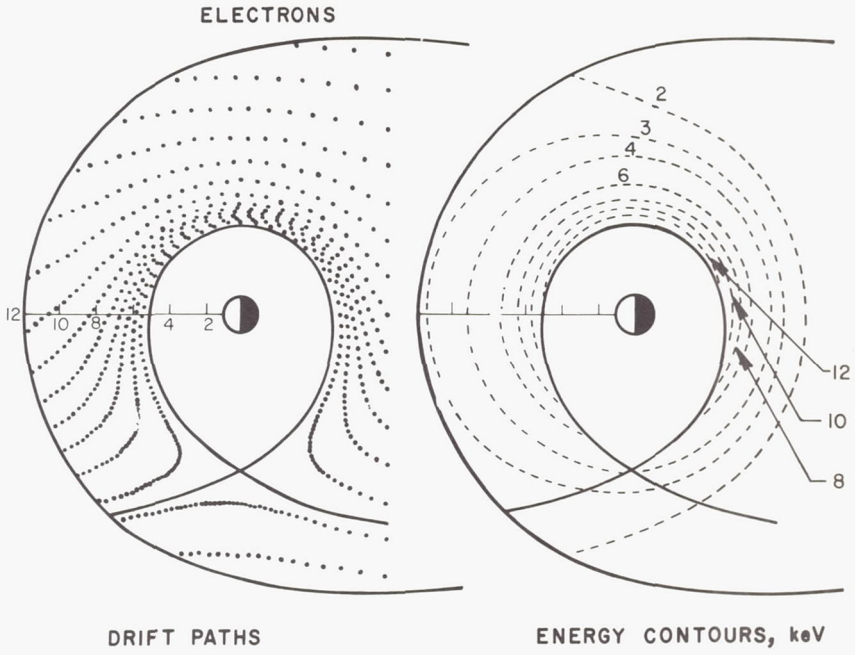


Figure 32.—**Possible drift paths in the magnetospheric equatorial plane for electrons of magnetic moment 0.05 keV/γ. A dawn-to-dusk electric field of 0.3 mV/m has been assumed (left). The magnetopause and the "forbidden" region are indicated by solid lines. Successive dots indicate the distance a particle drifts in 10 minutes. A possible return flow near the magnetopause is not indicated. Contours of constant energy for these electrons are shown on the right (Kavanagh et al., ref. 148).**

While the various convective flow models are reasonably close to agreement for plasma flow within the magnetosphere, there is considerable disagreement over the nature of the convective flow near the magnetopause. The Alfvén (ref. 144) model would have the magnetospheric plasma flow virtually unaffected by the presence of the boundary. The Axford (ref. 145) or Axford and Hines (ref. 149) model would have the boundary as an approximate electric equipotential, which forces the plasma flow approaching the boundary to be deviated to flow along the sides of the magnetospheric cavity. The Dungey (ref. 146) model would have some plasma deviated around the sides of the cavity, with other plasma flowing normal to the equatorial plane and out of the magnetopause through something like a boundary rotational discontinuity. An experimental observation from ATS–I of plasma flowing parallel to the boundary was discussed in a previous section in

connection with the magnetic storm of January 13 and 14, 1967, and was illustrated in figure 29. This observation appears to support either the Axford or the Dungey model. Since the instrument was incapable of detecting flow normal to the equatorial plane, it was not possible in a preliminary analysis to distinguish between the two.

The convective flow model has been used thus far in one way or another to explain auroral substorms, asymmetric ring currents, the position of the plasmapause, and the presence of a plasma sheet in the nightside outer magnetosphere. However, a major problem with the model is the fact that as energetic particles drift into the magnetosphere from the tail, the gradient in the magnetic field causes a charge separation to occur in the plasma. There is no general agreement at present on whether the excess charge should dissipate itself by flowing as electrical current along the magnetic-field lines, or whether the electric field formed by the charge separation should choke off the plasma convective flow altogether. The convection process is not expected to explain several other phenomena; one of these is the presence of large fluxes of protons of several hundred keV in the outer magnetosphere. These are presently thought to diffuse into the magnetosphere through scattering by magnetic- and electric-field fluctuations.

SOLAR COSMIC RAYS

Based on observations during the last solar cycle (ending in 1965), a phenomenological picture of solar cosmic ray production and propagation was developed. Impulsive acceleration of protons during the flash phase of a flare was assumed to be followed by immediate release of the protons into the interplanetary medium where particles were scattered by irregularities in the general spiral interplanetary magnetic field. Understanding of the scattering process was advanced by a number of theoretical studies (refs. 149a to 156). High-energy-particle scattering can be described roughly as a resonance with irregularities seen at the gyrofrequency of the particle, but mathematical difficulties remain, particularly in formulations using the Fokker-Planck equation in phase space (ref. 157). Although the predicted relation between the power spectrum of the magnetic irregularities measured near Earth and the modulation of energetic galactic cosmic rays is borne out by recent observations (ref. 158), the description of solar cosmic ray propagation, particularly at low energies (protons <100 MeV) is not yet resolved. For instance, modulation of galactic protons near the solar minimum could be explained by a measured power spectrum of magnetic-field fluctuations whose frequency dependence varied as f^{-1} (ref. 159); however, many solar-flare events were fit by a rigidity-independent mean-free-path λ (ref. 160), which required a frequency dependence such as f^{-2}, since the simple theory predicts $\lambda \propto R^{-2n}$ where R is the particle rigidity and the power spectrum varies as f^{-n}. (Fichtel and McDonald (ref. 161) give a

general review of solar cosmic ray observations prior to 1966.) Moreover, although the magnetic-scattering mechanism appears to be adequate to explain backscatter of low-energy flare particles from beyond 1 AU (ref. 162), the persistent anisotropies of early-arriving particles in some high-energy flare events (ref. 163) and of many lower energy proton events (refs. 164 and 165) suggest that there is less particle scattering inside 1 AU than beyond. Perhaps significantly, the first attempt to describe a flare event by diffusion (ref. 166) used a model with negligible scattering within the orbit of Earth. Although Burlaga (ref. 167) obtained a number of satisfactory bits to the history of high-energy particle events using solutions to an anisotropic diffusion equation, Reid (ref. 168) had pointed out that the proton onset of the flare of September 28, 1961, was consistent with two-dimensional diffusion across the solar surface (the flare was at 30° E), and Axford (ref. 169) combined this model of diffusion at the solar surface with one-dimensional diffusion along interplanetary-field lines to explain the latter phases of flare events.

These apparent discrepancies may be nearing resolution. The past 2 years have seen a considerable increase in our understanding of solar cosmic rays because of the greatly expanded observations of what might be called the "low-energy" component of solar-flare-associated radiations (protons <20 MeV, electrons ~ 40 keV, and X-rays ~ 20 keV). These particles serve as "tracers" of the coronal and interplanetary magnetic-field configurations because their small gyroradii effectively tie them to field lines. Their persisent presence is a clue to long-lived acceleration mechanisms in solar-active regions. The X-ray bursts are considered to be bremsstrahlung from electrons energized in flares, providing a valuable diagnostic of flare processes when combined with particle and radio observations.

There was an expected paucity of large-particle events following solar minimum in the medium- and high-energy ranges (protons >20 MeV, electrons >1 MeV, and X-rays >50 keV). However, improved detectors and more thorough coverage of these events by traditional means have brought out new aspects of solar acceleration and interplanetary propagation. Detailed study of radio and optical observations of particle-producing flares has revealed the development of magnetic-field and plasma configurations preceding and during the flare itself. These correlated studies have reached the point where an entire volume of collected observations will be devoted to a single event (July 7, 1966, in ref. 170).

The other species of solar cosmic rays have received greatly increased attention: neutrons, gamma rays, and neutrinos. Although only upper limits have been set on their fluxes, these limits are useful constraints on proposed models for solar processes.

In the following sections the observations of medium- and high-energy particles during 1965, 1966, and January 1967 are reviewed first on an event-by-event basis with occasional references to earlier events. Then

significant particle-related optical, radio, and X-ray observations are discussed, followed by a review of the recent satellite observations of low-energy proton and electron events and their relation to solar processes. A summary of neutron, gamma ray, and neutrino upper limits and their implications concludes this discussion of solar cosmic rays.

Medium- and High-Energy Particles

Simultaneous coverage of several events by widely separated satellites and probes added a new dimension to flare-event observations and permitted the separation of spatial from temporal variations of particle fluxes when conditions were favorable. In addition, improved techniques for ground-based particle detection have augmented the usefulness of these nearly continuous monitors.

The response of a standard IGY neutron monitor has been analyzed extensively (ref. 171) and the tendency of higher energy atmospheric secondaries to produce more than one neutron has been exploited in the neutron multiplicity monitor (ref. 172). The multiplicities can yield spectral information at high energies in intense flare events. Spectral information can also be obtained by a less-direct means, the latitude dependence of monitors during the isotropic phase of a large event such as that of February 23, 1956 (ref. 173). Independent measurements of primary cosmic rays have allowed refinement of monitor response functions (ref. 174). A major simplification has been noted by Wilson et al. (ref. 175). It appears that for a particular event, superneutron monitors may be compared at different altitudes and, moreover, that the percentage increase of a superneutron monitor and an IGY monitor for one solar event (January 28, 1967) were nearly identical.

Polar-cap-absorption (PCA) measurements (with riometers) have been especially useful in studying low-intensity proton events; see, for instance, the review by Obayashi (ref. 176) and the summary of recent events by Masley and Goedeke (ref. 177). Recent theoretical work (ref. 178) has established that riometers at 30 MHz respond predominantly to 10- to 25-MeV protons with a threshold sensitivity 10 protons/cm^2-sec-ster, and agreement of absolute fluxes with satellite observations has been attained (ref. 179). Moreover, the ratio of absorption caused by alphas versus protons is quite close to the alpha-to-proton ratio itself. Haurwitz (ref. 180) has made use of polar cap events (PCE) to continue the study of longitudinal distribution of flares begun by Dodson and Hedeman (ref. 181), Guss (ref. 182), and Warwick (ref. 183). Heeding the warning of Wilcox and Schatten (ref. 184) in analyzing the statistical significance of the apparent clustering tendency for a given choice of rotation period, Haurwitz still finds, as did his predecessors, a "dominant" hemisphere for the production of flares over the previous century in a longitude system based on a 27.213-day synodic

period. In corroboration, he notes that meter-wavelength radio bursts are statistically considerably stronger in the dominant hemisphere while the distribution of sunspot areas could well have occurred by chance. Further correlations of electromagnetic radiation with energetic particles are discussed after these summaries of large flare events.

February 5, 1965.—The event of February 5, 1965, was the first large event of the ascending part of solar cycle 20, but it was characterized by only a small proton flux increase above 80 MeV. It was recorded by satellite-borne detectors in the magnetosphere (Injun IV) (ref. 179), and also with similar detectors outside the magnetosphere (Explorer XXI and Mariner IV) (ref. 185). While Krimigis and Van Allen (ref. 179; see also refs. 186 and 187) were successful in obtaining a diffusion-type fit for protons with $E_p > 55$ MeV and Bostrom et al. (ref. 188) for protons with $E_p > 25$ MeV, the lower energy protons could not be fit thusly. Paulikas et al. (ref. 189) also noted for this event that proton intensities above 40 MeV decayed with a characteristic time considerably smaller than that applied to those above 20 MeV. The decay time was much less than expected on the basis of simple diffusion theory. O'Gallagher and Simpson (ref. 185) suggested that a difference in intensity profiles observed at the same energy ($E_p \sim 15$ MeV) at Earth and at 1.14 AU (fig. 33) could be explained by "corotation past the spacecraft of a magnetic region, containing enhanced proton flux and following the general spiral pattern of the interplanetary magnetic fields." This explanation implies a considerable spread in the azimuthal distribution of the particles. The flare occurred at 24° W, some and 40° and 50° east of the spiral line connecting to the Earth and Mariner IV, respectively. From this argument and the 3-day duration of the event, Krimigis and Van Allen concluded that the intensities must be essentially the same over a cone of full vertex angle of 70° if diffusion transverse to the average magnetic field is negligible to parallel diffusion.

This was the first event for which measurements of low-energy protons $E_p \sim 1$ MeV and electrons $E_e > 40$ keV were obtained. These are discussed after the next section. Comparison of fluxes within the magnetosphere with those on Mariner IV led Krimigis and Van Allen to regard, with qualifications, "the similarities in the absolute values of Mariner IV and Injun IV intensities as more remarkable than the differences."

All in all, this event proved to be a prototype for the simpler events that were to follow.

March 24, 1966.—The flare on March 24, 1966, gave additional evidence that the state of the interplanetary medium can strongly affect the propagation of medium-energy protons. The flare was not small (class 2) and was favorably located with regard to spiral field structure (22° N, 42° W). Consequently, the onset time of the protons (10 to 90 MeV) was about half an hour after the flare, almost simultaneous with the 40-keV electrons (ref. 190). Flare longitude was an important factor since there was a 1-hour

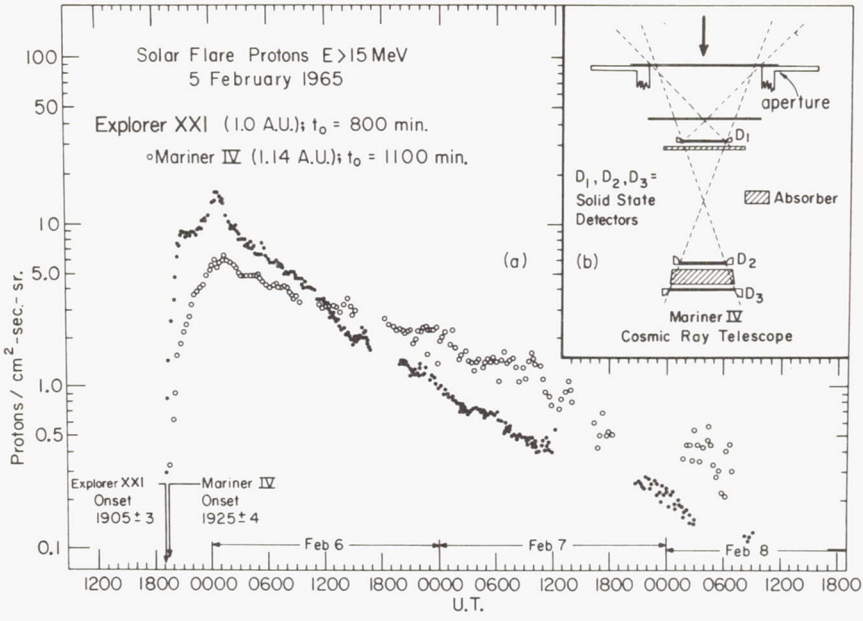


***Figure 33.*—(*a*) The decay time t_0, for proton fluxes from the February 5, 1965, event was observed by similar detectors to be shorter at Earth Explorer XXI (IMP–II) than at Mariner IV; (*b*) cross section of Mariner IV detector elements. Detectors D_1 and D_2 define a cone of acceptance of 40°. The telescope pointed directly away from the Sun throughout the mission (O'Gallagher and Simpson, ref. 185).**

delay in flux increase from a very similar flare at 32° N less than 4 hours earlier. The proton flux histories did not fit diffusion curves, exhibiting too rapid a decay. Although the time of maximum flux varied with energy roughly as $E^{-\frac{1}{2}}$, in accordance with classical diffusion theory, the root-mean-square path length thus derived was only about 2 AU. Diffusion analyses of flares at the end of the last solar cycle (ref. 191) yielded a distance of 10 AU. Kahler et al. concluded that the field lines could well have been "smoothed out" by outward moving plasma which caused a sudden commencement at 1133 UT on March 23, allowing more direct propagation. They noted that K_p was quite low on March 24, whereas it had been high for diffusive events, such as that of September 28, 1961. Directional measurements of protons ~10 MeV on Pioneer VI (refs. 164 and 165) showed very strong long-lived flux anisotropies with protons streaming predominantly outward from the Sun throughout the event.

A similar field configuration was deduced in the analysis of neutron moni-

tor increases for the event of May 4, 1960 (ref. 192), where 350-MeV protons appeared to experience well-ordered, scatter-free collimation within the filamentary structure, while the relativistic primaries (>4 BeV) passed through more than one magnetic filament per gyration. The individual filaments connecting the Sun and Earth were presumably smoothed out by the plasma from a west limb flare on April 29, 1960, that also produced a shock wave which preceded the flare particles (fig. 34). Another shock wave from a previous flare was invoked to explain additional increases during the decay phase on March 24, 1966. The shock producing a sudden commencement on March 23 would have been at 1.21 AU when the energetic protons arrived, possibly reflecting them back to the Earth. A "reflection coefficient" of 0.12 was deduced (ref. 190).

July 7, 1966.—The coverage of the flare of July 7, 1966, both ground-based and by satellite, was extraordinarily complete. Solar observations (photospheric fields, Hα and optical, radio, and X-rays) have furnished a detailed history of the active region for several days before and after the proton flare (ref. 170). The low-energy particle observations are discussed below.

Protons of energy greater than several GeV were produced since neutron monitors registered a small increase, less than 3 percent (refs. 170 and 193). Not only was this the smallest ground-level event ever distinguished, but it was the most northerly (47° W, 34° N). MeV flare electrons were definitely identified for the first time in this event (ref. 194); although they were probably present also on February 5, 1965.

While emphasizing that a diffusion-type fit does not necessarily imply interplanetary diffusion (because temporary storage at the Sun is possible), Cline and McDonald noted that not only did simple diffusion theory fit the electron history, but that intensities of electrons and 20- to 80-MeV protons gave congruent curves when plotted versus path length vt (fig. 35). The diffusion fit is quite sensitive to the choice of injection time, so it is striking that the optimum fit gave injection at the time (corrected for 8.3-minute light transit time) of the X-ray and microwave burst (ref. 195). Holt and Cline (ref. 196) argued that a differential kinetic energy electron spectrum E^{-3} or steeper could have produced both the observed X-ray spectrum above 80 keV (by bremsstrahlung) and the microwave intensity (by synchrotron radiation) if the source region is high in the chromosphere where the magnetic field is less than 500 gauss. Their analysis implies that most of the MeV electrons did not leave the Sun promptly. The deduced spectrum is consistent with that suggested by Takakura and Kai (ref. 197) in their analysis of the generation of the microwave radiation in flares.

August 28, 1966.—Cline and McDonald (ref. 194) point out that the flare of August 28, 1966, was similar to that of July 7, 1966, in both proton and X-ray output but lacked MeV electrons. The difference could be caused

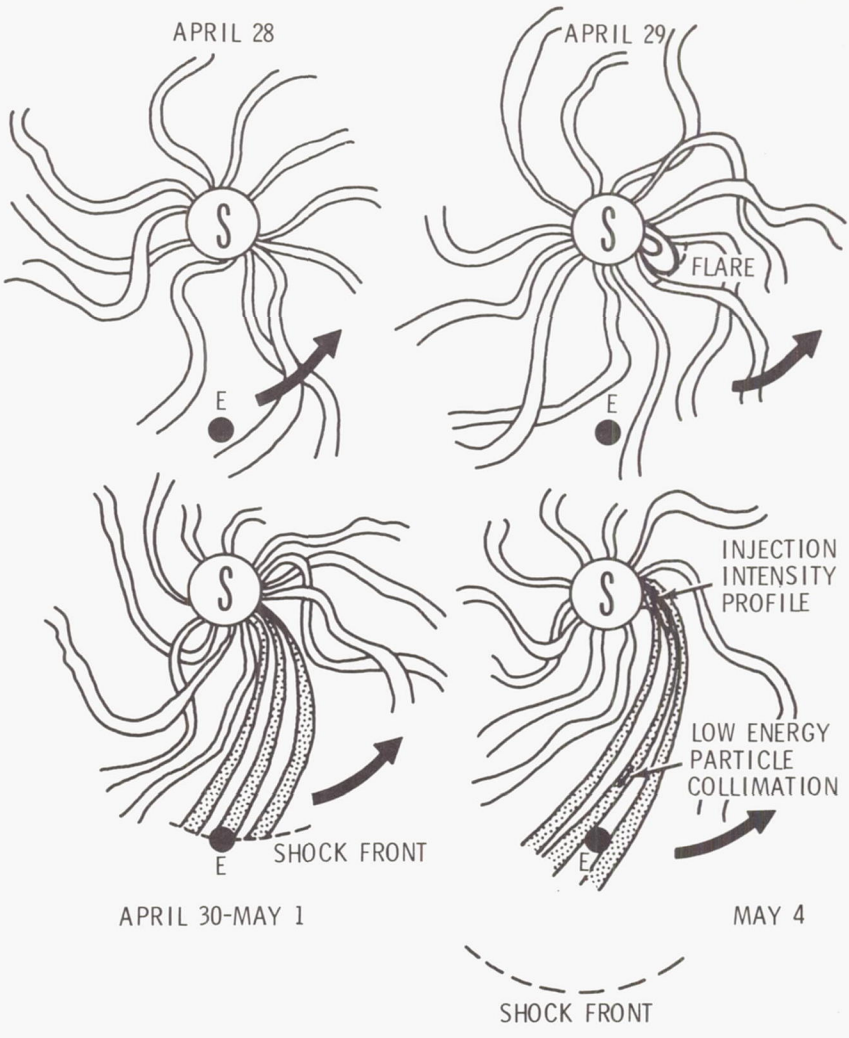


Figure 34.—A grossly exaggerated schematic representation of the time-history of the interplanetary magnetic-field configuration from late April to early May 1960. Solar particles generated in the flare event of May 4 are preferentially injected into a single well-ordered magnetic filament that was created by the west limb flare event of April 29 (Bukata and Palmeira, ref. 192).

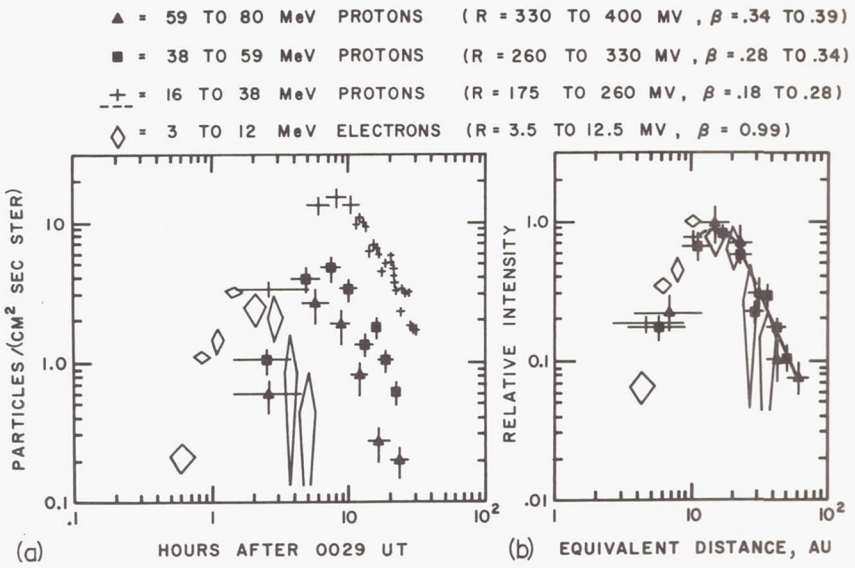


Figure 35.—(*a*) Intensity observations from Explorer XXVIII (IMP-III) on July 7, 1966, of protons with energies from 16 to 38 MeV, 38 to 59 MeV, 59 to 80 MeV, and of >3-MeV electrons plotted against time; (*b*) profiles of each relative intensity, I/I_{max}, plotted against distance traveled, $x = vt$, where v is the mean velocity for each energy group. The fit to a common curve is clearly seen. The velocities of the protons are between 0.18 and 0.4 that of the electrons ($\approx c$), but the rigidities of the protons (175 to 400 MV) are up to two orders of magnitude higher than those of the electrons (>3.5 MV) (Cline and McDonald, ref. 194).

by the more easterly location (23° N, 4° E) except that the March 24, 1966, event (which was more intense than that of July 7, 1966, in both high-energy X-rays and medium-energy protons and was ascribed to a flare at 37° N) also produced no detectable MeV electrons. However, both the events lacking MeV electrons occurred under large type I radio noise storms, a contingency that has proved important in classifying low-energy. (>40 keV) electron events (ref. 198).

Analysis of optical data for this flare (ref. 199) revealed that the Hα flare emission occurred "apparently close to the extremities of a feature which, if seen at the limb, possibly would have been described as the early phase of an ascending prominence," leading Dodson and Hedeman to suggest further study of the relationship between fast ejections recorded at the limb and the configuration of flares on the solar disk.

September 2, 1966.—Three rocket-borne emulsion measurements of protons and multiply charged nuclei (ref. 200) brought to five the number of events for which solar cosmic ray abundances are known. The event discussed here is that of September 2, 1966. The others are: September 3, 1960, November 12, 1960, November 15, 1960, and July 18, 1961 (ref. 33). As in previous observations the light elements (LiBeB) were missing and the helium-to-medium elements (CNO) ratio was about 60 (the weighted average of all observations in these five events was 59 ± 5). The solar cosmic ray abundances continue to agree well with photospheric abundances for $2\leq Z\leq 21$. This constancy of relative abundances does not appear in the proton-to-helium ratio which can vary by as much as a factor of 50 from event to event (ref. 33). Certainly, the propagation has something to do with these variations. The proton spectra obtained at three different times during this event (fig. 36) are considerably different at low rigidities, only the last one (35 hours after the flare) being mainly of the form exp $(-R/R_0)$ proposed by Freier and Webber (ref. 201; also see ref. 33) for higher rigidities. Protons of 10 MeV had almost an exponential decay over 7 days with a decay constant of 18.1 hours (ref. 165).

January 28, 1967.—The large event of January 28, 1967, has been ascribed to a flare on the invisible disk because of the lack of an adequate optical flare candidate, coupled with the unusually gradual rise to maximum ($\sim$4 hours) of the particle fluxes. It was easily observable by neutron monitors (refs. 175 and 193), and Lockwood (ref. 202) has extensively analyzed the sea-level measurements. He found an early anisotropy that defined an axis of symmetry at $65\pm15°$ due west of the Sun (fig. 37). The anisotropy disappeared about 3 hours after onset, and its value was much smaller than that of the May 4, 1960, event (ref. 203) in which the strong anisotropy lasted some 9 hours. The comparison is striking because the May 4, 1960, event resulted from a west limb flare (82° W). The early-phase ($\leq$5 hours) neutron-monitor intensity history was fit to a time dependence of the form t^{-N} exp $(-k/t)$, with N equal to either 5/2 (ref. 202) or 10/3 (ref. 193) while the later decay was exponential with a characteristic time of $\sim$6 hours. A fit to an anisotropic diffusion model by Burlaga (ref. 167) was consistent with a flare location about 60° beyond the western limb, the approximate location of an active center which was to produce a flare (February 13) on the next rotation.

This event was also observed by low- and medium-energy detectors on Explorer XXXIII near the Earth and Mariner IV some 82° west of the Earth at 1.59 AU (ref. 204). The Mariner IV coverage encompassed only a 4-hour interval some 8 hours after the onset of the high-energy event. The Geiger tube counting rates (attributed to penetrating protons $E_p>40$ MeV and an anisotropic flux of low-energy electrons $40<E_e<140$ keV) were the largest recorded on Mariner IV up to that date. They were larger

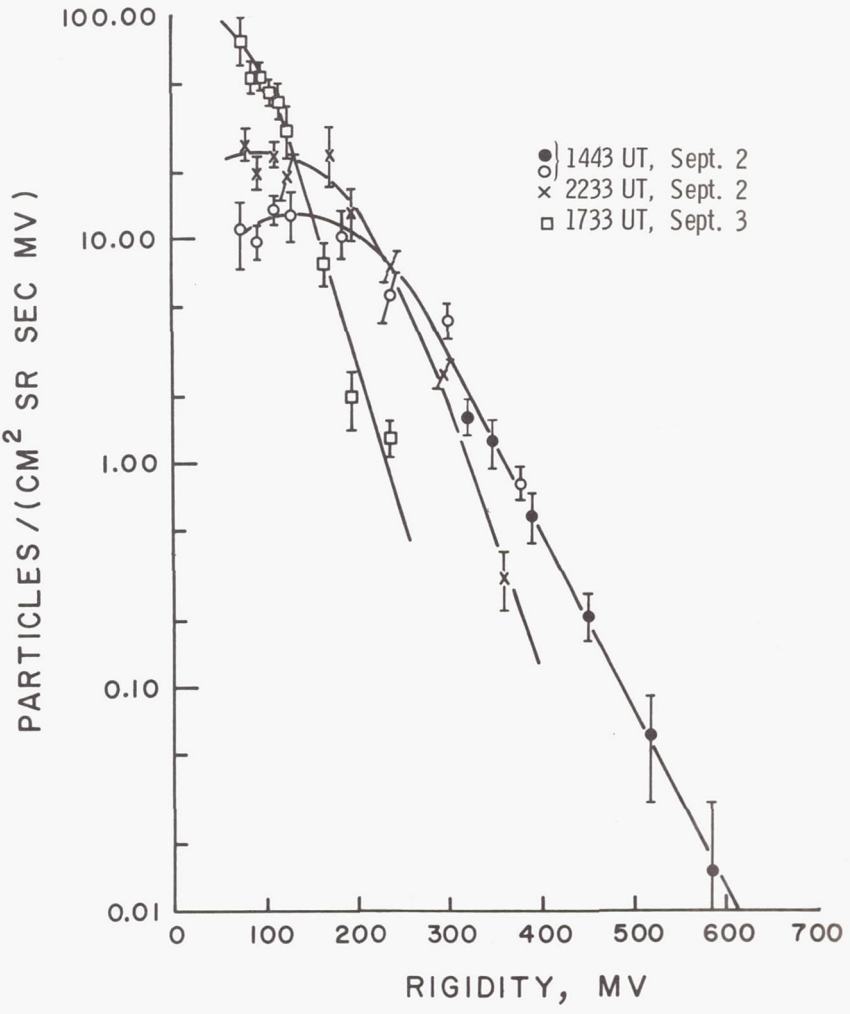


Figure 36.—Differential-rigidity spectra for particles from the flare of 0600 UT on September 2, 1966, observed with three sounding-rocket flights. Experimental points indicated by circles, crosses, and squares are for flights at 1443 Sept. 2, 2233 Sept. 2, and 1733 Sept. 3, respectively (UT). All data are for protons, except the solid circles, which represent fluxes of helium nuclei, multiplied by 10. Note that the spectra are exponential in form only at the higher rigidities (Durgaprasad et al., ref. 200).

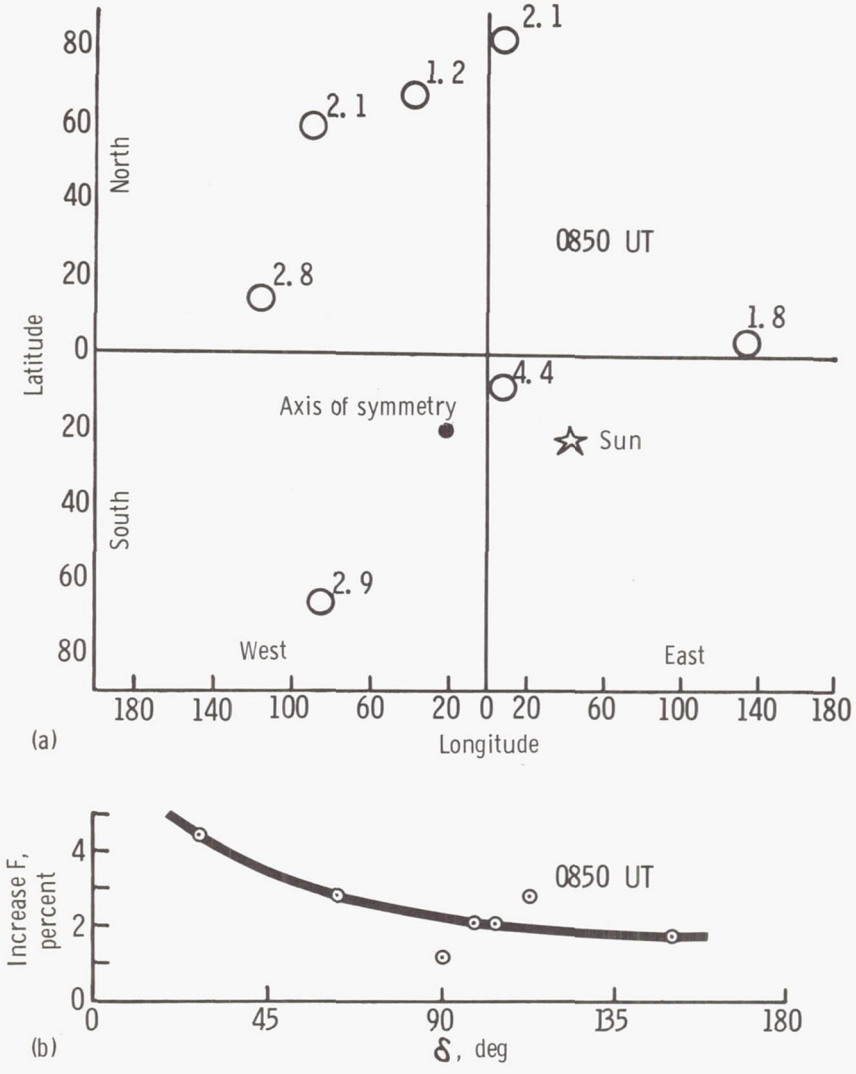


Figure 37.—Arrival anisotropies for flare of January 28, 1967, supposedly located beyond west limb of Sun. (*a*) Percent increase of the neutron-monitor counting rates at 0840 to 0850 UT as a function of asymptotic look direction; (*b*) percent increase in neutron-monitor rates versus δ, the angle between the axis of symmetry defined in (*a*) and the look direction of the station (Lockwood, ref. 202).

than those measured at the time by comparable detectors on Explorer XXXIII.

An unusual feature of the Explorer XXXIII measurements was a "proton precursor" which was also observed in Explorer XXVIII measurements (fig. 38 from ref. 194). Medium-energy proton fluxes began to rise at 0215 UT and 3 hours later reached a preliminary plateau that was more than an order of magnitude above background. The main proton increase, as well as the MeV electron increase, did not begin until about 0830 UT. A weak precursor had also been noted for the March 24, 1966, flare (ref. 194). The precursors have been attributed to preliminary acceleration at the Sun and/or a leak in a temporary storage region somewhere between the Sun and Earth. In this connection, Baird et al. (ref. 193) note that the onset of ~100 MeV protons (0822 UT) was earlier than that for energies of ~1 BeV (0833 UT), and they conclude that the acceleration mechanism therefore had to have a finite (as opposed to "impulsive") duration.

Following the event there was an extended "disturbed period," from February 1 to 7. Neutron monitors recorded extraordinarily large (>2 percent) diurnal variations with depressed fluxes from the sunward direction (ref. 202), while during this same period there were enhanced fluxes of MeV electrons, medium-energy protons (ref. 194), and low-energy protons (ref. 204).

Optical, Radio, and X-Ray Radiation

The previous discussion of the five most widely covered energetic particle events of the first 2 years of this solar cycle indicated that the behavior of particle fluxes near 1 AU was determined by conditions both in the interplanetary medium and at the Sun. For this reason the detailed optical studies of particle-producing flare regions by solar astronomers promise to prove increasingly helpful. In addition to those mentioned above (refs. 170 and 199), several analyses of flare regions were carried out by McKenna (ref. 205), Smith and Ramsey (ref. 206), Zirin and Acton (ref. 207), and Zirin and Werner (ref. 208). Flare structures exhibit continual activity (motions, brightening, surges, and waves (ref. 208); and "comparison between the incidence of $H\alpha$ brightenings and radio and ionospheric effects" associated with a particular solar region "showed that the frequency with which particles were accelerated to higher energies decreased markedly with the energy involved" (ref. 205). Despite continual variations, active regions often produce sequential "homologous" flares, showing a common pattern of structure and development (refs. 208 and 209).

Fokker (ref. 210) also found homology in centimeter, decimeter, and meter wavelength flare-associated radio events, suggesting that the dominant field structure is little changed over 1 or 2 days with nearly identical multiple-particle injections. Another consistency recently noted (and so far unexplained) is the tendency of proton-producing flares (indicated by

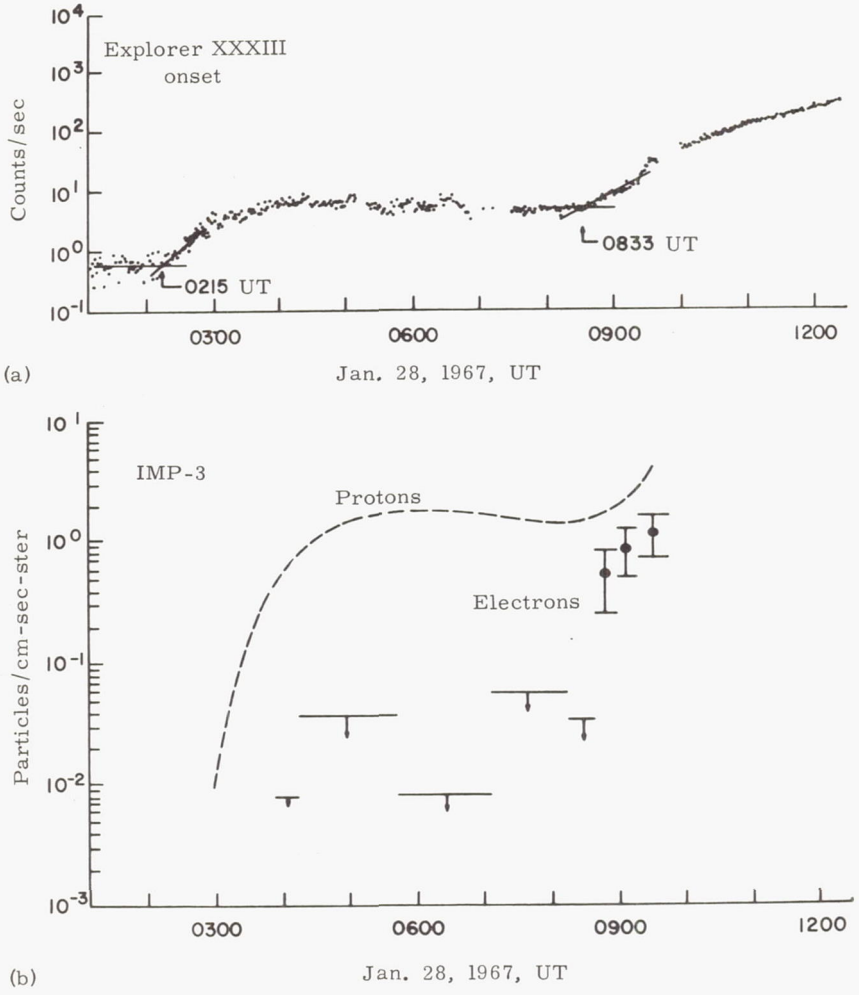


Figure 38.—**Proton precursor for the flare of January 28, 1967. (*a*) Counting rates of the Geiger tube (protons >40 MeV) on Mariner IV (Innanen, ref. 204). (*b*) Fluxes of protons >16 MeV and electrons >3 MeV on Explorer XXVIII (Imp III). The proton precursor is followed by an abrupt, large intensity increase which quickly becomes impossible to monitor, but in which some electron response is briefly indicated (Cline and McDonald, ref. 194).**

PCA's) to have U-shaped spectra for the flare-associated radio bursts (Castelli, Aarons, and Michael, refs. 211 and 212). The minimum intensity occurs at decimeter wavelength because of a much enhanced meter radiation (fig. 39). Castelli et al. point out that since U-shaped spectra are quite

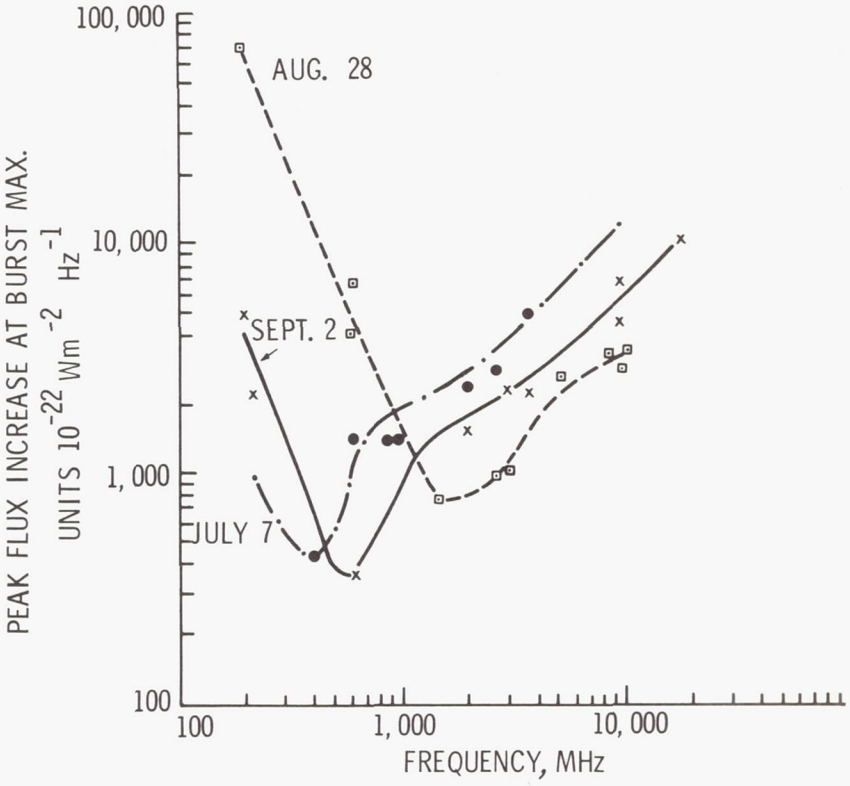


Figure 39.—**Radio spectra proton events, 1966. Each point for each event represents the maximum flux increase at the observed frequency, generally within a few minutes of each other and of the associated optical flare. Observations for these events were made at Sagamore Hill, the Netherlands, Nagoya, Tokyo, and the Dominion Radio Observatory, Canada (Castelli et al., ref. 211).**

common, absolute intensity must also be considered. A flux density >800 units in the microwave region up to 10 GHz is required for a high probability of associated proton production. The same authors reported that the unprecedentedly large radio bursts of May 23, 1967 (ref. 212), which were followed by a proton event also exhibited a U-shaped spectrum, as did several white-light flares between 1956 and 1960. Smerd (ref. 213) had noted earlier that meter-centimeter spectra associated with type III bursts showed an excess of meter radiation over those bursts not accompanied by type III bursts. This observation is consistent with the association of U-shaped spectra with energetic-particle production, since type III bursts are attributed to nearly relativistic electron streams escaping through the corona.

333-240 O—69——16

Warwick (ref. 214) has recently interpreted type V bursts (which only occur following type III bursts) as resulting from such streams passing through an outer coronal region already heated several-fold by the previous passage of type III-producing electrons. Kundu (ref. 215) discusses the large variety of solar radio emissions in terms of production mechanisms.

One of the most useful of the radio "fingerprints" of flare particle acceleration has been the impulsive microwave (centimeter) burst. Sakurai (ref. 216) has emphasized that type IV microwave bursts with fast rise and high intensity are more likely to be followed by X-ray effects in the ionosphere and the arrival at Earth of BeV protons than are bursts beginning in the decimeter range and then extending to centimeter wavelengths. He therefore suggests that rapid, intense development of the radio bursts is indicative of efficient particle acceleration. The microwave burst is often identified with flare X-rays and sudden ionospheric disturbances produced by X-rays (ref. 217); see the bibliography for early observations. Although recent authors attribute the microwave bursts to synchrotron radiation from nearly relativistic negative electrons (refs. 196 and 197), Lingenfelter and Ramaty (refs. 218 and 219) discussed the possibility of the radio bursts in large flares arising in part from relativistic ($20<\gamma<200$) positrons which are decay products of π^+ mesons from pp and $p\alpha$ reactions between energetic flare protons and solar hydrogen and helium. Hagen and Barney (ref. 220) have interpreted the frequency dependence of the preburst radio emission (decimeter and centimeter) as the rising of a hot region (10^6 to 10^7 °K). At some height in the corona the nonthermal burst occurs. The upward velocities derived from eight events varied between 1 and 150 km/sec.

If synchrotron radiation is to be used as a detailed diagnostic of particle acceleration, the influence of the solar atmosphere and magnetic field on the generation of the radiation must be taken into account, as was earlier recognized by Russian workers (ref. 221). One effect recently investigated is the low-frequency cutoff in type IV meter and decimeter bursts produced by relativistic electrons (refs. 222 and 223). Apparently there is a suppression of low harmonics. An opposite effect, "masing" of synchrotron emission, has been studied by McCray (ref. 224).

The most unambiguous indicator of flare-electron acceleration is the hard (>20 keV) X-ray bursts. Although there has been general agreement on bremsstrahlung as the mechanism since the first observation in March 1957 by Peterson and Winckler (ref. 225), controversy over thermal versus nonthermal sources still continues. Chubb et al. (ref. 226) interpreted the time dependence of their hard X-ray spectra (40 to 100 keV) from the flare of September 1, 1959, as free-free radiation from a plasma at 2.85×10^8 °K which they argued was also consistent with the 1957 event (originally considered nonthermal). Anderson and Winckler (ref. 227) in their detailed analysis found their three-point spectra (20, 50, and 150 keV) during the

bursts on September 28, 1961, inconsistent with any simple thermal model and supported their nonthermal model with association of types III and IV radio emission. Acton (ref. 228) argues that there is no evidence of temperatures above 5×10^6 °K in flare regions, and that the sharp temporal features of the bursts and good association with energetic flare particles at the Earth make nonthermal acceleration the likely candidate. At lower energies (7.7 to 12.5 keV), Hudson et al. (ref. 229) showed that the decay (only) of a burst (March 18, 1967) could be fit by a thermal cooling from 45×10^6 °K with a constant emission measure. (For some 50 events studied between March 9 and March 31, 1967, the emission measure is always within a factor of 2 of 10^{47} cm^{-3}.) De Jager (ref. 230) has emphasized the distinction between the soft X-rays (<10 keV) which are probably produced quasi-thermally and hard X-rays (>200 keV) which appear to be nonthermal. Boldt and Serlemitsos (ref. 231) have raised the interesting possibility that X-rays may be produced by energetic protons colliding with ambient electrons, a process certainly applicable to flares.

Van Allen's satellite-borne detectors (refs. 232 and 233) have provided increased detail on the temporal behavior of X-ray flares, and a new step in solar X-ray astronomy was reported by Vaiana et al. (ref. 234), who obtained X-ray images of a solar flare on June 8, 1968, with a rocket-borne grazing-incidence telescope. The general structure of the X-ray flare resembles the one in Hα. This relationship also holds for active regions, suggesting strong magnetic connection between the two emitting regions which must have a large difference in their degrees of ionization.

The continuous monitoring of the ion chambers on OGO–I and OGO–III allowed Arnoldy et al. (ref. 235) to study the correlation of hard X-ray bursts (threshold, 10 keV; peak response, $\sim$20 keV) with solar particle events from September 1964 to July 1966. In agreement with their earlier study (ref. 236), they found good correlation with the occurrence, intensity, and shape of centimeter radio bursts greater than 80 solar-flux units, but a negligible probability of detecting an X-ray burst above 3×10^{-7} ergs cm^{-2} sec^{-1} without a centimeter burst. Although for very large events both protons (>12 MeV) and low-energy electrons (>45 keV) follow the X-ray and radio bursts, the correlation with electrons is better than with protons for the smaller bursts; many solar proton events occurred without a detectable burst of energetic X-rays. Since all X-ray bursts for which no electrons were observed were assigned to flares near or east of central meridian, a propagation "cone" of some 30° to 90° as reported by Lin and Anderson (ref. 198) is suggested. Thus X-ray bursts are diagnostics not only of the particle acceleration mechanism but also of interplanetary propagation of low-energy solar cosmic rays.

Low-Energy Particles

In contrast to the sharp rise ($\sim$ hours) and smooth decay ($\sim$1 day) of fluxes of high-energy solar-flare particles, the low-energy events (protons, 0.3 to 10 MeV, and electrons, 20 to 100 keV) show, in addition to characteristic flare events, a rich variety of time profiles and may last as long as half a solar rotation. Some magnetic-storm-associated proton events follow several days after a large flare (ref. 237) and were called energetic storm particles (ESP) by Bryant et al. (ref. 160), who first observed them from satellites and by Rao et al. (ref. 238), who recently studied the events detected by Pioneers VI and VII. Others are associated with solar active centers themselves (ref. 164) and are reminiscent of the 27-day recurrence events prior to solar minimum (ref. 191).

Somewhat similar events are observed for electrons >40 keV (ref. 198) for which Anderson and Lin have found both "prompt" and "delayed" events. Prompt electrons arrive within an hour after a flare (approximately the transit time along the spiral field) and are usually from flares located in the interval 30° to 90° W. If the source flare is further east than 30° W, a type I radio noise region covering a substantial fraction of the solar disk is present. This radio emission is thought to be the result of plasma oscillations excited by fast electrons in the corona. The small gyroradii of these electrons in the interplanetary field suggests that they are confined to a "cone of propagation" of some 30° half-width above the flare (a "simple" event) unless there is a widespread radio region (a "complex" event) (fig. 40). Since strong flux anisotropies have lasted for >10 hours and the events last a day or so, Anderson and Lin concluded that the electrons must be stored at the Sun over a several-day period. The duration of the events above the detector threshold is consistent with corotation of a filled propagation cone; no "simple" event has lasted more than 2½ days (the time it takes a 30° cone to rotate past the Earth).

The corotation of a spatial structure over a flare region was deduced by Lin, Kahler, and Roelof (ref. 239) from low-energy detectors on three satellites (Explorer XXVIII (IMP–3), OGO–III, and Explorer XXXIII) near the Earth and the Moon. In addition to an "ordinary diffusive component" promptly following the flare at 0023 UT on July 7, 1966, there was a symmetric "halo" of protons and electrons that passed by the spacecraft all during the day of July 8 and a narrow "core," some 3° wide for electrons >40 keV in the midst of the halo, which occurred at the same time the flare region was at 60° W, the foot of the average interplanetary field line through the Earth (fig. 41). The structure was interpreted as the longitude injection profile near the Sun, with the core magnetically connecting back to the flare region. Svestka (ref. 240) considered the core to be electrons piled up behind a magnetic sector boundary preceding the core, although his argument is somewhat weakened by a misinterpretation of the charac-

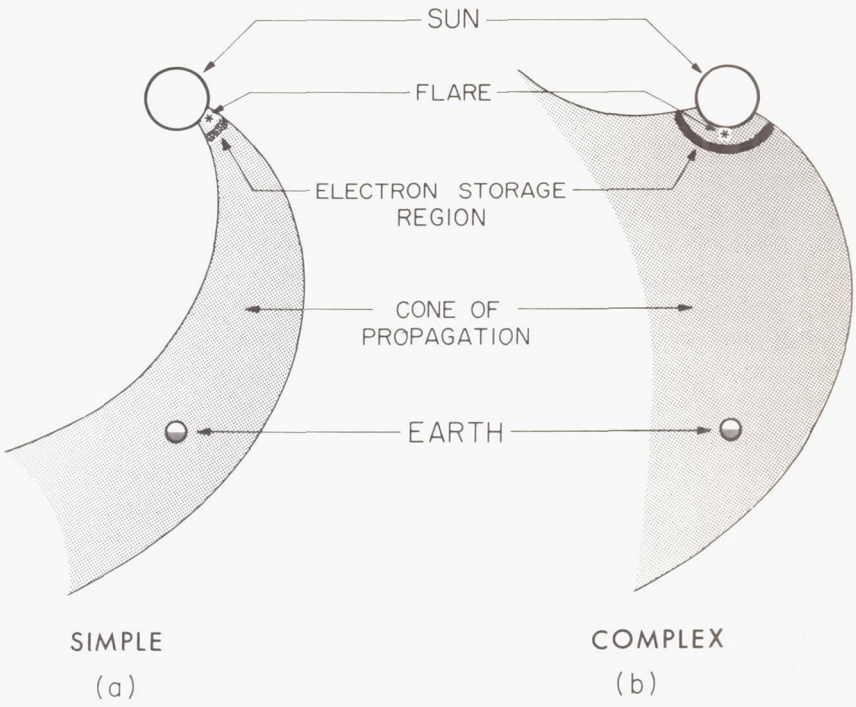


Figure 40.—**Low-energy (>40 keV) electron propagation within cones as deduced from satellite observations in which electrons arrive promptly (~½ hour) after an identifiable flare. Within the cones, electrons gyrate around the interplanetary field lines without appreciable scattering across field lines. (*a*) In the absence of type I radio noise storms, electron-producing flares are "simple," located within 30° of the foot of the average field line through the Earth. (*b*) "Complex" electron events occur within a wider cone when a type I noise storm covers a large portion of the solar disk (Lin and Anderson, ref. 198).**

teristics of the 45-keV electron detector (which he incorrectly assumed also counted protons), since the electron halo was seen on both sides of the sector boundary.

This picture of a corotating spatial structure may be carried over to the proton events (ref. 165), and Fan et al. (ref. 164) have established that the effective spread in longitude for 0.6- to 13-MeV protons can be as much as 100° to 180° (fig. 42). From an analysis of onsets of flare-associated events within the long-lived enhancements, they conclude that there must be a fast-propagation mode across the corona with negligible storage. Fast

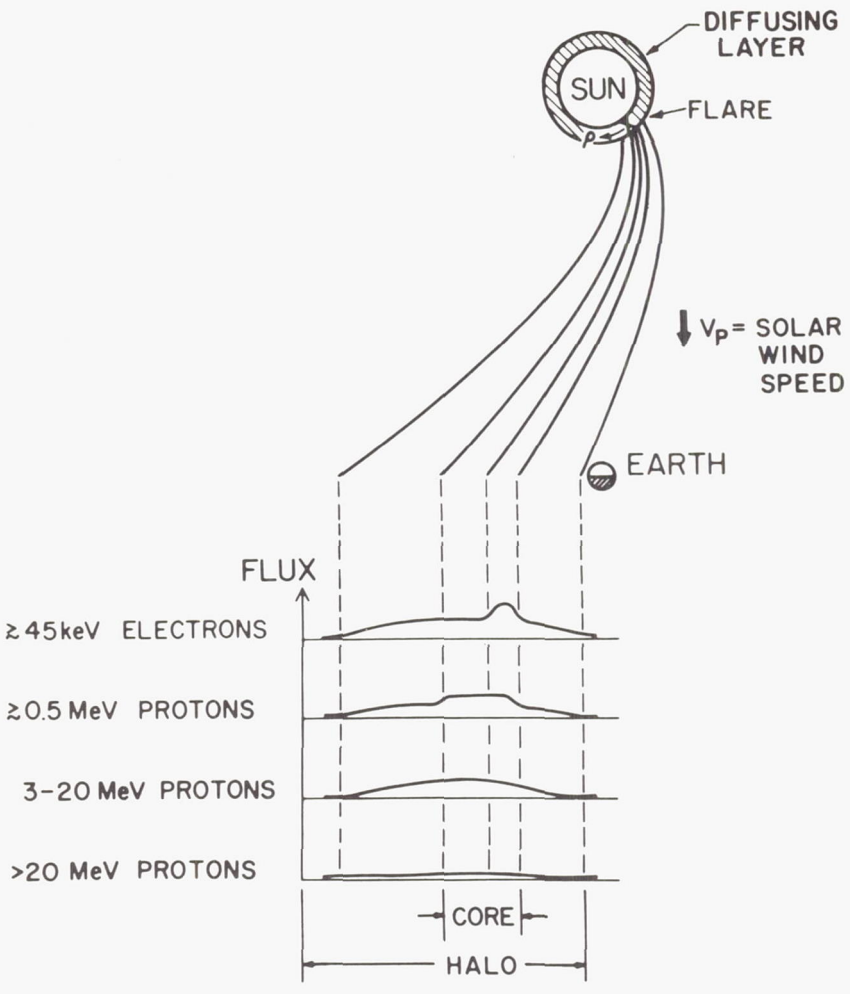


Figure 41.—A schematic of the core and halo of the energetic particle fluxes established by the flare of July 7, 1966, deduced from observations on OGO-III, Explorer XXVIII (IMP-III) and Explorer XXXIII. The core and halo are convected by the solar wind past the Earth, forming a corotating structure, populated by low-energy particles. The lower left graph indicates the spatial variation of the particle fluxes. The upper diagram shows the thin layer around the Sun in which particles diffuse as postulated by Reid (ref. 168) and Axford (ref. 169). From this layer energetic particles populate the interplanetary magnetic-field structure. The core (detected on July 8) connects directly to the flare region which was at 47° W at 0000 UT on July 7 (Kahler et al., ref. 239).

transverse propagation is also necessary to explain the rapid onsets (<2 hours) of >7.5 MeV protons from two flares at longitude 15° E (ref. 165) as well as the complex electron events (ref. 198). Lin and Anderson have suggested that the "flare wave" which Athay and Moreton (ref. 241) observed to move with speeds $\sim$1000 km/sec across the disk may locally energize the particles, while McCracken et al. suggest transverse diffusion. Negligible proton storage does not appear consistent with the postulated electron storage, but Fan et al. explain the wide longitudinal spread of protons by a dispersion of coronal field lines over the active center over nearly 180°.

The collimation of low-energy particles along interplanetary field lines has been well established, although late in flare events a radial "equilibrium anisotropy" is established in the outward convection of the particles by the magnetic-field irregularities in the solar wind (ref. 242). (See fig. 43.) Any longitudinal particle spread must be produced by the topology of the coronal and interplanetary field. McCracken et al. (ref. 165) detected

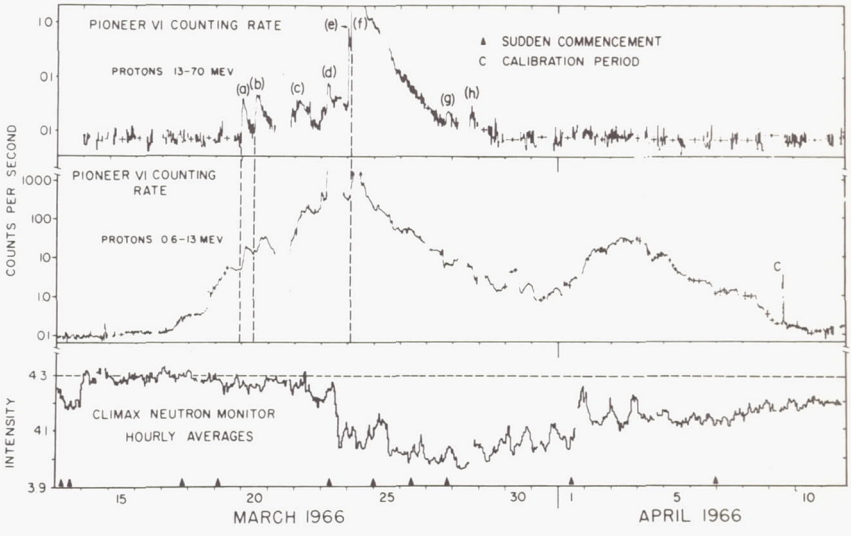


Figure 42.—An example of low-energy proton events associated with solar active centers. Thirty-minute averages of the counting rates are plotted for protons of 13 to 70 and 0.6 to 13 MeV. The enhanced flux of 0.6 to 13 MeV protons from March 15 to 31 is attributed to solar region 8207. The first evidence of enhanced flux from the following region (8223) appears on March 31. A magnetic sector boundary (Ness and Wilcox, ref. 12) occurs on March 31. Note at this time the abrupt change in the level of modulation at the Climax neutron monitor. Discrete flare and shock-wave events seen at 13 to 70 MeV are denoted by (*a*) to (*h*) (Fan et al., ref. 164).

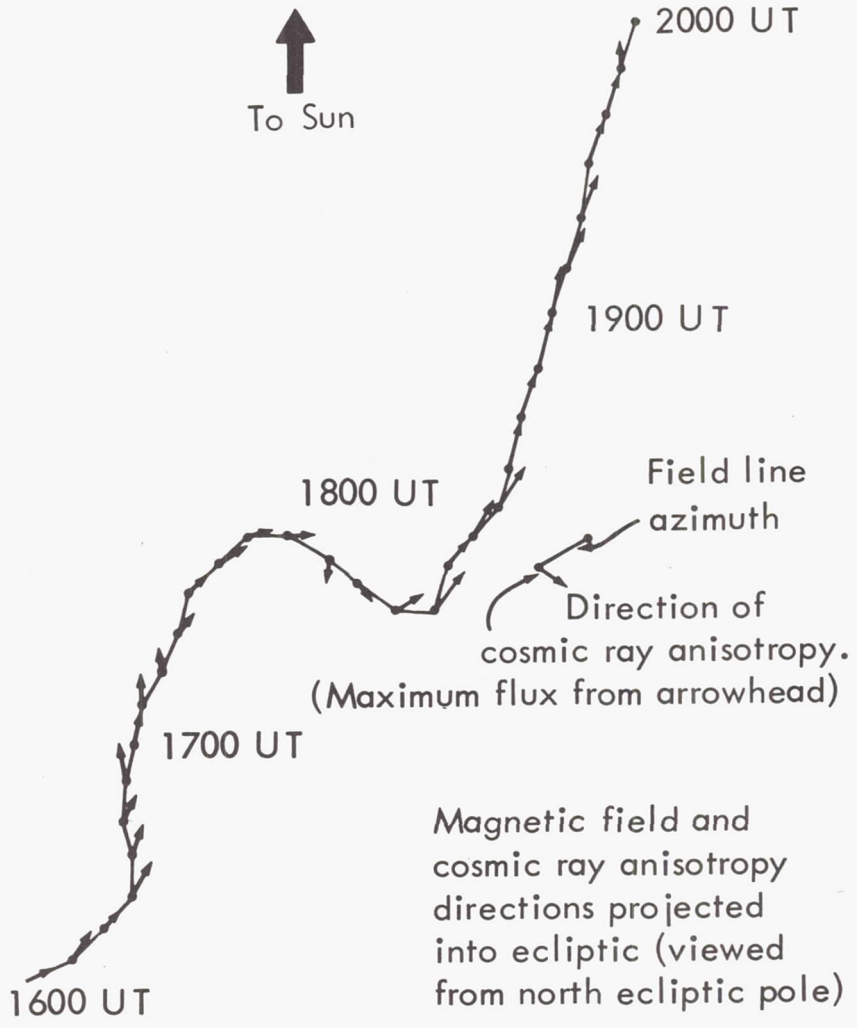


Figure 43.—Collimation of low-energy protons (>7.5 MeV) by the interplanetary magnetic field during the solar proton event observed by Pioneer VI on December 30, 1965. Note the very close correspondence of the two azimuths during the abrupt change in direction around 1800 UT (McCracken and Ness, ref. 13).

an event when Pioneers VI and VII were separated by 54° in solar longitude in which fluxes at the two spacecraft differed by over two orders of magnitude (fig. 44). Jokipii and Parker (ref. 16) ascribe the profile of one proton event reported by Fan et al. (ref. 164) to the random walk of photospheric field lines which was first considered by Leighton (ref. 243). Al-

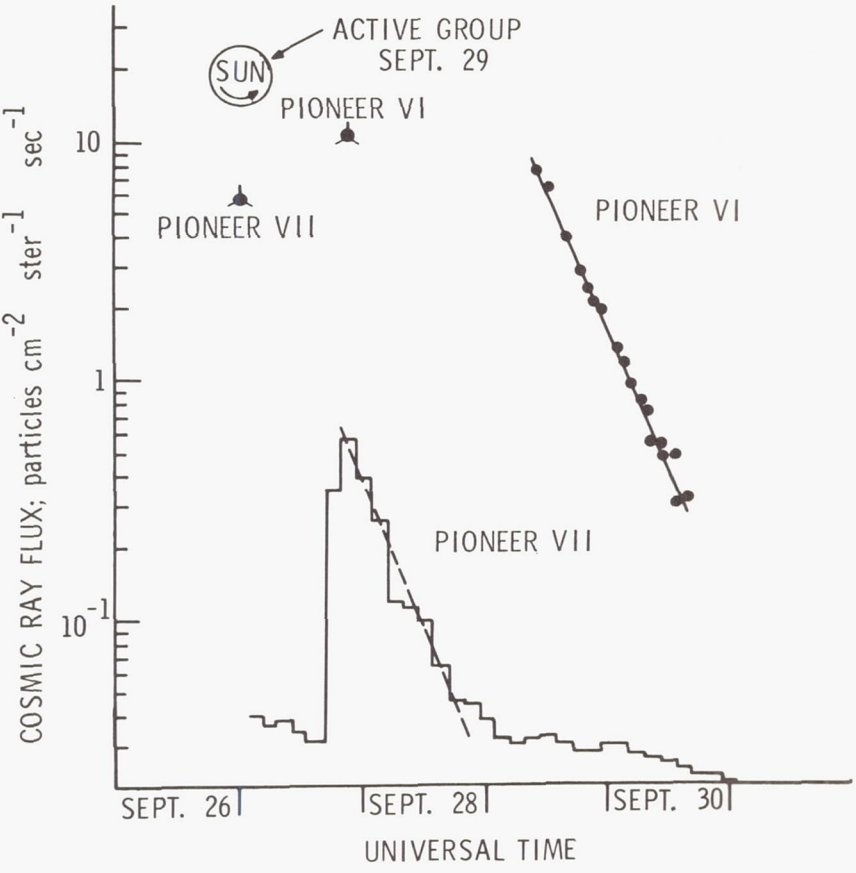


***Figure 44.*—The concurrent observation in September 1966 of cosmic rays of solar origin made by two Pioneer spacecraft separated by 54° of solar longitude. The relative positions of the two spacecraft and of a major sunspot group are shown in the insert. The difference of over two orders of magnitude in flux implies a strong azimuthal intensity gradient (McCracken et al., ref. 165).**

though the mechanism is undoubtedly operative, the quantitative agreement with Leighton's analysis is not quite satisfactory. Leighton emphasized that only the supergranulation activity could contribute to the motion of field lines above the chromosphere (the contribution of granulation was also invoked in ref. 16), and he gave a lifetime for the supergranulation twice as long as that quoted in Jokipii and Parker (ref. 16). All in all, the width predicted from Leighton's paper is closer to 4° than the observed 17°, a width closer to that of the "core" structure observed in a number of events, as discussed subsequently.

Anderson (ref. 244) has combined electron and proton observations of all genre of low-energy events in 1967. Occasionally there are only protons and very rarely only electrons; but when both species occur, the centroid of the electron flux precedes that of the protons. This separation in onset of 1 to 10 hours can be explained by particle drifts if the protons are stored for several days in a coronal region where there is a net poleward component of the field. The events show a structure like the delayed fluxes of July 8, 1966 (ref. 239), with a broad ($>70°$) smooth halo suggestive of a corona-stored population in diffusive equilibrium. The core shows large and quite rapid intensity variations (particularly for protons), suggesting that the core particles are not in equilibrium. The events are often associated with weak depressions in sea-level neutron intensities and occasionally with a well-developed Forbush decrease that usually occurs at the time of the core rather than the halo. This last-mentioned aspect is reminiscent of the recurrent Forbush decreases observed on Pioneer VI (ref. 245).

It is clear that the key to interpreting such events is an understanding of the coronal and interplanetary field. Work over the last several years (reviewed in ref. 6), has established the correlation of the gross features of the photospheric field and those in interplanetary space. Recently Schatten et al. (ref. 11) have extrapolated observations at 1 AU in to 0.4 AU and out to 1.2 AU using the "frozen-in" flux approximation. During late 1965 they found complex structures, some of loop form that represent a stage in the evolution of sunspots and magnetic bipolar regions on the Sun. The same authors (ref. 246) followed a suggestion of Newkirk (ref. 247) and used potential theory to map the photospheric field up through the corona to a "source surface" for the interplanetary field at 0.6 solar radius above the Sun. The calculated field shows considerable loop structure, since only about one-third of the photospheric flux is carried out into interplanetary space. Thus low-energy particles must experience rather complicated field configurations in the corona; whether they are adequate for long periods of storage is not yet known.

Another question remains unanswered: whether low-energy particles undergo energy changes in the interplanetary medium. Acceleration by dynamic processes has been suggested (refs. 248 and 249), and Fisk and Axford (ref. 250) concluded that deceleration may appreciably modify the spectrum of flare protons < 100 MeV late in an event. Rao et al. (ref. 238) invoke interplanetary acceleration to explain observed bidirectional field-alined flux anisotropies of energetic storm particles during the accompanying Forbush decrease. They suggest that recurrent proton events (refs. 179, 185, and 191) may be accelerated interplanetary particles. They observe, however, only recurrent decreases in proton flux at the appropriate times, three solar rotations later, corresponding to the last observed recurrent particle event of the previous series.

Further analysis is clearly required to decide if flare-associated energetic storm particles, protons associated with active centers, and delayed events involve fundamentally different processes or if they are simply different aspects of the same fundamental process.

Solar Neutrons, Gamma Rays, and Neutrinos

The exotic solar neutrons, gamma rays, and neutrinos, must exist because they are produced in known nuclear processes on the Sun (ref. 218) and in its interior (ref. 251). To date, however, only upper bounds on their fluxes have been set.

The most recent searches for solar neutrons (refs. 252 to 256) have given upper limits ~ 1 to 10 neutrons m^{-2} sec^{-1} MeV^{-1} in the range of 1 to 200 MeV; these limits are still several orders of magnitude above the theoretical limit (ref. 257) set by interplanetary proton measurements (since free neutrons decay in $\sim 10^3$ sec). Webber and Ormes (ref. 256) also set upper limits out to 1 BeV (fig. 45). Apparao et al. (ref. 258) reported a possible flare-associated neutron enhancement, but Holt (ref. 259) noted that the lower limit to the decay protons from the possible neutrons was well above the observed Geiger counter rates on OGO–I at the appropriate time.

Solar gamma rays are expected from n,p capture (2.2 MeV), electron annihilation (0.5 MeV), and other nuclear reactions (ref. 218). Recent searches (refs. 260 to 262) have yielded (ref. 260) an upper limit of 5×10^{-3} cm^{-2} sec^{-1} for the 2.2 MeV n,p capture gamma ray, which is consistent with the Ranger III measurement in 1962 (ref. 263).

Numerous solar nutrino experiments have been undertaken (ref. 264), and the most recent report on a ^{37}Cl (ν,e) ^{37} Ar experiment gives an upper limit of 2×10^6 neutrinos cm^{-2} sec^{-1} at Earth from ^8B decay in the Sun (ref. 252). From this figure, Bahcall (ref. 265) has concluded that the Sun does not derive most of its radiated energy from the CNO cycle and that the heavy-element mass fraction is less than 2 percent.

Summary of Solar Cosmic Rays

The conclusion that all but the highest energy solar cosmic rays are constrained to follow interplanetary field lines and undergo little scattering between the Sun and Earth has raised a host of new questions. For one, what is the configuration of the coronal magnetic fields? Radio observations for the same flare require storage of relativistic electrons high in the corona late in the event (type IV continuum), with simultaneous outward streaming of nearly relativistic electrons (type II and V bursts) and confinement to low coronal regions during the flash phase (microwave and X-ray bursts). For another, are protons stored in the corona? If they are free to escape, why are electrons trapped? Again, what is the relation between processes in

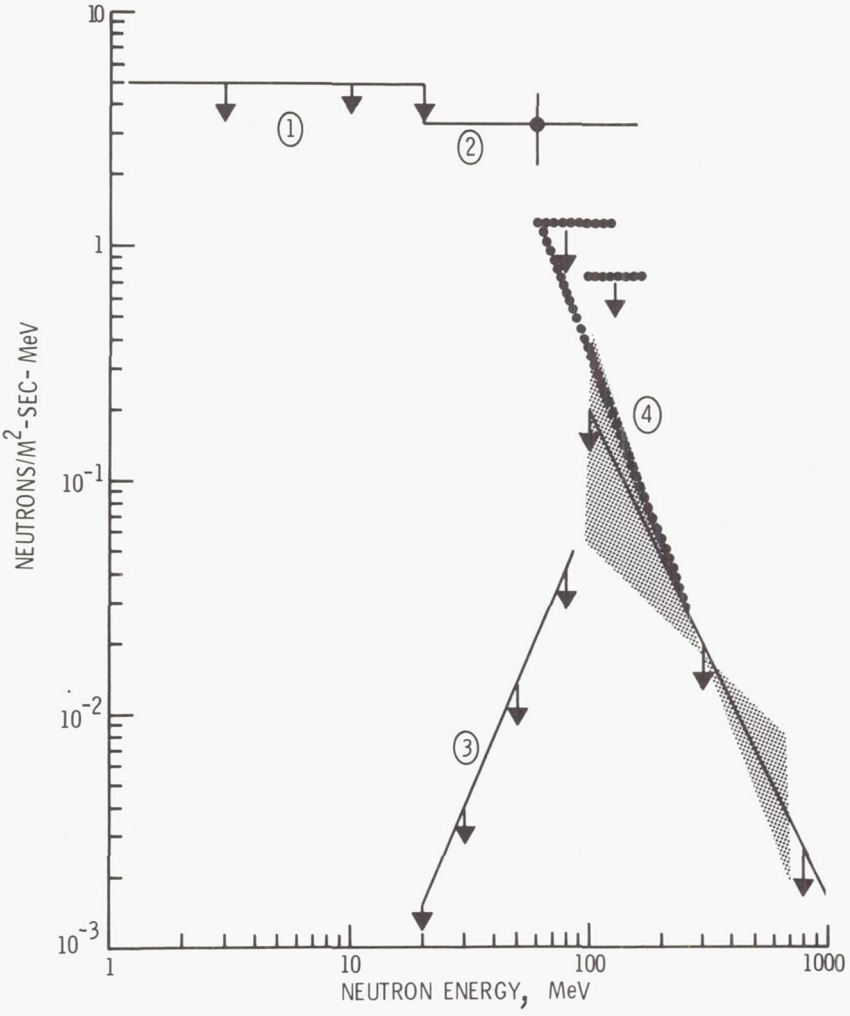


Figure 45.—**Recent limits on the differential intensities of solar neutrons at the Earth: (1) Bame and Asbridge (ref. 255); (2) a possible positive observation (Apparao et al., ref. 258); (3) theoretical upper limit based on quiet-time interplanetary proton fluxes (Roelof, ref. 257); and (4) Webber and Ormes (ref. 256).**

solar active centers and the low-energy electron and proton fluxes in interplanetary space? Finally, is the particle acceleration in active centers just a result of a small-scale flare mechanism, or is it fundamentally different from the explosive acceleration of BeV protons and MeV electrons in large flares? Does all acceleration take place at the flare site or do propagating waves energize particles at other locations on the Sun?

It is certainly too early to put forward a comprehensive description of this variety of phenomena, but sensitive particle detectors will provide additional information concerning flare and low-energy events so that the general pattern can be separated from the idiosyncrasies of individual events. There has been promising activity in correlating particle data with those of radio, optical, and X-ray observations. The influence of the solar atmosphere on these radiations is proving a valuable diagnostic of the locations and conditions of this emission.

At the present time one can say with confidence that the coronal fields are capable of both storage and fast propagation of particles, that acceleration of charged particles is a common phenomenon on the Sun, and that the interplanetary magnetic field offers little impediment to particle transport between the Sun and the Earth.

CONCLUSIONS

The particles and fields discipline originated from a study of ionizing radiations in space and of the magnetic fields that guide their trajectories. During the last few years this study has been rapidly evolving into an area of research that more appropriately may be called particle astrophysics. We are finding that information gained from these studies constitutes an essential part in our understanding of the universe. Classical astronomy, relying only on electromagnetic radiations, cannot investigate fully regions of space that are filled with a very tenuous medium such as interstellar and interplanetary space.

The study of the solar wind or interplanetary medium illustrates this point. Initially, the emission by the Sun of the solar wind appeared to be a curious but relatively unimportant phenomenon needed to explain the behavior of cometary tails and of geomagnetic storms that are observed periodically on Earth. We are now aware that a stellar wind can play an important role in the evolution of a star like the Sun and of planetary bodies that may surround it. The stellar wind provides a means of removing substantial amounts of angular momentum from the star. This can cause differential rotation of the surface and may also affect the magnetic-field configuration of the star. We are not yet able to assess the role of the stellar wind in the evolution of a young star, but observations of T-Tauri stars have shown that much stronger stellar winds can occur at that stage of evolution.

In the case of planetary evolution, a stellar wind can add angular momentum to a contracting cloud of cosmic dust. In our solar system it probably has contributed in some degree to the observed planetary periods, except for Mercury and Venus where special processes control the period of rotation. In the absence of a planetary magnetic field, the solar wind interacts directly with the atmospheres of the moons and planets, and in

some cases it may be responsible for removing a substantial fraction of the atmospheres during the evolution of these bodies.

The plasma properties of the solar wind are also of more general importance because studies of these properties permit us to test and develop plasma theory in a regime of astrophysical interest. As of now we have gained a phenomenological description of these properties between 0.7 and 1.5 AU from the Sun and have studied the interactions of the solar wind with four obstacles in its path: the Earth, the Moon, Venus, and Mars. We find that in many respects the solar wind may be characterized as a fluid even though it is a collisionless plasma. Clearly, this "fluid" is not in local statistical equilibrium as is illustrated by the inequality of temperatures measured perpendicular and parallel to the magnetic field. We found out further, in studying the solar-wind interactions with the Moon, that collective interactions between the particles do not have to be invoked in order to explain our observations.

Departure of plasma parameters from statistical equilibrium can trigger plasma instabilities and the growth of the waves associated with the instabilities. Only if the growth rate of the waves is fast compared with the time scale of the phenomenon will the solar wind behave like a fluid. Prediction of detailed properties of the solar wind outside the region that has been investigated directly depends, therefore, on our ability to predict theoretically the growth rates of the pertinent instabilities. Although progress has been made, we are not yet in a position to make such predictions with any degree of certainty. In general, growth rates of waves are quite sensitive to the density of the plasma. As the solar wind expands and becomes more tenuous, the "fluidlike" behavior should become less pronounced. We are not in a position, however, to predict whether this will have a major effect on the solar-wind interaction with the Jovian magnetic field and the resulting magnetosphere around Jupiter. The same problem faces us when we try to predict the interactions between the solar wind and the galactic medium. The conflicting information we have on the probable extent of the solar-wind-dominated domain indicates that our models of this process are still unrealistic.

Particles with energies from thermal to millions of BeV abound in the universe. Radio stars and galaxies, galactic and solar cosmic rays, and Van Allen belt particles are manifestations of this phenomenon. The existence of superthermal particles poses difficult theoretical problems because we are only now starting to identify some of the acceleration mechanisms. The study of mechanisms that can accelerate particles in the solar corona to hundreds of MeV has thus been of particular interest. During this period of increasing solar activity, a number of particle-producing flares have been observed in substantial detail. Although these events were not as intense as the large flares of the last solar maximum (1956 to 1962), they were

more informative because we have observations of the complete spectrum of particles emitted, as well as spectra of the X-ray and radio bursts.

A comprehensive attack on solar-flare and particle-acceleration mechanisms is now possible. It appears that solar processes resemble weather on Earth in the diversity of possible phenomena. It is to be expected that an understanding will emerge during the next few years. At this point we are still in the process of weeding out erroneous theories. For instance, it has been shown that protons do not have to be accelerated to their full energy in one step as had been assumed. Protons with energies from 0.1 to 10 MeV appear to be present almost continuously. From a theoretical point of view, it would be easier to explain a multiple-step process, rather than a one-step acceleration of thermal ions to an energy of 100 MeV.

The development of particle astronomy has greatly increased the interest in the particles and fields discipline. The more traditional problems, however, continue to be of substantial interest. For instance, we have found that the radiation hazards in space are normally not as great as had been feared from initial observations from 1958 to 1962. Solar-terrestrial relations, although not emphasized in this paper, are being studied actively. In addition to studying the Earth's space environment, thought is also being given toward finding ways to perturb and modify it. For instance, it has been shown theoretically that a transmitter in orbit around the Earth could precipitate electrons from the radiation belts into the atmosphere.

APPENDIX

Scientific Apparatus on Satellites and Space Probes

1963–38C (U.S. Navy-Launched Energetic Particle Satellite)

Protons: 1.2 to 100 MeV
Solid-state detectors

Electrons: 200 keV to >3.6 MeV
Solid-state detectors

Relay II (1964–3A; NASA Communications Satellite)

Protons: 1 to 60 MeV
Solid-state detector
Silicon p–n junction detectors
Scintillation counter

Electrons: 0.2 to 2 MeV
Solid-state detectors
Scintillation counters

Explorer XXVI (1964–86A; EPE–IV, Energetic Particle Explorer)

Protons: 30 keV to 110 MeV
- Scintillation detectors
- Silicon p–n junction detectors

Electrons: 10 keV to >5 MeV
- Scintillation detectors
- Silicon p–n junction detectors

Magnetic Fields: ±4000 gammas
- Flux-gate magnetometer

OGO–II and OGO–IV (1965–81A and 1967–73A; Orbiting Geophysical Observatory)

Cosmic Rays and Solar Protons: 0.5 to 1000 MeV
- Scintillation detectors
- Cerenkov counter
- Ionization chamber

Protons: 0.5 to 10 keV, 100 keV to 4.5 MeV
- Scintillation detectors
- Electrostatic analyzers (OGO–IV)
- Channel multipliers (OGO–IV)

Electrons: 75 eV to 100 keV and >120 keV
- Scintillation detectors
- Geiger-Mueller tubes
- Electrostatic analyzers (OGO–IV)
- Channel multipliers (OGO–IV)

Magnetic Fields: 10 000 to 65 000 gammas
- Rubidium-vapor magnetometer

Magnetic Micropulsations: 0.01 to 1000 hertz
- Triaxial search coil

Very-Low-Frequency Electromagnetic Radiation: 0.2 to 100 kHz
- Broadband receivers, 10-foot dipole antenna
- Stop frequency receivers, 9½-foot-diameter toroidal antenna
- Tunable narrowband receivers, 9½-foot-diameter toroidal antenna

OV3–1 (1966–34A; U.S. Air Force Orbital Vehicle)

Protons: 10 to 100 keV
- Electrostatic analyzer

Protons: 1 to 5 MeV and >30 MeV
- Scintillation spectrometer
- Geiger-Mueller tube

Electrons: 10 keV to 4 MeV
- Electrostatic analyzer

Electrons: 0.3 to 4 MeV and >3 MeV
- Scintillation spectrometer
- Geiger-Mueller tube

OV3–2 (1966–97A; U.S. Air Force Orbital Vehicle)

Electrons: 15 to 80 keV
- Electrostatic analyzer

Protons and Heavy Nuclei
- Mass spectrometer
- Langmuir probe
- Parallel plate retarding-potential analyzer

Magnetic Fields
- Three-axis magnetometer

OV3–3 (1966–70; U.S. Air Force Orbital Vehicle)

Protons: 10 eV to 10 keV and 100 keV to 5 MeV
- Faraday cup
- Magnetic spectrometer

Protons and Alpha Particles: 500 keV to 18 MeV and 25 to 250 MeV
- Telescopes

Electrons: 100 eV to 10 keV, 100 keV to 5 MeV, 200 keV to 3 MeV
- Faraday cup
- Magnetic spectrometer

Magnetic Fields
- Triaxial flux-gate magnetometer

OV3–4 (1966–52A; U.S. Air Force Orbital Vehicle)

Protons: 16 to 350 MeV
- Solid-state detectors

Electrons: 300 keV to 5 MeV
- Solid-state detectors
- Magnetic deflection spectrometer

Magnetic Fields
- Biaxial magnetometer

Aurora I (1967–65B; U.S. Navy Auroral Formation Satellite)

Electrons: 50 eV to 150 keV
- Channeltron detectors

Protons: 50 eV to 150 keV
- Channeltron detectors

ATS–I (1966–110A; Applications Technology Satellite)

Protons: 0.7 to 100 MeV
- Solid-state detectors
- Solid-state telescope

Electrons: 45 keV to 1.2 MeV
- Solid-state detectors
- Magnetic spectrometer
- Solid-state telescope

Suprathermal Protons and Ions: 0.25 to 50 eV
- Retarding potential analyzer

Magnetic-Field Variations: $\pm$400 gammas
- Biaxial flux-gate magnetometer

Electron Density
- Polarized phase-coherent VHF–UHF transmitter

333–240 O—69——17

Vela II and III (1964–40A+B, 1965–58A+B; Department of Defense Nuclear Test Detection Satellite)

Electrons and Positive Ions: 0.1 to 20 keV
- Electrostatic analyzer

Electrons: 45 to 430 keV
- Gold surface barrier solid-state detector
- Geiger-Mueller tubes
- Scintillation detectors

Protons: 180 to 500 keV and >800 keV
- Gold surface barrier solid-state detectors
- Scintillation detectors

Vela IV (1967–40A+B; Department of Defense Nuclear Test Detection Satellite)

Electrons and Positive Ions: 60 eV to 20 keV
- Electrostatic analyzer

Electrons: 27 to 700 keV
- Semiconductor telescopes
- Solid-state detector
- Geiger-Mueller tubes

Protons: 0.6 to 150 MeV
- Semiconductor telescopes
- Solar particle telescope

Alphas: 2 to 400 MeV
- Semiconductor telescopes
- Solar particle telescope

OGO–I and OGO–III (1964–54A and 1966–49A; Orbiting Geophysical Observatory)

Cosmic Rays and Solar Protons: 30 keV to 90 MeV
- Scintillation detectors
- Solid-state detector telescopes

Positrons: 0 to 3 MeV
- Gamma ray spectrometer

Protons: Thermal to 4.5 MeV
- Planar ion and electron trap
- Spherical retarding-potential analyzer
- Electrostatic analyzer
- Faraday cup
- Charged-particle telescope

Electrons: Thermal to 4 MeV
- Planar ion and electron trap
- Spherical retarding-potential analyzer
- Geiger-Mueller tubes
- Magnetic spectrometer

Magnetic Fields: ±500 gammas
- Flux-gate magnetometer
- Rb-vapor magnetometer 1 to 50 000 gammas (not operating on OGO–I)

Micropulsations: 0.01 to 1000 hertz
- Search-coil magnetometer

Very-Low-Frequency Electromagnetic Radiation
- Step-frequency receivers
- 0.2 to 100 kHz, toroidal antenna (OGO–I)
- 0.015 to 100 kHz, hexagonal antenna (OGO–III)

Explorer XXVIII, Explorer XXXIII, and Explorer XXXV (1965–42A, 1966–58A, and 1967–70A; IMP's III, AIMP I and II)

Cosmic Rays and Solar Protons: 50 keV to 200 MeV
- Solid-state detectors
- Scintillation detectors
- Geiger-Mueller tubes
- Ionization chamber

Electrons: Thermal to 210 eV and >40 keV
- Solid-state detectors
- Planar ion and electron trap
- Faraday cup (inoperative on Explorer XXVIII)
- Geiger-Mueller tubes

Protons: Thermal to 8 MeV
- Planar ion and electron trap
- Faraday cup (inoperative on Explorer XXVIII)
- Retarding potential analyzer (Explorers XXXIII and XXXV)

Magnetic Fields
- Flux-gate magnetometer
- Rubidium vapor: 3 to 500 gammas (Explorer XXVIII)
- Triaxial flux-gate magnetometer: 0.2 to 200 gammas (Explorers XXXIII and XXXV)

ERS XVIII (1967–40C; U.S. Air Force Radiation Research Subsatellite)

Electrons: >40 keV, >100 keV, and >500 keV
- Geiger-Mueller tubes
- Plastic scintillator
- Solid-state detector

Protons: 0.5 to 3 MeV and 7.5 to 15 MeV
- Surface barrier detector
- Solid-state detector

Alphas: >3.5 MeV
- Surface barrier detector

Explorer XXXIV (1967–51A; IMP–IV)

Cosmic Rays and Solar Protons: 0.4 to 400 MeV
- Solid-state detectors
- Ionization chamber
- Scintillation detectors
- Geiger-Mueller tubes

Protons: Thermal to 50 keV
- Electrostatic analyzer

Electrons: Thermal to 20 MeV
- Ionization chamber
- Geiger-Mueller tubes
- Scintillation detectors
- Electrostatic analyzer
- Solid-state detector

Magnetic Fields
Flux-gate magnetometer

Mariner IV (1964–77A; Mars Probe)

Protons: 30 eV to 10 keV
Faraday cup
Protons: 500 keV to 320 MeV
Solid-state detectors and telescope
Geiger-Mueller tubes
Ionization chamber
Electrons: 70 keV to >320 MeV
Solid-state detectors and telescope
Geiger-Mueller tubes
Ionization chamber
Alpha Particles: 2 to 60 MeV
Solid-state telescope
Ionization chamber
Magnetic Fields: ±360 gammas
Vector helium magnetometer

Mariner V (1967–60A; Venus Flyby)

Protons: 10 eV to 10 keV and 0.32 to 12 MeV
Faraday cup
Geiger-Mueller tubes
Solid-state detector
Electrons: >45 keV, >95 keV, and >150 keV
Geiger-Mueller tubes
Magnetic Fields
Triaxial helium magnetometer

Pioneer VI and Pioneer VII (1965–105A and 1966–75A; Interplanetary Probes)

Protons: 40 eV to 15 keV
Faraday cup
Electrostatic analyzer
Protons: 0.6 to 200 MeV
Solid-state detector telescope
Scintillation detector
Electrons: 3 to 2500 eV
Faraday cup
Electrostatic analyzer
Alpha Particles and Heavy Nuclei: 2.5 to 350 MeV
Solid-state detector telescope
Scintillation detector
Magnetic Fields: ±64 gammas
Flux-gate magnetometer

Pioneer VIII (1967–123A; Interplanetary Probe)

Protons: 200 eV to 16 keV
Electrostatic analyzer
Electrons: 3 eV to 1 keV
Electrostatic analyzer
Protons, Alpha Particles, and Heavy Nuclei: 1 keV to 1 MeV
Solid-state detector telescope
Scintillation detector
Magnetic Fields
Single-axis flux-gate magnetometer

Venera 4 (1967–58A; U.S.S.R. Venus Soft Lander)

Magnetometer (Flyby Only)
Plasma Detector (Flyby Only)
Trapped Radiation Detector
Cosmic-Ray Detector

REFERENCES

1. Hess, W. N.; Mead, G. D.; and Nakada, M. P.: Significant Achievements in Particles and Fields 1958–1964. NASA SP–97, 1966. (Also by the same authors: Particles and Fields Research in the Satellite Era. Rev. Geophys., vol. 3, 1965, p. 521.)
2. Schardt, A. W.; and Opp, A. G.: Particles and Fields. Significant Achievements in Space Science, 1965. NASA SP–136, 1967, p. 31. (Also by the same authors: Particles and Fields: Significant Achievements. Rev. Geophys., vol. 5, 1967, p. 411.)
3. Schardt, A. W.; and Opp, A. G.: Particles and Fields. Significant Achievements in Space Science, 1966. NASA SP–155, 1967, p. 205.
4. Dessler, A. J.: Solar Wind and Interplanetary Magnetic Field. Rev. Geophys., vol. 5, 1967, p. 1.
5. Axford, W. I.: Observations of the Interplanetary Plasma. Space Sci. Rev., vol. 8, 1968, p. 331.
6. Wilcox, J. M.: The Interplanetary Magnetic Field; Solar Origin and Terrestrial Effects. Space Sci. Rev., vol. 8, 1968, p. 258.
7. Wilcox, J. M.; and Ness, N. F.: Quasi-Stationary Corotating Structure in the Interplanetary Medium. J. Geophys. Res., vol. 70, 1965, p. 5793.
8. Coleman, P. J.; Davis, L.; Smith, E. J.; and Jones, D. E.: The Polarity Pattern of the Interplanetary Magnetic Field During Solar Rotations 1798–1808. J. Geophys. Res., vol. 72, 1967, p. 1637.
9. Neugebauer, M.; and Snyder, C. W.: Mariner 2 Observations of the Solar Wind—1. Average Properties. J. Geophys. Res., vol. 71, 1966, p. 4469.
10. Neugebauer, M.; and Snyder, C. W.: Mariner 2 Observations of the Solar Wind—2. Relation of Plasma Properties of the Magnetic Field. J. Geophys. Res., vol. 72, 1967, p. 1823.
11. Schatten, K. H.; Ness, N. F.; and Wilcox, J. M.: Influence of Solar Active Region on the Interplanetary Magnetic Field. Solar Phys., 1968 (in press).
12. Ness, N. F.; and Wilcox, J. M.: Interplanetary Sector Structure, 1962–1966. Solar Phys., vol. 1, 1967, p. 437.
13. McCracken, K. G.; and Ness, N. F.: The Collimation of Cosmic Rays by the Interplanetary Magnetic Field. J. Geophys. Res., vol. 71, 1966, p. 3315.

14. Bartley, W. C.; Bukata, R. P.; McCracken, K. G.; and Rao, U. R.: Anisotropic Cosmic Radiation Fluxes of Solar Origin. J. Geophys. Res., vol. 71, 1966, p. 3297.
15. Michel, F. C.: Model of Solar Wind Structure. J. Geophys. Res., vol. 72, 1967, p. 1917.
16. Jokipii, J. R.; and Parker, E. N.: Random Walk of Magnetic Lines of Force in Astrophysics. Phys. Rev. Letters, vol. 21, 1968, p. 44.
17. Colburn, D. S.; and Sonett, C. P.: Discontinuities in the Solar Wind. Space Sci. Rev., vol. 5, 1966, p. 439.
18. Burlaga, L. F.: Micro-Scale Structures in the Interplanetary Medium. GSFC Rept. no. X–612–67–524, 1967.
19. Siscoe, G.; Davis, L.; et al.: Power Spectra and Discontinuities of the Interplanetary Magnetic Field: Mariner 4. J. Geophys. Res., vol. 73, 1968, p. 61.
20. Burlaga, L. F.; and Ness, N. F.: Macro and Micro Structure of the Interplanetary Magnetic Field. Paper presented at the 10th International Conference on Cosmic Rays (Calgary, Alberta, Canada), June 1967.
21. Fairfield, D. H.: Simultaneous Measurements on Three Satellites and the Observation of the Geomagnetic Tail at 1000 R_e. J. Geophys. Res., vol. 73, 1968, p. 6179.
22. Ogilvie, K. W.; Burlaga, L. F.; and Wilkerson, T. D.: Plasma Observations on Explorer 34. J. Geophys. Res., vol. 73, 1968, p. 6809.
23. Lazarus, A. J.; and Binsack, J. H.: Observations of Interplanetary Plasma. Space Research VIII. North-Holland Publ. Co. (Amsterdam), 1968.
24. Gosling, J. T.; Asbridge, J. R.; et al.: Satellite Observations of Interplanetary Shock Waves. J. Geophys. Res., vol. 73, 1968, p. 43.
25. Van Allen, J. A.; and Ness, N. F.: Observed Particle Effects of an Interplanetary Shock Wave on July 8, 1966. J. Geophys. Res., vol. 72, 1967, p. 935.
26. Gringauz, K. I.; Bezrukikh, V. V.; and Musatov, L. S.: Solar Wind Observations With the Aid of the Interplanetary Station Venera–3. Komicheskiye Issledovaniya, vol. 5, 1967, p. 25.
27. Hundhausen, A. J.; Asbridge, J. R.; et al.: Vela 3 Satellite Observations of Solar Wind Ions: A Preliminary Report. J. Geophys. Res., vol. 72, 1967, p. 87.
28. Hundhausen, A. J.; Asbridge, J. R.; Bame, S. J.; and Strong, I. B.: Vela Satellite Observations of Solar Wind Ions. J. Geophys. Res., vol. 72, 1967, p. 1979.
29. Bame, S. J.; Hundhausen, A. J.; Asbridge, J. R.; and Strong, I. B.: Solar Wind Ion Composition. Phys. Rev. Letters, vol. 20, 1968, p. 393.
30. Lambert, D. L.: The Abundances of the Elements in the Solar Photosphere—I. Mon. Not. Astr. Soc., vol. 138, 1968, p. 143.
31. Hundhausen, A. J.; Gilbert, H. E.; and Bame, S. J.: The State of Ionization of Oxygen in the Solar Wind. Astrophys. J., vol. 152, 1968, p. 13.
32. Delache, Philippe: Contribution a l'Étude de la Zone de Transition Chromosphére—Couronne. Annales d'Astrophysique, vol. 30, 1967, p. 827.
33. Biswas, S.; Fichtel, C. E.; and Guss, D. E.: Solar Cosmic-Ray Multiply Charged Nuclei and the July 18, 1961, Solar Event. J. Geophys. Res., vol. 71, 1966, p. 4071.
34. Hundhausen, A. J.; Gilbert, H. E.; and Bame, S. J.: The Ionization State of Interplanetary Plasma. J. Geophys. Res., vol. 73, 1968, p. 5485.
35. Sturrock, P. A.; and Hartel, E. R.: Two-Fluid Model of the Solar Wind. Phys. Rev. Letters, vol. 16, 1966, p. 628.

36. HUNDHAUSEN, A. J.; BAME, S. J.; AND NESS, N. F.: Solar Wind Thermal Anisotropies: Vela 3 and IMP 3. J. Geophys. Res., vol. 72, 1967, p. 5265.
37. SCARF, F. L.; WOLFE, J. H.; AND SILVA, R. W.: A Plasma Instability Associated With Thermal Anisotropies in the Solar Wind. J. Geophys. Res., vol. 72, 1967, p. 993.
38. KENNEL, C. F.; AND SCARF, F. L.: Thermal Anisotropies and Electromagnetic Instabilities in the Solar Wind. J. Geophys. Res., vol. 73, 1968, p. 6149.
39. BREUS, T. K.; AND GRINGAUZ, K. I.: Estimate of Proton Temperature of Interplanetary Plasma According to Data Obtained on Spacecraft "Venera–3." Kosmicheskiye Issledovaniya, vol. 5, 1967, p. 948.
40. SCARF, F. L.; CROOK, G. M.; GREEN, I. M.; AND VIROBIK, P. F.: Initial Results of the Pioneer 8 VLF Electric Field Experiment. J. Geophys. Res., vol. 73, 1968, p. 6665.
41. SCARF, F. L.; CROOK, G. M.; FREDERICKS, R. W.; GREEN, I. M.; AND KENNEL, C. F.: Observations of Plasma Waves in Space. Paper presented to NATO Advanced Study Institute (Röros, Norway), Apr. 1968.
42. Coleman, P. J.: Hydromagnetic Waves in the Interplanetary Plasma. Phys. Rev. Letters, vol. 17, 1966, p. 207.
43. COLEMAN, PAUL J.: Variations in the Interplanetary Field: Mariner 2—1. Observed Properties. J. Geophys. Res., vol. 71, 1966, p. 5509.
44. COLEMAN, P. J.: Wave-Like Phenomena in the Interplanetary Plasma: Mariner 2. Planet. Space Sci., vol. 15, 1967, p. 953.
45. COLEMAN, PAUL J.: Turbulence, Viscosity, and Dissipation in the Solar-Wind Plasma. Astrophys. J., vol. 153, 1968, p. 371.
46. MONTGOMERY, M. D.; BAME, S. J.; AND HUNDHAUSEN, A. J.: Solar Wind Electrons: Vela 4 Measurements. J. Geophys. Res., vol. 73, 1968, p. 4999.
47. WOLFE, J. H.; AND MCKIBBIN, D. D.: Pioneer 6 Observations of a Steady-State Magnetosheath. Planet. Space Sci., vol. 16, 1968, p. 953.
48. WEBER, E. J.; AND DAVIS, L.: The Angular Momentum of the Solar Wind. Astrophys. J., vol. 148, 1967, p. 217.
49. PARKER, E. N.: Confinement of a Magnetic Field by a Beam of Ions. J. Geophys. Res., vol. 72, 1967, p. 2315.
50. SCHUBERT, G.; AND COLEMAN, P. J.: The Angular Momentum of the Solar Wind. To be published, 1968.
51. BRANDT, J. C.: Consequences of the Torque Exerted on the Sun by the Solar Wind. Astrophys. J., vol. 144, 1966, p. 1221.
52. ALFONSO-FAUS, A.: Rotation of the Solar Wind Plasma. Planet. Space Sci., vol. 16, 1968, p. 1.
53. ALFONSO-FAUS, A.: Effect of the Sun's Rotation on the Solar Wind. J. Geophys. Res., vol. 72, 1967, p. 5576.
54. MODISETTE, J. L.: Solar Wind Induced Torque on the Sun. J. Geophys. Res., vol. 72, 1967, p. 1521.
55. BRANDT, J. C.: Interplanetary Gas—XIV. On the Extent of Effective Corotation. Astrophys. J., vol. 148, 1967, p. 905.
56. DICKE, R. H.; AND GOLDBERG, H. M.: Solar Oblateness and General Relativity. Phys. Rev. Letters, vol. 18, 1967, p. 313.
57. DICKE, R. H.: The Sun's Rotation and Relativity. Nature, vol. 202, 1964, p. 432.
58. TURKEVICH, A. L.; FRANZGROTE, E. J.; AND PATTERSON, J. H.: Chemical Analysis of the Moon at the Surveyor V Landing Site. Science, vol. 158, 1967, p. 635.

59. Turkevich, A. L.; Patterson, J. H.; and Franzgrote, E. J.: Chemical Analysis of the Moon at the Surveyor VI Landing Site—Preliminary Results. Science, vol. 160, 1968, p. 1108.
60. Turkevich, A. L.; Franzgrote, E. J.; and Patterson, J. H.: Chemical Analysis of the Moon at the Surveyor VII Landing Site—Preliminary Results. Science, vol. 162, 1968, p. 117.
61. DeWys, J. N.: Results and Implications of Magnet Experiments on Surveyor V, VI, and VII Spacecrafts. Trans. AGU, vol. 49, 1968, p. 249.
62. Johnson, F. S.; and Midgley, J. E.: Notes on the Lunar Magnetosphere. J. Geophys. Res., vol. 73, 1968, p. 1523.
63. Gold, T.: The Magnetosphere of the Moon. The Solar Wind, R. J. Mackin, Jr., and M. Neugebauer, eds., Pergamon Press, 1966, p. 381.
64. Sonett, C. P.; and Colburn, D. S.: Establishment of a Lunar Unipolar Generator and Associated Shock and Wake by the Solar Wind. Nature, vol. 216, 1967, p. 340.
65. Ness, N. F.; Behannon, K. W.; Scearce, C. S.; and Cantarano, S. C.: Early Results From the Magnetic Field Experiment on Lunar Explorer 35. J. Geophys. Res., vol. 72, 1967, p. 5769.
66. Ness, N. F.: Lunar Explorer 35. GSFC rept. X–616–68–166, 1968.
67. Sonett, C. P.; Colburn, D. S.; and Currie, R. G.: The Intrinsic Magnetic Field of the Moon. J. Geophys. Res., vol. 72, 1967, p. 5503.
68. Behannon, K. W.: Intrinsic Magnetic Properties of the Lunar Body. J. Geophys. Res., vol. 73, 1968, p. 7257.
69. Ness, N. F.: Results From Lunar Explorer 35. GSFC rept. X–616–68–335, 1968.
70. Colburn, D. S.; Currie, R. G.; Mihalov, J. D.; and Sonett, C. P.: Diamagnetic Solar-Wind Cavity Discovered Behind Moon. Science, vol. 158, 1967, p. 1040.
71. Taylor, H. E.; Behannon, K. W.; and Ness, N. F.: Measurements of the Perturbed Interplanetary Magnetic Field in the Lunar Wake. J. Geophys. Res., vol. 73, 1968, p. 6723.
72. England, A. W.; Simmons, G.; and Strangway, D.: Electrical Conductivity of the Moon. J. Geophys. Res., vol. 73, 1968, p. 3219.
73. Lyon, E. F.; Bridge, H. S.; and Binsack, J. H.: Explorer 35 Plasma Measurements in the Vicinity of the Moon. J. Geophys. Res., vol. 72, 1967, p. 6113.
74. Ness, N. F.; Behannon, K. W.; Taylor, H. E.; and Whang, Y. C.: Perturbations of the Interplanetary Magnetic Field by the Lunar Wake. J. Geophys. Res., vol. 73, 1968, p. 3421.
75. Colburn, D. S.; Mihalov, J. D.; Sonett, C. P.; and Waid, S. H.: The Lunar Cavity in the Solar Wind. Trans. AGU, vol. 49, 1968, p. 234.
76. Whang, Y. C.: Interaction of the Magnetized Solar Wind With the Moon. GSFC rept. X–612–67–580, 1967.
77. Whang, Y. C.: Theoretical Study of the Magnetic Field in the Lunar Wake. GSFC rept. X–612–68–17, 1968.
78. Alfonso-Faus, A.; and Kellogg, P. J.: Interaction of the Solar Wind With the Moon. Univ. Minn. rept. no. CR–117, 1968.
79. Michel, F. C.: Shock Wave Trailing the Moon. J. Geophys. Res., vol. 72, 1967, p. 5508.
80. Michel, F. C.: Magnetic Field Structure Behind the Moon. J. Geophys. Res., vol. 73, 1968, p. 1533.
81. Wolf, R. A.: Solar Wind Flow Behind the Moon. J. Geophys. Res., vol. 73, 1968, p. 4281.

82. Bridge, H. S., Lazarus, A. J.; et al.: Mariner V: Plasma and Magnetic Fields Observed Near Venus. Science, vol. 158, 1967, p. 1669.
83. Jastrow, R.: The Planet Venus. Science, vol. 160, 1968, p. 1403.
83a. Gringauz, K. I.; Bezrukikh, V. V.; Musatov, L. S., and Breuse, T. K.: Plasma Measurements Conducted in the Vicinity of Venus on the Spacecraft "Venera–4." Kosmicheskiya Issledovaniya, vol. 6, 1968, p. 411.
84. Dolginov, S. S.; Yeroshenko, E. G.; and Zhuzgov, L. N.: Magnetic Field Investigations With AIS "Venera–4." Kosmicheskiya Issledovaniya, 1968. (To be published.)
85. Van Allen, J. A.; Krimigis, S. M.; Frank, L. A.; and Armstrong, T. P.: Observed Absence of Energetic Electrons and Protons Near Venus. Univ. Iowa rept. no. 67–66, 1967.
86. Van Allen, J. A.; Krimigis, S. M.; Frank, L. A.; and Armstrong, T. P.: Venus: An Upper Limit on Intrinsic Magnetic Dipole Moment Based on Absence of a Radiation Belt. Science, vol. 158, 1967, p. 1673.
87. Eshleman, V. R.; and Mariner Stanford Group: Venus: Ionosphere and Atmosphere as Measured by Dual-Frequency Radio Occultation of Mariner V. Science, vol. 158, 1967, 1678.
88. Kliore, A.; Levy, G. S.; Cain, D. L.; Fjeldbo, G.; and Rasool, S. I.: Atmosphere and Ionosphere of Venus From the Mariner V S-Band Radio Occultation Measurement. Science, vol. 158, 1967, p. 1683.
89. Smith, E. J.: Planetary Magnetic Field Experiments. Paper presented at meeting of Amer. Astron. Soc. (Ann Arbor, Mich.), Sept. 1968.
90. Smith, E. J.; Davis, L.; Coleman, P. J.; and Jones, D. E.: Magnetic Field Measurements Near Mars. Science, vol. 149, 1965, p. 1241.
91. Lazarus, A. J.; Bridge, H. S.; Davis, J. M.; and Snyder, C. W.: Initial Result From the Mariner 4 Solar Plasma Experiment. Space Research VII, North-Holland Publ. Co. (Amsterdam), 1967, p. 1296.
92. Dryer, M.; and Heckman, G. R.: Application of the Hypersonic Analog to the Standing Shock of Mars. Solar Phys., vol. 2, 1967, p. 112.
93. Kliore, A.; Cain, D. L.; et al.: Occultation Experiment: Results of the First Direct Measurement of Mars' Atmosphere and Ionosphere. Science, vol. 149, 1965, p. 1243.
94. Warwick, J. W.: Radiophysics of Jupiter. Space Sci. Rev., vol. 6, 1967, p. 841.
95. Ellis, G. R. A.: The Decametric Radio Emissions of Jupiter. Radio Sci., vol. 69D, 1965, p. 1513.
96. Franklin, K. L.: Jupiter's Radio Emission. Sci. American, vol. 211, 1964, p. 34.
97. Chang, D. B.; and Davis, L.: Synchrotron Radiation as the Source of Jupiter's Polarized Decimeter Radiation. Astrophys. J., vol. 136, 1962, p. 567.
98. Piddington, J. H.: Jupiter's Magnetosphere. Univ. Iowa rept. no. 67–63, 1967.
99. Bigg, E. K.: Influence of the Satellite Io on Jupiter's Decametric Emission. Nature, vol. 203, 1964, p. 1008.
100. Duncan, R. A.: Modulation of Jupiter Decametric Emission by the Satellite Io. Planet. Space Sci., vol. 13, 1965, p. 997.
101. Tiainen, P. O.: Dependence of Decametric Radio Emission From Jupiter on the Positions of the First Two Galilean Satellites. Nature, vol. 215, 1967, p. 1467.
102. Piddington, J. H.; and Drake, J. F.: Electrodynamic Effects of Jupiter's Satellite Io. Univ. Iowa rept. no. 67–64, 1967.
103. Burns, J. A.: Jupiter's Decametric Radio Emission and the Radiation Belts of Its Galilean Satellites. Science, vol. 159, 1968, p. 971.

104. Alfonso-Faus, A.: Solar Wind and Planetary Rotation. J. Geophys. Res., vol. 72, 1967, p. 5499.

105. Burns, J. A.; and Alfonso-Faus, A.: Discussion of paper by Antonio Alfonso-Faus, "Solar Wind and Planetary Rotation." J. Geophys. Res., vol. 73, 1968, p. 4449.

106. Giuli, T.: On the Rotation of the Earth Produced by Gravitational Accretion of Particles. Icarus, vol. 8, 1968, p. 301.

107. Alfven, H.: On the Origin of the Solar System. Univ. Calif., Berkeley, Space Sci. Lab. rept., 1967.

108. Alfven, H.: Partial Corotation of a Magnetized Plasma. Icarus, vol. 7, 1967, p. 387.

109. Patterson, T. N. L.; Johnson, F. S.; and Hanson, W. B.: The Distribution of Interplanetary Hydrogen. Planet. Space Sci., vol. 11, 1963, p. 767.

110. Hundhausen, A. J.: Interplanetary Neutral Hydrogen and the Radius of the Heliosphere. Planet. Space Sci., vol. 16, 1968, p. 783.

111. Asbridge, J. R.; Bame, S. J.; and Strong, I. B.: Outward Flow of Protons From the Earth's Bow Shock. J. Geophys. Res., vol. 73, 1968, p. 5777.

112. Anderson, K. A.: Energetic Electrons of Terrestrial Origin Upstream in the Solar Wind. J. Geophys. Res., vol. 73, 1968, p. 2387.

113. Oliven, M. N.; and Van Allen, J. A.: Paucity of Energetic Electron Clouds on the Sunward Side of the Magnetospheric Shock Front. Univ. Iowa rept. no. 68–19, 1968.

114. Heppner, J. P.; Sugiura, M.; et al.: OGO–A Magnetic Field Observations. J. Geophys. Res., vol. 72, 1967, p. 5417.

115. Smith, E. J.; Holzer, R. E.; McLeod, M. G.; and Russell, C. T.: Magnetic Noise in the Magnetosheath in the Frequency Range 3–300 Hz. J. Geophys. Res., vol. 72, 1967, p. 4803.

116. Tidman, D. A.: The Earth's Bow Shock Wave. J. Geophys. Res., vol. 72, 1967, p. 1799.

117. Tidman, D. A.; and Northrop, T. G.: Emission of Plasma Waves by the Earth's Bow Shock. J. Geophys. Res., vol. 73, 1968, p. 1543.

118. Freeman, J. W.; Kavanagh, L. D.; and Cahill, L. J.: An Observation of Transient Variations in the Magnetospheric Boundary Position. J. Geophys. Res., vol. 72, 1967, p. 2040.

119. Anderson, K. A.; Binsack, J. H.; and Fairfield, D. H.: Hydromagnetic Disturbances of 3- to 15-Minute Period on the Magnetopause and Their Relation to Bow Shock Spikes. J. Geophys. Res., vol. 73, 1968, p. 2371.

120. Sonnerup, B. U. O.; and Cahill, L. J.: Magnetopause Structure and Attitude From Explorer 12 Observations. J. Geophys. Res., vol. 72, 1967, p. 171.

121. Sonnerup, B. U. Ö.; and Cahill, L. J.: Explorer 12 Observations of the Magnetopause Current Layer. J. Geophys. Res., vol. 73, 1968, p. 1757.

122. Ballif, J. R.; and Jones, D. E.: The Magnetic Morphology of Solar Streams and Its Relation to Geomagnetic Storms. J. Geophys. Res., vol. 72, 1967, p. 5173.

123. Ballif, J. R.; Jones, D. E.; et al.: Transverse Fluctuations in the Interplanetary Magnetic Field: A Requisite for Geomagnetic Variability. J. Geophys. Res., vol. 72, 1967, p. 4357.

124. Schatten, K. H.; and Wilcox, J. M.: Response of the Geomagnetic Activity Index K_p to the Interplanetary Magnetic Field. J. Geophys. Res., vol. 72, 1967, p. 5185.

125. WILCOX, J. M.; SCHATTEN, K. H.; AND NESS, N. F.: Influence of Interplanetary Magnetic Field and Plasma on Geomagnetic Activity During Quiet-Sun Conditions. J. Geophys. Res., vol. 72, 1967, p. 19.
126. MAGUIRE, J. J.; AND CAROVILLANO, R. L.: Effect of the Interplanetary Field on the Energy of Geomagnetic Disturbances. J. Geophys. Res., vol. 73, 1968, p. 3395.
127. CUMMINGS, W. D.; AND COLEMAN, P. J.: Magnetic Fields in the Magnetopause and Vicinity at Sychronous Altitude. J. Geophys. Res., vol. 73, 1968, p. 5699.
128. LEZNIAK, T. W.; AND WINCKLER, J. R.: Structure of the Magnetopause at 6.6 R_e in Terms of 50–150 keV Electrons. J. Geophys. Res., vol. 73, 1968, p. 5733.
129. LANZEROTTI, L. J.; BROWN, W. L.; AND ROBERTS, C. S.: Energetic Electrons at 6.6 R_e During the January 13–14, 1967, Geomagnetic Storm. J. Geophys. Res., vol. 73, 1968, p. 5751.
130. PAULIKAS, G. A.; BLAKE, J. B.; FREDEN, S. C.; AND IMAMOTO, S. S.: Boundary of Energetic Electrons During the January 13–14, 1967, Magnetic Storm. J. Geophys. Res., vol. 73, 1968, p. 5743.
131. RUSSELL, C. T.; OLSON, J. V.; HOLZER, R. E.; AND SMITH, E. J.: OGO–3 Search Coil Magnetometer Data Correlated With the Reported Crossing of the Magnetopause at 6.6 R_E by ATS–1. J. Geophys. Res., vol. 73, 1968, p. 5769.
132. BAME, S. J.; ASBRIDGE, J. R.; HUNDHAUSEN, A. J.; AND STRONG, I. B.: Solar Wind and Magnetosheath Observations During the January 13–14, 1967, Geomagnetic Storm. J. Geophys. Res., vol. 73, 1968, p. 5761.
133. FREEMAN, J. W.; WARREN, C. S.; AND MAGUIRE, J. J: Plasma Flow Directions at the Magnetopause on January 13 and 14, 1967. J. Geophys. Res., vol. 73, 1968, p. 5719.
134. FREEMAN, J. W.: Observation of Flow of Low-Energy Ions at Synchronous Altitude and Implications for Magnetospheric Convection. J. Geophys. Res., vol. 73, 1968, p. 4151.
135. WARREN, C. S.: Plasma Flow at the Magnetopause. Master's thesis, Rice Univ., 1968.
136. SCHIELD, M. A.: Pressure Balance Between Solar Wind and Magnetosphere. To be published in J. Geophys. Res., 1968.
137. LAIRD, M. J.: Structure of the Neutral Sheet in the Geomagnetic Tail. Univ. N.H. rept. no. UNH–68–1, 1968.
138. MIHALOV, J. D.; COLBURN, D. S.; CURRIE, R. G.; AND SONETT, C. P.: Configuration and Reconnection of the Geomagnetic Tail. J. Geophys. Res., vol. 73, 1968, p. 943.
139. BEHANNON, K. W.: Mapping of the Earth's Bow Shock and Magnetic Tail by Explorer 33. GSFC rept. no. X–612–67–344, 1967.
140. MURAYAMA, T.; AND SIMPSON, J. A.: Electrons Within the Neutral Sheet of the Magnetospheric Tail. J. Geophys. Res., vol. 73, 1968, p. 891.
141. STÖRMER, C.: The Polar Aurora. Clarendon Press (Oxford), 1955.
142. HESS, W. N.: Energetic Particles in the Inner Van Allen Belt. Space Sci. Rev., vol. 1, 1962, p. 278.
143. FREDEN, S. C.; AND WHITE, R. S.: Trapped Proton and Cosmic-Ray Albedo Neutron Fluxes. J. Geophys. Res., vol. 67, 1962, p. 25.
144. ALFVÉN, H.: Some Properties of Magnetospheric Neutral Surfaces. J. Geophys. Res., vol. 73, 1968, p. 4379.

145. Axford, W. I.: Viscous Interaction Between the Solar Wind and the Earth's Magnetosphere. Planet. Space Sci., vol. 12, 1964, p. 45.
146. Dungey, J. W.: Interplanetary Magnetic Field and the Auroral Zones. Phys. Rev. Letters, vol. 6, 1961, p. 47.
147. Brice, N.: Bulk Motion of the Magnetosphere. J. Geophys. Res., vol. 72, 1967, p. 5193.
148. Kavanagh, L. D.; Freeman, J. W.; and Chen, A. J.: Plasma Flow in the Magnetosphere. J. Geophys. Res., vol. 73, 1968, p. 5511.
149. Axford, W. I.; and Hines, C. O.: A Unifying Theory of High-Latitude Geophysical Phenomena and Geomagnetic Storms. Can. J. Phys., vol. 39, 1961, p. 1433.
149a. Dolginov, A. Z.; and Toptygin, I. M.: Cosmic Rays in the Interplanetary Magnetic Field. Icarus, vol. 8, 1968, p. 54.
150. Dolginov, A. Z.; and Toptygin, I. M.: Diffusion of Cosmic Particles in the Interplanetary Medium. Geomag. and Aeron., vol. 7, 1967, p. 785.
151. Eviatar, Aharon: Scattering of Particles by Waves in the Presence of a Magnetic Field. J. Geophys. Res., vol. 72, 1967, p. 5997.
152. Hall, D. E.; and Sturrock, P. A.: Diffusion, Scattering and Acceleration of Particles by Stochastic Electromagnetic Fields. Phys. Fluids, vol. 10, 1967, p. 2620.
153. Hasselmann, K.; and Wibberenz, G.: Scattering of Charged Particles by a Random Electro-Magnetic Field—1. Theory. Zeit. Geophysik, 1968 (in press).
154. Jokipii, J. R.: Cosmic Ray Propagation—1. Charged Particles in a Random Magnetic Field. Astrophys. J., vol. 146, 1966, p. 480.
155. Roelof, E. C.: Transport of Cosmic Rays in the Interplanetary Medium. Can. J. Phys., vol. 46, 1968, p. S990.
156. Shisov, V. I.: Propagation of Highly Energetic Solar Protons in the Interplanetary Magnetic Field. Geomag. and Aeron., vol. 6, 1966, p. 174.
157. Noerdlinger, P. D.: Improved Model for Cosmic Ray Propagation. Phys. Rev. Letters, vol. 20, 1968, p. 1513.
158. Jokipii, J. R.; and Coleman, P. J., Jr.: Cosmic Ray Diffusion and Its Variation Observed With Mariner 4. J. Geophys. Res., vol. 73, 1968, p. 5495.
159. Jokipii, J. R.: Cosmic Ray Propagation—2, Diffusion in the Interplanetary Magnetic Field. Astrophys. J., vol. 149, 1967, p. 405.
160. Bryant, D. A.; Cline, T. L.; Desai, U. D.; and McDonald, F. B.: Explorer 12 Observations of Solar Cosmic Rays and Energetic Storm Particles Following the Solar Flare of September 28, 1961. J. Geophys. Res., vol. 67, 1962, p. 4983.
161. Fichtel, C. E.; and McDonald, F. B.: Energetic Particles From the Sun. Ann. Rev. of Astron. and Astrophys., vol. 5, 1967, p. 351.
162. Jokipii, J. R.: Back-Scatter and Diffusion of Cosmic Rays in a Random Magnetic Field. Astrophys. J., vol. 152, 1968, p. 997.
163. McCracken, K. G.: The Cosmic-Ray Flare Effect—3. Deductions Regarding the Interplanetary Magnetic Field. J. Geophys. Res., vol. 67, 1962, p. 447.
164. Fan, C. Y.; Pick, M.; et al.: Protons Associated With Centers of Solar Activity and Their Propagation in the Interplanetary Magnetic Field Regions Corotating With the Sun. J. Geophys. Res., vol. 73, 1968, p. 1555.
165. McCracken, K. G.; Rao, U. R.; and Bukata, R. P.: Cosmic Ray Propagation Processes—1. A Study of the Cosmic Ray Flare Effect. J. Geophys. Res., vol. 72, 1967, p. 293.

166. MEYER, P.; PARKER, E. N.; AND SIMPSON, J. A.: Solar Cosmic Rays of February 1956 and Their Propagation Through Interplanetary Space. Phys. Rev., vol. 104, 1956, p. 768.
167. BURLAGA, L. F.: Anisotropic Diffusion of Solar Cosmic Rays. J. Geophys. Res., vol. 72, 1967, p. 4449.
168. REID, G. C.: A Diffusive Model for the Initial Phase of a Solar Proton Event. J. Geophys. Res., vol. 69, 1964, p. 2659.
169. AXFORD, W. I.: Anisotropic Diffusion of Solar Cosmic Rays. Planet. Space Sci., vol. 13, 1965, p. 1301.
170. ANON.: Annals of the IQSY. Vol. 8, MIT Press, 1969.
171. HUGHES, E. B.; AND MARSDEN, P. L.: Response of a Standard IGY Neutron Monitor. J. Geophys. Res., vol. 71, 1966, p. 1435.
172. NOBLES, R. A.; ALBER, R. A.; ET AL.: Neutron Multiplicity Monitor Observations During 1965. J. Geophys. Res., vol. 72, 1967, p. 3817.
173. DORMAN, L. I.; AND MICROSHNICHENKO, L. I.: Method of Determining Solar Cosmic Ray Spectra in the High Energy Range. Geomag. and Aeron., vol. 6, 1966, p. 168.
174. LOCKWOOD, J. A.; AND WEBBER, W. R.: Differential Response and Specific Yield Functions of Cosmic Ray Neutron Monitors. J. Geophys. Res., vol. 72, 1967, p. 3395.
175. WILSON, B. G.; MATHEWS, T.; AND JOHNSON, R. H.: Intercomparison of Neutron Monitors During Solar Flare Increases. Phys. Rev. Letters, vol. 18, 1967, p. 675.
176. OBAYASHI, TATSUZO: The Streaming of Solar Flare Particles and Plasma in Interplanetary Space. Space Sci. Rev., vol. 3, 1964, p. 79.
177. MASLEY, A. J.; AND GOEDEKE, A. D.: The 1966–1967 Increase in Solar Cosmic Ray Activity. Proceedings of the 10th International Conference on Cosmic Rays. Can. J. Phys., vol. 48, 1968, p. S990.
178. ADAMS, G. W.; AND MASLEY, A. J.: Theoretical Study of Cosmic Noise Absorption Due to Solar Cosmic Radiation. Planet. Space Sci., vol. 14, 1966, p. 277.
179. KRIMIGIS, S. M.; AND VAN ALLEN, J. A.: Observations of the February 5–12, 1965, Solar Particle Event With Mariner 4 and Injun 4. J. Geophys. Res., vol. 72, 1967, p. 4471.
180. HAURWITZ, MARION H.: Solar Longitude Distribution of Proton Flares, Meteor Bursts, and Sunspots. Astrophys. J., vol. 151, 1968, p. 351.
181. DODSON, H. W.; AND HEDEMAN, E. R.: An Unexpected Effect in Solar Cosmic Ray Data Related to 29.5 Days. J. Geophys. Res., vol. 69, 1964, p. 3965.
182. GUSS, DONALD E.: Distribution in Heliographic Longitude of Flares Which Produce Energetic Solar Particles. Phys. Rev. Letters, vol. 13, 1964, p. 363.
183. WARWICK, C. S.: Longitude Distribution of Solar Flares. Astrophys. J., vol. 141, 1965, p. 500.
184. WILCOX, J. M.; AND SCHATTEN; K. H.: Longitude Distribution of Proton Flares as a Function of Recurrence Period. Astrophys. J., vol. 147, 1967, p. 364.
185. O'GALLAGHER, J. J.; AND SIMPSON, J. A.: Anisotropic Propagation of Solar Protons Deduced From Simultaneous Observations by Earth Satellites and the Mariner 4 Space Probe. Phys. Rev. Letters, vol. 16, 1966, p. 1212.
186. PARKER, E. N.: Interplanetary Dynamical Processes. John Wiley & Sons, Inc., New York, 1963.
187. KRIMIGIS, S. M.: Interplanetary Diffusion Model for the Time Behavior of Intensity in a Solar Cosmic Ray Event. J. Geophys. Res., vol. 70, 1965, p. 2943.

188. BOSTROM, C. O.; KOHL, J. W.; AND WILLIAMS, D. J.: The February 5, 1965, Solar Proton Event—1. Time History and Spectrums Observed at 1100 Kilometers. J. Geophys. Res., vol. 72, 1967, p. 4487.
189. PAULIKAS, G. A.; FREDEN, S. C.; AND BLAKE, J. B.: Solar Proton Event of February 5, 1965. J. Geophys. Res., vol. 71, 1966, p. 1795.
190. KAHLER, S. W.; PRIMBSCH, J. H.; AND ANDERSON, K. A.: Energetic Protons From the Solar Flare of March 24, 1966. Solar Phys., vol. 2, 1967, p. 179.
191. BRYANT, D. A.; CLINE, T. L.; DESAI, U. D.; AND MCDONALD, F. B.: Studies of Solar Protons With Explorers 12 and 14. Astrophys. J., vol. 141, 1965, p. 478.
192. BUKATA, R. P.; AND PALMEIRA, R. A. R.: The Effect of the Filamentary Magnetic Field Structure on the Solar Flare Event of May 4, 1960. J. Geophys. Res., vol. 72, 1967, p. 5563.
193. BAIRD, G. A.; BELL, G. G.; DUGGAL, S. P.; AND POMERANTZ, M. A.: Neutron Monitor Observations of High Energy Solar Particles During the New Cycle. Solar Phys., vol. 2, 1967, p. 491.
194. CLINE, T. L.; AND MCDONALD, F. B.: Relativistic Electrons From Solar Flares. Solar Phys., vol. 5 (in press), 1968.
195. CLINE, T. L.; HOLT, S. S.; AND HONES, E. W., Jr.: High Energy X-Rays From the Solar Flare of July 7, 1966. J. Geophys. Res., vol. 73, 1968, p. 434.
196. HOLT, S. S.; AND CLINE, T. L.: On the Generation of Synchrotron and X-Ray Emission With Energy Below mc^2 in Solar Flares. Astrophys. J., vol. 154, 1968. (In press).
197. TAKAKURA, T.; AND KAI, K.: Energy Distribution of Electrons Producing Microwave Impulsive Bursts and X-Ray Bursts From the Sun. Astron. Soc. Japan, vol. 18, 1966, p. 57.
198. LIN, R. P.; AND ANDERSON, K. A.: Electrons >40 keV and Protons>500 keV of Solar Origin. Solar Phys., vol. 1, 1967, p. 446.
199. DODSON, HELEN W.; AND HEDEMAN, E. RUTH: The Proton Flare of August 28, 1966. Solar Phys., vol. 4, 1968, p. 229.
200. DURGAPRASAD, N.; FICHTEL, C. E.; GUSS, D. E.; AND REAMES, D. V.: Nuclear Charge Spectra and Energy Spectra in the September 2, 1966, Solar Particle Event. Astrophys. J., vol. 154, 1968, p. 307.
201. FREIER, P. S.; AND WEBBER, W. R.: Exponential Rigidity Spectrum for Solar Flare Cosmic Rays. J. Geophys. Res., vol. 68, 1963, p. 1605.
202. LOCKWOOD, J. A.: Cosmic Ray Solar Flare Effect of January 28, 1967, as Recorded by Neutron Monitors. J. Geophys. Res., vol. 73, 1968, p. 4247.
203. MCCRACKEN, K. G.: The Cosmic-Ray Flare Effect—2. The Flare Effects on May 4, November 12, and November 15, 1960. J. Geophys. Res., vol. 67, 1962, p. 435.
204. INNANEN, WILLIAM G.: Solar Particle Observation From 24 January to 24 February 1967. Master's thesis, Univ. Iowa, 1968.
205. MCKENNA, SUSAN M. P.: East Limb Passage of an Active Solar Region, July 7–10, 1959. Astrophys. J., vol. 150, 1967, p. 1087.
206. SMITH, SARA F.; AND RAMSEY, HARRY E.: Flare Positions Relative to Photospheric Magnetic Fields. Solar Phys., vol. 2, 1967, p. 158.
207. ZIRIN, HAROLD; AND ACTON, LOREN W.: Spectrographic Observation of the Flare of July 20, 1961. Astrophys. J., vol. 148, 1967, p. 501.
208. ZIRIN, HAROLD; AND WERNER, SUSAN: Detailed Analysis of Flares, Magnetic Fields and Activity in the Sunspot Group of September 13–26, 1963. Solar Phys., vol. 1, 1967, p. 66.

209. Ellison, M. A.; McKenna, S. M. P.; and Reid, J. H.: Cape Lyot Heliograph Results–1. Light-Curves of 30 Solar Flares in Relation to Sudden Ionospheric Disturbances. Dunsin's Obs. Pub., vol. 1, 1960, p. 1.
210. Fokker, A. D.: Homology of Solar Flare-Associated Radio Events. Solar Phys., vol. 2, 1967, p. 316.
211. Castelli, J. P.; Aarons, J.; and Michael, G. A.: Flux Density Measurements of Proton-Producing Flares and Non-Proton Flares. J. Geophys. Res., vol. 72, 1967, p. 5491.
212. Castelli, J. P.; Aarons, J.; and Michael, G. A.: The Great Solar Radio Burst of May 23, 1967. Astrophys. J., vol. 153, 1968, p. 267.
213. Smerd, S. F.: Solar Radio Emissions. Research in Geophysics, vol. 1, MIT Press, 1963.
214. Warwick, James W.: Solar Radio Burst of Type V Interpreted as Type III's in Superheated Coronal Streamers. Astrophys. J., vol. 150, 1967, p. 1081.
215. Kundu, M. R.: Solar Radio Astronomy. Interscience (John Wiley & Sons, Inc.), New York, 1965.
216. Sakurai, K.: Development of Solar Flares and the Acceleration of Solar Cosmic Rays. Space Res. (Japan), vol. 21, 1967, p. 213.
217. Kundu, M. R.: Bursts of Centimeter-Wave Emission and the Region of Origin of X-Rays From Solar Flares. J. Geophys. Res., vol. 66, 1961, p. 4308.
218. Lingenfelter, R. E.; and Ramaty, R.: High Energy Nuclear Reactions in Solar Flares. Astrophysics, W. A. Benjamin, Inc. (New York), 1967.
219. Lingenfelter, R. E.; and Ramaty, R.: On the Origin of Solar Flare Microwave Radio Bursts. Planet. Space Sci., vol. 15, 1967, p. 1303.
220. Hagen, J. P.; and Barney, W. M.: Model for the Early Stage of Solar Radio Bursts. Astrophys. J., vol. 153, 1968, p. 275.
221. Ginzburg, V. L.; and Syrovatskii, S. I.: Cosmic Magneto-Bremsstrahlung. Ann. Rev. Astron. Astrophys., vol. 3, 1965, p. 297.
222. Ramaty, Reuven: Influence of the Ionized Medium on Synchrotron Emission of Intermediate Energy Electrons. J. Geophys. Res., vol. 73, 1968, p. 3573.
223. Ramaty, R.; and Lingenfelter, R. E.: The Influence of the Ionized Medium on Synchrotron Emission Spectra in the Solar Corona. J. Geophys. Res., vol. 72, 1967, p. 879.
224. McCray, R. A.: On the Possibility of Negative Absolution in Cosmic Radio Sources. Science, vol. 154, 1966, p. 1320.
225. Peterson, L. E.; and Winckler, J. R.: Gamma-Ray Burst From a Solar Flare. J. Geophys. Res., vol. 64, 1959, p. 697.
226. Chubb, T. A.; Kreplin, R. W.; and Friedman, H.: Observation of Hard X-Ray Emission From Solar Flares. J. Geophys. Res., vol. 71, 1966, p. 3611.
227. Anderson, K. A.; and Winckler, J. R.: Solar Flare X-Ray Bursts on September 28, 1961. J. Geophys. Res., vol. 67, 1962, p. 4103.
228. Acton, Loren W.: X-Ray and Microwave Emission of the Sun With Special Reference to the Events of July 1961. Astrophys. J., vol. 152, 1968, p. 305.
229. Hudson, H. S.; Peterson, L. E.; and Schwartz, D. A.: Solar and Cosmic Rays Above 7.7 keV (to be published). Sci. rept. UCSD–SP–684, 1968.
230. De Jager, C.: Note on Solar Hard X-Ray Bursts. Solar Phys., vol. 2, 1967, p. 347.
231. Boldt, E.; and Serlemitsos, P.: Suprathermal Proton X-Ray Bremsstrahlung. Astrophys. J. (in press), 1969.
232. Van Allen, J. A.: The Solar X-Ray Flare of July 7, 1966. J. Geophys. Res., vol. 72, 1967, p. 5903.

233. VAN ALLEN, J. A.: Solar X-Ray Flares on May 23, 1967. Astrophys. J., vol. 152, 1968, p. 185.
234. VAIANA, G. S.; REIDY, W. P.; ET AL.: X-Ray Structure of the Sun During the Importance in Flare of 8 June 1968. Science, vol. 161, 1968, p. 564.
235. ARNOLDY, R. L.; KANE, S. R.; AND WINCKLER, J. R.: Energetic Solar Flare X-Rays Observed by Satellites and Their Correlation With Solar Radio and Energetic Particle Emission. Astrophys. J., vol. 151, 1968, p. 711.
236. ARNOLDY, R. L.; KANE, S. R.; AND WINCKLER, J. R.: A Study of Energetic Solar Flare X-Rays. Solar Phys., vol. 2, 1967, p. 171.
237. AKASOFU, S. I.; AND YOSHIDA, S.: The Structure of the Solar Plasma Flow Generated by Solar Flares. Planet. Space Sci., vol. 15, 1967, p. 39.
238. RAO, U. R.; MCCRACKEN, K. G.; AND BUKATA, R. P.: Cosmic Ray Propagation Processes—2. The Energetic Storm Particles Event. J. Geophys. Res., vol. 72, 1967, p. 4325.
239. LIN, R. P.; KAHLER, S. W.; AND ROELOF, E. C.: Solar Flare Injection and Propagation of Low-Energy Protons and Electrons in the Event of 7–9 July, 1966. Solar Phys., vol. 4, 1968, p. 338.
240. SVESTKA, Z.: Effects Associated With the Sector Boundary Crossing on July 8, 1966. Solar Phys., vol. 4, 1968, p. 361.
241. ATHAY, R. G.; AND MORETON, G. E.: Impulsive Phenomena of the Solar Atmosphere—1. Some Optical Events Associated With Flares Showing Explosive Phase. Astrophys. J., vol. 133, 1961, p. 935.
242. MCCRACKEN, K. G.; RAO, U. R.; AND NESS, N. F.: Inter-Relationship of Cosmic Ray Anisotropies and the Interplanetary Field. J. Geophys. Res., vol. 73, 1968, p. 4159.
243. LEIGHTON, R. B.: Transport of Magnetic Fields on the Sun. Astrophys. J., vol. 140, 1964, p. 1547.
244. ANDERSON, K. A.: Electrons and Protons in Long-Lived Streams of Energetic Solar Particles. Univ. Calif., Berkeley, rept., June 1968.
245. MCCRACKEN, K. G.; RAO, U. R.; AND BUKATA, R. P.: Recurrent Forbush Decreases Associated With M-Region Magnetic Storms. Phys. Rev. Letters, vol. 17, 1966, p. 928.
246. SCHATTEN, K. H.; WILCOX, J. M.; AND NESS, N. F.: A Model of Interplanetary and Coronal Magnetic Fields, 1968 (to be published).
247. NEWKIRK, G. A., JR.: Structure of the Solar Corona. Ann. Rev. Astron. and Astrophys., vol. 5, 1967, p. 213.
248. PARKER, E. N.: Interplanetary Origin of Energetic Particles. Phys. Rev. Letters, vol. 14, 1965, p. 55.
249. WEDDELL, J. B.: Solar Proton Event Production by Hydromagnetic Shocks. Planet. Space Sci., vol. 13, 1965, p. 789.
250. FISK, L. A.; AND AXFORD, W. I.: Effect of Energy Changes on Solar Cosmic Rays. J. Geophys. Res., vol. 73, 1968, p. 4396.
251. BAHCALL, JOHN N.; AND SHAVIN, GIORA: Solar Models and Neutrino Fluxes. Astrophys. J., vol. 153, 1968, p. 113.
252. DAVIS, RAYMOND, JR.; HARMES, D. S.; AND HOFFMAN, K. C.: Search for Neutrinos From the Sun. Phys. Rev. Letters, vol. 20, 1968, p. 1205.
253. HAYMES, R. C.: Fast Neutrons in the Earth's Atmosphere—2. Time Variations at High Altitudes. J. Geophys. Res., vol. 69, 1964, p. 853.
254. HESS, W. N.; AND KAIFER, R. C.: The OSO–1 Solar Neutron Experiment. Solar Phys., vol. 2, 1967, p. 202.

255. BAME, S. F.; AND ASBRIDGE, J. R.: A Search for Solar Neutrons Near Solar Minimum. J. Geophys. Res., vol. 71, 1966, p. 4605.

256. WEBBER, W. R.; AND ORMES, J. F.: An Upper Limit on the Quiet Time Solar Neutron Flux at Energies >60 MeV. J. Geophys. Res., vol. 72, 1967, p. 3387.

257. ROELOF, E. C.: Effect of the Interplanetary Magnetic Field on Solar Neutron-Decay Protons. J. Geophys. Res., vol. 71, 1966, p. 1305.

258. APPARAO, M. V. K.; DANIEL, R. R.; VIJAYALAKSHMI, B.; AND BHATT, V. L.: Evidence for the Possible Emission of High Energy Neutrons From the Sun. J. Geophys. Res., vol. 71, 1966, p. 1781.

259. HOLT, S. S.: Satellite Protons as a Test of Solar Neutron Observations. J. Geophys. Res., vol. 72, 1967, p. 3507.

260. CHUPP, E. L.; LAVAKARE, P. J.; AND SEUKADY, A. A.: Limit on Continuous Solar Flux of the 2.2 MeV Neutron-Proton Capture Gamma Ray. Phys. Rev., vol. 166, 1968, p. 1299.

261. FROST, K. J.; ROTHE, E. D.; AND PETERSON, L. E.: A Search for the Quiet-Time Solar Gamma Rays From Balloon Altitudes. J. Geophys. Res., vol. 71, 1966, 4079.

262. FRYE, G. M., JR.; REINES, F.; AND ARMSTRONG, A. H.: Search for Solar and Cosmic Gamma Rays. J. Geophys. Res., vol. 71, 1966, p. 3119.

263. METZGER, A. E.; ANDERSON, E. C.; VAN DILLA, M. A.; AND ARNOLD, J. R.: Detection of an Interstellar Flux of Gamma-Rays. Nature, vol. 204, 1964, p. 766.

264. REINES, F.: The Search for the Solar Neutrino. Proc. Roy. Soc. (London), vol. 301A, 1967, p. 159.

265. BAHCALL, J. N.; BAHCALL, NITA A.; AND SHAVIN, GIORA: Present Status of the Theoretical Predictions for the ^{37}Cl Solar N° Experiment. Phys. Rev. Letters, vol. 20, 1968, p. 1209.

333-240 O—69——18

Page Intentionally Left Blank

PLANETARY ATMOSPHERES

F. S. Johnson, F. D. Colegrove, W. B. Hanson, R. R. Hodges, Jr.,
J. E. Midgley, A. Palm, and B. A. Tinsley

Southwest Center for Advanced Studies
Dallas, Texas

Page Intentionally Left Blank

Planetary Atmospheres

INTRODUCTION

During 1967 the following spacecraft were launched with experiments in the planetary atmospheres discipline: San Marco II, Ariel III, OGO–IV, Explorer XXXV, and Mariner V. Twenty-three sounding rockets were launched by NASA in investigation of the Earth's atmosphere under this discipline program, and about 55 rockets under the auspices of the meteorology program.

Significant new data and results were reported from experiments aboard spacecraft launched in previous years, and important new contributions have resulted from ground-based observations, theoretical studies, and laboratory research. The highlights of these results and the increase of our insight into the conditions and processes of planetary atmospheres are described in this report.

The most striking advance in knowledge of planetary atmospheres during 1967 resulted from spacecraft measurements of the planet Venus, disclosing that it has a massive, hot, dry atmosphere. The exact pressure and temperature at the surface remains in some doubt, but the pressure is within a factor of 2 of 100 atmospheres, and the temperature is within the range $650° \pm 100°$ K. There has also been steady, but less dramatic, progress in the development of knowledge of the atmospheres of Mercury and Mars. Observations around the Moon from Explorer XXXV show that the solar wind impinges directly on the lunar surface, and this permits the drawing of additional conclusions concerning the lunar atmosphere. In the case of the Earth's atmosphere, as the description of the upper atmosphere becomes more refined, additional significant features become recognizable. An example of this is the development of an increase in helium concentrations over the winter polar region, apparently as a result of large-scale circulation near the 100-kilometer level.

EARTH

Temperature and Density

Diurnal temperature changes in the atmosphere as a result of absorption of solar energy are relatively much larger above 150 kilometers than at lower altitudes. The increased temperature that occurs in the afternoon results in an expansion of the atmosphere, so that it becomes less confined by

the Earth's gravitational field. Also, a region of increased density (as well as temperature and pressure) develops at high altitudes; this is frequently referred to as a density bulge. There has been some uncertainty in recent years as to the proper description of this bulge.

Several years ago, Jacchia (ref. 1) put forth a description of the temperature pattern in the upper thermosphere, according to which the daytime temperature maximum followed the declination of the Sun with season, but lagged about 2 hours behind the Sun in local time. The pattern was nearly symmetric, with the daytime temperature maximum about one-third larger than the nighttime minimum. The principal lack of symmetry was that the nighttime minimum occurred at 0500 hours local time rather than at 0200 hours. The latitude of the minimum was equal to that of the maximum, but in the opposite hemisphere.

This view was questioned on the basis of additional satellite drag data. The new data indicated that the density bulge did not follow the Sun in declination. Keating and Prior (ref. 2) purported to show that the bulge occurred in the winter hemisphere with its center at the same latitude (but opposite sign) as the subsolar point. According to another interpretation of the data by Jacchia and Slowey (ref. 3), the bulge remained centered on the Equator and was not symmetrical, but rather elongated in latitude.

This rather confusing situation was clarified when Keating and Prior (refs. 4 and 5) recognized that a polar effect was involved; namely, an increase in helium content in the upper atmosphere over the winter polar region. Helium, because of its low mass and the effects of diffusive separation in the upper atmosphere caused by gravitational potential, dominates over heavier atmospheric constituents above some level that varies with the solar cycle. Satellites, flying at altitudes high enough so that the principal gas around them is helium, map out the distribution of helium, whereas satellites flying at lower altitudes map out the distribution of atomic oxygen. The oxygen distribution is principally controlled by the temperature distribution, so the lower altitude satellites provide data from which the global pattern of temperature in the upper thermosphere can be obtained. This temperature distribution is essentially that described by Jacchia in 1964, although the latitude of the temperature maximum appears to be a little nearer the Equator than the subsolar latitude.

Although it is superficially satisfying to find that the temperature maximum occurs near the subsolar latitude, it should be noted that this is not a satisfactory indication of atmospheric response to solar heating. Because of the greater length of the summer days at high latitudes, the maximum solar heating averaged over a day is at the summer pole, although the maximum is very flat, with nearly uniform heat input from 20° or 30° latitude to the pole. Consequently the temperature maximum would occur at much higher latitude than is observed if no other effects were involved besides solar

heating (ref. 6). Atmospheric circulation is presumably responsible for displacing the temperature maximum from high latitude to low latitude where it is observed.

There are other important heat inputs in the upper atmosphere besides solar heating. One of these is associated with geomagnetic activity; the actual mechanism of the heating is in some doubt, as it might be absorption of energy from hydromagnetic waves, energy input by energetic particles from the magnetosphere, or the solar wind. Jacchia, Slowey, and Veriani (ref. 7), using satellite drag data from Injun III, Explorer XIX, and Explorer XXIV, found a time delay of about 7 hours between the peak geomagnetic disturbance and the peak heating effect, with the time delay possibly somewhat greater at low latitudes than at high. The indices of magnetic activity that were used were the planetary indices K_p and a_p. For small magnetic perturbations ($K_p<5$), the temperature changes are nearly proportional to K_p and 15 to 25 percent larger at high latitudes than at low. This latitudinal dependence is much smaller than appeared to be the case with earlier data, when the effect of high latitudes appeared to be four or five times larger than at low (ref. 8). The variation of temperature at low latitude with magnetic activity is now described by the relations

$$\begin{aligned}\Delta T &= 28°K_p + 0.03° \exp(K_p) \\ &\approx 1.0°a_p + 100°[1 - \exp(-0.08a_p)]\end{aligned}$$

At high latitude, the variation is greater by a factor of about 1.2; this factor may be as large as 2.0 for occasional magnetic storms.

Some doubt has been cast upon the time of the diurnal temperature maximum. Satellite drag data indicate clearly that the maximum of the density bulge occurs near 1400 hours local time, and this has been interpreted as indicating a temperature maximum at that time. Ion temperatures can be determined throughout the upper ionosphere by means of Thomson scatter (incoherent radar backscatter), and these temperatures should be about the same or only slightly in excess of the neutral gas temperatures in the upper thermosphere. Carru, Petit, and Waldteufel (ref. 9) have presented data for an altitude of 300 kilometers indicating that the temperature maximum occurs near 1600 or 1700 hours. This is much closer to the time of the temperature maximum that would be expected if no lateral transport of energy were to occur as a result of diurnal wind systems.

Upper atmospheric data frequently have been organized by comparison with atmospheric models that are based upon fixed boundary conditions near 120 kilometers. This has been done because relatively few data have been acquired below satellite altitudes, so the region below about 200 kilometers is not very well mapped by comparison with the region above. Lacking knowledge of the lower region, some arbitrary assumption was needed,

and 120 kilometers was chosen as the altitude for that assumption because it was the lowest altitude down to which there was considerable confidence that diffusive equilibrium prevailed, and because what little evidence did exist suggested that conditions were relatively constant at that altitude. Atmospheric models were therefore constructed on that base. The large relative changes at higher altitudes caused by temperature changes usually greatly dominated over any change that might have been expected at 120 kilometers, so the procedure was generally quite satisfactory. With fixed boundary conditions at 120 kilometers, atmospheric models showed relatively little variation up to about 200 kilometers. Moreover, it was only at the higher altitudes that satellite data were available for comparison with the models. However, it is now becoming clear that atmospheric variations are important below 200 kilometers. King-Hele and Quinn (ref. 10) found an increase in density of about 30 percent at 220 kilometers over the period January–June 1966, by observing the orbital decay of the satellite Star-rad, 1962$\beta\kappa$; this increase is to be associated with the advance of the solar cycle. Further, King-Hele and Hingston (ref. 11) observed the orbital decay of a dense satellite, 1966–101G, whose perigee was 140 kilometers. They deduced greater air density by day than by night at 155 kilometers by a factor as large as 1.7; atmospheric models show little difference at that altitude, and that small difference tends to indicate larger density by night than by day. This is a clear indication of the inadequacies of atmospheric models based on fixed boundary conditions near 120 kilometers; although they are useful for organizing data and for predicting atmospheric behavior above 200 kilometers, they are of much less value below.

Composition

The most striking recent result concerning composition of the upper atmosphere as a factor influencing the major structure of the atmosphere has been the discovery of the helium bulge over the winter polar region (refs. 4 and 5). This was discovered by analysis of satellite drag data, which indicated that the region of maximum atmospheric density was to be found at low latitudes, when probing at altitudes below about 500 kilometers, and over the winter polar region, when probing at altitudes above 500 kilometers. Because the transition from atomic oxygen to helium as a major atmospheric constituent occurred near 500 kilometers at the time of the observation, which was near the minimum of the solar cycle, it was indicated that helium concentrations were enhanced over the winter polar region relative to other latitudes. With the advancing phase of the solar cycle, the transition region from oxygen to helium has raised in altitude, so similar observations can be made now only at higher altitudes, probably only above 1000 kilometers.

Direct measurements of atmospheric composition by Explorer XVII tend to substantiate the observation of enhanced helium concentrations over the

winter polar region (ref. 12). The separation of altitude, latitude, and local time is difficult because of the use of an eccentric satellite orbit, and the results are not as clear as might have been expected.

Measurement from the Earth's surface of resonantly scattered solar radiation by helium in the metastable 2^3S state by Tinsley (ref. 13) support the view that the helium concentrations are enhanced over the winter polar region and even down to latitudes as low as 30°. In addition to a marked maximum in the emission rate during the winter of 1966–67, the emission rates looking poleward at 34° latitude were observed to be significantly greater than looking equatorward.

Rocket measurements also show variations in helium content. Measurements below 200 kilometers at White Sands, N. Mex., by Nier showed an order of magnitude more helium in December 1966 than in July 1955. Hartmann, Mauersberger, and Müller (ref. 14) observed helium concentrations at 120 kilometers over Fort Churchill, Canada, on December 12, 1966, that were five times larger than the values adopted in the CIRA reference atmosphere; at the same time they observed argon concentrations within about 35 percent of the model values.

Measurements of the atomic oxygen content of the upper atmosphere have been questioned by von Zahn (ref. 15). He draws attention to the loss processes that exist in mass spectrometers for atomic oxygen—by trapping in the walls and by recombination to N_2O and CO_2. He suggests that the atmospheric concentrations deduced from mass spectrometer measurements therefore may be underestimated by a factor of several times.

Dynamics

There are many important dynamical effects in the upper atmosphere, among them tides and other internal gravity waves, turbulence, and large-scale circulation. The importance of eddy transport associated with turbulence has been recognized only recently, particularly with regard to heat transport and transport of atmospheric constituents. Large-scale circulation is obviously important in the transport of heat and atmospheric constituents, but these effects have not been worked out quantitatively. Tides and internal gravity waves may provide the energy source to stimulate turbulence, but the exact mechanism by which this is done remains in doubt.

In the vicinity of the turbopause near 100 kilometers, turbulence and eddy mixing act to transport atomic oxygen downward and molecular oxygen upward. A decrease in the rate of eddy mixing would allow atomic oxygen to accumulate in the region where it is formed more rapidly than it is lost by recombination, thus increasing the atomic to molecular ratio for oxygen; an increase in the rate of eddy mixing would act to remove atomic oxygen from its source region and transport it down to the vicinity of the 80-kilometer level where it is lost rapidly by recombination, thus decreasing the

atomic to molecular ratio near the turbopause. Eddy mixing also acts to transport helium from the region above the turbopause to the region below, so a rapid rate of eddy mixing acts to depress the helium content of the upper atmosphere, whereas a slow rate of eddy mixing allows helium to escape from below the turbopause to the region above it, increasing the helium content of the upper atmosphere.

When the excess of helium over the winter polar region was first observed, it was natural to suggest that this might be explained in terms of a reduction in the rate of eddy mixing or of a lowering of the turbopause. However, it appears that the reason for the helium bulge is more complex, as a reduction in the turbopause altitude would not supply a source of the required magnitude. When the helium concentrations build up over the winter polar region, there must be an outflow to lower latitudes, and this outflow will be mainly in the exosphere, because below the exosphere the flow is restricted by the requirement to diffuse horizontally through the neutral atmosphere. The magnitude of the outflow through the exosphere can be estimated from a study by McAfee (ref. 16), who was concerned mainly with the diurnal flow of atomic hydrogen and helium. From McAfee's calculations it is estimated that a vertical upward flux of about 4×10^8 atoms cm^{-2} s^{-1} would be required to maintain a 50-percent increase in the helium concentrations over the winter polar region. This is a factor of 4 greater than the rate at which helium can be released from the homosphere by diffusion; assuming a scale height of 7 kilometers, a molecular diffusion coefficient of 5×10^6 cm^2 s^{-1}, and a helium concentration of 10^7 cm^{-3} near the turbopause, this rate is about 10^8 atoms cm^{-2} s^{-1}. Therefore, a decrease in the rate of mixing would permit the escape of helium from the homosphere into the diffusosphere at a rate of about 10^8 atoms cm^{-2} s^{-1}, and this would cause an increase in the helium concentration of only about 10 percent, as lateral outflow in the exosphere would then carry helium away as fast as it is released. The magnitude of the helium bulge actually observed by Keating and Prior (ref. 5) is about a factor of 2 to 4 between the summer and winter poles. This is larger than can be explained by a decrease in the rate of eddy mixing. It should be noted that the vertical fluxes required to support a gradient in concentration in the exosphere are much larger than the escape flux to space, which is about 10^6 atoms cm^{-2} s^{-1}; therefore the flow problem is not significantly perturbed by helium escape.

A more powerful mechanism for concentrating helium over the winter polar region is provided by large-scale circulation near the altitude of the turbopause (ref. 17). The fact that the upper atmosphere over the winter polar region remains about as warm as that at low latitudes can be explained in terms of an average wind toward the winter pole, accompanied by downward motion and compressional heating at high latitudes; the return flow is accomplished at lower altitudes—perhaps in the troposphere where, because of the much greater density involved, the flow is too small to be recog-

nizable. Above the turbopause, where each atmospheric constituent is distributed according to its own molecular mass or scale height, the inflow toward the polar region for each constituent is proportional to the product of the inflow velocity (which is the same for all constituents), the concentration, and the scale height. The loss by downward motion is proportional to the product of the downward velocity and the concentration—but not the scale height. The downward velocity is related to the inflow velocity by the continuity requirement of the major constituents. Therefore, relative to the losses, there is an excess inflow of constituents lighter than the average and a deficiency in the inflow of constituents heavier than the average. Helium, having a molecular weight about one-seventh that of air, and hence a scale height above the turbopause about seven times that of the major constituent, has an excess inflow over outflow—the outflow downward is initially only one-seventh of the inflow, so six-sevenths of the inflow is excess and accumulates. As the helium concentrations build up, the loss by downward motion increases in proportion; if the concentration were to build up by a factor of 7, the downward flow would then equal the inflow. However, losses by outflow through the exosphere are also important, and the buildup must be limited to a factor well below 7.

There should be a similar, though smaller, buildup in oxygen concentration. This might prove a significant perturbation in the ionospheric chemistry. A decrease should be expected in the argon concentration; because of its heavy mass, the effect on argon is opposite to that on the lighter constituents. There might also be a significant increase in the hydrogen concentration, but the situation is less clear in this case because the hydrogen distribution is governed by the average scale height of the atmosphere well above the turbopause; this results from the rapid escape of hydrogen to space and the diffusive limitations on its rapid flow through the atmosphere (ref. 18).

In addition to the poleward winds in the winter hemisphere, there might be equatorward winds in the summer hemisphere, producing the opposite effects to those in the winter polar region. Such winds might exist in the summer hemisphere, as such a circulation could explain the presence of the temperature maximum at the lower latitudes where it is observed rather than at higher latitudes. Thus, there might be a depression of the helium and oxygen concentrations over the summar polar region.

Kohl and King (ref. 19) have calculated the diurnal winds to be expected at 300 kilometers as a result of the density or pressure bulge in the atmosphere. They considered the pressure gradient force caused by the bulge, Coriolis force, viscosity, and ion drag. In general, the computed wind pattern is from the region of the bulge to the minimum, and fairly symmetrical—the effect of ion drag being sufficient to counteract the effect of Coriolis force tending to make the system unsymmetrical. The calculated winds tend to be in the range 50 to 150 m/sec, with the maximum values appropriate to

solar minimum conditions because the ion drag is less then. It seems reasonable to expect that this diurnal wind system should also produce composition variations in the upper atmosphere similar to the polar wind system discussed above. This diurnal wind system does not necessarily interfere seriously with the polar wind system; the polar wind system that was described should exist in the average; requiring only that the inflow exceed the outflow sufficiently to yield an average inflow. Even the strongest winds calculated by Kohl and King cannot traverse the polar region before reversing.

Rocket measurements at high latitudes in Sweden and Alaska have shown very low summer mesopause temperatures (ref. 20). The distributions were consistent, with a temperature minimum of about 140° K near 85 kilometers, irrespective of the presence of noctilucent clouds. It is therefore concluded that the presence or absence of the clouds is dependent more upon the water vapor concentration than on the temperature, and that the variability in cloud occurrence is indicative of a variable water vapor content near the mesopause. Another possibility is that the meteoric dust influx is the controlling factor.

Geocorona

The distribution of gases above a height of about 110 kilometers is influenced by the effects of temperature on the processes of diffusion and escape (refs. 18, 21, 22, 23, and 24). In the case of hydrogen, given a constant production rate near 90 kilometers in the homosphere, large changes in density at high levels should accompany temperature variations over the course of a solar cycle. Similar density variations occur between dayside and nightside distributions, owing to diurnal temperature changes; in this case the lateral flow of exospheric constituents between dayside and nightside should decrease the magnitude of the effects calculated on the basis of the temperature change only (refs. 16 and 25).

Liwshitz and Singer (ref. 26) and Liwshitz (ref. 27) have calculated the effect of the nonequilibrium velocity distribution of exospheric constituents, caused by the appreciable escape rate, on the rate itself, and report that a factor of 2 or 3 more hydrogen should be present in the thermosphere compared to that calculated without considering the effect. However, Chamberlain and Campbell (ref. 28) have made similar calculations and find an effect of only 20 to 30 percent.

To predict the abundances of atmospheric constituents at high levels, the height of the turbopause (the level above which diffusive separation occurs) must be known. There is evidence that this level is variable (refs. 29 and 30), resulting in quite large changes in relative abundance. For gases other than helium and argon, it is necessary to know, in addition, the rates of production and removal by photochemical and other reactions. For

hydrogen, the rate of production cannot be reliably determined from considerations of the source chemistry (refs. 31 and 32), and it is necessary to normalize the theoretical altitude profiles to observational data.

In discussing the observational results which follow, comparisons will be made with the Kockarts and Nicolet (refs. 23 and 24) models, which arbitrarily assume a constant production rate below 100 kilometers for all phases of the solar cycle. They have a concentration of 10^7 cm^{-3} at 100 km, and an upward flow of 2.5×10^7 atoms cm^{-2} s^{-1} at 100 kilometers. Whenever thermospheric temperature is not deduced from the observation itself, a value from Jacchia's (ref. 33) relation between thermosphere temperature and solar 10.7-centimeter flux will be used in the following discussion.

Observational evidence on hydrogen concentrations come from many diverse sources. These are enumerated below:

(1) *Absorption Core in the Solar Lyman-α Line.*—Observations were made on July 21, 1959, at altitudes between 100 and 200 kilometers of the absorption core in the solar Lyman-α line (ref. 34). These daytime measurements indicate a concentration at 100 kilometers of about 10^7 cm^{-3} and a vertical column abundance of about 6×10^{12} atoms/cm^2 above 100 kilometers (ref. 18), in agreement with the Kockarts-Nicolet models for that time of observation.

(2) *Geocoronal Lyman-α Scattering.*—Starting in 1957, many measurements have been made in the United States and the U.S.S.R. on the brightness of the Lyman-α emission caused by resonant scattering of solar Lyman-α on hydrogen in the thermosphere and exosphere (the geocorona). Measurements were made under daytime, twilight, and nighttime conditions (when multiple scattering transports radiation around from the dayside). To interpret these measurements in terms of hydrogen abundance, it is necessary to compare them with model calculations of the multiple scattering in the spherical atmosphere, and also to know the flux of solar Lyman-α at the line center.

A discussion of the measurements up to 1965 is given by Donahue (ref. 35). Although there are difficulties and inconsistencies in interpreting the data, he states that the daytime abundance appears to have had a lower limit of 40×10^{12} atoms cm^{-2} in late 1964. It appears that the nighttime abundance increased from roughly 30×10^{12} atoms cm^{-2} in 1960 to a lower limit of 85×10^{12} atoms cm^{-2} in 1965. The 1964 and 1965 values are considered lower limits because the solar Lyman-α flux at solar minimum was not measured and was probably lower than the 1962 value used in interpreting the data. Increasing the solar minimum values by 50 percent results in their becoming about a factor of 3 greater than the Kockarts-Nicolet model values. The nighttime 1960 value is greater than the model value by a factor of 2.

Further measurements of geocoronal Lyman-α have been made from satellites, but only preliminary results and interpretations are at present available. Observations were made in 1966–67 on the OV1–10 satellite by Clark, Metzger, and Menigoz (ref. 36); on the OGO–III, OGO–IV and OSO–IV satellites by Mange (ref. 37); and on the Vela 4 satellites by Fuller, Chambers, Fehlau, and Kunz (ref. 38). Meier (ref. 39) has found that these measurements require an optical depth of $\sim$2.7 in Lyman-α above 700 kilometers during the daytime and greater amounts of hydrogen at night. The daytime value is an order of magnitude more than the corresponding Kockarts-Nicolet value for the period of observation.

(3) *Geocoronal Balmer-α Emission.*—Solar Lyman-β flux is multiply scattered in the geocorona in the same way as Lyman-α, except that it is nonconservatively scattered, with 12 percent of the scattering processes producing Balmer-α (6563 Å), which can be detected at the ground. Observations have been made for many years, with increasing spatial and temporal resolution, e.g., by Fishkova (ref. 40), Shcheglov (ref. 41), Armstrong (ref. 42), and Tinsley (refs. 43 and 44). The measurements are more consistent than the Lyman-α results, and they are capable of yielding good information on the hydrogen concentration and distribution. At present only preliminary interpretations are available, indicating a lower limit of 200×10^{12} atoms/cm^2 above 100 kilometers for 1965 nighttime conditions. Increasing this value by 50 percent results in a factor of 6 more than the Kockarts-Nicolet value. The Balmer-α measurements show a seasonal variation of about 30 percent with a maximum for the Northern Hemisphere in the summer and fall, and a minimum in the spring (ref. 44). The maximum can be interpreted as an enhanced abundance of hydrogen in the upper atmosphere at that time of year.

(4) *Mass Spectrometer Measurements of Hydrogen Ions.*—Measurements of the concentration of atomic hydrogen ions, combined with a knowledge of atomic oxygen neutral and ion concentrations, leads to values for the neutral atomic hydrogen concentration from considerations of charge exchange equilibrium. From the 1961 daytime measurements by Taylor, Brace, Brinton, and Smith (ref. 45), Hanson, Patterson, and Degaonkar (ref. 46) obtained the atomic hydrogen concentration of 7×10^4 at 500 kilometers at an exospheric temperature at 1235° K, which is an order of magnitude more than the Kockarts-Nicolet value.

From measurements made from Explorer XXXI, Hoffman (ref. 47) obtained an atomic hydrogen concentration of 5×10^6 cm^{-3} at 350 kilometers for a thermosphere temperature of 700° K in January 1964. This is on an order of magnitude more than the appropriate Kockarts-Nicolet value.

Brinton, Pharo, Mayr, and Taylor (ref. 48), in a rocket flight in March 1966, obtained a neutral hydrogen concentration of 3×10^5 cm^{-3} at 400

kilometers, along with a temperature in the range 700° to 800° K. The atomic hydrogen concentration is about the same as the Kockarts-Nicolet value for 750° K, though the agreement may be fortuitous, since a temperature of ~900° K would seem more appropriate for the time at observation.

(5) *Electron Cooling Measurement.*—Brace, Reddy, and Mayr (ref. 49) have arrived at an estimate of the atomic hydrogen concentration from arguments concerning the rate of electron cooling at sunset. They obtain 5×10^5 cm^{-3} at 1000 kilometers in early 1965, which is a factor of 5 more than the Kockarts-Nicolet value for 750° K.

(6) *Direct Measurement.*—Measurements have been made with a neutral mass spectrometer on the Explorer XXXII satellite. Reber, Cooley, and Harpold (ref. 50) find 2×10^6 cm^{-3} at 300 kilometers for 0900 local time May 1966, which is a factor of 20 more than the Kockarts-Nicolet value for 900° K.

(7) *Measurements Beyond 3000 Kilometers.*—Measurements have been made on three Soviet deep-space probes, Venus 2, Venus 3, and Zond 1, of geocoronal Lyman-α at distances from 1.5 (3200-km altitude) to 20 R_E (*Earth radii*). Kurt (ref. 51) has inferred from them hydrogen concentrations for November 1965, as follows: 2×10^3 cm^{-3} at 1.5 R_E, 10^2 cm^{-3} at 3 R_E, 10 cm^{-3} at 7.5 R_E, and 1.5 cm^{-3} at 20 R_E, along a trajectory roughly perpendicular to the Sun-Earth line.

Observations made by Swisher and Frank (ref. 52) of proton lifetimes between 2.5 and 4.8 R_E in July 1966, also give hydrogen concentrations, and these correspond very closely with the observations made by Kurt over the larger range. Kurt's values may be compared with Chamberlain's (ref. 53) model exosphere, which also extends to 20 R_E. The observations correspond to a temperature of 1000° K, and more closely to a model with all satellite orbits included (Chamberlain omits those with perigees above 2.7 R_E) than one without satellite orbits. It is of interest that a temperature of 1000° K was found at several Earth radii for 1965, while the temperature at 500 kilometers varied between daytime and nighttime values of 900° and 700° K. A situation that can be interpreted as a higher temperature corresponding to higher exospheric levels has been reported by Barth, Wallace, and Pearce (ref. 54) for the Venus exosphere.

In spite of difficulties and discrepancies in both the theory of the hydrogen distribution in the upper atmosphere and measurements of its absolute abundance, the broad outline of the height variation and solar cycle variation are well established. The absolute abundances are generally higher than the Kockarts-Nicolet models, except for the one measurement made by absorption near solar maximum. One might explain the discrepancies of the others by an increasing production rate with reduced solar activity, but at present this can only be speculation. Further work on multiple scattering

calculations should allow a much more detailed and critical evaluation of the optical data than is at present possible.

Airglow and Aurora

Sodium has been observed in the upper atmosphere through the emission of D-line radiation. Hunten and Wallace (ref. 55) and Donahue and Meier (ref. 56) have made the surprising observation that above the maximum of the layer near 90 kilometers the radiation falls off very rapidly with altitude, the scale height being about 3 kilometers during the daytime and at twilight. This rapid falloff with altitude cannot be explained in terms of conventional photochemical theory. Hanson and Donaldson (ref. 57) offer an explanation in terms of an upward flux of sodium atoms that undergo photoionization at such a rate as to cause the small scale height. To maintain continuity, they indicate that there is an equal downward flux of sodium ions that experience a rapidly increasing rate of recombination with decreasing altitude; they suggest that this results from a reaction with ozone whose concentration increases rapidly in the downward direction.

The oxygen green line at 5577 Å in the night airglow apparently has its minimum intensity near the Equator. This has been indicated by surface measurements in Ethiopia (ref. 58) and by satellite measurements (ref. 59). This line has its maximum emission near 95 kilometers and is thought to be caused by recombination of atomic oxygen into molecular form in three body collisions involving a third oxygen atom, which becomes excited. There is also a second layer of emission at a higher altitude, near 250 kilometers, confined to low latitudes, and probably caused by dissociative recombination of molecular oxygen ions (ref. 60). Hence a reduction in intensity near the Equator suggests that some mechanism is suppressing atomic oxygen recombination into molecules there. The reduction is quite marked. Weill, Fehrenbock, Morguleff, and Glaume (ref. 58) indicate an equatorial intensity seen from the surface of about 50 Rayleighs, a low value never reached at middle latitudes. Elliott, LaValle, and Williams (ref. 59) indicate an equatorial intensity of 150 Rayleighs as seen from above, compared with 500 Rayleighs at mid-latitude; their observing altitude was above the upper layer of equatorial emission, so the equatorial values of emission near 95 kilometers are probably well below 150 Rayleighs. No mechanism has been suggested to account for the suppression of oxygen recombination near the Equator; it might be accomplished by upward air currents, but it does not appear reasonable to have stronger large-scale upward currents near the Equator than in the summer hemisphere. If the phenomenon should prove to be equinoctial, the concept of upward flow over the Equator would appear more acceptable.

Infrasonic waves with periods from 20 to 80 seconds have been observed

occasionally by Wilson and Nichparenko (ref. 61) in connection with auroral activity. The amplitudes range up to 10 dynes/cm^2 and usually only a few cycles are observed. Events occur infrequently; occasionally several events are observed during one night, but on other nights none are observed. The generation seems to be associated with rapidly moving auroral forms, where the motion of the source is supersonic; this results from a movement of the energetic particle source and does not represent supersonic movement of the atmospheric gases. However, the supersonic motion of a source of sound waves should act to produce a shock wave, and this is presumably the generation mechanism for the infrasonic waves. The direction of arrival agrees with the concept that the source is in active, rapidly moving auroral forms, and the preferred direction of propagation is in the direction of motion of the auroral forms. The mechanism of formation of the pressure disturbance in the auroral form is not clear; it could, for example, be heating of the neutral atmosphere. The large amplitude of the waves—up to 10 dynes/cm^2—is difficult to explain in terms of a generation mechanism above 80 kilometers, where the ambient pressure is less than 10 dynes/cm^2. The fact that attenuation is to be expected because of geometric factors, and to a lesser extent because of absorption, makes the explanation even more difficult.

Ion temperatures in aurorae at altitudes between 200 and 500 kilometers have been measured by Knudsen and Sharp (ref. 62) and found to vary between 2000° and 6000° K; the measurements were made using an ion trap installed in a satellite. The high temperatures may result from bombardment by auroral particles or from electric current or drift effects.

MOON

The Moon has very little atmosphere, as indicated by the failure to detect from the Earth any refraction as stars are occulted by the Moon. The known limit on ion and electron concentration near the Moon has been steadily lowered as radio detection techniques have improved, and an upper limit of about 10 cm^{-3} is now applicable.

A notable advance in the understanding of the Moon and its environment occurred in 1967 when Explorer XXXV, the Anchored IMP, was placed in orbit around the Moon. The most significant observation was that there was no shock wave in the solar wind ahead of the Moon (refs. 63 and 64); this indicates that the solar wind impinges directly on the lunar surface. This has two important consequences with regard to the lunar atmosphere. First, the solar wind constitutes an atmospheric source through the recombination of ions and electrons on the lunar surface. Second, electric fields in the solar wind rapidly accelerate any atmospheric particle that becomes ionized, leading to very short lifetimes for ions in the vicinity of the Moon;

333-240 O—69——19

on this account, the degree of ionization of any ambient atmosphere must be very low. Consequently the concentration of neutral particles may be somewhat greater than one might otherwise anticipate on the basis of the low concentration of ions and electrons near the Moon. The lifetime of a neutral particle against ionization is of the order of 10^6 seconds, while the escape time of an ion, because of acceleration by the solar wind, varies from about 10 seconds for hydrogen up to 10^3 seconds for xenon; hence the degree of ionization should vary from about 10^{-5} for hydrogen to 10^{-3} for xenon. The limit on ion concentration near the Moon of less than 10 ions cm^{-3}, as determined by radio detection techniques, therefore is compatible with neutral particle concentrations near 10^6 cm^{-3} or pressures near 10^{-10} torr for hydrogen, decreasing to 10^4 cm^{-3} or pressures near 10^{-12} torr for xenon.

At the very least, the Moon must have some atmosphere caused by the neutralized solar wind. The exact composition of this source is not known, but it may be reasonable to assume normal solar abundances in the solar wind. The light constituents will escape predominantly because of their thermal energy, whereas the heavy constituents will escape predominantly because of ionization and acceleration by the solar wind, as this is much faster than thermal escape for heavy particles. On this basis, the lunar atmosphere may consist approximately of the following constituents, among others:

	Torr
H_2	10^{-13}
He	10^{-13}
Ne	10^{-11}
Ar	10^{-13}

In addition to the gases of solar origin, there may be constituents of internal origin, and these will be of great geochemical significance if they can be identified.

The average rate of release of water vapor and of carbon dioxide on Earth over geologic time has been about 10^{11} cm^{-2} sec^{-1} and 6×10^9 cm^{-2} sec^{-1}, respectively; the water has mainly condensed and formed oceans, and the carbon dioxide has mainly become bound up in carbonates and other geologic deposits. The average release rate of carbon dioxide on Mars has apparently been about 6×10^6 cm^{-2} sec^{-1}, assuming that none has been removed from the atmosphere by loss processes. The water release rate is unknown, as there may be substantial water deposits on Mars in the form of ice. The carbon dioxide release on Venus has apparently been of the same order of magnitude as on Earth. It is highly speculative to conjecture about possible gas release rates from the interior of the Moon on the basis of these figures; however, it is worth noting that a 10^6 seconds lifetime for molecules on the Moon (the approximate ionization lifetime)

would give rise to concentrations in excess of 10^5 cm^{-3} (or a pressure of about 3×10^{-12} torr) for a release rate of 10^6 cm^{-2} sec^{-1}, assuming a scale height in the range of a few tens of kilometers. Further, the release of gas from the lunar interior is probably intermittent, as suggested by the data compilation of Middlehurst (ref. 65); consequently the probability exists that gases of geochemical origin occasionally exist on the lunar surface at concentrations high enough to be measured. Middlehurst's compilation is of luminosity observed on the lunar surface that may be attributed to the luminescence of gas released from the lunar interior; such events occur several times a year, and certain locations, such as Aristarchus, are especially active.

The Pioneer VII spacecraft was occulted by the Moon, and this permitted an investigation of the electron concentration near the Moon (ref. 66). The refraction observed indicated that the electron concentrations were lower near the lunar surface than at altitudes well above it, in agreement with the concept put forth by Weil and Barasch (ref. 67) that ions are formed in neutral gases escaping from the Moon. However, this concept ignores the acceleration of ions by the electric field associated with the solar wind, which would sweep ions away very rapidly. If the Pioneer VII observation is accurate, it still requires explanation, perhaps in terms of a plasma sheath near the lunar surface.

VENUS

Great strides in the understanding of Venus were achieved in 1967. These resulted largely from the measurements made by Mariner V and by the Soviet probe Venera 4; the measurements complemented one another and brought about a situation in which the atmosphere of Venus is better known than that of Mars. Data acquired by remote sensing from the Earth's surface add still more to the picture. However, a few important discrepancies or uncertainties remain to be resolved.

Early reports of the Soviet measurements (ref. 68 and 69) indicated a temperature of 313° K and a pressure of 1 atmosphere at an altitude of 25 kilometers as determined by a radio altimeter, increasing to 553° K and 15 to 22 atmospheres at the surface. The composition was determined to be over 92 percent CO_2, less than 5 percent N_2, less than 1.6 percent (and probably less than 0.8 percent) H_2O, and over 0.4 percent O_2. More precise data were given later by V. V. Vakhmin, A. P. Vinogradov, A.D. Kuzmin, and V. S. Avduevsky at the Second Arizona Conference on Planetary Atmospheres, March 11 through 13, 1968. The most important data are a pressure of 550 millibars (0.72 atmosphere) and temperature 25°± 10° C at an indicated altitude of 26 kilometers, increasing to 18.5 atmospheres and 544° K at the point where the surface should have been encountered based upon the altitude determined at the beginning of the descent by

radio altimeter; this altimeter was a simple device that changed its response upon passing the preselected altitude of 26 kilometers. Coincidently, this was also the altitude at which the parachute opened and the data collection started. The water-vapor content was below 0.7 percent but above 0.1 percent, as indicated by two detectors, and above 0.05 percent as indicated by a third detector.

The temperature distribution was observed to be nearly dry adiabatic from the 0.72-atmosphere level down to the 18.5-atmosphere level, indicating that the atmosphere is mixed sufficiently to avoid control of the temperature distribution by radiation alone. Also, the atmosphere is very dry, as the moisture content could have been as high as 4.5 percent at the 26-kilometer level before producing saturation, thus the Soviet measurements indicate a relative humidity between 2 and 15 percent at that altitude. It therefore is reasonable that the dry adiabatic lapse rate might persist for some distance above the highest point of observation by Venera 4.

The Mariner V S-band occultation experiment (ref. 70) provided data on density and scale height that overlap the Venera 4 data down to the pressure level of about 7 atmospheres, and agree well. However, when radar data on the radius of Venus (ref. 71) are used to provide an altitude scale for the Mariner V data, a serious discrepancy with the Soviet height scale is noted. Whereas the Soviet data indicate a pressure of 0.72 atmosphere at an altitude of 26 kilometers, the Mariner V data indicate an altitude of 58 kilometers (the planetocentric distance of this pressure level was 6114 kilometers, which, when combined with a radar-derived radius of 6056 kilometers, gives an altitude of 58 kilometers). Stated otherwise, Mariner V data combined with radar data on the planetary radius indicate that the Soviet probe failed to reach the surface by 32 kilometers; corrections in the trajectory data will probably change this number some, but a discrepancy roughly of this magnitude appears likely to remain. Associated with this view is the possibility that the surface pressure on Venus is of the order of 100 atmospheres, within better than a factor of 2. The temperature may also be in excess of the 544° K measured by the Soviet probe at the pressure level of 18.5 atmospheres. It is speculative as to how far below the 18.5-atmosphere pressure level an adiabatic lapse rate may persist, so the surface temperature cannot be definitely related to the surface pressure.

The oxygen content observed by Venera 4 should be questioned. No atomic oxygen scattering of solar radiation was observed in the upper atmosphere of Venus by Mariner V (ref. 72), but this can be attributed to the relatively low upper atmospheric temperature and scale height. Similar measurements from Venera 4 also gave a very low value for the atomic oxygen concentration in the upper atmosphere. Further, spectrographic measurements generally indicate upper limits for molecular oxygen that are too low to be reconciled with the Venera measurements in the lower

atmosphere; Hunten (ref. 73) finds an oxygen abundance of 4×10^{-5}—100 times lower than the lower limit of 4×10^{-3} measured in Venera 4. For the present, the presence of oxygen in the Cytherean atmosphere should be regarded as questionable at best.

Venus appears to be cloud covered and is characterized by a temperature of about 230° K near the cloudtops (ref. 74). If the cloudtops mark the top of the convective region, the cloudtop height can be estimated from the lapse rate. If the water content were negligible, a dry adiabatic lapse rate would prevail, and this temperature would be reached at a planetocentric distance of 6122 kilometers or an altitude of 34 kilometers on the Soviet scale, where the pressure is about 200 millibars. Even if the water content were as large as the upper limit set by the Venera 4 observation, the cloudtop would be only slightly higher, as the water content is too small to very seriously perturb the dry adiabatic lapse rate by release of latent heat. Assuming convective-type clouds, the thickness of the clouds should be at least a kilometer if the water-vapor content were near the lower limit indicated by the Soviet measurements, and no more than about 4 kilometers if the water-vapor content were near the upper limit.

The Mariner V occultation measurement made by Kliore et al. (ref. 70) indicated a scale height of about 5.4 kilometers near the 1-millibar pressure level where the S-band telemetry link first showed a phase disturbance caused by the atmosphere. Kliore et al. assumed that the temperature could be no higher than the 230° K that applied near the cloudtops, and on this basis they calculated a molecular weight near 40 and concluded that carbon dioxide constitutes no more than 69 to 87 percent of the atmosphere. However, it is more reasonable to assume that the molecular weight is near 44, as indicated by the Soviet measurements lower down, and to use the measured scale height near 1 millibar to calculate a temperature; the resulting value is near 245° K. Thus one may conclude that above the cloudtops or haze layer, the temperature increases modestly to 245° K at a pressure level of 1 millibar; this pressure level would occur near a planetocentric distance of 6151 kilometers (or an altitude of 63 kilometers on the Soviet scale).

Above the 1-millibar pressure level, the only data readily interpretable in terms of temperature are those describing the distribution of Lyman-α intensity around Venus as measured during the Mariner V flyby (ref. 54). These data indicate a temperature of about 650° K well out in the exosphere. This observation is in excellent agreement with temperatures calculated by McElroy (ref. 75).

The temperature data for Venus are conveniently assembled in a very preliminary manner in figure 1. The distribution that was measured in Venera 4 is used between 6088- and 6114-kilometer planetocentric distance. Above this, the distribution is extrapolated to the cloudtop according to a

dry adiabatic lapse rate. The tropopause and the top of the cloud or haze layer occur at 6122 kilometers. Above the tropopause the temperature rises slowly and reaches a maximum of 245° K at 6150 kilometers, where the S-band occultation began indicating a scale height of 5.4 kilometers. Above 6150 kilometers, the temperature falls, agreeing with McElroy's calculations near the temperature minimum at 6175 kilometers and above. Approximate carbon-dioxide concentrations are also shown in figure 1.

Atomic hydrogen concentrations around Venus are less than those at comparable distances around Earth; Barth et al. (ref. 54) conclude that the hydrogen concentrations at 10 000 kilometers from the center of the planet on the dayside are about 200 cm^{-3}, whereas at this distance from Earth the concentrations vary in the range 10^3 to 10^4 cm^{-3}, depending on the phase of the solar cycle. The Soviet measurements made on the nightside indicate a lower concentration, 50 cm^{-3}. The day-night difference probably cannot explain the discrepancy between the two measurements, therefore one or both of the scales may have to be modified.

Debate continues on the composition of the clouds of Venus. Bottema, Plummer, Strong, and Zander (ref. 76) have presented spectroscopic evidence indicating that the clouds consist of ice crystals, a position supported by Sagan and Pollack (ref. 77). Rea and O'Leary (ref. 78) have reexamined the problem and conclude from the absorption structure that there is little probability that the scatterers are ice crystals. High resolution spectra by Connes, Connes, Benedict, and Kaplan (ref. 79) disclose the presence of HCl and HF; this opens the possibility that the clouds consist of chlorides or fluorides. However, the Soviet measurements reinforce the ice-crystal view, as the presence of water vapor and low temperature are very close to what is required to produce ice-crystal clouds.

The question of the rotation rate of Venus has been resolved beyond reasonable doubt. The radar measurements indicate a retrograde rotation with a period of 243 days and with the axis of rotation inclined only 2.2° from the ecliptic plane and 1.2° from the orbital plane (ref. 80). The rotation rate is locked to the Earth, with Venus on the average undergoing four revolutions as seen from the Earth between successive closest approaches of the two planets. The length of the solar day on Venus is 117 Earth days. This has been questioned in terms of visual observations, which indicate a rotation period near 4 days (ref. 81); however, these at best indicate cloud motions, while the radar obtains a firm return from the surface. If the visual observations actually indicate cloud motion around the planet in 4 days, this is puzzling and significant.

The high temperature at the surface of Venus can no longer be doubted, and this high temperature requires an explanation. Samuelson (ref. 82) has examined the greenhouse effect including scattering. He finds that dust scatterers can act powerfully to increase the intensity of the greenhouse effect, provided the total dust content is in the range 0.1 to 1.0 g/cm^2.

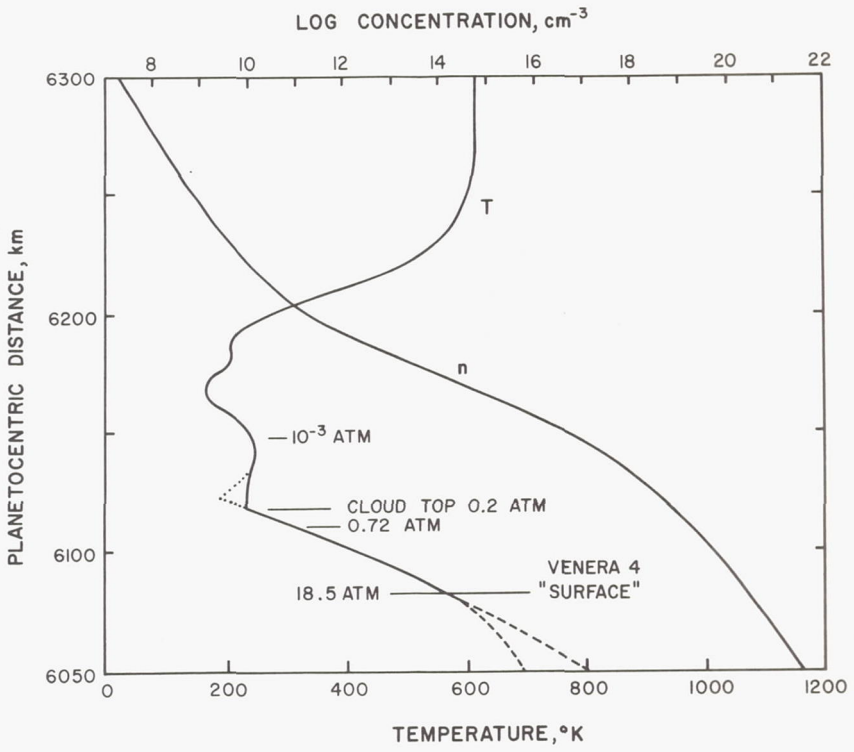


Figure 1.—A summary view of the atmosphere of Venus. Temperature and CO_2 concentrations are shown as functions of altitude. The region from 18.5 to 0.72 atm is based upon Venera 4 measurements, but on a planetocentric distance scale adjusted to fit Mariner V occultation data. From 0.72 to 10^{-3} atm, the distribution is based on Mariner V data but modified to agree with atmospheric structure concepts associated with cloud physics. At levels above the 10^{-3} atm pressure level, the distribution is in general agreement with the calculations by McElroy. The dotted portion of the temperature curve suggests a condition with cloudtop temperatures near 190° K, whereas the solid curve indicates 230° K. The dashed curves suggest possible temperature distributions below the lowest Soviet measurement, supposing that the Soviet probe did not actually reach the surface. Radar data indicate that the surface is located near the 6050-km value.

There are difficulties in explaining the presence of so much dust in the atmosphere and also in explaining the high albedo with likely dust materials. Further, the great pressure and the high carbon dioxide content of the atmosphere probably provide an adequate greenhouse effect without scatterers or other absorbers.

Another point of atmospheric interest regarding Venus arose from the dual-frequency occultation experiment (ref. 83). The main ionospheric layer was observed at a planetocentric distance of about 6220 kilometers on the nightside and 6210 kilometers on the dayside. Above the main ionospheric layer, an extensive upper ionosphere was observed, especially on the nightside. On the dayside, the upper ionosphere had electron concentrations of about 10^4 cm^{-3}, but this suddenly terminated between 6500- and 6600-kilometer planetocentric distance. The cause of this plasmapause at that point is probably the sudden termination of the planetary magnetic field there, so that any ions formed farther out are rapidly swept away by the solar wind, whereas those formed lower down have substantial lifetimes governed by recombination and diffusion processes. The planet does not have any recognizable intrinsic field, but probably has an induced field caused by an interaction between the ionosphere and the solar wind. It is to be anticipated that the ionospheric conductivity results in the buildup of magnetic-field strength above the ionosphere maximum; this is brought about by the rapid convection of the interplanetary field up to the planet and its slow passage through the ionosphere. The magnetic field should build up to the point where it is strong enough to turn aside the solar wind, causing a shock front to develop in front of the planet (ref. 84). The outer bound of the region of stagnation strength magnetic field may act as a magnetopause and give rise to the observed plasmapause. It should occur at an altitude that is sufficiently high so that the neutral concentrations are so low as not to interfere significantly with the unhindered flow of the solar wind around the induced magnetosphere. A neutral particle concentration of about 10^6 to 10^7 may be expected at this level. The implications of this with regard to the neutral atmosphere are threefold: (1) The flow of the solar wind is largely diverted around the atmosphere and so does not constitute an appreciable energy input into the upper atmosphere; (2) the solar wind is not a significant source of atmospheric particles; (3) the escape of atmospheric particles by the sweeping action of the solar wind is held to a modest level, the total escape by this mechanism over geologic time being of the order of a few tens of meters of gas at standard temperature and pressure. This entire concept of an induced magnetosphere must be regarded as highly tentative, as there is no general agreement as to the physics of the situation, and even the single relevant observation is not definitive.

The observed low scale height for the topside of the ionization maximum on Venus (refs. 70 and 83) is difficult to understand. The situation is similar to the daytime ionosphere on Mars, but even more aggravated. The observed daytime ionization maximum on Venus was about 5×10^5 cm^{-3}, and the scale height above the maximum was about 10 kilometers; whereas

the comparable figures for Mars were 9×10^4 cm^{-3} and 25 kilometers (ref. 85). The upward extension of the ionosphere consists of a region with concentrations about 10^4 cm^{-3} on the dayside, dropping suddenly near an altitude of 500 kilometers to an undetected value. A much more extended region of ionization exists on the nightside, but reliable concentration figures are not obtainable because the shape of the ionization cloud is not known; it surely cannot be spherically symmetric because of the solar-wind flow around the planet. Without knowledge of the shape of the cloud, the radio phase shift measurements cannot be satisfactorily interpreted in terms of electron concentration. If the results are interpreted in terms of a spherically symmetric cloud, the electron concentrations are in the vicinity of 300 cm^{-3}. Near the planet on the nightside, there is a sharp maximum with electron concentrations near 10^4 cm^{-3} at the maximum. The cause of this nighttime ionosphere is not known, but it could be caused by solar ultraviolet radiation scattered by the hydrogen corona around the planet.

MARS

The principal advances in the understanding of the atmosphere of Mars in 1967 were indirect, largely deductions that resulted from or were supported by the measurements made on Venus. A striking example of this was the observation of hydrogen in the outer atmosphere of Venus (ref. 54) that indicated an exospheric temperature of 650° K, a figure that agreed almost perfectly with calculations made by McElroy (ref. 75). This increases confidence in similar calculations made for Mars, also by McElroy (ref. 86), indicating an exospheric temperature in excess of 400° K. This same model indicates a mesopause or a temperature minimum of about 140° K at an altitude of 90 kilometers and a mean temperature of about 170° K between the surface and 100 kilometers.

The small scale height for the topside ionosphere observed in the Mariner IV occultation experiment (ref. 85) has its analog in the Mariner V observations of Venus (refs. 70 and 83); however, an even smaller scale height was observed on Venus, the values for the two planets being about 25 and 10 kilometers, respectively. In addition, a nighttime ionosphere was seen on Venus, and upward extensions to the ionosphere were seen on both the dayside and the nightside (ref. 83); this was made possible by the use of lower frequencies—50 and 200 MHz—than the 2000 MHz that was used in Mariner V. Mars may have a similar nightside ionosphere and similar extensions to both the dayside and nightside ionospheres, but these will not be observable until lower frequency occultation experiments are performed on Mars.

The physics of the Martian ionosphere remains a debated subject—particularly the question of whether it is analogous to one of the ionospheric

regions on Earth. McElroy (ref. 86) presents convincing arguments that it cannot be an F2 region, because the rate coefficient for the reaction

$$O^+ + CO_2 \rightarrow CO_2^+ + O$$

is much too large to permit F2 region chemistry to apply. The analogous situation does not occur on Earth because of the low concentration of CO_2 in the Earth's atmosphere and because the corresponding rate coefficients for O^+ reacting with molecular oxygen and nitrogen are about a thousand times smaller than for carbon dioxide. McElroy argues for an E-region interpretation, but the case for an F1 region interpretation is also reasonable; the issue may not be resolved until more data have been acquired.

Attention has been focused on the relatively short radiative relaxation times for Mars compared to those for Earth that apply in an atmosphere consisting mainly of carbon dioxide. Goody and Belton (ref. 87) have evaluated the relaxation times for perturbations of varying sizes containing varying amounts of carbon dioxide (i.e., for different pressures). They conclude that a diurnal temperature wave will propagate up from the surface of Mars because the radiative relaxation time is smaller than the diurnal period; the wave should attenuate above 1.5 kilometers. The corresponding wave on Earth is attenuated above 50 meters, so it is only a boundary layer phenomenon.

The relatively short radiative relaxation time mentioned above for Mars leads to an earlier breakdown than would otherwise occur in the equation normally used to compute eddy transport of heat. Eddy heat transport caused by turbulent motions is reduced to the extent that eddies relax radiatively and remain in thermal equilibrium with their surroundings rather than transport heat by advection. This occurs more readily in pure carbon dioxide than it does in air, because the heat capacity is less relative to the radiative capability when there is little or no oxygen and nitrogen present. The radiative relaxation times for eddies can be evaluated by using the computations of Goody and Belton (ref. 87). McElroy (ref. 86) has drawn attention to the effect of radiative relaxation of eddies on reducing eddy transport of heat and suggests that on this account mixing may occur to high altitudes on Mars without producing an associated heat transport. However, he apparently overestimates the importance of radiative relaxation of eddies by comparing the radiative relaxation times with the mixing time of the atmosphere as a whole, H^2/K, rather than with the lifetime of an eddy, L^2/K, where H is the scale height, L is the size of the largest turbulent eddy, and K is the eddy coefficient; because L probably does not exceed 200 meters and $H \approx 10$ km, the overestimate is by a factor of the order of 10^3 or more. It is also interesting to note that when radiative relaxation of eddies proceeds rapidly, buoyancy forces no longer act to restrict the development of turbulence; this effect has been referred to by Townsend (ref. 88) as radiative

destabilization of the atmosphere. Goody and Belton conclude that this destabilization phenomenon may occur in the lower atmosphere of Mars.

MERCURY

There has been speculation in recent years that Mercury might possess an atmosphere. Dollfus (ref. 89) has presented evidence for a surface pressure of about one millibar based on polarization measurements. Field (ref. 90) interpreted the relative warmth of the dark side of Mercury as indicative of an atmosphere, assuming the planet to have a synchronous rotation period of 88 days with the same side always in darkness. It is now known that the planet's rotational period is synchronized at two-thirds of the orbital period, making its solar day twice the orbital period; this can account for the relative warmth of the dark side.

Moroz (ref. 91) claimed to have observed carbon dioxide on Mercury by examining the 1.6-μ band. Spinrad, Field, and Hodge (ref. 92) examined the weak CO_2 band at 8689 Å and were able to set an upper limit of 57 m-atm for the CO_2 content on Mercury. They concluded that Moroz's data indicate an atmospheric pressure in excess of 3 millibars, but that this was inconsistent with the polarization observations by Dollfus.

Belton, Hunten, and McElroy (ref. 93) have examined the spectrum of Mercury near 1.049 μ and failed to find the head of the $\nu_1+2\nu_2+\nu_3$ band of CO_2. This places a limit of 5 m-atm on the CO_2 content and 0.35 millibar on the partial pressure. They also set a similar upper limit of 2 m-atm based on observation of the $2\nu_1+2\nu_2+\nu_3$ band by Binder and Cruikshank (ref. 94). Thus, these new observations indicate an upper limit of less than 1 millibar for the pressure of any atmosphere on Mercury, and they essentially supersede Moroz's earlier observations which indicated a larger pressure.

O'Leary and Rea (ref. 95) have examined the polarization properties of laboratory materials and conclude that the polarization observations by Dollfus do not require the presence of any atmosphere. In a more speculative vein they suggest that the dark color of the surface materials on Mercury and their photometric similarity to lunar-surface materials may be caused by direct bombardment by the solar wind; this would indicate a surface pressure below 10^{-5} millibar.

JUPITER

The most recent evaluation of the molecular hydrogen abundance on Jupiter derived from the quadrupole absorption is 240 km-atm in the optical path (ref. 96), which indicates an atmospheric content of 120 km-atm (ref. 97). The methane content is 150 m-atm (ref. 98). Greenspan and Owen (ref. 97) conclude that all the planet's atmospheric content is present in the form of methane, in which case the carbon-to-hydrogen ratio for

Jupiter's atmosphere is in agreement with the solar abundances. On the basis of that agreement, they suggest that all elements are present in Jupiter's atmosphere in their normal solar abundances excepting those that condense out; they conclude that the atmospheric constituents consist of fully reduced compounds. The calculated constituents of the atmosphere and their abundances are:

H_2	120 km-atm
He	23.5 km-atm
Ne	28.5 m-atm
CH_4	126 m-atm
NH_3	23 m-atm
H_2O	197.8 m-atm
H_2S	3.9 m-atm

Such an atmosphere appears to be in reasonably good agreement with the various optical measurements that have been made of the planet. Greenspan and Owen therefore conclude that Jupiter's atmosphere may constitute a good sample of solar material.

MICROMETEORITES

Data on micrometeorite impact rates on spacecraft have been brought into question by recognition of the fact that the microphone-type detectors most frequently used in spacecraft give rise to spurious output pulses when their temperatures are changed (ref. 99). Impact rates in general must be reexamined, along with the possibility of significant increases in count rate near Earth (ref. 100) and in the vicinity of the orbit of Mars (ref. 101).

Konstantinov, Bredov, and Mazets (ref. 102) performed an experiment in Cosmos 135 utilizing a target area that was well isolated acoustically from the remainder of the vehicle skin. The area was about 0.5 m^2. During the first 140 hours of operation in orbit between 260 and 650 kilometers, no impacts were observed, although 100 per day would have been expected on the basis of earlier data. After 140 hours, signals were detected, but they occurred preferentially at times of temperature change of the apparatus, so it was concluded that the equipment had degraded and that spurious responses were being obtained. A second detector, not acoustically isolated from the vehicle skin, gave signals from the beginning of the flight, but again clustering about times of changes in the thermal environment. The upper limit on impact rate from this experiment is 2.3×10^{-6} m^{-2} sec^{-1} above a threshold level of 6×10^{-3} dyne-sec impulse. This is to be compared with fluxes in the neighborhood of 10^{-2} m^{-2} sec^{-1} accepted earlier for 2×10^{-9} g particles (ref. 103), whose momenta would be 6×10^{-3} dyne-sec at 30 km/sec^{-1} velocity. A portion of this discrepancy probably results from the microphone detectors being more sensitive than was originally assumed, but most of the difference is probably caused by spurious responses associated with temperature changes.

Considerable uncertainty is associated with the conversion of micrometeorite flux rates into penetration rates, hence direct data on penetration of thin films are especially valuable, and such data have been acquired on several spacecraft. Data for thick films or sheets would be of even more value, but they cannot be acquired in any reasonable length of time because of the very low rates involved. On Explorer XVI over a 7½-month interval, there were 44 penetrations of 1-mil and 11 penetrations of 2-mil beryllium-copper foils (ref. 104). On Explorer XXIII, there were 43 penetrations of 1-mil and 54 penetrations of 2-mil foils. On Pegasus, capacitor-type penetration detectors were used with aluminum outer plates of thickness 1.6, 8, and 16 mil; the observed penetration rates for these various detectors (ref. 105) are given below:

Thickness of foil	*Penetration rate*
0.0038 cm (1.6 mil)	2.2×10^{-6} m^{-2}s^{-1}
0.02 cm (8 mil)	2.4×10^{-7}
0.04 cm (16 mil)	5.6×10^{-8}

These penetration rates are compatible with the Cosmos 135 results, if a penetration of a 1.6-mil (3.8×10^{-3} cm) aluminum foil is accomplished by a micrometeorite that would produce a 6×10^{-3} dyne-sec impulse on a detector microphone; because of the presence of ejecta that contribute to the pulse seen by the microphone, the actual incident momentum of the micrometeorite might be considerably less than this. A micrometeorite with a velocity of 30 km sec^{-1} would have to have a mass of 2×10^{-9} g to have an incident momentum of 6×10^{-3} dyne-sec and a smaller mass would suffice if the ejecta momentum is significant by comparison with incident momentum. Thus, the two results are compatible if the 1.6-mil foils are penetrated by meteorites with masses of about 10^{-9} g; this does not seem unreasonable.

The concept of a dust cloud, consisting of micrometeorites in orbit around the Earth, was based largely on a comparison of microphone data of impact rates near Earth with optical scattering (zodiacal light) by particles far from the Earth (refs. 100 and 101). These indicated particle concentrations near Earth about 10^4 greater than those far from Earth. However, the microphone data were apparently spurious, and the actual increase in the concentration of dust particles near Earth probably did not exceed a factor of 10 relative to the values in interplanetary space. This fits better with orbit theory, which could not satisfactorily explain the greater concentration of particles near Earth (refs. 106 and 107).

Measurements of meteorite impact on Mariner IV (ref. 101) indicated an increase in the impact rate over the range of heliocentric distance 1.36 to 1.43 AU, the values there being about four times those encountered over the distance range 1.00 to 1.25 AU. Owing to the relatively constant thermal environment on an interplanetary spacecraft compared to that encountered in Earth orbit, this result is probably valid even though the data obtained in Earth orbit with similar instrumentation are not.

CONCLUSIONS

By Robert F. Fellows

This report has summarized recent advances in knowledge of the nature and behavior of planetary atmospheres. Written 10 years after the start of a major effort in atmospheric research (the International Geophysical Year and the beginning of the space age), it is obvious that great strides have been made in understanding atmospheric phenomena. It is also obvious that many significant questions have not yet been adequately answered and, in fact, many questions have been raised that were not recognized or anticipated in 1957.

To treat these major questions in any sort of detail, or to discuss the many specific problems associated with the major questions, is beyond the scope and inappropriate to the purpose of this conclusion. An adequate discussion would probably occupy as many pages as required by the report.

It is more the intention, in the framework of a brief conclusion, to draw attention to important aspects of atmospheric research that have been emerging in recent years.

The most significant conclusion to be drawn from an appraisal of the status of aeronomy of the Earth's atmosphere is that future progress will be strongly dependent on the ability to obtain coordinated measurements of atmospheric phenomena. It has been shown that atmospheric phenomena are strongly coupled and dependent on the particular state of the atmosphere and on the intensity of incident solar electromagnetic and particulate radiations. The lack of solar-monitoring observations is a severe deficiency in this respect. Until detailed knowledge of the variations in solar-energy input to the atmosphere, especially in the ultraviolet, is available, all attempts to quantitatively explain and understand the processes occurring in the upper atmosphere can be nothing more than approximate explanations. It seems clear that continued progress will require experiments utilizing coordinated measurements of key phenomena and a detailed knowledge of incident solar energy at the time of the experiments.

An obvious gap in knowledge exists for the 90- to 150-kilometer region where both satellite and rocket measurements have been sparse and where some of the most important and least understood phenomena are occurring. Information concerning the short- and long-term variations of atmospheric temperature in this region is essential to arriving at an understanding of the role of turbulence and molecular conduction in thermal transport, and identification of the sources and sinks of energy in this region. A relation between temperature and geomagnetic activity has been found, but the nature of the coupling is not understood.

Many unanswered questions concerning the role and behavior of the constituents of the atmosphere exist. It now appears that horizontal flow

is a significant factor in determining the distribution of atomic oxygen, helium, and hydrogen in addition to the older concepts concentrating on vertical distribution parameters. Knowledge of the effect, distribution, and behavior of atomic oxygen and ozone in atmospheric processes below 200 kilometers is particularly weak. The role of carbon dioxide in determining the thermal characteristics of the atmosphere below about 150 kilometers is not well understood. A better understanding of the distribution and photodissociation properties is required. The quantitative role played by nitric oxide in D-region aeronomy is not known. The history of water vapor as it passes upward through the atmosphere culminating in eventual escape of hydrogen is not well understood, nor is the role that water-vapor processes play in phenomena of the D-region and higher. Likewise, important gaps and discrepancies exist in the understanding of the escape processes from the Earth of helium. The roles of metallic ions and particulate matter in the upper atmosphere are intriguing questions for whose significance we do not yet have an understanding.

It is now clear that the circulation processes of the thermosphere are significantly different from those of the troposphere and that many of the weaknesses in our understanding already mentioned must be remedied before circulation processes in the thermosphere will be understood on a global scale. What is the nature of the coupling of the neutral atmosphere and the ionosphere in this region? What is the relation between atmospheric temperatures at high latitudes and geomagnetic disturbances? Progress has been made in recognizing the features of turbulent mixing and horizontal flow in the thermosphere, and the phenomenon of tidal waves is being actively investigated, but a quantitative understanding does not exist. It is recognized that present theories may be incorrect to an unknown extent.

The increase in our understanding of the atmospheres of Mars and Venus represents a significant achievement. It has been possible to arrive at acceptable descriptions of the atmosphere of Mars and the upper atmosphere of Venus from rather limited experimental data obtained on a flyby mission to each planet supplemented by improved capability in ground-based astronomical observations. However, it was the knowledge of atmospheric processes on Earth that permitted the interpretation of the experimental data to be carried out in sufficient depth to arrive at models of these two atmospheres that are generally acceptable to aeronomists and planetary scientists. In the process many significant ideas concerning the similarities and differences among the planetary atmospheres have arisen as challenges to future studies.

While this conclusion has laid emphasis on an examination of some of the problems that still remain to be understood, it would be distorting the perspective of research if attention were not drawn to the fact that many of the important and significant questions discussed here were not recognized

10 years ago. Undoubtedly, new questions will become apparent in the coming years as research obtains answers to the questions of today and our knowledge progresses to the point where we can recognize what is not apparent at this time.

The next decade will see further advances resulting from use of coordinated experiments on rockets and satellites and the use of satellites capable of sustained operation in the 110- to 200-kilometer region. Atmospheric entry probes and orbiters to Mars and Venus will furnish information to develop further the models of the atmospheres as we now understand them, and to work toward an increased understanding of planetary atmospheres in general. Lastly, it is possible to anticipate flybys or orbiter investigations of the atmospheres of Mercury, Jupiter, and the outer planets, and to investigate what may be the most primeval atmosphere of all: the atmosphere of a comet. It does not require a prognosticator of great talent to predict that we shall find these atmospheres—known to be so different from those of the terrestrial planets—to be equally challenging and illuminating to science.

REFERENCES

1. Jacchia, L. G.: The Temperature Above the Thermopause. Smithsonian Astrophys. Obs. Special Rept. no. 150, 1964.
2. Keating, G. M.; and Prior, E. J.: Latitudinal and Seasonal Variations in Atmospheric Densities Obtained During Low Solar Activity by Means of the Inflatable Air Density Satellites. Seventh International Space Science Symposium (COSPAR) (Vienna, Austria), 1966.
3. Jacchia, L. G.; and Slowey, J.: The Shape and Location of the Diurnal Bulge in the Upper Atmosphere. Smithsonian Astrophys. Obs. Special Rept. no. 207, 1966.
4. Keating, G. M.; and Prior, E. J.: The Distribution of Helium and Atomic Oxygen in the Exosphere. Trans. AGU, vol. 48, no. 1, Mar. 1967, p. 188.
5. Keating, G. M.; and Prior, E. J.: The Winter Helium Bulge. Paper presented at 10th COSPAR meeting (London, England), 1967.
6. Lagos, C. P.; and Mahoney, J. R.: Numerical Studies of Seasonal and Latitudinal Variability in a Model Thermosphere. J. Atmos. Sci., vol. 24, no. 1, 1967, p. 88.
7. Jacchia, L. G.; Slowey, J. H.; and Veriani, F.: Geomagnetic Perturbations and Upper-Atmosphere Heating. J. Geophys. Res., vol. 72, no. 5, 1967, pp. 1423–1434.
8. Jacchia, L. G.; and Slowey, J.: Atmospheric Heating in the Auroral Zones: A Preliminary Analysis of the Atmospheric Drag of the Injun 3 Satellite. J. Geophys. Res., vol. 69, no. 5, 1964, pp. 905–910.
9. Carru, H.; Petit, M.; and Waldteufel, P.: On the Diurnal Variation of the Thermopause Temperature. Planet. Space Sci., vol. 15, 1967, pp. 944–945.
10. King-Hele, D. G.; and Quinn, E.: The Variation of Air Density at a Height of 220 km in the First Half of 1966. Planet. Space Sci., vol. 15, 1967, pp. 1067–1073.

11. KING-HELE, D. G.; AND HINGSTON, J.: Variations in Air Density at Heights Near 150 km From the Orbit of the Satellite 1966-101G. Planet. Space Sci., vol. 15, 1967, pp. 1883-1893.
12. REBER, C. A.; AND NICOLET, M.: Investigation of the Major Constituents of the April-May 1963 Heterosphere by the Explorer XVII Satellite. Planet. Space Sci., vol. 13, 1965, pp. 617-646.
13. TINSLEY, B. A.: Measurements of Twilight Helium 10,830 Å Emission. Planet. Space Sci., vol. 16, 1968, pp. 91-99.
14. HARTMANN, G.; MAUERSBERGER, K.; AND MÜLLER, D.: Evaluation of the Turbopause Level From Measurements of the Helium and Argon Content of the Lower Thermosphere Above Fort Churchill. Paper presented at 10th COSPAR Meeting (London, England), 1967.
15. VON ZAHN, U.: Mass Spectrometric Measurements of Atomic Oxygen in the Upper Atmosphere: A Critical Review. J. Geophys. Res., vol. 72, no. 23, 1967, pp. 5933-5937.
16. MCAFEE, J. G.: Lateral Flow in the Exosphere. Planet. Space Sci., vol. 15, 1967, pp. 599-609.
17. JOHNSON, F. S.: Significant Developments Concerning the Geocorona and Magnetosphere. Paper presented at IUGG General Assembly (Switzerland), Sept. 1967.
18. BATES, D. R.; AND PATTERSON, T. N. L.: Hydrogen Atoms and Ions in the Thermosphere and Exosphere. Planet. Space Sci., vol. 5, 1961, pp. 257-273.
19. KOHL, H.; AND KING, J. W.: Atmospheric Winds Between 100 and 700 km and Their Effects on the Ionosphere. J. Atmos. Terres. Phys., vol. 29, 1967, p. 1045.
20. THEON, J. S.; NORDBERG, W.; AND SMITH, W. S.: Temperature Measurements in Noctilucent Clouds. Science, vol. 57, 1967, p. 419.
21. JOHNSON, F. S., ED.: Satellite Environment Handbook. Stanford Univ. Press, 1961.
22. JOHNSON, F. S., ED.: Satellite Environment Handbook. Second edition, Stanford Univ. Press, 1965.
23. KOCKARTS, G.; AND NICOLET, M.: Le Problème Aéronomique de l'Hélium et de l'Hydrogène Neutres. Ann. Geophys., vol. 18, 1962, pp. 269-290.
24. KOCKARTS, G.; AND NICOLET, M.: L'Hélium et l'Hydrogène Atomique au Cours d'un Minimum d'Activité Solaire. Ann. Geophys., vol. 19, 1963, pp. 370-385.
25. HANSON, W. B.; AND PATTERSON, T. N. L.: Diurnal Variation of the Hydrogen Concentration in the Exosphere. Planet. Space Sci., vol. 11, 1963, pp. 1035-1052.
26. LIWSHITZ, M.; AND SINGER, S. F.: Thermal Escape of Neutral Hydrogen and Its Distribution in the Earth's Thermosphere. Planet. Space Sci., vol. 14, 1966, pp. 541-561.
27. LIWSHITZ, M.: The Effect of Thermal Escape on the Neutral Hydrogen Density Above 120 Kilometers. J. Geophys. Res., vol. 72, no. 1, 1967, pp. 285-293.
28. CHAMBERLAIN, J. W.; AND CAMPBELL, F. J.: Rate of Evaporation of a Non-Maxwellian Atmosphere. Astrophys. J., vol. 149, 1967, pp. 687-705.
29. REBER, C. A.: Thermosphere Conditions Deduced From Satellite Observations. J. Geophys. Res., vol. 72, no. 1, 1967, pp. 295-298.
30. REBER, C. A.: Helium Distribution and Dynamics in the Lower Thermosphere. Trans. AGU, vol. 49, 1968, p. 142.
31. BATES, D. R.; AND NICOLET, M.: The Photochemistry of Atmospheric Vapor. J. Geophys. Res., vol. 55, 1950, pp. 301-327.

333-240 O—69——20

32. HUNT, B. G.: Photochemistry of Ozone in a Moist Atmosphere. J. Geophys. Res., vol. 71, no. 5, 1966, pp. 1385–1398.
33. JACCHIA, L. G.: Density Variations in the Heterosphere. Ann. Geophys., vol. 22, 1966, pp. 75–85.
34. PURCELL, J. D.; AND TOUSEY, R.: The Profile of Solar Hydrogen-Lyman-α. J. Geophys. Res., vol. 65, no. 1, 1960, p. 370.
35. DONAHUE, T. M.: The Problem of Atomic Hydrogen. Ann. Geophys., vol. 22, 1966, pp. 175–188.
36. CLARK, M. A.; METZGER, P. H.; AND MENIGOZ, L. L.: Latitude and Directional Distribution of Lyman-α Radiation From the Hydrogen Geocorona. Trans. AGU, vol. 48, 1967, p. 150.
37. MANGE, P.: The Distribution of Lyman-α Radiation as Observed in the Sky From Satellites OGO 3, OGO 4 and OSO 4. Trans. AGU, vol. 49, 1968, p. 254.
38. FULLER, J. A.; CHAMBERS, W. H.; FEHLAU, P. E.; AND KUNZ, W. E.: Satellite Observations of Scattered Hydrogen Lyman-α Radiation at 17 R_E. Trans. AGU, vol. 49, 1968, p. 254.
39. MEIER, R. R.: Interpretation of Satellite Lyman-α Airglow Measurements. Trans. AGU, vol. 49, 1968, p. 254.
40. FISHKOVA, L. M.: On the Spatial Distribution and Variations of the Hα Emission in the Night Sky. Aurora and Airglow, vol. 10. Results of IGY, USSR Acad. Sci., 1963, pp. 35–39.
41. SHCHEGLOV, P. V.: The Concentration of Night Airglow Hα Emission Toward the Ecliptic and Radial Velocities of This Line. Sov. Astron., vol. 8, 1964, p. 289.
42. ARMSTRONG, E. B.: Observation of the Airglow Hα Emission. Planet. Space Sci., vol. 15, 1967, p. 407.
43. TINSLEY, B. A.: Initial Results of Geocoronal Balmer Alpha Observations. Planet. Space Sci., vol. 15, 1967, pp. 1757–1775.
44. TINSLEY, B. A.: Temporal Variations in Geocoronal Balmer Alpha. J. Geophys. Res., vol. 73, no. 13, 1968, pp. 4139–4149.
45. TAYLOR, H. A., JR.; BRACE, L. H.; BRINTON, H. C.; AND SMITH, C. R.: Direct Measurements of Helium and Hydrogen Ion Concentration and Total Ion Density to an Altitude of 940 Kilometers. J. Geophys. Res., vol. 68, no. 19, 1963, pp. 5339–5347.
46. HANSON, W. B.; PATTERSON, T. N. L.; AND DEGAONKAR, S. S.: Some Deductions From a Measurement of the Hydrogen Ion Distribution in the High Atmosphere. J. Geophys. Res., vol. 68, no. 22, 1963, pp. 6203–6205.
47. HOFFMAN, J. H.: A Mass Spectrometric Determination of the Composition of the Nighttime Topside Ionosphere. J. Geophys. Res., vol. 72, no. 7, 1967, pp. 1883–1888.
48. BRINTON, H. C.; PHARO, M. W., III; MAYR, H. G.; AND TAYLOR, H. A., JR.: Ion Concentrations in the Daytime F_2-Region Measured at a Time of Rising Solar Activity. Trans. AGU, vol. 49, 1968, p. 142.
49. BRACE, L. H.; REDDY, B. M.; AND MAYR, H. G.: Global Behavior of the Ionosphere at 1000-Kilometer Altitude. J. Geophys. Res., vol. 72, no. 1, 1967, pp. 265–283.
50. REBER, C. A.; COOLEY, J. E.; AND HARPOLD, D. N.: Preliminary Atmospheric Composition Data From the Explorer 32 Mass Spectrometers. Trans. AGU, vol. 48, 1967, p. 75.
51. KURT, V. G.: The Total Quantity of Neutral Hydrogen in the Earth's Upper Atmosphere. Cosmic Research, vol. 4, 1966, pp. 98–102.

52. SWISHER, R. L.; AND FRANK, L. A.: Charge-Exchange Lifetimes for Low-Energy Protons in the Outer Radiation Zone and Implications Concerning the Density of Atomic Hydrogen in the Terrestrial Exosphere. The Univ. of Iowa Rept. 68–3, 1968.
53. CHAMBERLAIN, J. W.: Planetary Coronae and Atmospheric Evaporation. Planet. Space Sci., vol. 11, 1963, pp. 901–960.
54. BARTH, C. A.; WALLACE, L.; AND PEARCE, J. B.: Mariner 5 Measurement of Lyman-Alpha Radiation Near Venus. J. Geophys. Res., vol. 73, no. 7, 1968, pp. 2541–2545.
55. HUNTEN, D. M.; AND WALLACE, L.: Rocket Measurements of the Sodium Dayglow. J. Geophys. Res., vol. 72, no. 1, 1967, pp. 69–79.
56. DONAHUE, T. M.; AND MEIER, R. R.: Distribution of Sodium in the Daytime Upper Atmosphere as Measured by a Rocket Experiment. J. Geophys. Res., vol. 72, no. 11, 1967, pp. 2803–2829.
57. HANSON, W. B.; AND DONALDSON, J. S.: Sodium Distribution in the Upper Atmosphere. J. Geophys. Res., vol. 72, no. 21, 1967, pp. 5513–5514.
58. WEILL, G.; FEHRENBOCK, M.; MORGULEFF, N.; AND GLAUME, J. CHRISTOPHE: The Forbidden Lines of OI and NI in the Night Airglow at the Magnetic Equator. Paper presented at IUGG General Assembly (Switzerland), Sept. 1967.
59. ELLIOTT, D. D.; LAVALLE, S. R.; AND WILLIAMS, R. L.: Latitude Distribution of the 3914-, 5577-, and 6300-A Nightglow. Trans. AGU, vol. 48, 1967, p. 150.
60. GULLEDGE, I. S.; PACKER, D. M.; AND HULBURT, E. O.: Observation of a New Ultraviolet Night Airglow Layer. Trans. AGU, vol. 47, 1966, p. 74.
61. WILSON, C. R.; AND NICHPARENKO, S.: Infrasonic Waves and Auroral Activity. Nature, vol. 214, 1967, pp. 1299–1302.
62. KNUDSEN, W. C.; AND SHARP, G. W.: Ion Temperatures Measured Around a Dawn-Dusk-Auroral-Zone Satellite Orbit. J. Geophys. Res., vol. 72, no. 3, 1967, pp. 1061–1072.
63. COLBURN, D. S.; CURRIE, R. G.; MIHALOV, J. D.; AND SONETT, C. P.: Diamagnetic Solar-Wind Cavity Discovered behind Moon. Science, vol. 158, no. 3804, 1967, pp. 1040–1042.
64. NESS, N. F.; BEHANNON, I. W.; SCEARCE, C. S.; AND CANTARANO, S. C.: Early Results From the Magnetic Field Experiment on Lunar Explorer 35. J. Geophys. Res., vol. 72, no. 23, 1967, pp. 5769–5778.
65. MIDDLEHURST, B. M.: An Analysis of Lunar Events. Rev. Geophys., vol. 5, no. 2, 1967, pp. 173–189.
66. POMALAZA-DIAZ, J. C.: Measurement of the Lunar Ionosphere by Occulation of the Pioneer VII Spacecraft. Stanford Electronics Laboratories Rept. SU–SEL–67–095, 1967.
67. WEIL, H.; AND BARASCH, M. L.: A Theoretical Lunar Ionosphere. Icarus, vol. 1, 1963, pp. 346–356.
68. NIKIFOROFF, C. C.: Venus 4: An Automatic Interplanetary Station. Trans. AGU, vol. 48, 1967, pp. 931–937.
69. DAVYDOV, V. D.: New View of Venus. Sci. Tech., no. 73, Jan. 1968, pp. 49–54.
70. KLIORE, A.; LEVY, G. S.; CAIN, D. L.; FJELDBO, G.; AND RASOOL, S. I.: Atmosphere and Ionosphere of Venus From the Mariner V S-Band Radio Occultation Measurement. Science, vol. 158, no. 3809, 1967, pp. 1683–1688.
71. ASH, M. E.; SHAPIRO, I. I.; AND SMITH, W. B.: Astronomical Constants and Planetary Ephemerides Deduced From Radar and Optical Observations. Astron. J., vol. 72, 1967, pp. 338–350.

72. BARTH, C. A.; PEARCE, J. B.; KELLY, K. K.; WALLACE, L.; AND FASTIE, W. G.: Ultraviolet Emissions Observed Near Venus From Mariner V. Science, vol. 158, no. 3809, 1967, pp. 1675–1678.
73. HUNTEN, D. M.: An Upper Limit for O_2 on Venus. J. Atmos. Sci., 1968, in press.
74. SINTON, W. M.; AND STRONG, J.: Radiometric Observations of Venus. Astron. J., vol. 131, 1960, pp. 470–490.
75. MCELROY, M. B.: The Upper Atmosphere of Mars. J. Geophys. Res., vol. 73, no. 5, 1968, pp. 1513–1521.
76. BOTTEMA, M.; PLUMMER, W.; STRONG, J.; AND ZANDER, R.: Composition of the Clouds of Venus. Astrophys. J., vol. 140, 1964, pp. 1640–1641.
77. SAGAN, C.; AND POLLACK, J. B.: Anisotropic Nonconservative Scattering and the Clouds of Venus. J. Geophys. Res., vol. 72, no. 2, 1967, pp. 469–477.
78. REA, D. G.; AND O'LEARY, B. T.: On the Composition of the Venus Clouds. J. Geophys. Res., vol. 73, no. 2, 1968, pp. 665–675.
79. CONNES, P.; CONNES, J.; BENEDICT, W. S.; AND KAPLAN, L. D.: Traces of HCl and HF in the Atmosphere of Venus. Astrophys. J., vol. 147, 1967, pp. 1230–1237.
80. SHAPIRO, I. I.: Resonance Rotation of Venus. Science, vol. 157, no. 3787, 1967, pp. 423–425.
81. SMITH, B. A.: Rotation of Venus: Continuing Contradictions. Science, vol. 158, no. 3797, 1967, pp. 114–116.
82. SAMUELSON, R. E.: Greenhouse Effect in Semi-Infinite Scattering Atmospheres: Application to Venus. Astrophys. J., vol. 147, 1967, pp. 782–798.
83. MARINER STANFORD GROUP: Venus: Ionosphere and Atmosphere as Measured by Dual-Frequency Radio Occultation of Mariner V. Science, vol. 158, no. 3809, 1967, pp. 1678–1683.
84. DESSLER, A. J.: Ionizing Plasma Flux in the Martian Upper Atomosphere. Atmospheres of Venus and Mars, J. C. Brandt and M. B. McElroy, eds., Gordon & Breach, London, 1967, p. 241.
85. KLIORE, A.; CAIN, D. L.; LEVY, G. S.; ESHLEMAN, V. R.; FJELDBO, G.; AND DRAKE, F. D.: Occultation Experiment: Results of the First Direct Measurement of Mars' Atmosphere and Ionosphere. Science, vol. 149, no. 3689, 1965, pp. 1243–1248.
86. MCELROY, M. B.: The Upper Atmosphere of Mars. Astrophys. J., vol. 150, no. 3, 1967, pp. 1125–1138.
87. GOODY, R. M.; AND BELTON, M. J. S.: Radiative Relaxation Times for Mars, a Discussion of Martian Atmospheric Dynamics. Planet. Space Sci., vol. 15, 1967, pp. 247–256.
88. TOWNSEND, A. A.: The Effects of Radiative Transfer on Turbulent Flow of a Stratified Fluid. J. Fluid Mech., vol. 4, 1958, pp. 361–375.
89. DOLLFUS, A.: Polarization Studies of Planets. Planets and Satellites, G. P. Kuiper and B. M. Middlehurst, eds., Univ. of Chicago Press, 1961, pp. 343–398.
90. FIELD, G.: The Atmosphere of Mercury. The Origin and Evolution of Atmospheres and Oceans, P. J. Brancazio and A. G. W. Cameron, eds., John Wiley & Sons, Inc., 1964, pp. 269–278.
91. MOROZ, V. I.: Infrared Spectrum of Mercury (λ=1.03–3.9μ). Soviet Astron. AJ, vol. 8, 1965, pp. 882–889.
92. SPINRAD, H.; FIELD, G. B.; AND HODGE, P. W.: Spectroscopic Observations of Mercury. Astrophys. J., vol. 141, 1965, pp. 1155–1160.

93. BELTON, M. J. S.; HUNTEN, D. M.; AND MCELROY, M. B.: A Search for an Atmosphere on Mercury. Astrophys. J., vol. 150, 1967, pp. 1111–1124.
94. BINDER, A. B.; and CRUIKSHANK, D. P.: Mercury: New Observations of the Infrared Bands of Carbon Dioxide. Science, vol. 155, 1967, p. 1135.
95. O'LEARY, B. T.; and REA, D. G.: On the Polarimetric Evidence for an Atmosphere on Mercury. Astrophys. J., vol. 148, 1967, pp. 249–253.
96. RANK, D. H.; FINK, U.; AND WIGGINS, T. A.: Measurements on Spectra of Gases of Planetary Interest II. H_2, CO_2, NH_3 and CH_4. Astrophys. J., vol. 143, 1966, pp. 890–899.
97. GREENSPAN, J. A.; AND OWEN, T.: Jupiter's Atmosphere: Its Structure and Composition. Science, vol. 156, 1967, pp. 1489–1494.
98. KUIPER, G. P.: Planetary Atmospheres and Their Origin. Atmospheres of the Earth and Planets, G. P. Kuiper, ed., Univ. of Chicago Press, 1952, pp. 306–405.
99. NILSSON, C.: Some Doubts About the Earth's Dust Cloud. Science, vol. 153, no. 3471, 1966, pp. 1242–1246.
100. WHIPPLE, F. L.: The Dust Cloud About the Earth. Nature, vol. 189, no. 4759, 1961, pp. 127–128.
101. ALEXANDER, W. M.; MCCRACKEN, C. W.; AND BOHN, J. L.: Zodiacal Dust: Measurements by Mariner IV. Science, vol. 149, no. 3689, 1965, pp. 1240–1241.
102. KONSTANTINOV, B. P.; BREDOV, M. M.; AND MAZETS, E. P.: Experimental Data as Evidence Against the Hypothesis on the Earth's Dust Cloud. Dokl A.N. SSR Geofizika, vol. 174, 1967, pp. 580–582 (NASA trans. ST–1D–1M–10696).
103. ALEXANDER, W. M.; MCCRACKEN, C. W.; SECRETAN, L.; AND BERG, O. E.: Review of Direct Measurements of Interplanetary Dust From Satellites and Probes. Space Research, vol. III, North-Holland Publ. Co., 1963, pp. 891–917.
104. D'AIUTOLO, C. T.; KINARD, W. H.; and NAUMANN, R. J.: Recent NASA Meteoroid Penetration Results From Satellites. Meteor Orbits and Dust, G. S. Hawkins, ed., NASA SP–135, 1967, pp. 239–252.
105. CLIFTON, S.; AND NAUMANN, R.: Pegasus Satellite Measurements of Meteoroid Penetration (Feb. 16–Dec. 31, 1965). NASA TMX–1316, Dec. 1966.
106. MCCRACKEN, C. W.: Conditions of Encounter Between Dust and Planets. Meteor Orbit and Dust, G. S. Hawkins, ed., NASA SP–135, 1967, pp. 213–224.
107. SHAPIRO, I. I.; LAUTMAN, D. A.; AND COLOMBO, G.: The Earth's Dust Belt: Fact or Fiction (Pts. 1–4). J. Geophys. Res., vol. 71, 1966, pp. 5695–5741.

Page Intentionally Left Blank

PLANETOLOGY

Edited by

L. S. Walter, B. M. French, and P. D. Lowman
Goddard Space Flight Center, NASA

Page Intentionally Left Blank

Planetology

INTRODUCTION

This report on the significant progress in the field of planetology during 1967 has been compiled by the staff of the NASA Goddard Space Flight Center. The various sections have been prepared by scientists with some degree of expertise in these fields. The sections in the order that they appear are: "The Planets," by R. Mueller; "The Earth," by C. R. Seeger, C. Schnetzler, L. S. Walter, and P. D. Lowman; "The Moon," by P. D. Lowman; "Impact Cratering and Metamorphism," by N. Short; "Iron and Stony-Iron Meteorites," by J. Goldstein; and "Stony Meteorites and Tektites," by L. S. Walter and C. Schnetzler. The "Summary" was prepared by S. E. Dwornik. The authors believe that a more complete and penetrating evaluation of the achievements could be made by a team of experts in the diverse fields of planetology. The editors believe this report will be of great use to investigators in the field, as well as to laymen interested in keeping up with the progress in planetology.

Planetology refers to the study of the condensed matter of the solar system. As such, the field encompasses not only the subjects in this report (i.e., the planets, their satellites, the asteroids, and meteorites) but also interplanetary condensed matter and the Sun itself. Because research on the interplanetary condensed matter has generally been restricted to particle counting, and because study of the Sun is held to be within the purview of the solar astronomers, they are reviewed in other disciplines in this report. In addition, the section on the Earth is relatively short in comparison with the large amount of literature that appears on the subject each year. As opposed to other areas of planetology, however, papers on the Earth are more often of restricted interest and applicability and, having confined the scope of this report to papers of broad interest, much work concerning the Earth has been passed over.

On the other hand, and despite the large number of references herein, much work of great value and of general interest concerning the Earth and other subjects has been omitted. The mass of data and ideas appearing in the literature regarding the planetology discipline area makes this unavoidable.

The report falls naturally into two general sections: the planets and the meteorites. Separate sections on the Earth and the Moon fall under the

category of "planetary studies," and the study of meteorites is divided into irons, stony irons, stones, and tektites. Tektites are included in this section because they are related to meteorites in that they contain meteoritic iron. A section on impact cratering and metamorphism spans the gap between planetary studies and meteorites.

THE PLANETS

The high point in the study of the planets during 1967 was, undoubtedly, the first sounding of the Venus atmosphere by the Soviet planetary probe Venera 4 and the simultaneous flyby of the U.S. Mariner V. However, other planetary research activities, both experimental and theoretical, have also moved at an accelerated pace.

Mars

Most activity concerning Mars was concentrated on sifting, correcting, and refining physical and chemical data on the atmosphere and surface of this planet. Barker (ref. 1) concluded from study of infrared spectra that the Martian atmosphere consists of nearly pure CO_2 at a surface pressure of approximately 5 millibars. Schorn and Gray (ref. 2), on the other hand, sought to explain certain apparent variations in the observed pressure by freezing out CO_2. Although it is not yet clear whether the icecaps on Mars consist of CO_2 or H_2O, Wells points out in reference 3 a relation between the caps and the frequency of occurrence of the white clouds of the atmosphere. He suggests that the maximum rate of mass transfer from each pole corresponds to the maximum frequency of these clouds.

The nature of the Martian surface is the subject of studies by de Vaucouleurs (ref. 4) and by Sinton (ref. 5). The work of de Vaucouleurs resulted in a detailed photometric map of Mars based on 3500 visual estimates in white, green, and red light made near favorable oppositions in 1941 and 1958. This map will aid in evaluating the atmospheric and surface temperatures. Sinton, on the other hand, offers an explanation for the color variation and absorption spectrum of the surface in terms of the mineral deposits. He concludes, as a result of observations with a birefringence interferometer, that the surface consists at least in part of hydrous minerals. Also, although iron oxides are regarded as only minor constituents of the surface, they probably account for the red colors observed.

The relation of the surface features of Mars to possible deep-seated subcrustal processes was studied by Miyamoto (ref. 6). His conclusion is that the surface structures are consistent with convection cells which adhere to third-order spherical harmonics.

Mercury

Observational data on Mercury continued to be sparse in 1967. Attempts to detect an atmosphere or to place an upper limit on its density were made by O'Leary and Rea (ref. 7) using a polarimetric method. Although no evidence for an atmosphere was obtained in these experiments, an upper limit of 1 millibar for the surface pressure was proposed.

Venus

The outstanding finding for the planet Venus resulted from the Soviet probe Venera 4 which confirmed the high surface temperatures previously inferred from Mariner II data and from a variety of terrestrial measurements. Other important data obtained from Venera 4 and the U.S. probe, Mariner V (ref. 8), include the total pressure, atmospheric composition, exospheric temperature and composition, and strength of the magnetic field. All these data have a critical bearing on the present physicochemical state and evolutionary history of the planet. They also provide interesting comparisons with our own planet since, in many ways, Venus is another "Earth experiment" run at a higher temperature.

Venera 4 entered the Venusian atmosphere on the dark side within 10° of the equator and approximately 80° from the terminator. (See refs. 9, 10, and 11.) At an altitude of 26 kilometers, as determined by a radar altimeter, temperature, total-pressure, and atmospheric-chemistry measurements were made. A second set of measurements was made at 23 kilometers and a third set very near the surface. The results of these measurements are presented in table I and in figures 1 and 2. These results are in general agreement with the data from Mariner V, except for the altitudes to which they refer. However, no explanation for these altitude inconsistencies has yet been proposed.

One of the most significant results from Mariner V is the conclusion that the intrinsic magnetic dipole of Venus is almost certainly less than 0.01 and probably less than 0.001 of that of Earth (ref. 12). It is likely that this result is directly related to the slow rotation of Venus, which corresponds to a sidereal period of 243 days. Another highly significant result is the determination of the relatively low temperature (600°–1100° K) inferred for the upper atmosphere (refs. 13 and 14), since it is this temperature which, in part, governs the rate of escape of hydrogen and helium. However, it is likely that these low upper atmospheric temperatures are more than compensated for by the high temperature of the lower atmosphere, a condition which favors a rapid upward transport of these constituents.

A terrestrial observation that supplements the planetary-probe data in

an interesting way is the detection and measurement of HCl and HF in the Venus atmosphere (ref. 15). It is estimated in reference 15 that, in the atmospheric region observed, the following mixing ratios yield:

$$\frac{HCl}{CO_2} \simeq 6 \times 10^{-7} \quad \text{and} \quad \frac{HF}{CO_2} \simeq 5 \times 10^{-9}$$

It is also reported in reference 15 that CH_4, CH_3, Cl, CH_3F, C_2H_2, and HCN, whose spectra all fall in the favorable region, were not detected and were thus estimated to be present in concentrations of less than 1 part per million.

The foregoing observations are of great interest in theoretical planetology because of their bearing on both meteorological- and chemical-model atmospheres and on the chemical and mineralogical nature of the surface. Indeed, Reese and Swan (ref. 11) have already obtained a fair fit of the pressure-altitude and temperature-altitude data (figs. 1 and 2) by assuming either constant- or adiabatic-lapse-rate models for the atmosphere. Of primary interest, however, are the chemical consequences which may be inferred from the high surface temperatures and the atmospheric-tempera-

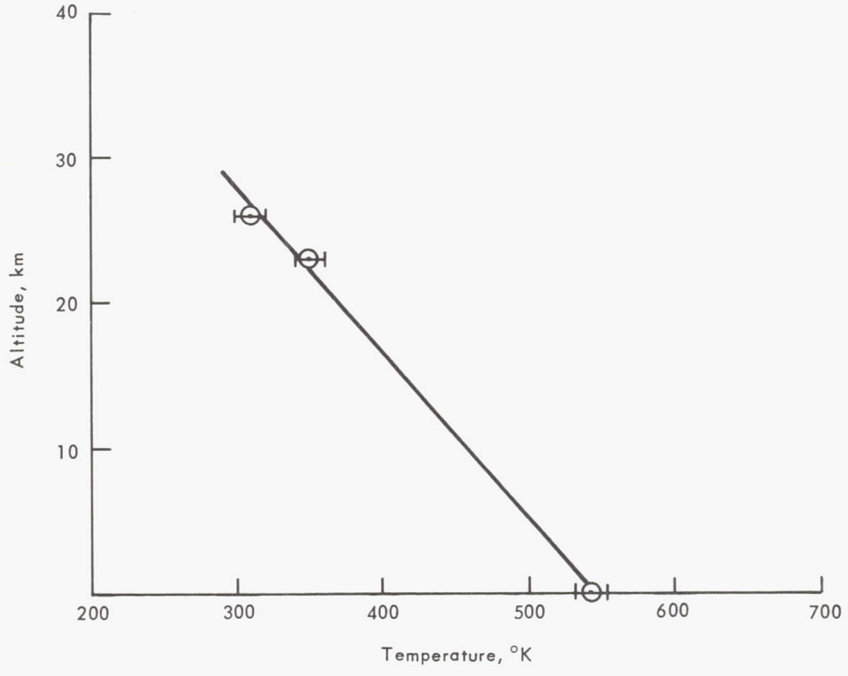


Figure 1.—**Temperature in Venus' atmosphere as a function of height above surface.**

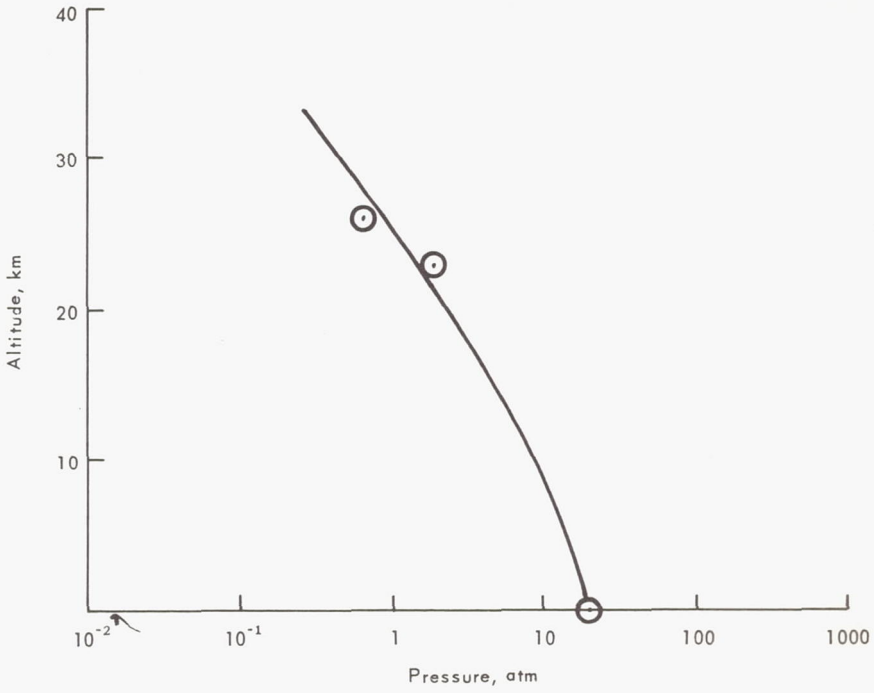


Figure 2.—**Pressure in Venus' atmosphere as a function of height above surface.**

ture profile. Because the kinetics of many inorganic chemical reactions are favored by the high surface temperatures, a chemical interaction between the lower atmosphere and the lithospheric minerals seems virtually assured (refs. 16 and 17). Furthermore, the rapid falling off of the temperature with altitude favors a trizonal chemical model (ref. 17). According to this interaction model, the surface CO_2 pressure is likely to fall within the range of 1 to 50 atmospheres, so that the observed measurements are in good agreement with those expected from an interaction with typical crustal material. Similarly, the low measured water and oxygen contents of the atmosphere are also in agreement, since these substances show a great affinity for silicate and oxide phases of the lithosphere. However, it seems likely that the measured oxygen content (table I) is still much too high because of errors inherent in the instrumentation.

Mueller has also shown (ref. 17) that the conditions of high temperatures, low water pressure, and the relatively oxidizing atmosphere implied by the high CO_2/CO ratio militate strongly against the occurrence of most hydrogen compounds so that the failure to detect them is also in harmony with pervasive chemical interaction with the lithosphere.

Table I.—*Measurements Made by Soviet Venera 4 on Its Approach to Venus*

[From refs. 9, 10, and 11]

Height, km	T, °K	Pressure, atm	Percent by volume of—			
			CO_2	H_2O	O_2	N_2
26	313±10	0.684	90 to 95	0.1 to 0.7	0.4 to 0.8	<7
23	353±10	1.98	90 to 95	0.1 to 0.7	0.4 to 0.8	<7
Near surface	543±7	20±2	90 to 95	0.1 to 0.7	0.4 to 0.8	<7

The idea of an approach to chemical equilibrium in the lower atmosphere of Venus was accepted by Lippincott, Eck, Dayhoff, and Sagan (ref. 18). They have, in fact, emphasized the equilibrium aspects of the problem to the virtual exclusion of the nonequilibrium processes. However, the rapid decrease of temperature with altitude shown by the Venera 4 and Mariner V data shows conclusively that the greatest part of the atmosphere cannot be in thermodynamic equilibrium. Indeed, it seems unlikely that even local equilibrium could prevail at more than a few kilometers above the surface. The molecular abundances in the greatest part of the atmosphere probably represent quenched equilibrium established in the part of the atmosphere immediately above or within the lithosphere.

In their discussion, Lippincott et al. (ref. 18) ignore the possibility of the interaction of certain gases such as CO_2 and H_2O with the lithosphere. In fact, they attempt to trace an evolutionary path for the atmosphere based solely on the escape of hydrogen and the reaction of oxygen with surface materials. If the interaction model holds, however, it is clear that the independent reaction of CO_2 and H_2O with the lithospheric minerals make all such evolutionary schemes meaningless.

The work of Goldreich and Peale (ref. 19) connects the contemporary state of Venus with its time of origin. These authors suggest that the sidereal period of Venus (~243 days) results from a resonance established with the period of Earth's revolution, since at approximately this resonance period (~243.16 days) the same axis of Venus would always point toward Earth at inferior conjunction. According to reference 19, this type of resonance results from a quadrupole component of the Venus gravity field and might be explained by an irregular geometric figure or by internal density variations. In the latter case, it is shown that trapping at the resonance can be understood if Venus possesses a fluid core similar to that of Earth. Maximum capture probability occurs if the core responds to changes in angular velocity of the mantle with a time lag of about 3×10^4 years. An interesting consequence of this is that if Venus is in such a

resonance, then mapping of its gravitational field will determine the direction of its primordial rotation and may also provide an estimate of its magnitude.

The Other Major Planets

Continued efforts were made to understand the atmospheres of the other major planets. Saslow and Wildey (ref. 20) emphasize the interaction of ultraviolet radiation with the highly reducing atmosphere of Jupiter and conclude that photochemical processes should result in the production of C_2H_4, C_2H_6, C_3H_8, and higher polymers. Trafton (ref. 21) discusses model atmospheres for the major planets and found that, in the case of Jupiter, He should dominate H_2, although a postulated small heat flux from the planet's interior would be consistent with a value of $(He/H_2) < 2$.

Further attempts were made to understand the complex radio-wave emissions from Jupiter. From analysis of the Io-related emission, Dulk (ref. 22) concludes that apparent change in Jupiter's rotation rate, as determined by these emissions, results from a beam in the form of a conical sheet which intersects the plane of the ecliptic.

Origin of the Planets

The general problem of the origin and development of the planets was the subject of a number of theoretical papers during 1967. Marcus (ref. 23) applied statistical methods to the accretion process and found planetary nuclei of from 0.42 to 0.60 of the mass of the whole planet. However, the same problem was approached quite differently by Harris and Tozer (ref. 24), who suggest that particle-size fractionation and magnetic forces between metallic grains played a role in the enrichment of iron in the region of the inner planets.

The chemical aspects of the problem were taken up again by Shimazu (ref. 25). However, his deduced scheme of mineral formation $Fe_2SiO_4 \rightarrow Fe \rightarrow Fe_2SiO_4$, with progressive loss of hydrogen, is probably of very limited applicability because it fails to take account of such important complicating factors as the nonstoichiometry of the phases involved.

An observation of some interest relative to the dynamics of the formation of the solar system was made by Hartmann and Larson (ref. 26). They found that if the asteroids are plotted on a logarithmic angular momentum-mass diagram, they fall near a straight-line curve whose extension also represents the large planets fairly well. According to these authors the observation agrees with the law of constant period proposed by Alfvén (ref. 27) and is explicable either by magnetohydrodynamic effects or by an approach to rotational instability at the time of origin.

Discussion

In confirming that the temperatures on Venus are high, the planetary probes have brought us face to face with the concept that Venus is an active planet since, upon it, chemical and petrogenic processes have the immediacy of laboratory experiments. The recorded temperatures of 500° to 600° K are encountered in large regions of the solid Earth during regional metamorphism, but then only at great depths within the crust where pressures are also high. However, on Venus, the analogous conditions should occur over wide regions of the surface where the pressure is comparatively low (by geologic standards) and the atmospheric chemistry is relatively constant.

The early evolution and continued development of the atmospheres of the terrestrial planets may be considered in terms of certain critical reactions between their gases and the lithosphere. Three of the most important reactions are the following:

$$\text{Oxidized rock} \rightleftarrows \text{Reduced rock} + O_2 \text{ (gas)} \quad (1)$$

$$\text{Carbonated rock} \rightleftarrows \text{Decarbonated rock} + CO_2 \text{ (gas)} \quad (2)$$

$$\text{Hydrated rock} \rightleftarrows \text{Dehydrated rock} + H_2O \text{ (gas)} \quad (3)$$

It is obvious that, in the case of the relatively cold planets, Mars and Earth, all three of these reactions are virtually suspended on the surfaces for kinetic reasons and that the quantities of gases in the atmosphere are governed instead by secondary reactions of the following types:

$$\text{Organisms} \rightleftarrows O_2 \text{ (gas)} \quad (4)$$

$$\text{Organisms} \rightleftarrows CO_2 \text{ (gas)} \quad (5)$$

$$CO_2 \text{ (ice)} \rightleftarrows CO_2 \text{ (gas)} \quad (6)$$

$$H_2O \text{ (liquid)} \rightleftarrows H_2O \text{ (gas)} \quad (7)$$

Even these reactions seldom approach equilibrium because of various dynamic and other perturbations. However, as is well known, reactions (4) and (5) play a dominant role in the O_2 and CO_2 economy of Earth and readily account for the great excess of O_2 in the atmosphere over that allowed by reaction (1). Similarly, reactions (6) and (7) probably govern the appearance and disappearance of icecaps on Mars and Earth, as previously discussed.

If Mercury is excluded, because of its tenuous atmosphere, only Venus appears hot enough for reactions (1), (2), and (3) to approach equilibrium. The result is that carbon on Venus is probably largely volatilized into the atmosphere as CO_2, whereas, on Earth, carbon abounds in the lithosphere and biosphere as carbonates and reduced carbon compounds. In fact, calculations show that if all known carbon compounds on Earth

were volatilized into the atmosphere as CO_2, the pressure of this gas would be close to that observed on Venus. On the other hand, the small quantity of water apparently present on Venus tells us either that this compound was in short supply from the start or that it was rapidly lost as would be commensurate with the high temperatures of the lower atmosphere. It has already been mentioned that the affinity of H_2O and O_2 for the lithospheric minerals is also great enough to account for the low partial pressures of these gases.

Finally, it should be emphasized that the interaction of planetary atmospheres and lithospheres is a two-way process. The gases are not simply lost from rock, by degassing, which corresponds to a slow secular leakage from the interiors according to reactions (1), (2), and (3). Indeed, it may have happened that great quantities of certain constituents were absorbed from the primordial atmospheres by these reactions, as O_2 and H_2O apparently are today on Venus. Hopefully, future planetary probes will answer these and other questions relative to the origin and development of the solar system.

THE EARTH

As usual, the study of the Earth led other subjects in the field of planetology in terms of the number of papers during 1967. Some of the more exceptional contributions are discussed here.

Determination of Age of the Earth

The uses and limitations of K/Ar and Rb/Sr mineral ages were the subject of several investigations. Hanson and Gast (ref. 28) made an extensive study of the effects of thermal metamorphism on both K/Ar and Rb/Sr mineral ages in the vicinity of two well-defined igneous contacts. They conclude that the temperatures required to effect essentially complete radiogenic daughter loss from biotite (a favorite mineral for K/Ar dating) in a simple thermal event are in excess of 300° C, and that the relative stability of mineral ages in a contact metamorphic zone is hornblende K/Ar> muscovite Rb/Sr>muscovite K/Ar>biotite Rb/Sr>biotite K/Ar. This latter conclusion is shown in figure 3. Livingston et al. (ref. 29) have shown that plagioclase feldspars from plutonic and pegmatitic environments can contain excess Ar^{40} with respect to that contained by cogenetic micas. This excess component is believed to have been occluded within these minerals at the time of their crystallization from the liquid magma, with the amount of excess Ar^{40} probably reflecting the partial pressure of Ar^{40} in the lithospheric gases. Livingston et al. (ref. 29) suggest that the use of several phases from the same rock body and their interpretation by graphical isochron diagrams are more informative than the simple calculation and comparison of K/Ar ages from the phases.

333-240 O—69——21

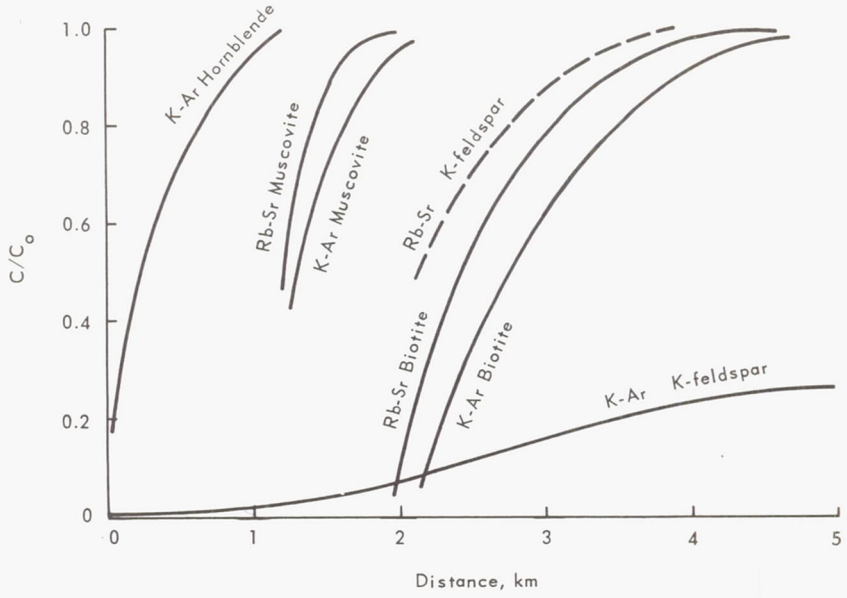


Figure 3.—**Generalized curves of concentration for Rb/Sr and K/Ar ages of biotite, muscovite, and potassium feldspar and the K/Ar ages of hornblende as a function of map distance from contact, Snowbank Lake, Minn. C/C_0 is concentration of the species under consideration at any time over the original concentration. All curves are drawn by visual best fit.**

Peterman et al. (ref. 30) have determined Rb, Sr, and Sr^{87}/Sr^{86} values for samples of eugeosynclinal sedimentary rocks, mostly graywackes. Their data are compatible with the theory that anatexis of eugeosynclinal sedimentary rocks in orogenic belts produces granitic magmas, provided that such melting occurs within several hundred million years after sedimentation. The low initial Sr^{87}/Sr^{86} ratios of these eugeosynclinal sedimentary rocks are probably related to the significant amounts of volcanogenic detritus present in them which probably was originally derived from the mantle.

A study by Ulrych (ref. 31) of the development of lead isotopic ratios in oceanic basalts yields an age for the Earth that is independent of the knowledge of the ages of the samples studied. The age is calculated to be 4530 ± 40 million years, which is in excellent agreement with several recent ages also obtained by studies of lead isotopes. Ulrych presents arguments as to why the age of 4750 million years obtained earlier by Tilton and Steiger (ref. 32) is too great. Ulrych also states that although the source

of the basalts studied is not generally homogeneous, the differentiation of this source from a closed system has occurred fairly recently, geologically. The oldest age obtained for any sample was 1230±350 million years for mid-Atlantic tholeiites.

By using radiometric ages to study possible continental drift, Hurley et al. (ref. 33) found that distribution of age values obtained by K/Ar and whole-rock Rb/Sr determinations was almost the same for West African basement rocks and for similar basement rocks at opposite locations in South America. When Africa and South America are "fitted together," the sharply defined boundary between the Eburnean (2000 million years) and the Pan African age (500 million years) provinces in West Africa strikes directly toward the corresponding age boundary in northeast Brazil. There is a suggestion of another age boundary in Cameroun-Gabon matching with the corresponding part of the east coast of Brazil, but the data are as yet insufficient. The authors state that these data support the hypothesis of continental drift and indicate the close proximity of these continents as recently as 500 million years ago.

Hakli and Wright (ref. 34) have studied the distribution of Ni between olivine, clinopyroxene, and glass from the Makaopuhi lava lake in Hawaii where the temperature of the crystallizing samples is measurable (1050° to 1160° C). The data strongly suggest that the distribution of Ni obeys the thermodynamic partition law and that the distribution coefficients permit the estimation of the crystallization temperature within an accuracy of 10° to 20° C. However, the authors point out that the application of these data to plutonic rocks and other volcanic rocks should be done with caution, because the effects of pressure and changing composition of the phases on the distribution coefficients are not known quantitatively.

In a very interesting study of an application of geochemical data, Hahn-Weinheimer and Ackermann (ref. 35) have used the analyses of Ti, Zr, P, Sr, Ba, Rb, K, and Na in 142 samples from Malsburg Granite and country rock to attempt to evaluate the intrusion mechanism and direction of differentiation. They have shown that this body crystallized from the margin to the core, and that there was a continuous process of crystallization differentiation.

In a study of the composition of ancient graywackes from Wyoming, Condie (ref. 36) suggests that the Precambrian continental crust did not change appreciably in composition from that of quartz diorite or granodiorite during the last 3.0 to 3.5 billion years. He suggests that pre-Cretaceous graywackes may represent a nearly unmodified sample of continental crust over the last 3.0 to 3.5 billion years and that the original chemical composition of the graywackes appears not to have been greatly affected by diagenesis and metamorphism.

Orbital Photography of the Earth

Although the Gemini Program was finished in 1966, interpretation of the nearly 1100 terrain photographs taken by the astronauts was just beginning in 1967. Preliminary study immediately indicates the most promising areas of geological application, as summarized in a review by Lowman (ref. 37). After discussing the unique advantages and disadvantages of orbital photographs, he concludes that they would be most useful in studies of continental drift and structure of rift valleys, and investigations of transcurrent faulting and other regional geologic problems. In another paper based on the Gemini photography, Lowman and Tiedemann (ref. 38) report on the use of orbital photographs in field mapping in northern Mexico. They found that, despite the small scale and relatively low resolution, such photographs could be used directly in the field with or without supplemental maps and photographs. They point out, however, that the inherent advantage of orbital photography, namely the great areal coverage per picture, could not be fully utilized unless very fast field transportation (such as helicopters) were available.

Because of its geological importance, the Great Rift Valley of Africa, part of which is occupied by the Red Sea, was a high-priority target for terrain photography during the Gemini flights. Abdel-Gawad (ref. 39) used several of the Gemini IV pictures of the northern Red Sea and adjacent parts of Egypt to construct a tectonic map of southeastern Egypt (fig. 4). He arrived at several conclusions about the regional geology, a major one being that many of the long depressions of the western desert are tectonically controlled. The parallel sand-dune belts may also be controlled by the regional structure. Using the Gemini photographs, Abdel-Gawad found granitic intrusives easy to delineate, and he also found it possible to trace gradations from metasedimentary granites into igneous granites. He concludes that the geologic value of the Gemini photographs had been clearly demonstrated.

Because of its great complexity and breadth, the problem of the origin of continents and ocean basins will probably not be solved (if it is solved) by any specific investigation directed to that end. The answers will come instead from many separate studies, some of which will probably appear at first to have no relation to the problem or even to geology. A number of papers published in 1967 illustrate this.

Determination of Age and Origin of Continents

Although the chain of reasoning about the origin of continents: (1) the continents are essentially granitic; (2) batholiths are essentially granitic; (3) therefore, the origin of batholiths is the origin of continents) is oversimplified and possibly fallacious, there is no doubt that batholith formation has major implications for continental growth. A major paper by Bate-

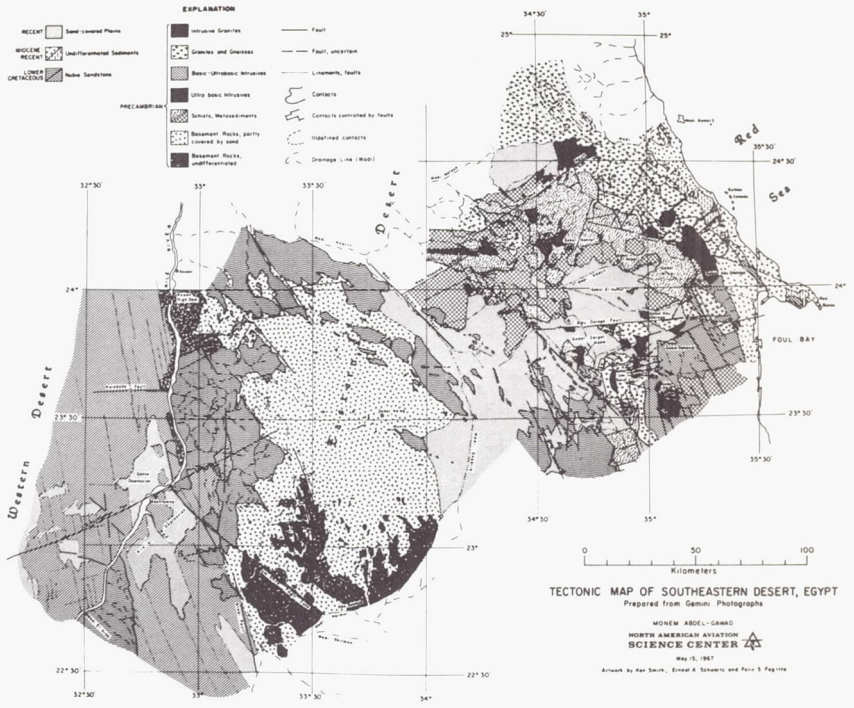


Figure 4.—**Tectonic map of southeastern desert in Egypt. Prepared from Gemini IV photographs.**

man and Eaton (ref. 40) on the Sierra Nevada batholith provides a clear picture of how continental accretion may take place. They present evidence indicating that the batholith and the associated geosynclinal sediments and volcanics are a net addition to North America at the expense of the Pacific basin. They propose that the batholith itself was formed by anatexis and related processes of the geosynclinal rocks, rather than coming from the mantle.

In a comprehensive review of the batholith problem, Hamilton and Meyers (ref. 41) show that batholiths may arise not only in miogeosynclinal environments, but completely outside geosynclines. They explain the nevertheless common association of eugeosynclines and batholiths as reflecting a related origin of the geosynclinal volcanics and the batholiths: "Batholiths form wherever temperatures are high enough at depth to melt the needed magmas, and eugeosynclines are only one setting in which these conditions are met."

In his presidential address to the Geological Society of Australia, S. R. Taylor (ref. 42) attacked the problem of origin and growth of continents directly. Reviewing a wide range of geophysical, geochemical, and geologi-

cal evidence, Taylor concludes that continent formation is essentially a process of multistage fractionation of the mantle. Specifically, growth is by addition of andesites in orogenic zones, followed by sedimentation, metamorphism, and eventual consolidation of the orogenic zone. The process stops when the underlying mantle has been depleted in the radioactive elements which are the chief heat sources. Taylor's mechanism operates over geologic time; however, it is nonuniformitarian to the extent that it requires an initial geochemical fractionation of the upper 1000 kilometers of the mantle.

Because of its size and geologic importance, the Pacific Ocean basin must have a central role in any comprehensive theory of continent or ocean-basin formation, as is brought out forcibly in several papers presented at the 11th Pacific Science Congress in 1966 (ref. 43).

From a general point of view, perhaps the major relation emphasized by the various papers presented to the Congress was the remarkable geologic unity of the Pacific basin, especially in the later geologic periods. The "ring of fire," applied to the chains of andesitic volcanoes surrounding the Pacific, is of course well known; what is not so well known, however, is the parallel ring of blue-schist facies metamorphic rocks. This facies, recognized only a few years ago, represents metamorphism at high pressures and relatively low temperatures and is characterized by such minerals as glaucophane, lawsonite, and aragonite. Blue-schist facies metamorphic rocks are found around the Pacific basin at widely separated localities including California, Japan, New Caledonia, and New Zealand. The circum-Pacific region is also characterized by major wrench faults, such as the San Andreas (California) and Alpine faults (New Zealand).

The papers presented at the Congress have a number of major implications for the origin of continents and ocean basins. Several papers specifically or implicitly contradicted the theory that continents grow by accretion of eugeosynclines and that the circum-Pacific orogenic belt (much of which arose from former eugeosynclines) represents the newest addition to the various continents. In a major study of the Canadian Cordillera, Roddick, Wheeler, Gabrielse, and Souther (ref. 44) found that continental (sialic) crust has existed near the present continental margin since Early Paleozoic or possibly Precambrian time, and concluded that there has been no appreciable westward accretion since the Paleozoic era. The geology of Taiwan, as shown by Ho (ref. 45), although dominated during the Tertiary by eugeosynclinal deposition and subsequent orogeny, does not indicate ensimatic continental growth, since the eastern part of the island (the oceanward side) is underlain by pre-Tertiary metamorphics. Similarly, New Zealand is underlain by relatively old continental rocks (ref. 46) with radiometric ages of 350 to 370 million years, and possibly much older ones, implied by the discovery of zircons with lead ages of 1270 and 1360 million years.

On the other hand, several authors, including Vassilkovsky (ref. 47) and Burgl (ref. 48), considered at least part of the circum-Pacific orogenic belt to be accretions to the continent.

Continental drift was a relatively minor topic at the Congress, in sharp contrast to meetings focused on the Atlantic Ocean. Hamilton (ref. 49) supports the existence of continental drift in eastern Asia and Alaska, but Fleming (ref. 50) found that the Mesozoic biogeography of the southwest Pacific could be interpreted either for or against drift.

The geologic history of the Pacific basin is of importance in planetology, not only as the largest single tectonic feature of the Earth but in relation to the origin of the Moon, since one version of Darwin's recently revived theory that the Moon was formed from the Earth holds the Pacific basin to be the birth scar. Although there was no mention of this theory in any of the papers presented at the Circum-Pacific Orogenesis Symposium, it is possible to draw a few inferences about the Darwin theory. In particular, it is almost certain that the supposed formation of the Moon from what is now the Pacific basin could not have happened later than the beginning of the Paleozoic era. This follows from a variety of evidence, the most important fact being the continuity and unity of circum-Pacific geologic history since the late Precambrian era. In addition, there appears to be nothing especially strange about the Pacific basin from a geologic viewpoint; its main peculiarity is the blue-schist zone surrounding it, and this zone is far too recent to have any direct relation to the supposed formation of the Moon. Perhaps the strongest evidence against the theory is subjective: the total omission of the theory from all the published papers. Although this omission could be interpreted as reflecting the conservatism of the authors, it is nevertheless striking that there is no major enigma about the Pacific basin which would appear to require a planetary catastrophe for its explanation.

The extremely interesting work of Lamar and Merifield clarified the origin of the Earth-Moon system (ref. 51). Using various dynamic models they calculate that the distance from Earth to Moon should have varied during geologic time as shown in figure 5. When combined with information on the length of the day during geologic time obtained by counting the growth rings of Paleozoic corals (fig. 6), they conclude that the age of the Earth-Moon system is 0.5 to 2 billion years.

They point out that origin by fission or close capture at such a late date should have left obvious indications in the geologic record, and evidence of this seems to be lacking. However, a noncatastrophic origin (Baldwin's capture-at-a-distance theory or MacDonald's aggregation of many smaller moons) would cause an abrupt increase in oceanic tidal action.

The greatly increased tidal ranges and tidal currents, together with the introduction of a lunar-light cycle, would strongly affect shallow-water marine invertebrates, which are highly sensitive to changes in their environment. Lamar and Merifield (ref. 51) therefore consider that a causal rela-

tionship is possible between the formation of the Earth-Moon system and the appearance of hard-shelled marine organisms in the Lower Cambrian era (500 to 700 million years ago). Lamar and Merifield point out that protective exoskeletons would certainly be an adaptive characteristic for shallow-water, bottom-dwelling organisms suddenly confronted with powerful tides. If the origin of the Earth-Moon system did provide the impetus for the development of hard-shelled organisms, then this origin must have occurred in Late Precambrian time (1.0 to 0.5 billion years ago); there is additional independent geological work to support this line of reasoning.

Paddack (ref. 52) notes that the analysis of 5 years of observation of the 1960 Iota-2 satellite shows that the motion of the node of the satellite's orbit is not measurably correlated with variations in the length of the day. These results indicate that there exists an irregular transfer of angular momentum between the solid and fluid parts of the Earth (for the periods of time involved), as has been suggested by Munk and MacDonald in 1960.

Finally, it can be noted that a substantial improvement in the precision of measurement of the rotation period of the Earth is now possible. Gold (ref. 53) discusses the method of radio interferometry on 10- to 60-centimeter wavelengths, by using independent high-precision clocks. MacDonald (ref. 54), in a companion paper, discusses the geophysical implications of such possible improved measurements. He points out that it would be possible to determine the changes in the rate at which the Earth's rotation is slowing and to make an improved calculation of the Earth's Love number,

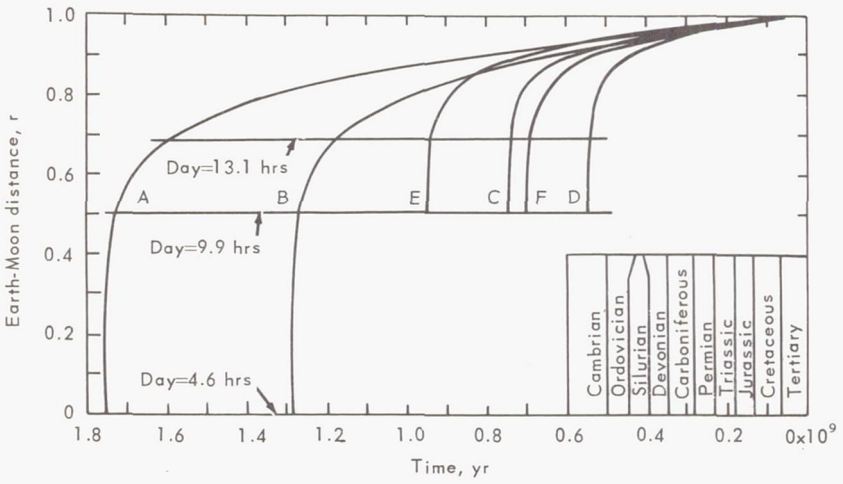


Figure 5.—Variation of Earth-Moon distance during geologic time. (Various models (A to F) depend on different assumptions as to values of torque and dissipation rates due to body tides and tidal currents.)

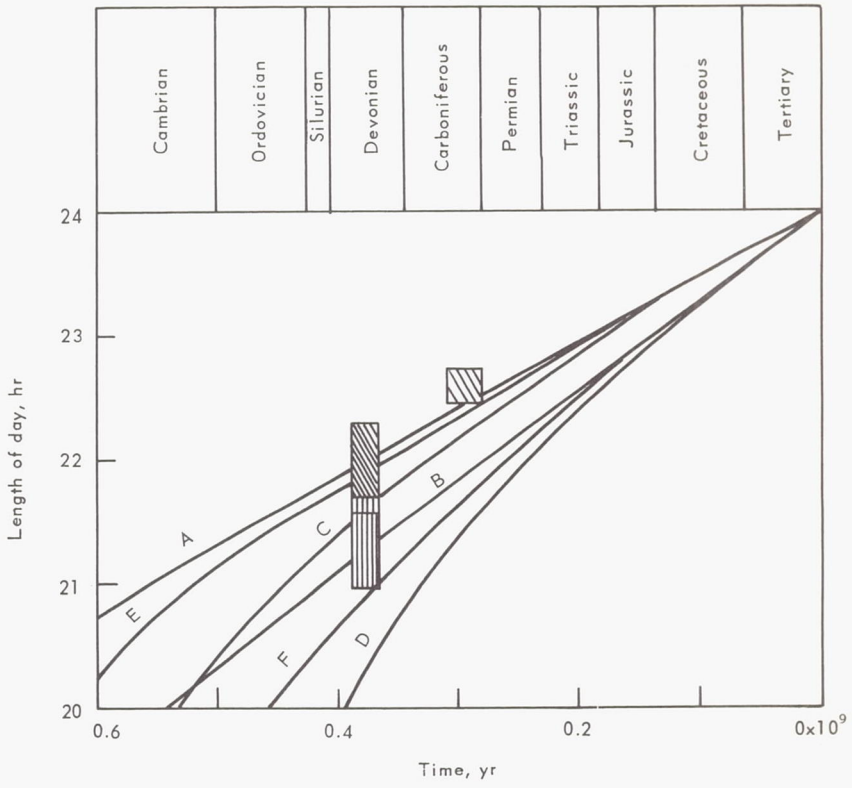


Figure 6.—**Variation in length of day during geologic time showing Wells' (diagonal lines) and Scrutton's (vertical lines) data on growth rings of Paleozoic corals.**

K, and its variation with frequency, and to measure changes in the angular momentum of the atmosphere for periods greater than 1 week. Further, such observations as suggested by Gold (ref. 53) and MacDonald (ref. 54), combined with the use of an optical corner reflector on the Moon (ref. 55), would improve our information about both the rotation of the Earth and the Moon. This combined information would thus greatly improve the basic dynamical data of the solar system.

Discussing the subject of the shape of the Earth, Lee and Kaula (ref. 56) present a table (shown herein as table II) which has refined some of the basic dimensions and elevations of the Earth, by using an analysis based on a spherical harmonic analysis of the topography of the Earth.

In the study of geomagnetism, Heinrich (ref. 57) has studied the natural remanent magnetism of 61 specimens of lava flows from a volcanic field on the eastern slope of the Sierra Nevada. The rocks are dated as Pliocene-Pleistocene in age. The values obtained for the magnetic vectors fall in two

Table II.—*Mean Values From Various Analyses of the Topography of Earth* [a]

[From ref. 56]

	Kossinna, 1933	Prey, 1921	Bruins (private communication)	Munk and MacDonald, 1960	Paper, 1966
Oceanic area, percent	70.80	(70.8)	(70.8)	71.43	70.92
Continental area, percent	29.20	(29.2)	(29.2)	28.57	29.08
Mean world elevation, meters	−2430	−2456	−2367	.....	−2300
Mean land elevation, meters	875	771	801	.....	756
Mean ocean depth, meters	−3800	−3787	−3674	.....	−3554

[a] Values in parentheses are assumed.

distinct groups (declination, $D=64°$; inclination, $I=-67°$ for one group, and $D=20°$, $I=+46°$ for the other group), which indicate that the first group represents an intermediate direction of magnetization during a magnetic reversal. Magnetic studies by Baksi, York, and Watkins (ref. 58) on volcanic specimens from Oregon similarly indicate a change from reversed to normal polarity in rocks which were dated by radioisotopes at 15.1 million years. On the other hand, Grommé, Merrill, and Verhoogen (ref. 59) determine the natural remanent magnetism of rocks dated at 142 to 129 million years from the Sierra Nevadas which indicate the same pole position as rocks as young as 84 million years. They conclude that polar wandering has not occurred in this period, but that apparent polar wandering determined in rocks from Australia and Africa is due to continental drift. Coe (ref. 60) studied the intensity of the paleogeomagnetic field preserved in volcanic rocks from the western United States. A value of 0.2 times the intensity of the present field, given by Miocene rocks, is evidence that the intensity of the geomagnetic field decreases during reversals. Other specimens bear evidence that the field may not have exceeded twice its present value during the past several million years.

In a recent paper, Cox and Dalrymple (ref. 61) develop a new statistical method for determining the ages of the boundaries between geomagnetic polarity epochs. Their best statistical estimates of the ages of the boundaries between epochs are: Gilbert-Gauss boundary, 3.36 million years, Gauss-Matuyama boundary, 2.5 million years; and Matuyama-Brunhes boundary, 0.70 million years. The duration of polarity events is estimated to vary from 0.07 to 0.16 million years, and the best estimate of the time required for the field of the Earth to undergo a complete change in polarity is 4600 years. The statistical analysis shows that if the geomagnetic-polarity time scale is to be extended much beyond its present limit of 3.6 million years, another method of dating the rocks, other than K-Ar, will probably have to be used;

this is certainly true if information is desired on the detailed polarity structure.

In a related study, Ozima et al. (ref. 62) report that the age difference between the lowermost flows of an upper normal-polarity group and the upper portion of the adjacent reversed group is about 0.05 million years, which they suggest is the maximum time for transition of the magnetic field of the Earth.

Sykes (ref. 63) has studied data from long-period seismographs on 17 earthquakes, solving for the mechanism of faulting. Ten of the earthquakes studied occurred on midoceanic ridges and, for these, the motion was predominantly strike-slip in character. The sense of the faulting was opposite to that expected for simple offset of the ridge crests along the fracture zones. The results of the study agree with the hypothesis of the growth of the sea floor at the crest of the midoceanic ridge system. Hodgson (ref. 64) has determined the direction of faulting in 65 earthquakes. He finds that of 75 earthquakes (10 were studied previously), all but 8 are the result of strike-slip faulting. For the strike-slip faults, the strike direction within any one area appears to be random. Hodgson points out that these results are incompatible with several theories on the mechanism for deep-focus earthquakes which require thrust or gravity faulting. These theories do not explain the appreciable amount of strike-slip faulting.

Hales and Doyle (ref. 65) have investigated the velocity of seismic-wave propagation and, in particular, the variations in the velocities of P- and S-waves in several regions of the United States. The arrival times are relatively early in central and eastern United States and relatively late in the west (differences range up to about 3 seconds for P-waves and 8 seconds for S-waves). The differences imply a variation in Poisson's ratio between the two regions and best fit a model in which the shear modulus varies at constant compressibility. The major part of the deviations may be due to differences in temperature in the upper part of the mantle under these regions—the west being at a higher temperature than the mantle under the central and eastern United States. Pollack (ref. 66) points out that the near equality of heat-flow measurements in continental and oceanic regions, giving rise to the implication that the temperatures under the oceans are greater than those under the continents, would indicate thermal displacements and stresses which would give rise to several tectonic features. Thus, the continents would be centers of relative contraction, while the ocean basins would be centers of expansion. In this model, normal shearing occurs on the surface of the expanding ocean basin and reverse shearing occurs on the continents. The zone of normal shearing which dips beneath the continental margin compares with the loci of earthquakes in the circum-Pacific seismic belt.

Anderson (ref. 67) has reexamined the question of a phase change as an explanation of seismic and density discontinuities in the mantle. He points

out that the velocity transition may be best explained by two transition regions, each about 75 to 90 kilometers thick and at depths of about 365 and 620 kilometers. Pressures and estimated temperatures at these depths agree very well with transition temperatures and pressures in the system $Mg_2SiO_4-Fe_2SiO_4$. This transition from olivine structure to spinel structure would take place at 1500° C at 365 kilometers depth and at 1900° C at 620 kilometers and indicates a possible increase in the fayalite content with depth.

Harris, Reay, and White (ref. 68) have found, in a study of inclusions of ultramafic rocks in extrusive rocks, evidence that there is geographic heterogeneity of mantle material. If such ultramafic xenoliths do, in fact, represent fragments of mantle material, the pyroxene peridotite zone of the upper mantle ranges in composition from 100 percent olivine to 65 percent olivine plus 35 percent pyroxene. The difference between this layer and a possible garnet peridotite layer which, from the mineralogical composition, should contain 55 percent olivine, may be real. The garnet peridotite xenoliths also contain less Ca and Al and have a higher Mg/Fe ratio.

Caner, Cannon, and Livingstone (ref. 69) have performed geomagnetic depth sounding (GDS) investigations; GDS involves the comparison of the variation in the three components of the geomagnetic field in order to obtain information on the electrical conductivity of subsurface layers. The authors recognized a highly conducting layer within 25 to 35 kilometers of the surface in the Cordillera region of North America.

Ergin (ref. 70) has used seismic data to investigate the structure of the Earth's core. The results indicate a layer of decreased seismic wave velocity below 4015 kilometers. Two other transitions in velocity are required at 4500 and 4685 kilometers in order to explain the refraction and reflection branches of the seismic waves. In general, the results suggest a layered transition zone between 4015 and 5140 kilometers below the surface within which the general level of velocity is lower than would be obtained by extrapolation of the velocities in the outer part of the outer core. Sacks (ref. 71) has used seismic P-waves diffracted by the core-mantle boundary to determine the radius of the core (3537 ± 9 km) and the velocity of the waves in the lower mantle (13.64 ± 0.045 km/sec). Irregularities in the arrival times of these diffracted waves indicate either variations of the velocities in the lower mantle or small differences in the radius of the core.

In a discussion of the thermal gradients of planetary bodies and the processes which took place during the formational stages of the planets, the condition of thermal energy, largely by radiation, is one of the most significant factors. Experimental difficulties, however, have resulted in a paucity of data on this subject. Aronson et al. (ref. 72) have now determined the radiative thermal conductivity of several minerals at temperatures up to 1500° K. Their results indicate considerable deviation from values based on room-temperature data. They point out that these values are more in

keeping with those necessary to explain the thermal history of the Earth.

Bullen and Haddon (ref. 73) present variations (B_1 and B_2) of an Earth model (B) which was constructed some years ago. This revision is based on new estimates of the moment of inertia of the Earth, density distribution in the core, and evidence from the free oscillation of the Earth. The difference in the two models is based on the values assumed for the density of the lower core: 15 gm/cm^3 for model B_1 and 13 gm/cm^3 for model B_2. The other parameters of these models are illustrated in figures 7 and 8.

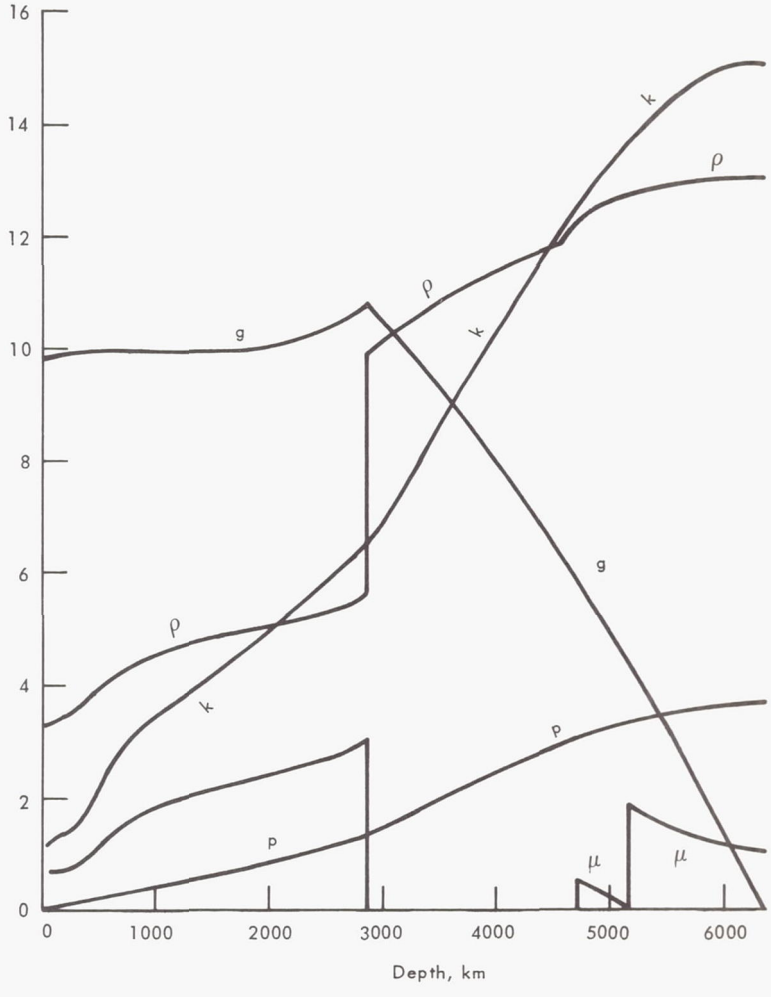


Figure 7.—Variation of pressure, p; density, ρ; incompressibility, k; rigidity, μ; and gravitational intensity, g, in Earth model B_1. Units in vertical scale are 10^{12} dyne/cm for p, k, and μ; g/cm^3 for ρ; and 100 cm/sec^2 for g.

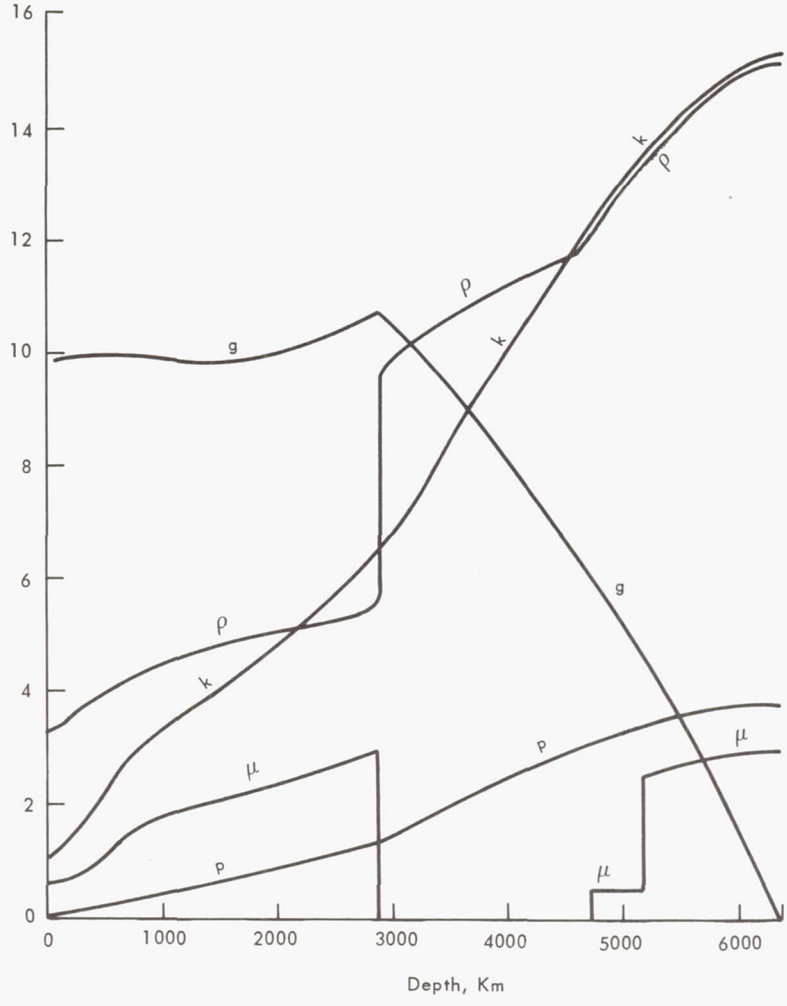


Figure 8.—Variation of pressure, p; density, ρ; incompressibility, k; rigidity, μ; and gravitational intensity, g, in Earth model B_2. Units in vertical scale are 10^{12} dyne/cm^2 for p, k, and μ; g/cm^3 for ρ; and 100 cm/sec^2 for g.

THE MOON

The year 1966 was marked by a number of firsts in lunar exploration, including the first soft-landing spacecraft and the first successful circumlunar orbital surveys. These programs were continued in 1967 with equal or greater success, with four more Surveyor spacecraft placed on the Moon and three more Lunar Orbiters placed in lunar orbit. In addition, an

unusually large number of astronomical investigations and theoretical studies of the Moon was published.

Spacecraft Investigations

Surveyor III

Following the unsuccessful Surveyor II flight in September 1966, Surveyor III made a successful landing on April 19, 1967, in Oceanus Procellarum at 2.94° S, 23.34° W, only 1.7 miles from the midcourse aiming point (ref. 74). The spacecraft actually made three distinct landings, the vernier engines continuing to fire after initial touchdown, an unexpected but valuable occurrence that gave additional information about the landing dynamics and consequently about the strength of the lunar surface. The final landing site was on the inner slope of a 200-meter-wide crater.

Perhaps the most important scientific finding of the Surveyor III mission was the demonstration that the inside of a subdued mare crater looks very much like the intercrater mare areas such as that on which Surveyor I landed (fig. 9). The surface at the Surveyor III site is relatively smooth, with occasional blocks, and is evidently unconsolidated to a depth of at least a few feet. The cumulative grain size resembles that of a repeatedly

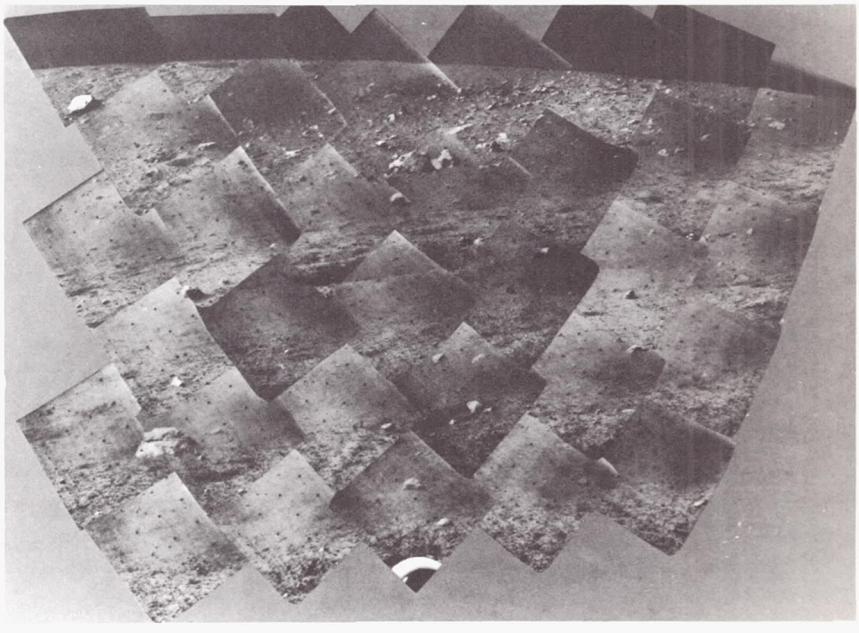


Figure 9.—Mosaic of narrow-angle pictures taken by Surveyor III camera. View to north, showing mare terrain.

impacted surface. This resemblance, together with the Surveyor III pictures which show various degrees of rounding for blocks in the field of view, suggests that the fragmental nature of the lunar surface is the result of primary and secondary impacts. A related phenomenon, first discovered by Surveyor III, is that of downhill creep of the lunar soil, indicated by the piling up of material on the uphill side of partly buried blocks. The cause for this creep is not known; meteoritic impacts and the attendant ground shock, temperature changes, and perhaps seismic activity, together with gravity, probably combine to produce it.

Another characteristic, discovered first by Surveyor I and confirmed by Surveyor III, is that the subsurface material exposed by either the footpads or the surface sampler is darker than the undisturbed surface (fig. 10). This discovery was a surprise, since it was believed, before the Surveyor landings, that the lunar surface darkens with time, probably as the result of sputtering. Shoemaker et al. (ref. 75) suggests that this "lunar varnish,"

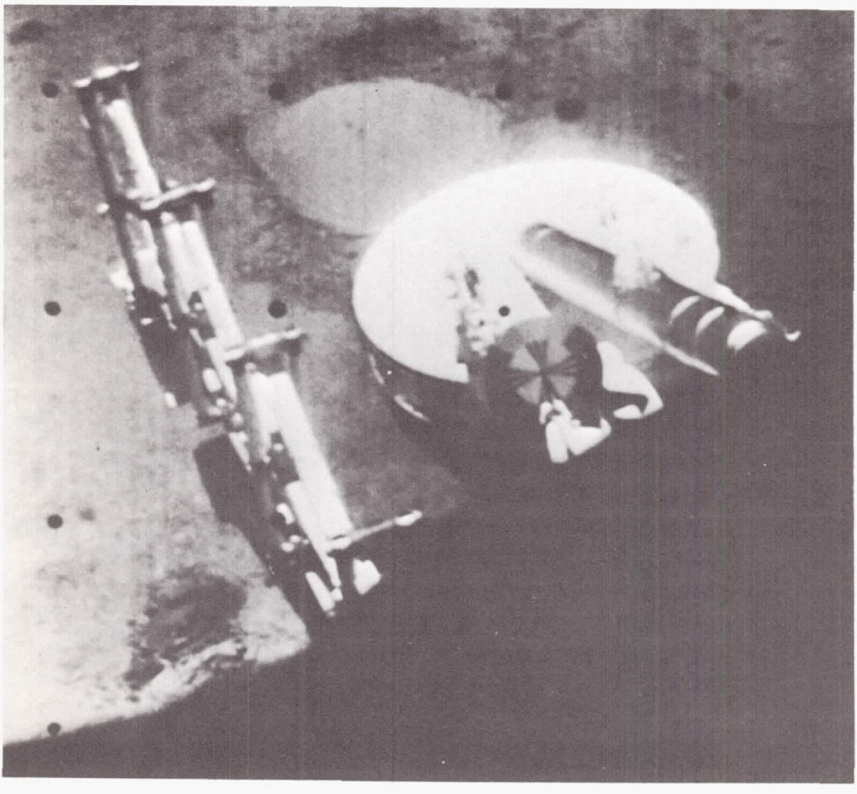


Figure 10.—Closeup Surveyor III picture showing footpad impression and dark material ejected by footpad. Surface sampler at left has made impression at lower left.

analogous to desert varnish on Earth, is the result of deposition of a dark substance by some unknown process, possibly involving gases from below or atoms knocked off by sputtering and redeposited just below the surface.

Perhaps the most interesting Surveyor III experiment was the surface sampler (fig. 11), the remotely controlled shovel carried for the first time on this flight. (See ref. 76.) Although this experiment was primarily an engineering test, the quantitative information it provided is of considerable scientific interest. The static bearing strength, for the conditions of the tests, was estimated to be between 2.5 and 3 psi. Furthermore, the material became noticeably stronger and denser at depths of about 3 inches, although there was no sign of changing grain size or other visible properties. The soil was slightly cohesive and was described in reference 76 as being similar to a fine-grained, granular terrestrial soil. The color of the soil, according to Rennilson (ref. 75), proved to be essentially gray, as shown by the filter wheel (fig. 12). Shoemaker (ref. 75) suggests that this result indicates that the iron is primarily in the reduced state, in contrast to the prevailing

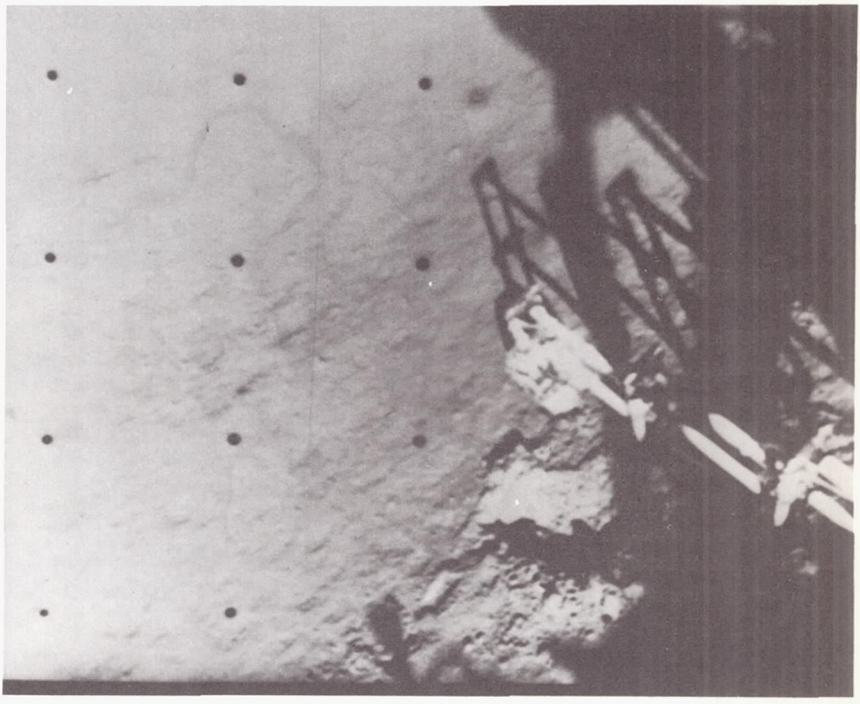


Figure 11.—Surveyor III surface sampler embedded in lunar surface. Trench at lower bottom is about 2 inches wide, 10 inches long, and 5 inches deep.

333-240 O—69——22

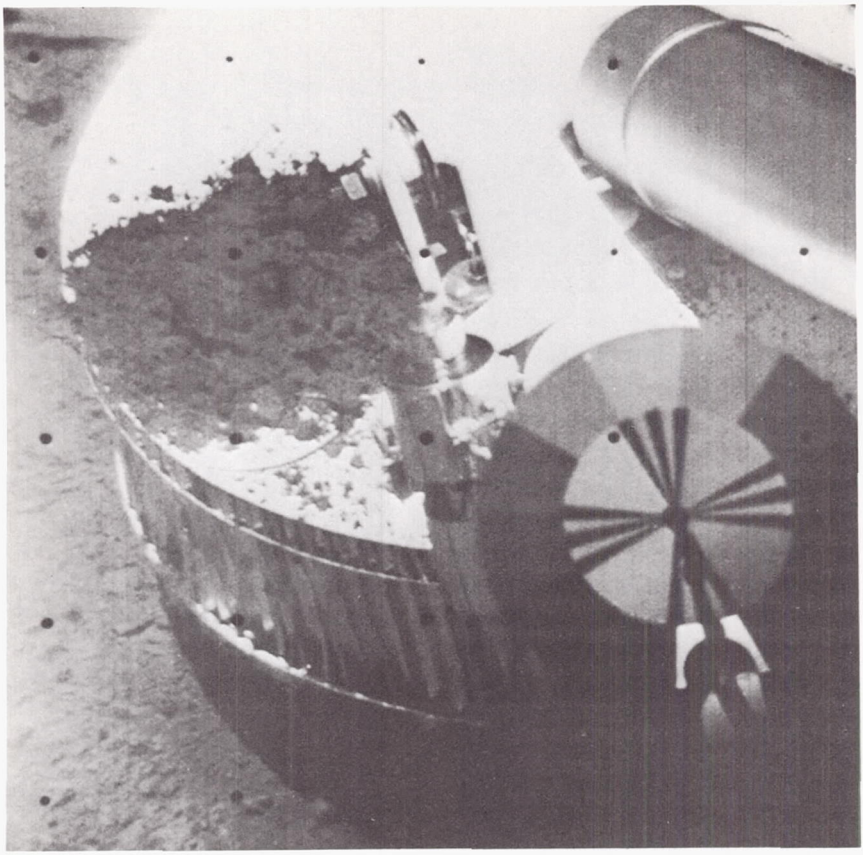


Figure 12.—**Lunar soil dumped on Surveyor III footpad by surface sampler to permit close examination. Note color calibration chart at lower right.**

oxidized state responsible for the characteristic reds, browns, and yellows of terrestrial soils.

Another first for Surveyor III was the photography, in color, of an eclipse of the Sun by the Earth, which is expected to be of scientific interest in the study of atmospheric scattering of light. The Surveyor III camera also served astronomers in returning pictures of the crescent Earth and of Venus.

To summarize, the Surveyor III mission was highly successful for a variety of reasons, perhaps the most important of which was the demonstration that the terrain photographed by Surveyor I was not an isolated, unusual region, but typical of a considerable number of areas. It also tended to confirm the generality of other characteristics and features found by Surveyor I, such as the relative darkness of subsurface material.

Surveyor V

On September 10, 1967, Surveyor V, the most successful of any soft-landing spacecraft to that date, touched down in a chain crater near the western border of Mare Tranquillitatis (fig. 13). Surveyor V was essentially similar to Surveyor III, with the addition of the first chemical-composition experiments to be carried on a soft-landing lunar probe: an alpha-scattering analytical instrument and a magnet fastened to a footpad. All the experiments were remarkably successful (ref. 77); the major results of the mission are discussed below.

Like Surveyor III, the Surveyor V spacecraft landed on the inner slope of a small crater, 9 by 11 meters; this crater was found from Lunar Orbiter V photographs to be a member of a string of subdued craters. The spacecraft landed just below the edge of the crater, tilted at 20° from the vertical, providing a good view of both the inside of the crater and the surrounding terrain, as well as views of the solar corona after sunset. The appearance of the inside of this chain crater (possibly two coalescing craters) was gen-

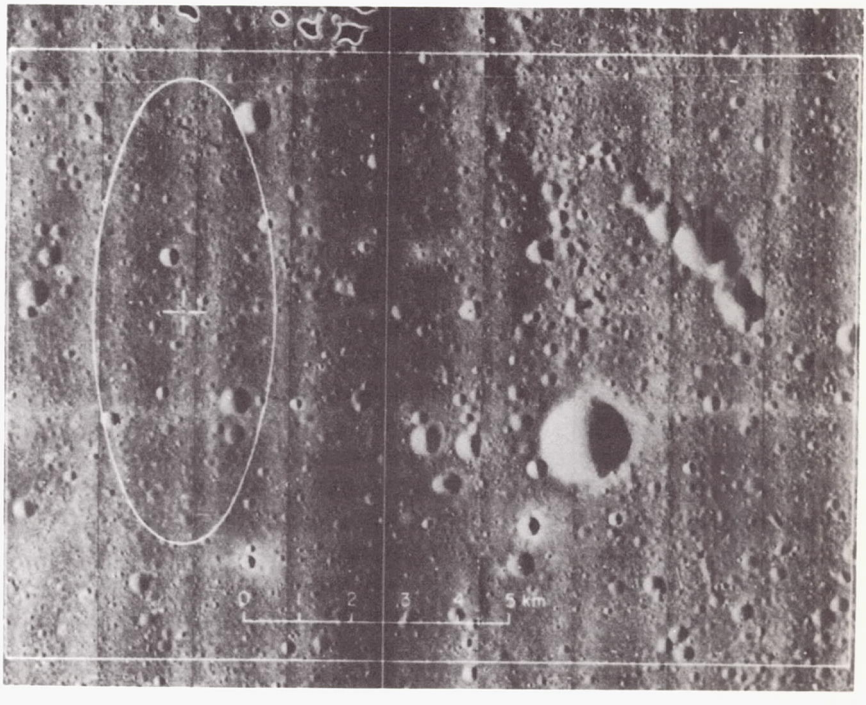


Figure 13.—Surveyor V landing site, photographed by Lunar Orbiter V medium-resolution camera, in southern Mare Tranquillitatis. Landing site lies in ellipse to 99 percent probability. Large crater at lower right is Sabine D.

erally similar to that of the Surveyor III crater, as shown in figure 14. It had no rim, a feature which, in conjunction with its alinement with the 45° N, west-trending Imbrian fracture system, led the experimenters to believe that it was formed by drainage into a tectonically controlled fissure.

The closeup views of the ground around the spacecraft were extraordinarily clear and provided new insights into the nature of the mare material. A lucky accident enhanced the value of these pictures (fig. 15): footpads 2 and 3 had dug trenches as the spacecraft slid down the side of the crater after landing, permitting close examination of the subsurface material. This material proved to be, as in the Surveyor I and III sites, fragmental debris with a wide range of grain sizes. Much of it appears to be aggregates, or clods, of finer grained material. Some of the smaller pieces look very much like glassy impactites from Meteor Crater and similar impact craters. Most of the larger fragments were thought to be rock. The overall nature of this regolith to a depth of a few meters appears to be the result

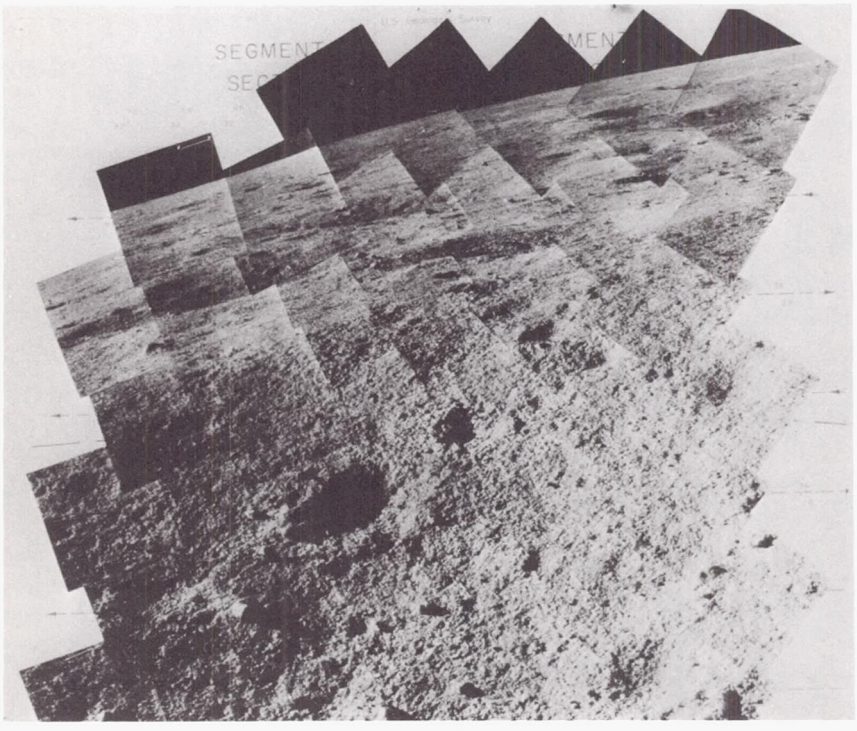


Figure 14.—Mosaic of narrow-angle pictures from Surveyor V showing northwest wall of crater in which spacecraft landed. Rim of crater is about halfway up picture and is marked by change in apparent texture caused by change in slope and distance.

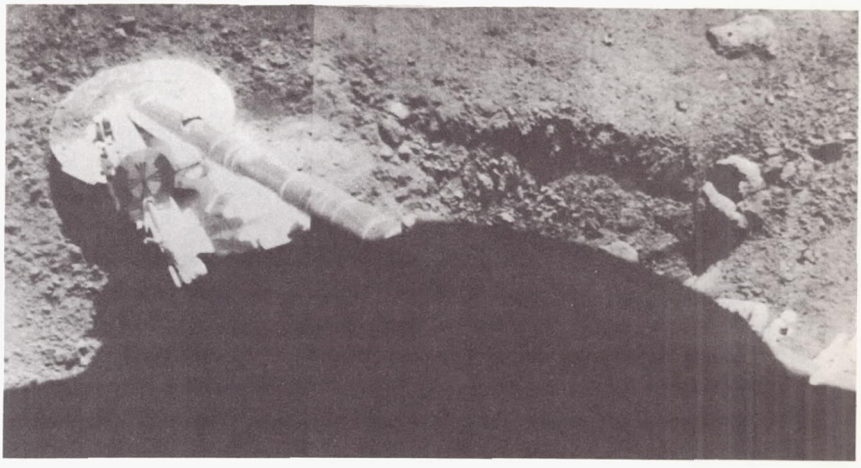


Figure 15.—**Trench dug by Surveyor V footpad during landing as it slid down slope.**

of repeated, superimposed impacts by meteorites and ejecta from other impact craters. This interpretation, if correct, has important implications for the alpha-scattering experiment. This apparatus analyzes one spot on the surface, unless moved by some means, and hence the significance of the analysis is open to question. If, however, the spot analyzed is a mechanical composite of material from a considerable area, as implied by the impact interpretation, the results are much more significant.

Also noticed in the closeup television pictures was the now-familiar lightening of the surface (or darkening of the subsurface), both in footpad ejecta and in the trench dug by footpad 2. The albedo of the dark material was estimated to be about 5 percent lower than that of the undisturbed surface (which was about 12 percent).

An interesting engineering soil test was performed 53 hours after the landing, by firing the vernier engines, for about half a second each. Although it was not possible to view the engine firings as they happened, study of pictures taken before and after permitted a detailed analysis of the effects (ref. 78). This analysis verified that the soil was somewhat cohesive and consisted largely of particles in the 2- to 60-micron-size range.

The major achievement of Surveyor V was, of course, the successful performance of the compositional experiments. The simpler of the two experiments was a magnet fastened to footpad 2 (fig. 16), to indicate the presence of magnetic material in the lunar soil. Data from this experiment will be used to help decide between two extreme views of the nature of the lunar-surface material: that it was formed wholly by meteoritic impact or that it was formed wholly by internal (i.e., essentially, volcanic) processes (ref. 79). A prevailing impact origin would indicate that considerable

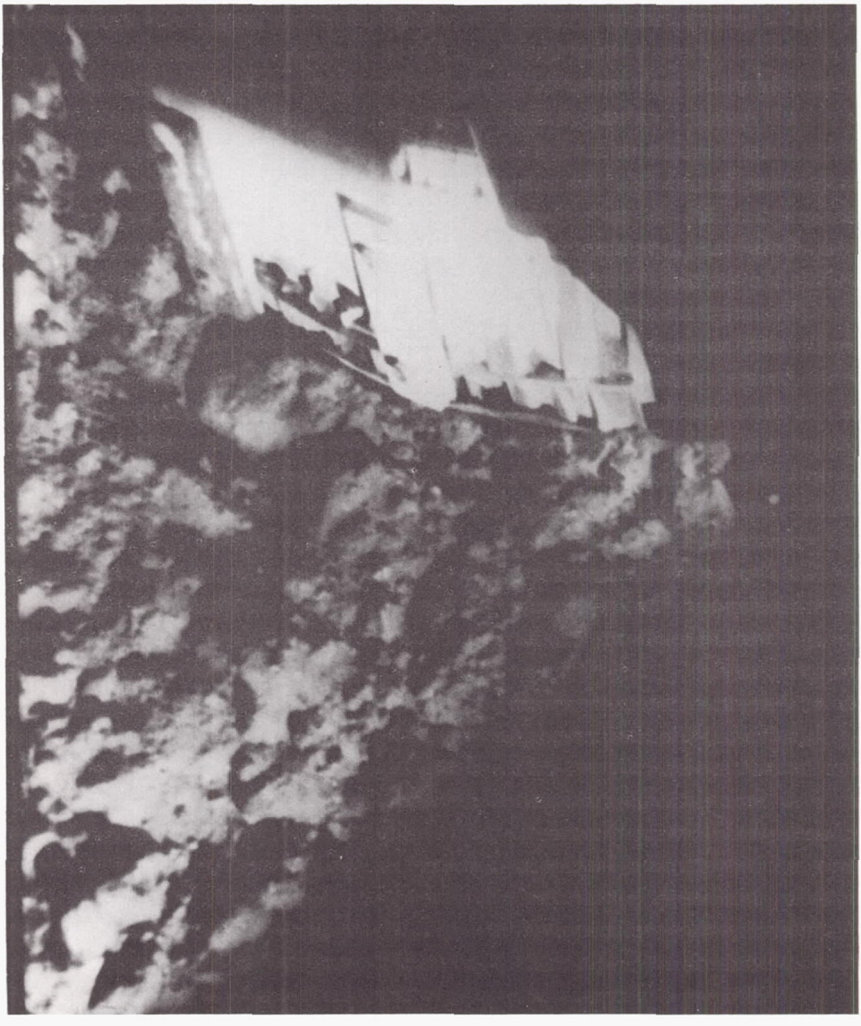


Figure 16.—Surveyor V footpad with attached magnet (left) and control bar (right). Note material sticking to magnet; control bar is clean.

meteoritic iron should be found in the lunar soil, whereas a volcanic soil would not contain much more iron than volcanic rocks. The magnet, which was paired with a nonmagnetic control bar of identical size and shape to eliminate confusion by nonmagnetic adhesion, was dragged through the soil when the spacecraft landed. A small amount of material stuck to the magnet. From the clean condition of the control bar and the fact that the material was not removed from the magnet by the vernier firing, the material was inferred to be magnetic metal or oxide. Comparison of the appearance of the magnet (fig. 17) on the television pictures with vacuum

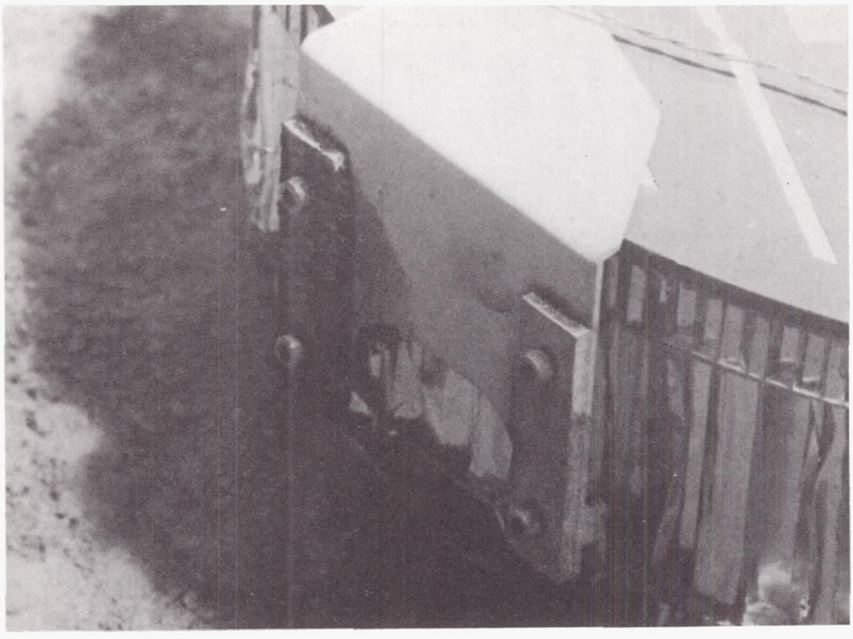
chamber tests of an identical magnet in a variety of rock powders, with varying amounts of added iron, indicated that the soil at the Surveyor V site contained not more than 1 percent by volume of metallic iron. From this comparison, reference 79 indicates that the mare material on which the spacecraft landed was not simply impact-pulverized nonvolcanic rock, but was more probably powdered volcanic rock such as basalt.

The experiment of greatest fundamental scientific importance on Surveyor V was the alpha-scattering experiment (fig. 18). The chemical composition of the Moon has long been one of the most refractory scientific problems; most remote analytical methods applied to it have given information about physical structure rather than composition. The pioneering gamma-ray survey by Luna 10 in 1966 indicated a basaltic composition, but had been very difficult to interpret because of the high background (ref. 80). Consequently, the results of the *in situ* alpha-scattering experiment were eagerly awaited.

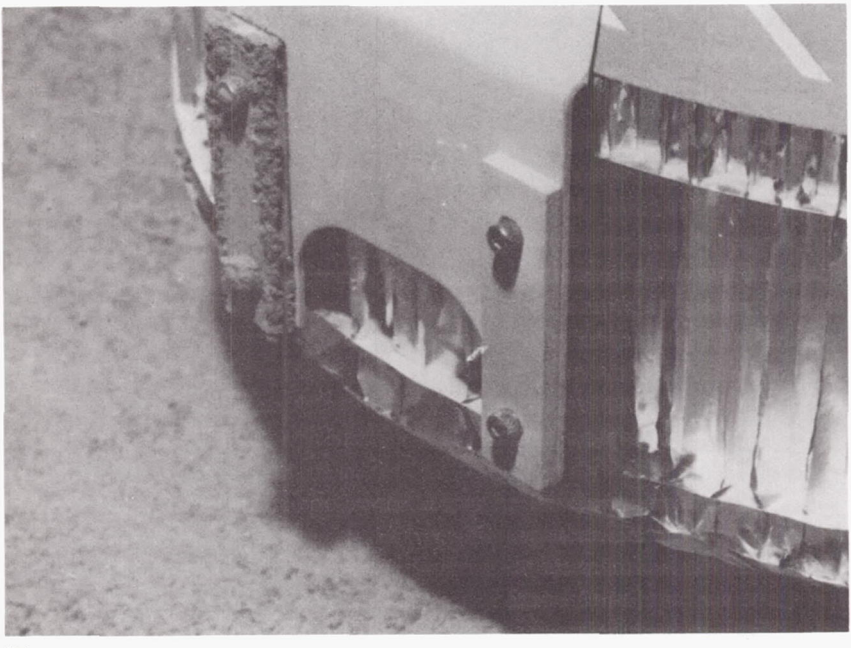
The experiment, as described by Turkevich et al. (ref. 81), depended on measurement of the energy spectra of alpha particles emitted by internal curium-242 sources and reflected by the surface material, as well as on measurement of protons produced in the surface by the alpha particles. The upper limit of alpha-particle energy is characteristic of elements in the atomic-weight range from 7 to 28, including oxygen, silicon, aluminum, and other elements common in the Earth's crust and in stony meteorites. To be interpreted, the energy spectra of a variety of materials had to be measured for comparison. During the mission, measurements were made of a standard sample of known composition carried on the spacecraft and of the background in the lunar environment, before the instrument was lowered to the surface to begin the actual analysis.

The experiment was highly successful. The instrument was placed on fragmental material thrown out by the footpad and thus analyzed a more representative sample than an undisturbed surface would be. Furthermore, the fragmental nature of the mare material in general implies that, at any one spot, the composition is a composite of the surrounding area. Nevertheless, Turkevich et al. (ref. 81) stress the preliminary nature of the analysis and the fact that it was of only one site on the Moon.

The results of the alpha-scattering experiment are shown in table III, and in figures 19 and 20. It is at once obvious that, as would have been expected, the composition of the material at this site is much more like that of the Earth's crust than that of the Sun's atmosphere. More significant is the comparison with various rock types and with tektites. It appears that ultrabasic rocks and chondritic meteorites can definitely be ruled out, that granitic rocks also can probably be eliminated. The most plausible analogs are basalts and basaltic achondrite meteorites, the latter having been previously suggested to come from the Moon by Duke and Silver in reference 82. In general, then, the mare material at the Surveyor V site has the



(a)



(b)

chemical composition of basalt. This interpretation is plausible for a variety of independent reasons. First, the magnet experiment already described had results consistent with powdered basalt. Second, the general physiography and distribution of the mare material is similar to that of volcanic rocks, as is the fine structure, if the fragmental nature can be accounted for.

This result indicates that the Moon is a differentiated body, since the mean density is too high for it to be basalt all the way through. More generally, it supports the concept of the Moon as a relatively warm, actively or recently evolving body—a school of thought that has been coming back into favor in the past few years (ref. 80).

Table III.—*Preliminary Study of Chemical Composition of Lunar Surface at the Surveyor V Landing Site*

[From ref. 81]

Element	Atoms, percent	Element	Atoms, percent
Carbon	<3	Aluminum	6.5 ± 2
Oxygen	58 ± 5	Silicon	18.5 ± 3
Sodium	<2	Sulfur→nickel [a]	13 ± 3
Magnesium	3 ± 3	Heavier than nickel	<0.5

[a] Iron, cobalt, and nickel, >3.

Lunar Orbiters III, IV, and V

The last three of five planned Lunar Orbiter spacecraft were sucessfully placed in orbit around the Moon during 1967, continuing the flood of new information begun by Lunar Orbiter I in 1966. The original program objective had been to obtain detailed photographs of potential Apollo landing sites, but owing to the success of the first three Orbiters, the last two were available chiefly for scientific photography of the front and back sides of the Moon, some of which is shown in figures 21 to 24. The program was essentially completed in 1967, although study of the results will continue for some time; therefore, the scientific results of the program as a whole will be summarized in the remainder of this section.

Figure 17.—Laboratory test of replicas of Surveyor V magnet and nonmagnetic control bar. Footpad was impacted in 37- to 50-micron powders of scoriaceous basalt (*a*) and basalt (*b*). Magnet (left) has material sticking to it.

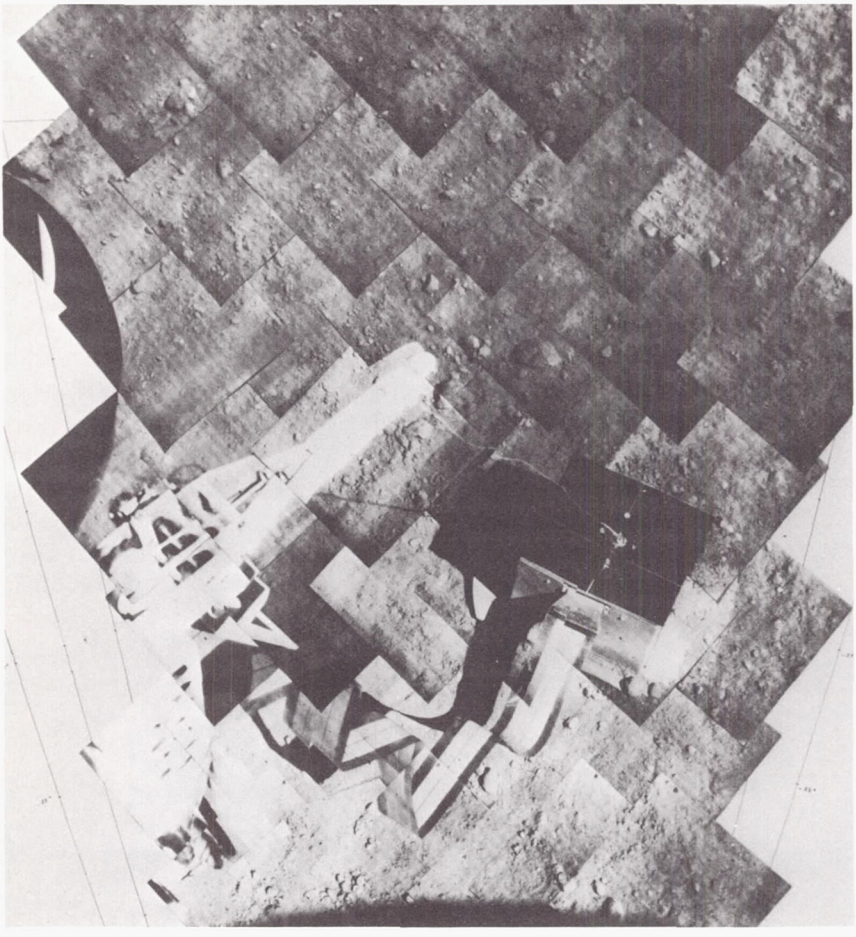


Figure 18.—Surveyor V alpha-scattering compositional experiment after firing of vernier engines, which moved the instrument.

In an indirect sense, the achievement of Apollo landing-site certification itself was—or will be—of great scientific importance. In addition to the expected scientific return from the manned landings, the Lunar Orbiter Program further confirmed the essential correctness of inferences made from Earth-based observations and earlier lunar probes such as the Ranger series. One of the most encouraging findings of all the precursor probes has been, in fact, the relative scarcity of totally unexpected discoveries that would affect the Apollo program.

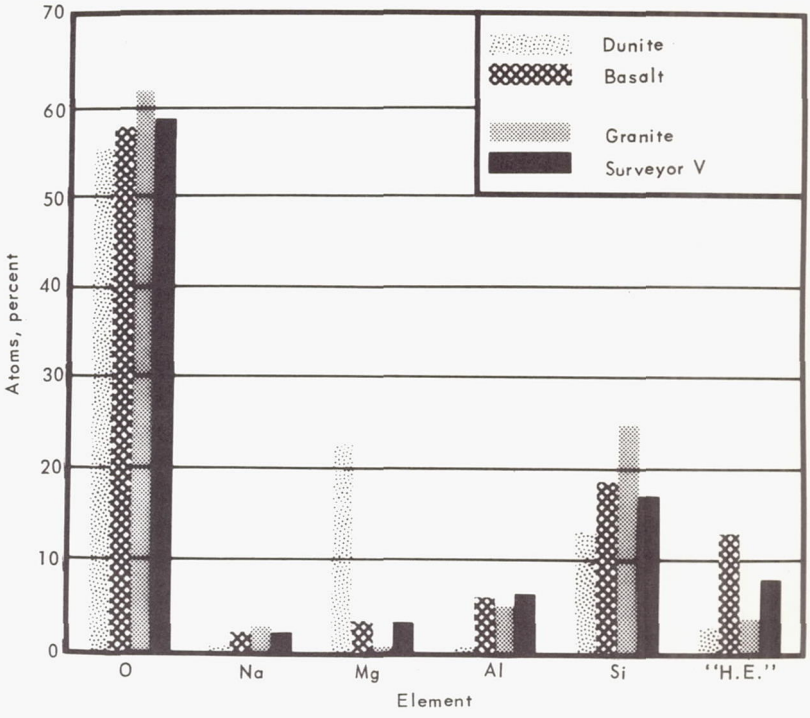


***Figure 19.*—Comparison of Surveyor V alpha-scattering experiment results from first spot (before vernier firing) with dunite, basalt, and granite.**

Some of the most scientifically significant results of the Lunar Orbiter Program are related to lunar geodesy, specifically the study of the Moon's gravitational field by analysis of tracking data. Knowledge of the Moon's mass distribution prior to the Orbiter program had been so unsatisfactory in some respects that it appeared the Moon became less dense toward the center—was more like a hollow sphere than like the Earth (ref. 83). However, studies by Michael et al. (ref. 84) indicate rather definitely that the Moon is nearly homogeneous, with similar density throughout. This homogeneity of course contrasts with the Earth, but is much more believable geophysically. Another preliminary deduction from the tracking data is that the radius of the Moon aimed toward the Earth is 1 or 2 kilometers less than previous estimates, implying that the center of mass is displaced (toward the Earth) from the center of figure. This may indicate that the Moon is in isostatic equilibrium, as previously deduced by O'Keefe and Cameron in

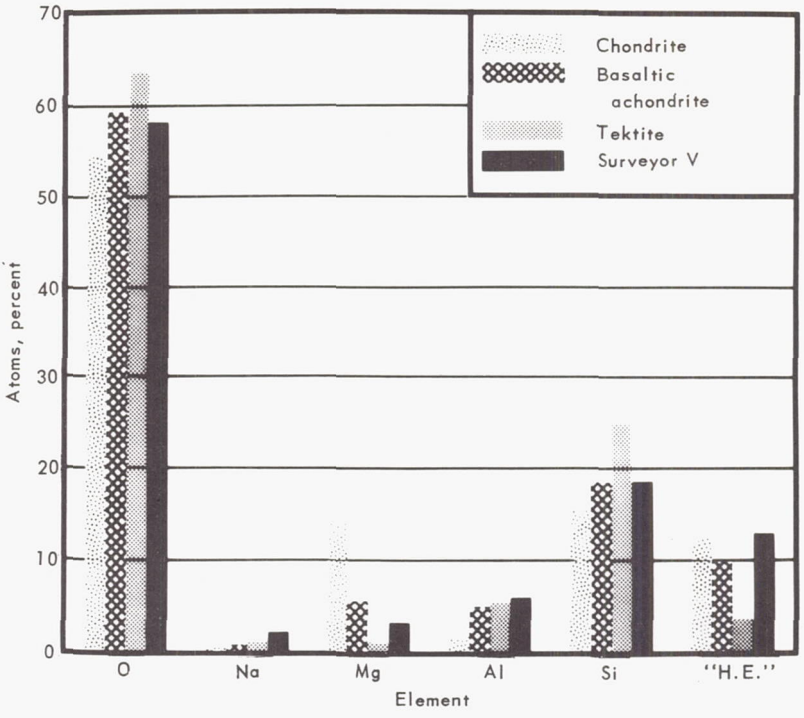


Figure 20.—**Comparison of Surveyor V alpha-scattering experiment results from first spot (before vernier firing) with chondritic meteorites, basaltic achondrites, and tektites.**

reference 85 and, from the Lunar Orbiter I tracking data, by Kaula (ref. 86). This theory would be in agreement with the abundant evidence of widespread volcanic activity uncovered by the Orbiters and other lunar probes, although, as Baldwin (ref. 87) points out, even nonisostasy would not preclude igneous activity.

The Lunar Orbiter spacecraft all carried micrometeoroid detectors of the "beer-can" type, in which hits are detected by loss of pressure when a pressurized cylindrical container made of 0.001-inch-thick copper is penetrated (ref. 88). As reported at the Lunar Orbiter V press conference, each spacecraft carried 20 of these cells with an exposed area of 2 square feet. Over the 14 months in which various members of the Lunar Orbiter fleet circled the Moon, 18 of the 100 detectors were punctured. The punctures were randomly oriented, showing no directional flux. This rate is less than one-half the flux measured in the near-Earth region by similar detectors

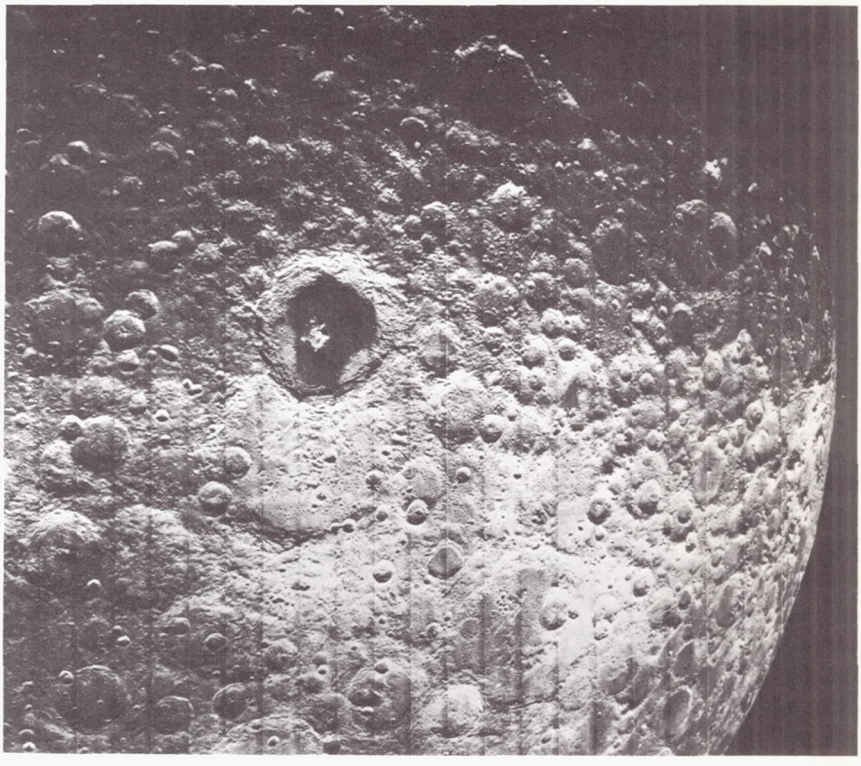


***Figure 21.*—Lunar Orbiter III photograph from 907 miles above the far side of Moon, showing crater Tsiolkovsky, 150 miles in diameter.**

on Explorers XVI and XXIII. Although the Lunar Orbiter micrometeoroid data are primarily of engineering value (providing, for instance, little knowledge of meteoroid mass or velocity), they are also of scientific interest.

Geology, which can be informally defined as what we see, in contrast to geophysics (what we don't see), is obviously the chief scientific beneficiary of the Lunar Orbiter Program. Because of the high quality of the Lunar Orbiter photographs and because there is no successor currently planned, geological study of these pictures will continue for several years. However, the main implications appear clear.

The major geologic importance of the Orbiter results is the new insight they provide about the extent and nature of lunar volcanic processes and mass wasting. Although the controversy about the origin of craters continues, it is clear that volcanism has played a major role in the formation of lunar rocks and landforms. Specific evidence for this comes from Orbiter

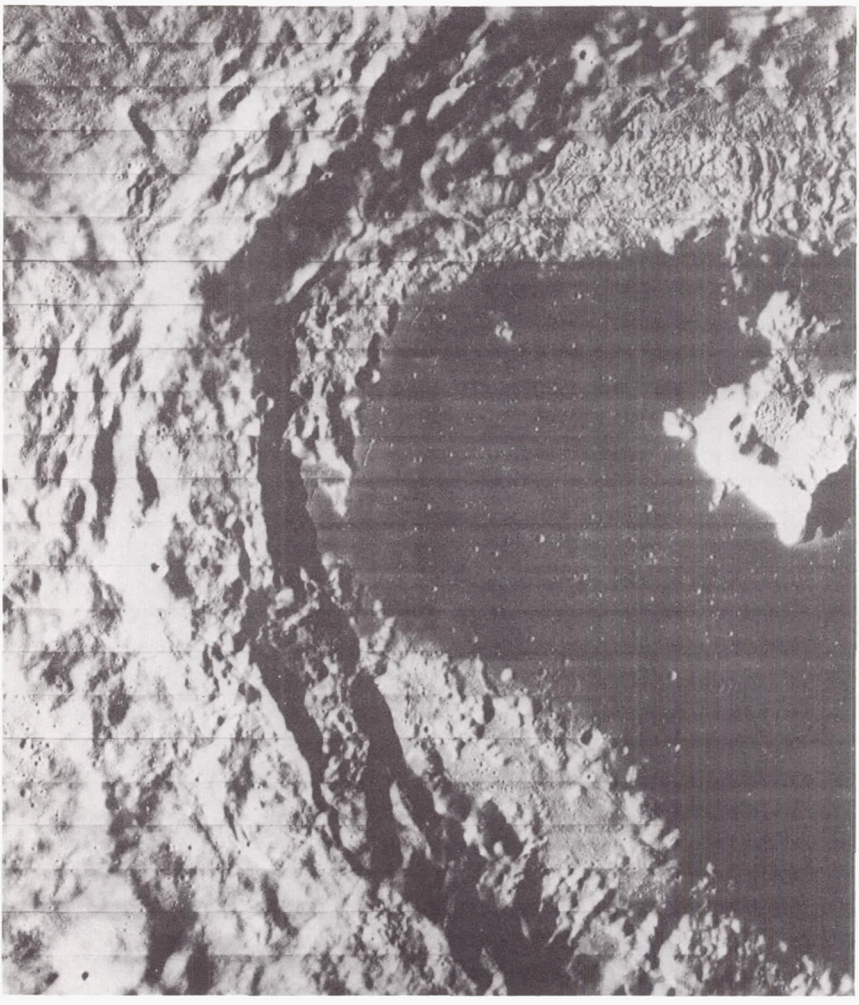


Figure 22.—**Closeup from Lunar Orbiter III with high-resolution camera of crater Tsiolkovsky. This crater apparently bridges gap between craters such as Tycho and mare-filled craters such as Archimedes.**

photographs of domes, craters, mare surfaces, and other features. Lunar domes, such as those of the Marius Hills (fig. 25), had long been considered to be of igneous origin (either shield volcanoes or laccoliths); as illustrated by McCauley (ref. 89), some of them closely resemble volcanoes when

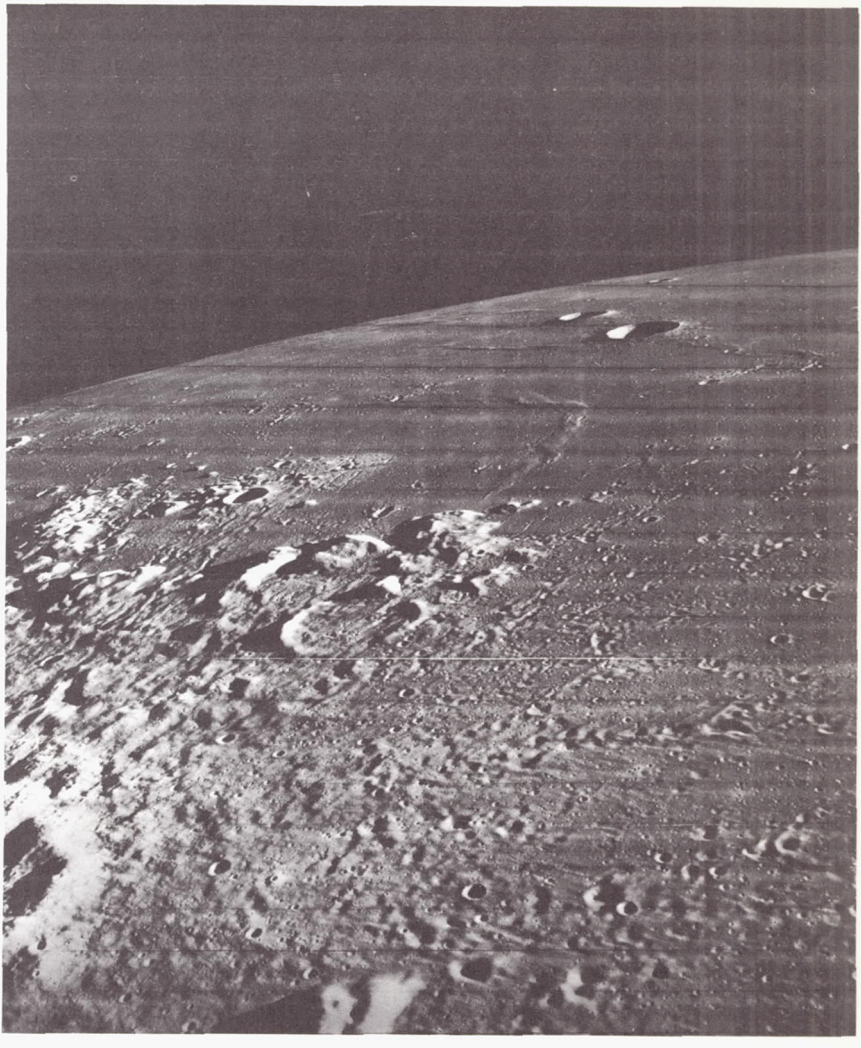


Figure 23.—View to north from Lunar Orbiter III showing part of Oceanus Procellarum, taken from altitude of 38 miles. Landing site of Luna IX, launched by the U.S.S.R. in 1966, is at center of photograph near highland-mare contact.

seen at high resolution. Several of the domes have a composite topography, consisting of relatively steep-sided upper parts superimposed on broad, gently sloping bases; these have been tentatively interpreted by McCauley (ref.

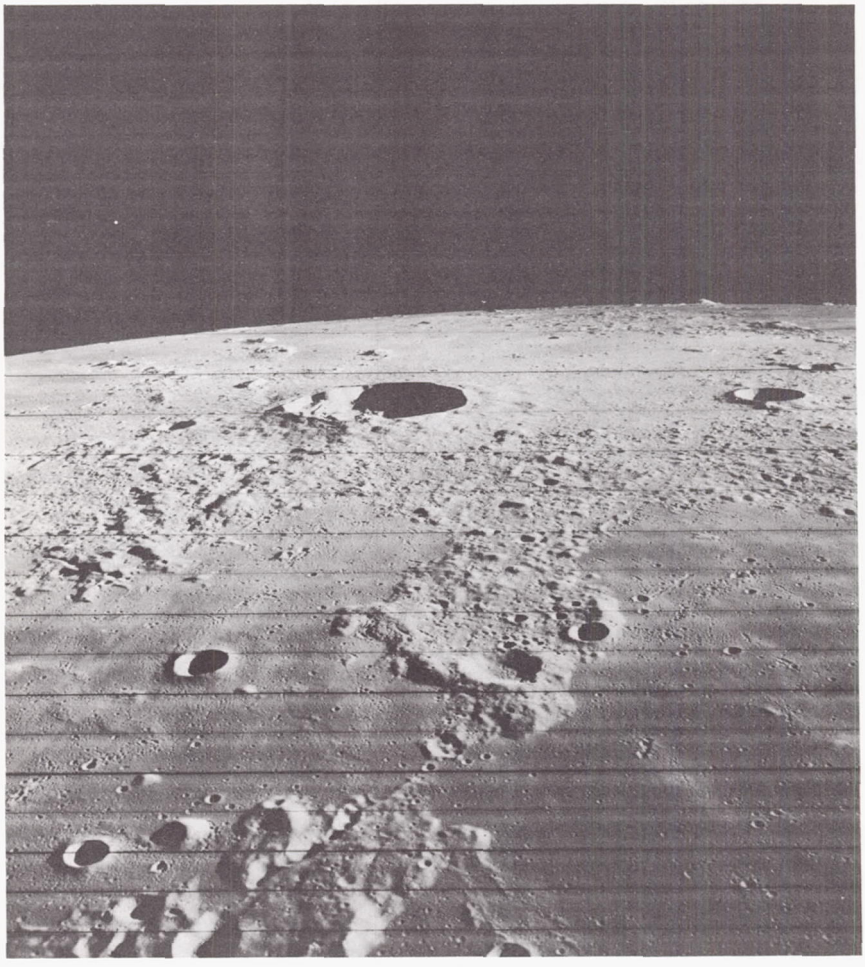


Figure 24.—Lunar Orbiter III view to north, showing crater Kepler in Oceanus Procellarum. Kepler is a Copernican-age crater with a diameter of approximately 20 miles. Clearly visible are its hummocky ejecta blanket and secondary craters.

89) as tholoids of intermediate to acidic lavas overlying basaltic shield volcanoes. The domes exhibit far more variety and complexity than had been evident in Earth-based telescopic photographs. Another interesting characteristic of the domes is the apparent absence of bedrock exposures; like the maria, they appear to be covered to some depth by unconsolidated material, perhaps produced by mass wasting.

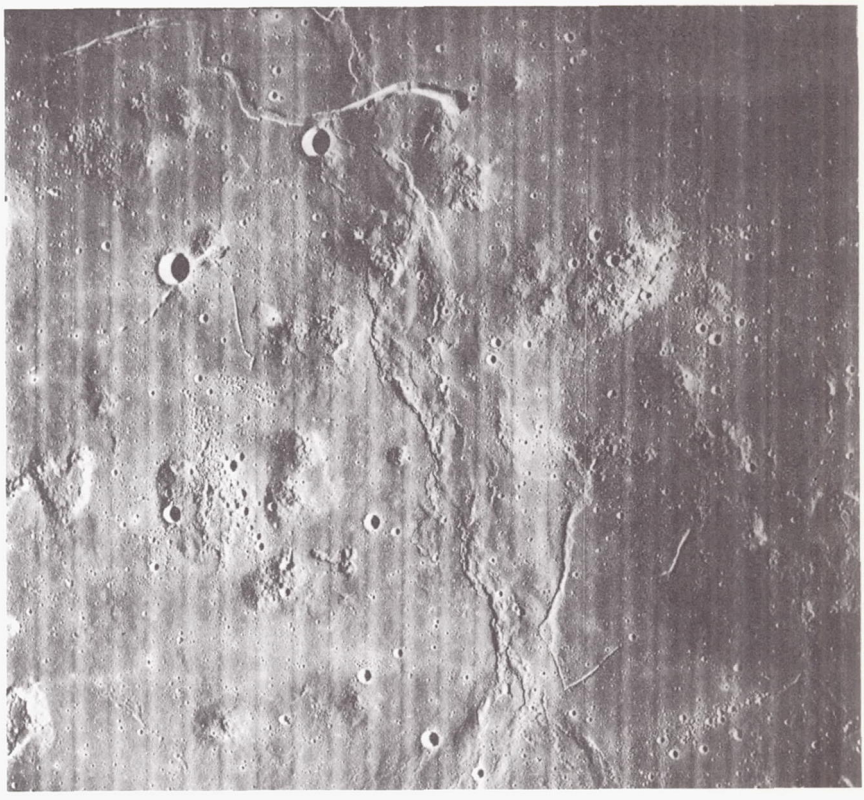


Figure 25.—Lunar Orbiter V wide-angle photograph of the Marius Hills. Various domes are considered volcanic features of some sort, possibly shield volcanoes. Notice prominent mare ridges at center.

Because they are favorable landing sites, the maria were of course repeatedly photographed by the Orbiters (fig. 26). A number of pictures show details of the "treebark structure," on both mare and highland terrain. Taken in conjunction with the Surveyor pictures, which show apparent downslope mass movement, the Orbiter pictures (fig. 27, for example) suggest that this structure is the result of mass wasting. A possible cause is the seismic disturbances set up by major meteorite impacts. Other mare features notable for their unexpected scarcity are flow fronts, finally photographed by the Orbiters. The existence of these features tends to confirm the Surveyor analyses indicating basalt as the mare material. The scarcity of flow fronts and other typical lava features on the maria is still not completely understood; the most favored explanation is that originally proposed

333-240 O—69——23



Figure 26.—**Lunar Orbiter IV photograph taken from an altitude of 2050 miles over the Moon's north pole. Earthward hemisphere is at top; large dark area is Mare Imbrium, with mare-floored crater Plato on its north rim.**

by Shoemaker (ref. 90) for the Ranger VII pictures of Mare Cognitum; namely, that the original topography has been largely destroyed by repeated impacts of meteorites and ejecta from meteorite impacts. However, some geologists believe that the eruption of the mare lavas was followed by major ash falls, which blanketed the originally rough topography. These two explanations are not necessarily contradictory; a compromise model consisting of lava overlain by ash, and saturated with impact craters, appears plausible.

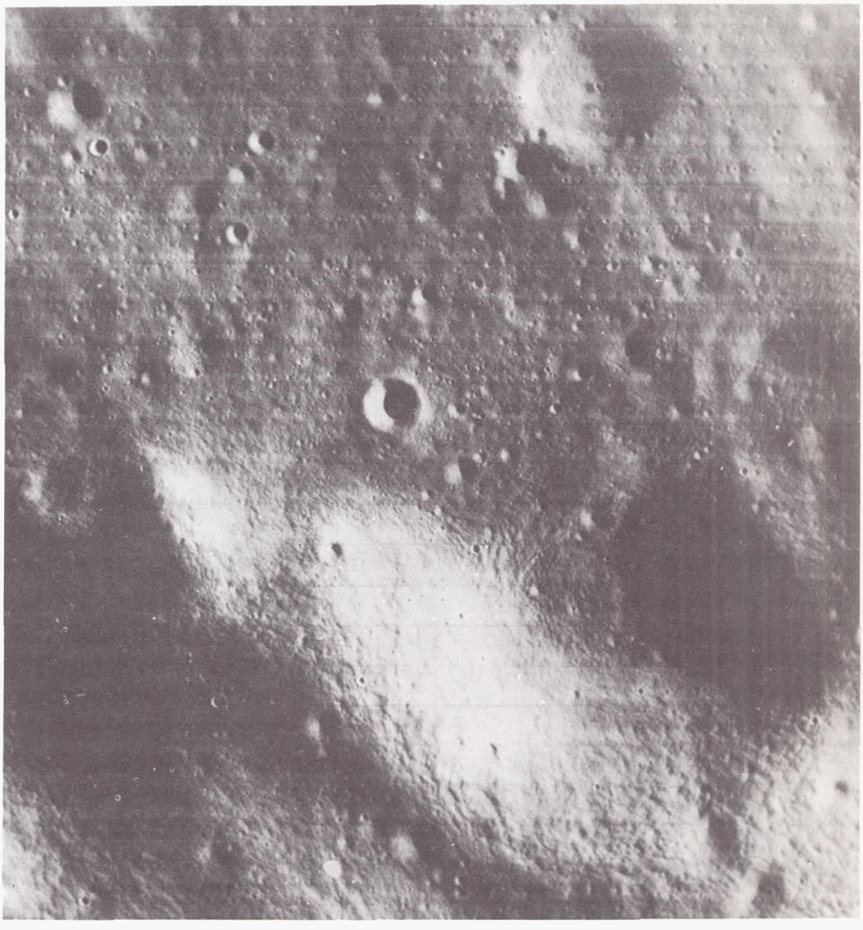


Figure 27.—High-resolution photograph from Lunar Orbiter III of a 9-square-mile highland area near crater Dembowski, at 6.6° E and 4° N on visible hemisphere. Note "patterned ground," believed by some geologists to be the result of downslope movement.

The theory of the origin of the Moon's craters continues to be controversial, despite, or to a degree because of, the many excellent crater pictures returned by the Lunar Orbiters, especially Orbiters IV and V. Of greatest interest are the vertical, high-resolution views of the craters Tycho, Copernicus, and Aristarchus (figs. 28 to 31). The Tycho photographs are discussed in some detail, since this crater, because of its relative youth, displays extremely well the topography common to all three. The most conspicuous

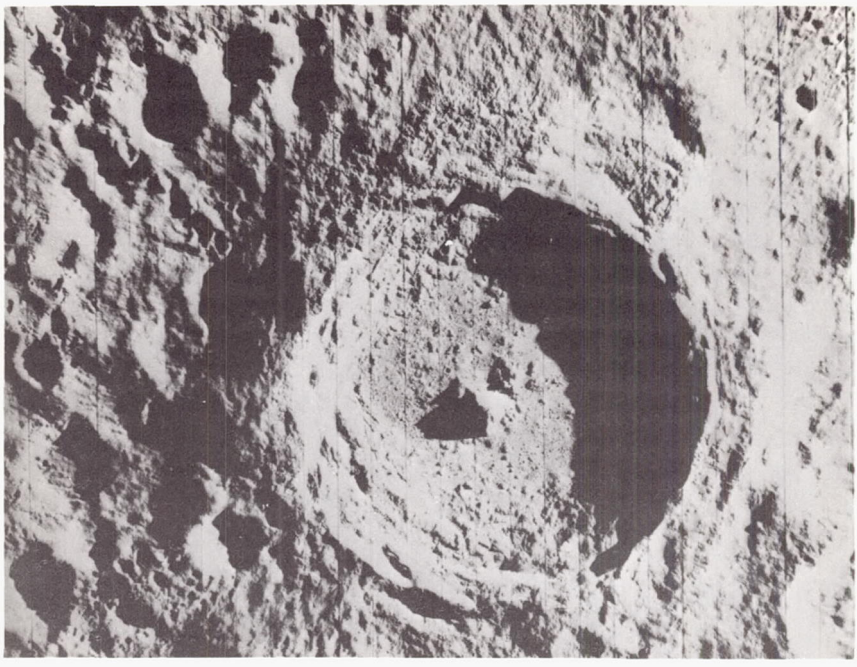


Figure 28.—**Lunar Orbiter V view of crater Tycho, with north at top and Sun at right. Tycho appears to be youngest of large craters.**

feature is the rough floor of the crater, which has a striking resemblance to terrestrial lava flows. It appears certain that some sort of relatively viscous liquid at one time covered much of the crater floor, but since there is evidence of large quantities of former melt in some terrestrial structures of suspected impact origin, such as the Manicouagan and Clearwater Lakes structures in Canada, the lava explanation is by no means unarguable. Other features for which a volcanic origin has been proposed include the small areas of what appear to be mare material which fill depressions in the outer flanks of Tycho. Here too, however, an impact origin—in this case from fallback as a "base surge"—is favored by some. The apparent flows on the outer flanks of the crater are of extreme interest, since Surveyor VII landed on one of them and returned an analysis indicating the elemental composition of a low-iron basalt.

In summary, Tycho (and to different degrees, Copernicus and Aristarchus) exhibits a number of topographic features strikingly similar to those of volcanic terrains. This result was rather unexpected, except by those who consider these craters to be large calderas, because these craters appeared, at telescopic resolution, to be relatively uncomplicated by possible volcanic activity, as are Archimedes and Plato (large, mare-material-filled craters). There appears a very real possibility that, even if the initial craters are



Figure 29.—**Lunar Orbiter V high-resolution view of floor of Tycho, with north at top and Sun at right. North-south distance in photo is approximately 14.7 miles. The ropy structure of crater floor resembles that of terrestrial lava flows and has almost certainly been formed by consolidation of some sort of liquid.**

formed by meteoritic or cometary impact, there has been substantial post-impact volcanic activity.

Zond 3

Results from two experiments carried on the Russian lunar probe, Zond 3, which flew by the Moon in 1965, were reported by the investigators in 1966 at the Vienna COSPAR meeting. Lebedinsky et al. (ref. 91) describe the ultraviolet spectrophotometer used and present typical spectrograms (a total of 15) obtained during the flight. The curves are similar to those of sunlight, although there are some differences. Another ultraviolet experiment carried by Zond 3 (ref. 92) covered the 2850- to 3550-Å region. This technique has potential value for compositional determina-

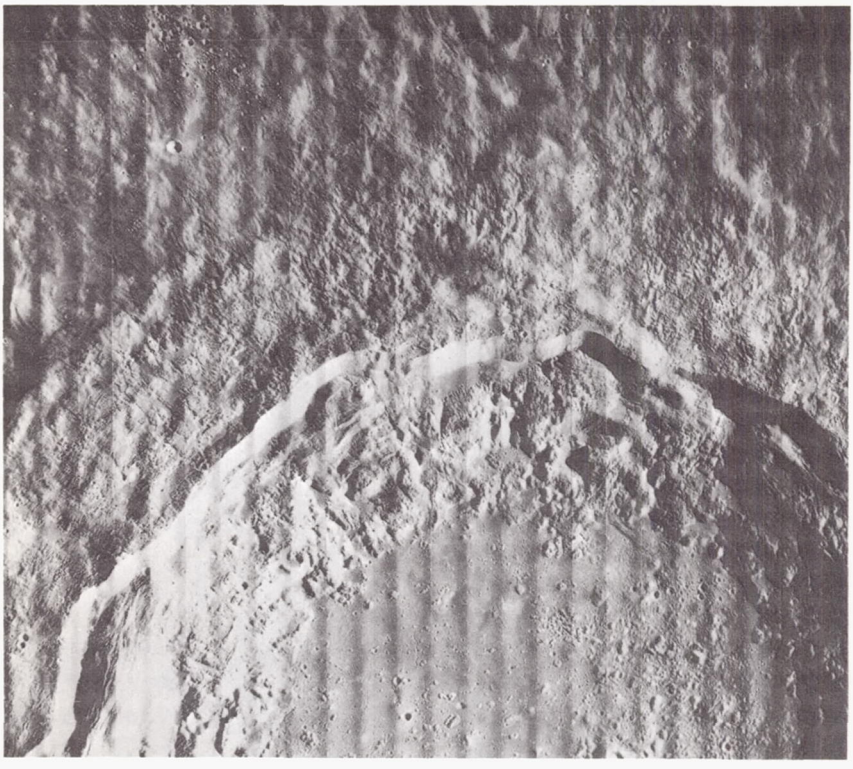


Figure 30.—Lunar Orbiter V view of northern part of crater Copernicus, whose greatest diameter in picture is about 55 miles. A number of typical crater features are shown exceptionally well, including the ejecta blanket and slump blocks produced by normal faulting of crater walls.

tions, according to the authors, but only preliminary analysis had been conducted at the time the paper was presented. A well-defined albedo versus wavelength curve was derived, showing a decrease from 4 percent to 3 percent in the 3550- to 3400-Å range, a leveling off at 3 percent, then a rapid decrease from 3 percent to 1 percent in the 3100- to 2850-Å range.

Explorer XXXV

On July 22, 1967, a spacecraft of the interplanetary monitoring platform type (IMP) was placed in orbit about the Moon and designated Explorer XXXV, or informally the Anchored IMP. Although the primary objective of this satellite was to study the space environment of the Moon and the interaction of the solar wind with the Moon, the information returned permitted significant inferences about the Moon itself. Preliminary results

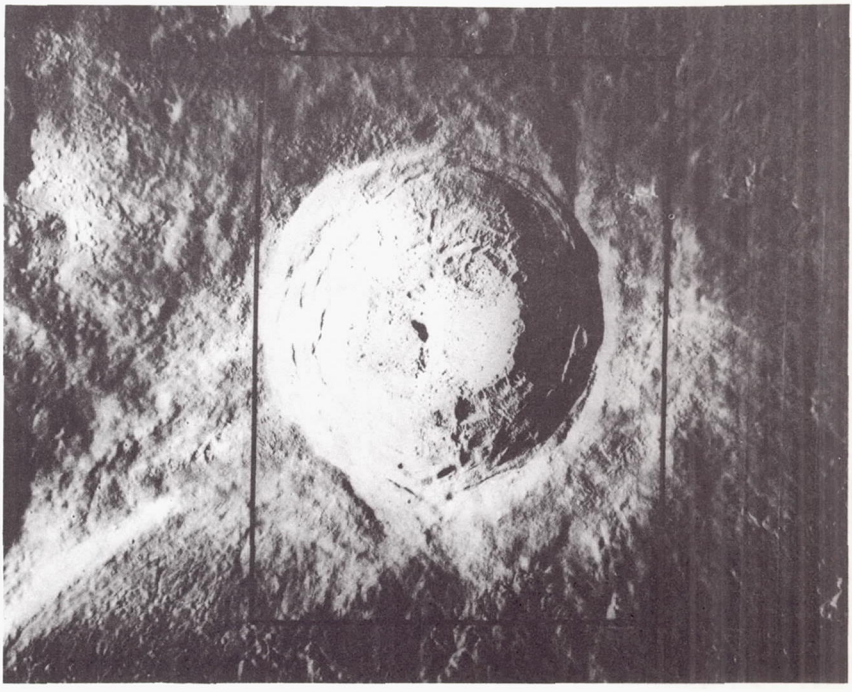


Figure 31.—**Lunar Orbiter V wide-angle photograph of crater Aristarchus, from an altitude of about 80 miles. Aristarchus, brightest large feature on the earthward hemisphere, is site of several confirmed transient events, in particular the famous "red spots" seen by Greenacre and Barr in 1963.**

of the magnetic-field experiment are reported by Ness et al. in reference 93.

Perhaps the major deduction from the magnetometer data was that the Moon has no strong magnetic field. Specifically, no field was detected at the periselene altitude of 800 kilometers, indicating, according to reference 93, that the intrinsic field at the surface is no more than 16 gammas. (For comparison, the interplanetary magnetic field during quiet Sun conditions is about 5 to 10 gammas.) This result had, in general, been expected, although Gold (ref. 94) had suggested that the Moon might accumulate the interplanetary magnetic field, and Dolginov et al. (ref. 95) interpret the Luna 10 results as indicating a field of 24 to 40 gammas near the Moon.

An extremely interesting indirect deduction about the interior of the Moon was also made by Ness et al. (ref. 93) from the magnetic data. Explorer XXXV detected no evidence of a bow-shock wave around the Moon such as is formed by the interaction of the Earth's magnetic field with the solar wind. This indicates that the interplanetary magnetic field diffuses through the Moon rapidly. From this diffusion time, Ness et al. calculate

that the electrical conductivity is no higher than 10^{-5} mho/meter. This in turn implies, assuming a temperature dependence of conductivity similar to that of olivine ($(Fe,Mg)_2\ SiO_4$) and periclase (MgO), that the average temperature of the Moon is less than 1000° K.

Whether this interpretation can be reconciled with the evidence of abundant past and present volcanic activity remains to be seen.

Optical Astronomy

Geological Mapping of the Moon

Despite the dramatic discoveries resulting from the analysis of the Lunar Orbiter and Surveyor photographs, telescopic mapping of the Moon remains an important project. For several years, the U.S. Geological Survey, in cooperation with the National Aeronautics and Space Administration (NASA) and the Aeronautical Chart and Information Center, has conducted a 1:1 000 000 scale lunar-mapping program based on relatively objective geological principles, such as observed superposition and transecting relationships. Several new maps in this series were published in 1967, including the following.

The Copernicus Quadrangle was completed by Schmitt, Trask, and Shoemaker in reference 96. This map (fig. 32) is of special interest since it shows what is probably the best-known and most thoroughly studied large crater on the Moon. The Lunar Orbiter II oblique photographs were used in the final revision of the map before publication. As a result of increasing experience and study, as well as new telescopic and spacecraft photography, the Copernicus map is remarkably detailed in comparison with similar maps developed only a few years earlier. Probably one of the most important things brought out in the map is the growing realization that lunar geologic evolution has been an extremely complex combination of internal and external processes. Although Copernicus itself and similar craters such as Eratosthenes and Reinhold are interpreted in reference 96 to be impact craters, they also exhibit features considered of internal origin, including the domes, sinuous rilles, dark-halo craters, and Eratosthenian chain craters. The mare material is as usual interpreted as volcanic, either pyroclastics or flows. The existence of craters such as Lansberg and Reinhold B which were clearly formed after the Imbrium Basin (since they are not cut by Imbrium sculpture or overlain by Imbrium ejecta), but before emplacement of the mare material, demonstrates that the mare material is not simply breccia from the impact formation of the mare basins—a misconception still encountered in some publications.

McCauley (ref. 97) completed the geologic map of the Hevelius region, which is on the western limb of the Moon (fig. 23). The Hevelius Quadrangle is of special interest for a number of reasons, a major one being the

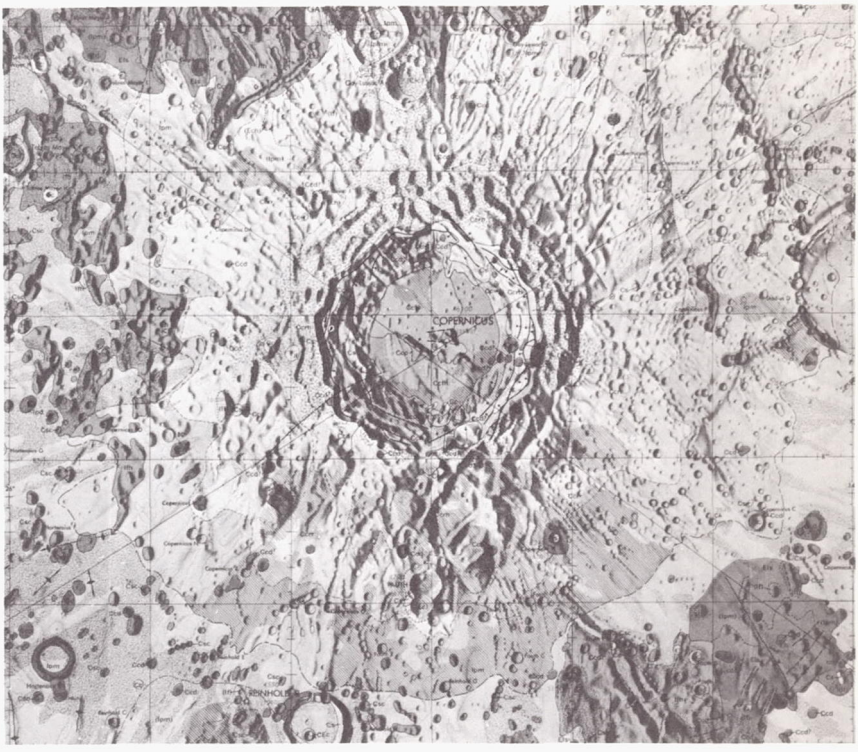


Figure 32.—Geologic map of crater Copernicus and vicinity, prepared by Schmitt, Trask, and Shoemaker (ref. 96).

abundance of apparently volcanic landforms found there. In addition to the part of Oceanus Procellarum included in the map area, there is a large dome field west of the crater Marius, many sinuous rilles, chain craters, and dark-halo craters, all of which are interpreted by McCauley as volcanic.

The Hevelius map is notable for the number of new mapping units introduced. Oldest of these is the Hevelius Formation, a relatively smooth material becoming rougher toward Mare Orientale, which is outside the Hevelius Quadrangle. It is interpreted by McCauley as ejecta from the impact believed to have formed the Orientale basin, and thus is analogous to the Fra Mauro Formation (around Mare Imbrium) and Vitello Formation (around Mare Humorum), as well as to the ejecta blankets of innumerable smaller craters. (McCauley discusses these interpretations in more detail in ref. 98.) Another new unit is the Marius Group, divided into four subgroups on the basis of topography. It includes the material of the Marius dome field, which McCauley interprets as volcanic flows, volcanoes, and tholoids, and in reference 98 as possible laccoliths.

The Cavalerius Formation, a very dark unit of Copernican age, is also interpreted as volcanic, chiefly pyroclastics. Luna 9, the Russian probe launched in 1966 (ref. 80), is thought to have landed on the Cavalerius Formation, although the uncertainty is such that it may be located on hills composed of relatively recent (Copernican) slope debris. The last new unit, named the Reiner Gamma Formation, designates the light-toned tadpole-shaped feature on Oceanus Procellarum whose nature has been speculated on for many years. McCauley (ref. 98) points out that this unit is unique on the Earthward hemisphere and has no obvious terrestrial analogs; he suggests tentatively that it may be an ash-flow deposit originating in the Marius Hills area.

Lying just north of the Hevelius Quadrangle is the Seleucus Quadrangle, a map of which was published by Moore in 1967 (ref. 99). Although no new formations were introduced, the Seleucus map is of interest because of the large number of apparently volcanic features it shows. The most important of these is the Aristarchus Plateau, a large raised area over 200 kilometers wide named from the crater Aristarchus on its east end. Part of the plateau had been mapped earlier by Moore (ref. 100); the Seleucus map shows the subsequent progress made in refining and subdividing the various rock-stratigraphic units. The most obvious difference between the two maps is the elimination of the Fra Mauro Formation (interpreted as Imbrium ejecta) except in cross section; the part of the Aristarchus Plateau which would have been formerly mapped as Fra Mauro is now designated as the Vallis Schroteri Formation. This is a five-member unit, generally dark and with a reddish color, which is typically exposed along Schroter's Valley (formally Vallis Schroteri), and including rock types and structures interpreted as volcanic flows, pyroclastics, maars, domes, and possibly laccoliths.

Another notable feature shown on the Seleucus map is the complex structure of the Aristarchus Plateau, which has apparently been cut by a large number of normal and reverse faults, which can be grouped, with other lineaments, in four main sets. Some of these are evidently relatively old, being related to the formation of the Imbrium basin, but some are younger than the plateau. This suggests again that the Moon is a tectonically active body—a concept in agreement with the well-known observations of present changes (the "red spots") near and in the crater Aristarchus in 1963 made by observers of the Aeronautical Chart and Information Center.

The area of Mare Humorum was mapped by Titley (ref. 101), who had previously mapped the adjoining Pitatus Quadrangle with Trask (ref. 102). This map includes all of Mare Humorum and a considerable part of the surrounding highlands, which Titley mapped as Vitello Formation, interpreted as being ejecta from the mare basin. A new unit in the Humorum

map is the Doppelmayer Formation, a very dark, smooth material blanketing the southwest part of Mare Humorum and adjacent craters. Ascribed by Titley to either the Imbrian or Eratosthenian system, it is interpreted as volcanic flows or pyroclastics or both. A number of craters are assigned to the Gassendi Group, including Gassendi itself, Doppelmayer, and Vitello. These are craters demonstrably younger than the mare basin but older than the mare material, and they are thus analogous to Archimedes and Plato; they are of genetic interest in furnishing additional evidence that a significant interval elapsed between formation of the mare basins and emplacement or eruption of the mare material. This point is of some importance in view of the residual doubts that the mare material is internally generated.

Although the Surveyor I color wheel verified that the lunar surface would be rather colorless to the eye at close range, there is nevertheless significant permanent color variation over large areas of the Moon. The most recent of many studies of lunar colors (excepting transient changes, which will be discussed separately) is reported by Evsyukov in reference 103. Using the 200-millimeter refractor of the Kharkov Observatory, Evsyukov photographed the Moon, at various phase angles, in the ultraviolet at 3700 Å and in the infrared at 1000 Å. He derived a color index for about 170 lunar surface features indicating whether they were greener or redder than the average Moon. Most features varied by no more than a 0.25 magnitude from the mean color index as measured by his equipment of −0.97 magnitude. However, a few objects—in particular, Aristarchus and Proclus—were much more strongly colored, which Evsyukov attributed to luminescence. He categorized a number of features, including individual craters, highland areas, and maria, as greenish or reddish compared with the average Moon and found his results agreeing with those of earlier workers such as Barabashov who had taken color photographs of the Moon. The older formations seemed to be chiefly reddish and the younger greenish; this suggests that "cosmic factors" diminish color contrasts and make the color more reddish.

Lunar Transient Phenomena

The problem of lunar colors is, of course, intertwined with that of observed color changes on the Moon. Rackham reports in reference 104 the continuation of his earlier work on the problem. He performed a photometric analysis of lunar negatives taken on 3 nights during the quiet Sun period of July 1964, at two passbands centered at 5700 and 6700 Å. Two hundred and five points were analyzed, lying chiefly in western Mare Imbrium, eastern Oceanus Procellarum, and adjoining areas. Analysis of the derived color indices showed evidence of considerable changes in color for a number of points during the period of observation, including Copernicus, Kepler, Gambart A, Diophantus B, and other craters. Aristarchus, interestingly,

did not show much change in color. Rackham pointed out that much more additional observational and interpretive work is needed to determine the cause of these color changes.

A major study of transient color changes is presented in reference 105, by McCord who used the Mount Wilson 60-inch telescope and a granting spectrometer during 6 lunations in 1965 to study 24 points on the Moon. The observation period included times of both modest solar activity and solar calm. McCord found no differences in line depth corresponding to changes in visible emission greater than about 5 percent of the reflected light, in contrast to earlier workers who had reported changes of from 5 to 17 percent. He did, however, find significant temporal and spatial variations in the 0.5- to 2.0-percent range indicating visible emission occurring on or near the surface (i.e., nonsolar). There was no obvious correlation of these changes with the changing observational parameters, preventing any unique conclusion as to the cause of the changes.

A retroactive search for changes on the Moon was conducted by Cameron (ref. 106), who collected more than 550 reports of lunar transient phenomena (LTP) extending back 400 years. This number included a series of lunar observations made by Bartlett (ref. 107) over the past 17 years. Cameron compared the occurrence of the LTP, which included color changes, brightenings, obscurations, and similar effects with the anomalistic period and with the distance from the terminator. She also plotted their location and found them concentrated around mare edges. She found it difficult to arrive at firm conclusions as to the cause of the LTP; however, she found no strong evidence of tide-induced degassing, first suggested by Green in reference 108. Possibilities remaining open include reaction of surface materials and/or gases with sunlight and luminescence caused by solar particles focused by the Earth's magnetic field (ref. 109).

In reference 110, Cameron and Gilheany present preliminary results of a more direct approach to lunar transient phenomena, Operation Moon Blink. This project uses an analog of the astronomical blink-microscope technique used to find motion of celestial objects; Tombaugh found the planet Pluto in 1930 with this method. The Moon Blink apparatus is designed to detect transient blue or red enhancements 2 percent greater than background. A confirmation network was set up to provide independent reports of any observed events. Twenty-five LTP were reported by Cameron and Gilheany, 16 of which were red spots, glows, or starlike flashes in or near Aristarchus (site of the 1963 observations). They found no good correlation between the sightings and either solar activity or the Moon's distance from the Earth. However, seven color events occurred during the 4.5-day period when the Moon was passing through the Earth's magnetic tail, tending to support the theory, previously mentioned in reference 109, that the Earth's magnetic field may focus solar particles on to

the Moon. Taking into account the historical survey of lunar transient phenomena by Burley and Middlehurst (ref. 111), Cameron and Gilheany believed that the tidal theory should also be retained as a working hypothesis. They pointed out the similarity of many of the phenomena—red glows and flashes—to ash-flow eruptions, which might leave little observable change on the Moon's surface, in contrast to eruptions of lava.

Some of the difficulty encountered by Cameron and others in correlating LTP with the Moon's orbit may be explained by the work of Tamrazyan (ref. 112), who studied the problem of whether terrestrial earthquakes (specifically in Transcaucasia) can be triggered by the Moon's gravity. Previous studies had found no simple correlation. However, Tamrazyan found that it is necessary to take into account simultaneously the position of the Moon with respect to the Earth *and* the Sun. By doing his, he discovered a significant increase in earthquakes at syzygy and the perigean third quarter of the Moon's orbit. This correlation is chiefly applicable to earthquakes with foci shallower than 400 kilometers. Tamrazyan's conclusion tends to strengthen the tidal theory of lunar degassing, since tectonic earthquakes are the result of movement along faults, and such movement in the Moon would presumably increase the chances of gas leakage.

Further progress in a previous study of historical records of about 400 lunar transient phenomena is reported by Middlehurst and Moore (ref. 113). By using most of the same records collected by Burley and Middlehurst (ref. 111) and by Cameron (ref. 106), they found that the LTP tended to be concentrated around the edges of maria (in agreement with Cameron), in ray craters, and in mare-floored craters such as Plato. An interesting negative finding was the absence of authenticated reports of LTP in the southeastern highlands. Middlehurst and Moore (ref. 113) conclude that the geographic distribution supports an internal cause, perhaps of volcanic nature.

The problem of correlating LTP was also attacked by Chapman (ref. 114), using a different approach. Chapman restricted his investigation to the crater Aristarchus, for which 27 sightings had been reported between 1963 and 1965, and attempted to find a correlation not only between the sightings and the Moon's distance, but also with the librations. He found that Aristarchus events tended to occur on the same day as tidal-gravity maxima and 1 day after the tidal-gravity minima. Concluding that there was a strong and predictable correlation, he suggested that Aristarchus be monitored closely on favorable times in 1970, when it should be more active.

It is apparent that the theory of an internal origin for lunar transient phenomena has been somewhat reinforced in the past 2 years, not only by the investigations just cited but also by Nash (ref. 115), who demonstrated that proton excitation was too inefficient to produce the observed effects. However, Palm (ref. 116) proposes that the latter difficulty might be cir-

cumvented if solar particles created color centers in lunar-surface materials, which might then produce either increased reflectance or photoluminescence.

Although not intended for that purpose, an investigation by Lipskii and Pospergelis (ref. 117) of lunar polarization throws possible light on the nature of LTP around Aristarchus. They used an electronic polarimeter to measure the Stokes parameters of polarization of various points on the Moon. On the night of June 31, 1964, the plane of polarization was rotated 12° from the polarization direction of adjacent areas; this phenomenon was not noticed on the other 13 nights on which measurements were made. Lipskii and Pospergelis interpreted that this effect was caused by a cloud of some scattering medium over the crater, possibly of volcanic origin. An interesting aspect of their method is that the discovery was made from only about 1 percent of the total light flux from the crater, which would not be possible with ordinary photometry.

A project of considerable potential value in determining the figure of the Moon is reported by Mills (ref. 118), who, with his colleagues, determined the absolute coordinates of 960 well-defined small craters. They used the stereoscopic method, in which the apparent positions of the chosen points are determined at greatly different librations, in order to determine the geometric or true figure of the Moon. A contour map prepared with the data from this study shows a 2-kilometer bulge just southeast of Alphonsus, which, they suggest, agrees with preliminary determinations of the lunar-gravity field from Lunar Orbiter I (although, Mills points out, there is no necessity for such agreement).

Infrared, Radio, and Radar Astronomy

Because they permit inferences as to the subsurface structure, infrared, radio, and radar investigations of the Moon continue to be of considerable importance, even after the ultra-high-resolution photographs returned by various lunar probes in 1966 and 1967.

A paper presented in 1966 at the Seventh International Space Science Symposium (COSPAR), but not published until 1967, describes infrared absorption studies by Markov and Khokhlova (ref. 119). They performed scans with the 125-centimeter Crimea telescope in the 0.8- to 13-micron region, much of which, however, is absorbed by the Earth's atmosphere. The most prominent feature of the Moon's absorption spectrum was a decided minimum at 3 to 4 microns (i.e., the lunar albedo is at a maximum in this region). They also found no evidence of limb darkening in the 0.8- to 13-micron range, confirming evidence from other methods that the surface is rough (dispersive) on this scale.

Saari and Shorthill in reference 120 summarize the results of an extensive program in which they mapped the visible face of the Moon in the far-infrared (10 to 12 micron) and visible (0.445 micron) regions. The

mapping was done with a focal-plane scanner, used with the 60-inch Mount Wilson and 74-inch Helwan Observatory telescopes, at 23 phases through a lunation. The results are presented as a series of isophotic and isothermal contour maps. These maps demonstrate the now-familiar correlation of thermal anomalies and high-albedo features, the optically bright areas being generally cooler on the illuminated disk (the reverse is true on the dark disk).

The thermal behavior of lunar-surface features is further clarified by the 8- to 14-micron observations of Salisbury and Hunt (ref. 121) in the Tycho region. Using an infrared imaging system which permitted precise location of thermal anomalies, they demonstrated that the well-known thermal anomaly is confined to Tycho and the immediate surroundings. Furthermore, they found that the crater walls that had been facing the Sun just before sunset stayed warmer than those that had been facing away, thus indicating that the anomaly is primarily solar rather than internal.

Another infrared reconnaissance in the 8- to 14-micron region, performed in 1964, is reported by Wildey et al. in reference 122. These investigators used a 24-inch telescope during July and August 1964, although only a few nights permitted good observations. They present a catalog of lunar nighttime thermal anomalies, all on the eastern half of the Moon (which was in the third quarter). Two features stand out from their data, which were also used to construct an 8- to 14-micron brightness-temperature map: an enhanced brightness for Mare Crisium and an absence of brightness temperature between highlands and maria. Further interpretation of these results are to be published.

The well-known Russian radio astronomer, V. S. Troitskii, with his colleagues V. D. Krotikov and N. M. Tseitlin (ref. 123), present results of their measurements of the Moon in the 30- to 60-centimeter wavelengths. Earlier studies had indicated that the apparent temperature rises to a depth corresponding to the penetration, or depth of emission, of 30-centimeter radiation. These observations indicate that, in the 30- to 60-centimeter band, the temperature is constant and independent of wavelength and averages 225° K.

Lunar thermal-radio emission can also be used to infer the electrical properties and roughness of the near-surface layer, as was done by Losovskii (ref. 124), who measured the polarization of 0.8-centimeter radio emission with a 22-meter radio telescope, finding a maximum polarization value of 4 ± 1 percent. Analysis of the data indicates a dielectric constant of 1.5 ± 0.2 and considerable diffuse scattering (caused by roughness) for waves shorter than 1 centimeter.

As pointed out by Eshleman in reference 125, a valuable review of radar astronomy, the problem of loss of echo strength with distance can be overcome by the bistatic technique, in which either the transmitter or receiver

is carried on a spacecraft to the vicinity of the body under study, the complementary equipment being on Earth. This technique was actually carried out for the first time on October 12, 1966, as reported by Tyler et al. (ref. 126) with Lunar Orbiter I. The returned signal was difficult to explain in terms of slope, roughness, or shadowing; Tyler et al. found instead that variations in reflectivity were probably responsible for the observed time-frequency variations. In physical terms, this may be the expression of patches of bare rock or dense soil. This result, while hardly surprising, demonstrates the potential value of bistatic radar for the mapping of planetary surfaces such as Venus.

The complex subject of interpretation and physical meaning of optical, thermal, radio, and radar observations of the Moon is reviewed by Cook in reference 127. This report, which is extensively referenced, concludes that there are no unique interpretations of the available data, although some general conclusions can be reached.

Interpretive, Experimental, and Theoretical Studies

It is axiomatic in many scientific fields that acquisition of information takes little time compared with the time needed to interpret the information. Space science is a prime example of this; the 1964–1965 Ranger probes sent back their pictures in a few minutes, but interpretation of these pictures was still continuing in 1967. Comparable interpretive studies were carried out for the other lunar probes, both Russian and American.

There are two comprehensive papers (refs. 89 and 128) on the geologic significance of the pictures returned by the Ranger, Surveyor, Lunar Orbiter, and Luna spacecraft. McCauley (ref. 89) covers much material that has already been summarized herein, and which will therefore not be repeated. However, his review contains two significant new interpretations. First, he proposes that the Orientale Basin, first photographed from directly overhead by Lunar Orbiter IV, is the youngest of the circular mare basins and that it was formed by the impact of an asteroid-sized body. The peculiar blanket of material surrounding the basin was, McCauley suggests, deposited by a base surge, analogous to the cloud of material that comes from the bottom of the cloud over an explosion crater. The concentric scarps, which are the most prominent feature of the Orientale Basin, were formed either by collapse or slumping shortly after the crater was excavated. A second contribution of McCauley's paper is also based on the Lunar Orbiter IV Mare Orientale photographs (figs. 33 and 34). There are two craters, one about 55 kilometers and the other about 35 kilometers in diameter, on the floor of the inner Orientale Basin. The larger of these is essentially similar to Copernicus, Eratosthenes, and other ray craters generally considered to be of impact origin, possessing terraced inner walls, humocky ejecta blankets, and a halo of secondary craters. The smaller crater has a

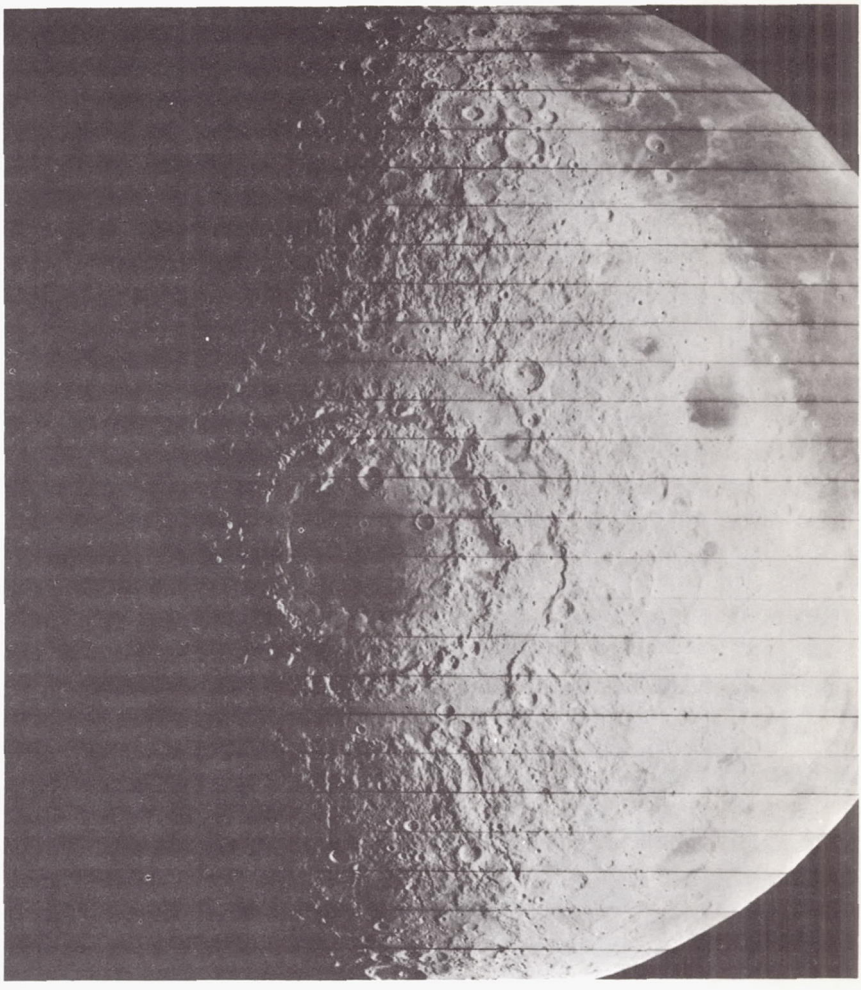


Figure 33.—Lunar Orbiter IV view of Mare Orientale, on western limb of Moon. This feature is only partly visible from Earth. It is believed to be the youngest of the large maria, which may have resembled Mare Orientale at an early stage in their evolution.

relatively smooth rim and none of the topographic features listed for the other crater, and it is floored by mare material. McCauley points out that both craters are youthful post-Orientale features and that the differences cannot therefore be explained by saying that the smaller crater is an eroded version of the larger. He suggests that the differences may reflect contrasting origins; the smaller crater may actually be volcanic. The interpretation,

333-240 O—69——24



Figure 34.—High-resolution Lunar Orbiter IV view of eastern part of Mare Orientale (north at top). In addition to structural details shown, this photograph illustrates differences between craters believed to be of impact origin (left edge) and volcanic origin (lower center).

if correct, is extremely important for two reasons. First, this pair of craters would furnish a type locality for comparison of impact and volcanic craters (assuming, of course, that the larger one is an impact crater). Second, it implies that there are many more large volcanic craters than previously recognized. Until the Lunar Orbiter IV pictures, it had been widely believed (ref. 129) that all large lunar craters were essentially similar to Copernicus, if allowance were made for subsequent mare flooding, isostatic uplift, impact erosion, and other postcrater events. McCauley's interpretation indicates that this may not be true.

The other paper summarizing results from the first three Lunar Orbiters, by Trask and Rowan (ref. 128), put more stress on mass wasting as a lunar geomorphic process. They call particular attention to the parallel ridges noticed on many mare slopes, which appear to follow contour lines, proposing that these, and the convex terraces seen at the base of many slopes, are the result of downslope movement of loose debris.

The fragmental nature of the mare material has been inferred for some time, especially since the availability of high-resolution photographs of the maria. However, there has been considerable variation among estimates of the thickness of this fragmental layer. A major contribution to this problem was made by Oberbeck and Quaide (ref. 130), who estimate the thickness of the fragmental layer in Oceanus Procellarum. They produced experimental craters in a variety of target materials and demonstrated that the shape of the craters depends largely on whether the material is completely fragmental or consists of upper fragmental material underlain by a solid layer. Craters in completely fragmental material are simple holes; craters that just reach a solid layer have flat floors, and those that penetrate the solid layer have one or more concentric terraces (fig. 35). Oberbeck and Quaide tabulated the number of craters with different shapes in the parts of Oceanus Procellarum photographed by various lunar probes, and by combining this tabulation with the experimental data, they estimated the areal extent of fragmental layers of different thickness. They found that 85 percent of the area studied has a fragmental layer between 5 and 15 meters thick, with a modal thickness of from 5 to 6 meters and an average thickness of 8 to 9 meters. Furthermore, they found craters with as many as three terraces, implying a mare structure with three alternating layers of hard rock and fragmental debris in the upper 100 meters.

These estimates are not only important for engineering purposes but they have interesting genetic implications. In particular, they indicate that there have been several periods of formation of mare material—a conclusion arrived at independently by geologists who have mapped the maria, such as Titley (ref. 101), whose Mare Humorum map has been discussed previously. Another implication, from the absence of concentric-terrace craters in the highlands, is that the highlands are underlain either by a very

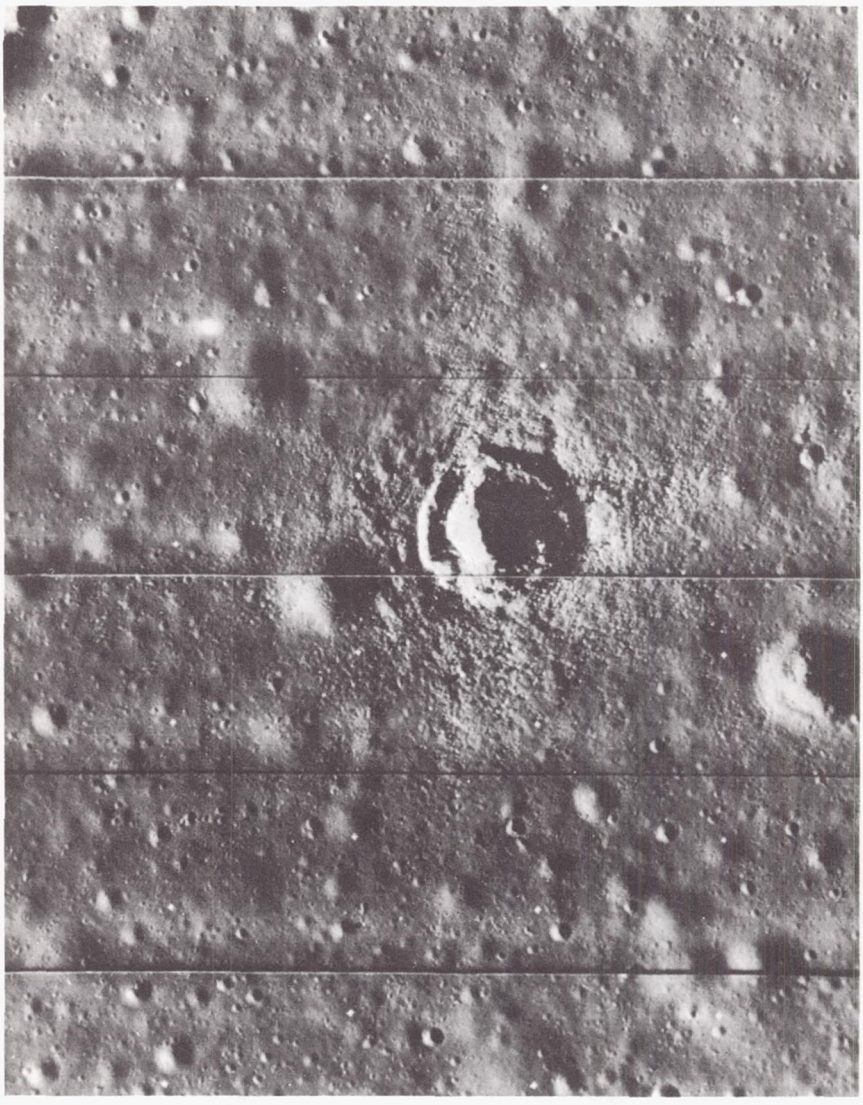


Figure 35.—Lunar Orbiter III high-resolution photograph of part of Oceanus Procellarum. Area shown measures about 3600 by 2800 feet. The well-preserved impact crater is about 500 feet in diameter. Its shape has been changed by peripheral slumping after formation.

thick fragmental layer or by none at all. The latter possibility seems unlikely, from the greater age of the highlands and from radar and infrared studies.

The Lunar Orbiter photographs, taken to find suitable Apollo landing sites, were not studied scientifically as rapidly as were the more science-oriented Ranger or Surveyor photographs, to which large teams of investigators were assigned. Consequently, geologic interpretation of the Orbiter photographs has been attempted by a large number of individuals and organizations. One of the first such attempts published in 1967 was by O'Keefe et al. (ref. 131), who studied the Lunar Orbiter I photographs of the Flamsteed Ring (figs. 36 and 37), or the Von Kármán crater as it has also been named. The Flamsteed Ring appears to be an extremely old, premare crater, of which only a few remnants of the former rim remain.

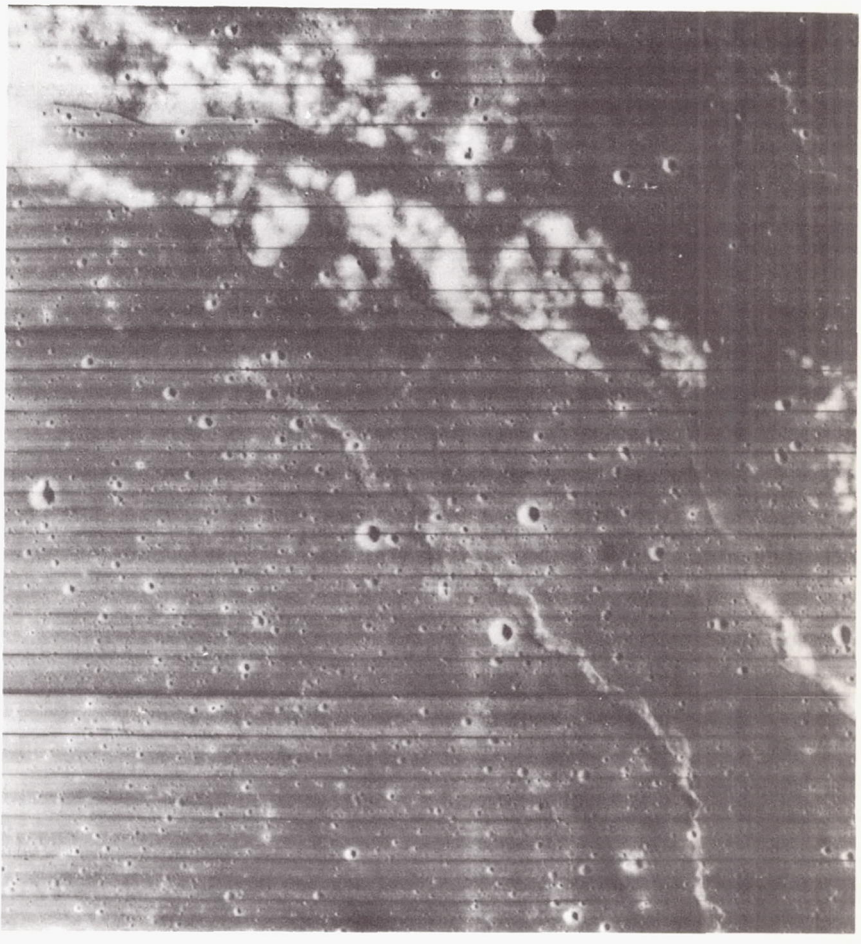


Figure 36.—Moderate-resolution photograph of Flamsteed Ring taken by Lunar Orbiter I. Only northeastern part of ring is shown. Area is about 32 by 38 kilometers. North at top.

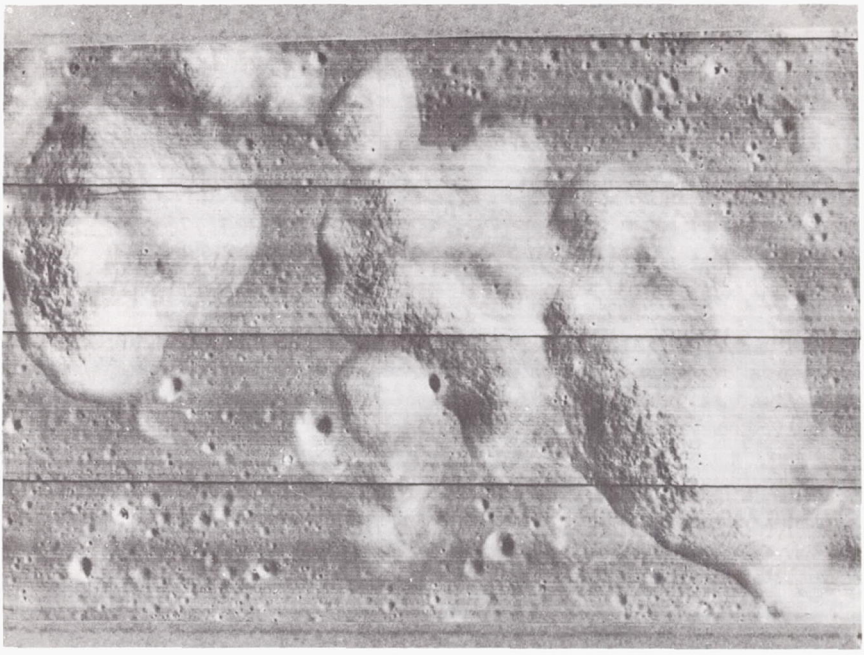


Figure 37.—**Enlarged portion of figure 36, emphasizing morphology of Flamsteed Ring. Of particular interest are convex slopes, low crater density on hills, and "patterned ground."**

However, O'Keefe et al. noticed that the rim material actually overlaps some mare craters, has a convex lower slope, and is remarkably crater free compared with the adjacent mare areas. They therefore suggest that it is a postmare extrusion of siliceous lava, such as andesite, dacite, or rhyolite. Fielder (ref. 132) published the same theory shortly after.

The theory that this apparently ancient crater is actually a young volcanic feature attracted some attention because of its novelty. Goles and Taylor (ref. 133) argue that the viscosity of the supposed lava could not reliably be used to infer its composition; Milton (ref. 134) suggests that the convex slope might be the result of seismic-induced landslides. Hartmann (ref. 135) also differs with the lava interpretation, pointing out that similar convex slopes were found on a number of other features whose volcanic nature seemed doubtful. (One of these, interestingly, was the crater Gambart, for which McCauley (ref. 98) had proposed a possible volcanic origin because of its similarity to the 35-kilometer-diameter crater in Mare Orientale, previously discussed.) The theory proposed by O'Keefe et al. may thus be in doubt; however, it demonstrates that resolution limits on Earth-based observation may limit the accuracy of superposition determinations;

previous studies of the Flamsteed Ring (ref. 136) had indicated that the mare material was later than the ring material, which the Lunar Orbiter photographs demonstrated to be untrue, at least locally.

Fulmer and Roberts (ref. 137) arrived at a somewhat similar conclusion to that of O'Keefe et al. in a study of the Lunar Orbiter photographs. They were primarily concerned with surface lineaments, which they found to be remarkably widespread, even in unconsolidated material. However, they also concluded that some craters, such as Gambart, might be the extrusive expression of ring dikes.

Another interpretation of the Lunar Orbiter photographs was published by Rackham (ref. 138), who studied a dark-halo crater located on the south flank of Copernicus. He suggests that the reason for the dark color of ejecta from the crater was that the impact which presumably formed it penetrated the light-colored Copernicus ejecta to bring up dark-colored mare material. Extending this to other craters, he points out that a similar mechanism might be applied to the large ray craters such as Copernicus itself, which might have been formed in an area of shallow mare material, the light-colored ejecta being in fact continental material excavated by the impact. Rackham also calls attention to the apparent stratum in the breached central peak of Copernicus.

A longtime advocate of lunar vulcanism as a crater-forming process, Green (ref. 139) published a survey of the evidence for this theory, with a discussion of the implications of lunar vulcanism for manned exploration of the Moon. He presents a discussion of caldera-forming processes on the Earth and pointed out how lunar conditions might affect them. Finally, he lists the economic advantages a primarily volcanic lunar terrain would have over an impact terrain, including the possible availability of extractable water, sulfur, and other materials, and even geothermal energy.

The famous controversy about lunar dust was somewhat muted by the confirmation that the surface material had substantial bearing strength, as shown by the behavior of Luna 9 and Surveyor I. However, the main features of the dust theory (originally developed by Gold on the basis of radar returns and thermal data) were in fact proven by the early soft-landing probes, in that the lunar soil was found to consist of unconsolidated, slightly cohesive material, to a depth of at least a meter in some places. Hapke (ref. 140), in a series of experiments, tried to demonstrate that virtually all the small terrain characteristics shown by the lunar-probe photographs could be duplicated by explosions or impacts in fine-grained Portland-cement powder. He produced a series of photographs with remarkable similarities to the lunar terrain, including the rocklike objects, which were compressed clots of dust. Furthermore, he pointed out that the optical, thermal, and radar properties of the Moon are nearly universal (this excludes the known anomalies, such as Tycho), indicating that if the maria are largely dust, the

highlands must also be largely covered with the same type of material. This implies an external origin; he favors specifically meteoritic impact.

The question of the structure and physical properties of the lunar soil, specifically of the maria, was also investigated by Jaffe (ref. 141). He combined the pre-Surveyor data with those from Surveyor I to arrive at a composite mare-surface model, with the following major features: A particulate nature, most particles being 100 microns or smaller; density ranging from 0.6 to 0.7 g/cm^3 at the surface to 2 to 3 g/cm^3 at depths of 1 to 10 meters; failure primarily by local shear; static bearing strength about 4×10^5 dynes/cm^2 for a 25-centimeter bearing diameter, increasing with depth; internal friction angle about 55°; and cohesion about 10^3 dynes/cm^2.

Jaffe's estimate for static bearing strength was roughly confirmed by a novel technique applied by Filice (ref. 142). Filice measured, on a Lunar Orbiter II photograph, the track length and width, and other pertinent quantities, of the trail left on the wall of the crater Sabine D by a 13-meter boulder that had rolled down the side of the crater. He found the effective bearing strength to be 4×10^6 dynes/cm^2, in rough agreement with the extrapolation of Jaffe's figure. This estimate is important because it applies to a distance of 650 meters, rather than to just one spot as do the estimates from Surveyor footpad behavior.

The question of the density of the upper layer of lunar soil was experimentally approached by Salisbury and Adler (ref. 143), who conducted a series of vacuum-chamber simulations. They concluded that the uppermost fine-grained surface layer probably has a density between about 0.3 and 1.5 g/cm^3, with grain shape having a major influence on the value.

Smith (ref. 144) studied the size-frequency distribution of boulders around the Luna 9 landing site, constructing a histogram to show the values derived. The diagram shows a sharp peak in the 2- to 5-centimeter range, differing somewhat from comparable Russian estimates.

The problem of determining the Moon's chemical composition is a classic one, which had never been approached directly until the delivery of analytical instruments to the vicinity of the Moon by Luna X and to the surface by Surveyor V. However, O'Keefe and Scott (ref. 145) developed a way to compare the radar reflectivity properties of the lunar surface with physical properties of soil to set limits to the chemical composition. This comparison was made by calculating soil porosity from the Surveyor I and III data and from this calculation the grain dielectric constant was found by means of the Böttcher formula which relates bulk and grain dielectric constant for granular materials. The most likely value for the grain dielectric constant was 4.3, which is inconsistent with chondritic meteorities, but consistent with either vesicular basalt or acidic rocks.

The albedo and color of lunar rocks could be used to infer chemical composition, according to Adams (ref. 146), who made a series of optical meas-

urements of various rock powders (ref. 147). Adams concludes that the main albedo difference between maria and terrae might be due to grain-size variations, but that there are also probably compositional variations within the maria. He found a basic or ultrabasic composition to best satisfy the optical properties of the maria and probably the highlands as well. Applying these findings to the soil disturbed by the Surveyor I landing pad, Filice (ref. 148) found a basic or ultrabasic composition most likely for this spot. Filice further concludes that albedo differences, including the light mare surface previously discussed, are probably largely the result of grain-size differences produced by micrometeorite bombardment.

Hartmann published a series of papers (refs. 149 to 151) presenting new studies of lunar and terrestrial craters. Crater counts in Alphonsus, from the Ranger IX photographs, suggest either accelerated crater destruction on the walls by mass wasting or an internal origin for some of the craters on the crater floor. Hartmann found it difficult to decide which of these was correct, but cited considerable evidence favoring the second; i.e., indicating an internal origin for many of the floor craters. He also suggests that the central ridge is an old, partially flooded horst (up-faulted block). In a second crater-count study, Hartmann found that there is similarity between the size-frequency slopes of the continental areas studied, the Alphonsus wall, and a mare area. If the cratering rate has been constant, the maria would be one-thirtieth of the age of the highlands, although Hartmann argues elsewhere that the early cratering rate was higher. In a third paper, Hartmann compares lunar craters with the Kapoho pumice cinder field in Hawaii that was repeatedly impacted by volcanic ejecta during the 1960 Kilauea eruption. He found that fields of fragments from meteoritic volcanic-ejecta impact would have about the same size-frequency distribution and that close examination would be necessary to distinguish the meteoritic from volcanic blocks. He comments on the close similarity in appearance between the volcanic field and the lunar terrain photographed by spacecraft. Most of the impact craters at Kapoho were formed by solid blocks, rather than unconsolidated masses, but the blocks were frequently buried out of sight. Subsidence craters, formed by drainage of pumice into cavities, were numerous.

It has been believed for several years that the darkening of lunar rays is the result of sputtering; i.e., the selective removal of oxygen atoms by the protons and alpha particles of the solar wind. However, an illuminating series of experiments by Nash (ref. 152), in which silicate rock powders were bombarded with 2- to 16-keV protons, throws considerable doubt on this theory. Nash found that the darkening was not only dose dependent but also rate dependent, and that the cause of the darkening was not sputtering, but more probably either carbon from decomposed hydrocarbons (such as vacuum-pump oil) or metal from the ion source. He concludes that earlier

experiments indicating darkening by sputtering were probably affected by contamination. In this connection, Nash points out that contamination darkening, either indirectly from lunar hydrocarbons or directly from the carbon fraction of the solar wind, appear quite possible, and that solar-wind darkening may not be effective at all, since the lunar photometric function has been shown to be not unique.

KenKnight et al. (ref. 153), who had previously conducted extensive experiments to investigate the cause of lunar-surface darkening, confirm the probable importance of carbon and hydrocarbons in this phenomenon. On the other hand, they present evidence that solar-wind bombardment probably has had considerable effect on the optical properties of the lunar surface, in particular on the color, whose uniformity may be due to the long-distance flight and redeposition of sputtered atoms. They estimate the erosion rate due to sputtering as 0.1 to 0.2 Å/year.

A third investigation of the sputtering problem was undertaken by Greer and Hapke (ref. 154). They confirm that contamination of the bombarded powders by metal and carbon could occur; however, they found inconsistencies in the experimental results which they believe preclude dismissal of all reports of ion darkening as due to contamination. They stressed the danger of prematurely extrapolating experimental results to predictions for the lunar surface.

The interaction of solar and cosmic particles with the lunar surface depends on the energy of the particles, among other things. Zeller and Ronca (ref. 155) simulated the bombardment of various minerals with protons and deutrons in the 1-MeV range (contrasted with the keV range of the sputtering experiments just described). They demonstrated that nuclear particles with such energies might be absorbed in the target material, rather than bouncing off, as would happen in sputtering; i.e., high-energy particles are additive rather than subtractive. Since most solar-wind particles are protons (hydrogen nuclei), the net result would be hydration, or space weathering. They suggest that chemical zonation similar to terrestrial-soil horizons could thus be formed, with the degree of hydration decreasing downward. Its depth would be on the order of a few millimeters. The importance of the Zeller-Ronca study is emphasized by the findings of Ness et al. (ref. 93) from Explorer XXXV that the solar wind probably impacts the lunar surface directly because of the absence of a lunar magnetic field.

It has been hoped that ultraviolet spectral surveys of the Moon, which would be possible outside the Earth's atmosphere, would provide lunar compositional information. However, Greenman et al. (ref. 156) conducted experiments to measure the ultraviolet reflectance of possible lunar-rock types and found little difference in the reflectance of different rocks. They conclude that compositional differences would have to be sought in the fine structure of the ultraviolet spectra if they exist.

Polarimetry of the Moon, a classic area of study, is still a fruitful one. Egan (ref. 157) demonstrates, with measurements made by a large device capable of registering the polarimetric response of samples up to 3.5 inches in diameter, that the polarimetric properties of the Moon could be duplicated by volcanic ash coated with fine grains of the same material.

Since many geologic processes, such as seismic activity, vulcanism, and perhaps internal convection currents, are driven by thermal energy, the study of a planetary body's thermal history is essentially a study of its internal geologic history in general. Several papers on the Moon's thermal history were published in 1967, including those discussed in the following paragraphs.

Fricker, Reynolds, and Summers (ref. 158) constructed several theoretical thermal models of the Moon, based on their earlier work on the Earth's thermal history. Previous studies, such as those of Urey, MacDonald, and Lowman (see bibliography of ref. 158), had considered the thermal regime of the Moon to the beginning of melting; the work of Fricker et al. took melting into account as well. Calculations by Fricker et al. indicate that even if the Moon had been initially cold, long-lived isotopes would eventually raise the temperature to the melting point. After partial melting, the thermal gradient would flatten and the radioactive materials would be segregated in the liquid fraction. The melting zone would gradually work its way outward, producing extensive volcanic activity peaking between 1 and 3 billion years ago. Their calculations indicate that the Moon should be largely solid now.

Miyamoto in reference 159 follows a different line of reasoning in studying the thermal evolution of the Moon (and Mars). He interprets the surface physiography of the Moon as indicating mantle convection currents corresponding to harmonics of the second and higher orders, as has been done for the Earth by Runcorn (bibliography of ref. 159). The circular maria and mare-floored craters would be the locus of converging currents.

Two other Japanese scientists, Iriyama and Shimazu (ref. 160), approached the problem of the Moon's thermal history by performing a series of numerical calculations with two different initial temperatures and a chondritic composition. Their treatment is unique, however, in taking into account the heat liberated by formation of the Moon's hypothetical core. From the calculations, they derive a series of curves showing variation of the surface heat flow through geologic time, for sudden and for gradual crust formation, as well as for different uranium concentrations.

Still another series of thermal calculations was carried out by Ornatskaya and Al'ber (ref. 161); following, in general, the methods and assumptions of earlier workers in this field, such as Levin, MacDonald, and Urey (bibliography of ref. 158), they solved the thermal-conductance equations for varying distributions of the radioactive elements in the Moon. Their

approach was somewhat similar to that of Fricker et al. (ref. 158), previously described, and some of their calculated thermal gradients are very similar. Ornatskaya and Al'ber found that the Moon would have been almost entirely melted at an early stage if the radioactive-element concentration had been high; with the lowest concentration, the Moon would not have been molten closer to the surface than 400 to 600 kilometers. An interesting result of their calculations is that the greater the concentration of the radioactive heat-producing elements, the more the Moon would have cooled by now. The reason for this is that with a high concentration of radioactive elements, the melting would have begun at a very early stage, providing more cooling time.

The ultimate question to be answered about the Moon is, of course, its origin. There has been an interesting tendency in recent years for theories of the Moon's origin to diverge, in contrast with those for the origin of the solar system, most of which are in substantial agreement on major points. (See ref. 162.) The main disagreement about the Moon centers on whether it has some close, genetic relation to the Earth or is a captured body from somewhere else in the solar system. The chief evidence favoring the capture theory is the apparent difference in bulk composition (inferred from the density difference) between the Earth and the Moon; the significance of this difference has been underlined by the growing body of evidence ruling out the phase-change theory proposed for the formation of the Earth's core.

Three papers published in 1967 all agree that the Moon was formed somewhere in the Earth's vicinity. References 163 and 164 are based on the fact that the angular momentum of the Earth-Moon system appears to conform to the relationship between angular momentum and masses of the planets, pointed out by MacDonald in reference 165.

The third paper by Ruskol (ref. 166) is an extension of his earlier work on the evolution of the Earth-Moon system. Ruskol concludes that the primeval lunar orbit was much closer to the Earth than is the present one, but always inclined to the Earth's equator. He finds no evidence, in the tidal variations of the lunar orbit, to support the capture theory, favoring instead an origin for the Moon in the vicinity of the Earth.

Summary of 1967 Studies of the Moon

The most spectacular scientific achievement in the study of the Moon during 1967 was without much doubt the chemical analysis performed by the experiments on Surveyor V. These are the first lunar-contact experiments of their kind ever performed, and as such are of historic significance.

From a broader viewpoint, it would seem that the greatest progress has been made in clarifying the nature and extent of volcanic processes on the Moon. It is generally (though not universally) agreed that the maria are at least partly basalt, but of volcanic origin whatever their bulk composition.

Their volcanic nature is emphasized by the high-resolution photographs of many minor features, in particular the dome fields and sinuous rilles, which appear to have some connection with volcanic processes. The role of volcanism in formation of the large ray craters remains disputed, the dispute being heightened by the discovery of features that have almost certainly resulted from fluid flow (the ropy textures in the floor of Tycho are the best example).

On the other hand, the high-resolution views of Mare Orientale have tied together the mare basins and the ray craters, and many believe that an impact origin of the Moon (with or without subsequent volcanism) is most probable. The curious paradox that more and more impact structures are being found on the Earth while more and more volcanic structures are found on the Moon continues; it is to be hoped that the mean to which both schools of thought are trending is the truth.

IMPACT CRATERING AND SHOCK METAMORPHISM

Considerable progress was made during 1967 in field and laboratory investigations of terrestrial craters. Interest in the study of meteorite impact craters and their associated shocked rocks continues to grow.

As in previous years, the most extensive studies have been carried out in Canada, where some 16 probable impact craters are now recognized. In 1967, a report on Lac Couture was issued by the Dominion Observatory in Ottawa (ref. 167). Drilling of three more holes at the Brent structure, under the supervision of M. R. Dence, provided additional core and subsurface data which add to the ranking of this crater as one of the most completely investigated impact sites in the world. Of particular interest was the K/Ar dating by J. B. Hartung of some highly shocked granite gneiss breccia fragments collected near the crater base. An age of 460 ± 10 million years obtained by this method corresponds reasonably well with the estimate of an early Ordovician age for Brent on the basis of sedimentary rocks of this period within the crater. Currie and Shafiqullah present in reference 168 chemical and petrographic evidence of a direct relation between the Brent structure and rock types associated with carbonatites and claim therefore that Brent has a purely endogenetic origin. Work on the West Hawk Lake structure involving petrographic and instrumental analyses of drill core from the breccia and rupture zones is reported by Short in reference 169. This structure, similar to Brent in size, shows in comparison somewhat lower and more varied shock damage owing to the presence of fine-grained quartz-mica schists and amphibole-rich rocks in the target material.

The field project to map and sample the Manicouagan structure in eastern Quebec, before it is partially inundated by backwaters from the world's third largest dam, was completed by the Quebec Geological Survey under the

direction of J. G. Murtaugh. Although the question of origin is still hotly debated, Murtaugh and others now believe that this structure, the largest of its kind known on Earth, is best explained as the consequence of a meteorite impact. A paleomagnetic study of thermoremanent magnetization of flow units from the Manicouagan group indicates that they have formed during a period of 10 000 years or less—a result not inconsistent with an impact origin in that it suggests rapid postimpact intrusion following the event, as may be expected from sudden off-loading. (See ref. 170.)

With the publication of a paper by French (ref. 171), describing shock effects in the Onaping tuff of the Sudbury, Ontario, structure, interest was greatly enlarged in the possibility of a meteorite impact origin of this famous nickel-copper ore locality, first proposed by Dietz in reference 172. Bray and staff (ref. 173) have now found over 50 shatter-cone localities around the Sudbury basin, and geologists there have also discovered shock features in the older rim units outside the irruptive. Because Sudbury is the first suspected impact structure to have major economic value (it has produced over $9 billion in ores since 1880), the search for further field evidence of shock and other features attributed to cratering is now being intensified as more geologists are beginning to consider seriously the impact hypothesis as a plausible explanation for other structures.

In the spring of 1967, a prospector reported finding some unusual rock fracturing in rocks along the St. Lawrence river. These features were identified by J. G. Murtaugh as shatter cones, thus marking the first time that these unique features, previously found only at presumed impact-crater sites, were initially responsible for calling attention to another possible impact structure. The structure, provisionally called La Malbaie after a town on the St. Lawrence some 110 kilometers northeast of Quebec City, was visited by P. B. Robertson (ref. 174) and M. R. Dence of the Dominion Observatory. They collected samples of mixed breccia containing abundant evidence of shock damage. A diameter of 37 kilometers, provisionally assigned to La Malbaie, makes this the third largest of the Canadian structures of the cryptoexplosion class (ref. 174). It is now inferred to be an impact crater of the complex type (exhibiting a central uplift) that strongly resembles Manicouagan.

Following identification in 1966 of a buried structure (Steen River) in northwest Alberta as a probable astrobleme because of the occurrence of shocked rocks in drill core, Canadian oil companies and other sources have reported as many as six other structures which possess similar characteristics. Most were found by geophysical methods and several have been drilled. These structures are now undergoing further examination in search of shock criteria which would place them in the putative impact-crater category.

In the United States, major field investigations of the Flynn Creek, Tennessee, and Sierra Madera, Texas, structures were completed in 1967

by the U.S. Geological Survey. Six shallow drill holes, emplaced at Flynn Creek, helped to confirm the presence of a central peak and the occurrence of relict mixed breccias (ref. 175). The map prepared by D. J. Roddy (ref. 175) emphasizes the style of deformation at Flynn Creek as being one of intense folding and faulting that dies out abruptly with depth. D. J. Roddy (see ref. 175) attributes the formation of Flynn Creek to impact by a cometary body rather than a meteorite. At Sierra Madera, Wilshire et al. (ref. 176) have mapped the central uplift in great detail, demonstrating the existence of a stratigraphic uplift of some 6400 meters associated with steep to overturned, complexly faulted beds in the central zone. Within this central zone, the Permian rocks appear to have moved both inward and upward to reach their present position. The uplift, now visible as rugged hills, is surrounded by a depressed ring of downdropped Cretaceous rocks and an outer zone of structurally higher rocks of similar age. The overall deformation at Sierra Madera dies out rapidly with depth, and this fact, coupled with the presence of possible shock-metamorphic features in mixed breccias, leads Wilshire et al. to favor impact as the most likely mode of origin.

Three papers were presented in 1967 by Seeger dealing with the Jeptha Knob structure, Kentucky. (See refs. 177 to 179.) A magnetic survey showed that there is probably no basement counterpart to the surface feature, and a gravity survey revealed a +1 milligal anomaly. The scant drilling information available indicates that the deformation is shallow and decreases with depth. Multiple hypotheses were used to eliminate any endogenetic origin, leaving hypervelocity impact by a meteorite or comet as the most probable explanation.

A gravity survey at the 6-kilometer-wide Serpent Mound, Ohio, structure indicates that density reductions are confined to the near surface and apparently do not extend into the basin or beyond the limits of the structural disturbance (ref. 180). In lieu of drilling, these survey data provide a subsurface picture suggesting a breccia lens which, together with the shatter cones and coesite reported in surface samples, best fits the impact crater model.

The group under Prof. W. v. Engelhardt at the University of Tübingen published several important papers in 1967 describing various aspects of their continuing study of the Ries structure in Bavaria. Förstner in reference 181 reports results of a detailed examination of suevite recovered from two drill holes at the Ries. His description of variations in particle-size distribution helps to characterize the mode of "sedimentation" associated with the fallback process. Stöffler in reference 182 carefully documents shock-induced changes observed in plagioclase in breccia fragments derived from the crystalline basement rocks beneath the Ries. He concludes that isotropization of these minerals takes place within the 300- to 500-kilobar pressure range, whereas selective melting occurs between 500 and 650

kilobars and total melting results at higher pressures. Engelhardt et al. in reference 183 present evidence for distinguishing between diaplectic glasses (those developed by solid-state isotropization) and glasses resulting from actual melting during the Ries cratering event. The diaplectic glasses have higher densities and indices of refraction than do normal glasses and may also preserve certain original or shock-induced internal structures. Engelhardt also reports in reference 184 chemical analyses of glass bombs from the Ries and elsewhere and identifies the bombs as shock-melted granitic basement rocks whose textures vary with cooling rate, extent of transformation, and degree of recrystallization. Engelhardt et al. present new evidence for a meteorite-impact origin of the Steinheim basin west of the Ries in reference 185; this includes discovery of planar features and other signs of shock damage in minerals from breccia fragments in drill core. Johnson and Vand report an analysis of topographic features at the Ries using a computerized Fourier data-smoothing technique which led to a mathematical reconstruction of the original crater shape (ref. 186). Their results indicate that one or more secondary rims developed at the Ries. They also state that their method permits calculation of the location of the center of impact and the direction of meteorite entry.

In 1967, Kraut first informed other investigators of a structure in central France containing crystalline rocks which show shock-damage effects very similar to those observed in the Ries (see ref. 187). Suevite-like breccias occur in outcrops near the towns of Rochechouart and Chassenon, west of Limoges. Neither the shape nor the diameter of the structure has been determined, but known outcrops range up to 12 kilometers apart. Although the schists and granite gneisses underlying the structure are geographically near volcanic terrane (including the Auvergne), there is no evident interrelation and the structure appears to be an ancient astrobleme.

Milton and Brett of the U.S. Geological Survey spent much of 1967 mapping the Gosses Bluff structure in central Australia (refs. 188 and 189). Samples from breccia and central peak outcrops there show profusely developed planar features in quartz and other signs of strong shock damage. The character of deformation in the ring of hills making up the central peak at Gosses Bluff is generally similar to that observed at Sierra Madera. Fractured plates of steep dipping to vertical bedrock units appear to have slid along radial and concentric faults. These fault-bounded plates have moved inward and upward from initially flat-lying positions. Brecciation has accompanied the movements which, in extreme cases, has led to blocks and plates being rotated and/or overturned. Drilling shows that this intense deformation diminishes with depth. Shatter cones abound at Gosses Bluff. A closely related feature there, called shatter fracturing, consists of sets of striated planar surfaces which intersect at nearly rhombohedral angles. There are all gradations between these resulting rhombohedral blocks and shatter cones.

Taylor reports in reference 190 that glass collected from the area of the Henbury, Australia, crater has a chemical composition which, after iron due to meteorite contamination is removed, matches the composition of certain graywackes exposed within the largest of the Henbury craters.

Bunch and Cassidy have found convincing evidence of a meteorite impact origin for the Monturaqui crater in Chile (ref. 191). Microprobe analysis confirms the presence of metallic nickel-iron as inclusions within the impactite glasses. Crystalline fragments in these glasses show planar features in quartz and feldspars, as well as thetomorphs of these minerals which have been formed by shock.

In the last few years the subject of meteorite-impact cratering has become closely entwined with that of the new field of shock metamorphism. Review articles on both topics appeared during 1967. Explosion craters, embracing both nuclear and impact craters, and astroblemes, i.e., eroded meteorite craters, are considered by Short in references 192 and 193. A review article on shock processes in geology appeared in late 1966 (ref. 194). Two important articles on shock metamorphism or impact metamorphism brought this subject to the attention of the general scientific community. (See refs. 195 and 196.) Barringer updates his earlier versions of a catalog of the world's meteorite craters in reference 197.

Several significant papers dealing with experiments in cratering were published in 1967. Diehl and Jones describe their detailed study of the Snowball chemical explosion crater, a 500-ton chemical-explosive surface burst over soil and clay sediments in the prairie terrain of Alberta, Canada (ref. 198). This explosion produced a shallow crater approximately 100 meters (apparent lip) in diameter. Of particular interest was the formation of a well-defined, strongly deformed central peak. Distinctive fracture patterns, consisting of circumferential and radial fractures, developed beyond the lip.

A nuclear explosion, code named "Palanquin," which formed a crater by a gas-erosion mechanism, was investigated by Hansen (ref. 199). Its importance lies in its similarity—except for the rapid development—to certain types of volcanic maar craters with respect to general mode of origin.

Baëta and Ashbee describe certain types of fracture in quartz produced by compression experiments at atmospheric pressure but at temperatures from 550° to 700° C. (See ref. 200.) Currie in unpublished works reports that similar features form in plagioclase at somewhat higher temperatures. From inspection of photomicrographs of these specimens, it would appear that they resemble planar features commonly found in shocked rocks; however, definitive orientation data are lacking. Greenwood in reference 201 describes deformation lamellae parallel to $\{10\bar{1}3\}$ and $\{0001\}$ planes in quartz—two frequent planes associated with features in shocked quartz—in rocks from the Belt series which have no apparent meteorite impact history. In reference 202, Bunch, Dence, and Cohen present data on the characteristics of

333-240 O—69——25

natural terrestrial maskelynite found in the presumed impact craters at Clearwater West and Manicouagan. Heating maskelynite at temperatures well below the melting point of the corresponding plagioclase causes a reversion to the crystalline state, indicating that a degree of structural disordering comparable to that in fused plagioclase glass has not been produced.

During 1967 students of terrestrial volcanic craters continued to examine calderas, maars, and vents and to compare the morphology and associated surface features of these formations with certain lunar craters. In references 203 and 204, Green, using both calculations and direct studies of terrestrial volcanoes which he considers analogous to certain lunar structures, presents a strong case for the origin of many lunar craters by endogenetic volcanic processes. Katterfeld analyzes morphological characteristics of many large terrestrial calderas, maars, and ring dikes, showing thus that these bear many similarities in shape and profile to some of the larger lunar craters whose origin he attributes to comparable volcanic processes. (See ref. 205.) Hartmann notes that, on aerial photos of the Kapoho region, the craters formed by impacts of ejecta from the explosive volcanic eruptions of Kilauea resemble many secondary craters visible in the probe photos of the lunar surface (ref. 206). Roddy calculates in reference 207 the energy needed to form the Ubehebe maar crater near Death Valley, Calif., which is roughly 730 meters wide and 230 meters deep, to be approximately 10^{22} ergs. He concludes that a volcanic eruption, operating by a similar gas escape mechanism, of this magnitude on the Moon would produce a much deeper and somewhat wider crater. Ronca in reference 208 examines the possible link between meteorite impact and induced volcanism in craters. He concludes that triggering or localizing of magmatic activity by impact is possible, but contends that very large impacts would be needed to remove sufficient overburden to activate melting; the crater size and effective removal of material needed to initiate the process depends largely on the geothermal gradient in the region of impact.

Studies in crater morphology, distribution, and formational processes on the Moon's surface were advanced in 1967 by new data from successful lunar probes, continuing telescopic mapping, model experiments, and theoretical analyses. (See ref. 209.) Trask in reference 210 classifies craters seen in Ranger VIII and IX photographs into four categories depending on the relative sharpness of the rim and the depth-diameter ratio. Most craters at 100 meters are broad-rimmed and have smaller depth-diameter ratios than the more common sharper-rimmed craters visible down to the resolution limit near 1 meter. Trask interprets this result to indicate an episode of destruction—volcanic activity and/or intense bombardment by asteroid fragments and micrometeorites—which has modified the 100-meter class of craters, obliterated most smaller ones, and produced a smoothed surface on which younger, sharper craters have formed.

Members of the staff of the U.S. Geological Survey's Branch of Astrogeology have proposed a model in which small craters will be degraded faster than larger ones, leading to the conclusion that smaller subdued craters could be contemporaneous with some larger sharp ones. (See ref. 211.) They propose a scheme in which relative crater age is related to both crater diameter and a set of definitive morphological criteria. (See fig. 38.) A family of crater types is thus defined, with relative age value specified by an index number. When superposition is evident, the higher index craters are almost always observed to be superposed on lower index craters. Certain modifying factors, e.g., mass-wasting effects on lunar slopes, can also vary the relative rates of degradation.

Walker analyzes crater distribution as a function of crater size and time of exposure to assumed fluxes of impacting bodies in reference 212. Until

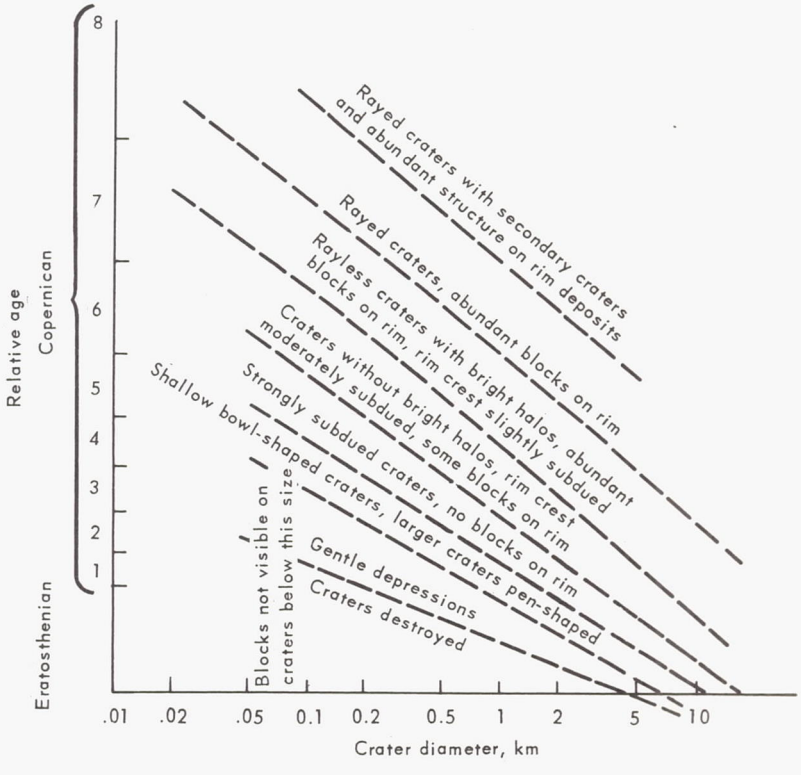


***Figure 38.*—Relation between diameters, properties, and ages of craters. Categories are intergradational. Age units are relative. Lower numbers correspond to older craters, as determined from morphology.**

the surface becomes saturated with craters, the distribution will correspond to the flux, but, from the time of saturation onward, the surface no longer reflects the continuing flux. Secondary craters up to 100 meters in diameter contribute significantly to the surface distribution, but their effects on saturation are distinguishable.

Chapman and Haefner object to the cumulative diameter-frequency curves commonly used to summarize crater distribution (ref. 213). They provide an improved plotting method which contains an adjustable exponent B in the crater equation $N=AD^B$ relating the number N of craters to size as diameter D.

In reference 214 Baldwin analyzes the energy requirements appropriate to the crater formed by the Ranger VIII impact on the Mare Tranquillitatis surface. He used a scaling-law equation derived from cratering-explosion experiments in soil-like materials to calculate the range of diameters expected for the energy involved in the Ranger impact at a speed below the hypervelocity limit (at 5 km/sec). When he applied the equation to the two fresh-looking craters close to the impact point which NASA cites as the most probable collision site for Ranger VIII, he concluded that the smaller crater would represent the size expected in a low cohesion material if normal cube-root scaling were used. However, Baldwin contends that fourth-root scaling, which takes into account the energy needed to overcome gravity in excavating material out of the crater, properly applies to those impacts on the Moon that produce larger craters if they still do not penetrate the local regolith or surface rubble layer. Baldwin furthermore minimizes the effects of variations of gravity (for different planetary masses) as a decisive factor in determining the actual crater diameter, in contrast to the earlier suggestions of other workers on the basis of experimental work. Baldwin, therefore, selects the larger (13-meter) fresh crater as the more likely Ranger VIII impact site, because it closely approximates the size expected from his gravity-scaling calculations.

Pike in reference 215 notes major discrepancies in the values of Schroeter's rule; i.e., the ratio of crater rim volume to true crater volume, normally supposed to be 1:1 for both terrestrial and lunar craters. This, he explains, results from one or more modifying processes, such as erosion, partial burial by extrusive products, and isostatic adjustments. Scott in reference 216 carries out a mathematical analysis of viscous flow of large craters which supports the role of isostasy in raising the central region and lowering the rim.

Walker presents evidence from experimental hypervelocity impacts into materials whose strengths vary in terms of target density and cohesion (ref. 217). His results indicate that rock or metal projectiles produce relatively deep craters in hard (solid) targets and shallow craters in granular, low-cohesion targets. From this he infers that smaller lunar craters are mostly emplaced in weak, soil-like layers. Oberbeck and Quaide use a similar ap-

proach to estimate the thickness of the surface regolith on the Moon (ref. 218). They note a systematic change in crater morphology as diameters increase. Flat-bottomed and ringed craters are produced wherever a solid "bedrock" layer is penetrated by a crater surface. Relative thickness of the fragmental cover can be estimated from ratios of crater diameter to layer thickness derived experimentally from laboratory impacts into sand layers of varying thickness overlying bonded material. Ratio boundaries are correlated with the different crater geometries so that, for craters normalized to constant diameter, it is possible to estimate the thickness of the fragmental layer overlying a cratered area on the basis of distribution and frequency of the various morphological types. As applied to parts of Oceanus Procellarum visible in Lunar Orbiter I photos, the thickness of the fragmental layer covering 85 percent of the area investigated ranges between 5 and 15 meters.

IRON AND STONY-IRON METEORITES

Iron Meteorites

Isotope Analyses

Rare gases in meteorites are divided into three types: primordial, radiogenic, and spallogenic. The primordial gases were incorporated into the meteorite when it was formed; the radiogenic gases were produced as daughters of radioactive parent elements after formation of the meteorite and are used to determine gas-retention ages. The spallogenic gases, formed as a result of exposure to cosmic rays in space, are used to determine cosmic-ray-exposure ages. Lammerzahl has recently reviewed the method and results of rare-gas-isotope studies on meteorites (ref. 219).

It has been shown that ^{3}H in irons and the iron phases of stones is low. Two explanations have been offered: (1) Diffusion of ^{3}H out of the iron phase during terrestrial descent and residence, and (2) solar heating of the meteorites in space. In reference 220, Fisher shows experimentally that the temperature-time history during atmospheric descent is not sufficient for the observed ^{3}H loss, but that long times on the surface of the Earth, aided by grain-boundary diffusion, is sufficient. Hintenberger et al. (ref. 221) measured He and Ne contents in 40 irons. The 12 hexahedrites investigated showed a definite loss of spallogenic ^{3}He. It was concluded that this loss indicates that these irons were always in the vicinity of the Earth or even closer to the Sun; i.e., that tritium loss occurs by solar heating in space. Schultz, in a study of ^{3}H losses, found a correlation between iron meteorites of low cosmic-ray-exposure ages, the amount of spallogenic ^{3}He, and the low spallogenic tritium content in freshly fallen iron meteorites. (See ref. 222.) Therefore, he concludes that solar heating of meteorites in space causes the tritium loss in iron meteorites.

The isotopic composition and abundance of Li was measured by Krankowsky and Müller on several chondrites as well as on the silicate and troilite inclusions in the Odessa octahedrite (ref. 223). The $Li^7:Li^6$ ratio of the meteorite samples, as well as the ratio of terrestrial diabase W–1 and granite G–1 agree to within ± 2 percent. Therefore, all these materials were exposed to the same proton flux even though they probably came from different regions of the solar system. Burnett and Manuel investigated the origin of noble-gas anomalies in the Canyon Diablo iron. (See ref. 224.) Using the measured $^{129}I:^{129}Xe$ ratios, they were able to date the formation interval (the time between nucleosynthesis and the time that the temperature of ^{129}Xe is low enough to be retained in the graphite) as 131 million years. The stone meteorites have formation intervals between 127 and 300 million years and show no appreciable differences from the Canyon Diablo (iron) meteorite.

Several other studies of spallogenic rare-gas isotopes were also carried out. Spallogenic isotopes of helium, neon, and argon were measured in 36 irons. and concentration of ratios of ^3He, ^4He, ^{21}Ne, and ^{38}Ar were determined (ref. 225). Munk determined Ne, A, K, and Xe in the Castilla Peak iron. He found a cosmic-ray-exposure age between 400 and 640 million years and a I–Xe formation interval of 230 million years (ref. 226). In an attempt to see if the Campo del Cielo strewn field and the North Chilean hexahedrites are related, Nyquist, Huneke, and Signer measured the rare gases in the El Taco (Campo del Cielo) meteorite (ref. 227). Based on observed differences in terrestrial ages, they concluded that the two groups were not from the same body.

Cosmic-ray-exposure ages (the time between breakup of the meteorite parent body and capture by the Earth) of 60 iron meteorites were determined by Voshage using the $^{41}K/^{40}K$ method (refs. 228 and 229). A histogram showing all the exposure age data is given in figure 39. Exposure-age data for the several structural and chemical groupings, Og+H (coarse octahedrite+hexahedrites), Om+Of (medium and fine octahedrites), Of IVa (fine octahedrites of chemical group IVa), and D (ataxites) are also included. Medium and fine octahedrites of chemical Group III are found in a peak at 550 to 750 million years, and fine octahedrites of Group IVa are in a peak at 400 million years. Presumably each of these groups was produced in a major collision. The correlation between structure, Ga-Ge chemical grouping, and cosmic-ray-exposure ages for Groups III and IVa suggest that each of these meteorites groups comes from the same parent bodies. Hexahedrites, coarse octahedrites of the chemical Group I, and ataxites have age distributions which are continuous. Voshage suggests that these three groups of meteorites are fragments of a multiplicity of nickel-iron inclusions within the surface layers of the Moon, Mars, and the asteroids.

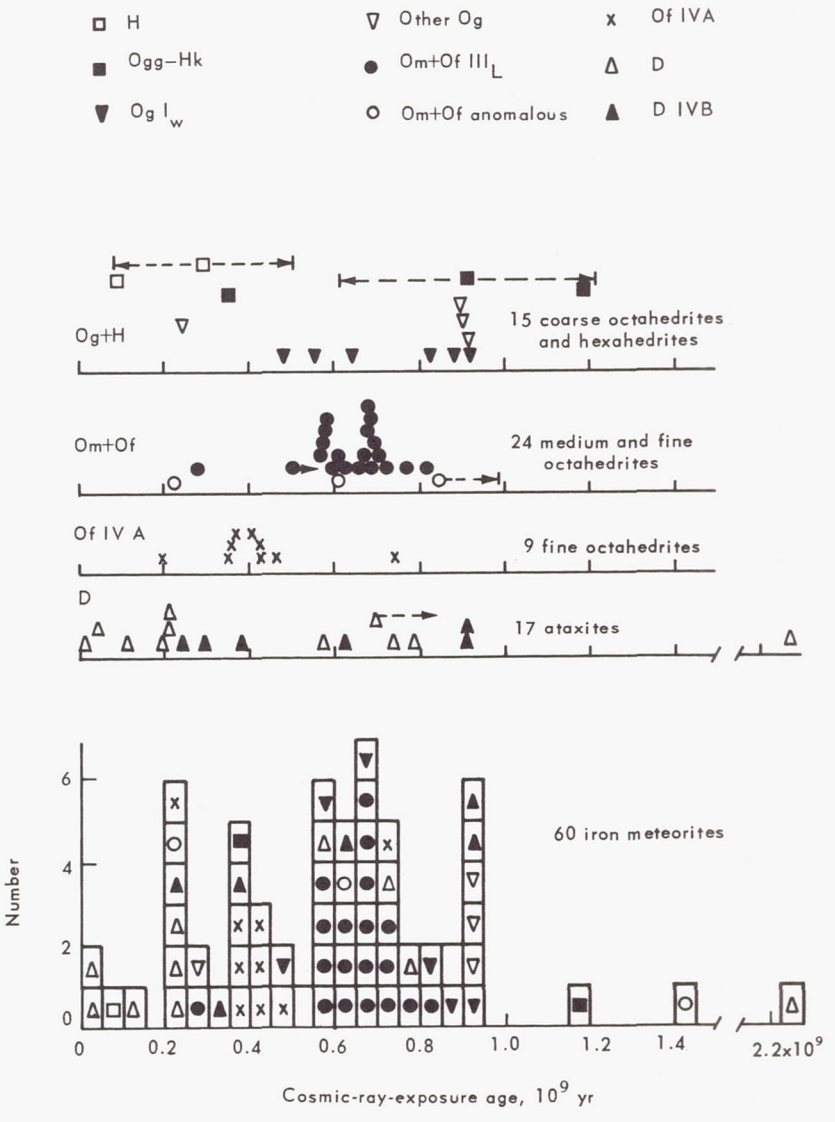


Figure 39.—Distribution of cosmic-ray exposure ages. Below: Histogram of the ages of 60 iron meteorites. Above: Age distribution of these 60 meteorites resolved into distributions of various classes; in addition, some poorly determined ages are included.

The cosmic-ray-exposure ages of stone meteorites are clustered between 1 and 30 million years, over one order of magnitude lower than the ages for the irons. To determine the effect of space erosion on the relative exposure rates of irons and stones, Comerford (ref. 230) investigated the effect of small-particle bombardment. He found that mass loss is much greater with brittle material (chondrites), but no quantitative data could be obtained as to rates of erosion.

Radiogenic gases (e.g., Ar^{40} for K/Ar dating) have been measured in order to obtain the formation or solidification age of iron meteorites. Recent K/Ar age data have indicated ages of from about 7 to 10 billion years, whereas the age of the solar system is generally well accepted at about 4.7 billion years. Rancitelli et al. measured a K/Ar age of about 100 billion years in the Weekeroo Station meteorites. (See ref. 231.) This value disagrees with the Sr/Rb age of 4.7 billion years determined from silicate inclusions of the same sample. Rancitelli et al., conclude that the K/Ar dating technique as applied to iron meteorites gives unreliable results. Recently, in references 232 and 233, Rancitelli and Fisher show that preferential leaching of K relative to Ar in irons by terrestrial weathering processes is a mechanism that may account for the old "ages" determined by the K/Ar age method. Bogard et al. measured the rare gases He, Ne, and Ar, as well as K, in silicate inclusions of several iron meteorites. (See ref. 234.) The K/Ar age of the silicate from Weekeroo Station is less than the Rb/Sr age of the same silicate fraction and does not agree with the high K/Ar ages measured by other investigators for this and other iron meteorites.

Burnett and Wasserburg have made Rb/Sr measurements on different types of silicate inclusions extracted from seven iron meteorites (ref. 235). Four Corners and Pine River have irregular patches of silicates; Toluca, Odessa, and Linwood have silicates as minor constituents of troilite or graphite nodules; and Colomera and Weekeroo Station have droplike silicate inclusions. Six of seven of these meteorites give 4.6 ± 0.2 billion-year isochrons, compatible with chondrite-achondrite ages. The strontium-evolution diagram for four of these meteorites is given in figure 40. Toluca and Odessa are typical octahedrites showing a well-developed Widmanstätten pattern.

Chemical Analyses of Irons

Chemical analyses have been performed on iron meteorites for hundreds of years. Only within the last 20 years, however, has the analyst possessed the necessary apparatus for performing analyses for both major elements (Fe, Ni, and Co) and minor elements (P, S, and C). Recently measurements of trace elements (Ga, Ge, Pt, Ir, Cr, Cu, etc.) in irons using such techniques as emission spectroscopy and neutron activation are being actively performed (ref. 236). These measurements may be ultimately more

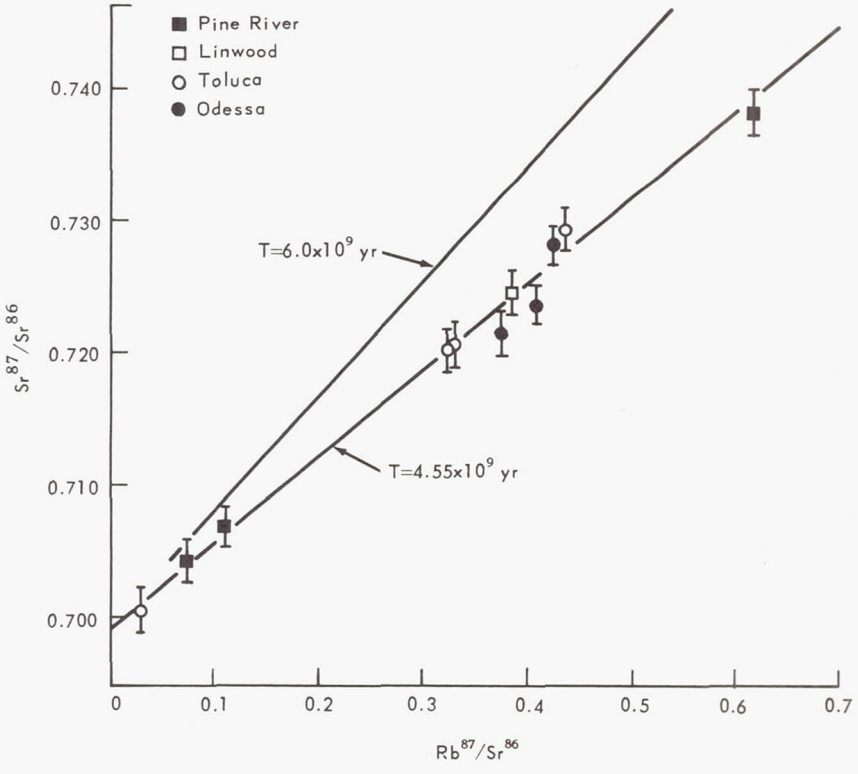


***Figure 40.*—Strontium-evolution diagram for silicate inclusions from four iron meteorites. Meteorites should be considered singly as well as collectively.**

useful than major-element analyses since they help to differentiate several groups of irons from each other.

With respect to trace elements Tanner and Kohman have determined the Hg and Bi abundances in 20 iron meteorites. (See ref. 237.) They found Hg contents in the range of 0.03 to 13 ppm and Bi contents in the range of 0.04 to 0.10 ppm. Rao spectrographically determined the siderophilic element Os in three iron meteorites, and his results agree with those determined by neutron activation (ref. 238). In measurements of the abundance and distribution of Cl in iron meteorites by neutron activation, Berkey and Fisher found that terrestrial processes have, through weathering, locally raised the Cl abundance in some meteorites (ref. 239). The Cl content ranged in value from <0.005 ppm to 10^4 ppm and was segregated mainly at grain boundaries, cleavages, and Neumann bands.

Since the initial discoveries of the "quantization" of Ga in iron meteorites by Goldberg et al. (ref. 240) and the correlation of Ga-Ge by Lovering et al. (ref. 241), several investigators have proposed that members of Ga-Ge groups are related genetically. The authors of references 242 to 245 have all attempted, by measurements of various combinations of trace elements, to further define these chemical groups.

Cobb (ref. 242) has measured Co, Cu, As, Ga, Ir, and Au in 33 iron meteorites by neutron activation. The trace-element values were compared for meteorites within each of the structural groups of iron meteorites: hexahedrites; coarse, medium, and fine octahedrites; and ataxites. He found a good correlation between Au, Ir, and Ga and the structural groups—hexahedrites, coarse octahedrites, and medium octahedrites. The complexity of trace-element distribution between structural groups is proposed as an argument for a number of parent bodies. For the hexahedrites and coarse octahedrites, the trace-element composition of the melt and the conditions of crystallization were similar. Cobb also postulates a melt of different trace-element compositions for the medium and fine octahedrites. The lack of trace-element uniformity in the ataxites could be due to any individual ataxite being a late-stage portion of any one of the starting melts. Due to the small number of meteorites studied, further refinement of the groups was not possible.

Smales, Mapper, and Fouche (ref. 243) measured Ga, Ge, As, Sb, Cu, Cr, Mo, Ag, In, Zn, and Pd by neutron activation on 67 iron meteorites. The elements Ge, Zn, Ga, As, Sb, Ag, and In are more concentrated in the coarse octahedrites; Cr is least concentrated; and Mo and Cu are not correlated with the structure of the irons. Smales et al. point out that $\sim$40 percent of the meteorites studied do not belong to the Ga-Ge groups as set out by Lovering et al. in reference 241, and that a correlation between two trace elements is not sufficient to define a chemical group. By considering possible correlations between trace elements, they found that Ge-Zn, As-Sb, and As-Pd were strongly correlated. They also found chemical groupings between some of the members within each of the broadly defined Ga-Ge groups.

Wasson (ref. 244) has measured Ga and Ge in 34 iron meteorites by neutron activation, and Wasson and Kimberlin (ref. 245) measured Ga-Ge and Ir contents by neutron activation, and Ni content by atomic absorption, in 69 additional irons and 8 pallasites. They define chemical groups when (*a*) the differences in trace-element composition are smaller than for meteorites as a whole, (*b*) the major and trace elements vary coherently with each other, and (*c*) the member meteorites have similar textures. Results for five resolved groups are given in table IV.

Table IV.—*Chemical Characteristics of 5 Groups of Iron Meteorites Resolved by Trace-Element Analysis*

[From refs. 244 and 245]

Chemical group	Ni variation, percent by weight	Ga, ppm	Ge, ppm	Ir, ppm	Correlation with Ni, as Ni increases, of—		
					Ga	Ge	Ir
IIIa	8.65 to 7.53	22 to 17	47 to 33	0.4 to 13	Increase	Increase	Decrease.
IIIb	9.3 to 10.7	20 to 16	38 to 28		Decrease	Decrease	
IVa	7.4 to 9.2	1.6 to 2.2	0.09 to 0.135	1.9 to 2.8	Increase	Increase	
IVb	16.2 to 18.2	0.18 to 0.31	0.03 to 0.06		Increase	Increase	
P	8.8 to 12.3	26 to 13	72 to 11	0.1 to 0.25	Decrease	Decrease	

Group IIIa may be resolvable into smaller groups and Groups IIIa and IIIb may come from the same parent body. A plot of the Ge-Ni and Ga-Ge variation for all the meteorities studied is shown in figure 41. Many meteorites are not members of chemical groups. The fractionation processes which may be responsible for the formation of the Ni-Ga-Ge-Ir correlations are discussed briefly.

Since so much emphasis has been placed on the importance of Ge abundances, several studies have been conducted to see if Ge is distributed, as has been assumed, totally within the metallic phases. Goldstein, using the electron probe, studied the Ge distributions in 10 iron meteorites with bulk Ge contents between 8 and 2000 ppm (ref. 246). He found that Ge is not

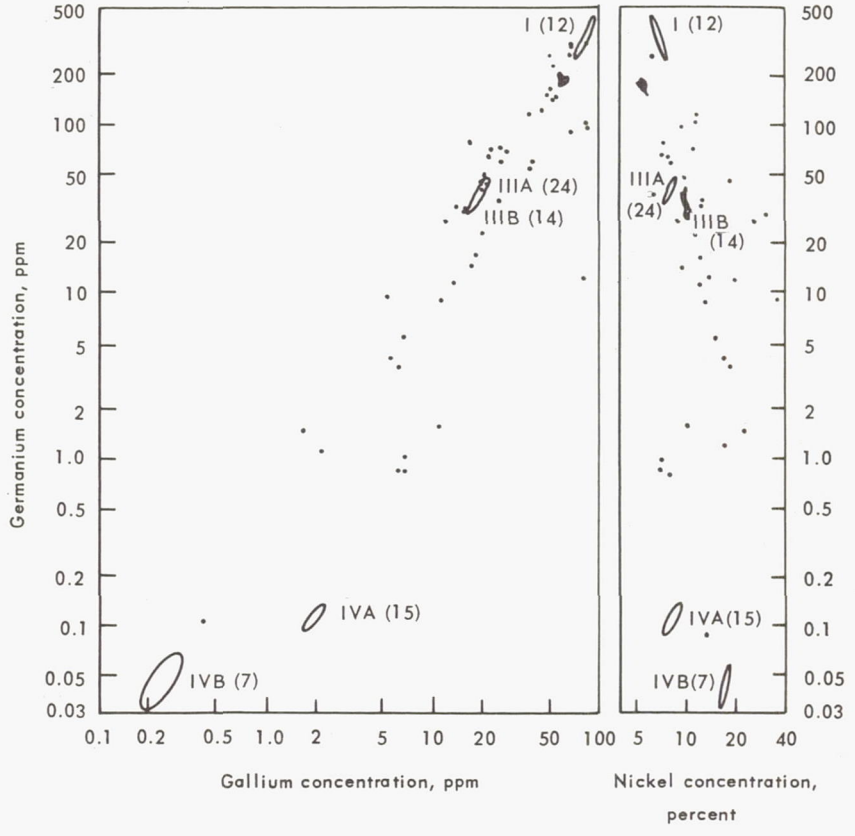


Figure 41.—**Plots of germanium concentration and gallium concentration for about 150 iron meteorites and of germanium concentration and nickel concentration for about 100 iron meteorites. Resolved chemical groups are circled and labeled with the population of the group given in parentheses.**

detectable (<20 ppm) in either schreibersite, troilite, or cohenite, and that it is concentrated in the metallic phases. During the formation of the Widmanstätten pattern, Ge was redistributed preferentially into the parent taenite phase. Wai et al. performed laboratory studies on the equilibrium distribution of trace amounts of Ge between iron-silicate and Fe-FeS at controlled temperature, pressure, and oxygen fugacity. (See ref. 247.) In both experiments Ge was observed to be strongly siderophile, being found in the iron phase. From these results it seems that a one-stage oxidation-reduction process is unlikely to cause the extremely low Ge content in some iron meteorites.

Trace-element concentrations have also been used to establish whether separate meteorites fell to Earth in the same shower. In one study, Wasson (ref. 248) showed that the Boxhole, Henbury, and Wolf Creek, Australia, meteorites are unique in composition and each associated crater was caused by a unique event. Wasson and Goldstein (ref. 249), using Ni, Ga, Ge, and Ir determinations, combined with microprobe and structural studies, showed that the North Chilean hexahedrites have not resulted from a single shower, but rather from a minimum of four falls. There appears to be no connection between these hexahedrites and the Campo del Cielo, Argentina, irons. In a study of the Ni, Ga, and Ge contents in a series of Canyon Diablo and Odessa meteorite specimens, Wasson (ref. 250) found that Canyon Diablo and Odessa are members of the same chemical group but are not likely to be from the same fall.

In order to determine the possible differences between Canyon Diablo specimens located on the rim of Meteor Crater and those on the surrounding plains, Moore, Birrell, and Lewis analyzed Ni and C in a large number of separate iron specimens and determined the volume percent of various phases. (See ref. 251.) They found more taenite and less oxide in the rim specimens than in the plains specimens. The C content was also significantly higher for the rim specimens (0.33 percent by weight) than the plains specimens (0.11 percent by weight). They were not able to tell whether the difference between rim and plains specimens are gradual or sharp. Total sulfur content for 100 iron meteorites was determined by Moore et al. using an oxygen combustion technique (ref. 252). The values ranged from 0.001 to 0.063 percent by weight of S with the majority of samples containing less than 0.0075 percent by weight of S.

Nonmetallic Minerals

Many nonmetallic minerals have been found in iron meteorites. The other surrounding minerals, provide independent data on the conditions composition and oxidation state of each mineral, as well as its relation to under which the iron meteorites formed.

Reed in reference 253 reviews the evidence from iron meteorites which bears on the nature of meteorite parent bodies up to 1966. Olsen found amphibole (richterite) as a primary mineral enclosed in a graphite nodule in the Wichita County iron (ref. 254). Terrestrially, this mineral indicates formation temperatures between 300° and 800° C and water pressures between 100 and 300 atmospheres. In reference 255, Olsen and Fuchs estimate the oxidation states of two iron meteorites (Mount Stirling and Odessa) which contain chlorapatite-silicate-schreibersite assemblages. Although many thermodynamic uncertainties were present, they conclude that phosphate-bearing metallic meteorites represent approximately the same range of oxidation as do the ordinary chondrites. Most iron meteorites represent more reduced regions in a parent body. Two new phosphate minerals were discovered in the Dayton meteorite (Fuchs et al., ref. 256). The authors estimated the oxidation state of this iron and found that it also has an oxidation state similar to ordinary chondrites. El Goresy (ref. 257) analyzed coexisting sphalerite, daubreelite, and troilite in the Odessa iron meteorite with the electron microprobe. He found that the minerals had variable compositions and had formed under nonequilibrium conditions. Therefore, the FeS-ZnS system, which has been used as a geological thermometer, could not be used. El Goresy (ref. 258) also found K-feldspar grains in graphite-troilite nodules in Odessa. Bence and Burnett (ref. 259) have studied the compositions of silicate inclusions in two irons, Four Corners and Kodaikanal, with the electron microprobe. The Four Corners silicates represent a more typical silicate assemblage, with homogeneous minerals, two species of pyroxene, and lesser amounts of olivine and feldspar. The Kodaikanal silicates are predominantly alkali feldspars which are nonhomogeneous and have excess SiO_2.

Mason (ref. 260) describes a general classification for silicates commonly found in iron meteorites. Except for the rounded droplike silicate inclusions in Colomera, Kodaikanal, and Weekeroo Station samples, these inclusions are similar to those of chondritic meteorites. This similarity suggests that chondritic material was incorporated into the metal and recrystallized during slow cooling. Possibly these meteorites represent a border zone between a metallic core and a silicate mantle in one or more asteroids. Brett and Henderson (ref. 261) found two types of troilite (FeS) in iron meteorites: narrow, long inclusions; and elongated bodies. The Widmanstätten pattern is noncontinuous across the narrow long inclusions, but is continuous across the elongated bodies. Evidence is presented to show that the narrow long lamellae form from this liquid and that octahedrites containing elongated bodies of troilite have faster cooling rates.

Up until a few years ago, the presence of diamonds in several meteorites and the presence of cohenite (Fe_3C), which is unstable at low pressures, was considered evidence for the formation of iron meteorites at high pressures.

However, recent studies have shown that diamond can be produced by shock. The following papers present different types of evidence all bearing on the formation of diamonds and cohenite in iron meteorites. Lipschutz (ref. 262) has observed that cohenite grains in Canyon Diablo show evidence of shock-induced alterations. The nature and extent of these were determined by x-ray diffraction, using eight artificially shocked Odessa iron standards. Marvin (ref. 263) has also observed by x-ray diffraction analysis that the grains of ureyite and sphalerite from small diamond-bearing specimens of Canyon Diablo meteorite also show evidence of shock transformation. Hexagonal diamond, a new polymorph of carbon, was discovered by Hanneman, Strong, and Bundy in the Canyon Diablo meteorite (ref. 264). Their results provide strong evidence that these hexagonal diamonds were produced by intense shock pressures acting on crystalline graphite inclusions present in the meteorite before impact, rather than by disintegration of larger statically grown diamonds. Brett presents in reference 265 a thorough study of cohenite, its occurrence and origin. If cohenite is stabilized by high pressures, then it should be present in all meteorites with sufficiently high C contents. In fact, Brett finds that cohenite is present almost entirely in iron meteorites with Ni contents between 6 to 8 percent by weight of Ni. On the basis of phase diagrams and kinetic data, it is proposed that temperatures were too low for cohenite to form in meteorites containing over 8 percent by weight of Ni and that any cohenite which formed in meteorites having Ni contents lower than 6 percent by weight of Ni decomposed because of the high temperature during cooling of the meteorite. The absence of cohenite in meteorites containing both metal and graphite requires low pressures during cooling, implying that these meteorites cooled in small parent bodies of asteroidal size or near the surface of large bodies.

Brett and Higgins (ref. 266) studied the formation of cliftonite in iron meteorites. Some investigators have considered cliftonite to be a pseudomorph after diamond and have used the diamond ancestry of cliftonite as evidence of a high-pressure origin for iron meteorites. However, Brett and Higgins synthesized cliftonite as a decomposition product of Fe_3C (cohenite) in evacuated tubes at 550° C. Cliftonite was only produced at low oxygen fugacities and in the presence of Ni. Cliftonite has not been found in meteorites with more than 8 percent by weight of Ni since no cohenite is present. The authors suggest that meteorites containing cliftonite formed at low pressures.

Metallic Minerals

Metallographic examination of iron meteorites yields information on structural relationships and the heat treatment of the samples. In a study of the Goose Lake meteorite and the Goose Lake fragments, Axon and

Rieche (ref. 267) found, by metallographic techniques, that the structure of the fragments was consistent with that of the main mass. Buchwald (ref. 268) studied six iron meteorites which had been reheated to varying degrees by metallographic techniques. Axon and Faulkner (ref. 269) have investigated hot working or thermal-mechanical recrystallization in the parent taenite of iron meteorites. Annealing twins were found in Laurens County, Toluca, and Gibeon. Nonoctahedral kamacite, which predates the formation of the Widmanstätten pattern, was also found in Gibeon (refs. 269 and 270). The nonoctahedral kamacite was caused by slip deformation on the cube plane at high temperatures.

Two papers discuss the structure of the plessite phase formed by the decomposition of taenite at low temperature. Duerr and Ogilvie (ref. 271) investigated the formation of plessite in the octahedrite Carbo. They determined the orientation of the martensite in taenite and attributed the morphology of plessite to the presence of carbon. Goldstein (ref. 272) used the scanning electron microscope to look at plessite structures at high magnifications. Three regions and types of plessite were delineated and the mechanisms for each of these were outlined. In an attempt to determine whether shock pressures up to 228 kilobars changed the Ni contents of kamacite-taenite interfaces, Axon and Boustead examined cohenite-rich, cohenite-poor, and cohenite-free, artificially shocked meteorites with the electron probe (ref. 273). They found that the interface relations were not altered by shock.

Jaeger and Lipschutz (ref. 274) investigated shock effects by metallographic and X-ray diffraction techniques in five octahedrites. All but one was shocked by preterrestrial collisions to at least 130 kilobars. In a much more complete study (ref. 275), Jaeger and Lipschutz investigated 65 octahedrites. Most of the shocked (>130 kilobars) meteorites are in Ga-Ge Group III defined by Lovering et al. (ref. 241). (See fig. 42.) These shocked meteorites also cluster around a 650±60-million-year exposure age and may be from the same parent body. Since the majority of the hypersthene chondrites have a 520-million-year exposure age, Jaeger and Lipschutz postulate that the parent bodies which contained the hypersthene chondrites and the Group III irons were involved in a collision and provide the majority of the iron meteorites.

Development of the Widmanstätten Pattern in Iron Meteorites

Since the advent of the electron microanalyzer, it has been found that the growth of the Widmanstätten pattern in meteorites is incomplete. The existence of large Ni and Fe gradients, combined with models for the growth of the Widmanstätten pattern, have enabled investigators to estimate the rate at which irons have cooled within their parent bodies. Investigations on major and minor element redistribution in the metal phase and on cooling-rate distributions have been continued.

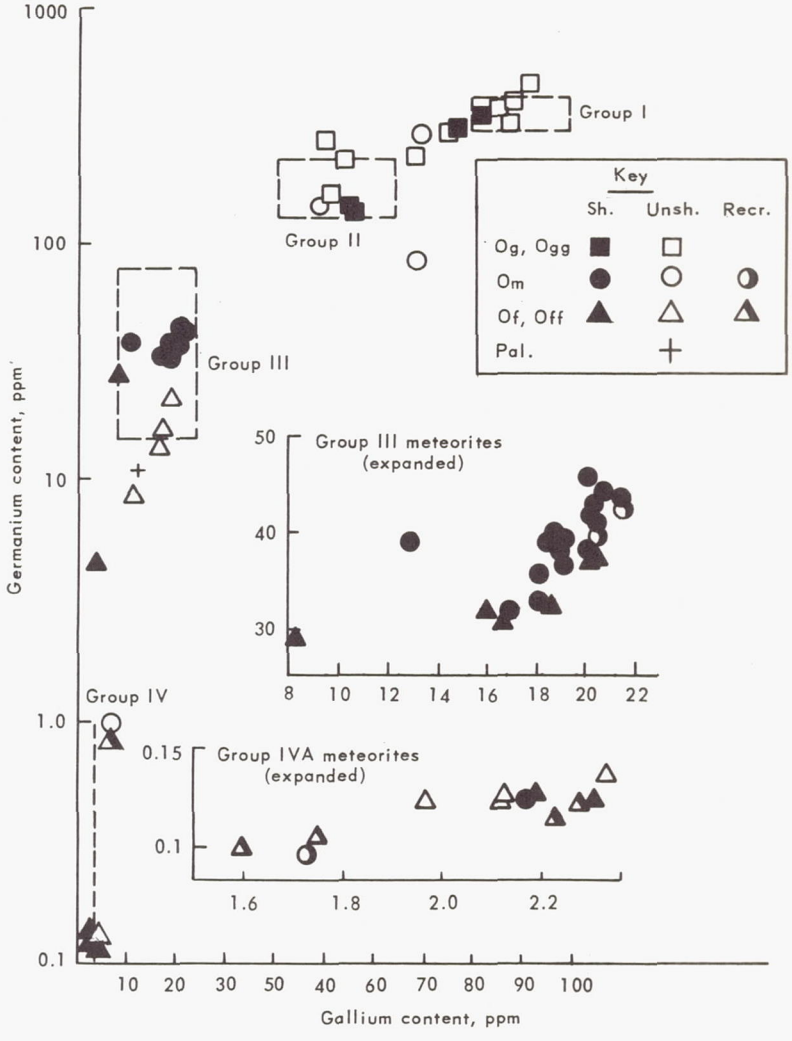


Figure 42.—**Germanium and gallium contents, shock histories, and structures of 61 octahedrites.**

Axon and Yardley (ref. 276) examined the Ni distribution at phase interfaces in the Brenham County pallasite. They found that the Ni distribution in taenite is identical, regardless of whether the taenite is in contact with olivine or with kamacite. The results also suggest the possibility of enhanced Ni diffusion along phase interfaces. The effect of phosphorus on the development of the Widmanstätten pattern is not well known. Reed (ref. 277) measured the P distribution in the Mount Edith octahedrite with

the electron microprobe. He found that kamacite contains 0.09 to 0.10 percent by weight of P and taenite contains 0.02 to 0.03 percent by weight of P. The P and Ni gradients in kamacite near schreibersite inclusions are consistent with the formation of schreibersite as a solid-state precipitation.

Goldstein and Short (ref. 278) have determined cooling rates for 27 iron and stony-iron meteorites. The cooling rates were obtained by comparing measured Ni gradients at kamacite-taenite boundaries with those gradients calculated by a theoretical growth analysis. A wide range of cooling rates was found (0.4° to 40° C/10^6 years). Three groupings were found: (1) Fine octahedrites (chemical Group IVa), 9° to 40° C/10^6 years; (2) fine and medium octahedrites, 1° to 5° C/10^6 years; and (3) pallasites, 0.4° to 1° C/10^6 years. These groups of meteorites developed their Widmanstätten pattern in different thermal environments and under conditions of low pressure.

Short and Goldstein (ref. 279) developed two rapid and simple methods for the determination of approximate cooling rates of iron phases in meteorites without the need for extensive computer calculations. They used one of these methods to determine the approximate cooling rates of 193 iron meteorites (ref. 280). About two-thirds of the meteorites cooled between 1° and 10° C/10^6 years, although the total variation in cooling rates is 0.4° to 500° C/10^6 years. These variations indicate that meteorites formed in more than one body, and that the Widmanstätten pattern formed at low pressures. Evidence was given that meteorites within each chemical (Ga-Ge) group are further correlated by bandwidth, plessite structure, and cooling rate. The variation in cooling rate and Ni content for meteorites in the five chemical groups is shown in figure 43.

The cooling-rate variations in both Group I and IIIb iron meteorites are small (2° to 3° C/10^6 years and 1° to 2° C/10^6 years, respectively) and independent of chemical composition. These meteorites probably formed in the cores of their parent bodies. The cooling-rate variations in both Groups IIIa and IVa are large (1.5° to 10° C/10^6 years and 7° to 90° C/10^6 years, respectively) and vary with the Ni content, decreasing as the Ni content increases. These meteorites probably formed in isolated regions spread throughout their parent bodies.

Stony-Iron Meteorites

The stony-iron meteorites, including the pallasites and mesosiderites, constitute less than 5 percent of the number of known meteorites. However, their unusual mineralogy and the possibility that they are a link between the two major groups of meteorites make them important. The petrology

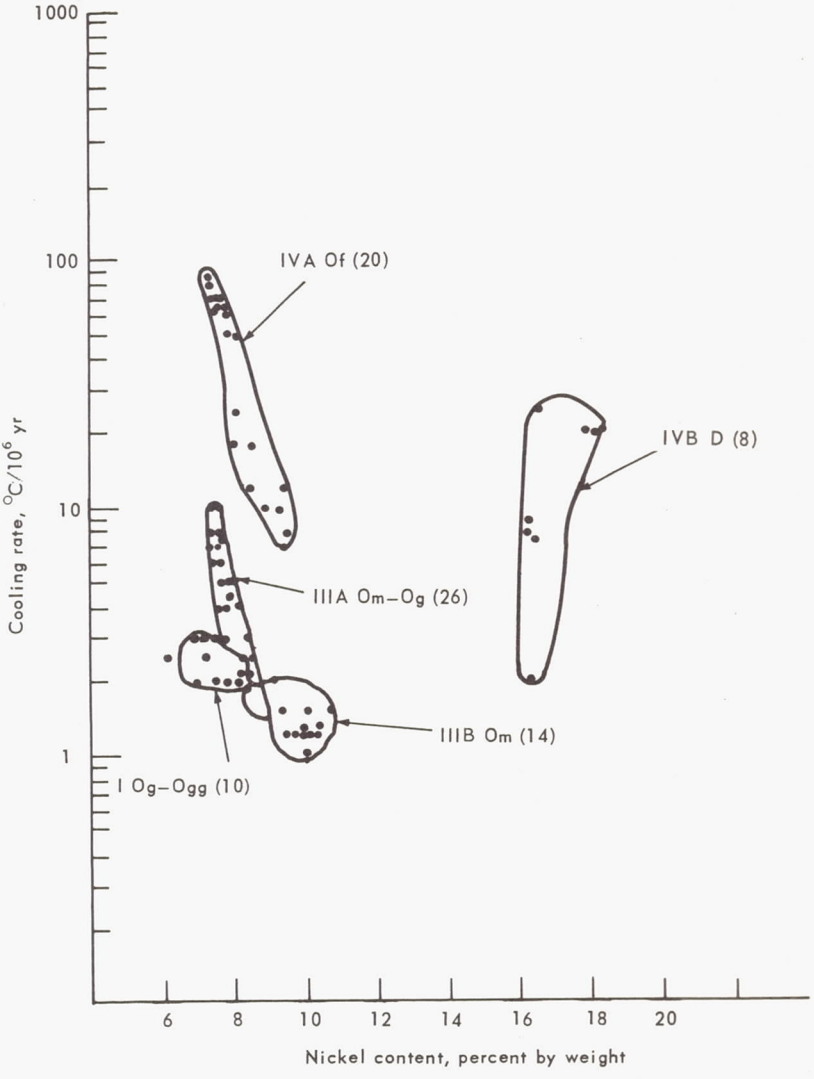


Figure 43.—Variation of cooling rate and nickel content for meteorites in the five gallium-germanium groups. (Numbers in parentheses indicate the number of meteorites studied in each group.) Each gallium-germanium group plots coherently and is outlined on graph.

and chemistry of eucrites, howardites (calcium-rich achondrites), and mesosiderites is described by Duke and Silver in reference 281. They conclude that the principal mineralogical and textural properties are due to original magmatic crystallization followed by complex fragmentation and recrystallization episodes. The authors suggest that these meteorites come from the Moon, probably originating as surficial material. Preliminary Surveyor data tend to confirm in part this suggestion. Powell and Weibler examined microscopically 10 mesosiderites (ref. 282). They also analyzed most of these with the electron microprobe to determine the major-element compositions of all major minerals and of certain accessory minerals. A large variety of structures was observed, and they conclude that the individual mesosiderites have had dissimilar histories.

Several investigations on the pallasites are also published. Stanfieldite, a new phosphate mineral, was found by Fuchs in one mesosiderite and six pallasites (ref. 283). A new pallasite, Marburg, was also described chemically and mineralogically by Buseck et al. in reference 284. Buseck and Goldstein examined the olivine and metal phases in over 75 percent of the known pallasites with an electron microprobe (ref. 285). The olivine compositions and homogeneity data indicate that the pallasites were derived from a limited number of parent bodies. The lower cooling rates of pallasites indicate that they formed in a site more thermally insulated than the iron meteorites. Wasson and Kimberlin determined Ni, Ga, Ge, and Ir contents in six pallasites and conclude that the pallasites are all members of a single genetic group (ref. 245). However, their data are only marginally consistent with the previously observed correlation that the fayalite content of the pallasitic olivine increases with increasing Ni content of the metal.

In a paper on the Bununu meteorite (ref. 286) and in an article on meteorites (ref. 287), Mason proposes that most of the stony-iron meteorites and achondrites, other than the enstatite achondrites, can be derived by melting and fractional crystallization of one or more parent bodies with the overall composition of the chrondites. In this way a continuum of structures and meteorite types develops from the core of the parent body to the surface. Pallasites are then found in the center of the body and are surrounded by howardites and then eucrites. The mesosiderites are close to the surface and are breccias of the eucrites and howardites.

STONY METEORITES

As in previous years, the research on stony meteorites centered around the search for those types which represent the most primary material and which will thus yield the most significant data concerning the origin of the elements, the solar system, and meteorites.

A new classification scheme for chrondritic meteorites was proposed by Van Schmus and Wood in reference 288 which depends on essentially

two parameters: the chemistry and the petrologic type. On the basis of chemistry (the Fe/SiO_2 and MgO/SiO_2 ratios in the bulk analyses and the ratio of $FeO/FeO+MgO$ in olivines and pyroxenes), the meteorites are categorized into enstatite, carbonaceous, high (-iron), low (-iron) and low-low (-iron) groups. Each of these is further divided by petrologic type as shown in table V. The use of this classification has, in a short time, gained wide acceptance and, as will be noted here, can be correlated with many of the results of analyses on chrondritic meteorites. The existence of the distinctive features (which result in types 1 to 6 in table V) is, for the most part, unquestioned. On the other hand, the origin of these features is the subject of some controversy. Van Schmus and Wood attribute them to postformational metamorphism which increases progressively from type 1 to type 6. This, they believe, is consistent with increasing homogeneity of the silicates, the disappearance of glass, and the disappearance of low-calcium clinopyroxene in the higher groups. Dundon and Walter have likewise correlated the higher petrologic types with an increased ordering of Fe and Mg between two dissimilar cation sites in pyroxenes from these meteorites (ref. 289). This is indicative of a lower equilibration temperature for these meteorites. Van Schmus and Koffman (ref. 290) used the constant of equilibration, K, for the distribution of Fe and Mg between high-calcium (clino-)pyroxenes and low-calcium (ortho-)pyroxenes to determine the approximate temperature of equilibration. The use of K, where:

$$K=\frac{X_{Fe_{clinopyx}}X_{Mg_{orthopyx}}}{X_{Fe_{orthopyx}}X_{Mg_{clinopyx}}}$$

assumes ideal mixing for which there is some evidence. Van Schmus and Koffman found, from previous microprobe analyses, that, for the equilibrated ordinary chondrites (those in types 5 and 6), K varied between 0.55 and 0.65. Using the curve shown in figure 44, which is based on thermodynamic data, they derived a value of $820\pm50°$ C for the equilibration temperature.

In a general survey of the unequilibrated ordinary chondrites, Dodd, Van Schmus, and Koffman (ref. 291) present evidence (fig. 45) that, as the heterogeneity of the olivine of a chondrite decreases, the average FeO content of the olivine increases. (The heterogeneity is determined by the point-to-point variation in the microprobe analysis of many olivine grains of the various chondrites and is presented as the percent mean deviation of these analyses. Dodd et al. maintain that this parameter is inversely correlated with the degree of metamorphism.) Thus, they conclude, the high- (H), low- (L), and low-low (LL)-iron groups represent three distinct metamorphic series which involve a general increase in the oxidation state. Wood, on the other hand, finds that, in type II carbonaceous chrondrites, the average FeO content of the olivine decreases as hetero-

Table V.—*Chemical-Petrologic Classification for Chondritic Meteorites*

[From ref. 288]

Characteristic	Petrologic type—					
	1	2	3	4	5	6
Homogeneity of olivine and pyroxene compositions.	.....	Greater than 5% mean deviations		Less than 5% mean deviations to uniform	Uniform	
Structural state of low-calcium pyroxene.	.....	Predominantly monoclinic		Abundant monoclinic crystals	Orthorhombic	
Degree of development of secondary feldspar.	.....	Absent		Predominantly as microcrystalline aggregates		Clear, interstitial grains
Igneous glass.....	.....	Clear and isotropic primary glass; variable abundance		Turbid if present	Absent	

Metallic minerals (maximum Ni content).	.....	<20% (taenite absent or very minor)	>20% (kamacite and taenite present)			
Sulfide minerals (average Ni content).	.....	>0.5%	<0.5%			
Overall texture.....	No chondrules...	Very sharply defined chondrules		Well-defined chondrules	Chondrules readily delineated	Poorly defined chondrules
Texture of matrix.....	All fine-grained, opaque	Much opaque matrix	Opaque matrix	Transparent microcrystalline matrix	Recrystallized matrix	
Bulk carbon content.....	~2.8%	0.6 to 2.8%	0.2 to 1.0%	<0.2%		
Bulk water content.....	~20%	4 to 18%	<2%			

Dotted lines between columns indicate gradational transitions.

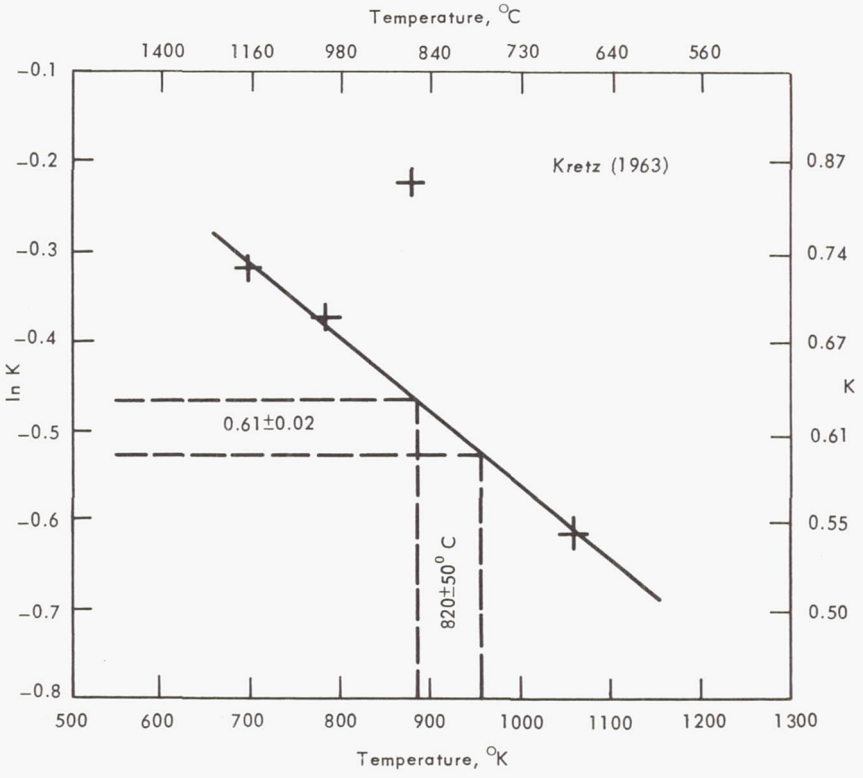


Figure 44.—**Estimated dependence of distribution coefficient K with temperature.**

geneity decreases. He proposes that metamorphism of these meteorites took place in a reducing atmosphere of modified solar composition. (See ref. 292.)

The analyses of water, carbon, and Ar^{36} in unequilibrated ordinary chondrites made by Dodd et al. (ref. 291) is shown herein as table VI. These are seen to decrease with increasing metamorphic grade and decreasing percent mean deviation. Suess and Wänke, however, point out in reference 293 that the argon-xenon ratio does not change with degree of metamorphism, although argon would diffuse much more rapidly than xenon. In response to this argument, Wood (ref. 294), suggests that xenon might be, in effect, walled into the crystalline structures to the extent that iron and magnesium could be redistributed during metamorphism without affecting the xenon. Otting and Zahringer (ref. 295), however, show that, while there are no reports of primordial Xe^{132} in H6 chondrites, there is a steady decrease in primordial Ar^{36} from the H3 to the H6 types.

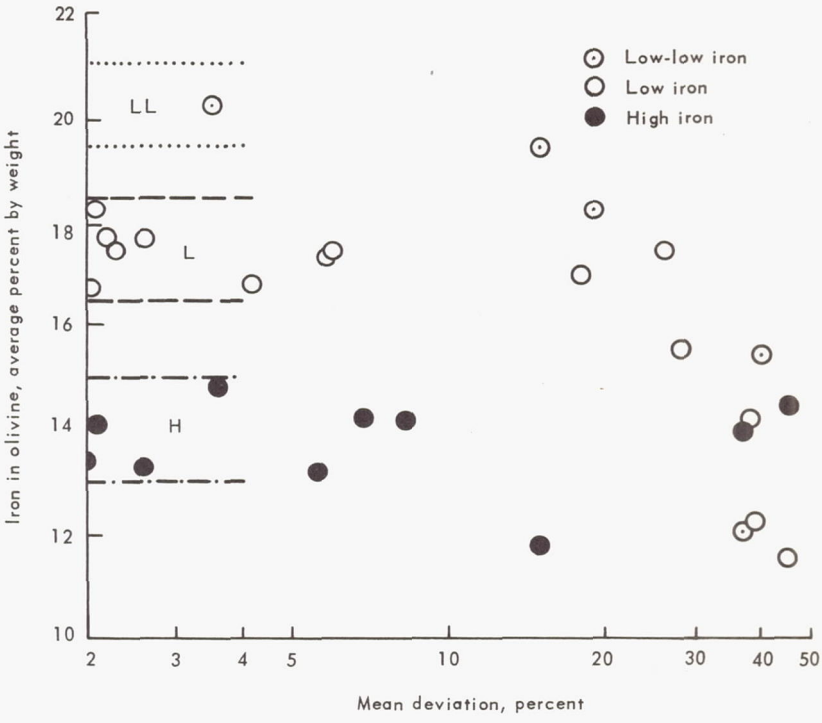


Figure 45.—**Plot of average iron content of olivine versus percent mean deviation for olivine compositions in chondrites. Note the trend toward lower iron contents for the olivine in the most unequilibrated LL-group chondrites and L-group chondrites, while olivines from the H-group chondrites show little change. The dashed line pairs above and below the letters LL, L, and H denote approximate range in compositions of olivine from equilibrated samples.**

This decrease holds true for both primordial Xe^{132} and Ar^{36} in L-group chondrites. Finally, Heymann and Mazor (ref. 296) have shown that the noble gases are strongly fractionated in the unequilibrated chondrites relative to their cosmic abundances. However, the more unequilibrated the chondrite, the greater the primordial component of solar gas. They conclude that the original rare-gas content of even the most unequilibrated chondrites is probably not entirely primordial, indicating that even these chondrites have been heated to some degree. This is in agreement with the absence of a primordial neon component which presumably was lost during this mild heating. (Table VII summarizes these analyses to show the percentage of meteorites in the H3 to H6 groups of chondrites which exhibit solar rare-gas ratios.)

Table VI.—*Water, Carbon, and Primordial Argon Contents in Unequilibrated Ordinary Chondrites*

[From ref. 291]

Chondrite	Olivine, percent mean deviation	H_2O, percent by weight	C, percent by weight	Primordial Ar^{36}, 10^{-8} cc
High group				
Tieschitz	45	0.88	0.25	22
Sharps	37	2.03	.95	.....
Bremervörde	15	.23	.22	.....
Prairie Dog Creek	6.9	.....	.35	.....
Clovis No. 1	5.6	.....	.22	.....
Castalia	3.6	.43	.27	.....
Geidam	(*)	.57	.....	.....
Sindhri	(*)	.....	.....	.....
Weston	(*)	.98	.28	.....
Low group				
Krymka	45	.....	0.27	52
Bishunpur	39	1.10	.53	55
Hallingeberg	38	.95	.26	.....
Manych	26	.....	.....	12
Mezö-Madaras	21	.....	.45	51
Khohar	18	1.16	.32	.....
Carraweena	6.0	.....	.09	3.0
Ioka	5.8	.....	.12	.....
Barratta	4.2	.....	.09	5.6
Goodland	2.6	.....	.07	6.7
Cynthiana	(*)	.....	.10	.....
Tennasilm	(*)	.51	.10	.....
Bjurböle	(*)	.....	.....	2.5
Lua	(*)	.....	.11	.....
Modoc	(*)	.....	.16	.....
Low-low group				
Ngawi	40	1.40	0.39	.....
Semarkona	37	1.22	.57	.....
Chainpur	32	1.00	.44	5.0
Parnallee	19	.....	.10	1.5
Hamlet	3.5	.04	.16	9.5

*The olivines of these meteorites are believed to be completely equilibrated.

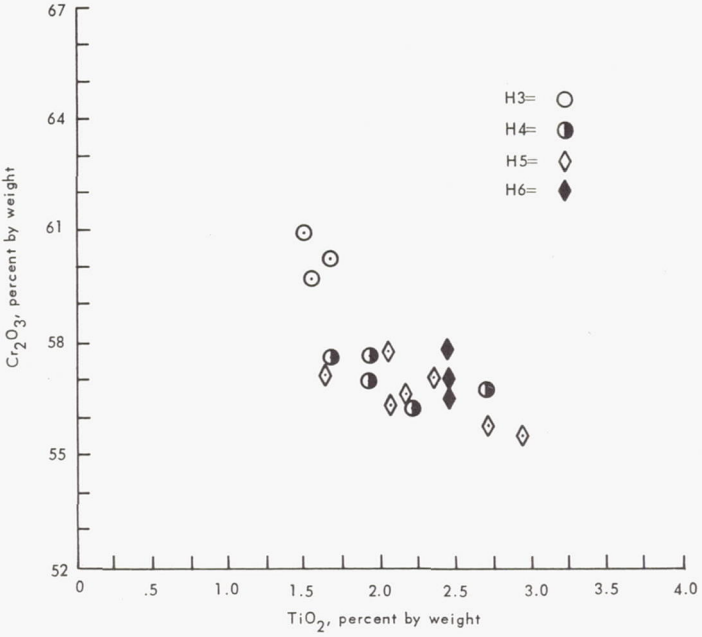
Table VII.—*Number and Percentage of H-Group Chondrites Containing Solar Rare Gases*

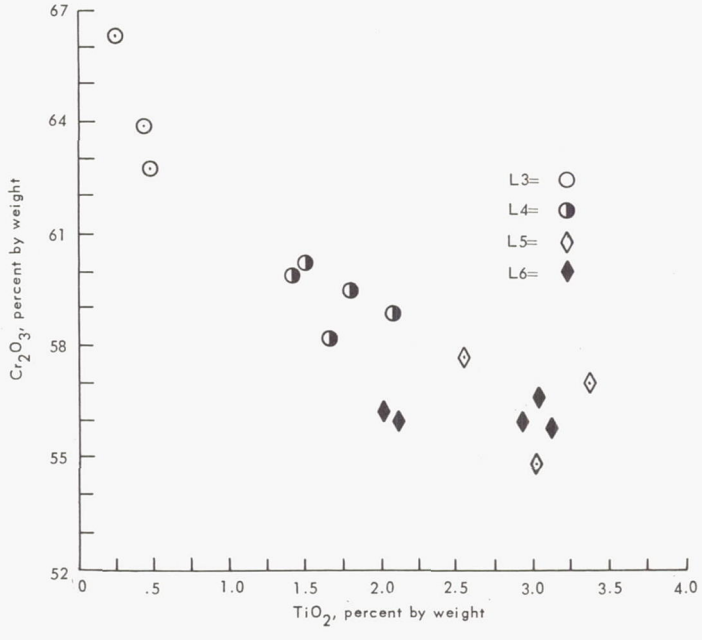
[From refs. 291 to 296]

Petrologic group	Total number of meteorites	Number analyzed	Meteorites with solar gases	Number with solar rare gases, percent
H–3	8	6	1	17
H–4	33	21	3	14
H–5	74	45	6	13
H–6	44	25	0	0

Wood was also forced to propose a heating period for the unequilibrated chondrites (ref. 297). In a study of diffusion at the boundaries between taenite and kamacite metal grains in chondrites, he found that equilibrated meteorites have apparently cooled through the temperature of 500° C at a greater rate than the unequilibrated chondrites (2° to 10° C per million years for the former; 0.2° to 2° C per million years for the latter). The temperature for partial equilibration of Ni in the metal phase (500° C) is substantially lower than the temperatures below which mobilization in the silicate phase ends (approximately 800° C) so that reheating to a temperature between these values would permit retention of the disequilibrium silicate phases in the unequilibrated chondrites. Slow cooling in these would cause equilibration of the metal phase, while fast cooling in the equilibrated (in terms of the silicate phase) chondrites would result in disequilibrium (in the metal phase). Binns (ref. 298) differentiates between "primitive" and "transitional" groups and notes that, in the latter, the striated structure of the orthopyroxene was evidence that it had formed by inversion from clinopyroxene. This supports the contention that the more metamorphosed (transitional) chondrites were reheated. In a study of chromite in ordinary chondrites, Bunch et al. (ref. 299) found definite variations in the trace-element content of this mineral as a function of petrologic type (fig. 46) as well as chemical group. They were unable to conclude, on the basis of their study, whether these systematic variations were the result of primary crystallization or metamorphism.

Kurat (ref. 300) reemphasizes the possibility that the homogeneous distribution of olivine and pyroxene compositions in the equilibrated chondrites might be the natural result of a fast quench of a silicate liquid, so that crystallization took place at temperatures below the solidus. The unequilibrated meteorites, on the other hand, may have cooled more slowly, having time to develop compositional heterogeneity as crystals slowly separated from the melt. Kurat points out that many of the mineral phases in "equilibrated" meteorites are in disequilibrium.


67
64
61
58
55
52
0
.5
1.0
1.5
2.0
2.5
3.0
3.5
4.0
Cr_2O_3, percent by weight
TiO_2, percent by weight
H3=
H4=
H5=
H6=


67
64
61
58
55
52
0
.5
1.0
1.5
2.0
2.5
3.0
3.5
4.0
Cr_2O_3, percent by weight
TiO_2, percent by weight
L3=
L4=
L5=
L6=

Reid and Fredriksson (ref. 301) point out that, in order to derive an equilibrated from an unequilibrated chondrite, considerable redistribution of iron must take place, especially since the average FeO content of pyroxenes in unequilibrated chondrites is substantially lower than that of equilibrated types. The chondrite Bjurböle, which contains low-calcium clinopyroxene but homogeneous silicates, has chondrules which are quite distinct and could not have withstood the migration of iron. In addition, because the matrix of Bjurböle consists of ground-up chondrules while the matrix of Chainpur, an unequilibrated chondrite, consists of fine-grained carbonaceous material, Bjurböle could not have been produced from the latter material by simple metamorphism. Reid and Fredriksson also question how glass in the Bjurböle chondrite could have been preserved during metamorphism. The temperature of equilibration, as determined by the composition of coexisting orthopyroxenes and clinopyroxenes, is higher than the crystallization temperature of gabbro (according to the same data used by Van Schmus and Koffman in ref. 290), thus raising the question of how such temperatures might have existed without causing extensive remelting in the meteorite.

The Shaw meteorite, according to Fredriksson and Mason (ref. 302), has coexisting orthopyroxenes and clinopyroxenes which indicate a temperature of crystallization of 1100° C. It has no chondritic structure but contains equilibrated olivine and pyroxene which characterize the chondrite as L-group. The total iron, however, is low so that it might be classified as LL–group. The authors propose that the iron content was high originally, but that iron sulfide drained away during the melting process.

There have been several interesting studies on meteorites which exhibit shock effects and brecciation. Van Schmus (ref. 303) presents a petrographic description of the unequilibrated ordinary chondrite, Mezö-Madaras, and, in particular, describes several breccia inclusions which occur in that meteorite. Glass in the chondrules is close to albite ($NaAlSi_3O_8$) in composition but does contain some iron and magnesium. The glass lies close in composition to the eutectic composition in the phase systems forsterite-silica-nepheline and fayalite-albite. The glass is, therefore, the result of quenching rather than shock. One inclusion he describes resembles the Murray Type II carbonaceous chondrite, bearing olivine and pyroxene of variable composition. Another, and more common inclusion has homogeneous olivines and pyroxenes and contains distinct chondrules. A third

---

Figure 46.—**Correlation between chromite composition and petrographic subgroup classification of chondritic meteorites. With decreasing Cr_2O_3 content, TiO_2 content of chromite from H- and L-subgroups increases.**

type has less distinct chondrules and glass which contains appreciable FeO, MgO, and CaO, indicating a relatively high temperature of formation. This type of inclusion contains globular sulfides. The petrography of the Mezö-Madaras chondrite, he concludes, indicates the following sequence of events: (1) deposition of unequilibrated chondrules; (2) heating of regions of the parent body to 800° to 1200° C causing local homogenization and partial melting; (3) breakup and reaccumulation.

Binns (ref. 304) describes inclusions of cristobalite in the Farmington meteorite. These are surrounded by rims of diopsidic pyroxene. The meteorite also exhibits cavities into which globular metal particles project. Experimental heating of the Parnallee meteorite caused melting and produced blackened voids similar to those in Farmington. Binns believes that the heat which caused melting in Farmington was probably not due to shock, since this would have destroyed the voids. Ortho-clinopyroxene equilibration temperatures indicate that the chondrite was heated to 1000° C. The origin of the calcium which forms the diopside surrounding the cristobalite is unknown—however, the cristobalite is definitely foreign and was injected into the meteorite.

In reference 305, Buseck discusses the postformational history of the hypersthene chondrite Beenham which, according to petrographic study, has been subjected to strong shock effects. He presents the following chronology for this chondrite: (1) formation of metal-free chondrules (this agrees with Wood's model); (2) crystallization of metal; (3) formation of kamacite from taenite in the metal phase; (4) formation of sulfides (which selectively replace kamacite); (5) shock event and the formation of Neumann bands; and (6) shock melting.

Metallographic studies by Heymann (ref. 306) indicate that the blackened hypersthene chondrites have been strongly shocked (from a few hundred to over a thousand kilobars shock pressure). During this shock process, these meteorites experienced helium loss to varying degrees. The He^3 and He^4 contents, when corrected, give an isochron for this shock event at 520 ± 60 million years. The concordance of many K/Ar dates of the hypersthene chondrites with this value indicates that approximately one-third of these meteorites were involved in this shock event.

Tanenbaum (ref. 307), however, made a statistical study of analyses of cosmic-ray-induced activities of chondrites and concludes that the clustering of cosmic-ray-exposure ages of hypersthene chondrites may well be random, although clustering of these ages for bronzite chondrites at 4 million years is probably statistically significant.

The Rb/Sr age method has been useful in defining the time of crystallization of meteorites. However, in the majority of previous investigations, it has been necessary to assume that at least two meteorites are genetically related in order to calculate an age. If different portions of one meteorite can be found to contain different Rb/Sr ratios, it is possible to determine when

the different portions became closed systems (time of crystallization or metamorphism), without assuming any relationship between meteorites. In the past several years, the techniques of Rb/Sr dating have been improved to the point where very small samples may be analyzed so that the analysis of the component parts of meteorites is feasible. During 1967 three important papers have reported work of this type. The internally determined ages for three chondrites (ref. 308), an achondrite (ref. 309), and silicate inclusions in six iron meteorites (ref. 310) are all compatible with the generally accepted ages of meteorites, as determined by assuming genetic relations between meteorites—about 4.5 billion years.

Hohenberg et al. (ref. 311) irradiated samples of several meteorites and determined the release of xenon as a function of temperature. They found that, although xenon has been lost from the low-temperature sites in meteorites to varying degrees, the high-temperature sites have retained their xenon, giving an original I^{129}/I^{127} ratio of 10^{-4}.

Morgan and Lovering (ref. 312) determined uranium and thorium abundances in carbonaceous chondrites by neutron-activation analysis. The type I carbonaceous chondrites were found to be quite variable in uranium concentration, even for separate samples from the same meteorite. The mean Th/U ratios for type I and II carbonaceous chondrites were found to be 3.2 ± 0.7 and 3.5 ± 0.5, respectively. The abundances are considerably lower than predicted by nucleosynthetic theory, which could mean either that the carbonaceous chondrites are not primary or that the nucleosynthetic theory must be revised.

By contrast, Tanner and Ehmann (ref. 313) have analyzed antimony in a number of meteorites, including two type I carbonaceous chondrites, and on the basis of these two latter analyses they suggest a cosmic abundance for Sb of 0.40 ($Si=10^6$). This value is considerably higher than is predicted by current theories of nucleosynthesis. They point out that the recent experimental abundances in the type I carbonaceous chondrites for the mass region bracketing the isotopes of Sb are generally two to six times the calculated values (see fig. 47), but they point out the atomic-abundance curve for the type I carbonaceous chondrites matches, in a relative sense, the previously calculated cosmic-abundance curve of Clayton and Fowler much better than the curve for the type II carbonaceous chondrites. They suggest that the theories of nucleosynthesis should be reexamined to reconcile the approximately fourfold greater experimental abundances in this mass region.

Other studies reported during 1967 which bear on the questions of cosmic abundances of the elements and fractionation of the elements among the various types of meteorites include studies on I, U, and Te (ref. 314); Rb, Pd, Os, Ir, Pt, and Au (ref. 315); Cl, Br, and I (ref. 316); Li (ref. 317); Re and Os (ref. 318); Fe, Ni, Co, Ca, Cr, and Mn (ref. 319); and Si (ref. 320).

The isotopic composition of tin in a variety of meteoritic and terrestrial samples has been studied by DeLaeter and Jeffery (ref. 321). They found

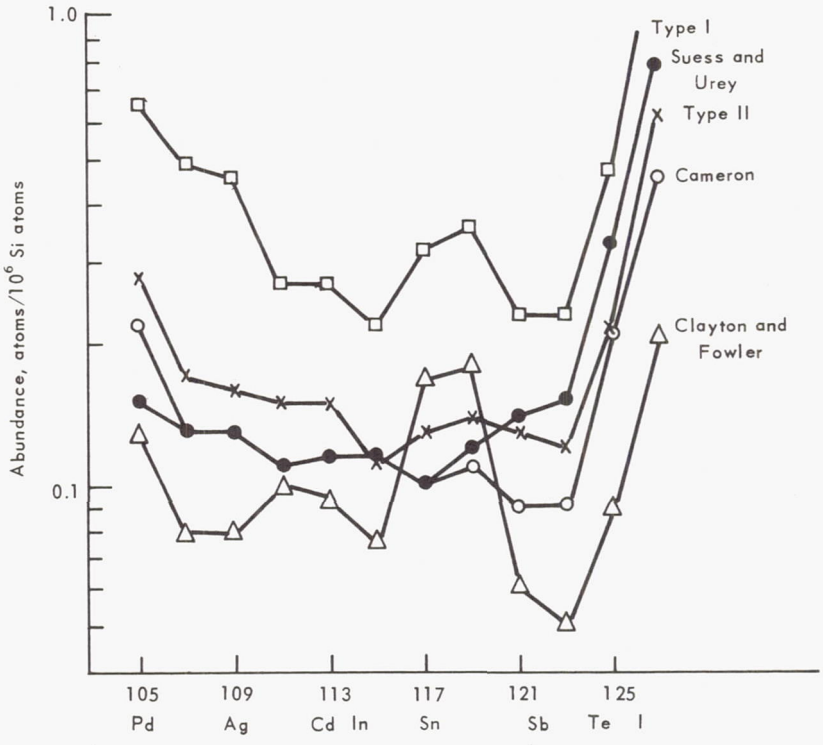


Figure 47.—**Experimental and predicted atomic abundances in the mass region 105 to 126. Experimental abundances were derived from a compilation given by Larimer and Anders except for indium (Akaiwa, and unpublished data summarized by Schmitt and Smith) and antimony which is from the present paper.**

no evidence of significant variations resulting from inhomogeneities in galactic or solar-system processes. Tin was chosen specifically because each of its various isotopes is produced by one of the major synthesizing processes: *r*, *s*, and *p*. From the lack of isotopic anomalies in tin, the authors question the validity of the Fowler-Greenstein-Hoyle (FGH) model of nucleosynthesis. From a study of the lithium isotopic composition in meteoritic matter, Krankowsky and Müller (ref. 317) have reached a similar conclusion concerning inhomogeneities; that is, if the FGH model is correct, then the postulated proton flux must have been constant over several astronomical units, or large-scale mixing processes must have occurred over the same distances.

Greenland (ref. 322) has analyzed many specimens of all types of chondritic meteorites for several trace elements. He found that fractionation of these elements during formation of the meteorites cannot be explained on the

basis of a one-step separation. He concludes that several of the elements in chondritic meteorites (Cd, Bi, Pb, and Tl) must have been separated from the chondrites independently of each other and independently of the other fractionated elements in response to individual elemental characteristics, while there is also evidence for additional fractionation of entire groups of other elements. The former type of fractionation might be explained as due to a sulfide-extraction process, as suggested by earlier workers. The latter fractionation of groups of elements may be due to a mixing of a high-temperature chemical fraction with a low-temperature chemical fraction of cosmic (primordial) composition. This view is consistent with the idea that type I carbonaceous chondrites and certain types of enstatite chondrites are the most primitive types of meteorites.

Mueller and Olsen (ref. 323) have compared the amount of normative olivine in chondrites of types H, L, and LL with the oxidation states of the meteorites. They find that these factors are related according to a corollary of Prior's rule—that the olivine content increases as the oxidation state increases. The same relationship holds for all these types, indicating that they are quite homogeneous. This factor must be taken into account in theories of meteorite origin.

Ahrens (ref. 324), on the other hand, has found significant fractionation of calcium (relative to silicon) between carbonaceous chondrites (Ca/Si=10.1) and ordinary chondrites (Ca/Si=15.5), representing a fractionation of 54 percent between the two groups. The ratios Si/Mg and Si/Al vary by 10 percent and 27 percent, respectively, between these groups.

Larimer (ref. 325) has made a study of the thermodynamics of condensation of material from a gas of solar composition. His results are summarized in figure 48 and are given for condensation during both fast cooling and slow (equilibrium) cooling. In both cases, metallic iron precipitates at the highest temperatures (after the precipitation of several minor compounds). This relative sequence may not conform to several petrographic studies, but relative fractionation of volatiles can be used to explain the extreme depletion of Pb, Bi, In, and Tl in ordinary chondrites. The evidence, Larimer concludes, supports the hypothesis of the existence of a mixture of two fractions: volatile and involatile. Larimer and Anders point out in reference 326 that, in the sequence, type I carbonaceous chondrites, type II carbonaceous chondrites, type III carbonaceous chondrites, type I enstatite chondrites, 31 volatile elements decrease by the factors, 1: 0.6: 0.3: 0.7. The volatile contents of the meteorites, when applied to the data of Larimer (ref. 325), indicate that carbonaceous chondrites condensed at temperatures below 400° K; enstatite chondrites (type I) between 400° and 480° K, ordinary and type II enstatite chondrites between 530° and 650° K, and unequilibrated ordinary chondrites above 530° K. Larimer and Anders point out that these temperatures are higher than the blackbody temperature of objects in the asteroid belt. These temperatures and the proportion

333-240 O—69——27

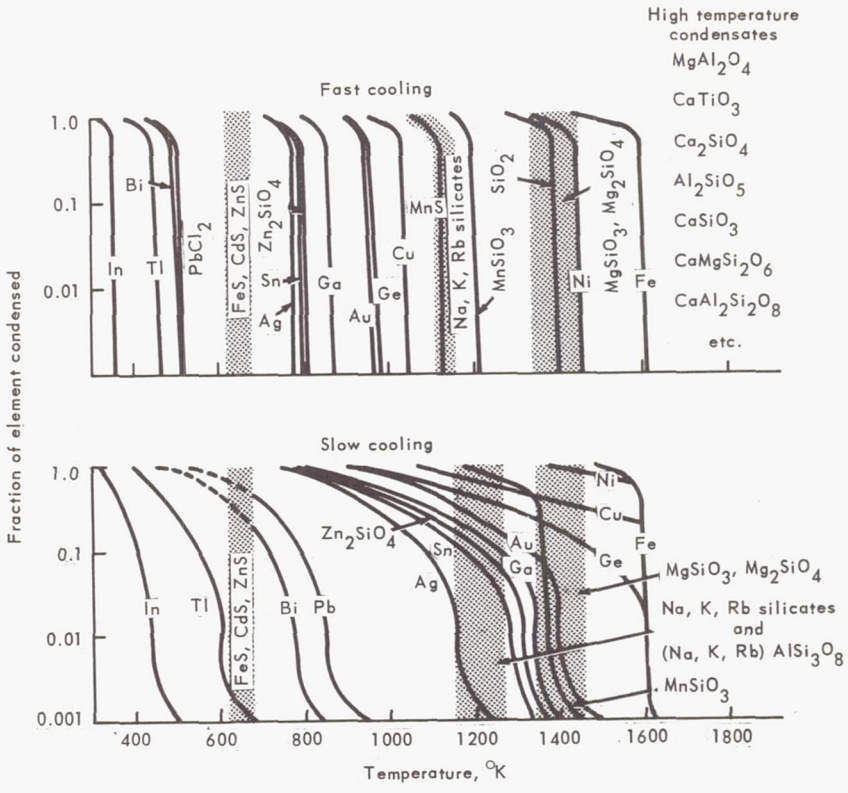


Figure 48.—**Condensation of the elements as a function of temperature and cooling rate. In fast cooling, successive layers of pure elements or compounds condense on grain surfaces with little or no diffusion into the grain interior. Condensation range for each element is quite narrow. In slow cooling, newly condensed elements diffuse into grain interior forming solid solutions. Activity in condensed phase is lowered, leading to higher condensation temperatures and broader condensation ranges.**

of volatile (A) and nonvolatile (B) fractions in various meteorite types and the Earth, as determined by their trace elements, are presented in table VIII.

Blander and Katz also discuss in reference 327 a model for the condensation of primordial gas of solar composition to form the chondrules, taking into account the difficulties such a slowly condensing gas has in finding nucleation sites. The Blander and Katz mechanism of disequilibrium condensation seems to explain several perplexing aspects of the formation of chondrules. (Equilibrium condensation of a low-density solar gas takes place at temperatures at which crystalline silicates are stable. Thus, in

Table VIII.—*Formation Conditions of Meteorites and the Earth*

[From refs. 325 and 326]

Class	Fraction A,[a] %[b]	Features diagnostic of—			Inferred condensation or accretion temperature, °K	
		Fraction A[a]		Fraction B[a]		
		H_2O	Tl, Bi, and In in "normal" abundance?	Na, K, and Rb lost?	Fraction A	Fraction B
Carbonaceous I	[c] ≥80	Yes	Yes	([c])	≤315	([c])
Carbonaceous II	55	Yes	Yes	Yes	≤315	>1300
Carbonaceous III	32	Yes	Yes	Yes	≤400	>1300
Enstatite I	66	No	Yes	No	400 to 470	~1200
Enstatite II	48	No	No	Yes	530 to 650	>1300
Ordinary	27	No	No	No	530 to 650	~1200
Eucrites, howardites	<10		No?	Yes	>530?	>1300
Irons I, II	50 to 100		No		>530	≥1100
Irons III	20		No		>530	≥1100
Irons IV	2		No		>530	≥1100
Earth (surface)	~10	Yes	Yes	Yes	≤400	>1300

[a] Fraction A is considered "volatile" by the authors (refs. 325 and 326); Fraction B is considered "nonvolatile."

[b] Inferred from abundance of normally depleted elements.

[c] Type I carbonaceous chondrites seem to contain most elements, including alkalis, in their cosmic proportions. The simplest interpretation would be that they consist of pure fraction A. However, the data are not accurate enough to preclude the possibility of a slight (≤20%) depletion, and consequently a minor admixture of fraction B.

order to form chondrules which have obviously been molten, a reheating stage is required.) They point out that, in disequilibrium condensation, liquids can form metastably below the solidus of the system, enabling liquid chondrules to condense directly from the solar gas. Furthermore, it may be more difficult for iron to start nucleation sites so that, while under equilibrium conditions, iron would precipitate at high temperatures (ref. 325), iron would, under disequilibrium conditions, begin to condense only after most silicates. This process would agree with the petrographic evidence (ref. 305) and, because it would result in an increase in the activity of FeO in the gas, it would also explain the high and variable FeO content of primitive meteorites (the FeO content being higher than predicted by the oxygen pressure of the solar gas).

Urey (ref. 328) also has discussed the origin of chondrules, pointing out that their accretion to form meteorites must have taken place in a gravitational field of appreciable strength. He proposes that chondrules are formed by the collision of objects in space (one of them, probably, the Moon) and that the temperatures of these objects were, at the time of collision, close to their melting points. Repeated collisions with the parent body result in a surface covered with chondrules and matrix (ground-up chondrules). Since the starting material for the formation of chondrules consists essentially of two phases—olivine and pyroxene—the droplets, being a small sample of this material, cool to form the same homogeneous minerals in varying proportions (explaining the mineralogical homogeneity and chemical heterogeneity of chondrules). As the material at the surface cools it absorbs inert gases of solar composition. The metal (which may have been derived from the colliding smaller objects) undergoes the transition from taenite to kamacite. The theory has one major advantage—it explains the accretion of the chondrules. As the author points out, collision between two asteroids might form droplets such as chondrules but would result in the scattering of these droplets throughout space.

TEKTITES

During 1967 several interesting discoveries were made concerning tektites. Of major importance was the discovery by Glass (ref. 329) of microtektites—glass particles in the size range of 50 to 100 microns with the shapes and indices of refraction of tektites. These particles were found in core samples from the ocean floor around Australia and were dated at about 700 000 years by their proximity to a geomagnetic reversal. This age agrees, essentially, with the potassium-argon age for the Southeast Asian tektite strewnfield. Calculation of the mass required to form the observed distribution of both microtektites and tektites has greatly increased the mass of material required to form the strewnfield. In addition, the size of the object or objects striking the Earth and the association with the magnetic reversal suggested to Glass and Heezen (ref. 330) that the reversal occurred

because the shock caused alterations in the currents which cause the magnetic field. Periodic changes in the direction of the field indicate that, energetically, the vector is not very stable. Thus, a huge impact, such as that which produced the Southeast Asian field, may have imparted sufficient energy to the Earth to reverse the field.

Nininger and Huss (ref. 331) discovered several tektite specimens (fig. 49) which indicate that they were partially molten at the time of landing. Others (fig. 50) show fractures in what must have been a hardened skin, as well as the formation of a meniscus in what was a molten interior at the time of impact. If the flattening and fractures occurred at the time of impact with the Earth's surface, the tektites could not have come to the Earth as individual fragments because, in that case, they would have been hardened throughout at the time of impact. These tektites do indicate that the surface sculpturing of tektites is the result of aerodynamic ablation rather than weathering since the meniscus surfaces (fig. 50) are smooth relative to the rest of the surface of these specimens.

Gentner, Kleinman, and Wagner (ref. 332) have compiled new fission-track age determinations together with older age determinations of tektites and impact-crater glasses. The results, given in table IX, show a very good correlation between the ages of moldavite tektites and the Ries crater, Germany, glass on one hand, and Ivory Coast tektites and the Bosumtwi crater, Ghana, glass on the other. This evidence lends strong support to a terrestrial origin for these tektites. Kolbe et al. (ref. 333) determined the Rb/Sr isochron age of metamorphism of the country rock around the Bosumtwi crater and found it to be 2110 million years—in general agreement with the Rb/Sr isochron age for both the Bosumtwi crater glass and the Ivory Coast tektites. This result, again, relates the Ivory Coast tektites to the impact event at the Bosumtwi crater.

Table IX.—*K/Ar and Fission-Track Ages of Impact Glasses and Tektites*

[From ref. 332]

Material	Number	Age-type	Age, yr	Range, yr
Moldavite tektites	5	Fission track	$14.1 \pm 0.6 \times 10^6$	13.4 to 14.5×10^6
Moldavite tektites	.....	K/Ar	14.7 ± 0.7	
Ries impactite glass	5	Fission track	14.0 ± 0.6	13.7 to 14.6
Ries impactite glass	.....	K/Ar	14.8 ± 0.7	
Ivory Coast tektites	15	Fission track	1.02 ± 0.1	
Ivory Coast tektites	15	K/Ar	1.1 ± 0.1	
Bosumtwi crater impactite glass.	.....	Fission track	1.04 ± 0.2	
Bosumtwi crater impactite glass.	.....	K/Ar	1.3 ± 0.3	

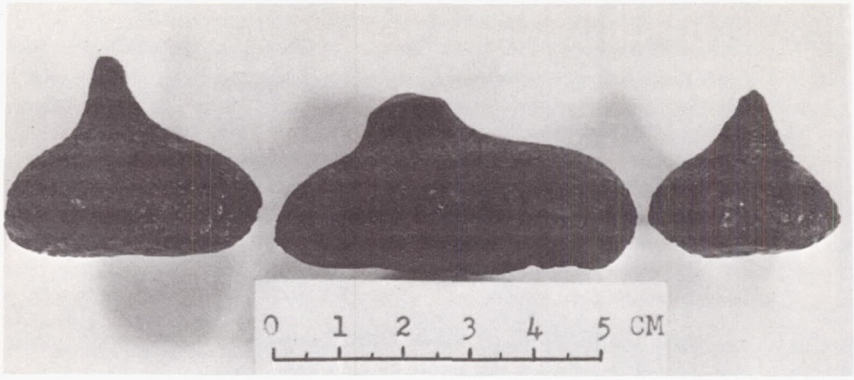


Figure 49.—Tektites with bulbous drops that show plastic flattening and external spallation after completion of aerial sculpturing. Photograph courtesy of the American Meteorite Laboratory.

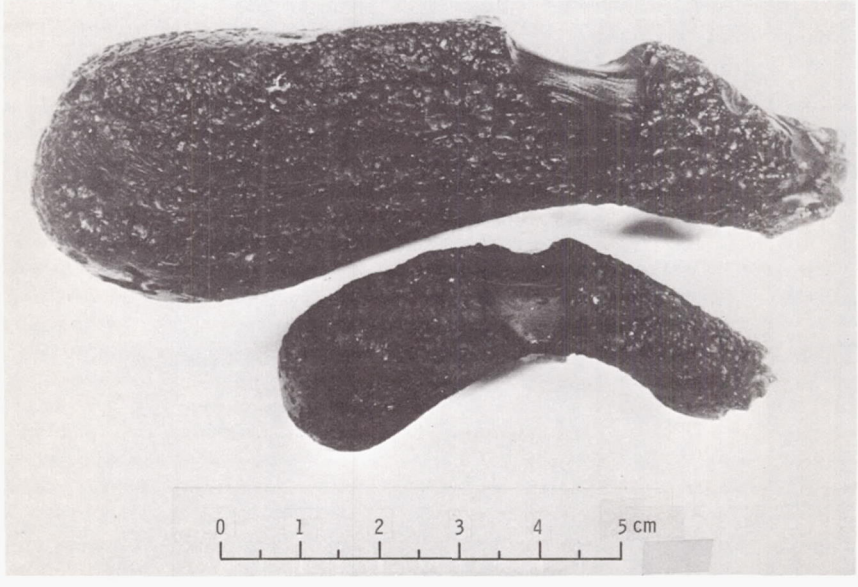


Figure 50.—Tektites that suffered surface breaks and interior stretching during plastic bending. Note the lack of sculpturing within breaks. Photograph courtesy of the American Meteorite Laboratory.

Finally, Walter (ref. 334) reported the results of the vapor fractionation of silicate melts at high temperatures. In this work, material of the composition of the most siliceous tektites was subjected to high temperatures (2800° C) in a solar furnace. The residual glass was then analyzed by microprobe and the variation of other oxides was plotted against silica content (fig. 51). The resulting trends are quite similar to trends for the analyses of tektites within strewn fields such as the North American tektites (fig. 52). This similarity is strong evidence that all tektites (except, perhaps those from the Ivory Coast) were derived from an extremely siliceous starting material through a high-temperature vaporization process.

SUMMARY

The Planets

Of major importance in the study of the planets was the sounding of Venus' atmosphere by the Soviet planetary probe Venera 4 and the simultaneous flyby of the U.S. Mariner V. These missions provided information concerning surface temperature, total pressure, atmospheric composition,

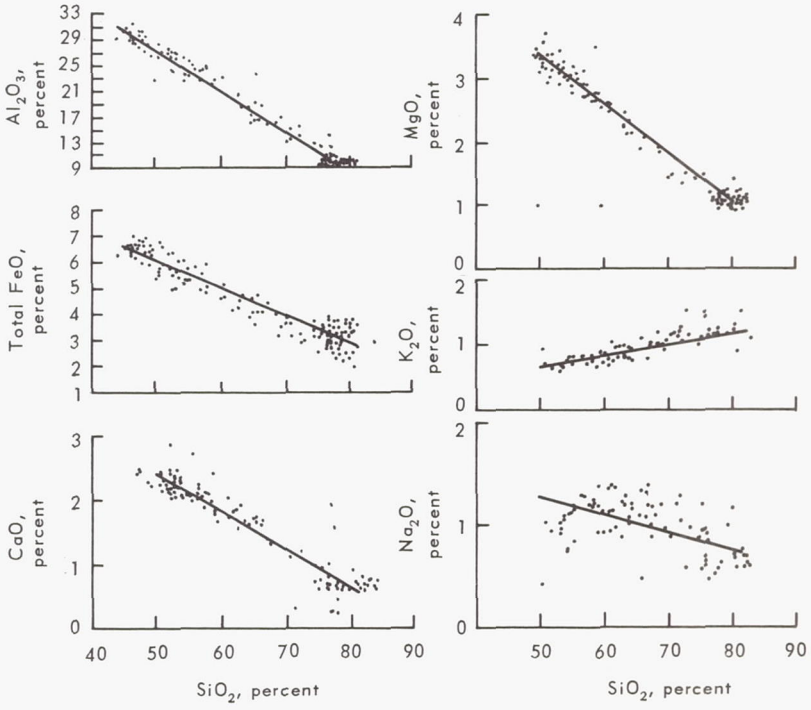


Figure 51.—Vapor fractionation of silicate melts containing 82 percent SiO_2 performed at 2800° C.

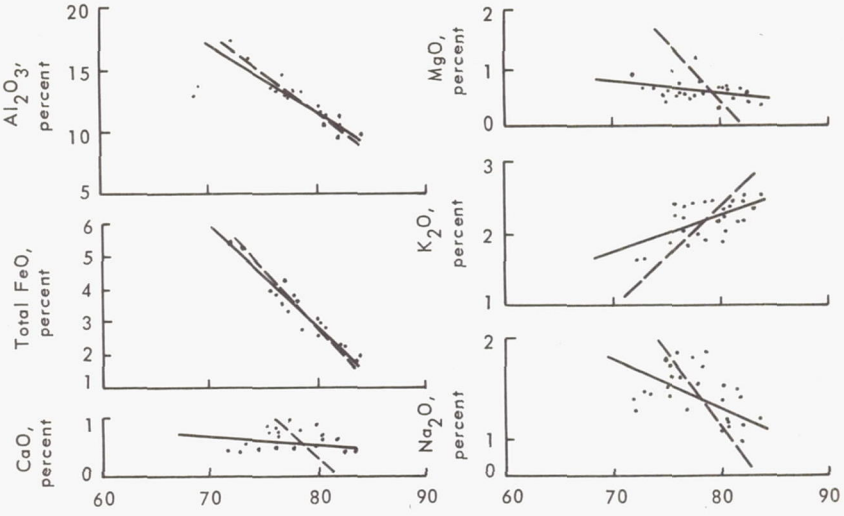


Figure 52.—**Major oxide-silica correlations for North American tektites.**

exospheric temperature and composition, and strength of the magnetic field. These data have a critical bearing on study of the present physicochemical state and evolutionary history of the planet. Terrestrial observations supplemented the planetary probe data by detecting and measuring hydrogen chloride and hydrogen fluoride in the atmosphere of Venus.

Study of infrared spectra of Mars indicates a nearly pure carbon dioxide atmosphere at a surface pressure of approximately 5 millibars. Although it is yet not clear whether the icecaps on Mars consist of carbon dioxide or water, a positive correlation was proven between the icecaps and the frequency of occurrence of the white clouds. A detailed photometric map of the Martian surface was compiled based on 3500 visual estimates in the white, green, and red regions of the spectrum. As a result of observations with a birefringence interferometer, it is concluded that the surface consists at least in part of hydrous minerals, and although iron oxides are regarded as only minor constituents of the surface, they probably account for the observed red coloration.

The Moon

In 1967, four Surveyor spacecraft landed in mare regions of the Moon, and three Lunar Orbiters were placed in orbit around the Moon. Surveyor III found that the inside of a subdued mare crater had the characteristics of the intercrater mare areas photographed by Surveyor I, confirmed the Surveyor I discovery that the lunar-subsurface material was darker than the surface material, and showed that the unconsolidated material was slightly cohesive and became noticeably stronger and more dense at depths

of about 3 inches. The Surveyor V alpha-scattering experiment provided the first lunar chemical compositional data. In general, the mare material at the Surveyor V site has the chemical composition of basalt. A magnet attached to the Surveyor landing leg attracted magnetic particles in amounts that correlated with those expected from basaltic rocks. These results, along with observation of the general physiography of the landing site region, indicate that the Moon is a differentiated body.

Lunar Orbiters provided Apollo landing-site information and new insight concerning the extent and nature of lunar volcanic processes and mass wasting. Although the controversy about the origin of craters continues, it is clear that volcanism has played a major role in the formation of lunar rocks and terrain features. Significant geodesy data related to the study of the Moon's gravitational field were obtained through an analysis of the Lunar Orbiter tracking data.

Despite the dramatic discoveries made by the Surveyors and Lunar Orbiters, telescopic mapping of the Moon remains an important project with several new maps being published in 1967: those of the Copernicus Quadrangle, Hevelius region, Seleucus Quadrangle, and Mare Humorum. There were several new approaches to studying lunar transient phenomena. Because they permit inferences as to the subsurface structure, infrared, radio, and radar investigations of the Moon continue to be of considerable importance.

Earth

Studies of terrain photographs obtained during the Gemini Earth orbital missions indicate that their most promising geological applications are in studies of continental drift, structure of rift valleys, investigations of transcurrent faulting, and other regional geologic problems. The geologic history of the Pacific basin is of importance in planetology not only as the largest single tectonic feature of the Earth, but in relation to the origin of the Earth-Moon system.

Interest in field and laboratory investigations of meteorite impact craters and associated impact metamorphism continues to grow. The most extensive of these studies have been carried out in Canada where 16 probable impact craters are now recognized. In the United States, major field investigations of the Flynn Creek, Tennessee, and of the Sierra Madera, Texas, structures were conducted. Drill holes have confirmed the presence of a central peak and occurrence of breccia in the Flynn Creek structure. At Sierra Madera, investigators have mapped the central uplift in great detail, demonstrating the existence of a stratigraphic uplift of 6400 meters associated with steep, overturned, complexly faulted beds in the central zone.

Studies of the Earth per se have led to a number of significant contribu-

tions to knowledge in the field of planetology. Studies concerning the uses and limitations of potassium/argon and rubidium/strontium mineral age dating indicate that in a contact metamorphic zone the relative stability of mineral ages is dependent upon the mineral species and age system under consideration (i.e., hornblende K/Ar>muscovite Rb/Sr>muscovite K/Ar>biotite Rb/Sr>biotite K/Ar). The use of several cogenetic phases from the same rock body and their interpretation by graphical isochron diagrams is more informative than the simple calculation and comparison of potassium/argon ages from the phases. Rubidium and strontium data support the theory of anatexis of eugeosynclinal sedimentary rocks in orogenic belts to produce granitic magmas, if melting occurred within several hundreds of million years after sedimentation.

Analysis of 5 years of observation of the 1960 Iota-2 satellite and radio interferometry has provided a substantial improvement in the precision of measurement of the rotation period of the Earth.

In geomagnetism, a new statistical method has been developed for determining the ages of the boundaries between geomagnetic polarity epochs. The statistical analysis shows that if the geomagnetic polarity time scale is to be extended much beyond its present limit of 3.6 million years, another method, other than potassium/argon, of dating the rocks will probably have to be used.

Studies of data from long-period seismographs on 17 earthquakes support the hypothesis of the growth of the sea floor at the crest of the midoceanic ridge system. Investigations of the velocity of seismic-wave propagation and the variations in the velocities of P- and S-waves in several regions of the United States showed variations which may be due to differences in temperatures in the upper mantle under these regions. Heat-flow measurements in continental and oceanic regions indicate that thermal displacements and stresses give rise to several tectonic features. Concerning the question of a phase-change as an explanation of seismic and density discontinuities in the mantle, the velocity transition may be best explained by two transition regions, each about 75 to 90 kilometers thick and at about 365 and 620 kilometers depth. Seismic data were used to investigate the structure of the Earth's core and the results suggest a layered transition zone between 4015 and 5140 kilometers below the surface.

Iron and stony-iron meteorite studies have indicated that the ^{3}H in irons and the iron phases of stones is low. Two explanations are offered: diffusion of ^{3}H out of the iron phase during terrestrial descent and residence, and solar heating of the meteorites in space. Isotopic composition and lithium abundance were measured on several chondrites as well as on the silicate and troilite inclusions in the Odessa octahedrite.

Chemical analysis of iron meteorites using emission spectroscopy, neutron activation, and other elemental analysis techniques has been performed for both major (Fe, Ni, Co) and minor elements (P, S, C), and for trace ele-

ments (Ga, Ge, Pt, Ir, Cr, Cu, etc.). Many nonmetallic minerals have been found in iron meteorites. Studies of the composition and oxidation state of each mineral, as well as its relationship to other surrounding minerals, have provided independent data on conditions under which the iron meteorites were formed. Metallographic examination of iron meteorites has yielded information concerning thermal-mechanical recrystallization of Goose Lake fragments. Two rapid and simple methods have been developed for the determination of approximate cooling rates of iron phases in meteorites without the need for extensive computer calculations.

The unusual mineralogy of stony-iron meteorites suggests their possible link between the two major groups of meteorites. Studies of the principal mineralogical and textural properties indicate that they are due to original magmatic crystallization followed by complex fragmentation and recrystallization episodes. Minor element abundances (Ni, Ga, Ge, and Ir) in six pallasites indicate that the pallasites are all members of a single genetic group. It is also proposed that most of the stony-iron meteorites and achondrites, other than enstatite achondrites, can be derived by melting and fractional crystallization of one or more parent bodies with the overall composition of chondrites.

Research on stony meteorites has centered around the search for those types which represent the most primary material because these can yield the most significant data concerning the origin of the elements, the solar system, and meteorites. A new classification of chondritic meteorites which depends on essentially two parameters (the chemistry and petrologic type) has been proposed and widely accepted. Evidence from a general survey of the unequilibrated ordinary chondrites indicates that they represent three distinct metamorphic series which involve a general increase in the oxidation state. Retention of disequilibrium silicate phases in the unequilibrated chondrites supports the contention that the more metamorphosed chondrites were reheated. Experimental studies indicate that in order to derive an equilibrated from an unequilibrated chondrite, considerable redistribution of iron must take place, since the average ferrous oxide content of pyroxenes in unequilibrated chondrites is substantially lower than that of equilibrated types.

One of the several mineralogic and petrographic studies on meteorites which exhibit shock effects and brecciation indicates the following sequence of events: deposition of unequilibrated chondrules; heating of regions of the parent body from 800 to 1200° C, causing local homogenization and partial melting; and breakup and reaccumulation.

Metallographic studies indicate that the blackened hypersthene chondrites have been strongly shocked (from a few hundred to over a thousand kilobars shock pressure) and that these meteorites experienced varying degrees of helium loss during the shock process.

Mean thorium/uranium ratios for carbonaceous chondrites, determined

by neutron activation analysis, were found to be considerably lower than predicted by nucleosynthetic theory. In contrast, cosmic abundances for antimony were found to be considerably higher than predicted by current theories of nucleosynthesis.

Other studies on the isotopic composition of tin in a variety of meteoritic and terrestrial samples indicate no evidence of significant variations resulting from inhomogeneities in galactic or solar system processes. Tin was chosen specifically because each of its various isotopes is produced by one of the major nuclear synthesizing processes.

Study of the thermodynamics of condensation of material from a gas of solar composition supports the hypothesis of the existence of a mixture of two fractions: volatile and involatile. Volatility data can provide a model for the condensation of primordial gas of solar composition to form chondrules, taking into account the difficulties such a slowly condensing gas has in finding nucleation sites. It would explain an increase in the activity of ferrous oxide in the gas, and the high and variable ferrous oxide content of primitive meteorites (the ferrous oxide content being higher than predicted by the oxygen pressure of the solar gas). Another viewpoint proposes that chondrules are formed by collisions between objects in space and that the temperatures of these objects were close to their melting points at the time of collision.

The discovery of microtektites in core samples from the ocean floor around Australia is of major importance to the study of tektites. Their age, 700 000 years, agrees with the potassium/argon age for the Southeast Asian tektite strewnfield. A huge meteoritic impact, such as that which produced the Southeast Asian field, may have imparted sufficient energy to the Earth to reverse the magnetic field.

Prospectus

It is axiomatic in the many scientific fields that acquisition of information takes little time, compared to the time needed for interpretation. A prime example of this is that the early Rangers sent back their pictures in a few minutes in 1964 and 1965, but interpretation of those pictures will continue beyond 1967. Thus with the masses of data obtained, analyzed, and reported during 1967, and the accelerated activities in the field of planetology, these can and have led to more questions than answers—a challenge to the planetologist in the study of the condensed matter of the solar system.

REFERENCES

1. BARKER, E. S.: A Determination of the Martian CO_2 Abundance. Astrophys. J., vol. 147, 1967, pp. 379–381.
2. SCHORN, R. A.; AND GRAY, L. D.: The Martian Surface Pressure. Astrophys. J., vol. 148, 1967, pp. 663–667.
3. WELLS, R. A.: Some Comments on Martian White Clouds. Astrophys. J., vol. 147, 1967, pp. 1181–1183.
4. DE VAUCOULEURS, G.: A Low-Resolution Photometric Map of Mars. Icarus, vol. 7, 1967, pp. 310–349.
5. SINTON, W. M.: On the Composition of Martian Surface Materials. Icarus, vol. 6, 1967, pp. 222–228.
6. MIYAMOTO, S.: Lunar and Martian Crust and Mantle Convection. Icarus, vol. 6, 1967, pp. 50–55.
7. O'LEARY, B. J.; AND REA, D. G.: On the Polarimetric Evidence for an Atmosphere on Mercury. Astrophys. J., vol. 148, 1967, pp. 249–253.
8. KLIORE, A.; LEVY, G. S.; CAIN, D. L.; FJELDBO, G.; AND RASOOL, S. I.: Atmosphere and Ionosphere of Venus From the Mariner V S-Band Radio Occultation Measurement. Science, vol. 158, 1967, pp. 1683–1688.
9. ANON.: Tass, Izvestia, Oct. 31, 1967.
10. ANON.: Tass, Pravda, Oct. 22, 1967.
11. REESE, D. E.; AND SWAN, P. R.: Venera 4 Probes Atmosphere of Venus. Science, vol. 159, 1968, pp. 1228–1230.
12. VAN ALLEN, J. A.; KRIMIGIS, S. M.; FRANK, L. A.; AND ARMSTRONG, J. P.: Venus: An Upper Limit on Intrinsic Magnetic Dipole Moment Based on Absence of a Radiation Belt. Science, vol. 158, 1967, pp. 1671–1675.
13. BARTH, C. A.; PEARCE, J. B.; KELLY, K. K.; WALLACE, L., AND FASTIE, W. G.: Ultraviolet Emissions Observed Near Venus from Mariner 5. Science, vol. 158, 1967, pp. 1675–1678.
14. MARINER STANFORD GROUP: Venus: Ionosphere and Atmosphere as Measured by Dual-Frequency Radio Occultation of Mariner 5. Science, vol. 158, 1967, pp. 1678–1683.
15. CONNES, P.; CONNES, V.; BENEDICT, W. S.; AND KAPLAN, L. D.: Traces of HCl and HF in the Atmosphere on Venus. Astrophys. J., vol. 147, 1967, pp. 1230–1237.
16. ADAMCIK, J. A.; AND DRAPER, A. L.: The Temperature Dependence of the Urey Equilibrium and the Problem of the Carbon Dioxide Content of the Atmosphere of Venus. Planetary Space Sci., vol. 11, 1963, pp. 1303–1307.
17. MUELLER, R. F.: A Chemical Model for the Lower Atmosphere of Venus. Icarus, vol. 3, 1964, pp. 285–298.
18. LIPPINCOTT, E. R.; ECK, R. V.; DAYHOFF, M. O.; AND SAGAN, C.: Thermodynamic Equilibrium in Planetary Atmospheres. Astrophys. J., vol. 147, 1967, pp. 753–764.
19. GOLDREICH, P.; AND PEALE, S.: Spin-Orbit Coupling in the Solar System. II. The Resonant Rotation of Venus. Astron. J., vol. 72, 1967, pp. 662–668.
20. SASLOW, W. C.; AND WILDEY, R. L.: On the Chemistry of Jupiter's Upper Atmosphere. Icarus, vol. 7, 1967, pp. 85–93.
21. TRAFTON, L. M.: Model Atmospheres of the Major Planets. Astrophys. J., vol. 147, 1967, pp. 765–781.
22. DULK, G. A.: Apparent Changes in the Rotation Rate of Jupiter. Icarus, vol. 7, 1967, pp. 173–182.
23. MARCUS, A. H.: Formation of Planets by Accretion of Planetesimals—Some Statistical Problems. Icarus, vol. 7, 1967, pp. 283–296.

24. HARRIS, P. G.; AND TOZER, D. C.: Fractionation of Iron in the Solar System. Nature, vol. 215, 1967, pp. 1449–1451.
25. SHIMAZU, Y.: Thermodynamical Aspects of Formation Processes of the Terrestrial Planets and Meteorites. Icarus, vol. 6, 1967, pp. 143–174.
26. HARTMANN, W. K.; AND LARSON, S. M.: Angular Momentum of Planetary Bodies. Icarus, vol. 7, 1967, pp. 257–260.
27. ALFVÉN, H.: On the Formation of Celestial Bodies. Icarus, vol. 3, 1964, pp. 57–62.
28. HANSON, G. H.; AND GAST, P. W.: Kinetic Studies in Contact Metamorphic Zones. Geochim. Cosmochim. Acta., vol. 31, 1967, pp. 1119–1153.
29. LIVINGSTON, D. E.; DAMON, P. E.; MANGER, R. L.; BENNETT, R.; AND LAUGHLIN, A. W.: Ar^{40} in Cogenetic Feldspar—Mica Mineral Assemblages. J. Geophys. Res, vol. 72, 1967, pp. 1361–1375.
30. PETERMAN, Z. E.; HEDGE, C. E.; COLEMAN, R. G.; AND SNAVELY, P. D., JR.: Sr^{87}/Sr^{86} Ratios in Some Eugeosynclinal Sedimentary Rocks and Their Bearing on the Origin of Granitic Magma in Orogenic Belts. Earth Planetary Sci. Letters, vol. 2, 1967, pp. 433–439.
31. ULRYCH, T. D.: Oceanic Basalt Leads: A New Interpretation and an Independent Age for the Earth. Science, vol. 158, 1967, pp. 252–256.
32. TILTON, G. R.; AND STEIGER, R. H.: Lead Isotopes and the Age of the Earth. Science, vol. 150, 1965, pp. 1805–1807.
33. HURLEY, P. M.; DE ALMEIDA, F. F. M.; MELCHER, G. C.; CORDANI, V. G.; RAND, J. R.; KAWASHITA, K.; VANDORAS, P.; PINSON, W. H.; AND FAIRBAIRN, H. W.: Test of Continental Drift by Comparison of Radioactive Ages. Science, vol. 157, 1967, pp. 495–500.
34. HAKLI, T. A.; AND WRIGHT, T. L.: The Fractionation of Ni Between Olivine and Augite as a Geothermometer. Geochim. Cosmochim. Acta, vol. 31, 1967, pp. 877–884.
35. HAHN-WEINHEIMER, P.; AND ACKERMANN, H.: Geochemical Investigation of Differentiated Granite Plutons of the Southern Black Forest–II. The Zoning of the Malsberg Granite Pluton as Indicated by the Elements Titanium, Zirconium, Phosphorus, Strontium, Barium, Rubidium, Potassium, and Sodium. Geochim. Cosmochim. Acta, vol. 31, 1967, pp. 2197–2218.
36. CONDIE, K. C.: Composition of the Ancient North American Crust. Science, vol. 155, 1967, pp. 1013–1015.
37. LOWMAN, P. D., JR.: Geologic Applications of Orbital Photography. NASA TN–D–4155, 1967.
38. LOWMAN, P. D., JR.; AND TIEDEMANN, H. A.: Field Mapping From Orbital Photographs (Abstract). Paper presented at 1967 Annual Meeting of Geological Society of America, New Orleans, La., Nov. 20–22, 1967, p. 134.
39. ABDEL-GAWAD, M.: Geologic Exploration and Mapping From Space. Paper presented to American Astronautical Society, 1967.
40. BATEMAN, P. C.; AND EATON, J. P.: Sierra Nevada Batholith. Science, vol. 158, no. 3807, Dec. 1967, pp. 1407–1417.
41. HAMILTON, W.; AND MEYERS, W. B.: The Nature of Batholiths. Shorter Contributions to General Geology, U.S. Geological Survey Professional Paper 554–C, 1967, pp. C1–C30.
42. TAYLOR, S. R.: The Origin and Growth of Continents. Tectonophys., vol. 4, no. 1, 1967, pp. 17–34.
43. MATSUMOTO, T., ED.: Age and Nature of Circum-Pacific Orogenesis. Tectonophys., vol. 4, nos. 4–6, 1967, pp. 317–623.

44. Roddick, J. A.; Wheeler, J. O.; Gabrielse, H.; and Souther, J. G.: Age and Nature of the Canadian Part of the Circum-Pacific Orogenic Belt. Tectonophys., vol. 4, nos. 4–6, 1967, pp. 319–337.
45. Ho, O. S.: Structural Evolution of Taiwan. Tectonophys., vol. 4, nos. 4–6, 1967, pp. 367–378.
46. Aronson, J. L.: Absolute Ages of the Plutonic and Metamorphic Rocks of New Zealand (Abstract). Tectonophys., vol. 4, nos. 4–6, 1967, p. 499.
47. Vassilkovsky, N. P.: On the Geological Nature of the Pacific Mobile Belt. Tectonophys., vol. 4, nos. 4–6, 1967, pp. 583–593.
48. Burgl, H.: The Orogenesis in the Andean System of Columbia. Tectonophys., vol. 4, nos. 4–6, 1967, pp. 429–443.
49. Hamilton, W.: Continental Drift in Eastern Asia and Alaska (Abstract). Tectonophys., vol. 4, nos. 4–6, 1967, p. 569.
50. Fleming, C. A.: Biogeographic Change Related to Mesozoic Orogenic History in the Southwest Pacific. Tectonophys., vol. 4, nos. 4–6, 1967, pp. 419–427.
51. Lamar, D. L.; and Merifield, P. M.: Cambrian Fossils and Origin of Earth-Moon System. Bull. Geolog. Soc. Am., vol. 78, 1967, pp. 1359–1368.
52. Paddack, S.: On the Angular Momentum of the Solid Earth. J. Geophys. Res., vol. 72, 1967, pp. 5760–5762.
53. Gold, T.: Radio Method for the Precise Measurement of the Rotation Period of the Earth. Science, vol. 157, 1967, pp. 302–304.
54. MacDonald, G. J. F.: Implications for Geophysics of the Precise Measurement of the Earth's Rotation. Science, vol. 157, 1967, pp. 304–305.
55. Alley, C. O.; Bender, P. L.; Dicke, R. H.; Faller, J. E.; Franken, P. A.; Plotkin, H. H.; and Wilkinson, D. T.: Optical Radar Using a Corner Reflector on the Moon. J. Geophys. Res., vol. 70, 1965, p. 2267–2269.
56. Lee, H. K.; and Kaula, W. M.: A Spherical Harmonic Analysis of the Earth's Topography. J. Geophys. Res., vol. 72, 1967, pp. 753–758.
57. Heinrich, D.: Paleomagnetism of the Plio-Pleistocene Lousetown Formation, Virginia City, Nevada. J. Geophys. Res., vol. 72, 1967, p. 3277–3294.
58. Baksi, A.; York, D.; and Watkins, N. D.: Age of Steens Mountain Geomagnetic Polarity Transition. J. Geophys. Res., vol. 72, 1967, pp. 6299–6308.
59. Grommé, C. S.; Merrill, R. T.; and Verhoogen, J.: Paleomagnetism of Jurassic and Cretaceous Plutonic Rocks in the Sierra Nevada, California, and Its Significance for Polar Wandering and Continental Drift. J. Geophys. Res., vol. 72, 1967, pp. 5661–5684.
60. Coe, R. S.: Paleo-Intensities of the Earth's Magnetic Field Determined From Tertiary and Quaternary Rocks. J. Geophys. Res., vol. 72, 1967, pp. 3247–3262.
61. Cox, A.; and Dalrymple, G. B.: Statistical Analysis of Geomagnetic Reversal Data and the Precision of K-Ar Dating. J. Geophys. Res., vol. 72, 1967, pp. 2603–2621.
62. Ozima, M.; Kono, M.; Kaneoka, I.; Kinoshita, H.; Kobuyashi, K.; Nagata, T.; Larson, E. E.; and Strongway, D.: Paleomagnetism and K-Ar Ages of Some Volcanic Rocks From the Rio Grande Gorge, New Mexico. J. Geophys. Res., vol. 72, 1967, pp. 2615–2621.
63. Sykes, L. R.: Mechanism of Earthquakes and Nature of Faulting on Mid-Oceanic Ridges. J. Geophys. Res., vol. 72, 1967, pp. 2131–2153.
64. Hodgson, J.: Nature of Faulting in Large Earthquakes. Bull. Geolog. Soc. Am., vol. 68, 1957, pp. 611–644.

65. HALES, A. L.; DOYLE, H. A.: P and S Travel Time Anomalies and Their Interpretation. Geophys. J. Roy. Astronom. Soc., vol. 13, 1967, pp. 403–415.
66. POLLACK, H. N.: Tectonic Implication of a Thermal Contrast Between Continents and Oceans. J. Geophys. Res., vol. 72, 1967, pp. 5043–5049.
67. ANDERSON, D. L.: Phase Changes in the Upper Mantle. Science, vol. 157, 1967, pp. 1165–1173.
68. HARRIS, P. G.; REAY, A.; AND WHITE, I. G.: Chemical Composition of the Upper Mantle. J. Geophys. Res., vol. 72, 1967, pp. 6359–6369.
69. CANER, B.; CANNON, W. H.; AND LIVINGSTONE, C. E.: Geomagnetic Depth Sounding and Upper Mantle Structure in the Cordillera Region of Western North America. J. Geophys. Res., vol. 72, 1967, pp. 6335–6351.
70. ERGIN, KAZIM: Seismic Evidence for a New Layered Structure of the Earth's Core. J. Geophys. Res., vol. 72, 1967, pp. 3669–3687.
71. SACKS, I.: Diffracted P-Wave Studies of the Earth's Core. J. Geophys. Res., vol. 72, 1967, pp. 2589–2594.
72. ARONSON, J. R.; ECKROAD, S. W.; AND ERNSLIE, A. G.: Radiative Thermal Conductivity in Planetary Interiors. Nature, vol. 216, 1967, pp. 1096–1097.
73. BULLEN, K. E.; AND HADDON, R. A.: Earth Models Based on Compressibility Theory. Phys. Earth Planet. Interiors, vol. 1, 1967, pp. 1–13.
74. MILWITZKY, B.; AND DWORNIK, S. E.: Introduction. Surveyor III—A Preliminary Report, ch. 2, NASA SP–146, 1967.
75. SHOEMAKER, E. M.; BATSON, R. M.; HOLT, H. E.; MORRIS, E. C.; RENNILSON, J. J.; AND WHITAKER, E. A.: Surveyor III—A Preliminary Report, ch. 3, NASA SP–146, 1967.
76. SCOTT, R. F.; ROBERSON, F. I.; AND CLARY, M. C.: Surveyor III—A Preliminary Report, ch. 4, NASA SP–146, 1967.
77. JAFFE, L. D.; BATTERSON, S. A.; BROWN, W. E., JR.; CHRISTENSEN, E. M.; DWORNIK, S. E.; GAULT, D. E.; LUCAS, J. W.; NORTON, R. H.; SCOTT, R. F.; SHOEMAKER, E. M.; SUTTON, G. H.; AND TURKEVICH, A. L.: Surveyor V—A Preliminary Report, ch. 1, NASA SP–163, 1967.
78. CHRISTENSEN, E. M.; BATTERSON, S. A.; BENSON, H. E.; CHOATE, R.; HUTTON, R. E.; JAFFE, L. D.; JONES, R. H.; KO, H. Y.; SCHMIDT, F. N.; SCOTT, R. F.; SPENCER, R. L.; AND SUTTON, G. H.: Surveyor V—A Preliminary Report, ch. 4, NASA SP–163, 1967.
79. DE WYS, J. N.: Surveyor V—A Preliminary Report, ch. 4, NASA SP–163, 1967.
80. WALTER, L. S.; AND LOWMAN, P. D., JR.: Planetology. Significant Achievements in Space Science, 1966. NASA SP–155, 1967.
81. TURKEVICH, A. L.; FRANZGROTE, E. J.; AND PATTERSON, J. H.: Chemical Analysis of the Moon at the Surveyor V Landing Site. Science, vol. 158, no. 3801, 1967, pp. 635–637.
82. DUKE, M. B.; AND SILVER, L. T.: Petrology of Eucrites, Howardites, and Mesosiderites. Geochim. Cosmochim. Acta, vol. 31, 1967, pp. 1637–1665.
83. MACDONALD, G. J. F.: Interior of the Moon. Science, vol. 133, no. 3458, 1961, pp. 1045–1050.
84. MICHAEL, W. H.; TOLSON, R. H.; AND GAPCYNSKI, V. P.: Lunar Orbiter: Tracking Data Indicate Properties of the Moon's Gravitational Field. Science, vol. 153, 1966, pp. 1102–1103.
85. O'KEEFE, J. A.; AND CAMERON, W. S.: Evidence From the Moon's Surface for the Production of Lunar Granites. Icarus, vol. 1, 1962, pp. 271–284.
86. KAULA, W.: The Geometric and Dynamical Figures of the Moon. Preprint 66–189, Am. Astronaut. Soc., 1966.

87. BALDWIN, R. B.: The Measure of the Moon. Univ. of Chicago Press (Chicago), 1963, p. 488.
88. CORLISS, W. R.: Scientific Satellites. NASA SP–133, 1967.
89. MCCAULEY, J. F.: The Nature of the Lunar Surface as Determined by Systematic Geologic Mapping. Mantles of the Earth and Terrestrial Planets, S. K. Runcorn, ed., Interscience Pub. (New York), 1967, pp. 431–460.
90. HEACOCK, R. L.; KUIPER, G. P.; SHOEMAKER, E. M.; UREY, H. C.; AND WHITAKER, E. A.: Experimenters' Analyses and Interpretation. Ranger VII, pt. II, ch. 4, Jet Propulsion Lab. Tech. rept. 38–700, 1965.
91. LEBEDINSKY, A. I.; KRASNOPOLSKY, V. A.; AND KRYSKO, A. A.: The Spectrophotometric Measurements of the Moon in the 1900–2750 Å range from the Zond 3 Automatic Space Probe. Moon and Planets. A Session of the Seventh International Space Science Symposium, A. Dollfus, ed., North-Holland Publ. Co., 1967, pp. 59–64.
92. LEBEDINKY, A. I.; ALESHIN, G. M.; IOZENAS, V. A.; KRASNOPOLSKY, V. A.; SELIVANOV, A. S.; AND ZASETSKY, V. V.: The Lunar Ultraviolet Spectrum in the Range of 2850–3550 Å According to the Data Obtained From the Zond 3 Automatic Space Probe. Moon and Planets. A Session of the Seventh International Space Science Symposium, A. Dollfus, ed., North-Holland Publ. Co., 1967, pp. 65–70.
93. NESS, N. F.; BEHANNON, K. W.; SCEARCE, C. S.; AND CANTARANO, S. C.: Early Results From the Magnetic Field Experiment on Lunar Explorer 35. J. Geophys. Res., vol. 72, no. 23, 1967, pp. 5769–5778.
94. GOLD, T.: The Magnetosphere of the Moon. The Solar Wind, R. J. Mackin, Jr., and N. Neugebauer, eds., Pergamon Press, 1966, pp. 381–392.
95. DOLGINOV, SH. SH.; YEROSHENKO, YE. G.; ZHUZGOV, L. N.; AND ZHULIN, I. A.: Possible Interpretation of the Results of Measurements in the Near Lunar Satellite AMS Luna 10. Geomagnetizm Aeronomiya, vol. 7, 1967, pp. 436–441.
96. SCHMITT, H. H.; TRASK, N. J.; AND SHOEMAKER, E. M.: Geologic Map of the Copernicus Quadrangle of the Moon. U.S. Geological Survey, Map I–515 (LAC–58), 1967.
97. MCCAULEY, J. F.: Geologic Map of the Hevelius Region of the Moon. U.S. Geological Survey, Map I–491 (LAC–56), 1967.
98. MCCAULEY, J. F.: Geologic Results From the Lunar Precursor Probes. AIAA Paper No. 67–862, 1967.
99. MOORE, H. J.: Geologic Map of the Seleucus Quadrangle of the Moon. U.S. Geological Survey, Map I–527 (LAC–38), 1967.
100. MOORE, H. J.: Geologic Map of the Aristarchus Region of the Moon. U.S. Geological Survey, Map I–465 (LAC–39), 1965.
101. TITLEY, S. R.: Geologic Map of the Mare Humorum Region of the Moon. U.S. Geological Survey, Map I–495 (LAC–93), 1967.
102. TRASK, N. J.; AND TITLEY, S. R.: Geologic Map of the Moon. U.S. Geological Survey, Map I–485 (LAC–94), 1966.
103. EVSYUKOV, N. N.: Color Contrasts on the Lunar Surface. Soviet Astron.—AJ, vol. 10, no. 5, Mar.–Apr. 1967, pp. 840–843.
104. RACKHAM, T. W.: Color on the Moon. Icarus, vol. 7, 1967, pp. 297–309.
105. MCCORD, T. B.: Observational Study of Lunar Visible Emission. J. Geophys. Res., vol. 72, no. 8, Apr. 1967, pp. 2087–2097.
106. CAMERON, W. S.: Observations of Changes on the Moon. Paper presented at the Fifth Annual Meeting, Working Group on Extraterrestrial Resources, NASA Marshall Space Flight Center (Huntsville, Ala.), Mar. 1967, pp. 47–56.

333–240 O—69——28

107. BARTLETT, J. C., JR.: Aristarchus: The Violet Glare. The Strolling Astronomer, vol. 20, no. 1–2, Jan.–Feb. 1966, pp. 20–28.
108. GREEN, J.: Tidal and Gravity Effects Intensifying Lunar Defluidization and Volcanism. Ann. N.Y. Acad. Sci., vol. 123, art. 2, July 1965, pp. 403–469.
109. SPEISER, T. W.: Particle Trajectories in Model Current Sheets, 2. Analytical and Numerical Applications to Auroras Using a Geomagnetic Tail Model. Doc. 641–65–451, NASA Goddard Space Flight Center, 1965.
110. CAMERON, W. S.; AND GILHEANY, J. J.: Operation Moon Blink and Report of Observations of Lunar Transient Phenomena. Icarus, vol. 7, July 1967, pp. 29–41.
111. BURLEY, J. M.; AND MIDDLEHURST, B. M.: Apparent Lunar Activity, Historical Review. Proc. Nat. Acad. Sci., vol. 55, no. 5, 1966, pp. 1007–1011.
112. TAMRAZYAN, G. P.: Tide-Forming Forces and Earthquakes. Icarus, vol. 7, no. 1, July 1967, pp. 59–65.
113. MIDDLEHURST, B. M.; AND MOORE, P. A.: Lunar Transient Phenomena: Topographical Distribution. Science, vol. 155, no. 3761, Jan. 1967, pp. 449–451.
114. CHAPMAN, W. B.: Tidal Influences at the Lunar Crater Aristarchus. J. Geophys. Res., vol. 72, no. 24, 1967, pp. 6293–6298.
115. NASH, D. B.: Proton-Irradiation Darkening of Rock Powders: Contamination and Temperature Effects, and Applications to Solar-Wind Darkening of the Moon. J. Geophys. Res., vol. 72, no. 12, 1967, pp. 3089–3104.
116. PALM, A.: Enhanced Luminance of the Moon. Icarus, vol. 7, no. 2, Sept. 1967, pp. 188–192.
117. LIPSKII, P. K.; AND POSPERGELIS, M. M.: Some Results of the Total Stokes Vector for Details of the Lunar Surface. Soviet Astron.—AJ, vol. 11, no. 2, 1967, pp. 324–326.
118. MILLS, G. A.: Absolute Coordinates of Lunar Features. Icarus, vol. 7, no. 2, Sept. 1967, pp. 193–220.
119. MARKOV, M. N.; AND KHOKHLOVA, V. L.: The Lunar Surface Absorption Spectrum in the Range of 0.8 to 13 Microns. Moon and Planets. A Session of the Seventh International Space Science Symposium, A. Dollfus, ed., North-Holland Publ. Co., 1967, pp. 53–58.
120. SAARI, J. M.; AND SHORTHILL, R. W.: Isothermal and Isophotic Atlas of the Moon; Contours Through a Lunation. NASA CR–855, 1967.
121. SALISBURY, J. W.; AND HUNT, G. R.: Infrared Images of Tycho on Dark Moon. Science, vol. 155, no. 3766, Mar. 1967, pp. 1098–1100.
122. WILDEY, R. L.; MURRAY, B. C.; AND WESTPHAL, J. A.: Reconnaissance of Infrared Emission From the Lunar Nighttime Surface. J. Geophys. Res., vol. 72, no. 14, 1967, pp. 3743–3749.
123. TROITSKII, V. S.; KROTIKOV, V. D.; AND TSEITLIN, N. M.: Measurement of Radio Emission From the Moon in the 30–60 cm Band. Soviet Astron.—AJ, vol. 11, no. 2, 1967, pp. 327–328.
124. LOSOVSKII, B. YA.: Observations of Polarization of Lunar Radio Emission at 0.8 cm With High Resolution. Soviet Astron.—AJ, vol. 11, no. 2, 1967, pp. 329–331.
125. ESHLEMAN, V. R.: Radar Astronomy. Science, vol. 158, no. 3801, Nov. 1967, pp. 585–597.
126. TYLER, G. L.; ESHLEMAN, V. R.; FJELDBO, G.; HOWARD, H. T.; AND PETERSON, A. M.: Bistatic-Radar Detection of Lunar Scattering Centers With Lunar Orbiter I. Science, vol. 157, no. 3785, July 1967, pp. 193–195.

127. Cook, J. J.: A Survey of Lunar Geology. Earth Resources Survey Program Technical Letter, NASA–95, NASA Manned Spacecraft Center, 1967.
128. Trask, N. J.; and Rowan, L. C.: Lunar Orbiter Photographs: Some Fundamental Observations. Science, vol. 158, no. 3808, Dec. 1967, pp. 1529–1535.
129. Lowman, P. D., Jr.: Lunar Impact Craters. The Encyclopedia of Atmospheric Sciences and Astrogeology, R. W. Fairbridge, ed., Reinhold Publ. Co. (New York), 1967, pp. 629–633.
130. Oberbeck, V. R.; and Quaide, W. L.: Estimated Thickness of a Fragmental Surface Layer of Oceanus Procellarum. J. Geophys. Res., vol. 72, no. 18, 1967, pp. 4697–4704.
131. O'Keefe, J. A.; Lowman, P. D., Jr.; and Cameron, W. S.: Lunar Ring Dikes From Lunar Orbiter I. Science, vol. 155, no. 3758, 1967, pp. 77–79.
132. Fielder, G.: Volcanic Rings on the Moon. Nature, vol. 213, no. 5074, 1967, pp. 333–336.
133. Goles, G.; and Taylor, S. R.: Properties of Lunar Surface Rocks. Science, vol. 156, 1967, pp. 1134–1135.
134. Milton, D. J.: Slopes on the Moon. Science, vol. 156, no. 3778, 1967, p. 1135.
135. Hartmann, W. K.: Extrusive Lunar Ring Structures. Science, vol. 157, no. 3790, 1967, p. 841.
136. Marshall, C. H.: Geological Map and Sections of the Letronne Region of the Moon. U.S. Geological Survey, Map I–385 (LAC–75), 1963.
137. Fulmer, C. V.; and Roberts, W. A.: Surface Lineaments Displayed on Lunar Orbiter Pictures. Icarus, vol. 7, no. 3, Nov. 1967, pp. 394–406.
138. Rackham, T. W.: Lunar Orbiter Photography. Icarus, vol. 7, no. 2, Sept. 1967, pp. 263–267.
139. Green, J.: Calderas as Related to Lunar Exploration. U.S. Bureau of Mines, Contract P.O. Minn. 788–67, Advanced Research Laboratories, McDonnell Douglas Corp., Huntington Beach, Calif., Apr. 20, 1967.
140. Hapke, B: Surveyor I and Luna IX Pictures and the Lunar Soil. Icarus, vol. 6, no. 2, 1967, pp. 354–369.
141. Jaffe, L. D.: Surface Structure and Mechanical Properties of the Lunar Maria. J. Geophys. Res., vol. 72, no. 6, Mar. 1967, pp. 1727–1731.
142. Filice, A. L.: Lunar Surface Strength Estimate From Orbiter II Photographs. Science, vol. 156, no. 3781, June 1967, pp. 1486–1487.
143. Salisbury, J. W.; and Adler, J. E. M.: Density of the Lunar Soil. Nature, vol. 214, no. 5084, Apr. 1967, pp. 156–158.
144. Smith, B. G.: Boulder Distribution Analysis of the Luna 9 Photographs. J. Geophys. Res., vol. 72, no. 4, Feb. 1967, pp. 1398–1399.
145. O'Keefe, J. A.; and Scott, R. F.: Chondritic Meteorites and the Lunar Surface. Science, vol. 158, no. 3805, Dec. 1967, pp. 1174–1176.
146. Adams, J. B.: Lunar Surface Composition and Particle Size: Implications From Laboratory and Lunar Spectral Reflectance Data. J. Geophys. Res., vol. 72, no. 22, Nov. 1967, pp. 5717–5720.
147. Adams, J. B.; and Filice, A. L.: Spectral Reflectance 0.4 to 2.0 Microns of Silicate Rock Powders. J. Geophys. Res., vol. 72, no. 22, Nov. 1967, pp. 5705–5715.
148. Filice, A. L.: Observations on the Lunar Surface Disturbed by the Footpads of Surveyor I. J. Geophys. Res., vol. 72, no. 22, Nov. 1967, pp. 5721–5728.
149. Hartmann, W. K.: Lunar Crater Counts. I. Alphonsus. Communications of the Lunar and Planetary Laboratory, Univ. of Arizona (Tucson, Ariz.), no. 80, Mar. 20, 1967, pp. 31–38.

150. HARTMANN, W. K.: Lunar Crater Counts. II. Three Lunar Surface Type Areas. Communications of the Lunar and Planetary Laboratory, Univ. of Arizona (Tucson, Ariz.), no. 81, Apr. 5, 1967, pp. 39–41.
151. HARTMANN, W. K.: Secondary Volcanic Impact Craters at Kapoho, Hawaii, and Comparisons With the Lunar Surface. Icarus, vol. 7, no. 1, July 1967, pp. 66–75.
152. NASH, DOUGLAS B.: Proton Irradiation Darkening of Rock Powders: Contamination and Temperature Effects, and Applications to Solar Wind Darkening of the Moon. J. Geophys. Res., vol. 72, no. 12, 1967, pp. 3089–3104.
153. KENKNIGHT, C. E.; ROSENBERG, D. L.; AND WEHNER, G. K.: Parameters of the Optical Properties of the Lunar Surface Powder in Relation to Solar-Wind Bombardment. J. Geophys. Res., vol. 72, no. 12, June 1967, pp. 3105–3129.
154. GREER, R. T.; AND HAPKE, B. W.: Electron Microprobe Analyses of Powders Darkened by Simulated Solar-Wind Irradiation. J. Geophys. Res., vol. 72, no. 12, June 1967, pp. 3131–3133.
155. ZELLER, E. J.; AND RONCA, L. B.: Space Weathering of Lunar and Asteroidal Surfaces. Icarus, vol. 7, no. 3, Nov. 1967, pp. 372–379.
156. GREENMAN, N. N.; BURKIG, V. W.; AND YOUNG, J. F.: Ultraviolet Reflectance Measurements of Possible Lunar Silicates. J. Geophys. Res., vol. 72, no. 4, Feb. 1967, pp. 1355–1359.
157. EGAN, W. G.: Polarimetric Measurements of Simulated Lunar Surfaces. J. Geophys. Res., vol. 72, no. 12, June 1967, pp. 3233–3245.
158. FRICKER, P. E.; REYNOLDS, R. T.; AND SUMMERS, A. L.: On the Thermal History of the Moon. J. Geophys. Res., vol. 72, no. 10, May 1967, pp. 2649–2663.
159. MIYAMOTO, S.: Lunar and Martian Crusts and Mantle Convection. Icarus, vol. 6, no. 1, 1967, pp. 50–55.
160. IRIYAMA, J.; AND SHIMAZU, Y.: A Note on the Thermal History of the Moon. Icarus, vol. 6, no. 3, May 1967, pp. 453–457.
161. ORNATSKAYA, O. I.; AND AL'BER, YA. I.: Thermal History of the Moon. Soviet Astron.—AJ, vol. 11, no. 1, 1967, pp. 122–127.
162. LOWMAN, P. D., JR.: Origin of the Moon. The Encyclopedia of Atmospheric Sciences and Astrogeology, L. W. Fairbridge, ed., Reinhold Publ. Co. (New York), 1967, pp. 658–662.
163. FISH, F. F., JR.: Angular Momenta of the Planets. Icarus, vol. 7, no. 2, Sept. 1967, pp. 251–256.
164. HARTMANN, W. K.; AND LARSON, S. M.: Angular Momenta of Planetary Bodies. Icarus, vol. 7, no. 2, Sept. 1967, pp. 257–260.
165. MACDONALD, G. J. F.: The Internal Constitutions of the Inner Planets and the Moon. Space Sci. Rev., vol. 2, 1963, pp. 473–557.
166. RUSKOL, E. I.: The Tidal History and Origin of the Earth-Moon System. Soviet Astron.—AJ, vol. 10, no. 4, 1967, pp. 659–665.
167. BEALS, C. S.; DENCE, M. R.; AND COHEN, A. J.: Evidence for the Impact Origin of Lac Couture. Publ. Dominion Observatory (Ottawa), vol. 31, no. 10, 1967, pp. 409–426.
168. CURRIE, K. L.; AND SHAFIQULLAH, M.: Carbonatite and Alkaline Igneous Rocks in the Brent Crater, Ontario. Nature, vol. 215, 1967, pp. 725–726.
169. SHORT, N. M.: The Anatomy of a Meteorite Impact Crater—West Hawk Lake, Manitoba, Canada (Abstract). 30th Ann. Meeting, Meteorit. Soc., 1967.
170. LAROCHELLE, A.; AND CURRIE, K. L.: Paleomagnetic Study of Igneous Rocks From the Manicouagan Structure, Quebec. J. Geophys. Res., vol. 72, no. 16, 1967, pp. 4163–4169.

171. French, B. M.: Sudbury Structure, Ontario: Some Petrographic Evidence for Origin by Meteorite Impact. Science, vol. 156, no. 3778, 1967, pp. 1094–1098.
172. Dietz, R. S.: Sudbury Structure as an Astrobleme. J. Geol., vol. 72, no. 4, 1964, pp. 412–434.
173. Bray, J. G.; and Zoological Staff: Shatter Cones at Sudbury. J. Geol., vol. 74, no. 2, 1966, pp. 243–245.
174. Robertson, P. B.: The Malbaie Structure, Quebec—An Ancient Meteorite Impact Site (Abstract). 30th Ann. Meeting, Meteorit. Soc., 1967.
175. Anon.: Flynn Creek Crater. Crater Investigations, Astrogeologic Studies, Ann. Progress Rept., Part B. U.S. Geol. Survey, July 1, 1966–Oct. 1, 1967, 1967, pp. 28–30.
176. Wilshire, H. G.; Cummings, D.; Offield, T. W.; and Howard, K. A.: Geology of the Sierra Madera Cryptoexplosion Structure (Abstract). Ann. Meeting, Geol. Soc. Am. (New Orleans), 1967, p. 239.
177. Seeger, C. R.: The Jeptha Knob Structure, Kentucky. I. Subsurface Structure (Abstract). Trans. Am. Geophys. Union, vol. 48, no. 1, 1967, p. 147.
178. Seeger, C. R.: The Jeptha Knob Structure. II. Rock Deformation (Abstract). 30th Ann. Meeting, Meteorit. Soc., Oct. 1967.
179. Seeger, C. R.: The Jeptha Knob Stucture. III. Origin. Ann. Meeting, Geol. Soc. Am. (New Orleans), 1967, p. 199.
180. Bull, C.; Corbato, C. E.; and Zahn, J. C.: Gravity Survey of the Serpent Mound Area, Southern Ohio. Ohio J. Sci., vol. 67, no. 6, 1967, pp. 359–371.
181. Förstner, U.: Petrographische Untersuchungen des Suevit aus den Bohrungen Deiningen und Wörnitzostheim in Ries von Nördlingen. Contrib. Mineral. Petrol., vol. 15, 1967, pp. 281–308.
182. Stöffler, D.: Deformation und Umwandlung von Plagioklas durch Stosswellen in den Gesteinen des Nördlinger Ries. Contrib. Mineral. Petrol., vol. 16, 1967, pp. 51–83.
183. Engelhardt, W. v.; Arndt, J.; Stöffler, D.; Muller, W. F.; Jeziorkowski, H.; and Gubser, R. A.: Diaplektische Gläser in den Breccien des Ries von Nördlingen als Anzeichen fur Stosswellenmetamorphose. Contrib. Mineral. Petrol., vol. 15, 1967, pp. 93–102.
184. Engelhardt, W. v.: Chemical Composition of Ries Glass Bombs. Geochim. Cosmochim. Acta, vol. 31, 1967, pp. 1677–1689.
185. Engelhardt, W. v.; Bertsch, W.; Stöfler, D.; Groschopf, P.; and Reiff, W.: Anzeichen für den Meteoritischen Ursprung des Beckens von Steinheim. Naturwissenschaften, vol. 8, 1967, pp. 198–199.
186. Johnson, G. G.; and Vand, V.: Application of a Fourier Data Smoothing Technique to the Meteoritic Crater Ries Kessel. J. Geophys. Res., vol. 72, no. 6, 1967, pp. 1741–1750.
187. Kraut, F.: Sur l'origin des clivages du quartz dans les brèches "volcaniques" de la région de Rochechouart. C. R. Acad. Sci. Paris, vol. 264, 1967, pp. 2609–2612.
188. Anon.: Gosses Bluff Structure. Crater Investigations, Astrogeologic Studies, Part B, Ann. Progress Rept. U.S. Geol. Survey, July 1, 1967, 1967, pp. 31–35.
189. Dietz, R. S.: Shatter Cone Orientation at Gosses Bluff Astrobleme. Nature, vol. 216, no. 5120, 1967, pp. 1082–1084.
190. Taylor, S. R.: Composition of Meteorite Impact Glass Across the Henbury Strewnfield. Geochim. Cosmochim. Acta, vol. 31, 1967, pp. 961–968.

191. BUNCH, T. E.; AND CASSIDY, W. A.: Petrographic and Electron Microprobe Study of the Monturaqui Impactite (Abstract). 30th Ann. Meeting, Meteorit. Soc., Oct. 1967.

192. SHORT, N. M.: Explosion Craters. Encyclopedia of Atmospheric Sciences and Astrogeology, R. Fairbridge, ed., Reinhold Publ. Corp. (New York), 1967, pp. 373–378.

193. SHORT, N. M.: Astroblemes and Meteorite Craters. Encyclopedia of Atmospheric Sciences and Astrogeology, R. Fairbridge, ed., Reinhold Publ. Corp. (New York), 1967, pp. 40–43.

194. SHORT, N. M.: Shock Processes in Geology. J. Geol. Edu., vol. 14, no. 4, 1966, pp. 149–166.

195. CHAO, E. C. T.: Shock Effects in Certain Rock-Forming Minerals. Science, vol. 156, no. 3772, 1967, pp. 192–202.

196. CHAO, E. C. T.: Impact Metamorphism. Researches in Geochemistry, P. H. Abelson, ed., vol. 2, John Wiley & Sons, Inc. (New York), 1967, pp. 204–233.

197. BARRINGER, R.: World's Meteorite Craters. Meteoritics, vol. 3, no. 3, 1967, pp. 151–158.

198. DIEHL, C. H. H.; AND JONES, G. H. S.: The Snowball Crater: I. General Background Information. II. Profile and Ejecta Pattern, Defence Res. Estab. Canada, Suffield Tech. Notes, nos. 187 and 188, 1967.

199. HANSEN, S. M.: A Nuclear Crater Formed by a Gas-Erosion Mechanism (Abstract). 30th Ann. Meeting, Meteorit. Soc., 1967.

200. BAËTA, R. D.; AND ASHBEE, K. H. G.: Plastic Deformation and Fracture of Quartz at Atmospheric Pressure. Philosoph. Mag., vol. 14, 1967, pp. 931–938.

201. GREENWOOD, W.: Deformation Lamallae Parallel to $(10\bar{1}3)$ and (0001) in Quartz of the Coeur d'Alene District, Idaho. Science, vol. 158, 1967, p. 1180.

202. BUNCH, T. E.; DENCE, M. R.; AND COHEN, A. J.: Natural Terrestrial Maskelynite. Am. Mineralogist, vol. 52, 1967, pp. 244–253.

203. GREEN, J.: Moon—Lunar Volcanism. Encyclopedia of Atmospheric Sciences and Astrogeology, R. Fairbridge, ed., Reinhold Publ. Corp. (New York), 1967, pp. 651–658.

204. GREEN, J.: Moon—Lunar Geology. Encyclopedia of Atmospheric Sciences and Astrogeology, R. Fairbridge, ed., Reinhold Publ. Corp. (New York), 1967, pp. 623–629.

205. KATTERFELD, G. N.; Types, Ages and Origins of Lunar Ring Structures—Statistical and Comparative Geological Approach. Icarus, vol. 6, 1967, pp. 360–380.

206. HARTMANN, W. K.: Secondary Volcanic Impact Craters at Kapoho, Hawaii and Comparisons with the Lunar Surface. Icarus, vol. 7, 1967, p. 66–75.

207. RODDY, D.: Minimum Energy of Formation of Ubehebe Crater, Death Valley, California. Ann. Meeting, Geological Soc. Am. (New Orleans), 1967, p. 187.

208. RONCA, L. B.; Meteorite Impact and Volcanism. Icarus, vol. 5, 1967, pp. 515–520.

209. LOWMAN, P. D., JR.: Moon—Lunar Impact Craters. Encyclopedia of Atmospheric Sciences and Astrogeology, R. Fairbridge, ed., Reinhold Publ. Corp. (New York), 1967, pp. 629–633.

210. TRASK, N. J.: Distribution of Lunar Craters According to Morphology From Ranger VIII and IX Photographs. Icarus, vol. 6, 1967, pp. 270–276.

211. ANON: Apollo Site Mapping. Lunar and Planetary Investigations. Astrogeolog. Studies, Ann. Progress rept., pt. 2, U.S. Geol. Survey, July 1, 1966–Oct. 1, 1967, 1967, pp. 18–25.
212. WALKER, E. H.: Statistics of Impact Crater Accumulation on the Lunar Surface Exposed to a Distribution of Impacting Bodies. Icarus, vol. 7, 1967, pp. 233–242.
213. CHAPMAN, C. R.; AND HAEFNER, R.: A Critique of Methods for Analysis of the Diameter-Frequency Relation for Craters With Special Application to the Moon. J. Geophys. Res., vol. 72, no. 2, 1967, pp. 549–558.
214. BALDWIN, R.: Ranger VIII and Gravity Scaling of Lunar Craters. Science, vol. 157, 1967, pp. 546–548.
215. PIKE, R.: Schroeter's Rule and the Modification of Lunar Crater Impact Morphology, J. Geophys. Res., vol. 72, no. 8, 1967, pp. 2099–2106.
216. SCOTT, R. F.: Viscous Flow of Craters. Icarus, vol. 7, 1967, pp. 139–148.
217. WALKER, E. H.: The Structure of the Lunar Surface as Indicated by the Geometry of Impact Craters. Icarus, vol. 7, 1967, pp. 183–187.
218. OBERBECK, V. R.; AND QUAIDE, W. L.: Estimated Thickness of a Fragmental Surface Layer of Oceanus Procellarum. J. Geophys. Res., vol. 72, no. 18, 1967, pp. 4697–4704.
219. LAMMERZAHL, P.: Rare-Gas Isotope Studies on Meteorites. Mantles of the Earth and Terrestrial Planets, S. K. Runcorn, ed., Interscience Publ., 1967, pp. 49–61.
220. FISHER, D. E.: Cosmogenic Tritium Problem in Iron Meteorites. J. Geophys. Res., vol. 72, 1967, pp. 1351–1354.
221. HINTENBERGER, H.; SCHULTZ, L.; WÄNKE, H.; AND WEBER, H.: Helium- und Neonisotope in Eisenmeteoriten und der Tritium verlust in Hexaedriten. Naturforschung, vol. 22a, 1967, pp. 780–787.
222. SCHULTZ, L.: Tritium Loss in Iron Meteorites. Earth and Planetary Sci. Letters, vol. 2, 1967, pp. 87–89.
223. KRANKOWSKY, D.; AND MÜLLER, O.: Istopic Composition and Abundance of Li in Meteoritic Matter. Geochim. Cosmochim. Acta, vol. 31, 1967, pp. 1833–1842.
224. BURNETT, J. H.; AND MANUEL, O. K.: On the Origin of Noble Gas Anomalies in Canyon Diablo Graphite. Earth and Planetary Sci. Letters, vol. 3, 1967, pp. 95–100.
225. SCHULTZ, L.; AND HINTENBERGER, H.: Edelgasmessungen an Eisenmeteoriten. Naturforschung, vol. 22a, 1967, pp. 773–779.
226. MUNK, M.: Spallation of Ne, A, K, and Xe in an Iron Meteorite. Earth and Planetary Sci. Letters, vol. 2, 1967, pp. 301–309.
227. NYQUIST, L. E.; HUNEKE, J. C.; AND SIGNER, P.: Spallogenic Rare Gases in the El Taco Meteorite. Earth and Planetary Sci. Letters, vol. 2, 1967, pp. 241–248.
228. VOSHAGE, H.: Bestrahlungsälter und Herkunft der Eisenmeteorite. Naturforschung, vol. 22a, 1967, pp. 477–506.
229. VOSHAGE, H.: Cosmic Ray Exposure Ages and Origin of Iron Meteorites, Radioactive Dating and Methods of Low-Level Counting. Int. Atomic Energy Agency Symposium, 1967, pp. 281–295.
230. COMERFORD, M. F.: Comparative Erosion Rates of Stone and Iron Meteorites Under Small-Particle Bombardment. Geochim. Cosmochim. Acta, vol. 31, 1967, pp. 1457–1471.

231. RANCITELLI, L.; FISHER, D. E.; FUNKHOUSER, J.; AND SCHAEFFER, O. A.: Potassium Argon Dating of Iron Meteorites. Science, vol. 158, 1967, pp. 999–1000.

232. RANCITELLI, L.; AND FISHER, D. E.: Problems in the K/Ar Dating of Iron Meteorites (Abstract). 30th Ann. Meeting, Meteorit. Soc., Oct. 1967.

233. RANCITELLI, L. A.; AND FISHER, D. E.: Potassium Argon Ages of Iron Meteorites. Abstract of 48th Ann. Meeting, Am. Geophys. Union, 1967, p. 167.

234. BOGARD, D. D.; BURNETT, D. S.; EBERHART, P.; FANALE, F.; AND WASSERBURG, G. J.: K-Ar Ages and Rare Gas Contents of Silicate Inclusions in Iron Meteorites. Abstract of 48th Ann. Meeting, Am. Geophys. Union, vol. 48, 1967, p. 167.

235. BURNETT, D. S.; AND WASSERBURG, G. J.: ^{87}Rb-^{87}Sr Ages of Silicate Inclusions in Iron Meteorites. Earth and Planetary Sci. Letters, vol. 2, 1967, pp. 397-408.

236. KORNBLUM, J. J.: Neutron Produced Isotopes in Iron Meteorites (Abstract). 30th Ann. Meeting, Meteorit. Soc., Oct. 1967.

237. TANNER, J. T.; AND KOHMAN, T. P.: Determination of Mercury and Bismuth in Iron Meteorites by Neutron Activation. 30th Ann. Meeting, Meteorit. Soc., Oct. 1967.

238. RAO, M. N.: Osmium in Three Iron Meteorites. J. Geophys. Res., vol. 72, 1967, pp. 5758–5759.

239. BERKEY, E.; AND FISHER, D. E.: The Abundance and Distribution of Chlorine in Iron Meteorites. Geochim. Cosmochim. Acta, vol. 31, 1967, pp. 1543–1558.

240. GOLDBERG, E.; UCHIYAMA, A.; AND BROWN, H.: The Distribution of Nickel, Cobalt, Gallium, Palladium, and Gold in Iron Meteorites. Geochim. Cosmochim. Acta, vol. 2, 1951, pp. 1–25.

241. LOVERING, J. F.; NICHIPORUK, W.; CHODOS, A.; AND BROWN, H.: The Distribution of Gallium, Germanium, Cobalt, Chromium, and Copper in Iron and Stony-Iron Meteorites in Relation to Nickel Content and Structure. Geochim. Cosmochim. Acta, vol. 11, 1957, pp. 263–278.

242. COBB, J. C.: A Trace-Element Study of Iron Meteorites. J. Geophys. Res., vol. 72, 1967, pp. 1329–1341.

243. SMALES, A. A.; MAPPER, D.; AND FOUCHE, K. F.: The Distribution of Some Trace Elements in Iron Meteorites, as Determined by Neutron Activation. Geochim. Cosmochim. Acta, vol. 31, 1967, pp. 673–720.

244. WASSON, J. T.: The Chemical Classification of Iron Meteorites with Low Concentrations of Gallium and Germanium. Geochim. Cosmochim. Acta, vol. 31, 1967, pp. 161–180.

245. WASSON, J. T.; AND KIMBERLIN, J.: The Chemical Classification of Iron Meteorites—II. Irons and Pallasites With Germanium Concentrations Between 8 and 100 ppm. Geochim. Cosmochim. Acta; vol. 31, 1967, pp. 2065–2093.

246. GOLDSTEIN, J. I.: Distribution of Germanium in the Metallic Phases of Some Iron Meteorites. J. Geophys. Res., vol. 72, 1967, pp. 4689–4696.

247. WAI, C. M.; WETHERILL, G. W.; ERNST, G. W.; AND WASSON, J. T.: The Distribution of Trace Quantities of Ge Between Iron, Silicate and Sulfide Phases. 30th Ann. Meeting, Meteoritic. Soc., Oct. 1967.

248. WASSON, J. T.: Differences of Composition Among Australian Iron Meteorites. Nature, vol. 216, 1967, pp. 880, 905.

249. Wasson, J. T.; and Goldstein, J. I.: The North Chilean Hexahedrites: Variations in Composition and Structure. 30th Ann. Meeting, Meteorit. Soc., Oct. 1967.

250. Wasson, J. T.: Concentrations of Ni, Ga and Ge in a Series of Canyon Diablo and Odessa Meteorite Specimens. J. Geophys. Res., vol. 72, 1967, pp. 721–730.

251. Moore, C. B.; Birrell, P. J.; and Lewis, C. F.: Variations in the Chemical and Mineralogical Compositions of Rim and Plains Specimens of the Canyon Diablo Meteorite. Geochim. Cosmochim. Acta, vol. 31, 1967, pp. 1885–1892.

252. Moore, C. B.; Lewis, C. F.; and Gans, M.: Total Sulfur Content of Iron Meteorites. 30th Ann. Meeting, Meteorit. Soc., Oct. 1967.

253. Reed, S. J. B.: Chemical and Mineralogical Evidence From Iron Meteorites on the Nature of the Parent Body. Mantles of the Earth and Terrestrial Planets, S. K. Runcorn, ed., Interscience Publ., 1967, pp. 15–33.

254. Olsen, E.: Amphibole: First Occurrence in a Meteorite. Science, vol. 156, 1967, pp. 61–62.

255. Olsen, E.; and Fuchs, L. H.: The State of Oxidation of Some Iron Meteorites. Icarus, vol. 6, 1967, pp. 242–253.

256. Fuchs, L. H.; Olsen, E.; and Henderson, E. P.: On the Occurrence of Brianite and Panethite, Two New Phosphate Minerals From the Dayton Meteorite. Geochim. Cosmochim. Acta, vol. 31, 1967, pp. 1711–1719.

257. El Goresy, Ahmed: Quantitative Electron Microprobe Analyses of Coexisting Sphalerite, Daubreelite and Troilite in the Odessa Iron Meteorite and Their Genetic Implication. Geochim. Cosmochim. Acta, vol. 31, 1967, pp. 1667–1676.

258. El Goresy, A.: Quantitative Electron Microprobe Analyses of K-Feldspar Grains From the Odessa Iron Meteorite. 30th Ann. Meeting, Meteorit. Soc., Oct. 1967.

259. Bence, A. E.; and Burnett, D. S.: The Compositions of Silicate Inclusions in Iron Meteorites. 30th Ann. Meeting, Meteorit. Soc., Oct. 1967.

260. Mason, B.: The Woodbine Meteorite, With Notes on Silicates in Iron Meteorites. Mineralog. Mag., vol. 36, 1967, pp. 120–126.

261. Brett, R.; and Henderson, E. P.: The Occurrence and Origin of Lamellar Troilite in Iron Meteorites. Geochim. Cosmochim. Acta, vol. 31, 1967, pp. 721–731.

262. Lipschutz, M. E.: X-Ray Diffraction Analysis of Cohenite From Iron Meteorites. Geochim. Cosmochim. Acta, vol. 31, 1967, pp. 621–634.

263. Marvin, U. B.: Shocked Crystals of Ureyite and Sphalerite in the Canyon Diablo Iron Meteorite. Abstract of 48th Ann. Meeting, Am. Geophys. Union, vol. 48, 1967, pp. 167–168.

264. Hanneman, R. E.; Strong, H. M.; and Bundy, F. P.: Hexagonal Diamonds in Meteorites: Implications. Science, vol. 155, 1967, pp. 995–997.

265. Brett, R.: Cohenite: Its Occurrence and a Proposed Origin. Geochim. Cosmochim. Acta, vol. 31, 1967, pp. 143–160.

266. Brett, R.; and Higgins, G. T.: Cliftonite in Meteorites: A Proposed Origin. Science, vol. 156, 1967, pp. 819–820.

267. Axon, H. J.; and Rieche, R.: The Goose Lake Meteorite and the Goose Lake Fragments. Nature, vol. 215, 1967, pp. 379–380.

268. Buchwald, U. F.: Study of Six Iron Meteorites. Analecta Geologica, No. 2, Mineralogist Museum (Copenhagen), 1967.

269. Axon, H. J.; and Faulkner, D.: Hot Working Effects in the Parent γ-Phase of Iron Meteorites. Geochim. Cosmochim. Acta, vol. 31, 1967, pp. 1539–1542.
270. Frost, M. J.: Oriented Lamellae in the Gibeon Meteorite. Mineralog. Mag., vol. 36, 1967, pp. 607–612.
271. Duerr, J. S.; and Ogilvie, R. E.: Martensitic Transformation Studies in Meteorites. 30th Ann. Meeting, Meteoritic. Soc., 1967.
272. Goldstein, J. I.: Scanning Electron Microscope Studies of Plessite in Iron Meteorites. 30th Ann. Meeting, Meteoritic. Soc., 1967.
273. Axon, H. J.; and Boustead, J.: Kamacite-Taenite Relationships in Iron Meteorites. Nature, vol. 213, 1967, pp. 166–167.
274. Jaeger, R. R.; and Lipschutz, M. E.: Pressure History of Some Iron Meteorites. Nature, vol. 213, 1967, pp. 975–977.
275. Jaeger, R. R.; and Lipschutz, M. E.: Implications of Shock Effects in Iron Meteorites. Geochim. Cosmochim. Acta, vol. 31, 1967, pp. 1811–1832.
276. Axon, H. J.; and Yardley, E. D.: The Distribution of Nickel at Phase Interfaces in the Brenham County Pallasite. 30th Ann. Meeting, Meteoritic. Soc., Oct. 1967.
277. Reed, S. J. B.: The Distribution of Phosphorus in the Mount Edith Octahedrite. Geochim. Cosmochim. Acta, vol. 31, 1967, pp. 1969–1974.
278. Goldstein, J. I.; and Short, J. M.: Cooling Rates of 27 Iron and Stony-Iron Meteorites. Geochim. Cosmochim. Acta, vol. 31, 1967, pp. 1001–1024.
279. Short, J. M.; and Goldstein, J. I.: Rapid Methods of Determining Cooling Rates of Iron and Stony-Iron Meteorites. Science, vol. 156, 1967, pp. 59–61.
280. Goldstein, J. I.; and Short, J. M.: The Iron Meteorites, Their Thermal History and Parent Bodies. Geochim. Cosmochim. Acta, vol. 31, 1967, pp. 1733–1770.
281. Duke, M. B.; and Silver, L. T.: Petrology of Eucrites, Howardites, and Mesosiderites. Geochim. Cosmochim. Acta, vol. 31, 1967, pp. 1637–1665.
282. Powell, B. N.; and Weibler, P. W.: On the Petrology of Mesosiderites, 30th Ann. Meeting, Meteoritic. Soc., Oct. 1967.
283. Fuchs, L. H.: Stanfieldite: A New Phosphate Mineral From Stony-Iron Meteorites. Science, vol. 158, 1967, pp. 910–911.
284. Buseck, P. R.; Moore, C. B.; and Goldstein, J. I.: Marburg—A New Pallasite. Geochim. Cosmochim. Acta, vol. 31, 1967, pp. 1589–1593.
285. Buseck, P. R.; and Goldstein, J. I.: Olivine Compositions and Cooling Rates of Pallasitic Meteorites. Abstract of 48th Annual Meeting, Am. Geophys. Union, 1967, p. 165.
286. Mason, B.: The Bununu Meteorite, and a Discussion of the Pyroxene-Plagioclase Achondrites. Geochim. Cosmochim. Acta, vol. 31, 1967, pp. 107–115.
287. Mason, B.: Meteorites. Am. Sci., vol. 55, 1967, pp. 429–455.
288. Van Schmus, W. R.; and Wood, J. A.: A Chemical-Petrologic Classification for the Chondritic Meteorites. Geochim. Cosmochim. Acta, vol. 31, no. 5, 1967, pp. 747–766.
289. Dundon, Robert W.; and Walter, L. S.: Ferrous Ion Order-Disorder in Meteoritic Pyroxenes and the Metamorphic History of Chondrites. Earth and Planetary Sci. Letters, vol. 2, 1967, pp. 372–376.
290. Van Schmus, W. R.; and Koffman, D. M.: Equilibration of Iron and Magnesium in Chondritic Meteorites. Science, vol. 155, 1967, pp. 1009–1011.

291. Dodd, R. T., Jr.; Van Schmus, W. R.; and Koffman, D. M.: A Survey of Unequilibrated Ordinary Chondrites. Geochim. Cosmochim. Acta., vol. 31, 1967, pp. 921–951.
292. Wood, J. A.: Olivine and Pyroxene Composition in Type II Carbonaceous Chondrites. Geochim. Cosmochim. Acta, vol. 31, 1967, pp. 2095–2108.
293. Suess, H. E.; and Wänke, H.; Metamorphosis and Equilibration in Chondrites. J. Geophys. Res., vol. 72, no. 14, 1967, pp. 3609–3612.
294. Wood, J. A.: Criticism of Paper by H. E. Suess and H. Wänke, Metamorphosis and Equilibration in Meteorites. J. Geophys. Res., vol. 72, no. 24, 1967, pp. 6379–6383.
295. Otting, W.; and Zahringer, J.: Total Carbon Content and Primordial Rare Gases in Chondrites. Geochim. Cosmochim. Acta, vol. 31, 1967, pp. 1949–1960.
296. Heymann, D.; and Mazor, E.: Primordial Rare Gases in Unequilibrated Ordinary Chondrites. Science, vol. 155, 1967, pp. 701–702.
297. Wood, J. A.: Chondrites: Their Metallic Minerals, Thermal Histories and Parent Bodies. Icarus, vol. 6, 1967, pp. 1–49.
298. Binns, R. A.: Structure and Evolution of Non-Carbonaceous Chondrite Meteorites. Earth and Planetary Sci. Letters, vol. 2, 1967, pp. 23–28.
299. Bunch, T. E.; Keil, K.; and Snetsinger, K. G.: Chromite Composition in Relation to Chemistry and Texture of Ordinary Chondrites. Geochim. Cosmochim. Acta, vol. 31, 1967, pp. 1569–1582.
300. Kurat, G.: Zur Enstehung der Chondren. Geochim. Cosmochim. Acta, vol. 31, 1967, pp. 491–502.
301. Reid, A. M.; and Fredriksson, K.: Chondrules and Chondrites. Researches in Geochemistry, vol. 2, P. H. Abelson, ed., John Wiley & Sons, Inc. (New York), 1967, pp. 170–203.
302. Fredriksson, Kurt; and Mason, Brian: The Shaw Meteorite. Geochim. Cosmochim. Acta, vol. 31, 1967, pp. 1705–1709.
303. Van Schmus, W. R.: Polymict Structure of the Mezö-Madaras Chondrite. Geochim. Cosmochim. Acta, vol. 31, 1967, pp. 2027–2042.
304. Binns, R. A.: Farmington Meteorite: Cristobalite Xenoliths and Blackening. Science, vol. 156, 1967, pp. 1222–1226.
305. Buseck, P. R.: The Post-Formational History of a Hypersthene Chondrite—Beenham. Geochim. Cosmochim. Acta, vol. 31, 1967, pp. 1583–1587.
306. Heymann, Dieter: On the Origin of Hypersthene Chondrites: Ages and Shock Effects of Black Chondrites. Icarus, vol. 6, 1967, pp. 189–221.
307. Tanenbaum, Andrew S.: Clustering of the Cosmic Ray Ages of Stone Meteorites. Earth Planetary Sci. Letters, vol. 2, 1967, pp. 33–35.
308. Shima, M.; and Honda, M.: Determination of Rb-Sr Age of Chondrites Using Their Separated Components. Earth Planetary Sci. Letters, vol. 2, 1967, pp. 337–343.
309. Bogard, D. P.; Burnett, D. S.; Eberhardt, P.; and Wasserburg, G. J.: Rb^{87}-Sr^{87} Isochron and K^{40}-Ar^{40} Ages of the Norton County Achondrite. Earth Planetary Sci. Letters, vol. 3, 1967, pp. 178–189.
310. Burnett, D. S.; and Wasserberg, G. J.: Rb^{87}-Sr^{87} Ages of Silicate Inclusions in Iron Meteorites. Earth Planetary Sci. Letters, vol. 2, 1967, pp. 397–409.
311. Hohenberg, L. M.; Podosek, F. A.; and Reynolds, J. H.: Xenon-Iodine Dating: Sharp Isochronism in Chondrites. Science, vol. 156, 1967, pp. 223–236.
312. Morgan, J. W.; and Lovering, J. F.: Uranium and Thorium Abundances in Carbonaceous Chondrites. Nature, vol. 213, 1967, pp. 873–875.

313. TANNER, J. T.; AND EHMANN, W. D.: The Abundance of Antimony in Meteorites, Tektites and Rocks by Neutron Activation Analysis. Geochim. Cosmochim. Acta, vol. 31, 1967, pp. 2007–2026.

314. CLARK, R. S.; ROWE, M. W.; GANAPATHY, R. G.; AND KURADA, P. K.: Iodine, Uranium and Tellurium Contents in Meteorites. Geochim. Cosmochim. Acta, vol. 31, 1967, pp. 1605–1614.

315. CROCKETT, J. H.; KEAYS, R. R.; AND HSIEH, S.: Precious Metal Abundances in Some Carbonaceous and Enstatite Chondrites. Geochim. Cosmochim. Acta, vol. 31, 1967, pp. 1615–1624.

316. GOLES, G. G.; GREENLAND, L. P.; AND JEROME, D. Y.: Abundances of Chlorine, Bromine, and Iodine in Meteorites. Geochim. Cosmochim. Acta, vol. 31, 1967, pp. 1711–1778.

317. KRANKOWSKY, D.; AND MÜLLER, O.: Isotopic Composition and Abundance of Lithium in Meteoritic Matter. Geochim. Cosmochim. Acta, vol. 31, 1967, pp. 1831–1842.

318. MORGAN, J. W.; AND LOVERING, J. F.: Rhenium and Osmium Abundances in Chondritic Meteorites. Geochim. Cosmochim. Acta, vol. 31, 1967, pp. 1893–1910.

319. NICHIPORUK, W.; CHODOS, A.; HELIN, E.; AND BROWN, H.: Determination of Fe, Ni, Co, Ca, Cr, and Mn, in Stony Meteorites by X-Ray Fluorescence. Geochim. Cosmochim. Acta, vol. 31, 1967, pp. 1911–1930.

320. SCHMITT, R. A.; SMITH, R. H.; EHMANN, W. D.; AND MCKOWN, D.: Silicon Abundances in Meteoritic Chondrules. Geochim. Cosmochim. Acta, vol. 31, 1967, pp. 1975–1986.

321. DELAETER, J. R.; AND JEFFERY, P. M.: Tin: Its Isotopic and Elemental Abundance. Geochim. Cosmochim. Acta, vol. 31, 1967, pp. 969–985.

322. GREENLAND, L.: The Abundances of Selenium, Tellurium, Silver, Palladium, Cadmium and Zinc in Chondritic Meteorites. Geochim. Cosmochim. Acta, vol. 31, no. 5, 1967, pp. 849–860.

323. MUELLER, R. F.; AND OLSEN, E.: The Olivine, Pyroxene and Metal Content of Chondritic Meteorites as a Consequence of Prior's Rule. Mineralog. Mag., vol. 36, no. 279, 1967, pp. 311–318.

324. AHRENS, L. H.: Notes on the Fractionation of Some of the Abundant Lithophile Elements in Chondrites With Particular Reference to La and Al. Geochim. Cosmochim. Acta, vol. 31, 1967, pp. 861–868.

325. LARIMER, JOHN W.: Chemical Fractionation in Meteorites. I. Condensation of the Elements. Geochim. Cosmochim. Acta, vol. 31, 1967, pp. 1215–1238.

326. LARIMER, JOHN W.; AND ANDERS, EDWARD: Chemical Fractionations in Meteorites. II. Abundance Patterns and Their Interpretation. Geochim. Cosmochim. Acta, vol. 31, 1967, pp. 1239–1270.

327. BLANDER, M.; AND KATZ, J. L.: Condensation of Primordial Dust. Geochim. Cosmochim. Acta, vol. 31, 1967, pp. 1025–1034.

328. UREY, H. C.: Parent Bodies of the Meteorites and the Origin of Chondrules. Icarus, vol. 7, 1967, pp. 350–359.

329. GLASS, BILL: Microtektites in Deep-Sea Sediments. Nature, vol. 214, 1967, pp. 372–374.

330. GLASS, BILL; AND HEEZEN, BRUCE: Tektites and Geomagnetic Reversals. Nature, vol. 214, 1967, p. 372.

331. NININGER, H. H.; AND HUSS, G. I.: Tektites That Were Partially Plastic After Completion of Surface Sculpturing. Science, vol. 157, 1967, pp. 61–62.

332. GENTNER, W.; KLEINMAN, B.; AND WAGNER, L. A.: New K-Ar and Fission Track Ages of Impact Glasses and Tektites. Earth Planetary Sci. Letters, vol. 2, 1967, pp. 83–86.

333. KOLBE, P.; PINSON, W. H. JR.; SAUL, JOHN; AND MILLER, ELLIOTT: Rb-Sr Study on Country Rocks of the Bosumtwi Crater. Geochim. Cosmochim. Acta, vol. 31, 1967, pp. 869–876.

334. WALTER, L. S.: Tektite Compositional Trends and Experimental Vapor Fractionation of Silicates. Geochim. Cosmochim. Acta, vol. 31, 1967, pp. 2043–2063.

Page Intentionally Left Blank

SOLAR PHYSICS

G. K. Oertel
Office of Space Science and Applications, NASA

R. G. Teske
University of Michigan

Harold Glaser
Office of Space Science and Applications, NASA

Page Intentionally Left Blank

Solar Physics

INTRODUCTION

There has been a great deal of progress in the field of solar physics during 1967. It is difficult to do justice to all investigations that have directly or indirectly contributed to that progress. In general, the authors have had to restrict themselves to research results published during the calendar year 1967; however, there are some exceptions. The most notable one is the Orbiting Solar Observatory program. The "OSO Program" in this report concentrates on the results obtained from OSO–III and OSO–IV, which were launched in 1967 and which constitute the most successful single program in solar physics in any year. Naturally, very few publications appeared during 1967, although large amounts of data were obtained during the year. The preliminary results that had been reported by the experimenters in preliminary reports, letters, and oral presentations have been included as 1967 results in this document as long as they were obtained primarily during that year. In the remaining sections the deadline has generally been the end of 1967; thus, work that was published later, or is as yet unpublished, was included only where we had easy access to it and believed it would materially add to the discussion by clarifying, amplifying, or perhaps disproving published results. Unpublished results were also included, in some cases, when they were considered to be of particular interest. On the other hand, it is probable that some good work, published or unpublished, has been overlooked, or its significance to solar physics not fully realized.

A number of review articles on various topics of solar physics have not been reviewed. There are two reasons for these omissions. First, most of the information contained in the reviews is of necessity older than that normally included in this document. More important, a review of the reviews would have been repetitious without adding to the clarity, while necessarily reducing the comprehensiveness of the articles. It was considered more appropriate to refer the reader to the original articles. Included are comprehensive articles on ultraviolet and X-rays from the Sun by Goldberg (ref. 1), on magnetic fields by Howard (ref. 2), on the solar corona by Newkirk (ref. 3), on solar X-rays by Underwood (ref. 4), and on the long and exciting history of space research at the Naval Research Laboratory by Tousey (ref. 5).

333–240 O—69——29

This introduction gives some of the philosophy that motivates the solar physics program in the direction and support of solar research. The introductory paragraphs of the individual sections outline some of the rationale for carrying on the respective types of solar physics research.

In general, the complete dependence of terrestrial life on the Sun as a producer of energy and on its capability to continue this function without significant variation is enough reason for serious attempts to learn as much as possible about the physical mechanisms and phenomena that comprise solar physics. Moreover, solar activity has given rise to such varied phenomena on Earth as radio-communication blackouts, aurorae, proton streams that pose hazards to space flight as well as travel in supersonic transport planes, magnetic storms, and even changes in the climate with the cycle of solar activity. The study of solar physics is, therefore, a vital part of man's efforts to understand and control his environment.

Solar physics is concerned with the evolution, structure, and behavior of the Sun. The principal task of NASA's solar physics program is to analyze the electromagnetic radiation emitted by the Sun in order to deduce the physical processes underlying these observations and to infer models explaining the structure of the solar photosphere and atmosphere and models explaining solar activity. Studies of the interplanetary magnetic field and the transient effects in the interplanetary medium are also related to solar activity. However, the study of the characteristics of charged particles and plasma emitted by the Sun is considered to be the responsibility of the particles and fields program.

Solar-terrestrial relationships involve the overlap between solar physics, particles and fields, and the geophysics disciplines. Solar physics thus includes monitoring solar events that would be of primary interest to other disciplines.

Some solar phenomena can be studied actively. The corona can be probed by reflecting radar signals from it; it can also be studied by observing its effects on transmitted radio signals, as in the planned Sunblazer program. Active techniques for the study of the corona are included in the solar physics discipline.

Research on the Sun is primarily empirical at this time. The macroscopic physics underlying the observed phenomena is, in a large measure, beyond our present physical understanding and especially our laboratory experience. Also, at times we are not certain in our observations because of instrumental and environmental filtering of particle and electromagnetic radiations from the Sun. Theoretical guidance and understanding come primarily through phenomenological models of various observed effects. These models are necessarily restricted in applicability and have an ad hoc character.

A significant aspect of solar research is that data on solar phenomena are obtained by remote sensing of solar emanations; there are no in situ measurements on solar phenomena to date. Thus, most facts obtained about the Sun come from observations in the electromagnetic spectrum

because electromagnetic radiations are most readily transmitted through the interplanetary medium. As an almost empirical area of research, the most interesting facts are expected from observations of increasingly finer structures (spatially, temporally, and spectrally) and from observations in new wavelength regions of the spectrum. Consequently, researchers are continually motivated to make observations that require larger aperture telescopes, faster spectrographic instruments, and more sensitive and faster detectors; and to develop means for observing and detecting a new wavelength regions, such as the low-frequency radio, millimeter, infrared, hard X-ray and gamma-ray regions.

To obtain increased spatial and wavelength resolution, the scientific instrumentation tends to become increasingly larger and heavier. Also, as detectors increase in sensitivity, apertures tend to increase in size to observe energetically weaker phenomena without having to increase integrating times. To observe and measure in new wavelength regions at first does not necessarily require relatively large instrumentation. However, subsequent observations in these new spectral regions seem to follow the same general tendencies mentioned above.

The solar physics program maintains an effort to develop instrumentation for ever-increasing spatial, temporal, and wavelength resolution, and to design experiments utilizing these instruments. The current understanding of the physics underlying solar phenomena is poor. Nevertheless, it is possible to define problems whose solutions will significantly improve the understanding of solar behavior. The current state of knowledge is such that a limit on spatial resolution can be set for some types of problems that require high spatial resolution. This limit is in the range of 0.05 to 0.10 arc-second which further sets a limit on telescope aperture size of about 1.5 meters in the visible spectrum. This limit is set by the interstices of the photospheric granular structure and by the filaments lying over sunspot penumbral regions. In the time and wavelength domains, no lower limits on resolution can be set with any degree of confidence.

As solar observations become finer and finer in detail, it is essential to their interpretation that there be a correspondingly increased effort in theoretical and laboratory research. The area of high-resolution spectroscopy especially requires a larger effort, as solar observational spectroscopy tends to higher spectral resolution and increased spectral coverage. Such advanced theoretical and laboratory work is largely lacking. This lack is currently obstructing progress in solar astronomy.

To observe wavelengths to which the Earth's atmosphere is opaque, instrumentation must be carried above the atmosphere on rockets, satellites, and probes. In the ultraviolet and X-ray spectra, the shorter wavelengths correspond generally to higher levels of the Sun's envelope. The radiation at high X-ray and gamma-ray energies provides more information on different processes than is revealed by observations in the visible spectrum.

On the ground, spatial resolution of details on the Sun is limited because of atmospheric turbulence. By placing telescopes above the atmosphere, it becomes possible to attain theoretical limits of resolution for perfect lenses or mirrors. These limits decrease as wavelengths get shorter, so that a perfect ultraviolet telescope has roughly twice the resolution of a visible light telescope of the same aperture.

Some studies require continuity in time over days or months or years, as in studies of cyclic solar activity. Ultimately, instrumentation for these studies must be carried in satellites into orbits where they will be independent of diurnal effects.

Another reason for performing observations of the Sun from rockets and satellites can be found in atmospheric scattering. The atomic and molecular constituents and dust of the Earth's atmosphere scatter the Sun's visible radiation. This scattered radiation can obscure radiations from phenomena that are inherently dim; in particular, the zodiacal light and radiations from the corona. This background light is minimized on space platforms because they are above most of the scattering elements of the Earth's atmosphere.

Observations of any celestial source in the radiofrequencies below about 10 MHz must be conducted above the radiation-reflecting and absorbing ionosphere of the Earth. This electrically conducting plasma absorbs the solar radio emissions below the critical plasma frequency that diminishes with height. Large-scale density irregularities and time variations produce scintillations that mask solar radio phenomena during ground observations above the plasma frequency. Also, low-frequency ground observations of cosmic radio signals are greatly confused by terrestrial emissions, which are scattered and reflected downward by the ionosphere, so that an orbiting low-frequency solar radio telescope benefits also from diminished background noise.

The possibility of some in situ measurements of solar coronal activity is approaching realization through the planned Sunblazer program. Although the Sunblazer itself would not provide for in situ measurements, the spacecraft would approach to within one-half of an astronomical unit of the Sun. This program would point the way for technological developments that will permit spacecraft to get in even closer to the Sun and for the consideration of in situ measurements in the corona. This is in a class of measurements that is scientifically highly desirable. Programs of this kind will permit the direct measurement of parameters necessary to specify the solar atmosphere. Only with a large uncertainty can values of these parameters be inferred from observations made in terrestrial orbits.

The division of this chapter according to solar physics topics was chosen over the organization by the different observing techniques because it seemed more amenable to the discussion and comparison of different papers of related contents in terms of solar phenomena. The notable exception is the OSO part which stands by itself with only occasional cross-references

to other topical sections. This emphasizes the magnitude of the contribution made by the solar experiments on OSO in observational solar astronomy. At the same time it reflects the preliminary nature of the results, many of which have not been analyzed in terms of their relevance to the different aspects of solar physics. The choice of the other headings is somewhat arbitrary.

"Neutrino Observations" deals with the observations of the solar neutrinos that have had a surprising negative result, although the sensitivity is now sufficient to permit observation of solar neutrinos if the accepted model of the solar interior, composition, and energy production is correct. This exciting nonobservation is rivaled in importance by the observation of the solar oblateness that is discussed in "Solar Rotation." While intended to test different approaches to general relativity, it may turn out to complement the neutrino observations in providing clues to the interior structure of the Sun. The next two parts deal with the solar atmosphere, starting from the lower levels and reaching to the corona and solar wind. Spicules are included in the discussion, but generally the two sections deal with the homogeneous solar atmosphere. The discussion of phenomena that are usually summed up as solar activity begins in "The Solar Cycle." Next we deal with sunspots, prominences, and flares, respectively. Two topics in activity-related observational solar physics have been singled out: the neutron flux and the X-rays in the following two sections. The important field of solar radio astronomy has not been singled out but instead is discussed in connection with the aspects of solar structure to which it relates. The evaluation of observations and their interpretation in terms of physical mechanisms would be impossible without supporting laboratory and theoretical work. Discussion of such work has been restricted to some highlights and to results that have a direct bearing on solar physics research.

ORBITING SOLAR OBSERVATORY PROGRAM

The purpose of the Orbiting Solar Observatory (OSO) program is to study the physical phenomena on the quiet and active Sun and the solar-terrestrial interactions by observing the particle and electromagnetic radiations over a wide range of energies. This broad objective is achieved by accommodating a range of different experiments by different investigators on each spacecraft in the program. Experiments of interest to other research areas are often accommodated if space is available, such as the experiment to determine the effect of space environment on different surface coatings on OSO–IV.

With two OSO's launched in 1967 with a total of 18 working experiments, the OSO program has been the most successful and fruitful one in solar physics during the calendar year 1967. Not only did all experiments perform and return data initially, but many did so far beyond the designed

lifetime of the spacecraft and experiments. The scientific return has been gratifying. Even a cursory look at the large amounts of data transmitted to Earth has led to major discoveries and great increases in scope, precision, and resolution of solar observational material in the wavelengths that cannot be observed from the ground.

The OSO program has eight approved spacecraft. Four have now been successfully launched and designated OSO–I, OSO–II, OSO–III, and OSO–IV. OSO–I and OSO–II were launched in 1962 and 1965, respectively. OSO–III and OSO–IV were launched in 1967. A fifth spacecraft failed to achieve an orbit. Three remaining spacecraft are to be launched in 1968, 1969, and 1970, respectively. A full complement of experiments has been selected for each of these remaining spacecraft.

Table I shows some of the data on the first four OSO's as well as the OSO–F spacecraft that is scheduled to be launched in 1969. The indicated improved performance of the OSO–F spacecraft reflects minor updating of the spacecraft in terms of increasing some of those capabilities that proved to be pacing experiment utilization. OSO–III and OSO–IV, in fact, meet or exceed their respective design specifications. All experiments on OSO–III and OSO–IV returned data during 1967, and many are still operating.

It will be some time before the full scientific impact of the OSO results will be appreciated; in fact, not until all of the data can be evaluated. Most results reported to date were presented orally at scientific meetings rather than published as journal articles or letters. Thus, here we include few references but a large number of graphs and tables. Those unpublished were made available by the experimenters. (Credit is given in the figure captions or in the text.) Any discussion here, therefore, reflects interpretations by the present authors and not necessarily those of the experimenters, unless references are given.

In the OSO program the individual experiments are proposed for each OSO spacecraft by the scientific community and selected on a competitive basis of scientific merit and technical capability. Those selected are integrated into an OSO experiment payload to function with the housekeeping services provided by the spacecraft, such as data storage and telemetry, power supply, and stabilization and pointing. The spacecraft has two primary sections: a pointing section which points at the Sun and a rotating wheel section. Each section contains experiments, but those in the wheel section share that space with spacecraft housekeeping hardware. Some of the OSO's provide a raster scan capability that enables the pointing section of the spacecraft to scan the Sun. Spatially resolving experiments in the nonrotating sail or pointing section can thus piece together spectroheliograms with a resolution limited by pointing accuracy and experiment design. Later OSO's will also have an offset pointing capability for the observation of preselected regions of interest on the Sun. Figure 1 is a picture

Table I.—*OSO Satellites*

Designation	OSO–I	OSO–II	OSO–III	OSO–IV	OSO–F
Launch	Mar. 7, 1962	Feb. 3, 1965	Mar. 8, 1967	Oct. 18, 1967	1969.
Orbit apogee, kilometer	593	633	570	577	550.
Orbit perigee, kilometer	553	551	540	542	550.
Pointing accuracy, min	1	1	0.7	0.5	0.5.
Raster capability	No	256 sec	No	307.2 sec 40×40 min.	307.2 sec 40×40 min.
Sail experiments, data returned	5 (5)	3 (2)	2 (2)	3 (3)	3.
Wheel experiments, data returned	8 (8)	5 (5)	7 (7)	6 (6)	3.
Data recording rate, bits per second	Analog	400	400	400	800.
Data playback rate	18 times recorded rate.	7200	7200	7200	14 400.
Bit storage, 10^6 bits		2.16	2.16	2.16	4.32.
Power for experiments, watts	9	12	15.3	15	15.

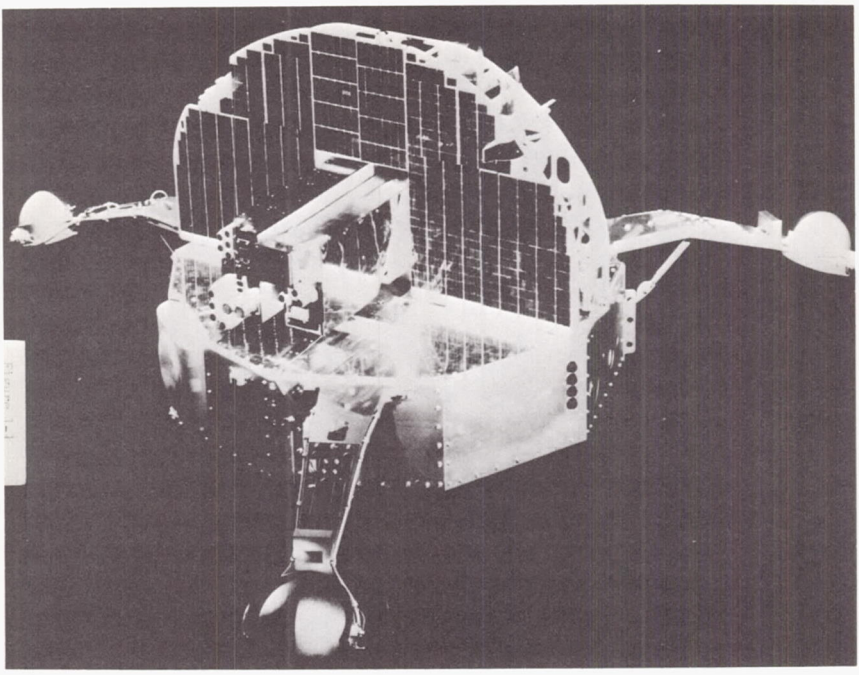


Figure 1.—Orbiting Solar Observatory spacecraft.

of a typical OSO spacecraft, showing the pointing section with the solar cells as well as the wheel section with its various experiment compartments.

X-ray experiments on board have permitted the study of the solar atmosphere, particularly the corona, during quiet periods as well as during flare and other activity of the active Sun. The results constitute valuable material for comparison with the predictions of various existing and future flare and corona models. In addition to fulfilling their mission to study the quiet Sun, its structure and composition, and to aid in establishing model atmospheres, the extreme ultraviolet experiments have also contributed to studies of solar activity. The supporting experiments, e.g., those measuring cosmic rays, trapped-particle radiation, and Lyman-alpha night-sky glow, have provided valuable information on solar-terrestrial relationships. The following brief description of experiments and preliminary results for OSO–III and OSO–IV demonstrate the spectacular success of the program.

OSO–III, launched on March 8, 1967, does not have a raster scan capability. The experiments on OSO–III are particularly productive in observations of solar activity. Excellent flare spectra in a wide range of X-ray energies were obtained, and EUV enhancement, or EUV flares, were discovered. Although the preliminary experimental results reported below are restricted to solar physics; many interesting stellar, galactic, and tech-

nological results were also obtained as a byproduct or by specially designed experiment packages on the wheel. For example, the high-energy (larger than 50 MeV) MIT gamma-ray experiment of Clark, Garmire,[1] and Kraushaar [2] has indicated a clustering of such gamma rays from the direction of the galactic center, suggesting that it is a source of such high-energy photons.

A spectrometer experiment by Neupert and White of the Goddard Space Flight Center, for the 1- to 400-Å region, occupies one-half of the pointing section of OSO–III. It has no spatial resolution on the Sun, but has good time resolution, better than 1 second overall, and precisely 0.32 second in the 20- to 400-Å interval. It also has good wavelength resolving power: 200 at 2 and 10 Å, and 800 at 400 Å. The extended wavelength coverage for OSO–III is achieved by a combination of instruments as follows: 1.3- to 3.1-Å crystal spectrometer (LIF), 3- to 8-Å crystal spectrometer (EDDT), ion chamber (integrated flux), 6- to 25-Å crystal spectrometer (KAP), and 20- to 400-Å grating spectrometer. The basic dispersing elements are crystals and a grazing-incidence grating. The detection equipment includes an ion chamber, Bendix photomultipliers, and conventional photomultipliers coupled with phosphors. This equipment permits basically two types of observations: the recording of the line spectrum associated with X-ray bursts on the quiet Sun by scanning in wavelength; and the recording of the time history of emission at some selected wavelengths during solar X-ray bursts with the full time resolution.

Figure 2 shows two consecutive (within 5 min.) scans of the 1.3- to 3-Å spectrum during a flare of importance 3b on March 22, 1967. The increasing activity during the observation period is plainly indicated by the hardening of the spectrum. The strong emission lines and possible weak emission lines are indicated, and they are superimposed on an apparent continuum. The expected positions of the hydrogenlike Lyman-alpha lines of some abundant elements are indicated on the figure for comparison. The rich emission spectrum between 7 and 20 Å during the same flare is shown in figure 3. It may be compared with experimental laboratory spectra as discussed in "Supporting Laboratory and Theoretical Research." The superimposed quiet Sun spectrum dramatically illustrates the hardening of the spectrum during flare events. The emission of hydrogenlike ion lines in significant intensities may, in fact, be caused by K-shell transitions in less highly ionized iron.

A typical time history of X-ray emission lines is shown in figure 4 as observed during the May 6, 1967, flare. The slow increase of the softer compared with the harder emission may have to be explained in terms of an inhomogeneous model. A homogeneous model would require peaking of the softer component before and after the peak for the harder component.

[1] Now at the California Institute of Technology.

[2] Now at the University of Wisconsin.

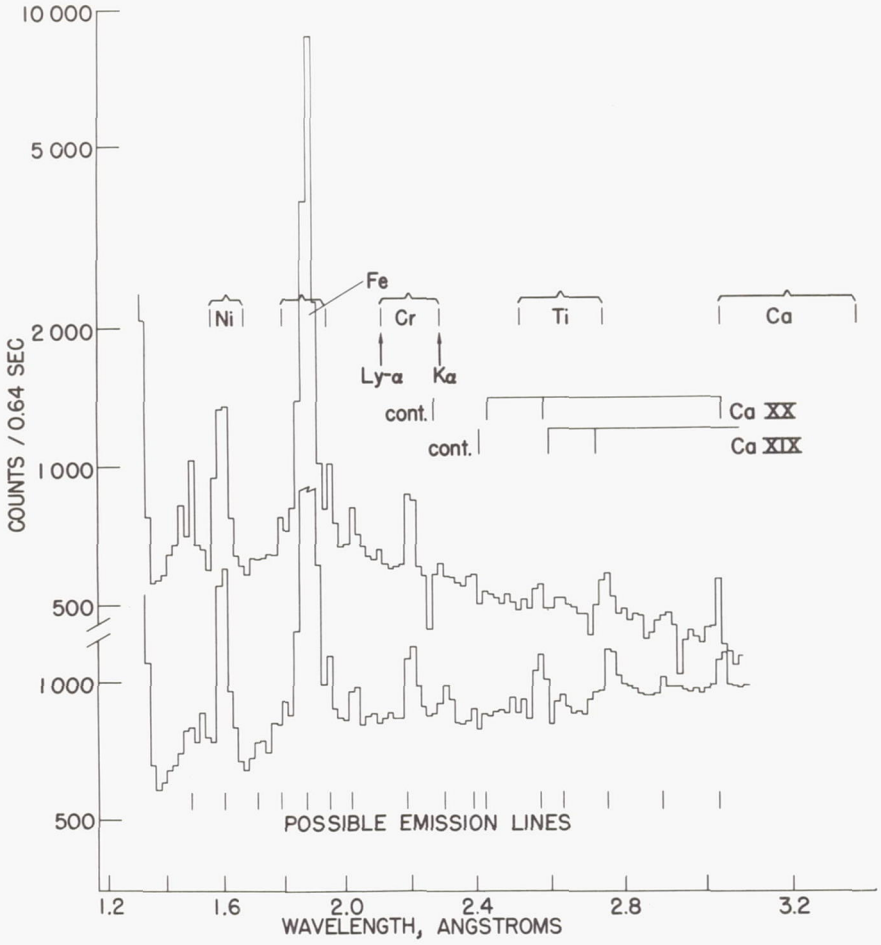


Figure 2.—**Solar flare spectra, March 22, 1967, from OSO-III (Neupert, Goddard Space Flight Center).**

Further details about the observations may be found in a letter by Neupert, Gates, Swartz, and Young (ref. 6).

An ion-chamber photometer mounted in the OSO–III wheel provided by Teske, University of Michigan, monitored the soft X-ray flux between 8 and 12 Å. No angular resolution of sources on the Sun was permitted by the design; the time resolution was 1.8 seconds. The instrument was very stable during the first year's operation.

The data show that during times when no reportable optical events occur on the Sun, the solar soft X-ray background flux may still undergo some variations. These fluctuations become greater in amplitude and occur more

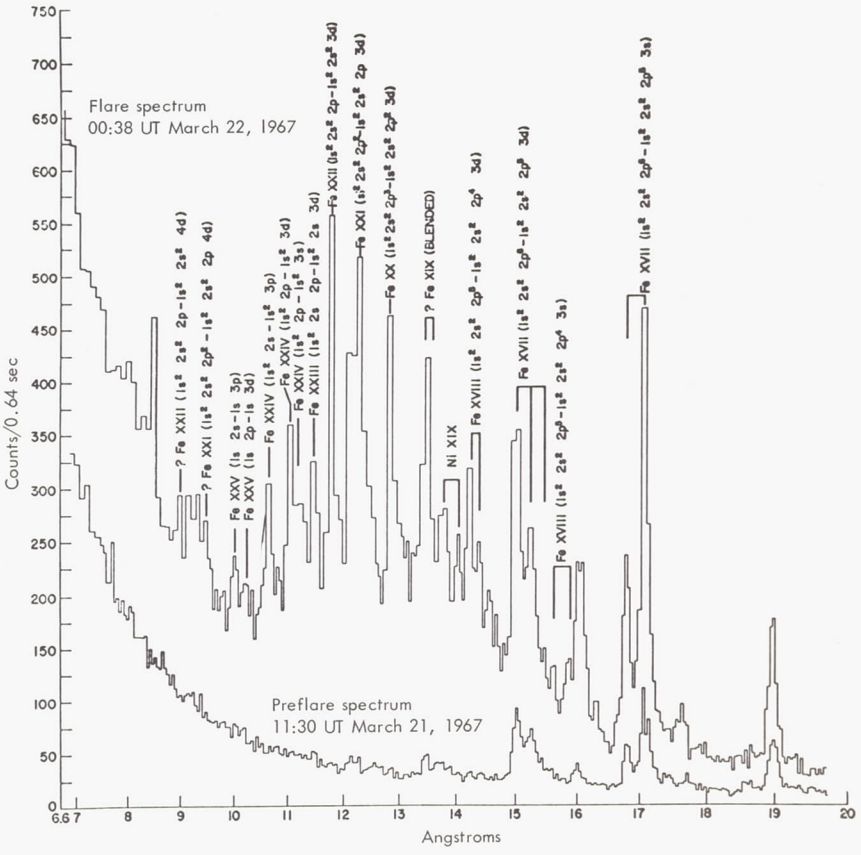


Figure 3.—**Solar flare spectra, March 22, 1967, from OSO-III (Neupert, Goddard Space Flight Center).**

frequently as solar activity increases, although there is not always a visible H-alpha plage fluctuation accompanying them. Preliminary study of the available information indicates that soft X-radiation accompanies flares probably 100 percent of the time. On the other hand, it does not appear that all soft X-ray enhancements are accompanied by reportable flares or other transient events. Regarding flares, the H-alpha and soft X-ray events tend to begin together. In about 80 percent of the cases, the H-alpha peak intensity precedes or coincides with X-ray flux maximum. The X-ray event tends to outlast the H-alpha event by a margin that increases with increasing flare importance. Usually, the peak microwave flux resulting from the flare occurs on the rising portion of the X-ray flux curve. The X-ray flux tends to peak at the onset of the microwave postburst increase, if the increase occurs. Otherwise, the X-ray flux peaks after the radio maximum. A

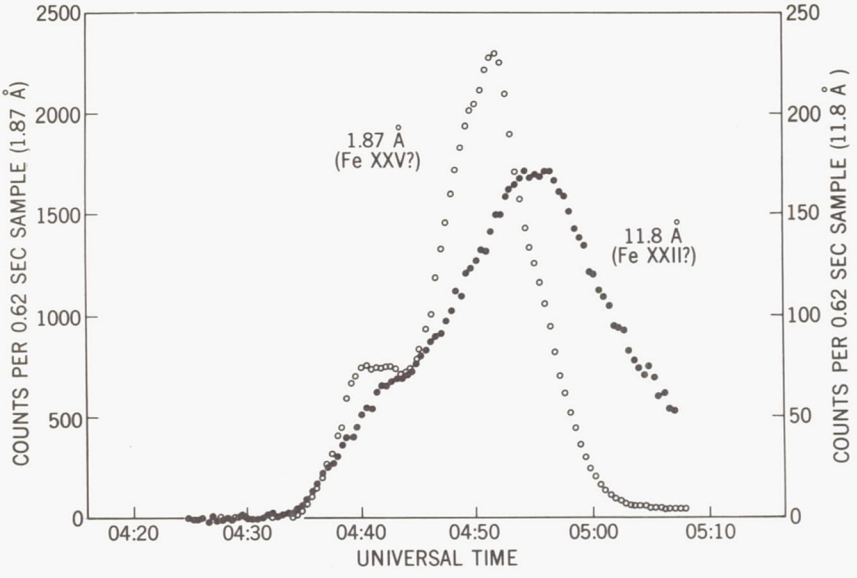


Figure 4.—**Solar X-ray line emission at two wavelengths, May 6, 1967 from OSO-III (Neupert, Goddard Space Flight Center).**

detailed comparison of X-ray, H-alpha, and microwave emission in a flare that took place July 25, 1967, is shown in figure 5. The data from this experiment are being used in a detailed study of the phenomenological relationships of solar active events simultaneously observed at optical, radio, and X-ray wavelengths.

A scanning spectrometer built by Hinteregger and Hall, Air Force Cambridge Research Laboratories, for observations of the 250- to 1300-Å region is sharing the pointing section with the Goddard Space Flight Center experiment. It provides good time resolution, sampling for 0.12 second every 0.16 second, looking at the entire Sun without spatial resolution. The spectral resolving power increases from 250 at the short-wavelength end to more than 400 at the other end of the observed spectrum. The counting rate, as indicated by figure 6, is sufficiently high to provide essentially noise-free data. Thus, there is very little difference between the results of a single scan and the average over four scans. To a somewhat lesser extent, this is also true at the short-wavelength end of the spectrum, figure 7. Preliminary results indicate that the presence of EUV bursts from the Sun could not be observed previously with the very short and intermittent sounding rocket coverage of this spectral region. These bursts have typical 1-minute rise times and several minutes' decay times, and change the total flux integrated over the Sun by only a small amount, typically 10 percent. In terms of local

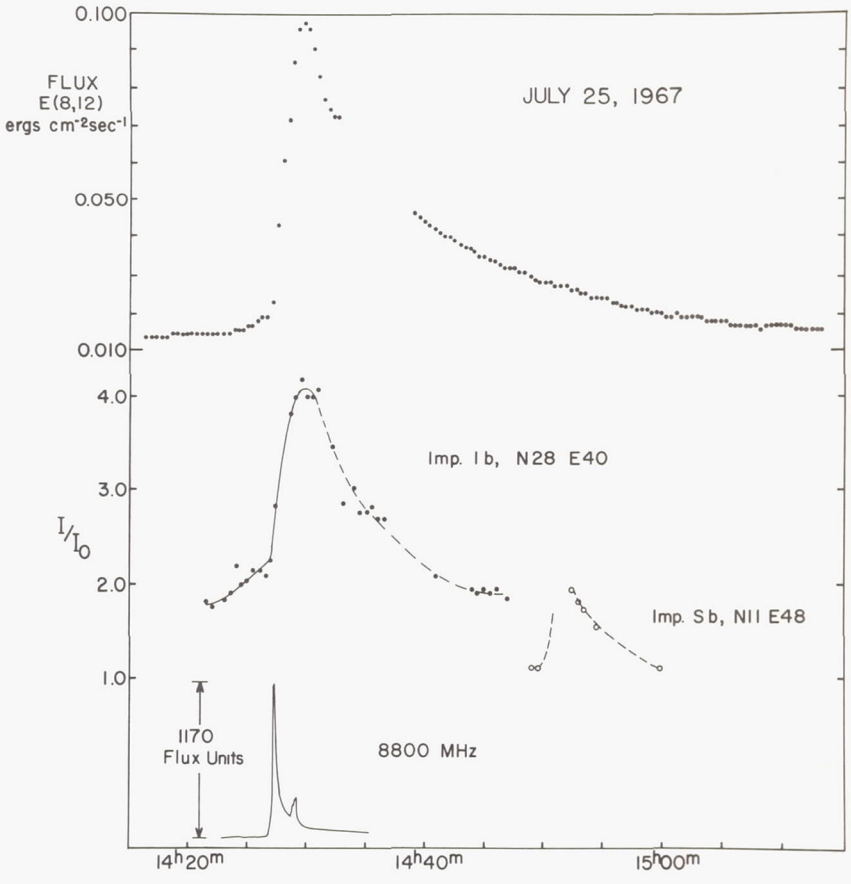


Figure 5.—X-ray flux, 8 to 12 Å, July 25, 1967, from OSO-III (Teske, University of Michigan).

emission on the Sun, this amounts to a significant enhancement. Prominent enhancements occurred, for example, in the He II 304-Å resonance line, but time-resolved observations also were made in He I and ionic lines of C, O, Ne, Mg, Si, and Fe. As might be expected, a number of the EUV bursts coincided with optical and X-ray events, such as on March 22, 1967, and May 6, 1967.

Besides providing a wealth of spectral and, in many cases, time-resolved information about the Sun, this experiment also furnishes extremely valuable information on the structure of the Earth's atmosphere through the measurements of occultation of the ultraviolet (UV) Sun by the atmosphere during satellite sunrise and sunset. In fact, this was the primary scientific motivation behind this experiment.

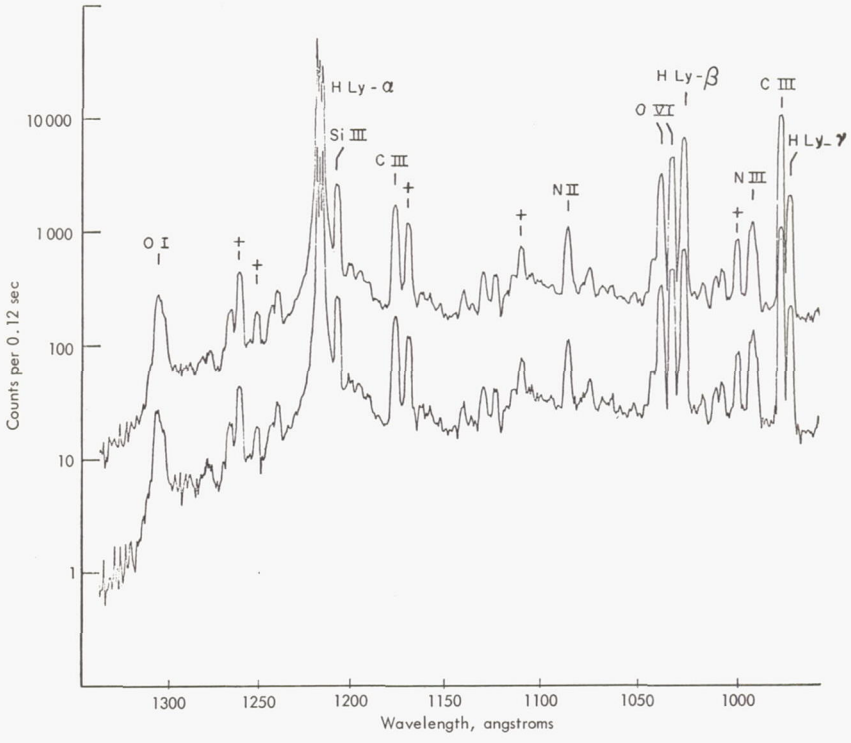


***Figure 6.*—Solar EUV spectra, March 9, 1967, from OSO-III. Upper trace average of four scans; lower trace single scan, shifted by one decade; + indicates higher orders (Hinteregger, Air Force Cambridge Research Laboratories).**

Also on the wheel of OSO–III is an X-ray and gamma-ray detector built by Peterson, University of California at San Diego, and designed for solar as well as galactic observations of photons in the 7.7- to 210-keV range. It provides a map of the sky as well as valuable solar observations. The detector consists of a scintillator with anticoincidence shielding; it has 0.15-steradian directionality. A pulse-height analyzer is used for spectral resolution in six channels.

The variability of solar emission at these photon energies is illustrated by the fact that the Sun appeared invisible against the cosmic background on May 11, 1967, but completely saturated the electronics during the March 22 class 3 flare, although the dynamic range of the instrument is at least 50 000:1. The extreme variability of the flux is indicated in table II where the counting rates and fluxes are compared for various sources. For comparison with the results obtained by Neupert et al. (ref. 6) and by other OSO–

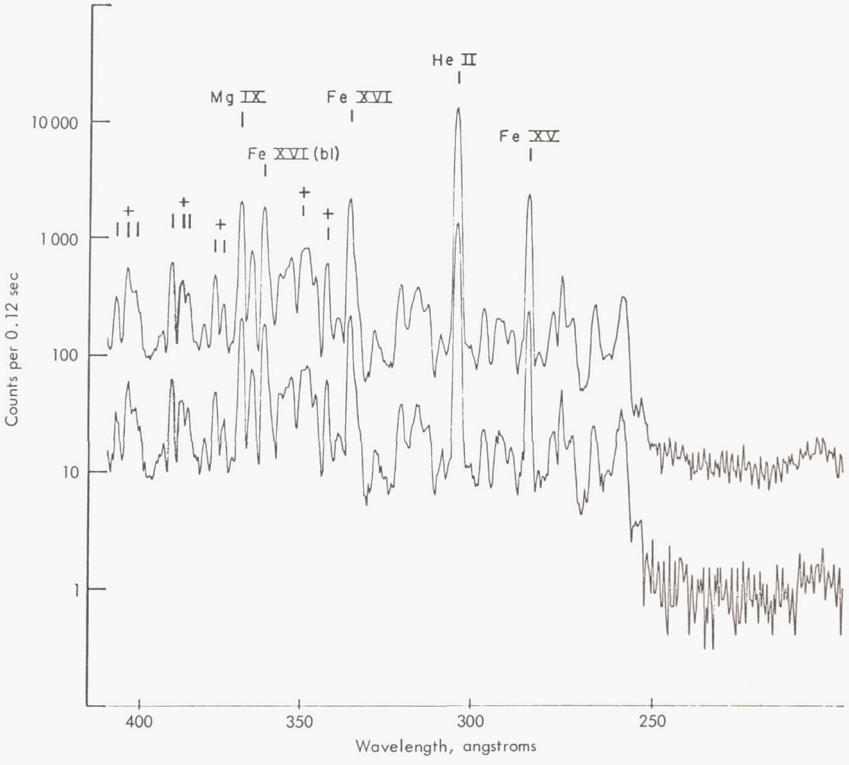


Figure 7.—**Solar EUV spectra, March 9, 1967, from OSO-III (Hinteregger, Air Force Cambridge Research Laboratories).**

III experimenters, the results from the solar X-ray event of March 22, 1967, and the 2700-MHz radio observations are shown in figure 8. The softening of the spectrum with time is clearly indicated.

Table II.—*Channel 2—7.7 to 12.5 keV*

Source	Rate, counts/cm²/sec	Flux, ergs/cm²/sec
Cosmic-sky background	0.2	3×10^{-9}
Quiet Sun, Mar. 15	3.0	50×10^{-9}
Bursts, 5/day	80	1.2×10^{-6}
Bursts, 0.6/day	1000	15×10^{-6}
Saturation	3000	50×10^{-6}

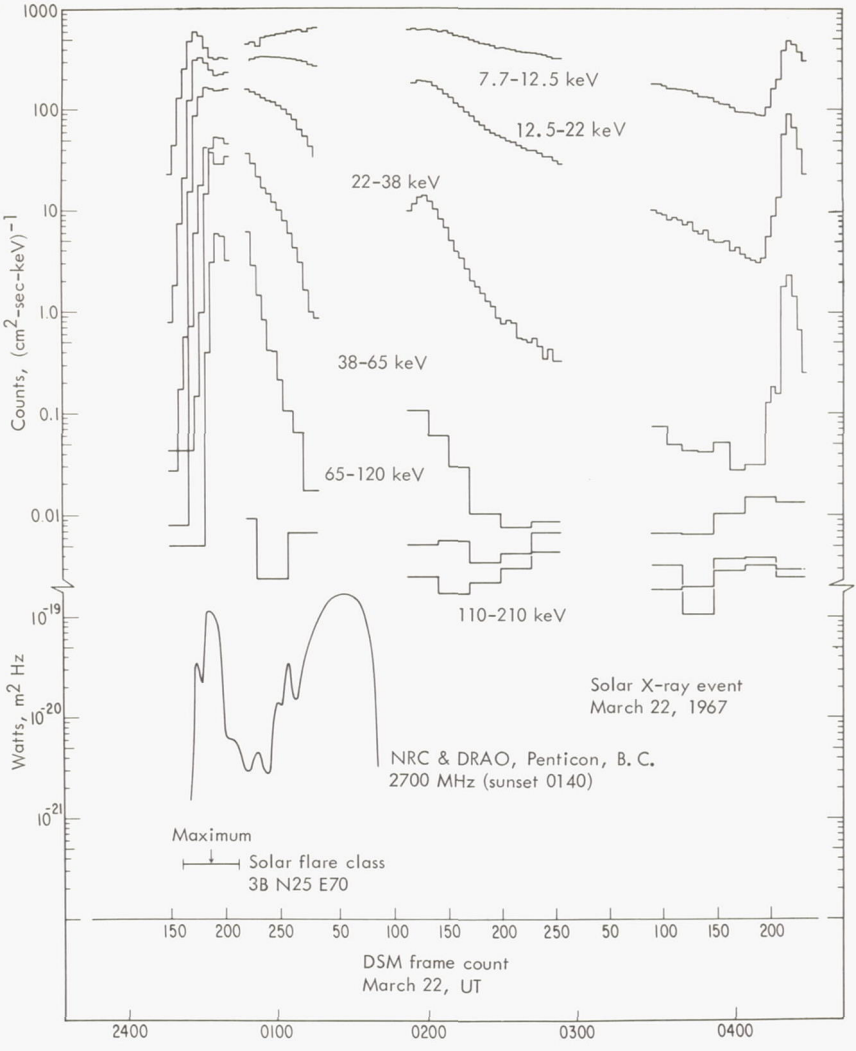


Figure 8.—**X-ray flux from pulse-height analysis, Mar. 22, 1967, from OSO-III (Peterson, University of California).**

The lower energy channels remained saturated for hours; even near 100 keV the emission lasted for about 1 hour. In addition to solar data, the experiment provided the first map of the celestial sphere in this X-ray energy interval. The cosmic X-ray source Lupus XR–1 was observed over a 40-day period and exhibited no significant time variations. An upper limit to the hard X-ray flux from the peculiar galaxy M 87 was also obtained.

Gamma rays with energies in excess of 50 MeV and cosmic-ray-charged particles with energies in excess of 400 MeV/nucleon are detectable by a scintillator device (Kaplon, Deney, and Dennis, University of Rochester) which is also located on the wheel of OSO–III. Anticoincidence and Cerenkov devices permit discrimination against other particles and between the desired species. An upper limit of 5.5×10^{-5}/cm^2/sec has been established for the solar gamma-ray intensity above 50 MeV, assuming that it originated in π° decay. On the same assumption, the upper limit for diffuse primary gamma radiation is 3.2×10^{-4} gammas/cm^2/sec. Cosmic-ray protons and alpha particles have been observed. The proton spectrum is flatter than the alpha particles spectrum; the ratio of protons to alpha particles increases slowly from approximately 6 at 3 BeV to 8 at 15 BeV. Further results will include cosmic-ray spectra for heavier nuclei in three charge ranges: 3 to 5, 6 to 9, and above 10, in the energy range 3 to 18 BeV.

For the MIT gamma-ray experiment by Kraushaar, Garmire, and Clark, which is responsive to energies above 50 MeV, there are only preliminary results as yet. Long integration times are required to separate the cosmic gamma-ray flux from instrumental effects and from the secondary gamma rays created in the Earth's atmosphere under the influence of cosmic rays. The tentative result that the center of the galaxy is a source of gamma rays is most exciting. The large amount of data obtained from the experiment should permit confirmation of this result by integrating and averaging techniques.

The OSO–III wheel includes other space experiments: one for a study of the effects of space environment on 12 different temperature-control surfaces in order to clarify the mechanism and rate of degradation, especially in regard to emissivity and reflectance (Neel and Hillard, Ames Research Center); and an experiment to measure the Earth's albedo between 3200 and 4800 Å (Neel and Griffin, Ames Research Center).

OSO–IV was launched on October 18, 1967, with a total of nine experiments on board, of which three are in the pointing section, and all nine have returned data to the Earth. One of the sail experiments, the Harvard College Observatory (HCO) spectrometer and spectroheliograph, is discussed in "Photosphere and Chromosphere" in connection with chromospheric observations. The spectral information and the spectroheliograms obtained in the HCO experiment permit studies of both the chromosphere and the corona, and many of them are of interest in connection with solar activity. (See "Flares.") Sample spectroheliograms are shown in figures 9 through 11.

A second experiment on the OSO–IV pointing section, provided by Giacconi and Paolini, American Science & Engineering, Inc., produces heliograms in wide-wavelength bands between 3 and 70 Å units. It consists of a Wolter-type grazing-incidence telescope with two reflecting surfaces, parabo-

333–240 O—69——30

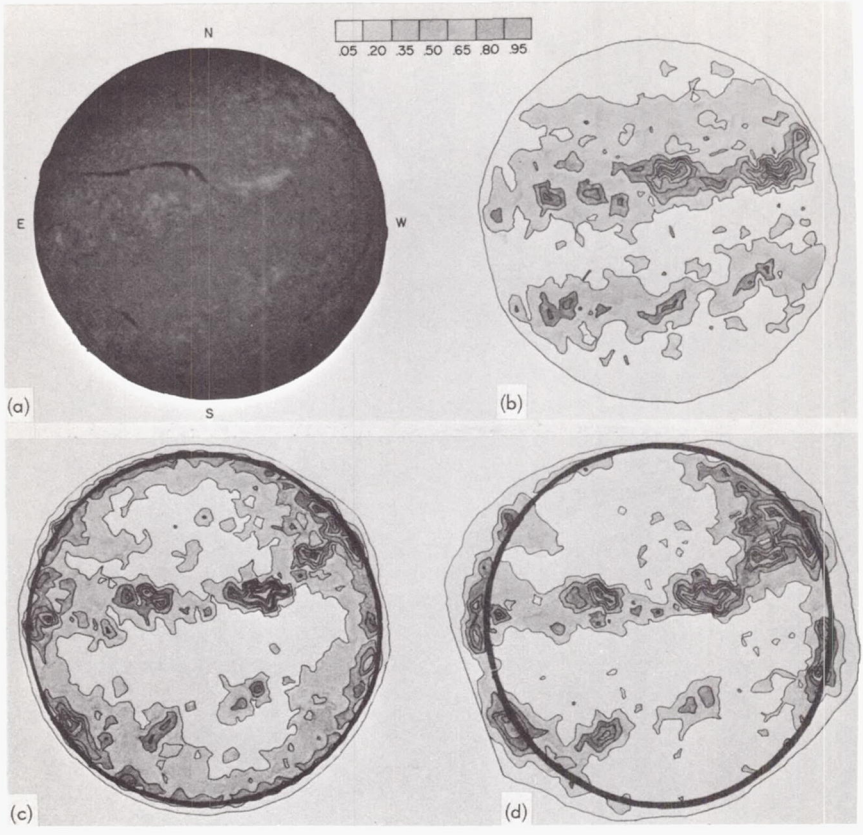


Figure 9.—(*a*) **Hydrogen-alpha spectroheliogram from OSO-IV (Sacramento Peak Observatory, October 25, 1967) compared with spectroheliograms (Goldberg, Harvard College Observatory); (*b*) in Lyman continuum, 897 Å, October 27, 1967; (*c*) in oxygen VI, 1032 Å, October 25, 1967; and (*d*) in magnesium X, 625 Å, October 25, 1967.**

loid and hyperboloid of revolution; a set of filters that provide the wavelength resolution in bands of 3 to 13, 3 to 21, and 44 to 70 Å; an electro-optical image converter device for image intensification; and a photomultiplier for data recording. Inflight calibration is provided by an Fe^{55} X-ray source on board. The instrument observes a small region on the Sun in a single channel; the heliogram results from the raster scan of the solar disk by the entire pointing section. Apertures permit resolution of 4 (coarse) and 1 (fine) minutes of arc.

The coarse mode is particularly well suited for the study of the less luminous (in X-rays) plage regions, while the fine mode with its lesser sensitivity but better resolution is well adapted to flare observations where the lu-

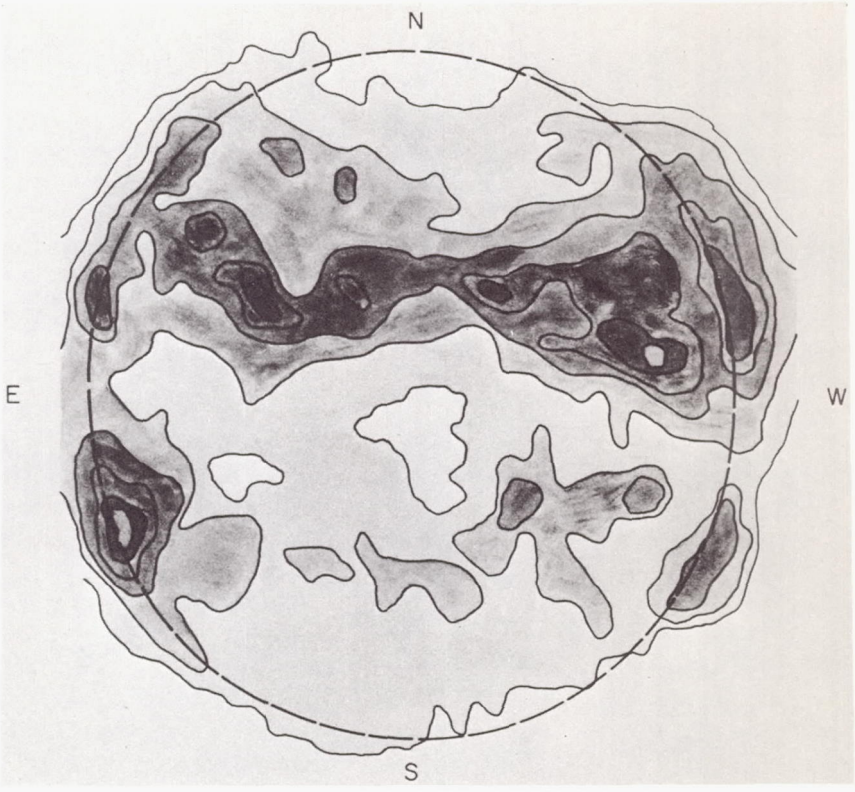


Figure 10.—**Spectroheliogram in Si XII 499 from OSO-IV (Goldberg, Harvard College Observatory), November 22, 1967. Contour interval 0.3 in $\log_{10}$ I.**

minosity is much greater. Figure 12 shows the progress of plage areas over the apparent disk in a sequence of heliograms, the first set of successive solar X-ray pictures ever obtained. In the heliograms, the darker the gray, the brighter the region. The brightest plage in picture 1 of this figure (early afternoon, Oct. 25, 1967) reached the limb in picture 2 (midmorning, Oct. 28) while intensifying. It reappears on the eastern limb in picture 3 (midnight, Nov. 10) and can be seen progressing over the disk in the remaining five pictures, taken around midnight on November 11, 12, 14, 15, and 16, respectively. This plage was observed for 2.75 rotations as of December 14, 1967, and has produced a number of flares. By means of observations in different-wavelength intervals, plages could be classified in terms of the hardness of the X-ray emission. A hardness index may be defined as the ratio of counts at shorter wavelength intervals to counts at longer wavelength intervals. Variations of an order of magnitude were found in an empirical

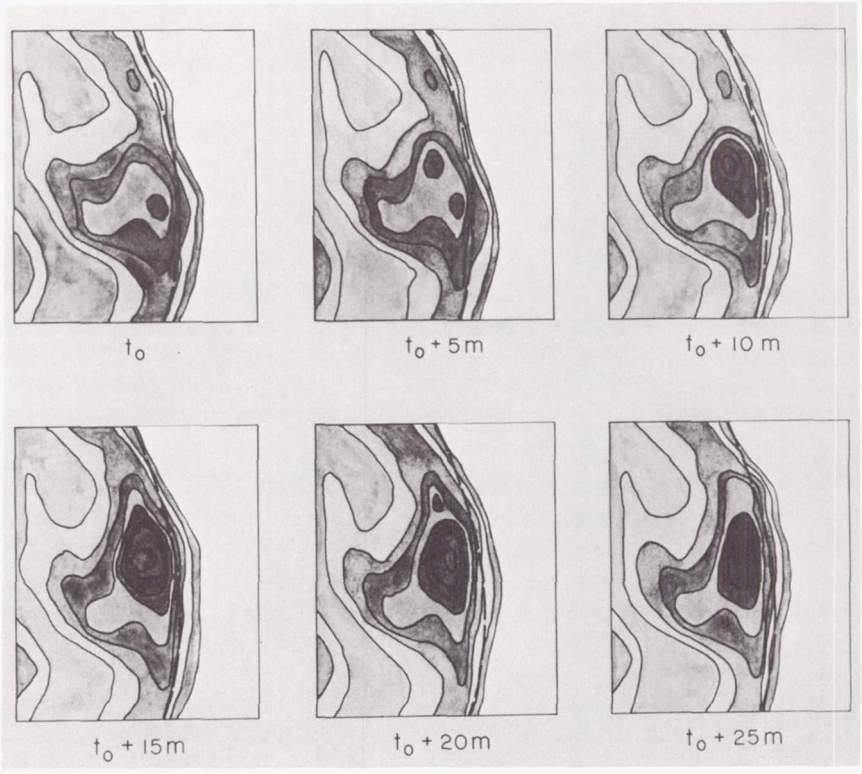


Figure 11.—**Spectroheliograms of a class 2b flare from OSO–IV (Goldberg, Harvard College Observatory), November 29, 1967; O VI, 1032 Å. Contour interval 0.21 in $\log_{10}$ I.**

hardness index, and it was observed that the harder plages live longer and produce more flares.

A large number of flare observations was made both in the heliographic mode and in the monitoring mode in which the solar emission is monitored intermittently in the different available passbands. Figure 13 shows the development of a flare on October 28 that occurred at about 0825 near the limb. The individual heliograms were taken at −100, +10, 30, 40, 50, and 110 minutes with respect to 0825, respectively. The peak enhancement was by a factor of more than 20, and the *e*-fold rise and decay times were 17 and 25 minutes, respectively. The indicated size of the flare itself is consistent with an angular extent of no more than 1 minute of arc, probably much less. No flare observations with time sequencing had ever been made before, nor could they have been made except with a satellite-borne instrument and raster scan capability.

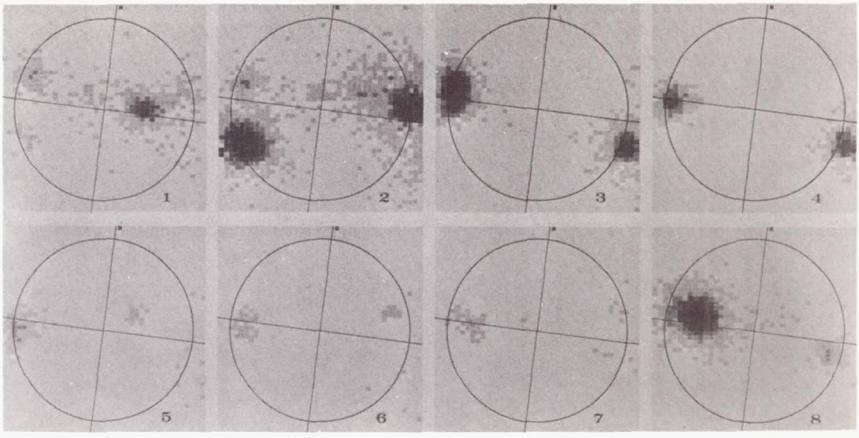


Figure 12.—X-ray heliograms from OSO-IV (Giacconi, American Science & Engineering, Inc.), nos. 1 to 8 taken on October 25 and 28, and November 10, 11, 12, 14, 15, and 16, 1967, respectively.

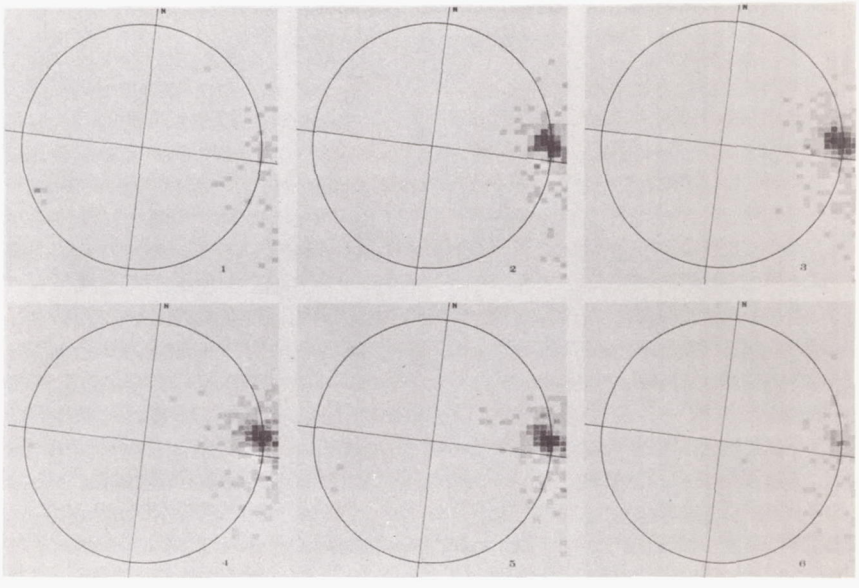


Figure 13.—X-ray heliograms during a flare on October 28, 1967, at times −100, +10, 30, 40, 50, and 110 minutes with respect to the starting time of 0825, respectively, from OSO-IV (Giacconi, American Science & Engineering, Inc.).

A third experiment on the pointing section of OSO–IV (Friedman, Chubb, Kreplin, and Meekins, U.S. Naval Research Laboratory) features two Bragg crystal spectrometers for X-ray observations between 1 and 8 Å, looking at the entire Sun. The dependence of Bragg-reflected wavelength on angle prevents simple data reduction of this experiment when the OSO is in the raster scanning mode. Nevertheless, computer reduction of the data can correct for this. An example of a spectrum obtained during raster scanning when a flare of class 3b was in progress on November 16, 1967, at 2125 UT is shown in figure 14. The most important emission lines are identified, many as hydrogenlike or heliumlike transitions in highly ionized medium mass elements, Na to Fe. The abrupt background changes at spectrometer positions 170 and 550 are instrumental. The absolute intensities in the preliminary data are derivable within a factor of about 10; the relative line intensities, within a factor of 2. Spectra were also obtained during other flares and during periods of relative calm, many of these in a pointing rather than raster scanning mode of operation.

The Naval Research Laboratory pointing experiment is supplemented by a wheel experiment (Chubb, Kreplin, and Friedman, U.S. Naval Research Laboratory) that measures solar X-rays in bands of 0.5 to 3, 2 to 8, 8 to 16, and 44 to 60 Å with the aid of ionization chambers and filters. Besides providing absolute intensity measurements in these bands as a means of calibrating the spectra obtained in the pointing experiment, the wheel experiment furnishes important basic data for aeronomy in terms of energy inputs to the atmosphere in these soft X-ray bands.

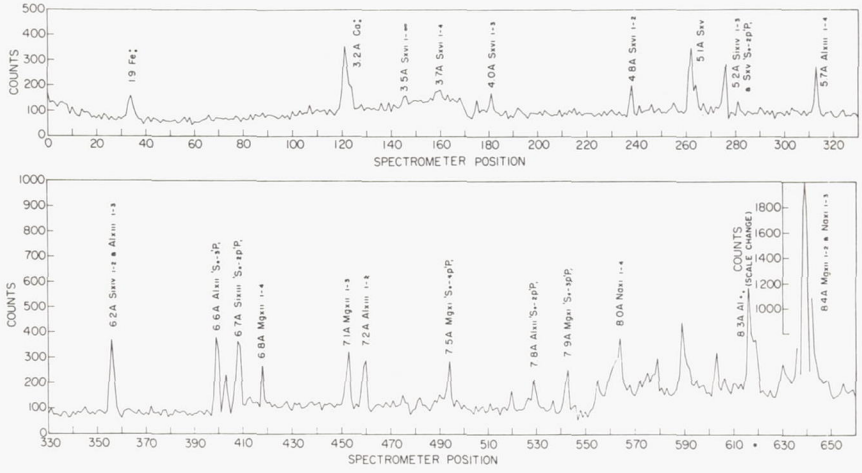


Figure 14.—EUV spectrum during November 16, 1967, flare from OSO-IV (Friedman, Naval Research Laboratory).

Still another OSO–IV wheel experiment by Boyd, University College, London, and Stewardson and Pounds, Leicester University, observed X-ray emission in the bands 1.2 to 3.6, 3 to 9, 6 to 18, 44 to 55, and 44 to 70 Å by means of proportional counters. Pulse-height analysis provides further spectral resolution within these bands. Figure 15 shows a typical time history in the 3.3- to 4-Å band, including a small flare and occultation by the atmosphere.

A precision experiment for the monitoring of the He II 304-Å resonance line is also located on the OSO–IV wheel (Boyd, University College, London). The measurement of absolute intensities at this wavelength is extremely difficult, both in view of the lack of intensity standards for preflight calibration and because of the degradation of optical surfaces in the space environment. The device uses a grating, ruled in gold with 1200 lines per millimeter, in grazing incidence with entrance and exit slits on a 25-cm-diameter Rowland circle. For an inflight check on the constancy of the equipment, the 1216-Å Lyman-alpha radiation is measured periodically with the same grating and detector that is also used for the 304-Å observations. The signal is compared with the readings from a nitric oxide, Lyman-alpha ionization chamber. This comparison would lend credence to any observed slowly varying component at 304 Å. The precision should be ± 20 percent. Excellent results on atmospheric absorption of the 304-Å radiation are obtained during orbit eclipses. There are indications of interesting variations in the 304-Å intensity near flare times. This is illustrated by figure 16 in which the 304-Å and the 1- to 3-Å X-ray intensities are compared for the importance 3b optical flare of November 16, 1967.

Other OSO–IV wheel experiments include a proton-electron detection experiment designed to measure the flux and angular distribution of protons and electrons in eight channels between 1.87 and above 36.7 MeV, and between 93 and above 5000 keV, with the aid of scintillator-photomultiplier combinations, pulse-shape discrimination between electrons and protons, and pulse-height analysis. The principal investigator was Waggoner, University of California, Lawrence Radiation Laboratory. This experiment serves to study the buildup and loss mechanisms of radiation trapped near the Earth, and the effect of solar-cycle variations on the trapped flux. The night-sky glow in Lyman-alpha is observed by another wheel experiment on OSO–IV (Mange, Chubb, and Friedman, U.S. Naval Research Laboratory) for the purpose of studying the properties of the geocorona. A survey of the night sky for cosmic sources of X-rays in the 0.5- to 30-keV range (Giacconi and Gursky, American Science & Engineering, Inc.) is intended to record possible point sources on a general background in this energy range. The preliminary results are inconclusive.

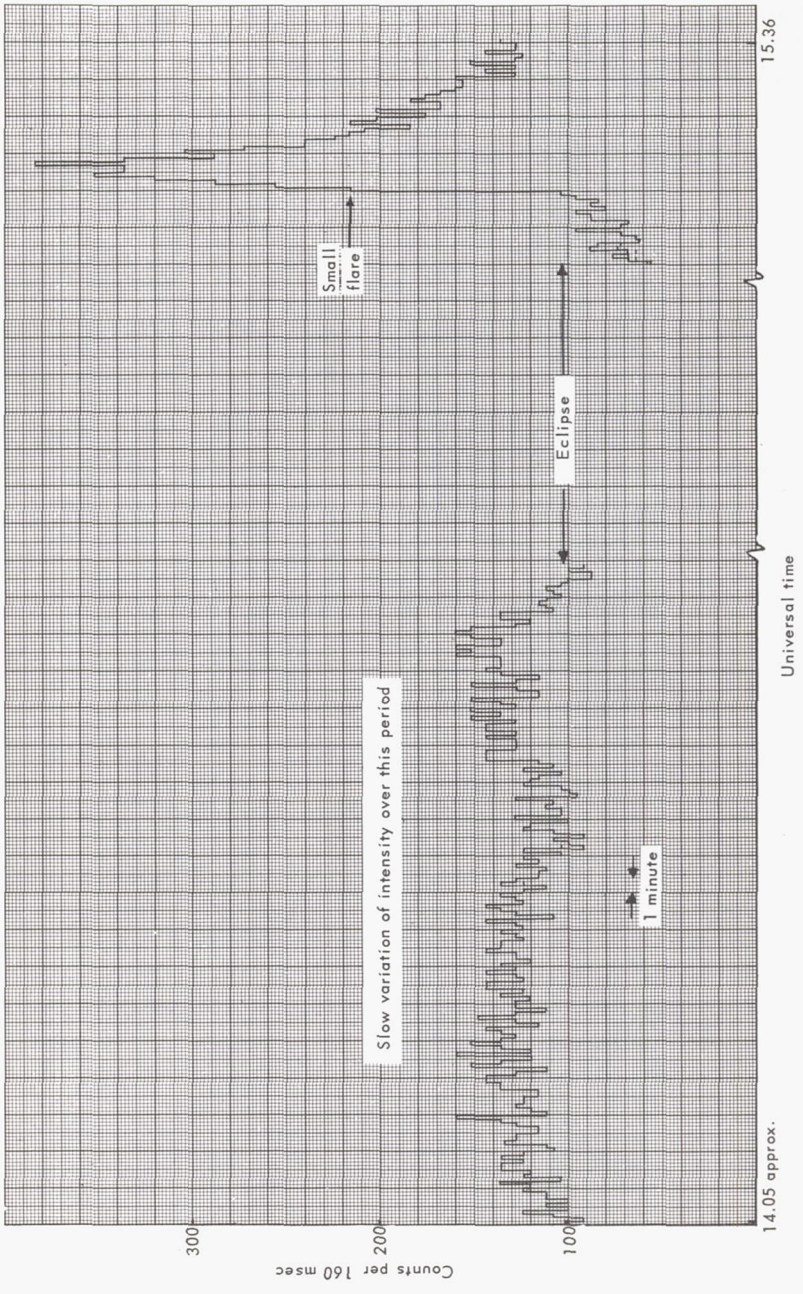


Figure 15.—X-ray emission, broadband 3.3 to 4 Å for orbit 75 from OSO-IV (Boyd, University College, London, and Pounds, Leicester University).

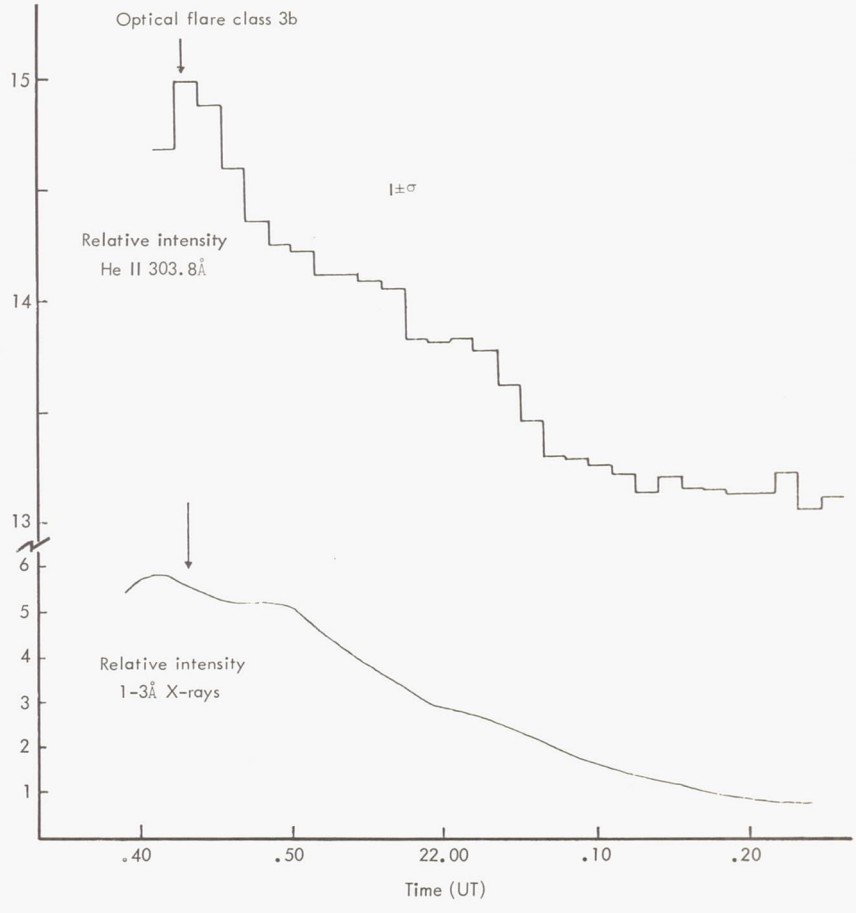


Figure 16.—**Comparison of He II 304-Å radiation with broadband X-radiation in the 1- to 3-Å band according to Boyd, University College, London, and Stewardson and Pounds, Leicester University, OSO-IV, November 16, 1967.**

NEUTRINO OBSERVATIONS

It is usually taken for granted that solar observations are limited to the outermost layers of the Sun: the corona, chromosphere, and photosphere. This assumed limitation on observations arises from the small size of mean free paths for charged particles and photons when compared with the dimensions of the Sun. The notable exception to this rule is the neutrino, the mean free path of which in solar material is of the order of many light-years. This extraordinarily long mean free path is a result of the weakness

of the neutrino's interaction with matter and, as a consequence, neutrino detection is an exceedingly difficult task. On the other hand, the observation of neutrinos offers great promise to solar physics, providing perhaps a unique opportunity to examine the interior of the Sun. This presupposes that neutrinos are indeed being produced in the Sun, such as is predicted by the nuclear reaction chains in the hydrogen-helium and carbon-nitrogen cycles. A computation of solar neutrino flux must rely on a model for the interior of the Sun and on computations and measurements of solar abundances and various cross sections (Bahcall, Cooper, and Demarque, ref. 7). If abundances in the interior of the Sun are assumed to be the photospheric ones, then the neutrino flux which is expected (Davis, Harmer, and Hoffman, ref. 8), along with other quantities of importance, is listed in table III. It can be seen that the neutrinos produced in the beta decay of B^8 in the Sun are most easily detected in the neutrino capture reaction Cl^{37} (ν, e^-) Ar^{37}.

The most rigorous experiment for the detection of this neutrino flux was carried out by Davis et al. (ref. 8), who used 390 000 liters of C_2Cl_4 as chlorine supply for the observation of the capture reaction; this experiment was located in a South Dakota gold mine to reduce background effects caused by cosmic rays. The detection consists of separating the argon-reaction products from the tetrachlorethylene in the tank. The predicted rate of capture of solar neutrinos is two to seven per day. Consequently, the recovery of the resulting few argon atoms from the vast storage tank is in itself a formidable task (ref. 8), the details of which will not be discussed here. The recovered argon, which contains only a few of the Ar^{37} product atoms along with a great amount of natural impurity Ar^{36}, is detected by its beta decay. An upper limit of only 0.5 capture per day was established in the longer of two experimental runs. Accepting the model and the Goldberg, Mueller, and Aller (ref. 9) abundances implies that at most only 9 percent of the solar energy is actually generated in the carbon-nitrogen cycle (ref. 8). The use of more recently obtained abundances (Lambert, ref. 10) leads to a smaller predicted neutrino flux which, as a result of the large error brackets, is still consistent with the accepted energy production mechanism.

Bahcall, Bahcall, and Shaviv (ref. 11) discuss some of the important uncertainties and list some of the important experiments that should be done to reduce the uncertainties in the theoretical calculations. In particular, the neutron lifetime, the low-energy cross section for the $Be^7(H^1,\nu)B^8$ reaction, and the heavy element abundance on the surface of the Sun should be measured with improved accuracy. Such measurements, combined with the fundamental solar neutrino flux measurements by Davis et al. (ref. 8), will reveal whether the current understanding of stellar (solar) interiors is adequate.

Table III.—*Solar Neutrino Fluxes and Cross Sections for the Cl^{37} (ν, e^-) Ar^{37} Reaction*

Neutrino source	Cross section, cm^2	Neutrino flux at the Earth, cm^{-2}/sec^{-1}	$\sigma\varphi\times10^{-35}$ sec^{-1}
$H+H+e^-\rightarrow D+\nu$	1.72×10^{-45}	1.7×10^{8}	0.03
Be^7 decay	2.9×10^{-46}	3.9×10^{9}	.11
B^8 decay	1.35×10^{-42}	$1.3(\pm0.6)\times10^{7}$	$1.8(\pm0.6)$
N^{13} decay	2.1×10^{-46}	1.0×10^{9}	.02
O^{15} decay	7.8×10^{-46}	1.0×10^{9}	.08
			$\Sigma\varphi\sigma=2.0(\pm0.6)\times10^{-35}$ sec^{-1}

On the basis of model calculations, Bahcall et al. (ref. 11) have already drawn a number of important conclusions from the Davis et al. (ref. 8) results. Independent of the model (Bahcall, ref. 12), the solar neutrino flux should exceed the observed upper limit (ref. 8) if most of the energy of the Sun was derived from the carbon-nitrogen cycle; thus the Sun does not derive most of its energy from this cycle. If the model of the solar interior is correct, the heavy element mass fraction in the solar interior must be less than 2 percent by mass, and with this number assumed to be 1.9 percent the primordial helium mass fraction can be deduced to be 0.22 ± 0.03 (22 percent), the uncertainty being caused by the stellar model. Other investigations related to the solar neutrino problem include Shaviv, Bahcall, and Fowler (ref. 13) and Iben, Kalata, and Schwartz (ref. 14).

Further refinements in the neutrino flux measurements may be looked for with great anticipation because they provide an opportunity to study the interior structure of the Sun, its source of energy, its interior composition, and the composition of the material from which it was formed.

SOLAR ROTATION

There has been considerable research on two aspects of the solar rotation problem. The question of the loss of solar angular momentum caused by solar wind has been considered in a number of investigations. (See "Corona.") More dramatic has been the observation of solar oblateness by Dicke and Goldenberg (ref. 15) and the continuing discussion on the interpretation of their experiment in terms of differential solar rotation and the implications of a possible solar quadrupole moment for general relativity.

Dicke and Goldenberg (ref. 15) used the device illustrated in figure 17 for a determination of solar oblateness. They were careful to eliminate all possible sources of error such as instrumental and atmospheric distortions of the solar image, the effects of "seeing," an oblate corona or chromosphere, prominences on the limb, shear stresses caused by velocity and magnetic fields, and others. The results are shown in figure 18. Each point represents an average over 10 days, and the combined points represent the observation time from June to September 1966. They can be explained by assuming a solar oblateness of $5 \pm 0.7 \times 10^{-5}$. In the process of eliminating the possible effect of a difference between the radiation temperatures of the Sun at the equatorial and polar limbs, Dicke and Goldenberg found that it was too small to be detected; i.e., less than $\pm 3°$ K, in contrast to earlier measurements.

The observed solar oblateness implies a sizable solar gravitational quadrupole moment that, in turn, would result in a perihelion advance of 3.4 seconds of arc per century for the planet Mercury. If this is subtracted from

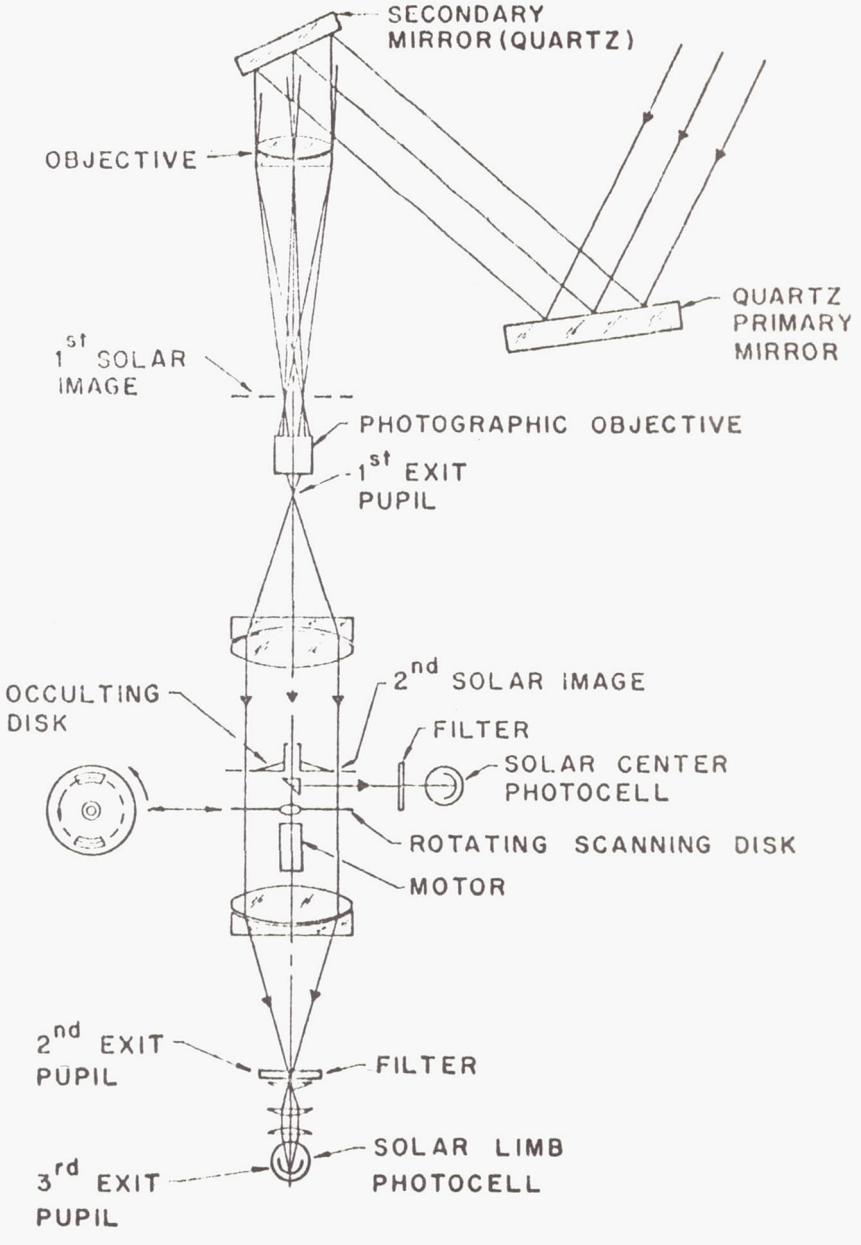


Figure 17.—Optical system apparatus (ref. 15). The primary mirror tracks the Sun.

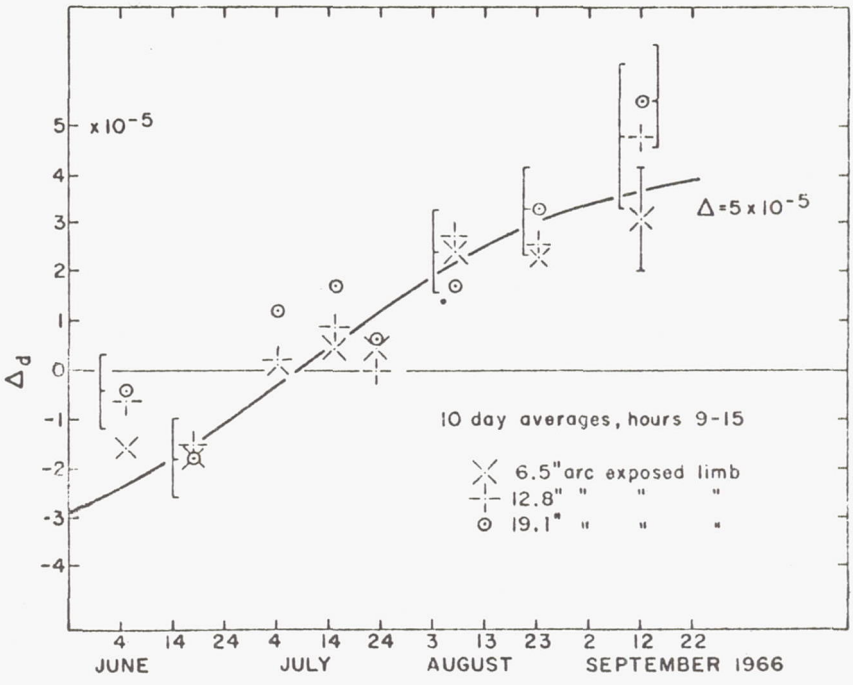


Figure 18.—Diagonal component of the solar oblateness (ref. 15).

the observed residual value not caused by planetary perturbations, there remains a presumably relativistic effect of 39.6 seconds of arc per century. This would be in good agreement with the predictions of the scalar-tensor theory of general relativity (Jordan, ref. 16; Brans and Dicke, ref. 17; and Dicke, ref. 18), while it falls short of Einstein's value by 8 percent. Before the correction for the solar quadrupole moment, the agreement with Einstein's value was much better: within approximately 1 percent.

If the solar oblateness observed by Dicke is interpreted in terms of a more rapid rotation of the solar interior compared with the rotation determined from the progress of active photospheric regions, there would have to be a large differential rotation between surface and interior of the Sun. Howard, Moore, and Spiegel (ref. 19) claim that in this situation the "spindown process" (Greenspan and Howard, ref. 20) would quickly damp the differential rotation by so-called "Ekman pumping" (as in a stirred cup of tea). Dicke (ref. 21) refutes this argument on the grounds that the large density gradients and the large spatial dimension would prevent the formation of an Ekman layer.

Sturrock and Gilvarry (ref. 22) discuss the possible interpretation of the observed solar oblateness in terms of magnetic stresses in the interior, and

they conclude that this alternate to the rapid interior rotation hypothesis cannot be ruled out. Continued measurements over at least 22 years would give an indication of possible changes during the solar cycle. Such changes would imply that magnetic stresses play a major role in producing the observed oblateness. Gilvarry and Sturrock (ref. 23) also discuss critically what effects the solar quadrupole moment would have on the orbits of different planets by pointing out that the quadrupole moment axis may not coincide with the axis of solar rotation. The gravitational field of a solar interior with large magnetic stresses would probably not be well represented by a quadrupole moment superimposed on the zero-order gravitational field. Verification of the quadrupole moment by natural planets such as Icarus seems hopeless because the effects are too small. Artificial "planets" with highly elliptic orbits would be required for this purpose. This would entail the consideration of such otherwise negligible effects as solar radiation pressure, charge, and neutral drag in the corona. Arguments for (Roxburgh, refs. 24 and 25) and against (Dicke and Goldenberg, ref. 26) the assumption of uniform solar rotation as the cause of the observed solar oblateness have been exchanged.

In the search for independent tests of the Dicke hypothesis of a solar quadrupole moment, Audretsch, Dehnen, and Hoenl (ref. 27) showed that it would lead to a regression of the node in the orbit of Mercury of 3.4 seconds of arc per century. They suggested that the observed regression should be untangled from possible planetary and relativistic effects and compared with this prediction. O'Connell (ref. 28) pointed out, however, that this value is relative to the Sun's equatorial system. With respect to the observed ecliptical system of coordinates, the regression rate is only 0.27 second of arc per century and presently is unobservable. Richard (ref. 29) showed that the quadrupole moment would lead to a precession in the lunar orbital node of -0.008 second of arc per century, also an unobservable effect.

PHOTOSPHERE AND CHROMOSPHERE

The photosphere and chromosphere form the lower layers of the Sun's atmosphere and are the sources of most of the solar radiation in the infrared, visible, and near-ultraviolet regions of the spectrum. Most of the total energy output of the Sun occurs in this region. The photosphere is also the innermost layer of the Sun that can be inspected with conventional observational techniques. The large energy output, which reaches a maximum in the visible, would permit very detailed observations from the ground if these were not degraded by the effects of "seeing," a distortion of the solar image by the Earth's atmospheric fluctuations. Furthermore, the Earth's atmosphere absorbs most of the radiation in the infrared and near ultraviolet. This limitation of ground-based observations to a narrow-wavelength interval and to the resolution that can be obtained with a good

telescope of only a few inches' aperture has been removed by balloon, rocket, and satellite flight opportunities that have become available in increasing number and improving capabilities during the past 10 years. In particular, flights of balloon-borne telescopes have resulted in observations with higher spatial resolution in the visible, and rocket and satellite observations have extended the wavelength coverage far into the ultraviolet and infrared. Concurrent observational and theoretical studies serve for the development of an accurate model of the solar atmosphere, based on an understanding of the physical processes involved and on the detailed knowledge of the emitted spectrum. Detailed results of the model would be relevant to such important questions as the mechanism of solar energy production (see "Neutrino Observations"), and of the Sun's chemical composition, origin, and interaction with the Earth.

Here we are concerned primarily with the homogeneous portion of the solar atmosphere below the chromospheric temperature minimum, specifically excluding the aspects connected with detailed structure such as the chromospheric network and centers of activity. From an observational standpoint it is limited to the ultraviolet above about 1500 Å, the visible, and the near-infrared regions of the spectrum but excluding again isolated features that originate in centers of activity such as the heliumlike $2\ ^3S$ to $2\ ^3P$ emission lines; e.g., of oxygen VII near 1640 Å. As a classical photospheric effect, the granulation is discussed in this context, although its possible magnetic properties might eventually establish a relation with some forms of solar activity. The related topics of model atmospheres and abundances are elaborated because they received attention again in 1967. The spicules are included as a specifically chromospheric feature.

MODEL ATMOSPHERES

The vast store of solar observations in the visible and, more recently, also in the infrared and ultraviolet regions of the spectrum, including center-to-limb variations and resolution of spectral line profiles, provides the foundation on which a complete solar model will eventually be built. Spectroheliograms reveal that the solar atmosphere is inhomogeneous at many wavelengths (ref. 30) and, in fact, show rather well-defined structure on a scale that seems always to be as small as the best currently available instruments can resolve. It is likely that a successful solar model atmosphere must take account of the fine structure in the various layers. The ensuing complexity and the large number of parameters that would have to be fit to construct such a detailed model are a strong argument for continued solar observations to obtain center-to-limb data in both line profiles and in the continuum for as many wavelengths as possible. However, most current solar models deal with homogeneous atmospheres and account for the small-scale structure

only in terms of average quantities such as macroturbulence and microturbulence, which are determined so as to provide a best fit to the observations.

Even homogeneous model atmospheres are difficult to analyze. A solution of the problem of radiative transfer is required in conjunction with thermodynamic consideration. The most important question in this connection is whether at least local thermodynamic equilibrium (LTE) holds; i.e., are the Saha equation and the Boltzmann factor applicable? In fact, the question is: Up to what height in the chromosphere may these relations be applied (de Jager and Neven, ref. 31). Nevertheless, LTE is postulated for most model atmospheres if for no other reasons than that it must be valid at a sufficient depth in the chromosphere and that this assumption greatly simplifies computations. While the merits of homogeneous LTE model atmospheres are being questioned, the very questioning and challenging have led to fruitful discussions, to new and more precise measurements, and to improved models. Zirin (ref. 30) discusses the merits of model atmospheres, homogeneous and otherwise. While structure and non-LTE effects should certainly be included, a reliable model atmosphere has not emerged as a result of the physical complexity of the problem. Most of the recent non-LTE work, for example, by Athay (ref. 32), Jefferies (ref. 33), and Thomas (ref. 34), has served to lay the groundwork for such a model and to point out just how misleading the assumption of LTE can be in particular situations.

A new homogeneous LTE model atmosphere was worked out by a large group of astronomers at the International Study Week, April 17 to 21, 1967, at Bilderberg near Arnhem, the Netherlands. It resulted in the Bilderberg continuum atmosphere (BCA) model, replacing the previously used Utrecht reference model of the photosphere and lower chromosphere (URP) that was in need of revision (Gingerich and de Jager, ref. 35). The BCA is limited to the solar continuum. Some shortcomings in the explanation of line shapes were recognized from the start and so conflicting line-shape information was excluded. Nevertheless, the BCA provides predictions of the absolute intensity versus wavelength, including limb darkening and predictions of line profiles. Gingerich and de Jager (ref. 35) point out that the agreement with line profiles may reflect the meagerness of the available data more than the quality of the model. They also call for more complete observations in the ultraviolet and infrared continuum in order to determine whether the electron and excitation temperatures in the resonance lines are the same.

The BCA model is illustrated in figure 19 and its prediction of the solar continuum in figure 20. The extent of the various commonly distinguished portions of the atmosphere is defined in terms of the optical depth near 4000 Å photosphere, $t=-1$ or larger; chromosphere, $t=-2$ to -4.

The temperature rise to the corona begins at $t=-4$. The minimum temperature is 4600° K, which may be derived from the color temperature

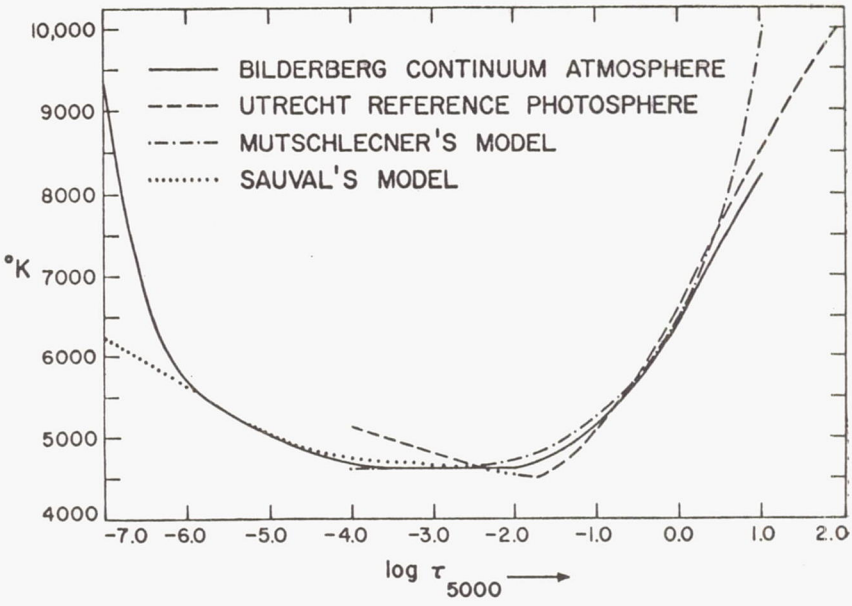


Figure 19.—**The BCA temperature distribution compared to other models examined at the Bilderberg study week.**

at 1600 Å (Gingerich and Rich, ref. 36) and the carbon monoxide spectrum (Rich, ref. 37). Limb darkening in the infrared (Noyes, Beckers, and Lowe, ref. 38) and in the ultraviolet suggests a broad minimum. The model assumes a hydrogen-to-helium ratio of 10. Reliable information on temperature fluctuations, turbulence velocity, convection velocity, and vibrational velocity was found to be lacking, and isotropic velocities of 2 km/sec for macroturbulence and 1 km/sec for microturbulence were assumed. Withbroe (ref. 39) analyzed CH features and deduced microturbulence and macroturbulence velocities for the upper photosphere on the basis of a homogeneous model, finding 1.2 ± 0.2 km/sec microturbulence, isotropically, and 1.0 ± 0.5 and 1.7 ± 0.5 km/sec macroturbulence velocity in radial and tangential directions, respectively. Temperature fluctuations could not be included. Photospheric pictures, with about 0.1 second of arc resolution, might reveal such fluctuations. Currently available pictures fall short by a factor of about 3.

A systematic method for the analysis of high-resolution Fraunhofer lines is presented by de Jager and Neven (ref. 40). It is shown how the model atmosphere parameters—macroturbulence velocity, damping constant, abundance distribution function of convective velocity, source function, and microturbulence velocity—may be obtained from different portions of the profiles of Fraunhofer multiplets. The method is applied to a carbon I multiplet. The proposed method permits, to a large extent, the untangling

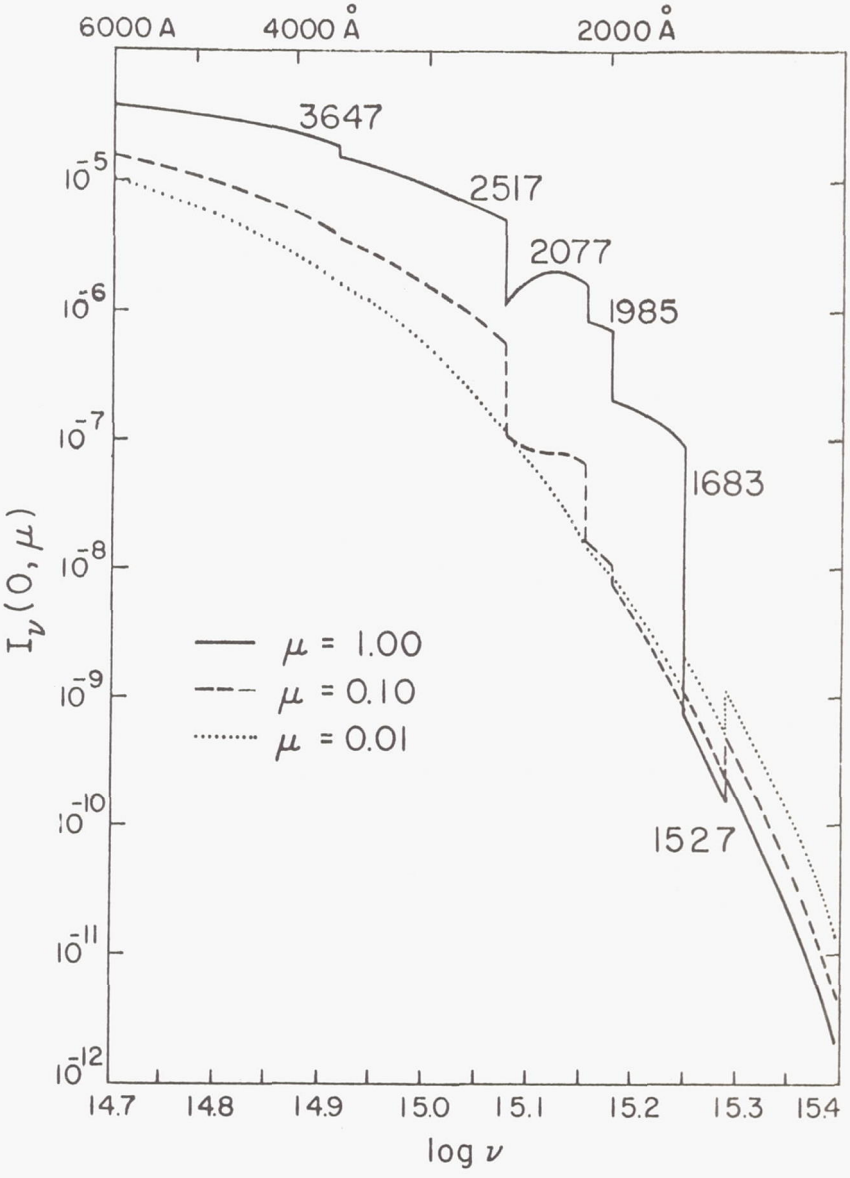


Figure 20.—**Specific intensities in the UV spectrum predicted from the BCA for the center and limb of the solar disk.**

of the influences of these parameters, all of which have an important effect on the profile, but more so on some parts than on others.

A large number of observations relevant to model atmospheres were reported in 1967 and will be discussed in the next section. Model atmo-

spheres were directly challenged or supported in a number of evaluations of previous and new results (Lena, ref. 41). For example, Gingerich and Rich (ref. 36) criticize the URP and demonstrate better agreement of rocket ultraviolet observations (1400 to 2100 Å) with the BCA model, while Elste (ref. 42) proposes a model that further improves the BCA in predictions of limb darkening in the visible and infrared between 4500 and 25 000 Å in the solar spectrum.

The available solar continuum data from 900 Å to 13 microns at the solar disk center were analyzed and compared with the BCA and URP models by Sauval (ref. 43). The agreement with BCA is better, notably in the infrared and ultraviolet; however, there is little difference between the two models (7 percent) in the infrared. Withbroe (ref. 44) compares five different models in an analysis of the center-to-limb variation of C_2, CH, CO, MgH, and other molecules, finding best agreement with an unpublished three-stream model by Elste.

Representative of the non-LTE approach to model atmospheres is the work of Jefferies and White (ref. 45) on the analysis of line profiles when limb-darkening observations are available. LTE is not assumed but is included as a special case, so that an evalution of the effect of the assumption of LTE becomes possible. Curtis and Jefferies (ref. 46) apply this method to an analysis of the sodium D lines in the Sun, giving a great amount of detail on the atmospheric structure with consistency. It is shown that the assumption of LTE in the analysis of the sodium D lines would give the correct abundance within a factor of 2 (see "Solar Abundances" below). A monograph by Jefferies (ref. 33) on the subject is forthcoming. Athay (ref. 47) illustrated the importance of non-LTE effects most dramatically when he indicated that under certain circumstances emerging Lyman-alpha photons originate deeper in the atmosphere than Lyman-beta photons.

The LTE model atmosphere can be used for detailed predictions only if basic atomic information on absorption coefficients is available. For spectral lines, this means that *f*-values and line-broadening parameters must be known with reasonable precision. The requirement for such data becomes even greater in non-LTE models, where ionization, excitation, and recombination rate coefficients are required for the analysis. While significant progress is being made both theoretically and in the laboratory, there is a continuing need for further measurements and computations. For example, little information on van der Waals' broadening and resonance broadening is available, and *f*-values for some important elements such as the rare earths are virtually nonexistent. (For some progress, see "Supporting Laboratory and Theoretical Research.")

While it is clear that the goal of a model atmosphere that can predict the absolute intensity of the solar photospheric and chromospheric spectrum, including center-to-limb variations and line profiles, is far from achieved,

there has been significant progress, both in the understanding of line formation and non-LTE conditions and in the establishment of simple homogeneous, LTE model atmospheres. Further progress in both directions depends heavily on observations with better precision and spatial and spectral resolution, supported by theoretical and laboratory programs for the determination of the basic atomic quantities that must be known if an analysis is to be carried out with confidence.

SOLAR ABUNDANCES

The abundances of the elements in the Sun are important in theories of the origin of the Sun, its chemical composition, its energy-production mechanism, and the possible production of heavier elements by nuclear reactions on the Sun. The abundances may be derived from the photospheric spectrum of the Sun in the visible, using either a model atmosphere or a curve-of-growth technique. Independent determinations use the forbidden coronal lines in the visible and vacuum ultraviolet and soft X-ray spectra. Abundances are customarily given as logarithms (base 10) with a hydrogen abundance of 12 as a reference.

Dupree and Goldberg (ref. 48) determined coronal abundances from the ultraviolet and X-ray emission, including the dielectronic recombination mechanism in their analysis. They found agreement with photospheric GMA abundances (Goldberg, Mueller, and Aller, ref. 9), using a corona model including localized high-temperature regions. There are alternate interpretations of the ultraviolet spectra as evidenced by the exchanges between Pottasch and Athay (refs. 32, 49, 50, and 51). Pottasch's abundances are larger than those of Goldberg, Mueller, and Aller, and agree with determinations from forbidden coronal-line intensities in the visible. It may become necessary to revise upward the effective transition probabilities of some of the forbidden visible coronal lines. (See "Supporting Laboratory and Theoretical Research.") The abundances of lithium and of lead are of particular interest with regard to nuclear reactions in the Sun. Daehler (ref. 52) reports on his search for lithium in the solar spectrum. He observed the solar disk near 6708 Å with a resolving power exceeding 100 000 and with a photometric precision of 0.01 percent of continuum, using the McMath solar telescope at the Kitt Peak National Observatory with a combination of a spectrometer and a Fabry-Perot interferometer but failed to find any lithium lines. Peach (ref. 53) computed an upper limit of log $N_{Li}=0.38$ for the solar lithium abundance on the basis of the hydrogen abundance log $N_H=12.00$. Grevesse (ref. 54) used new measurements with the solar spectrometer on the Jungfraujoch and the BCA model atmosphere to redetermine the abundance of lead in the photosphere. His value is log $N_{Pb}=2.00$, up from the previous 1.63. However, more recently, Ross, Aller, and Mohler (ref. 55) found a value of 1.76 in an analysis of the existing data.

Ross and Aller (ref. 56) also redetermined the solar chromium abundance as 4.73 ± 0.26. The problem of solar helium abundance in relation to the primordial helium abundance was reviewed by Lambert (ref. 57). On the basis of unpublished results, he estimates the solar helium-to-hydrogen abundance ratio as $N_{He}/N_H = 0.063 \pm 0.015$.

A comprehensive series of articles on solar abundances has been written by Lambert and Warner (refs. 10, 58, 59, and 60), in which new values are reported for C, N, O, Na, Al, P, S, K, and the iron group. The new abundances for C, N, and O are somewhat smaller than those derived by Goldberg, Mueller, and Aller; Lambert and Warner's relative values are still (as are Goldberg, Mueller, and Aller's) in agreement with measurements of relative cosmic-ray abundances by Biswas and Fichtel (ref. 61). The major difference between the treatments is in the line damping, which was previously found to affect abundances (Mugglestone and O'Mara, ref. 62). Lambert and Warner investigated the errors introduced by uncertainties in their solar model and in atomic quantities, *f*-values, and line-broadening parameters and found the latter to be generally more important. They included molecular as well as atomic lines in their analyses and found very satisfactory consistency. Differences between abundances derived from weak (forbidden) and strong lines can be traced to shortcomings of the model in allowing for detailed structure, but are not of excessive magnitude. Lambert and Warner called for a more comprehensive investigation that takes account of center-to-limb variations and is based on the wings of the lines as well as equivalent widths. This would provide a source of more consistent abundances and more detailed information about the structure of the atmosphere. Abundances are compared in table IV for the most important elements in the Sun.

Unexpected evidence on abundances has turned up from a different field, the solar neutrino experiments. (See "Neutrino Observations.") A neutrino flux from the Sun has never been positively measured. However, the upper limit is below the flux that results when the Goldberg, Mueller, and Aller abundances for the photosphere are accepted and used in a model of the solar interior for a neutrino flux prediction on the basis of the excepted mechanism for solar energy generation. If, instead, the Lambert-Warner abundances are employed, the computed neutrino flux is barely consistent with its present upper limit. Refinements in the neutrino experiments are, therefore, being anticipated.

Abundance determinations will continue to be of great interest. The controversy surrounding the relatively abundant elements such as iron is still unresolved as far as many workers in this field are concerned. Less abundant but equally or more important elements are even more difficult to determine quantitatively in the Sun. Basic atomic quantities relating to the physical processes that play a role in line formation are lacking for many elements. (See "Supporting Laboratory and Theoretical Research.")

Table IV.—*Comparison of Solar Abundance Results Obtained by Different Investigators*

Atomic no.	Element	Log N_E/N_H		
		Goldberg, Mueller, and Aller (ref. 9)	Lambert and Warner (refs. 10, 58, 59, and 60)	Others
1	H	12.00	12.00	
3	Li	.96	.....	<0.38 (ref. 53)
6	C	8.72	8.55	
7	N	7.98	7.93	
8	O	8.96	8.77	
11	Na	6.30	6.18	
12	Mg	7.40	.....	
13	Al	6.20	6.40	
14	Si	7.50	7.55	
15	P	5.34	5.43	
16	S	7.30	7.21	
19	K	4.70	5.05	
20	Ca	6.15	.....	
21	Sc	2.82	3.04	
22	Ti	4.68	4.50	
23	V	3.70	3.92	
24	Cr	5.36	5.47	4.73 (ref. 56)
25	Mn	4.90	4.88	
26	Fe	6.57	6.51	
27	Co	4.64	3.53	
28	Ni	5.91	5.08	
82	Pb	1.33	.....	2.0 (ref. 54) 1.76 (ref. 55)

Uncertainties in the model atmospheres also affect abundance determinations from the photospheric and chromospheric absorption spectrum. The discovery of the dielectronic recombination mechanism illustrates how excitation, ionization, and recombination rates may be significantly altered by the discovery of competing physical processes as well as by better theoretical or experimental results. The current controversy surrounding coronal abundances deduced from ultraviolet and "forbidden" visible emission lines for the corona may well be resolved in a similar way.

OBSERVATIONS

More ground-based, balloon, rocket, and satellite observations of the Sun were made and reported in 1967 than perhaps in any preceding year. One

of the most important developments is the successful flight of a combined spectrometer and spectroheliograph by Harvard College Observatory on board OSO–IV. The time interval between observation of the Sun and data inspection at Harvard has been as short as 20 minutes. This has permitted some firsthand studies to be made with a minimum of delay. Watts (ref. 63) has reported initial results obtained during the first weeks of OSO–IV operation. Typical spectroheliograms are shown with an H-alpha spectroheliogram in figure 9. They were made from points in a 40 x 48 raster pattern that was obtained in 4½ minutes with a resolution of 1 minute of arc. The spectroheliograms shown are in the oxygen VI line at 1032 Å, the hydrogen-Lyman continuum at 897 Å, the Mg X line at 625 Å, and, in figure 10, in the Si XII line at 499 Å. These lines are formed in regions with temperatures of 0.32, 1.4, and 2.3 million degrees Kelvin, respectively. Active regions can be recognized, and limb brightening is indicated. The excellent results, even in the shorter wavelength regions, are made possible by a 4-square-centimeter grating, ruled in gold with 18 000 lines per centimeter, blazed for 800 Å. The detection system can count photons with the aid of a magnetic electron multiplier in windowless operation. As a spectrometer, the Harvard instrument scans the solar spectrum in one-half hour in steps of 0.1 Å from 300 to 1400 Å. While the Harvard results may prove to be most useful in the study of active regions, the spectroheliograms in the long wavelength end of the working range can contribute to tests of model atmospheres.

Lemaire and Blamont (ref. 64) used a balloon-borne stigmatic spectrograph stabilized by a biaxial pointing system for precision observations of the Mg II doublet at 2795.5 and 2802.7 Å. The best profile measurement had a resolution of 0.02 Å. Limb darkening over the profile was observed with a spatial resolution of 1 minute of arc. Bonnet, Blamont, and Gildwarg (ref. 65) obtained limb darkening information for the 1800- to 2800-Å range with a resolution of 20 seconds of arc, using a Veronique rocket. The scan over the entire Sun came within 1 minute of arc of the disk center. Particular attention was given to the discontinuity at 2076 Å, the ionization limit of aluminum I, which was found to have an intensity ratio of 5 to 6 across the discontinuity. The lack of continuum intensities in the range 1525 to 1700 Å, from which the solar temperature minimum can be deduced, led Sandlin and Widing (ref. 66) to make rocket observations in the range 1510 to 1750 Å on July 27, 1967. The results are excellent, but only a preliminary evaluation has been made. In another rocket observation relating to the solar temperature minimum, Porter, Tilford, and Widing (ref. 67) observed 14 CO bands in the ultraviolet spectrum of the Sun. They concluded that the ultraviolet spectrum may be classed as photospheric above 1525 Å and chromospheric below this wavelength.

In a typical ground-based observation, Appenzeller and Schroeter (ref. 68) measured photoelectrically the center-to-limb variation of faint iron lines and other Fraunhofer lines and continuum bands across the polar and equatorial diameters of the solar disk. The temperatures of polar and equatorial limbs were found to differ by less than 6° K. They reported a large limb effect for H-beta, larger than 6 km/sec, which they do not attempt to explain pending a better knowledge of velocity fields. Zirker (ref. 69) concludes from the Sacramento Peak 12-inch coelostat and 13-meter spectrograph profiles of the H and K lines of Ca II that the optical depth of formation of the H_2 and K_2 wings must be very shallow. The width of the line is large and increases toward the limb. In the region of formation of the lines, the opacity of the chromosphere is very small.

Burton, Ridgeley, and Wilson (ref. 70) flew a stabilized Skylark rocket with a normal incidence spectograph for an observation of the solar spectrum between 950 and 2950 Å above the limb by about 10 seconds of arc. They listed the wavelengths and estimated intensities of about 300 emission lines in this range, with identification for about 75 percent of them, and the spectrum is compared with disk spectra previously obtained. They were able to make a number of new identifications, particularly of intercombination lines in the corona. The list of wavelengths includes emission lines near 1623, 1638, and 1640 Å where Elton (ref. 71) reported the laboratory observation of the important heliumlike 2 ^{3}S to 2 ^{3}P resonance lines of the triplet system. However, this identification cannot be made positively, since strong He II and Fe II lines are present. Measurements further off the limb might show these heliumlike lines, as well as perhaps the heretofore unobserved Ne IX isoelectronic lines, and might provide an opportunity to map the corona in these strong emission lines with time, space, and wavelength resolution not readily available at much shorter wavelengths at which most of the radiation of these ions normally occurs.

A number of other observations that relate to the solar photosphere and chromosphere are discussed elsewhere in this paper in the context of the aspects of solar physics for the benefit of which they were performed and are not repeated here.

A reanalysis of previously published data can often give useful new results. For example, Lambert and Swings (ref. 72) report the first observation in either the laboratory or space of the forbidden transition at 8727.13 Å in the 2 ^{2}S to 2 ^{2}P configuration of carbon I. The line was found in the solar spectrum. Houtgast (ref. 73) reported that crowding of Fraunhofer lines can be shown to reduce significantly the Balmer jump in the solar spectrum reported by Labs (ref. 74) by a reanalysis of his data.

This situation is likely to recur more frequently in the future, as some space experiments provide more data than can be quickly analyzed. On the other hand, the scarcity or nonexistence of information on some vitally

important regions of the spectrum continues to hamper the development of improved model atmospheres.

Velocity fields in the solar atmosphere were studied in detail by Howard (ref. 75). In particular, he studied various types of oscillations. The 300-second vertical oscillations in the chromospheric supergranulation were confirmed in nearly 250 hours' observing time. The size of the elements is typically 5 to 10 seconds of arc. Some phase changes were observed, but no correlation with observed magnetic fields was detected. At the disk center the period of oscillation is 200 to 400 seconds, while it is only about 100 seconds at the limb—possibly to be interpreted as a height effect. The amplitudes fall off toward the limb. Roddier (ref. 76) observed the oscillations in the Sr 4607-Å and Ca 4227-Å lines. He suggests the possible interpretation as an oscillation between two metastable states, one convective with a shifted asymmetrical line profile, the other quiet with an unshifted, symmetrical profile. He notes that the calcium line is formed higher in the photosphere as compared with the strontium line and reports that the oscillations look entirely different in the two lines but that they have the same period.

Howard (ref. 75) also reported short-period oscillations (SPO) in bursts of 1 or 2 minutes' duration with 0.05 to 0.1 km/sec amplitudes, and suggested that these may be responsible, in part, for the microturbulence that must be assumed in model atmospheres to account for line broadening. The physical size of the cells having SPO's is less than that of the cells having the 300-second oscillations, and the SPO's cannot be interpreted as resulting from the high-energy end of the 300-second oscillation distribution function. Howard discusses and eliminates the possible nonsolar origin of the SPO's.

GRANULATION

Exciting results on photospheric granulation were reported in 1967. R. J. Roesch of Pic du Midi showed motion picture films of the development of individual granules, showing that subsequent, virtually identical granules appear at the same position and with the same shape going through the same developmental stages. Similar results on supergranulation were reported by Janssens, Rogers, and Vrabec (ref. 77), who obtained movie coverage of the Sun over a continuous period of 62 hours at Thule. Evans (ref. 78) tried to find whether simultaneous one-dimensional scans at separate wavelengths showed the same bright-dark granular structure. Simultaneous measurements at 3954 Å and at 5888 Å show a high correlation, in contradiction with the results of Vassiljeva (ref. 79). Evans suggests that Vassiljeva's results may be in error as a result of the effects of differential atmospheric refraction.

The dark intergranular spaces may be more stable and long lived than had been suspected. The attainment of sufficiently high resolution for

granulation studies is very difficult. There are indications that better resolution will lead to the discovery of further structure. It is interesting in this context to note magnetographic observations of the solar disk. Bumba (ref. 80) reports on magnetic field measurements carried out with the Kitt Peak McMath telescope. These measurements show magnetic fields of the order of 1200 gauss in small sunspots that had not been previously resolved because of poor seeing, and that could now be seen with high resolution in the stable 80-centimeter solar image at Kitt Peak's McMath telescope. Broadening of the Fe I 6312.5-Å line suggests large but unresolved magnetic fields in the intergranular space. Similarly, Sheeley (ref. 81) also reports on findings with the solar image at Kitt Peak, including the presence of small scale, of the order of 500 kilometers, magnetic fields of several hundred gauss well removed from sunspots, weakened Fraunhofer lines, and darkened continuum combined with enhanced Ca II K emission, probably occurring at pores and dark lanes between granulation. This confirms results obtained earlier by Sheeley (ref. 82) with Leighton's method.

Zwaan (ref. 83) suggests that the small regions with large magnetic fields between granules correspond to the "invisible" sunspots predicted by Hale and Nicholson (ref. 84). Similar small-scale fields up to 1500 gauss were also reported by Beckers and Schroeter (ref. 85).

SPICULES

Still enigmatic is the source of the chromospheric spicules and the role they play in the energy balance of the chromosphere and corona. Kuperus and Athay (ref. 86), in a qualitative discussion, suggested that spicules have their origin in the response of the chromosphere to energy input from both above and below.

The steep temperature gradient across the chromosphere-corona interface gives rise to a conductive flux of energy backward into the chromosphere of about 3×10^5 ergs cm^{-2} sec^{-1}, a value comparable with the radiative energy flux from the upper chromosphere. Because mechanical energy is also deposited in the upper chromosphere, it appears necessary to invoke an additional mechanism for energy loss from those layers that will permit their existence at the observed relatively low temperature. It is suggested that the loss mechanism is one in which energy is expended by accelerating matter, thus the spicules. At the base of the transition region the chromosphere is forced into a dynamic configuration, resulting in an outflow of kinetic energy that roughly equals the inward conductive flux.

CORONA

Although not yet completely solved in detail, the classical problem of the structure and maintenance of the solar corona viewed as a spherically symmetric envelope is well enough in hand that significant progress can be made in understanding physical processes in the corona and in discussing its struc-

tural inhomogeneities. Chief among the problems is the extension of the corona into interplanetary space, the relative abundances of chemical elements, the density and temperature inhomogeneities associated with active centers, and the details of energy balance near the chromospheric-coronal interface. Major contributions to the clarification and solution of these problems are being made through rocket- and satellite-based observations. Ground-based radio and optical observations, however, continue to provide a significant bulk of the information on coronal structure. Much of the detailed ground-based information is obtained during solar eclipses.

Eclipses

Although there exist ground-based instruments capable of observing the solar corona outside of eclipses, and although it is now possible to observe the corona against the disk in the far ultraviolet, solar eclipses still offer the opportunity to gather information on the physical state of the corona that can be obtained in no other way. Coronagraphs are not sufficiently large to suppress diffraction around occulting disks. During 1967 the results of eclipse observations made in February 1961, May 1965, May 1966, and November 1966 were reported.

During the total solar eclipse of February 15, 1961, broad passband photographs of the solar corona were taken by observers from the Observatoire du Pic du Midi. Kawaguchi (ref. 87) analyzed one photographic plate that showed a dome formation or coronal arch over a group of small prominences. Around the prominences the corona was darker—presumably deficient in electron density (see "Prominences")—while at greater heights in the dome a brightening of the corona was interpreted as caused by a higher-than-average electron density; the electrons were trapped within the magnetic-field lines overarching the small prominences.

On May 30, 1965, Eddy and Malville (ref. 88) observed the polarization of the infrared Fe XIII 10 747-Å coronal line. It should exhibit complete resonance polarization when entirely radiatively excited, with the plane of the electric vector along the radial direction. Collisional excitation, line-of-sight integration, and presence of a coronal magnetic field will decrease the observed degree of polarization. Eddy and Malville found that the degree of polarization was below that predicted for a zero-magnetic field corona at all heights $1.2 \leqq p \leqq 1.72$, suggesting the presence of nonradial fields at those levels, where p is the distance from the disk center in terms of the solar radius. These results were confirmed by Eddy, Firor, and Lee (ref. 89) during the November 12, 1966, eclipse. From the observed line-to-continuum intensity ratios, Eddy and Malville deduced from their 1965 data an iron abundance $\log N_{Fe} = 7.9$ on a scale $\log N_H = 12.0$, in agreement with the higher coronal values then being found. (See "Photosphere and Chromosphere.")

In recent years it has been possible to extend eclipse-observing times by flying in jet aircraft at high altitudes along the eclipse path. Conway, Morris, and Andrews (ref. 90) obtained spectra in the wavelength region 3000 to 6750 Å on such a flight on November 12, 1966. The Ca II H- and K-lines were seen 1 solar radius from the limb. This observation is reminiscent of that made by Deutsch and Righini (ref. 91) during the total solar eclipse of July 20, 1963, in which an emission line at the position of the Ca II K-line was seen extending from the limb to a height of about 1 solar radius. Both observations are unexplained. During the November 12, 1966, eclipse and from a different aircraft, Münch, Neugebauer, and McCammon (ref. 92) sought to detect the presence of predicted coronal lines due to Si X and Mg VIII. The lines were observed with signal-to-noise ratios, respectively, of 50/1 and 3/1, and the wavelengths were found to be:

$$\text{Si X: } \lambda_{obs} = 1.4305 \pm 0.0004\ \mu; \quad \text{Mg VIII: } \lambda_{obs} = 3.0275 \pm 0.0020\ \mu$$

The abundances of silicon and of magnesium implied by the observed intensities of these lines is in agreement with photospheric abundances as derived by Goldberg, Mueller, and Aller rather than with some coronal abundances. (See "Photosphere and Chromosphere.")

Radio Radiation

Radiofrequency radiation from the corona is generated through a variety of processes. In general, the frequency of the radiation is directly related to the coronal level at which it arises. Often the source of radiation is highly localized, and analysis of eclipse data yields important information on the relation of source positions to positions of other features on the Sun.

Radio observations were made from the ground at 4.28 centimeters by Kaufmann, Matsuura, and Marques dos Santos (ref. 93) during the November 12, 1966, eclipse. Radiation at this wavelength arises in the solar chromosphere. However, the time difference between the second and third optical and radio contacts indicated that there is a significant 4.28-centimeter emission at a height of 85 000 kilometers above the photosphere. During totality the residual radio flux density, which came from heights about 16 000 kilometers, was 12.2 percent of the uneclipsed Sun.

During the partial phases of the May 20, 1966, eclipse, the Moon's limb as seen from the Ondrejov Observatory occulted a type I noise-storm source. In their analysis of data obtained at 260 MHz, Letfus, Tlamicha, and Valuicek (ref. 94) demonstrated that the meter-wave source was located at a position close to a plage visible near the solar east limb.

An excellent review article, "Theory of Solar Bursts," was prepared by Takakura (ref. 95) with an extensive bibliography. Takakura pointed out that some parts of the theories are not firmly established and that improvements in both observational material and in theoretical background are highly desirable.

One such improvement during 1967 was the theoretical investigation of the Razin effect (defined below) and its detection in the solar corona. Ramaty and Lingenfelter (ref. 96), considering the low-frequency cutoff ν in the spectral distribution of power in type IV events, suggested that under ambient coronal conditions of electron density N_e and magnetic field H the criterion $\nu << 20N_e/H$ for neglect of the influence of the medium might not be satisfied, and that it is necessary to incorporate into the theory the influence of the departure from unity of the plasma index of refraction. When this is done, the theory predicts a significant decrease of synchrotron emission at low frequencies. They computed radiofrequency spectra for monoenergetic electrons and for an exponential rigidity spectrum, taking into account deviations of the refractive index from unity (fig. 21). Since Razin (ref. 97) appears to have been the first to suggest this effect, Ramaty and Lingenfelter called it the Razin effect.

Warwick (ref. 98) pointed out that there is a strong morphological similarity between meter-wave bursts of type III and of type V. He proposed that the latter arises through the same physical mechanism as that which produces type III and in the same coronal volume. The apparent difference in frequency versus time structure between the two is caused by prior heating of the emitting volume by particles which give rise to the parent

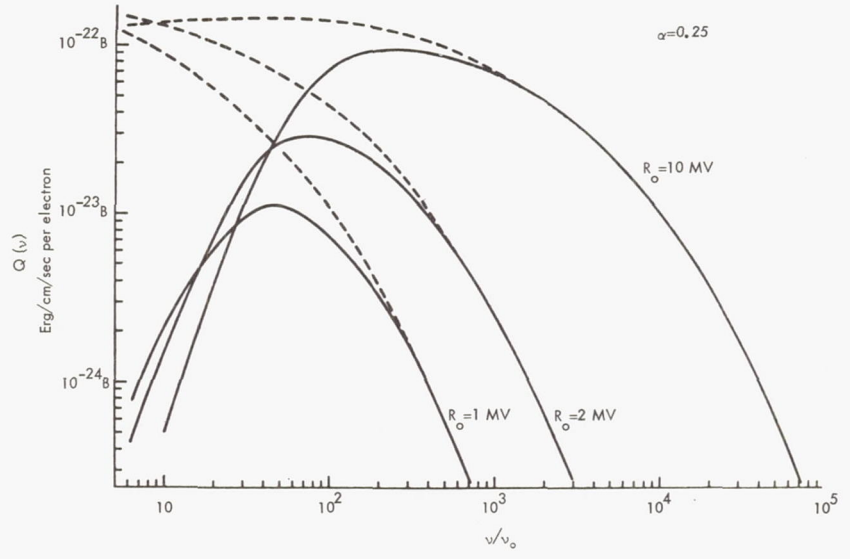


***Figure 21.*—Razin effect: synchrotron-emission spectra of electrons having an exponential rigidity distribution in vacuum (dashed lines) and in a medium with $\alpha = 0.25$ (solid curves) (ref. 96). R_0 = rigidity of spectrum in megavolts; B = magnetic field in gauss.**

type III event. Warwick calculated that particle-particle collisions between the exciter stream and material in a coronal streamer lead to a sufficient heating, lasting long enough to provide the observed type V duration.

Bursts of short duration, approximately 1 second, and narrow bandwidth, less than 200 kHz, have been observed near 38 MHz by Yoh and James (ref. 99). The bursts are associated with solar-noise storms and at least some of them are circularly polarized, indicating a strong magnetic field at the source. Because of their structure, they are not type III events, although about 1 percent show frequency drift rates between .1 and .5 MHz sec^{-1}, intermediate between types II and III.

Ultraviolet Data

The solar ultraviolet spectrum contains a wealth of information concerning the structure of the solar corona. Present problems, beyond achieving the observations, are the identification of lines, a description and classification of their association with centers of activity and/or the quiescent corona, and measurement of absolute spectral intensities. Much work has already been accomplished, and the data are being used in enlarging our understanding of coronal physics.

The solar UV line intensities have been used by several investigators in determining the relative abundance of chemical elements in the solar corona. This work, based on Pottasch's interpretation of UV spectra or variations of it, has been discussed in "Photosphere and Chromosphere." Athay (ref. 100) introduced a formulation that permits the determination of the temperature distribution in the chromosphere-corona transition region from the UV line data. Using that formulation and newer calculations, Dupree and Goldberg (ref. 101) have also found that the transition from chromospheric to coronal temperatures occurs in a very narrow region of the order of 10^3 kilometers thickness. They inferred a maximum temperature for the homogeneous corona of 1.2×10^6 °K.

Models of the solar corona above an active region containing a spot of Zürich type E and above an old, quiescent plage were constructed by Neupert (ref. 102) using EUV spectra from OSO–I and ground-based decimetric radio flux-density measurements. The time history of EUV and radio emission from active centers was reviewed. Emission from the highest stage of ionization observed, Fe XVI, increases rapidly at the onset of the active plage life along with a rapid increase in radio emission. These are most intense at the time of greatest activity; the highest coronal temperatures and electron densities associated with the active center occur then. As activity declines, lines of Fe XV and Fe XIV become more prominent while decimetric radio emission decreases, indicating a reduced temperature and density in the coronal condensation. For the regions observed by Neupert, the period of maximum activity was about 2 weeks long, while the interval of reduced activity was 2 months or longer.

Electron temperatures were deduced from the EUV spectra using ionization-equilibrium calculations including dielectronic recombination. Electron densities were obtained using the electron temperature and the radio data. Table V reproduces the model parameters. Finally, the models were used to predict the flux in the Fe XV and Fe XVI lines at 284 and 335 Å (fig. 22), respectively, achieving good agreement with the observations.

Solar Wind and Coronal Rotation

The realization that the corona must be in dynamic equilibrium has led to significant reorientation in our understanding of the content of interplanetary space and to a greater knowledge of the dominating role played by the corona in the physics of the interplanetary plasma. In an excellent review article, Parker (ref. 104) reviewed developments that led to the prediction of the solar wind and discussed in detail the hydrodynamics of the problem. More recently, attention has been focused upon the rotation of the corona.

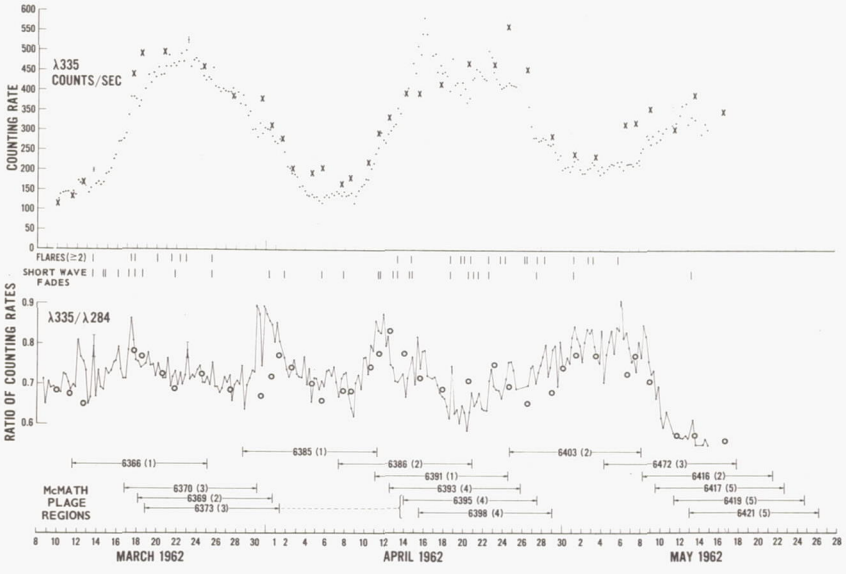


Figure 22.—Comparison of observed Fe XVI, 335 Å, and Fe XV, 284 A, emission with predicted values (large symbols) based on Neupert's (ref. 102) models. The ratio (lower half) is much more sensitive to temperature than to density of electrons. Sharp increases in this ratio (Mar. 13, 1962) often coincide with those solar flares which show "gradual rise and fall" at microwave frequencies.

333-240 O—69——32

Table V.—*Properties of Coronal Models*

	Active region	Quiescent region	Undisturbed corona
Active sunspot group	E38	None	None
Diameter of active region	150 000 km	250 000 km	
T_e, EUV data (Burgess and Seaton, ref. 103)	$3.8–4.0\times10^6$ °K	$2.5–2.9\times10^6$ °K	$1.0–2.0\times10^6$ °K
T_b, 2000 MHz radio data	1.9×10^6 °K	1.8×10^5 °K	4.4×10^4 °K
Mean electron density	11.2–12.2 n_q	2.8–3.4 n_q	n_q: 0.66 of Newkirk's at n_e sunspot maximum

A major difficulty in the theory of the solar wind has been the specification of that level in the solar corona at which energy input effectively ceases. Usually in the theory the corona is treated as a polytropic gas to avoid the need to specify its energy source in detail (Weber and Davis, ref. 105). The solar radar observations by James (ref. 106) have been taken by Brandt (ref. 107) to indicate that energy deposition into the corona by shock waves effectively ceases at around $R=1.6\ R_\odot$.

Brandt (ref. 108) has tried to deduce the solar-wind velocity from a study of the orientation of type I ionic comet tails. The assembled information indicates a mean plasma velocity of 500 ± 50 km sec^{-1} with an azimuthal component of about 10 km sec^{-1} at 1 AU. A lower limit to the plasma velocity of 150 ± 50 km sec^{-1} seems to exist.

The effect of the coronal and interplanetary magnetic field on solar-wind flow was not included in early models, which treated only the hydrodynamics of the problem. More recent models have included the effects of magnetic stresses in the plasma, which are expected to have a significant effect on the coronal rotation. The most complete treatment during 1967 was given by Weber and Davis (ref. 105).

Starting with Maxwell's equations, the conservation of mass, the balance of azimuthal momentum and azimuthal magnetic force, and the radial momentum equation, Weber and Davis derived the radial gradient of the radial component of flow, du/dr, in the plane of the solar equator. Fluid viscosity is ignored. The equation has a family of solutions with three critical points at $r_c<r_a\leq r_z$. At r_c the critical fluid velocity equals the speed of a slow-mode, magnetoacoustic wave; this point is analogous to Parker's (ref. 104) critical point. At r_z the critical fluid velocity is the speed of a fast-mode wave. At r_a the radial Alfvenic Mach number $M_a=u/B_r\sqrt{4\pi\rho}$ is unity. The consistent solution must pass through all three critical points (fig. 23). A polytropic equation of state was adopted and numerical calculations were carried out based on observed conditions at 1 AU. The resulting velocity field and pressure resemble Parker's models very closely. No rigid corotation can exist in the model.

A spiral magnetic-field pattern was predicted by this model (ref. 105) in which the field lines at 1 AU lag by 62° behind their points of connection on the Sun. The azimuthal velocity of the plasma at first increases very rapidly from 2 km sec^{-1} to a maximum of 4 km sec^{-1} and then declines monotonically (fig. 24). The magnetic torque in the wind flow exceeds by a large factor the angular momentum convected away by the wind (fig. 25). In this model the time scale for braking of the solar rotation is $\sim7\times10^9$ years.

A spiral interplanetary magnetic-field pattern was deduced from IMP–I observations by Wilcox and Ness (ref. 109). During three rotations of the Sun between November 27, 1963, and February 15, 1964, a persistent sector structure in the interplanetary field was discerned. An autocorrelation

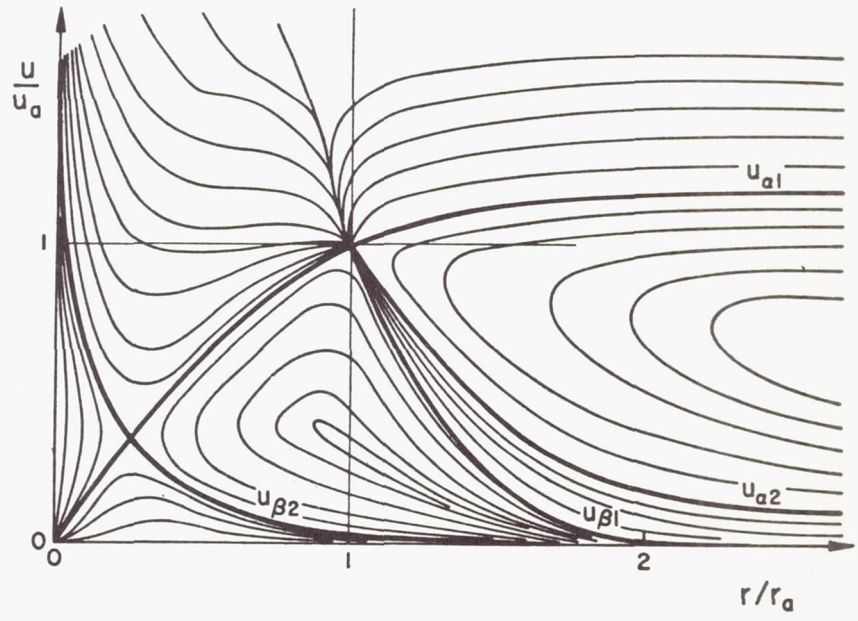


Figure 23.—Flow velocity u divided by the Alfvén speed u_a as a function of the distance r from the solar surface, divided by r_a (ref. 105).

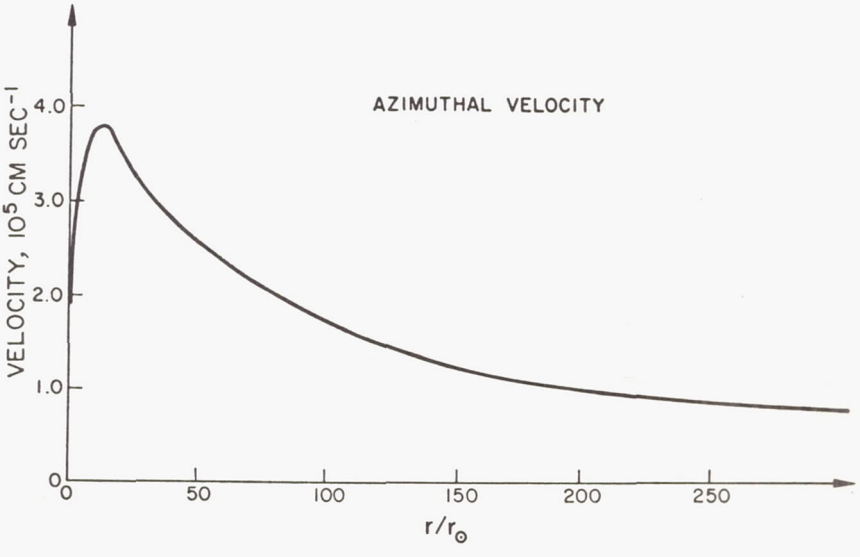


Figure 24.—Azimuthal velocity of the solar wind as a function of distance above the surface (ref. 105).

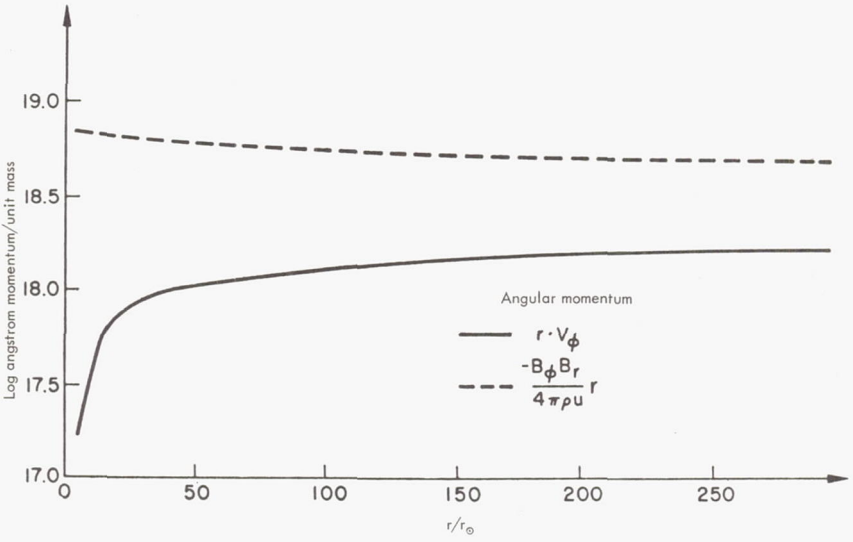


Figure 25.—**Angular momentum and magnetic torque as functions of distance above the solar surface (ref. 105).**

analysis of the data strongly indicated that the field structure corotates with the Sun: it has a period of rotation of about 27 days. Autocorrelation analyses of solar photospheric magnetic fields observed at the Mount Wilson Observatory were compared with the IMP–I data. The comparison suggested the interplanetary field was most strongly related to photospheric fields near 15° North latitude. Since the spacecraft was located above a considerably lower heliographic latitude, Wilcox and Ness suggested the data demonstrate a meridional component in the solar-wind flow.

Theoretical results similar to those of Weber and Davis were obtained by Modisette (ref. 110). Both reach the essential conclusion that the rotating corona is equivalent, in terms of angular momentum transfer, to an envelope which rotates rigidly out to a level where the wind velocity and Alfvén speed are equal; beyond that level the flow preserves constant angular momentum. Modisette calculated that 80 percent of the braking effect on solar rotation is in the torque exerted by the magnetic-field lines: the braking time scale is again 7×10^9 years.

Brandt (ref. 111) has argued that the data from comet tails (ref. 109) should not be overlooked. If the flow has a 10 km sec^{-1} azimuthal component at 1 AU, then the angular momentum convected away from the Sun is about equivalent to the magnetic torque, and the rotational braking time is halved. While the Weber-Davis theory (ref. 105) predicts an azimuthal flow somewhat lower than this, the precise value is determined by conditions

near the Sun. Brandt (ref. 112) showed that if instead one uses the measured values (at 1 AU) of interplanetary field strength and direction, solar-wind speed and density, and extrapolates these backward toward the Sun, the resulting predicted azimuthal flow speed is consistent with comet-tail results and compatible with the Weber-Davis theory. The distance from the Sun of the point r_a may be somewhat larger ($20 < r_a < 40\ R_\odot$) than that derived by Weber and Davis ($r_a = 24.3\ R_\odot$).

Ferraro and Bhatia (ref. 113) consider corotation and solar wind in the corona and in the interplanetary medium, and conclude that corotation can exist only if there is no solar wind, but that approximate corotation occurs where the solar-wind velocity is much less than the Alfvén speed. There is no corotation in the opposite limit. They also recover Parker's result (ref. 114).

There does not appear to be a significant inconsistency between theory and observation.

THE SOLAR CYCLE

The cyclic nature of solar activity has been recognized for more than a century, first from the variation in sunspot numbers. It has become increasingly obvious that the change in solar activity has a profound influence on certain phenomena on Earth such as the frequency of large cyclones. This is surprising in view of the small variations in the total solar energy output as a result of the activity. Some clues may be derived from the observation that the large cyclones occur most frequently in a circular band around the magnetic rather than the geographic north (and presumably also south) pole. Evidence of the solar cycle can also be found in tree rings and in sediment layers in rivers. These effects, along with the marked influence on the probability of occurrence of solar flares, provide ample grounds for continued interest in this periodicity.

Our knowledge of the solar cycle is at present largely empirical, and the causes for the cycle remain the subject of much speculation. Attempts have been made to correlate the tidal effects of planetary motions with the solar cycle, and even with the occurrence of flare events, which these forces may serve as one of perhaps many possible trigger mechanisms. The physical mechanisms which might explain the reported correlations remain doubtful (Blizard, refs. 115 and 116; Head, ref. 117; Jose, ref. 118; Trellis, ref. 119; and Wood and Wood, ref. 120). It can be further presumed that, should a definite cause-effect relationship between solar activity and planetary motions be established (Bigg, ref. 121), an observation of activity on other stars might give a clue on the presence of planets near them.

The observation of similar cycles on other stars would certainly be interesting. Sheeley (ref. 122) suggests the use of the Ca II K_2 emission because he found from an observation of the average profile that the relative in-

tensity varies by about 40 percent between solar minimum and maximum. Similarly, Bumba and Ruzickova-Topolova (ref. 123) presented preliminary results on the variability of the K_2 emission with solar rotation (disappearance of active regions behind the limb) which indicate a definite relation between the integrated Ca II K_2 emission and presence of plages on the visible hemisphere. Weeks (ref. 124) reviewed rocket measurements and satellite measurements of the solar Lyman-alpha emission between 1955 and 1966 and found a correlation with the solar minimum and maximum, providing perhaps an alternate method for detecting activity in other stars. Weeks' results are illustrated in figure 26.

The maxima and minima in the solar cycle are not particularly well defined, and they depend, to some extent, on the indicator that is used. Thus, Gnevyshev (ref. 125) reviews the case for two maxima in the solar cycle, which actually implies a shallow minimum at the peak of the ordinary sunspot number cycle. The evidence includes the emission in the 5303-Å coronal line, the frequency of large area sunspots, the occurrence of proton flares, and the number of large cyclones on Earth. On the other hand, Forbush (ref. 126) asserts that the cosmic-ray diurnal anisotropy varies with a period of two solar cycles (1937 to 1961).

The question of whether or not the general solar magnetic field reverses at the maximum of each solar cycle is still being debated. Godoli and Mazzuconi (ref. 127) present their study of bright surges on the limb (BSL's) as further evidence in favor of reversal. Polar BSL's are more frequent near the minimum of the solar cycle when the magnetic field is largest, the polar faculae are more frequent, and the polar coronal rays are visible.

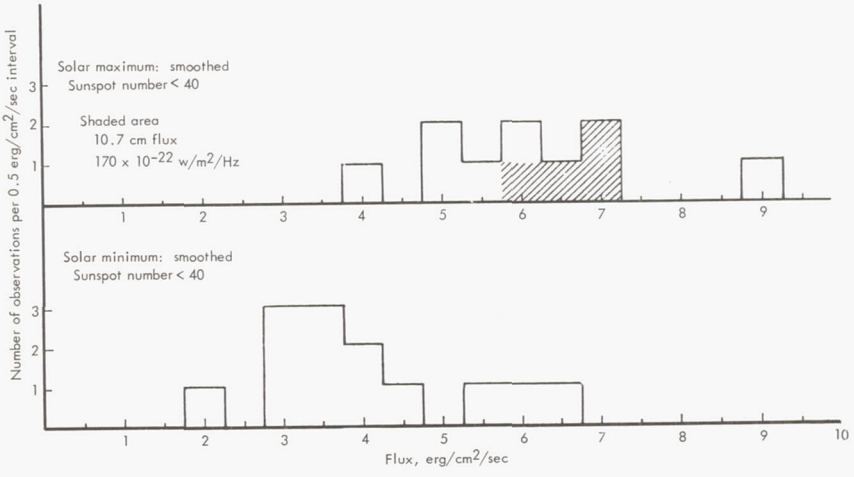


Figure 26.—**Solar Lyman-alpha flux from rocket measurements with ion chambers (ref. 124).**

SUNSPOTS

Studies of sunspots currently devote the greatest share of attention to theoretical investigations of spot structure. It may be conceded that much of the observational material for erection and testing of hypotheses is already available, although improvement of the observational data is still desirable. Spot models are becoming considerably sophisticated. Some of the difficulties being encountered, however, are the understanding of which physical processes to include and what boundary conditions should be applied.

Yun (ref. 128) sought to improve the magnetohydrostatic model of Deinzer (ref. 129) by revising the surface boundary condition; in other respects the procedures and assumptions were similar. Deinzer had neglected the horizontal pressure difference between spot and photosphere at the surface; Yun has taken this difference into account. The resulting models are in better accord with observations in regard to predicted magnetic-field strength and the variation of area and surface brightness with field strength.

In Yun's model, magnetic stresses arising from field-line curvature are taken into account. A model proposed by Chitre and Shaviv (ref. 130) does not contain this feature. Their model is developed from the hypothesis that the magnetic field interferes with convection; within the spot the convective flux is $C_s = \beta C_{ph}$, where C_{ph} is the photospheric convection flux and β is a monotonic function involving magnetic energy and internal energy. Furthermore, the convection, radiative, and magnetic flux all decrease with altitude as the magnetic field diverges. Elste (private communication) has pointed out that the model that he computed does not predict the observed visible light intensity ratio of umbra to photosphere.

While a great store of information on spot spectra, relative intensities, areas, and temperatures is available in the literature, continued attempts are made to improve our knowledge of the distribution and configuration of magnetic fields in and near sunspots. As Yun (ref. 128) has pointed out, this information is of critical interest to spot theories.

A photographic technique was employed by Rayrole (ref. 131) to determine the complete field parameters H, ψ, and Φ of magnetic fields in sunspots. He applied the technique to investigation of the relation of magnetic field to the Evershed flow field in a large spot.

With the exception of Treanor's method (ref. 132), Adam (ref. 133) presents methods employed in the measurement of magnetic-field direction on the Sun that depend, in part, on the relative intensities in magnetically split Fraunhofer lines. It is generally accepted that the π-components have anomalous intensities. Hence, it is of considerable interest to investigate the problem of possible peculiarities in the profiles of magnetically split lines.

For a single spot, Adam (ref. 134) obtained the field distribution by using Treanor's method for deducing field direction. For this same spot, absorption-line profiles were also obtained. The magnetic-field data were used to predict, by means of Stepanov's theory, absorption-line profiles for comparison with the spectrum profiles (Bray and Loughhead, ref. 135). When scattered light and instrumental polarization were taken into account, there was no discrepancy between theory and observation.

An improvement in the theory of formation of absorption lines in a magnetic field has been accomplished by Kjeldseth Moe (ref. 136). He found a new method for solving the transfer equations for polarized light that permits the derivation of the Stokes parameters without any special assumptions regarding the model atmosphere. The method, while allowing use of any model atmosphere, is restricted to the case of a homogeneous field.

Small sunspots are best observed with the largest images of the Sun. For this work, the McMath telescope at Kitt Peak National Observatory is ideally suited. Small sunspots with diameters of 1 to 7 arc-seconds seen with that telescope appear to have fields in excess of 1000 gauss, in contrast to earlier results, according to Bumba (ref. 80). (See "Photosphere and Chromosphere.") He believes that the broadening of the 6302.508-Å line in dark intergranular lanes is caused by concentration of magnetic fields there. The Evershed effect, so pronounced in the larger sunspots, is absent in small young spots (Bumba, ref. 137). There is, rather, a motion of material inward, at least at the photosphere level.

New observational material concerning the Evershed effect has led to a reevaluation of the interpretation of the line shifts. Maltby and Erickson (ref. 138) suggested that longitudinal compression waves, rather than material motion, must be invoked. Because it is difficult to understand how material flow can be maintained in presence of a magnetic field, they consider that the "Evershed flow" may be a wave phenomenon.

Spectrum lines formed in a field of pressure oscillations such as sound waves were previously studied by Erickson and Maltby (ref. 139). These lines are displaced and asymmetric, qualitatively like lines seen in the Evershed effect. Maltby and Erickson conclude that possibly the observations would be satisfied if sound waves of sufficient amplitude propagate parallel to the solar surface, in the direction of umbra to photosphere. Possibly the light and dark penumbral filaments are sound waves of different intensity. These horizontal waves could be excited by vertically directed Alfvén waves flowing through the spot umbra and may contribute importantly to the spot's heat balance. However, Musman (ref. 140) considered the importance of Alfvén waves in sunspots and concluded that they cannot be a significant mechanism for energy transport within spots.

The electrical conductivity of sunspots may have been previously overestimated, with serious consequences for their theoretical understanding. Some years ago, Schroeter (ref. 141) calculated that the electrical conduc-

tivity in spots may be as low at 10^{-2} mho per meter, a factor of 10 000 below the previously acceptable value. Altschuler (ref. 142) undertook a series of calculations to determine the effect of such low electrical conductivity on the magnetic structure of spots. He found that gradients of the conductivity then play an important role in the diffusion of the field.

PROMINENCES

Solar prominences take extremely varied forms which, however, are probably constrained by magnetic fields arching upward from the photosphere. They may be placed into two broad categories of quiescent and active prominences. These categories generally separate the prominences as to the dominant electron temperature regime: quiescent prominences are dominated by radiative and collisional processes occurring at an electron temperature of about 10 000° K, while in active prominences it is about 30 000° K. Recognition of the essential role that magnetic fields play in the formation and maintenance of prominences of all types has led to currently fruitful work in which prominences are seldom discussed separately from the magnetic field structures with which they are associated.

Quiescent Prominences

Our present understanding of quiescent solar prominences is based on their observed association with photospheric magnetic fields (Rust, ref. 143), their spectra (Zirin, ref. 144), and their observed morphology and life history (de Jager, ref. 145). The mechanisms for formation and maintenance of quiescent prominences have been worked out qualitatively and quantitatively and, to some extent, are confirmed by observations. Currently, efforts are being directed toward obtaining further observational information, toward evaluating models in terms of new data, and toward incorporation of promising theoretical results into the models. It does not appear that there are fundamental difficulties in the general concepts which invoke a pressure equilibrium between coronal material and prominence material, and which suppose that the latter is supported by magnetic-field lines that pass between regions of opposite magnetic polarity.

Kuperus and Tandberg-Hanssen (ref. 146) suggested that prominence material initially condenses in the neutral plane between vertically directed fields of opposite sign. There, the coronal gas cannot be in thermal equilibrium. The material is compressed by the external field, becomes a more effective radiator, and cools. They calculate cooling times on the order of 1 day, depending on the ratio of magnetic pressure to gas pressure; as this ratio increases, the cooling time is shortened. The resulting prominence configuration is unstable against the "tearing" mode instability (Furth, Killeen, and Rosenbluth, ref. 147) in which the magnetic field exhibits a tendency to form closed loops: lines of force that are initially distinct link

up during the perturbation. The growth rate of this instability is sufficiently small so that the fluid flow remains subsonic. Kuperus and Tandberg-Hanssen cite Sturrock as being the first to suggest the importance of the "tearing" mode instability in prominence structures. By equating growth time to cooling time, they showed that the fine filamentary structures thus formed in the prominence should have diameters near 300 kilometers (fig. 27). The filamentary features are of fundamental importance to maintenance of the prominence. These help to limit conductive heating by the corona by excluding free electrons from access to the cooler prominence material.

The model requires that there is a coronal streamer with every prominence and that there is a dark space surrounding the streamer and prominence. Both of these requirements are fulfilled by the structures shown in the eclipse picture obtained by Dunn and Newkirk during the 1966 solar eclipse. (See fig. 28.) The dramatic picture which shows streamers extending far out into the corona was made possible by the use of a neutral density filter in which the density decreases gradually with the radius.

Rust (ref. 143) reported magnetographic observations of quiescent prominence fields with the High Altitude Observatory's Climax Observatory coronagraph. In polar crown prominences and in newly formed prominences bordering old active centers, he found fields typically of 5 gauss, while the fields in sunspot-zone prominences were typically 8 gauss and ranged upward to 60 gauss. Field polarities were in agreement with what could be deduced from studies of the longitudinal component of the photospheric field, but the field direction through the prominence is neither parallel to nor perpendicular to the prominence axis—rather, it is directed somewhere between these extremes.

A vertical gradient of the horizontal field component was found in most of the prominences studied by Rust; it is about $\delta H/\delta r \sim 10^{-4}$ gauss per kilometer in the sense that the horizontal component increases with height (fig. 29). There was no indication that the solar magnetic fields above the photosphere are "wrapped up" by the effects of differential rotation. Thus, reconnections of field lines must be frequent.

In general, Rust's observations tend to confirm the model of Kippenhahn and Schlüter (ref. 148). A feature of this model is that the maximum stable height of quiescent prominences is related to the separation of magnetic poles in which the supporting fields originate. Thompson and Billings (ref. 149) used observational data to test the prediction and found that prominences, in fact, tend to obey the predicted relationship quantitatively.

Prominence Activity

Physical processes which produce moving and active prominences are little understood. Here, attempts still center, to a great extent, on providing observational material and on organizing it in a meaningful way. Active

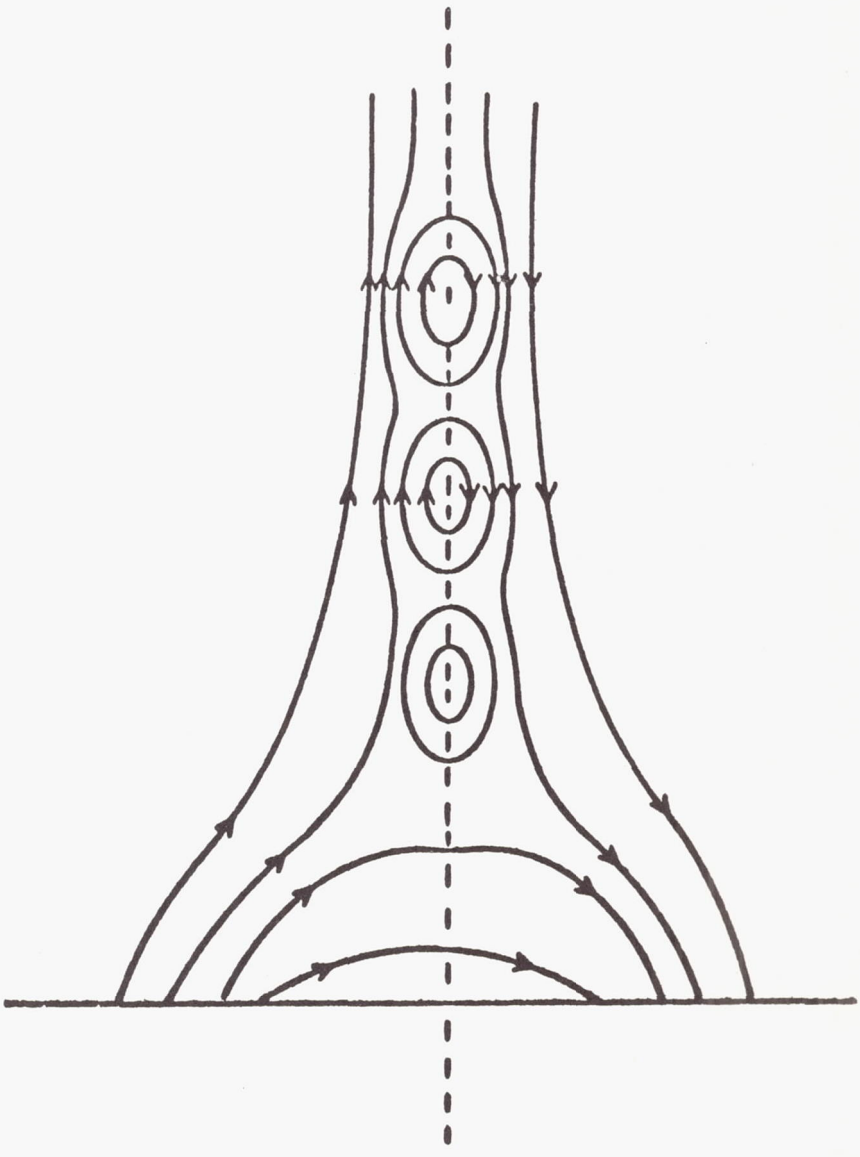


Figure 27.—Schematic representation of the field configuration during the formation of a quiescent prominence (ref. 146).

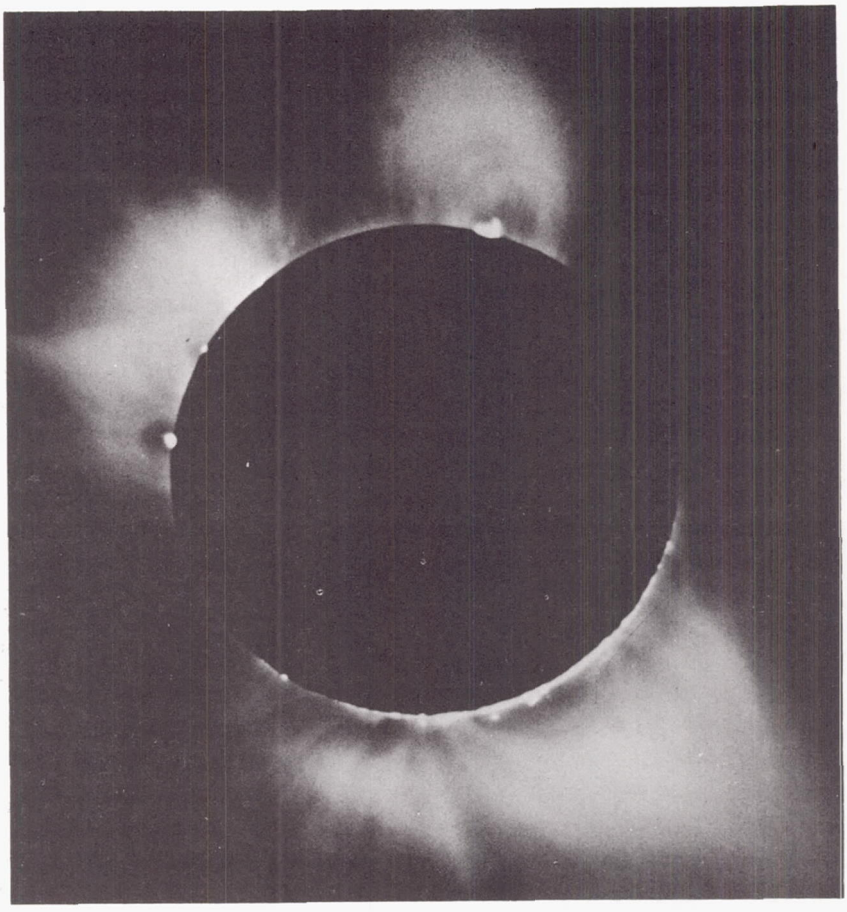


Figure 28.—**The solar corona during the 1966 eclipse.**

prominences occur in great variety. They are short lived and may be broadly classed into two types. One originates through the condensation of material in or injected into the corona such as loops and "coronal rain." The second type arises from acceleration of cool dense material by some process causing flare puffs and surges.

Bruzek (ref. 150) has collected and described photographic material on relatively short, very dark H-alpha filaments seen in young spot groups. These filaments appear to be organized into systems in the interspot region of young, developing bipolar groups and extend generally between the innermost spots of opposite polarity. The systems of filaments are arch shaped and dynamic and exhibit both a mass flow, with velocity at least of the order of 50 kilometers per second along the arches, and an expansion. The ex-

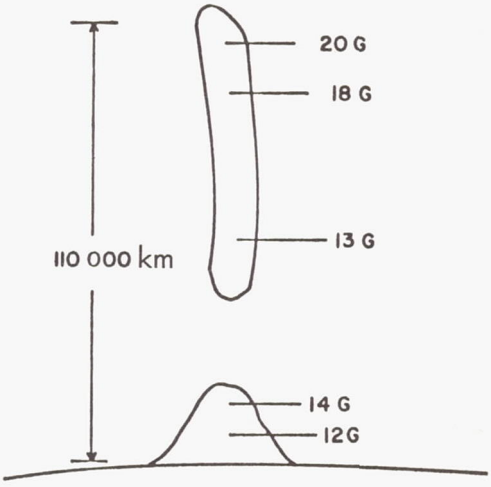


Figure 29.—**Magnetic field in a large, quiescent spike prominence of October 6 to 10, 1965, according to magnetographic measurements by Rust (ref. 143). Notice that the field strength increases with height above the limb. The prominence appeared as a small circular filament on the disk.**

pansion is not detectable at low levels and has a velocity of at least about 5 km/sec at high levels. The mass flow along the arches is in the same direction for all filaments within a given spot group. Normally developing bipolar groups show conspicuous arch-filament systems of this kind for about 3 days only; the general configuration of the system remains unchanged for several hours while individual filaments last only for about a half hour.

Arch-filament systems are probably associated with the emergence of bipolar magnetic flux loops from the photosphere that rise upward into the corona during the evolution of a bipolar spot group. The systems are perhaps closely related to fibrils and to threads; they also have a number of characteristics in common with loop prominence systems.

The sequence of events leading from a solar flare to a loop prominence has been described at length by Bruzek (ref. 151) and a model for the event proposed by Jefferies and Orrall in a series of papers (refs. 152 to 154). It is believed that the loops, found generally correlated with cosmic-ray flares, are the manifestation of the temporary storage of fast particles in the corona (ref. 152). Olson and Lykoudis (ref. 155) have offered an alternate model in which the loop prominences are the result of a process of compression that

gives rise to the flare. Their model would apply at low heights in the corona with a transition to the Jefferies-Orrall model at greater heights.

In the Olson-Lykoudis model, it is assumed that opposite magnetic poles on the photosphere are somehow transported toward one another. These poles are the bases of flux tubes to which coronal material is frozen. The flux tubes are shortened by this motion and the plasma contained in them is compressed. Through an equation developed from the first law of thermodynamics, Olson and Lykoudis computed cooling curves for the gas, assuming compression times of 500 and 1000 seconds. This model demonstrates that the higher loops should take longer to cool to temperatures at which H-alpha is able to radiate. This accounts for the observation that a loop system grows upward by the successive appearance of higher and higher loops. No quantitative description of matter flux in the loops is attempted, although it is estimated that up to loop heights of the order of 30 000 kilometers, sufficient material to maintain the prominence is available in the coronal condensation itself. Loops which appear above this level would probably have to be formed by the fast particle injection model of Jefferies and Orrall.

It is therefore possible that more than one mechanism may be involved in the production of systems of loop-type prominences. The appearance of loop structures, however, is almost certainly associated in some way with acceleration and storage of energetic particles.

FLARES

Solar flares, the most energetic of transient solar phenomena, continue to be of primary observational and theoretical interest. In addition to their visible and radiofrequency radiations detectable at the Earth, many flares exercise a considerable influence on the terrestrial and interplanetary environments through the copious emission of high-energy electromagnetic radiations and high-energy particles. The former radiations produce an excess ionization in the Earth's ionosphere that may severely disrupt short-wave radio communication. The high-energy particles pose a radiation hazard to biological organisms that are not protected by the atmosphere such as astronauts and passengers in high-altitude supersonic transports. Flares of large area on the Sun are often followed by geomagnetic storms, which are the result of the acceleration of an ionized plasma that reaches the Earth within 2 to 4 days after the flare. Magnetic compasses are strongly affected during the more severe storms and radio communications may be strongly influenced. Displays of the aurorae borealis may be observed.

Although many of these effects are, to some extent, statistically predictable, individual flare events are not. Therefore, current efforts are being directed, as they have been for many years, toward understanding the

physical processes that go on in flares and toward attempting to find suitable ways to predict the occurrence of energetic flares and the phenomena that often accompany them. These efforts range from the worldwide cooperation of flare observers who provide detailed information on individual events for statistical evaluation to theoretical and laboratory work that bears on possible mechanisms of flare production.

In this section, reports of optical, radio, and particle observations are discussed together with new theoretical investigations. X-ray observations are summarized in "Observations."

Descriptive and Statistical Data

Reports of solar flares from the worldwide flare-patrol network are received, collated, and published in the United States by the Environmental Science Services Administration. These reports are made by individual observing stations in a fashion that is intended to provide a homogeneous body of data. Sawyer (ref. 156) has, however, detected systematic errors in the reported values of flare importance and area as judged at the individual stations. The errors arise from a number of causes and manifest themselves in various ways. A statistical analysis of flare reports by computers has been directed toward making empirical corrections that may be applied to flare reports from each observatory. This applies also to assembled flare reports. Systematic errors that are present in the data can thus be smoothed out. When applied to the body of flare reports, these corrections give a flare rate that is uniform throughout the day (fig. 30) and that is uniform in central meridian distance (fig. 31). The usefulness of corrected flare areas in assessing flare importance has also been investigated by Sawyer (ref. 157), especially for flares close to the limb. Statistically, it appears that the apparent area of a flare depends only on its distance from the center of the disk and not on the flare importance itself. A daily flare index (Sawyer, ref. 158) may thus be defined in terms of the mean standardized flare areas given in the NBS flare lists without reference to other quantities.

To develop a view of flare activity on the Sun during successive solar cycles, Křivský and Knoška (ref. 159) have prepared time-latitude diagrams of distribution of flares for cycles 18 and 19. Figures 32 and 33 illustrate that well-separated maxima occur in the distribution of flares, which suggest a correlation of flare occurrence with time in the solar cycle.

Individual events have been discussed at length by many authors. One of the great flares of the last solar cycle occurred at the west limb on July 20, 1961. Spectroscopic observations of the event were reviewed by Zirin and Acton (ref. 160), who cited references to the voluminous literature on the flare and its accompanying effects, which included the observation of cosmic rays at ground level.

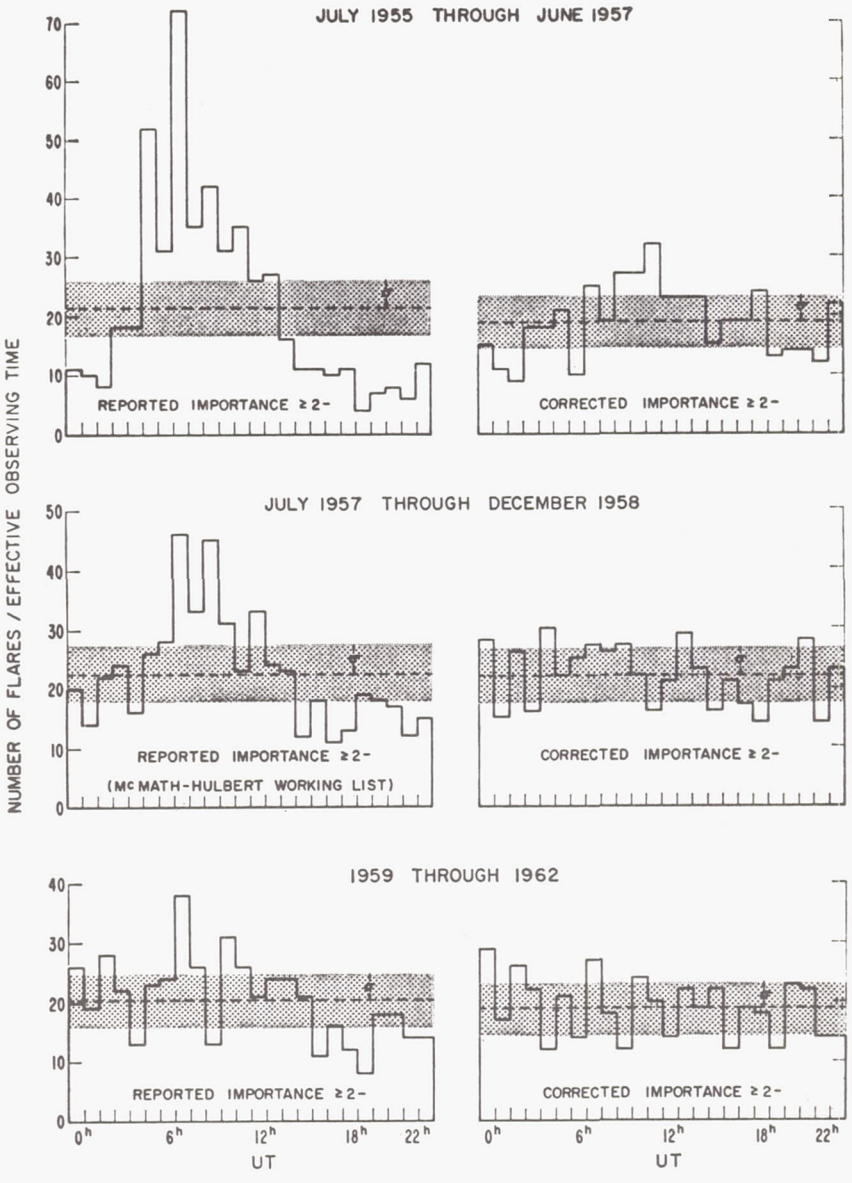


Figure 30.—Occurrence-frequency distribution of flares of importance 2 or higher beginning in each hour of universal time according to mean reported importance (left) and according to mean corrected importance (right) (ref. 156). A correction has been applied to allow for less than complete patrol coverage. The shaded band indicates the standard deviation.

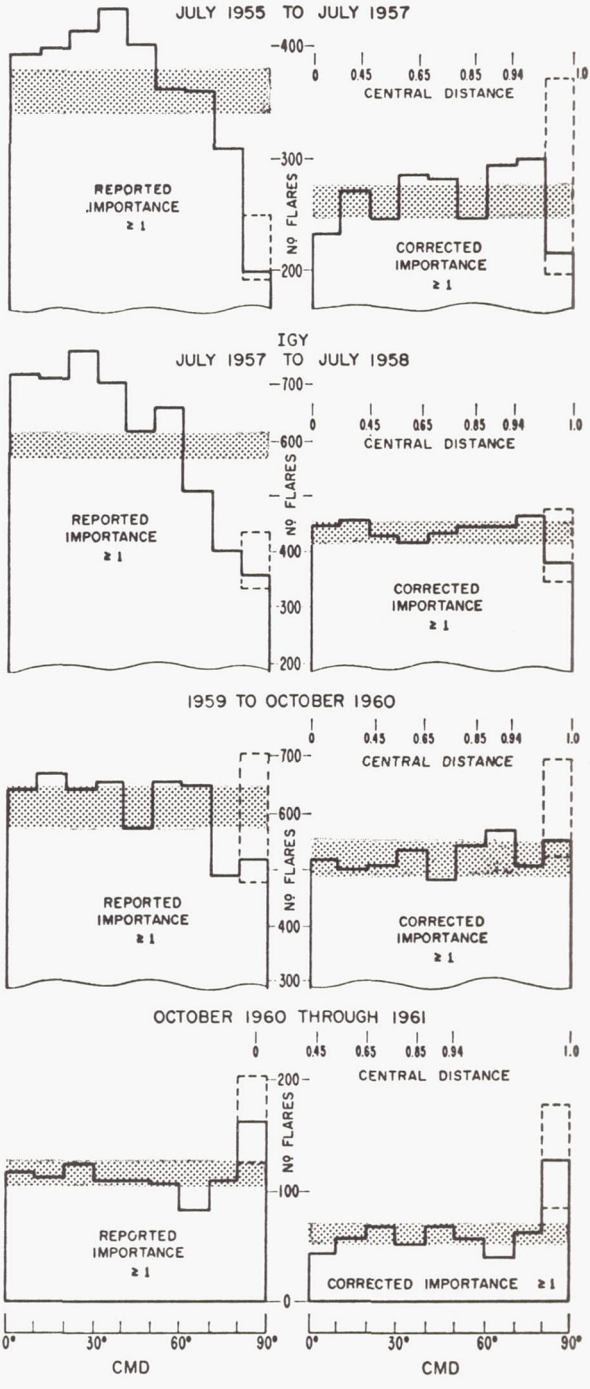


Figure 31.—Number of flares of importance 1 or higher in each interval of central meridian distance in each of four periods (ref. 156).

333-240 O—69——33

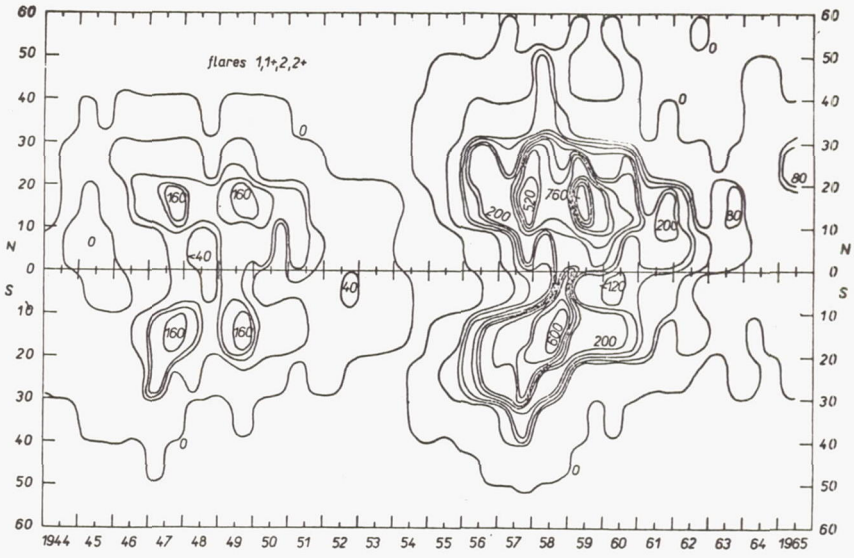


Figure 32.—Time-latitude distribution of the number of 1 to 2+ importance flares. The isolines are drawn at each 40 up to 200 and at each 80 above 200 (ref. 159).

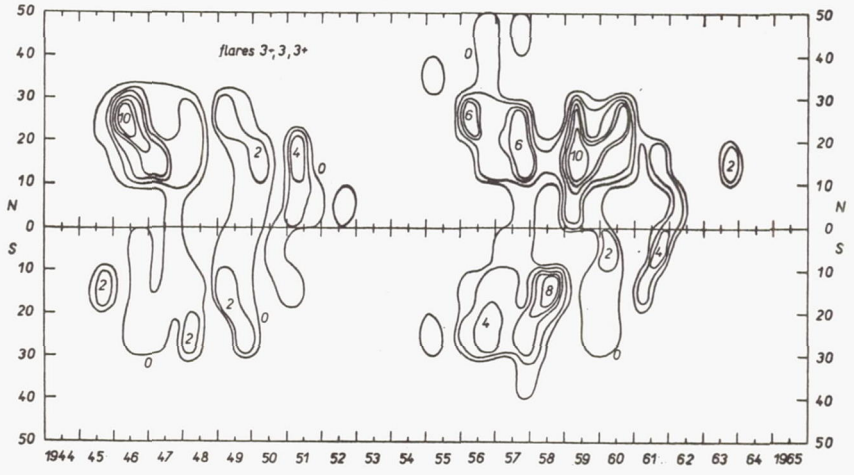


Figure 33.—Time-latitude distribution of flares of importance 3−, 3, and 3+. The isolines are drawn by values of 2 (ref. 159).

An importance 2 flare on September 20, 1966, is described by Tandberg-Hanssen (ref. 161), who studied filtroheliograms, spectra, and magnetographic data connected with the event. The major parts of the flare were intimately associated with active filaments found in the region. Its brightest segment occurred over a sunspot umbra. Ohman, Stiber, and Kussofsky (ref. 162) discussed a flare spray observed at Capri on July 11, 1966. It was probably related to a flare behind the limb. Coronagraphic observations made at 5300 Å in the continuum indicated the presence of polarized radiation that was produced by Thomson scattering in the flare spray.

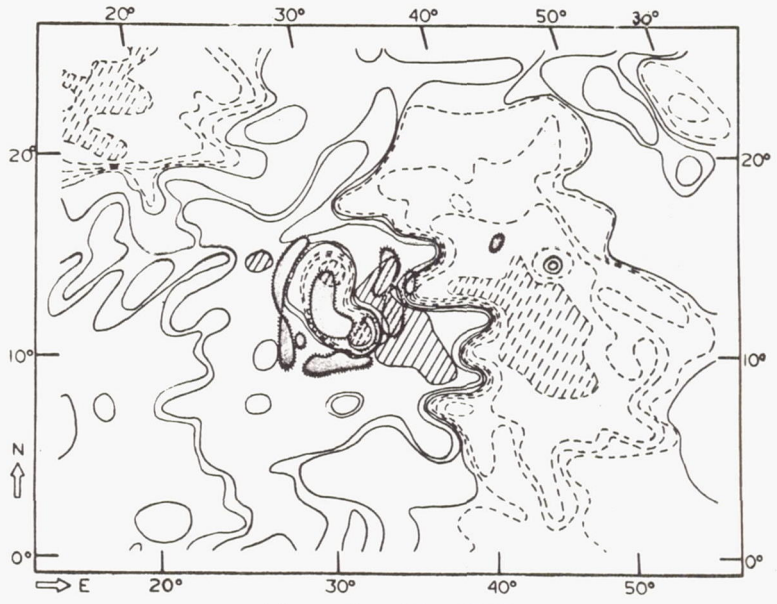
A very unusual series of observations is presented by Gurtovenko (ref. 163). While making a spectrum tracing of the Fraunhofer sodium D_2 line, he observed a flarelike brightening that was confined to the vicinity of the center of the line. There was no evidence of an H-alpha flare at the same place on the disk. However, a plage appeared at that place one rotation later, and on the next rotation an actively flaring region was observed at the original site of the sodium flare.

A new cinematographic technique for flare observations, which is being used by Janssens and Rogers (ref. 164), is a further evolution of the familiar wavelength-scanning technique already in use at many observatories. In making their observations, they rapidly scanned the H-alpha line by tuning the Lyot filter. The resulting movies contain a wealth of detail on flare brightness and on Doppler motions of material.

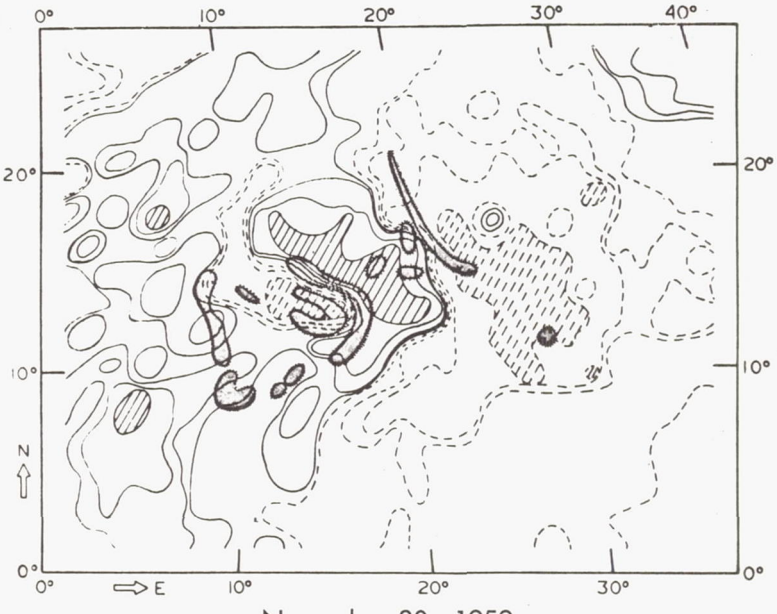
The Harvard College Observatory spectroheliograph on OSO–IV (see "OSO Program" and "Photosphere and Chromosphere") has provided a unique flare observation in the light of the oxygen VI resonance line at 1032 Å. Figure 11 shows a series of contour spectroheliograms obtained in time intervals of 5 minutes during a class 2b optical flare that occurred near the west limb on November 29, 1967. The complex structure of the event indicates that spatial resolution is essential for an understanding of flare events.

Association With Magnetic Fields

The configuration of magnetic fields with which flares are associated is important for understanding the flare-production mechanism. Thus, much emphasis has been attached to the determination of the field structure. In general, flares occur near neutral lines which separate regions of different magnetic polarities in active regions. Smith and Ramsey (ref. 165) have studied the problem of flare location with respect to magnetic-field configuration. Photographic flare observations were superimposed on isogauss maps from the Mount Wilson scanning magnetograph. Figure 34 is representative of Smith and Ramsey's results. They found a strong tendency for the major flares they studied to occur adjacent to, but not exactly at, the neutral line in the magnetic field. Each flare was divided into several seg-



November 28, 1959



November 30, 1959

ments on either side of the neutral line. The segment contours appeared to be conditioned by the shape of the neutral line. The flare patches usually occupied regions of steep gradient in the longitudinal magnetic-field component. Material was seen to move both along and perpendicular to the field gradient, but moving material never crossed a neutral line.

McKenna (ref. 166) prepared a detailed description of activity in the region which produced the July 10, 1959, proton event. She reviewed phenomena in the active region between its east limb appearance on July 7 and the proton flare 3 days later. On the basis of the deduced association of prominence material and flares with the chromospheric network, she proposes that the active region was enclosed by an "onion dome" of magnetic loops that extended to great heights. Prominence material and fast particles could be stored in these loops.

Zirin and Werner (ref. 167) discussed cinematograms of the active region of September 1963 in connection with radio, magnetic, and optical data. Their description reveals that much of the activity that occurred in this region between September 13 to 26 was interrelated in a complex way. Waves of activity moving within the region produced filament agitation, brightening, surges, and displacement of material. Thus, much of the activity was triggered by events elsewhere in the region. A significant number of flares were produced, many of them homologous. The flare of September 18, for which a detailed magnetic map had been prepared, occurred very close to the steepest field gradients. Its most energetic portion lay near the neutral line. De Jager (ref. 168) reported on an X-ray burst associated with the same flare.

Fokker (ref. 169) has extended the concept of homology from optical flares to flare-associated radio events. It implies a detailed similarity in burst phenomena: the bursts extend over about the same frequency range or ranges and produce, at each frequency, responses of the same magnitude and duration. Homologous radiofrequency phenomena typically occur within less than 48 hours of one another. This probably indicates that there has been no appreciable change in the magnetic-field structure during this time. It might constitute an upper limit to the time scale for variation of the magnetic configuration in a flare-producing center.

Figure 34.—**Flare drawing superimposed on isogauss map of the longitudinal component of photospheric magnetic fields (ref. 165). Most of the flare segments lie adjacent to the neutral lines where the field changes from positive polarity (solid lines) to negative polarity (dashed lines). From outer to inner, the contour lines represent magnetic fields of approximately 2, 6, 15, and 45 gauss. (Top) November 28 and (bottom) November 30, 1959.**

It is possible that the emergence of a bipolar magnetic flux loop in the vicinity of a preexisting old active center on the photosphere creates an unstable magnetic configuration. This might be a potential source of flares. The suggestion was investigated by Banos (ref. 170) with reference to an importance 2 flare on October 4, 1965.

The magnetic-field structure that is associated with very high energy flares is of special interest. It is now generally believed that such flares are accompanied by type IV radiation from relativistic electrons. All active regions that produced type IV radiation in association with flares during the interval 1956 to 1963 were classified by Antalová (ref. 171) according to the sunspot group's Zürick type. The regions with large, complex spots and also with spots of types H and E are most likely to produce flares with type IV radiation. This radio emission preferentially accompanies flares produced in active regions with two or more spot groups as reported by Kleczek and Olmr (ref. 172). The magnetic field of the entire active region seems to contribute to the production of the synchrotron emission.

Warwick (ref. 173) has presented evidence that proton flares have a tendency to take place at favored intervals of Carrington longitude on the Sun. Wilcox and Schatten (ref. 174) have analyzed the data in a recurrence-period calculation. They cast doubt on Warwick's hypothesis and suggest that there is no significant evidence for a long-term clustering of proton-producing regions on the Sun.

Deductive Investigations

In two lengthy papers, Hyder (refs. 175, 176) has revived and discussed evidence for the hypothesis that flares have their origin in the disparition brusque phenomenon. Sudden changes in the magnetic field that supports prominences in active regions lead to destabilization and ascent of the prominence. Then, under the force of gravity, the prominence material descends along the field lines into the chromosphere. The dissipation of its kinetic energy produces compression, heating, and a flarelike brightening on impact (fig. 35). The model predicts ribbonlike chromospheric brightening placed symmetrically on either end of the disappearing filament. Sufficient potential energy is available in the prominence material to supply all or a significant part of the flare energy even if the process is not efficient. If this model is correct, material should be observed falling into flare-bright regions at speeds of 50 to 200 kilometers per second. Hyder (ref. 176) examined the observational evidence and found support for the model. Several flare events, notably the cosmic-ray flare of August 28, 1966, are discussed in this connection. In general, however, observations for detailed verification of the model have not been made.

The electron density in flares is related to the mass density in the emitting region. It must be known for a determination of the number of

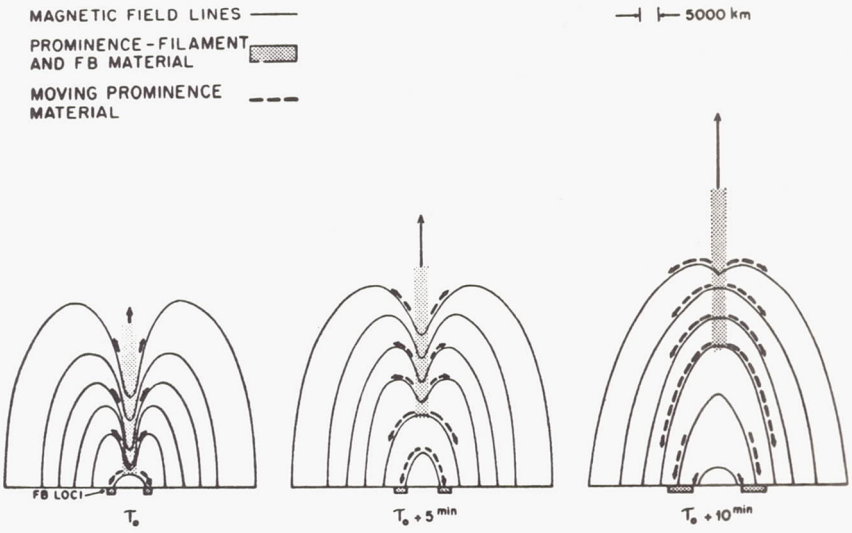


***Figure 35.*—Schematic prominence field-line changes and gas flows expected during the eruption of a Kippenhahn-Schlueter prominence in a disparition brusque (refs. 175 and 176).**

electrons that are available for acceleration in the flare and provides information on the amount of compression that has taken place. Svestka at Ondrejov Observatory has developed a technique for estimating electron densities in flares by measurement of the half-widths $\Delta\lambda_H$ of higher members of the hydrogen Balmer series. Švestka and Fritzová-Švestková (refs. 177, 178) discussed the measurement of Balmer-line widths and examined the effects which influence the inferred electron densities N_e. They felt that errors do not exceed several tens of percent, although they considered the theory relating N_e to $\Delta\lambda_H$ as approximate. However, recent work by Greig, Lim, Moo-Young, Palumbo, and Griem (ref. 179) and by Kepple and Griem (ref. 180) suggests that the line-broadening theory is significantly more accurate than Švestka and Fritzová-Švestková assumed. An application of their method (ref. 178) to a number of flares indicates that the electron density is somewhat correlated with flare importance. The greatest flares have N_e in excess of 3×10^{13} electrons per cubic centimeter. At any given time N_e appears not to vary significantly within the flare. In a flare of July 12, 1961, N_e reaches a maximum at peak H-alpha intensity.

Particle Data, Energetic Events

Generally, flares with the greatest areas and densities are most successful in accelerating high-energy particles. It was recently discovered that some solar events are followed by the appearance of high-energy electrons in

interplanetary space. Lin and Anderson (ref. 181) reviewed the observations and concluded that there are two distinct classes of solar flare electron events: those for which the electrons arrive at the Earth within an hour after the optical flare, and those for which they are delayed by about a day. The prompt electron events with electron energies in excess of 40 keV are usually accompanied by protons with energies of more than 500 keV. A comparison showed that the behavior of the two-particle events is strikingly different and can be traced to differences in their origin and/or propagation in the solar atmosphere. The electrons are probably not released from the same region in which protons are accelerated. On at least one occasion (March 16, 1964), the electrons apparently were ejected from the Sun before the protons. Delayed electrons are usually followed a few hours later by low-energy protons. The delayed electrons appear about 20 to 40 hours after flares of importance ≥ 2 and within a few minutes of a sudden commencement in the ionosphere. Lin and Anderson provide a table of solar electron events that were observed between March 1964 and September 1966.

Observations of individual solar cosmic ray events were reported by Kahler, Primbsch, and Anderson (ref. 182); Bostrom, Kohl, and Williams (ref. 183); Baird, Bell, Duggal, and Pomerantz (ref. 184); and Goedeke, Masley, and Adams (ref. 185).

Protons in the energy range 10 to 100 MeV were released by the March 24, 1966, flare and observed by Kahler, Primbsch, and Anderson (ref. 182) on OGO–I. This flare also gave rise to prompt electrons that were observed by Lin and Anderson (ref. 181). Kahler and his colleagues concluded that the proton scattering by the interplanetary field was small, and that the ordinary diffusion theory cannot account for the temporal variation of the observed flux. Some variations might possibly be explained as due to reflection from a shock front which passed the Earth on March 23.

On January 28, 1967, Baird, Bell, Duggal, and Pomerantz (ref. 184) observed an enhancement of secondary neutrons by 18 percent above the background. The primary protons might possibly have originated in a flare on the back side of the Sun. If so, this would be the first ground-level observation of such a flare. However, an application of ordinary diffusion theory (Krimigis, ref. 186) indicates that the particle ejection might have occurred in a subflare on the disk.

The first great solar proton event of cycle 20 occurred on February 5, 1965. Protons were observed on satellite 1963–38C (ref. 183) and on the ground by means of riometers in polar regions (ref. 185). Goedeke, Masley, and Adams (ref. 185) report this event. They also list 32 other PCA events of low energy and intensity that occurred during the IQSY.

Spike radio bursts at 345 and 230 MHz were observed with rapid-run recorders at the University of Michigan during the type IV event of February 5, 1965. Malville, Aller, and Jensen (ref. 187) interpreted the observed radio burst decay times of 0.055 and 0.085 second at 345 and at 230

MHz, respectively, in terms of stream velocities for the radiating electrons between $1.6-6\times10^4$ km/sec.

It is generally accepted that the synchrotron emission mechanism is responsible for type IV radio bursts. The frequency distribution of flux density decreases toward higher frequencies in accordance with the energy spectrum of the radiating electrons. On September 14, 1966, Boischot and Clavelier (ref. 188) observed a low-frequency type IV event in which the spectrum decreased steeply toward low frequencies as well (fig. 36). They interpreted the low-frequency cutoff as caused by the Razin effect (Ramaty and Lingenfelter, ref. 189) (see "Corona"), and computed an electron density to magnetic-field ratio of 2×10^7 per cubic centimeter per gauss from the critical frequency. They inferred a magnetic field of approximately 0.5 gauss at the origin of the radiation, about 1 solar radius above the limb.

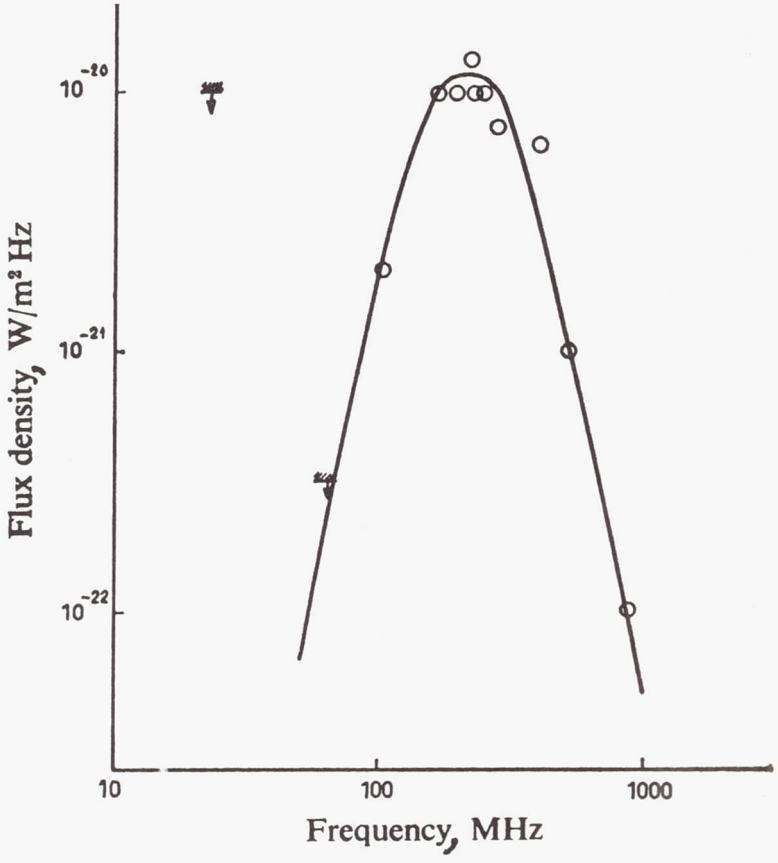


Figure 36.—The Razin effect: spectrum of the metric type IV burst of September 14, 1966 (ref. 188).

Castelli, Aarons, and Michael (ref. 190) deduced the radio spectra of three proton flares in 1966 from single frequency measurements. These spectra have a typical U-shape at the time of maximum flux density with a minimum at decimeter wavelengths (see also Castelli and Michael's report, ref. 191). It appears that a majority of proton flares have radiofrequency spectra of this shape. The fact that the nonproton flare of importance 4b on February 13, 1967, did not have a U-shaped spectrum indicates that the typical spectrum is not a property of flare areas alone.

Theory

It is generally accepted that the mechanisms that give rise to solar flares must be closely associated with magnetic fields in active centers. One of the most promising of the many flare models was proposed by Petschek (ref. 192). Field lines reconnect across a neutral sheet accompanying ohmic dissipation. The neutral sheet is resolved into two slow-mode stationary hydromagnetic shock waves. Green and Sweet (ref. 193) have attempted to generalize this flare model for nonuniform fields. They conclude that the Petschek mechanism will not operate unless one introduces a reversal of the tangential component of the field across the shock waves. The magnetic field is bowed in the region between the waves. Petschek and Thorne (ref. 194) suggested that the flow can be resolved into a combination of slow shocks and intermediate waves that form ahead of the shocks. The intermediate waves are invoked to change the sign of the tangential field component without changing its magnitude. It is thus possible to obtain a consistent solution of the flow equations.

The difficulties that beset magnetic theories of flare production have led to the consideration of alternate models. Hyder's model (refs. 175, 176) has already been discussed. Other hypotheses have recently been examined by Alfvén and Carlquist (ref. 195) and by Pneuman (ref. 196).

Currents of 10^{11} amperes are found near sunspots. Alfvén and Carlquist (ref. 195) suggest that solar flares occur by disruptions of such currents at a location where the current density exceeds the maximum value that the plasma can carry in a stable way. A major portion of the magnetic energy is released near the point where the interruption occurs. Quantitative estimates indicate that about 0.5×10^{30} ergs may be released. The voltage drop across the flaring region should initially be of the order of 10^9 volts.

Pneuman (ref. 196) advanced the hypothesis that flares are the result of temporary storage of hydromagnetic wave energy in the magnetic field of an active center. The mechanical energy flux from the photosphere into active centers is about 3×10^8 ergs/cm^2/sec. A substantial fraction of this energy may be in the form of slow-mode Alfvén waves and slow-mode shocks that must propagate along the magnetic-field lines. The rate of dissipation of this energy will then be less than the rate of input. This

would lead to a net increase of energy density above the active center. When the energy density of the accumulating waves exceeds that of the magnetic field, the waves can no longer be contained and the field is disrupted. The energy in the small-scale motions can then be liberated in a flare. In the first "flash" phase there is an explosive increase in the energy density of small-scale motions in the initial, stationary region. The subsequent expansion or "flare decline" reduces the energy density. It is a unique feature of this model that energy input continues even during the decline of the H-alpha event.

Among the various theories that attempt to explain the physical processes that cause solar flares, all invoke the necessary presence of magnetic lines of force: flares are never seen to occur away from the transient centers of activity and their magnetic fields. It is likely that the definitive test of at least some theories may be made to stand on observation of the time history of small-scale magnetic structure in a flare. In addition, a detailed description of the thermodynamic structure and its history will be needed to test certain aspects of the theories. The outlook for gathering this information is bright, and it is discussed in the section "Outlook."

SOLAR NEUTRON FLUX

As evidence for thermonuclear reactions or nonequilibrium nuclear reactions in the solar atmosphere, the direct observation of solar neutrons would be a valuable result, providing important constraints on any model of solar activity. In particular, the emission of neutrons in solar flare events would provide a possible basis for a decision between existing flare models—or help in the establishment of a new model.

The observation of solar neutrons is hampered in that those neutrons that are easiest to detect—those of relatively low energy—will decay before they can travel 1 AU from the Sun to the vicinity of the Earth. The first positive result was obtained by Apparao, Daniel, Vijayalakshimi, and Bhatt (ref. 197). Negative results obtained since then have led Holt (ref. 198) to discuss these results critically, casting doubt on whether they actually detected neutrons. Holt recommends that future experiments should provide for simultaneous measurement of protons. In other experiments, Webber and Ormes (ref. 199) set an upper limit on 24 solar neutrons/m^2/sec with energies of 100 MeV or more on the basis of their balloon observations. Similarly, Hess and Kaifer (ref. 200) placed an upper limit of 20 neutrons/m^2/sec on the solar flux in the energy range 10 keV to 10 MeV during March to May 1962, deduced from data obtained with their OSO–I experiment, using BF_3 counters. They note, however, that there was no proton flare event during that period. They suggest that Apparao et al. made some misinterpretation in their emulsion experiment that flew during the same time period.

Daniel, Joseph, Lavakare, and Sunderrajan (ref. 201) found a positive result in a balloon flight on April 15, 1966, carrying a high-energy neutron detector (larger than 50 MeV). An increase in the counting rate was observed approximately in coincidence with a possible subflare on the Sun. The rise was about a factor of 3 above the expected background. During the 1.5 hours of observation, they measured an average solar neutron flux of $1000/m^2/sec$ in the 50- to 500-MeV energy range.

There are now some first results on the solar neutron flux, most of them in the form of upper limits under quiet Sun conditions. The observed neutron production in connection with a flare event is a first indication for transient nuclear reactions in the solar atmosphere. An isolated observation can probably do little more than establish that nuclear reactions can occur. The details, such as the thermal or nonthermal nature and the physical state of the emitting region, probably can be deduced only when comprehensive observations of a single neutron-producing flare are available. These observations should include fluxes from the radio to the hard X-ray regions of the electromagnetic spectrum as well as fluxes of neutrons and other particles.

SOLAR X-RAYS

The aim of solar X-ray astronomy is to locate on the Sun the sources of X-ray emission, to measure their total rate of radiation and the energy distribution with wavelength, and to monitor the temporal variations of these quantities. Production of thermal X-radiation involves, generally, only the most highly ionized atomic species that are formed at temperatures exceeding 10^6 °K; nonthermal X-rays are generated by fast electrons that are accelerated during solar flares. Hence solar X-radiation provides significant information about the hottest parts of the solar corona and about the physical state of flares. The study of solar radiation at the shortest wavelengths, begun in 1948, has been increasing in pace during the last few years and is an important contribution to the solution of problems of coronal and flare structure. Goldberg (ref. 1) has recently reviewed the status of solar X-ray studies. Here, we report on the orientation of current work and some of the results that have been achieved.

Quiet Sun and Nonflare Data

One of the primary needs has been for a high-resolution telescope to operate at X-ray wavelengths and for an accurate, triaxially stabilized rocket platform [1] on which such instruments may be mounted. Underwood and

[1] Recommendation 1(a) of the Working Group on Solar Astronomy in Space Research, Directions for the Future, report submitted by the Space Science Board, NAS–NRC, Jan. 1966. The recommendation states, in part, ". . . that highest priority be given to the development of triaxially stabilized rocket attitude controls. . . ."

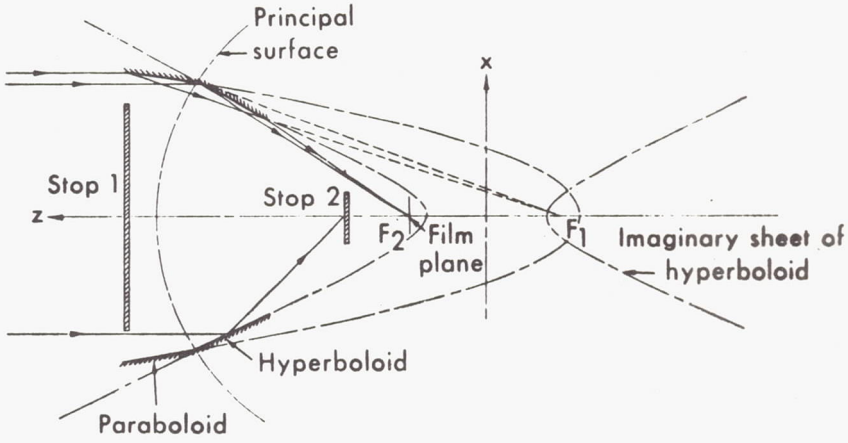


Figure 37.—**Optical configuration of X-ray telescopes.**

Muney (ref. 202) have reported successful photographs of high quality made on May 20, 1966, with a glancing-incidence telescope (fig. 37) on a triaxial mounting in an Aerobee. Reidy, Vaiana, Zehnpfennig, and Giacconi (ref. 203) have quantitatively analyzed a photograph that was made with similar equipment on March 17, 1965. Figure 38 shows the high quality of X-ray photographs that can now be taken and demonstrates the scientific benefit of having developed the long-needed triaxial pointing control.

The four photographs in figure 38 show the development of solar activity early in cycle 20 as seen at soft X-ray wavelengths. The most prominent features are the regions of enhanced emission that correspond closely in position and extent with the chromospheric plages and with local areas of thermal microwave emission. Limb brightening, which at these wavelengths is related to the increase toward the limb of the total number of emitting ions along the line of sight, is also pronounced, as is the persistent absence of such brightening at the southern polar cap prior to October 1967. It is of interest to recall in this connection that, early in cycle 20, the northern hemisphere was far more productive of active regions than was the southern hemisphere, and that while the northern polar cap had a measurable poloidal field component, that in the southern hemisphere was very weak.

Solar X-ray photographs made with a pinhole camera on a triaxial mounting were discussed by Broadfoot (ref. 204). On the date of the Aerobee flight, June 23, 1965, five coronal condensations were detected that were closely correlated in position with regions of microwave emission. The height of the X-ray sources was estimated by Broadfoot to be $2.2 \pm 0.3 \times 10^4$ kilometers above the photosphere.

The solar minimum of 1964 was only the second to occur since the ob-

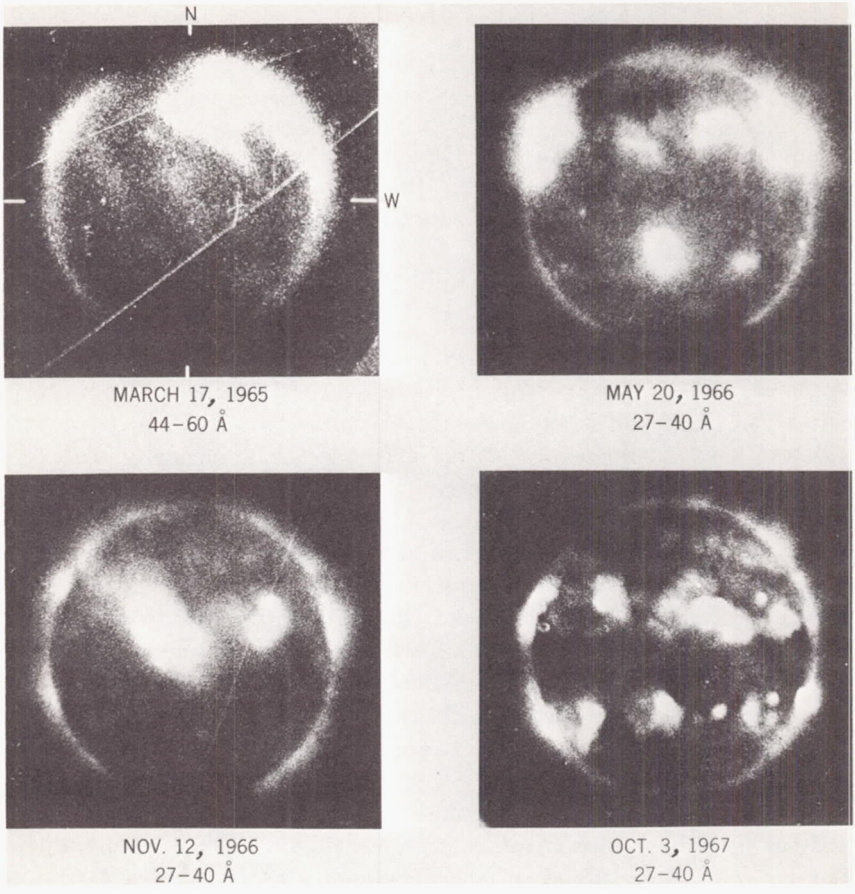


Figure 38.—**Solar X-ray photographs from rockets.**

servational study of solar X-rays was initiated in 1948, and hence has played an important role in helping to fix values for minimum X-ray flux levels from the Sun. Solar minimum data were made available in 1967 by Landini, Russo, and Tagliaferri (ref. 205), by van Gils and de Graaff (ref 206), and by Edwards and McCracken (ref. 207).

Landini et al. (ref. 205) monitored at the Arcetri Observatory transmissions of X-ray data obtained by the NRL 1964–01–D Solar Radiation Satellite (Solrad 7A) during the period March 1, 1964, through February 28, 1965. During this period the 44- to 60-Å flux declined to a broad minimum that appears centered early in the summer of 1964, and then rose again toward the end of the year, in good correlation with the 10.7- and 20-centimeter radio flux densities.

In May 1964 the 44- to 60-Å fluxes reached 2.3×10^{-2} erg cm^{-2} sec^{-1}. (According to Gregory and Kreplin (ref. 210), the flux in this band was 0.07 erg cm^{-2} sec^{-1} by 1966.) The 8- to 12-Å fluxes were almost always below the photometer threshold of 1×10^{-4} erg cm^{-2} sec^{-1} during the same period, occasionally rising to a few times threshold for brief intervals. Similarly, the 0- to 8-Å fluxes were always below threshold except during flares and during one brief nonflare period.

On November 4, 1964, van Gils and de Graaff (ref. 206) launched broadband proportional counters in a Veronique rocket, measuring fluxes of 1.5×10^{-3} erg cm^{-2} sec^{-1} (8 to 15 Å) and 1.8×10^{-2} erg cm^{-2} sec^{-1} (44 to 60 Å) at about 1635 UT. This latter flux value was less than one-half the flux level monitored at Arcetri on the same date by Landini et al. (ref. 205).

Shortly after solar minimum in mid-1964 and while sunspot numbers were still very low, a balloon-borne X-ray telescope was launched by Edwards and McCracken (ref. 207). Observing in the 26- to 45-keV range on April 2, 1965, the detector did not respond to a solar flux component, although other sources were seen. Edwards and McCracken concluded that at solar minimum the integral flux of X-rays $E>30$ keV is below 0.01 photon cm^{-2} sec^{-1}.

The nonflare solar X-ray emission below 5 Å was measured on May 15, 1966, by Bowles, Culhane, Sanford, Shaw, Cooke, and Pounds (ref. 208) from a rocket launched by ESRO. The spectral distribution, determined by means of proportional counters, fitted a Wien curve for $T_e=3\times10^6$ °K. The total flux computed for the 0- to 8-Å band was 1.4×10^{-4} erg cm^{-2} sec^{-1}, in agreement with data secured by Explorer XXX (Solrad 8).

The quiet-Sun flux on March 15, 1967, measured in the range 7.7 to 12.5 keV by Peterson, Hudson, and Schwartz (ref. 209) on OSO–III was 5×10^{-8} ergs cm^{-2} sec^{-1}. The equivalent temperature deduced was 3.6×10^6 °K, requiring an emission measure $N_e{}^2V=10^{46}$ cm^{-3}. Further details concerning this experiment were given in "OSO Program."

Ion chambers in Explorer XXX (ref. 210) and in OSO–III (ref. 211) have shown that the solar X-ray emission may vary appreciably on a short time scale in the absence of flares. Gregory and Kreplin (ref. 210) found that in the 1- to 8-Å region, changes of up to 40 percent occur on a time scale of 1 to 2 minutes, while changes of 20 percent occur in the 8- to 16-Å bandpass on a somewhat longer time scale. Teske (ref. 211) reported small fluctuations in the 8- to 12-Å flux on a time scale of tens of minutes which sometimes accompany changes in H-alpha plage brightness but often do not.

Fazio and Hafner (ref. 212) attempted to detect solar photons of energy $E>50$ MeV on OSO–I in mid-1962. During several solar flares accompanied by hard X-ray bursts, no gamma rays were seen by their detector.

However, during one flare of importance 3, which was not accompanied by an X-ray burst, an excess of gamma photons from the direction of the Sun was observed. Higher rates of counting were consistently recorded from the direction of the Sun throughout the experiment though than were detected from adjacent sectors of the sky. The excess counts were roughly proportional to the level of solar activity, so that for a relative, sunspot number $R_{A'}=40$, the gamma-ray flux from the Sun is 3×10^{-3} photons cm^{-2} sec^{-1}.

X-Ray Spectroscopy

Until recently, only the gross characteristics of the solar X-ray spectral distribution could be obtained by means of broadband photometers sensitive to different regions of wavelength, or by means of proportional counting techniques. Use of Bragg crystal spectrometers in rockets and satellites has, during the past few years, permitted the spectrum to be observed in detail down to around 1-Å wavelength. These observations have shown the presence in the solar corona of extremely highly ionized species of atoms requiring ionization temperatures, in the case of the quiet Sun, of up to 7×10^{6} °K and, in the case of solar flares, of up to 10^{8} °K. Table VI is a compilation of measured wavelengths and line identifications from two different reports and predicted in a third report.

Development of phase gratings (see "Supporting Laboratory and Theoretical Research") for glancing-incidence X-ray spectroscopy promises to provide an excellent means for obtaining solar X-ray spectra with high time resolution, since they permit photography of the spectrum to less than 1-Å wavelength with a single setting. At present, however, crystals are being used as dispersing devices.

Two NRL crystal spectrometers were carried in an Aerobee rocket on October 4, 1966, to cover the wavelength range 1.9 to 25 Å. Numerous emission lines were observed and most were identified (table VI). Rapid variations in the emission spectra of some active regions were observed during the flight, although no flares were occurring at that time. It was found that the ratio of line intensity to continuum intensity was about one-half in the wavelength range 10 to 20 Å, as compared to the theoretical prediction of 3/1. Fritz et al. (ref. 213) did not attempt to explain this apparent problem. It is possible that the high continuum intensity is produced by the two-photon process as described by Elton. See "Supporting Laboratory and Theoretical Research."

A Bragg crystal spectrometer was flown on Satellite 1966–111B by Walker and Rugge (ref. 214). Of 57 emission lines detected between 8 and 25 Å, all but 8 were identified (table VI). Virtually all of the lines in these spectra were highly variable during solar flares, especially at the shorter wavelengths.

Absolute intensities for 28 identified and 4 unidentified lines (table VI) between 11 and 22 Å, measured on May 5, 1966, were reported by Pounds and Evans (ref. 215). They interpreted the lines of O VII as arising from the general corona at $T_e \sim 1.5 \times 10^6$ °K with an emission measure $N_e^2V \leq 1.5 \times 10^{49}$ cm^{-3}, while all the other lines were associated with an active region. The observed intensities of the active region lines are satisfactorily represented by $T_e = 3 \times 10^6$ °K, $N_e^2V = 1.7 \times 10^{48}$ cm^{-3} when autoionization and dielectronic recombination are taken into account. A two-component model, in which a small part of the emitting volume is at $T_e = 4 \times 10^6$ °K, was proposed as possibly also representing the data. Such a model minimizes the abundances of Fe and Ni in which $Fe/H = 1.4 \times 10^{-4}$, Fe/Ni = 6. Both ratios are higher than the corresponding photospheric ratios as given by Goldberg, Mueller, and Aller. (See "Photosphere and Chromosphere.")

Information about the spectral distribution of X-rays may be obtained by combining broadband photometer observations made during atmospheric occultation of the Sun. As was shown by Venables (ref. 216), the terrestrial ionospheric density profile revealed by solar X-ray observations is highly variable, both in topocentric position and in time; thus it is difficult to use a model atmosphere in deducing X-ray spectra with any confidence. Landini (ref. 217) was able to avoid this problem in dealing with data from Solrad 7 and Solrad 8, which carried detectors sensitive to more than one wavelength band. The atmospheric density profile was deduced from occultation data in the 8- to 16-Å channel, and this information was used to obtain spectrum information from the signal in the 44- to 60-Å channel. The results were in good agreement with spectral observations made by others.

Two crystal spectrometers on OSO–III covered most of the wavelength range 1.6 to 25 Å. This experiment was described in "OSO Program," where figures 3 and 4 illustrated the remarkable spectra obtained by Neupert, Gates, Swartz, and Young (ref. 218) during an importance 3 flare on March 22, 1967.

Most of the flare spectrum emission lines were identified as arising from transitions in highly ionized iron; the predicted wavelengths for the strongest expected lines of Fe XIX–Fe XXV fall within 1 percent of the positions of strong emission lines observed during the solar flare. Laboratory spectra secured by Feldman and Cohen (ref. 219) (see "Supporting Laboratory and Theoretical Research" and fig. 42) have tended to confirm these observations. In the flare spectrum the highest stages of ionization (Fe XXIV, Fe XXV) are found to increase most rapidly at the beginning of the flare, while lower stages are observed later in the event. It thus appears that the initial flare ionization produces predominantly Fe XXV as observed in emission at 1.87 Å (fig. 3) and that subsequent recombination of ions gives rise to successively lower stages of ionization as the flare cools.

333–240 O—69——34

Table VI.—*X-Rays*

Fritz, Kreplin, Meekins, Unzicker, and Friedman (ref. 213)		Walker and Rugge (ref. 214)		Pounds and Evans (ref. 215)	
Observed λ(Å)	Identification	Observed λ(Å)	Identification	Predicted λ(Å)	Identification
1. 91	.....				
2. 26	.....				
2. 33	Ca XX [a]				
2. 64	Ca XX				
3. 05	Ca XX, Ar XVIII				
3. 77	Ar XVIII				
4. 41	.....				
5. 73	.....				
5. 85	.....				
6. 11	Si XIV				
6. 52	.....				
6. 58	.....				
6. 70	Si XIII				
6. 74	.....				
7. 05	.....				
7. 42	Mg XI				
7. 70	Na XI				
7. 73	Al XII				
7. 79	Na XI				
7. 82	Na XI				

8. 06	Na XI				
		8. 44	Mg XII		
			Na XI		
		8. 55	Mg XII (satellite?)		
9. 15	Mg XI				
		9. 18	Mg XI		
9. 19	Mg XI				
9. 32	Mg XI (satellite)				
	Ne X				
9. 33	Ne X	9. 33	Ne X		
			Mg XI (satellites) [a]		
		9. 53	Ne X		
9. 71	Ne X				
		9. 75	Ne X		
		10. 05	Na XI		
			Ni XIX [a]		
		10. 25	Ne X		
		10. 61	.....		
		10. 82	.....		
		11. 05	Na X [a]		
		11. 18	Na X (satellite)		
		11. 31	.....		
11. 56	Ne IX			11. 56	Ne IX
	Ni XIX [a]	11. 57	Ne IX		
			Ni XIX [a]		
		11. 76	Ne IX (satellite?)		
				12. 12	Fe XVII
12. 13	Fe XVII			12. 13	Ne X
	Ne X	12. 14	Fe XVII		
			Ne X	12. 24	Ni XIX

See footnote at end of table.

Fritz, Kreplin, Meekins, Unzicker, and Friedman (ref. 213)		Walker and Rugge (ref. 214)		Pounds and Evans (ref. 215)	
Observed λ(Å)	Identification	Observed λ(Å)	Identification	Predicted λ(Å)	Identification
12. 26	Fe XVII			12. 26	Fe XVII
		12. 27	Fe XVII		
		12. 45	Ni XIX		
				12. 53	
		12. 64	Ni XIX	12. 64	Ni XIX
				12. 80	Ni XIX
		12. 85	Ni XIX		
		13. 01	.....		
13. 44	Mn XVI				
	Ne IX			13. 45	Ne IX
		13. 48	Ne IX [a]		
				13. 55	Ne IX
13. 56	Ne IX				
	Mn XVI			13. 65	(Possibly Ne VIII)
13. 70	Ne IX (satellite)				
		13. 71	Ne IX (satellite)		
				13. 77	Ni XIX
13. 82	Ni XIX	13. 82	Ni XIX	13. 82	Fe XVII
	Fe XVII		Fe XVII		
	Ne IX (satellite)		Ne IX (satellite)		

13. 87	Fe XVII
14. 08	Ni XIX
14. 23	Fe XVIII
14. 57	O VIII [a]
14. 82	O VIII
15. 01	Fe XVII
	Cr XV
15. 13	O VIII
15. 25	Cr XV
	Mn XVI [a]
	Fe XVII
15. 45	Fe XVII
15. 69	Mn XVII
	Fe XVIII

13. 92	Fe XVII
14. 02	Ni XIX
14. 10	Ni XVIII
14. 27	Fe XVIII [a]
14. 39	Ni XVIII
	Fe XVIII
14. 56	.....
14. 68	O VIII
15. 00	Fe XVII
15. 25	Fe XVII
15. 45	Fe XVII
15. 61	Fe XVIII
15. 88	Fe XVII

14. 03	Ni XIX
14. 25	Fe XVIII
14. 40	Fe XVIII
14. 82	O VIII
15. 01	Fe XVII
15. 17	O VIII
15. 26	Fe XVII
15. 45	Fe XVII

See footnote at end of table.

Fritz, Kreplin, Meekins, Unzicker, and Friedman (ref. 213)		Walker and Rugge (ref. 214)		Pounds and Evans (ref. 215)	
Observed λ(Å)	Identification	Observed λ(Å)	Identification	Predicted λ(Å)	Identification
16.00	O VIII Fe XVIII	16.01	O VIII Fe XVIII	16.01	O VIII
16.07	Mn XVIII				
		16.30	.....	16.3	
				16.6	
		16.77	Fe XVII	16.77	Fe XVII
16.86	Fe XVII Mn XVI Cr XV				
17.04	Cr XV Fe XVII			17.05	Fe XVII
		17.06	Fe XVII		
17.11	O VII Mn XVI				
17.41	O VII				
		17.42	Fe XVI [a]		
17.64	Mn XVII	17.64	Mn XVII [a] Badly blended		
17.78	Mn XVII O VII	17.78	O VII	17.77	O VII
		18.35	Mg XI (λ9.17, 2d order)		
		18.54	Real?		

18.63	N VII [a]			18.63	O VII
	O VII	18.64	O VII		
	Mn XVI				
18.96	N VII [a]	18.96	O VIII		
	Mn XVI			18.97	O VIII
	O VIII				
	Cr XV				
20.87	Cr XV				
	N VII	20.90	N VII		
21.60	O VII	21.60	O VII	21.60	O VII
21.80	O VII	21.80	O VII	21.80	O VII
22.07	Ca XIV				
		22.08	Ca XIV		
		23.12	Ne IX (λ11.56, 2d order)		
23.28	(O_K line?)	23.29	(O VII?)		
23.74	N VI				
		24.22	Fe XVII (λ12.12, 2d order)		
		24.28	Ne X (λ12.13, 2d order)		
		24.58	Fe XVII (λ12.26, 2d order)		
24.78	N VII	24.78	N VII		
24.98	N VI				

[a] More than one line (blended) of this ion.

Flare-Associated X-Rays

Hard X-ray bursts from solar flares in the energy range 10 to 50 keV were observed on OGO–I and OGO–III (Arnoldy, Kane, and Winckler, ref. 220). The data again demonstrate and make more certain that there is a close relationship between microwave radio bursts and the emission of hard X-rays. Figure 39, taken from the results of Arnoldy, Kane, and Winckler (ref. 220), illustrates data for the March 20, 1966, flare. Valnicek (ref. 221) found that in this flare the X-ray and microwave maxima occurred at the time of most rapid H-alpha flare expansion. Arnoldy et al. examined the total time-integrated fluxes of microwaves and hard X-rays, finding that there is a quantitative relationship between the two sets of data (fig. 40). An analysis of the relationship of hard X-ray bursts with solar electron events revealed that all seven of the largest electron events observed on IMP had associated hard X-ray bursts, although four very small electron events did not have X-ray bursts nor microwave emission. On the other hand, 12 hard X-ray bursts for which no electron event was recorded on IMP–I were all produced by flares east of the solar central meridian.

De Jager (ref. 222) has suggested an elaboration of his earlier X-ray burst classifications, proposing that they be subdivided as soft X-ray bursts (quasi-thermal, $N_e^2V \sim 10^{48}$–10^{49} cm^{-3}), deka-keV bursts (nonthermal, $N_eV \sim 10^{35}$–10^{36}) and deci-keV bursts (nonthermal, $N_eV \sim 10^{35}$). There appears to be no fundamental difference between the latter two except as to their photon energies. The quasi-thermal bursts, though, may arise in volumes of considerably greater extent than the volumes within which nonthermal bursts are generated.

A burst of very hard X-rays (their energy seemed to be $E \sim 0.5$ MeV) on September 18, 1963, has been discussed by de Jager (ref. 223) in connection with a wealth of optical, magnetic, radio flux-density and ionospheric observations. Only a very weak microwave burst accompanied the X-rays. De Jager concluded that the X-ray burst was produced by acceleration of $\sim 3 \times 10^{35}$ electrons within a volume of $\sim 5 \times 10^{25}$ cm^3; the acceleration time scale was about 1 minute and the relaxation time scale—the decay of the burst was exponential—was 86 seconds. The data are consistent with the hypothesis that the acceleration took place within only a very small volume embedded in a part of the active region near the neutral line where magnetic-field gradients were very steep.

Hard X-ray bursts were observed by Peterson and his colleagues (ref. 209) on OSO–III. The typical event observed by them had a fast rise time and a slower decay, with a duration of about 15 minutes. At these energies as at others, the burst frequency decreases rapidly with burst size.

The solar proton flare of July 7, 1966, was recorded at wavelengths 2 to 12 Å by Van Allen (ref. 224) with Geiger-Mueller tubes on Explorer XXXIII. Comparison of his X-ray curve with the 2700-MHz burst reveals a general

resemblance, but there are differences in the details of the two curves. The total X-ray energy from the flare was 1.4×10^{29} ergs. Van Allen (ref. 225) has reported that X-ray flare events are intimately related to the H-alpha flare reports and to terrestrial SID effects. In comparing photometric H-alpha flare intensity curves with soft X-ray flux curves (8 to 12 Å), Teske (ref. 211) found that for at least some flares there is a good time relation between the H-alpha event and the soft X-ray event. (See fig. 5.)

The extremely valuable information from solar X-ray observations illustrates the important interplay between observations from space and in the laboratory, and theoretical investigations. Because of these complementary efforts, solar X-ray data are presently contributing significantly to our understanding of solar physics and solar activity.

SUPPORTING LABORATORY AND THEORETICAL RESEARCH

Laboratory research, ground-based observations, and theoretical work are essential for the evaluation and interpretation of data obtained by space vehicles as well as for the understanding of basic physical processes that take place in the observed objects, such as the solar atmosphere. A supporting research and technology effort must, therefore, be an integral part of any successful program in space research. While the cost is small compared with that of most space experiments, the scientific merits are comparable. Some of the most significant future developments in space physics may take place in the laboratory on Earth. The ground-based laboratory and space-vehicle efforts are interrelated; and the success of the solar physics program depends on a well-balanced effort.

The supporting research and technology in solar physics includes such diverse efforts as instrument development, the development of new gratings, laboratory plasma spectroscopy and similar research, as well as purely theoretical work, and evaluation of results obtained from space experiments.

Some Instrument Component Developments

Among the many instrument components that were further developed, the grating might be singled out as particularly important. A most comprehensive review article on the subject was prepared by Stroke (ref. 226); it emphasizes gratings for normal-incidence applications.

Considerable progress has been made in the manufacture of gratings over the past few years. In particular it has become possible to reduce problems with grating ghosts, to rule more lines per millimeter, to obtain larger grating surfaces for special purposes, and to greatly enhance the efficiency of individual gratings by a suitable change in the geometry of the grating grooves (blazing). While further refinements in these techniques have led to bigger and better gratings in the past year, the most exciting development perhaps has taken place in grazing-incidence diffraction gratings for soft X-rays.

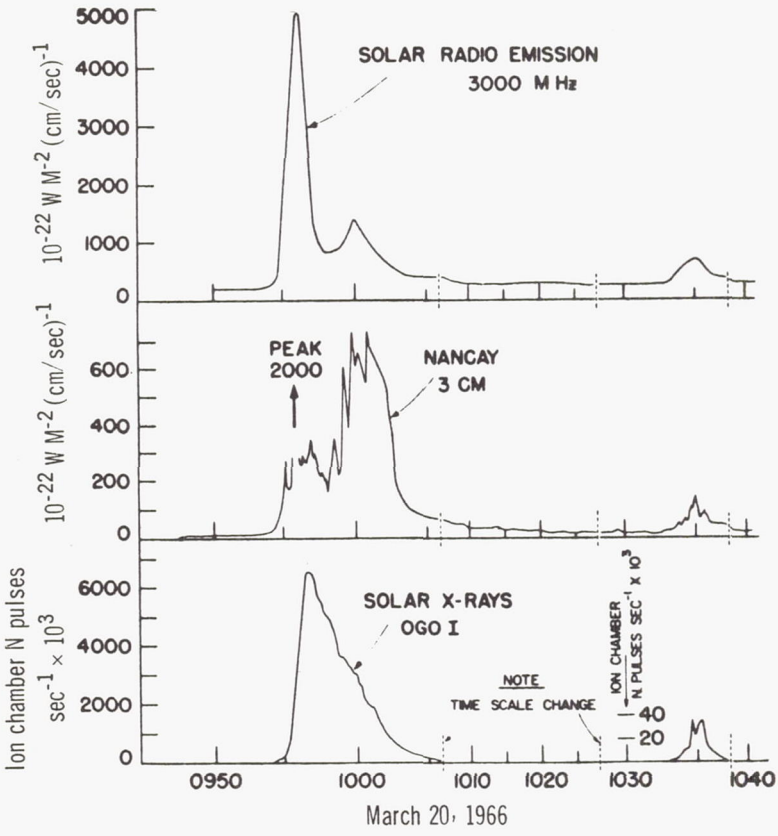


Figure 39.—**X-ray emission from the March 20, 1966, flare (ref. 220).**

A. Franks (ref. 227) has demonstrated that the effectiveness of X-ray diffraction gratings can be severely impaired by imperfections in the diffracting surfaces, even though these imperfections may be so small as to leave the gratings perfectly acceptable for use in the visible. It is difficult to improve much on the smoothness of grating surfaces if a mechanical ruling engine is used to rule the grooves. Franks has applied chemical etching techniques, combined with multiple replication and coating, to make gratings of significantly smoother surface characteristics. He is now incorporating an ion-bombardment technique which he expects to be more controllable. Gratings produced by these methods have a surface smoothness that allows them to be used efficiently at glancing angles as small as 5 minutes of arc. This enables the observation of spectral lines of wavelengths down to about 0.5 Å and constitutes a gain of about an order of magnitude in the spectral range of gratings toward harder X-rays. It extends the range to the point where overlap with more stable and reliable crystals occurs.

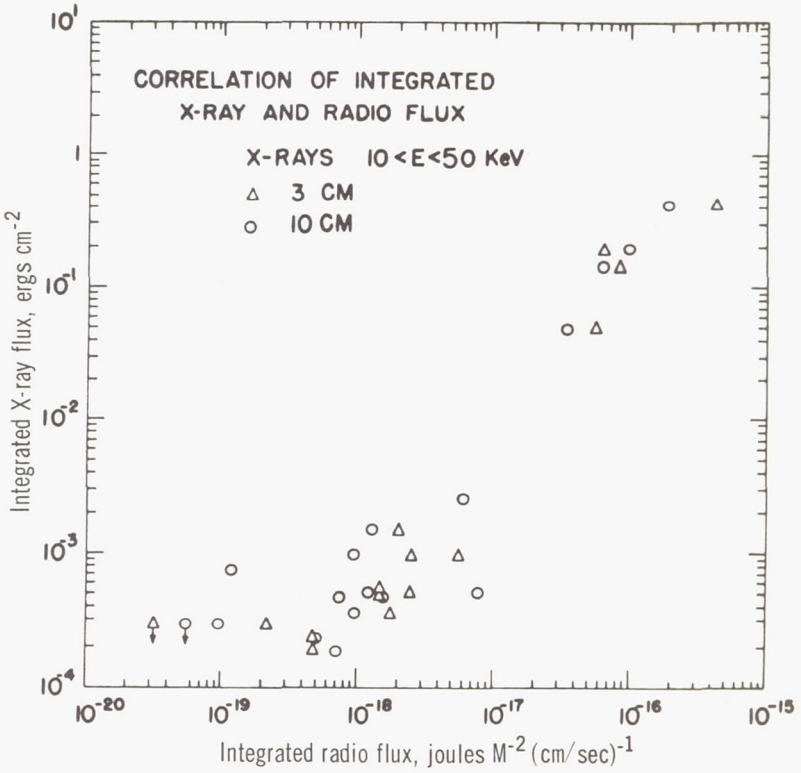


Figure 40.—**Time-integrated X-ray and microwave fluxes (ref. 220).**

So-called phase gratings utilize diffraction from both the grooves and the unruled regions between the grooves. This increases the efficiency at certain wavelengths by constructive interference.

The new gratings have already played a role in the analysis of some of the new laboratory sources of X-rays and will find application in space experiments in due time. In particular, with these gratings it will become possible to photograph the intense X-ray flare spectrum at wavelengths longer than 0.5 Å with a single instrument setting. This would eliminate the photoelectric scanning that is now required in crystal instrument observations.

Laboratory Sources and Simulation

A number of laboratory plasma experiments, most developed originally for controlled fusion applications, have proved to be valuable sources of electromagnetic radiation for purposes of generating the spectra observed from the Sun and for measuring basic atomic quantities. Examples are various pinch devices and, more recently, the plasma focus device discovered by J.

Mather (ref. 228) at Los Alamos. For example, Peacock and Speer (ref. 229) have used such a plasma-focus device for recording emission spectra of highly stripped ions in a high-temperature laboratory plasma. The density of more than 10^{19} electrons per cubic centimeter and a temperature of approximately 10 million degrees Kelvin permitted observation of an iron spectrum very similar to the flare spectrum observed by Neupert et al. (ref. 218). The great advantage of the plasma focus over the more conventional spark is the fact that not only insulator and electrode materials but also gases (such as noble gases) can be highly ionized. Thus, the spectra of argon XVII and XVIII have been observed in three orders by Peacock and Speer with the grazing-incidence grating spectrometer and the new Franks grating mentioned above. The intensity of the plasma-focus source is so high that it was possible to observe the Ne IX resonance lines and satellites up to the 14th order. The correspondingly high resolution makes it possible, in principle, to study the line shape.

Burgess, Fawcett, and Peacock (ref. 230) have shown that laser-produced plasmas reach coronal temperatures at densities of the order of 10^{20} per cubic centimeter. Thus it is possible to observe Stark broadening of coronal ions. While this interferes with the precision that is desirable in line-identification work, there is a unique feature in the laser spark that aids this work. There is a good correlation between laser power input and the stage of ionization. There is usually little emission from stages of ionization other than the dominant one. The assignment of observed transitions to stages of ionization is expedited and simplified by this property of the laser spark plasma.

In an attempt to observe the "forbidden" magnetic dipole emission line of argon XIV at 4412 Å, another experiment was carried out by Conrads and Oertel (ref. 231) on the mega-joule theta pinch magnetic compression device at the NASA Langley Research Center. The line is observed in the solar corona. None of the visible solar corona emission lines had been previously observed in any laboratory. They found emission at 4412 Å that could not be attributed to any mechanism other than possibly the sought-after argon XIV emission line. They were not able to definitely conclude that this emission was due to the argon XIV line, since grazing-incidence equipment, which would have permitted the simultaneous observation of argon XIII and XIV line emission in the X-ray region, was not available. No alternative explanation has been suggested since Conrads and Oertel were able to show that the emission is caused by argon in a stage of ionization higher than argon XII. If it is assumed that the observed emission is indeed caused by the argon XIV 4412-Å line, then the transition probability is at least a factor of 4, possibly a factor of 10, larger than the theoretical value of 109 per second. Such a finding would have a significant effect on abundance determination in the solar corona from forbidden line emission. It should be emphasized, however, that there is no obvious reason why the theoretical values should be off by such a large factor for argon XIV.

Still another X-ray-producing laboratory source was discovered by Lie and Elton (ref. 232). It is a device similar to the plasma focus that emits a spectrum similar to that of small vacuum spark devices. Some of the observed emission may be interpreted as heliumlike copper XXVIII and hydrogenlike copper XXIX resonance emission lines.

Line Identification

Many of the solar vacuum ultraviolet and soft X-ray spectral lines that are observed by rockets and satellites are still not identified as to their element, stage of ionization, and atomic transition. The information on atomic energy levels and the ultraviolet line spectrum for any given element is still very sketchy except for the first few stages of ionization, although laboratory observations have been made for many years by Edlén and coworkers at Uppsala, Sweden. Therefore, much line identification work remains to be done in the vacuum ultraviolet and soft X-ray regions. Progress is being made with the aid of the new sources that were discussed in the previous paragraph, as well as conventional sources. Cowan (ref. 233) classified vacuum ultraviolet lines in the range 100 to 200 Å based on results obtained by Feldman and Fraenkel (ref. 234) in a conventional spark device. Deutschmann and House (ref. 235) identified resonance lines of highly ionized sulfur, barium, argon, and potassium in the High Altitude Observatory theta pinch. Feldman and Cohen (ref. 236) identified the neon I isoelectronic sequence from titanium XXI through nickel XXVII, as well as some other ion transitions.

The spectra obtained by Cohen, Feldman, Swartz, and Underwood (ref. 237) have been compared with the flare spectrum observed by Neupert et al. (ref. 6) on OSO–III. The line-identification work in the laboratory is a good example of how laboratory observations directly support flight programs. It would be impossible to interpret all the X-ray spectra obtained by the OSO's without the identification data that can only be obtained in the laboratory with the necessary level of confidence. The X-ray spectra of Neupert et al. from OSO–III and by Cohen et al. (ref. 237) are compared in figure 41.

Over the years, the well-known compilations of energy levels and multiplet tables by Moore-Sitterly have proved a most valuable aid to every spectroscopist. This monumental work is, naturally, evolving continuously. A similar compilation by R. Kelly (ref. 238) for the soft X-ray and vacuum ultraviolet lines appeared recently and should be useful for coronal and chromospheric work.

Oscillator Strengths and Transition Probabilities

Knowledge of the oscillator strength (f-value) and the related transition probability is essential for the quantitative interpretation of all solar spectra. For example, the oscillator strengths of visible lines are important because

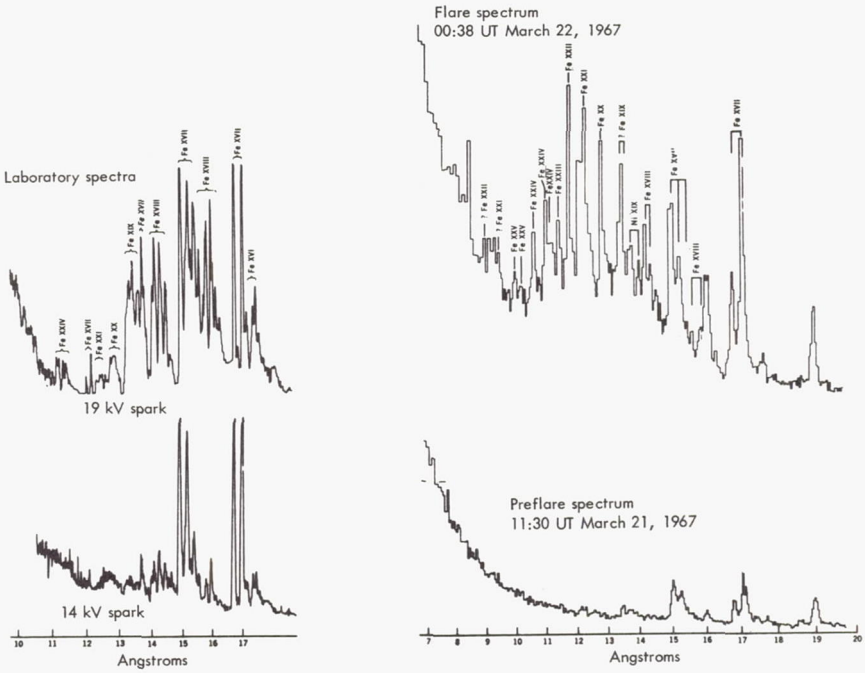


***Figure 41.*—Laboratory spark spectra of Cohen et al. (ref. 237) are compared with flare and preflare spectra from OSO-III (Neupert et al., Goddard Space Flight Center).**

they influence the details of radiative transfer in the region of line formation. While experimental and theoretical research on oscillator strengths is in progress at many institutions throughout the country and the world, there are still many elements for which this information is virtually nonexistent. It would be beyond the scope of this report to mention all research groups which have made contributions to oscillator strength determinations during 1967. However, the work of Bengtson (ref. 239) and Miller (ref. 240) might be singled out. They used a conventional shock tube in their respective investigations of the spectra of neutral and ionized Cl, O, P, S, Si, and others. They obtained a large number of oscillator strengths of considerable reliability as a result of their comprehensive evaluation technique that makes use of virtually all the spectral information recorded on the plate and arrives at a self-consistent picture of temperature, density, and abundances. They also obtained as a byproduct numerous Stark widths and a large portion of all Stark shifts that were measured to date.

The enormous task of analyzing and coordinating the available theoretical and experimental information on oscillator strengths has been taken over by

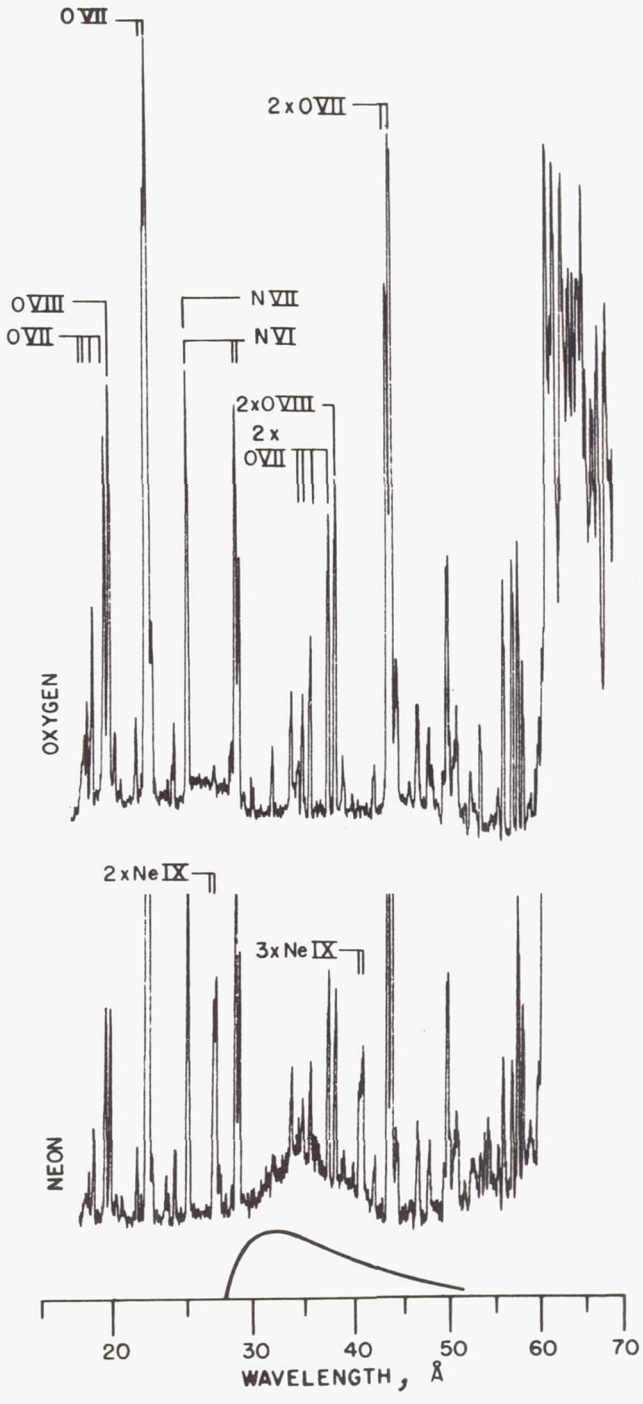
Wiese and coworkers at the National Bureau of Standards, Gaithersburg, Md.

Transition probabilities in the vacuum ultraviolet and soft X-ray regions are even harder to come by. Recent contributions include the computation of heliumlike ionic intercombination line oscillator strengths by Elton (ref. 71) and intermediate coupling calculations by House (ref. 241) and by Kastner (ref. 242). However, only very few experimental determinations exist. In this context, the beam-foil excitation technique for measuring lifetimes of excited levels directly by observing light-decay curves of fast traveling atoms or ions excited by a foil (Bashkin, ref. 243) holds great promise. The usual difficulties associated with excitation in a plasma with its radiative transfer problems and collisional processes are avoided. The usual objection is that cascading from higher levels would distort the simple exponential decay curve and require analysis in terms of many exponential decay curves with different decay constants. Chupp, Dotchin, and Pegg (ref. 244) have therefore applied the technique to measurements of radiative lifetimes in hydrogen which are known with high precision from theory. The effects of "cascading," different foil material, aging of foil material, etc., could therefore be evaluated quantitatively. The conditions were indicated under which reliable measurements are possible. Even more so than in the line-identification area, the lack of transition probabilities will leave room for theoretical and experimental research for many years to come.

One of the more exciting developments has been the observation of the two-photon emission (Smith, ref. 245) from heliumlike neon IX ions by Elton, Palumbo, and Griem (ref. 246). It has long been predicted that two-photon decay of metastable, excited singlet states in helium contributes to the X-ray continuum emission under the low-density conditions which exist in the corona. Elton's demonstration of the effect in a laboratory (theta pinch) plasma (see fig. 42) will lead to an experimental verification of the theoretical prediction of transition probability and spectrum (Shapiro and Breit, ref. 247), and will have an important bearing on the interpretation of solar spectra. A feature in the solar spectrum in the region 8 to 25 Å obtained by Rugge and Walker (ref. 248) may be interpreted as a solar observation of the two-photon continuum. The laboratory demonstration and the possible solar significance of the process are reviving interest in more accurate and comprehensive theoretical calculations of the two-photon decay probability and spectrum.

Cross Sections

In the solar corona, as well as in parts of the chromosphere, it is not possible to assume that thermodynamic equilibrium exists. Therefore, it becomes important to know cross sections for collisional ionization, excitation, and recombination for many of the constituent atoms and ions. Computa-


O VII
2 x O VII
O VIII
O VII
N VII
N VI
2 x O VIII
2 x
O VII
OXYGEN
2 x Ne IX
3 x Ne IX
NEON
20
30
40
50
60
70
WAVELENGTH, Å

tion, as well as measurement of these quantities, is difficult in all but the simplest (hydrogenic) configurations. It is difficult enough to derive wave functions with sufficient accuracy for a determination of energy eigenvalues. It is much harder to increase the precision to the point where the overlap integrals that are required for cross sections as well as transition probabilities can be derived. Nevertheless, techniques for computation as well as measurement have been developed and are beng applied. Bely (ref. 249) and Bely and Bely (ref. 250) demonstrated that discrepancies between computed and measured line-intensity ratios in the Sun could be reduced by the use of electron-excitation cross sections for Fe XVII that they derived within the Coulomb-Born approximation. Measurements of excitation rate coefficients of 2s to 2p, 2s to 3s, 2s to 3p, and 2s to 3d transitions in lithiumlike nitrogen V ions were carried out on Zeta by Boland, Jones, and McWhirter (ref. 251) within ± 70 percent. Similar work was done by Kunze (ref. 252) on a theta pinch under similar conditions as prevailed in Kunze's previous measurements (Kunze, Gabriel, and Griem, ref. 253) on beryllium-like ions. The analysis is based on a simplified approach to the rate-equation problem that restricts the applicability to the most important lines. The agreement with theoretical results obtained by Burke, Tait, and Lewis (ref. 254) and by Bely (ref. 255) is generally well within the experimental accuracy.

Ionization rate coefficients have been measured in the Stellerator for Ne II–Ne VII, O II–O V, N II–N IV, and C II–C III over a fairly wide temperature range. The early work was published by E. Hinnov (refs. 256 and 257). More complete results were reported by D. L. Mickey (ref. 258). Both found that the data for low-ionization stages agree well with expected values such as those given by Lotz (ref. 259). For ions of higher ionization stages, however, the measured coefficients are considerably larger and depend less strongly on temperature than expected.

Burgess (ref. 260) has demonstrated that dielectronic recombination is an important mechanism in the solar corona as well as in many high-temperature laboratory plasmas. It exceeds radiative recombination by an order of magnitude or more in many cases. As a consequence, the large difference between ionization and Doppler temperatures in the solar corona was significantly reduced. Ionization equilibria for elements of interest (O, Ne, Si, Fe) with and without dielectronic recombination were computed and compared by Allen and Dupree (ref. 261). The effect on coronal abun-

---

Figure 42.—**Theta-pinch-produced laboratory spectra with addition of ◊ oxygen (top) and neon (bottom) to the hydrogen gas filling. An estimated two-photon continuum is shown just below the bottom spectrum for comparison (ref. 246).**

333–240 O—69——35

dance determinations has already been mentioned. (See "Photosphere and Chromosphere.") A comparison between dielectronic and radiative recombination and between collisional and autoionization for O IV–O VI, Si IX, and Fe XV ions versus temperature was presented by van Rensbergen (ref. 262). Dielectronic recombination usually dominates, while autoionization rates are at most equal to, usually much smaller than, ordinary electron collisional ionization rates according to this analysis.

The influence of solar-physics-related research on other disciplines is exemplified by the investigation of the possible importance of dielectronic recombination in H II regions by Goldberg and Dupree (ref. 263). They show that overpopulation of large principal quantum number ($n=110$) levels in C I by dielectronic recombination can explain the large observed radio emission without the assumption of a significantly larger carbon abundance than is found in the Sun.

A measurement of the rate coefficient for the reaction $H^- + H \rightarrow H_2 + e$ was carried out by Schmeltekopf, Fehsenfeld, and Ferguson (ref. 264). The measured value is approximately four times as large as the theoretical estimate. This extends the range of validity of local thermodynamic equilibrium at 5000 Å in the solar continuum from 50 kilometers to 300 kilometers above the limb.

Line Broadening

Pressure broadening, in particular Stark broadening, van der Waals' broadening, and resonance broadening, is important for a large number of solar lines whenever the line formation occurs in an optically thick layer. While the Stark broadening of hydrogen lines and of isolated lines was considered to be in fairly good condition since the work of Griem (ref. 265), some discrepancies have shown up in the laboratory. This is true for isolated ion lines (Jalufka, Oertel, and Ofelt, ref. 266) and also for isolated lines of some of the more complex neutrals such as Cl I (Bengston, refs. 267 and 268). On the other hand, careful experimental work, as for example by Greig et al. (ref. 179) on hydrogen and helium, as well as more consistent computations by Kepple and Griem (ref. 180) for hydrogen, and Cooper and Oertel (ref. 269) for isolated neutral lines, have removed some of the discrepancies (ref. 270). The problems often arise not in line-broadening theory but rather in difficulties with computations of some of the required matrix elements and with missing levels in the compilations. Theoretical work on broadening of isolated ion lines has been published by Griem (ref. 271), Cooper and Oertel (ref. 272), Brechot-Sahal (ref. 273), and Davis and Roberts (ref. 274), and others. However, the subject remains in a less than satisfactory state since experimental and theoretical results still differ by factors of 2. The theoretical approaches are often of marginal applicability or have only semiempirical foundation.

Van der Waals' broadening is very important in certain layers of the Sun where most of the broadening is caused by collisions of neutral hydrogen atoms with radiating atoms. For example, this is the case for the sodium-D lines (O'Mara, ref. 275). The theoretical computations are not reliable because of a lack of input data. There is a great need for experiments to study van der Waals' and resonance broadening (Kusch and Meinhold, ref. 276).

Conclusions

Some exciting developments have occurred in laboratory and theoretical work, and some very important quantities have been measured. This has often led to a drastic revision of the existing set of numbers, and has had great repercussions on the interpretation of measurements from the Sun. The data from many solar experiments could not have been evaluated at all, or could not have been interpreted, without some of the more recent results of laboratory and theoretical work. It has become clear that the data obtained by many rockets and satellites are of limited use without the information that can be supplied only by the laboratory experimenter and theorist on the ground. Much additional work is needed before observational data can be successfully interpreted and understood in terms of the processes that take place on the Sun and that make it possible to arrive at realistic models for the solar atmosphere, structure, and activity.

OUTLOOK

Solar Activity

The time variation of nonthermal and nonstationary processes on the Sun is not understood in relation to the Sun's gross structure and evolution, nor well understood phenomenologically. Nearly every known fact concerning solar activity leads to questions to which answers are not known. For example, the intensity of solar activity varies with an approximate 11-year periodicity, but it cannot be shown how this period results from basic physical considerations. One goal of the solar physicist is to discover how the Sun's basic observable parameters—diameter, luminosity, surface temperature, and rotation rate—relate to the time scale and energy scale of solar activity. Equally unexplained is the familiar migration of centers of activity from solar middle latitudes toward the solar equator during the 11-year cycle. The outstanding tasks of this discipline are all concerned with some form of solar activity. Included in the research are attempts to answer the following questions:

What causes a solar flare?

How are solar protons accelerated and expelled?

What causes a persistent plasma emission from some activity centers?

Solar Magnetic Fields

These fields appear to be closely linked to solar activity, but the relationship is poorly understood. Sunspots exhibit strong magnetic fields on the surface. However, sunspot groups seldom appear as simple magnetic dipoles, or as the result of simple electric current systems. An elementary theory of magnetic diffusion suggests a natural lifetime of a sunspot to be a few hundred years, in contrast to their observed lifetimes of weeks or months. Theories on the origin and dispersal of sunspot magnetic fields have to account for the inhibiting character of the photospheric plasma. Customarily one invokes hydromagnetic and/or acoustical processes of bulk transport of magnetized material to explain rapid changes. The relation of solar magnetism to velocity distributions and thermal structures remains one of the most pressing tasks of solar astronomy. The spatial scale of such correlative observations from the ground is too coarse by about a factor of 10 for what is believed to be the physical scale that should be observed. This implies that the spatial resolution of ground-based telescopes is too low by a factor of 10 to see the true spatial scale of the solar phenomena believed to be important. The limiting factor is the relatively poor "seeing" on the ground. Important questions concern magnetic structures in the size range of a few hundred kilometers (prominence fibers, granules) through a few thousand kilometers (sunspots, plages). Many specific questions concerning solar magnetism remain unanswered. We must discover the cause of the alternation of leading spot polarity between successive sunspot cycles. A theory of sunspot magnetism must account for the observation that some spots are bipolar and others are much more complex.

At the other end of the known size scale, we do not yet know whether the photospheric granules or the chromospheric spicules are discretely magnetized. The relationship of their magnetic and geometric properties to their kinematic behavior is necessary for any theory of these phenomena, and probably of gross forms of solar activity, as well. Ultimately we seek to learn the origin of the Sun's magnetic fields. Solar rotation and convective transport of subphotospheric plasma have been suggested as the basic mechanism but these models, in fact, cannot yet predict the observed character of magnetic fields in spots or the general field, nor their slow variation. In this general area of research, exploratory observations will probably spearhead advances for some time to come.

Atmospheric Inhomogeneities and Turbulence

At the limit of attainable resolution at ballooning altitudes, photospheric granulation reveals the vital role played by convective energy transport in the Sun. Higher in the solar atmosphere, the offband hydrogen-alpha

spectroheliograms disclose the vertical transport of microscopic turbulent energy into a larger scale process. The supergranulation has been discovered to be intermediate between these small-scale motions and the grosser inhomogeneities of sunspots and activity centers. The relationship between the supergranulation, solar magnetism, and active centers is only known in a crude way and is not understood at all. The most difficult problems of making solar observations occur in this area. Weak field magnetometry of small structures, high angular resolution, multiple monochromatic time-lapse pictures, and observations of Doppler shifts must be made continuously over extended periods of time.

In the higher layers of the solar atmosphere, different characteristic inhomogeneities begin to dominate. In the chromosphere, the spicules correspond to the small-scale turbulent velocity field surrounding active regions. During the preceding decade, monochromators and high-resolution spectrographs were applied effectively to study spicules at the limb. Quite recently offband techniques combined with stop-motion time-lapse photography have provided meaningful new observations of spicules on the disk. The new data have not, however, conclusively answered the basic question of why they occur. (See "Photosphere and Chromosphere.")

The corona has been observed, at many total solar eclipses, to display structure in the form of a general ellipticity and also to have discrete radial streamers. The observed size and distribution of the features vary not only as a function of solar cycle but also from day to day as the Sun rotates and as the individual activity centers evolve. Indirect evidence of inhomogeneities in the corona is provided by variations in the temperature of the solar wind and large-scale structure observed in the interplanetary plasma. These variations have been observed directly by interplanetary spacecraft and inferred from their effect on the Earth's magnetic field. The mechanism of this interaction is not understood.

More highly organized forms of matter in the corona are familiar as prominences, which are readily observed and interpreted to be condensations of partially ionized gas. Almost everything about them is puzzling—why they form, how they persist, their relationship to activity centers in the chromosphere, details of their fine structure, and their response to chromospheric impulsive activity.

The Flare Phenomenon

Flares occupy a large share of the solar astronomer's attention because they appear to be the result of nonstationary and nonthermal physical processes that are difficult to understand, and because the largest flares produce quite spectacular geophysical effects.

A flare is a localized, sudden brightening of the chromosphere observed in hydrogen-alpha or the calcium K-line. Large flares often produce radio

noise bursts, sometimes are associated with sudden magnetic storms, usually produce flashes of X-rays, occasionally eject energetic protons, and disturb prominences in the neighboring corona. The observed X-ray emissions have revealed clues to the fundamental physical flare process, but raise as many questions as they answer. The certainty, duration, and spectral energy of flares and X-rays correlate only in a loose way with optical, radiofrequency and corpuscular characteristics of individual events. The relative roles of bremsstrahlung, synchrotron, and quasi-thermal processes of X-ray emission are unknown. A vast amount of observational detail is known concerning these chromospheric brightenings, but, at present, solar physicists can only guess how a flare is formed and why, where, and when it occurs. The answers to this particular set of questions continue to rank among the principal objectives of solar astronomers.

Numerous theories of flares have been advanced during the past few years, some of which admit of possible direct observational tests. Typical are theories of converting magnetic energy into streams of charged particles via plasma mechanisms such as pinch discharges and the Fermi process. Information on the details of the solar magnetic field could conceivably test the validity of such theories. A goal of this branch of solar astronomy is to follow promising lines of specialized observations to test such theories. Synoptic magnetic field maps, accurate to a few gauss and spatially resolved to a few hundred kilometers, could test some theories by comparing preflare with postflare magnetic field configurations.

Another class of flare observation concerns the nuclear composition of flare-ejected matter as it arrives at the Earth. Some measurements of the abundances of deuterium, tritium, helium, and neutrons have been made. Thus, the direct measurement of relative abundances of nuclear species in the interplanetary plasma is a test of some theories.

More familiar techniques of spectroscopy and cinematography will continue for a long time to play a major role in flare studies. This is particularly true as advances in technology or superior observing sites permit a significant improvement in observational capability. For some questions, an increase in resolution in the visible spectrum could be as important as extending more modest resolution observations to an unexplored spectral region. In general, however, the greatest promise for understanding flares is offered by high angular and high time-resolution studies of the beginning phases of flares in X-ray and ultraviolet spectral regions, including the analysis of spectral line profiles of critical emissions. This observational objective can be stated in terms of numerous specialized observations of which the following are only typical: 5 and 1 arc-second-resolution X-ray pictures of flares, both in resonance lines as Lyman-alpha, C VI or O VIII, and in the continuum near 1 and 10 Å; maps of the profile of the Lyman-alpha line of hydrogen, especially the extended faint wings, with spatial resolution as small as 100 kilometers; panchromatic spectrograms in the entire extreme ultraviolet region

(100 to 1000 Å), of the hottest portions of flares, to obtain time variations of equivalent widths of multiplets over the whole range of excitation and ionization energies; and polarization observations of the continuum in spectrum emitted from flaring regions.

The radiofrequency emission of flares had been energetically investigated during the past solar cycle. Together with direct measurements of solar protons, radiofrequency observations have revolutionized our outlook on flares, the Sun, and even the universe. Because of the very long wavelengths involved, angular resolution at metric and longer wavelengths is only adequate to locate radio bursts relative to activity centers. In theory, very large radio telescopes used at centimetric wavelengths could provide detailed maps of flares in radio emission, so as to provide information for the study of their nonthermal and their quasi-thermal processes. Important information on underlying physical mechanisms will be obtained by using polarization analysis with high-angular-resolution studies to investigate local magnetic fields and to discriminate between radiative processes. At very long wavelengths, low-resolution spectral observations may provide additional evidence on the nature of the radiofrequency radiation.

Relation Between Ground and Space Observations of the Sun

From ground observatories we see principally the radiations of the Sun as a result of processes that occur at relatively low temperatures, 4000° to 10 000° K. The highly energetic emissions, which contain much of the desired information on the phenomena of solar activity, lie near the threshold of detectability in the visible wavelengths. Only with the most refined monochromators are we able to measure and monitor the chromosphere and corona. This is because the Sun's spectral luminosity reaches a peak near 5200 Å, right at the center of this atmospheric window in the visible spectrum. At the extremes of the electromagnetic spectrum, in the X-ray and in the radiofrequency spectral regions, the quasi-blackbody radiation is much weaker in comparison to the nonthermal radiations. Some long-wavelength radiation can be detected in the radio spectrum by ground observations, but none of the shortwave components penetrate through the atmosphere.

Despite this handicap, ground-based observations must, for many years to come, play a significant role in solar research. Angular resolution of a high order is required to study the structures associated with solar activity, such as spots and flares, and structures on the quiet Sun, such as spicules and granulation. The atmosphere allows us to utilize apertures up to about 20 centimeters, equivalent to a spatial resolution of about 1 second of arc in the visible spectrum. To achieve higher resolution than about 1 arcsecond, larger apertures must be carried above the atmosphere. This will be done at first using balloons. However, the most efficient way to obtain

significant quantities of data at high resolutions is by carrying sophisticated experiments in spacecraft outside the Earth's atmosphere. Thus, one can foresee a scientific and technical program developing toward the goal of a solar observatory in space. In the meantime, solar observations from space vehicles serve best in the spectral regions not accessible to ground-based instruments, utilizing the relatively modest angular resolution possible by the size of telescope and precision of stabilization available. Ground-based observations of radio emissions from the Sun offer a powerful tool to discover and to monitor nonequilibrium processes. Investigations at sufficiently high angular resolution of structures of the size of spicules, prominences, spots, and granules cannot be attained at centimeter and decameter wavelengths. This is because high-resolution radio telescopes for such long wavelengths grow to prohibitive dimensions.

Even today satellite observations can, in principle, excel ground observations in another way. Continuity of observation is essential to study adequately the unpredictable solar events of special interest such as flares. Our understanding of the supergranulation is presently hampered by inadequate observations of its time development, as any one observatory can follow the evolution of an element only through part of its lifetime during a single day. Satellites carrying large telescopes in continually sunlit orbits might eventually permit studies to proceed over long times without interruption by sunsets and cloudy days.

In the meantime, simple satellites permit continual observation of the X-ray brightness of the Sun and could, if desired, provide the equivalent of a chromospheric flare patrol in hydrogen light. That function is currently performed more efficiently from the ground, because no firm requirements exist for complete monitoring. By tolerating a few gaps in coverage, up to a few hours' duration, a relatively inexpensive hydrogen-alpha patrol network can satisfactorily take the place of a more expensive orbiting monitor. This situation may change as operational requirements generate firm requirements for reliable, full-time monitoring.

Magnetometry of the Sun is a specialized application of spectrometry. It requires the measurement of optical line splitting, simultaneously with achievement of high spatial and time resolution. Thus, very large telescopes and spectrographs and freedom from atmospheric "seeing" limitations are required. Until a very large orbiting telescope can provide a significant improvement in angular resolution, ground-based astronomy alone must provide definitive solar magnetic field measurements. A new technique of solar magnetometry, perhaps by a photographic subtraction process, may enable a small telescope and spectrograph to exceed, by orbital observations, the very best resolution achieved now on the ground. Should this technique be realized, magnetic monitoring to a limit of about 1 arc-second by an orbiting telescope would be a desirable goal, because large

ground-based telescopes cannot obtain this resolution except at very rare times of best seeing, and then for only very short periods.

The solar corona can be observed in visible light from the ground and from balloons, but under a great handicap. Satellite observations of the brightness, polarization, and form of the visible corona will be limited by the telemetry capability of satellites in the next few years. The search for flare blast waves in the lower corona must be conducted in the near future from the ground. Ground-based coronagraphic techniques can provide pictures with about 5-arc-second resolution, at 2-minute intervals during a couple of hours on about 200 days a year, at two or three selected mountaintop observatories. Clearly, this observational opportunity is not sufficient, even at solar maximum, to assure detection of a sufficient number of typical events. Eventually an Earth-orbiting observatory must do this task. Observations of outer coronal brightness and ray structures require lower background sky brightness than is normally possible from high-altitude balloons or from orbit except during total eclipses. In the coming decade infrequent ground and balloon observations will offer higher resolutions than satellites, but orbiting coronagraphs will supplement these by daily or hourly synoptic low-resolution surveys.

Airplanes and balloons, as vehicles for instrumentation, have special roles to serve in our investigation of the Sun in the period of the OSO and ATM programs. Balloons permit searching for energetic solar X-rays and gamma rays which can penetrate the atmosphere to about 33 to 50 kilometers. With balloons, Anderson and Winckler discovered the hard X-rays emitted during solar flares, and thus stimulated a number of satellite experiments that are planned to fly in future years. Stratoscope I observed solar granulation through a 30-centimeter telescope, and obtained the finest sequences of high-resolution, white-light pictures ever made of the Sun. As mentioned above, the observation demands far more telemetry bandwidth than unmanned solar satellites will provide for some years to come. Balloons can overcome this difficulty, and indeed the projected Spectro-Stratoscope flight program will exploit that advantage in the coming years. A major disadvantage of balloon observations is the short period of observation they allow. It is inadequate to monitor large flares, or to integrate fluxes over a long time when it is necessary to discriminate against a noisy background. The study of the Sun's corona has already been discussed as an especially suitable use of balloons as carriers for astronomical instruments. The sky is nearly 100 times darker at peak balloon altitude than even from good mountaintop observatories. Thus the disadvantage of infrequent, short-duration flight is compensated by the ability to recover abundant photographic observations from a balloon mission. In the near infrared, balloons open up the atmospheric window so widely that there exists some compulsion to pursue that technique intensively before undertaking major infrared projects on satellites.

All that has been said of balloon solar astronomy applies, in some degree, to observations from aircraft. Engine vibration, navigational tracking errors, and air turbulence all conflict with the goals of high angular resolution; however, servo suntrackers and short exposures, when they can be tolerated, will probably enable aircraft observations to emulate at least the work of Stratoscope I. The present jet aircraft already can double the duration of totality of a solar eclipse; when supersonic flight is achieved, durations up to 90 minutes will permit immensely valuable height resolution in the chromosphere, or long-exposure monochromatic coronal observations. At an altitude of 13 kilometers, highly significant research in the infrared region down to a few microns becomes possible, even with modest telescopes and spectrographs. The possibility of pursuing eclipse studies almost free of interference by clouds is a major advantage of airplane-borne astronomical instruments.

The ultimate goal for research at high spatial resolution and maximum spectral coverage is the installation of a space solar observatory that would be at least as powerful as any now on Earth. It should permit a diversified series of observational programs to be conducted by a large number of solar investigators.

Such a major technological development must, however, be preceded by long years of experimentation in astronomical engineering in space. Large telescopes are too delicate to launch in an erected, operable condition and too costly to use in only an automatic, remote-controlled fashion, then discarded after the first failure of a critical component or subsystem. The large space telescopes of the future must be erected, serviced, and maintained by astronauts. In the near future, the Apollo Applications Program may permit initial trials with a combination of man and telescope. Such problems as attitude control, data acquisition, local environment contamination (by life-support system leakage, by dust dispersion, electrostatic discharge, etc.) and modes of services and repair must be explored. These engineering experiments can be performed with real research tasks, utilizing the special opportunities of early manned astronomy missions to work under otherwise unattainable conditions.

REFERENCES

1. Goldberg, L.: Ultraviolet and X-Rays From the Sun. Ann. Rev. Astron. Astrophys., vol. 5, 1967, p. 279.
2. Howard, R.: Magnetic Field of the Sun (Observational). Ann. Rev. Astron. Astrophys., vol. 5, 1967, p. 1.
3. Newkirk, G., Jr.: Structure of the Solar Corona. Ann. Rev. Astron. Astrophys., vol. 5, 1967, p. 213.
4. Underwood, J. H.: Solar X-Ray. Science, vol. 159, 1968, p. 383.
5. Tousey, R.: Some Results of Twenty Years of Extreme Ultraviolet Solar Research. Astrophys. J., vol. 149, 1967, p. 239.

6. Neupert, W. M.; Gates, W.; Swartz, M.; and Young, R.: Observation of the Solar Flare X-Ray Emission Line Spectrum of Iron From 1.3 to 20 Å. Astrophys. J. Letters, vol. 149, 1967, p. L79.
7. Bahcall, J. N.; Cooper, M.; and Demarque, P.: Dependence of the ^{8}B Solar Neutrino Flux on Heavy Element Composition. Astrophys. J., vol. 150, 1967, p. 723.
8. Davis, R., Jr.; Harmer, D. S.; and Hoffman, K. C.: A Search for Neutrinos From the Sun. Phys. Rev. Letters, vol. 20, 1968, p. 1205.
9. Goldberg, L.; Mueller, E.; and Aller, L. H.: The Abundances of the Elements in the Solar Atmosphere. Astrophys. J. Suppl., vol. 5, 1960, p. 1.
10. Lambert, D. L.: The Abundances of the Elements in the Solar Photosphere. I. Carbon, Nitrogen and Oxygen. Monthly Notices Roy. Astron. Soc., vol. 138, 1968, p. 143.
11. Bahcall, J. N.; Bahcall, N. A.; and Shaviv, G.: Present Status of the Theoretical Predictions for the ^{37}Cl Solar Neutrino Experiment. Phys. Rev. Letters, vol. 20, 1968, p. 1209.
12. Bahcall, J. N.: Solar Neutrinos. Phys. Rev. Letters, vol. 17, 1966, p. 398.
13. Shaviv, G.; Bahcall, J. N.; and Fowler, W. A.: Dependence of the ^{8}B Solar Neutrino Flux on the Rate of the Reaction $^{3}He(^{3}He, 2p)\,^{4}He$. Astrophys. J., vol. 150, 1967, p. 725.
14. Iben, I., Jr.; Kalata, K.; and Schwartz, J.: The Effect of Be^{7} K-capture on the Solar Neutrino Flux. Astrophys. J., vol. 150, 1967, p. 1001.
15. Dicke, R. H.; and Goldenberg, H. M.: Solar Oblateness and General Relativity. Phys. Rev. Letters, vol. 18, 1967, p. 313.
16. Jordan, P.: Fuenf-dimensionale Kosmologie. Astron. Nachr., vol. 276, 1964, p. 193.
17. Brans, C.; and Dicke, R. H.: Mach's Principle and the Relativistic Theory of Gravitation. Phys. Rev., vol. 124, 1961, p. 925.
18. Dicke, R. H.: Mach's Principle and Invariance Under Transformation of Units. Phys. Rev., vol. 125, 1962, p. 2163.
19. Howard, L. N.; Moore, D. W.; and Spiegel, E. A.: Solar Spindown Problem. Nature, vol. 214, 1967, p. 1297.
20. Greenspan, H.; and Howard, L. N.: On a Time-Dependent Motion of a Rotating Fluid. J. Fluid Mech., vol. 17, 1963, p. 385.
21. Dicke, R. H.: The Solar Spin-Down Problem. Astrophys. J. Letters, vol. 149, 1967, p. L121.
22. Sturrock, P. A.; and Gilvarry, J. J.: Solar Oblateness and Magnetic Field. Nature, vol. 216, 1967, p. 1280.
23. Gilvarry, J. J.; and Sturrock, P. A.: Solar Oblateness and the Perihelion Advance of Planets. Nature, vol. 216, 1967, p. 1283.
24. Roxburgh, I. W.: Implications of the Oblateness of the Sun. Nature, vol. 213, 1967, p. 1077.
25. Roxburgh, I. W.: Solar Oblateness. Nature, vol. 216, 1967, p. 1286.
26. Dicke, R. H.; and Goldenberg, H. M.: Differential Rotation and the Solar Oblateness. Nature, vol. 214, 1967, p. 1294.
27. Audretsch, J.; Dehnen, H.; and Hoenl, H.: Crucial Test for the Existence of a Solar Quadrupole Moment. Astrophys. J. Letters, vol. 150, 1967, p. 127.
28. O'Connell, R. F.: Regression of the Node of the Orbit of Mercury Due to a Solar Quadrupole Moment. Astrophys. J. Letters, vol. 152, 1968, p. L11.
29. Richard, J. P.: Solar Oblateness and the Moon Precession. Icarus, vol. 7, 1967, p. 274.

30. ZIRIN, H.: The Solar Atmosphere. Blaisdell Publ. Co., 1966.
31. DE JAGER, C.; AND NEVEN, L.: Source Functions in the Cores of Infrared Fraunhofer Lines. Solar Phys., vol. 3, 1968, p. 159.
32. ATHAY, R. G.: Theoretical Line Intensities. V. Solar UV Emission Lines of Heavy Elements. Astrophys. J., vol. 145, 1966, p. 784.
33. JEFFERIES, J. T.: Spectral Line Formation. Blaisdell Publ. Co. (New York), 1968.
34. THOMAS, R. N.: Nonequilibrium Phenomena in Stellar Atmospheres. *In*: Physics of Many Particle Systems, E. Meeron, ed., Gordon & Breach (New York), 1965.
35. GINGERICH, O.; AND DE JAGER, C.: The Bilderberg Model of the Photosphere and Low Chromosphere. Solar Phys., vol. 3, 1968, p. 5.
36. GINGERICH, O.; AND RICH, J. C.: The Far Ultraviolet Spectrum of the Sun. Solar Phys., vol. 3, 1968, p. 82.
37. RICH, J. C.: Silicon and Carbon Monoxide Absorption in the Solar Ultraviolet Spectrum. Paper presented at Harvard College Observatory, 1966.
38. NOYES, R. W.; BECKERS, K. N.; AND LOWE, F. J.: Observational Studies of the Solar Intensity Profile in the Far Infrared and Millimeter Regions. Solar Phys., vol. 3, 1968, p. 36.
39. WITHBROE, G. L.: An Analysis of CH in the Solar Atmosphere. Astrophys. J., vol. 147, 1967, p. 1117.
40. DE JAGER, C.; AND NEVEN, L.: A Systematic Method for the Analysis of High-Resolution Fraunhofer Line Profiles. Solar Phys., vol. 1, 1967, p. 27.
41. LENA, P. J.: Observations of the Center-to-Limb Variation of the Solar Brightness in the Far Infrared (10 to 25 Microns). Solar Phys., vol. 3, 1968, p. 28.
42. ELSTE, G.: Comments on the Bilderberg Continuum Atmosphere. Solar Phys., vol. 3, 1968, p. 106.
43. SAUVAL, A.: The Solar Continuum from 900 to 130,000 Å and the Photospheric Temperature Model. Solar Phys., vol. 3, 1968, p. 89.
44. WITHBROE, G. L.: The Center-Limb Behavior of Solar Molecular Lines. Solar Phys., vol. 3, 1968, p. 146.
45. JEFFERIES, J. T.; AND WHITE, O. R.: The Analysis of Spectral-Line Profiles. I. A Generalized Theory of the Solar Case. Astrophys. J., vol. 150, 1967, p. 1051.
46. CURTIS, C. W.; AND JEFFERIES, J. T.: The Analysis of Spectral-Line Profiles. II. An Application to the Solar Sodium D-Lines. Astrophys. J., vol. 150, 1967, p. 1061.
47. ATHAY, R. G.: Astronomical Plasmas. Paper presented at the Second Internatl. Conf. on VUV and X-ray Spectroscopy, Univ. of Maryland, 1968.
48. DUPREE, A. K.; AND GOLDBERG, L.: Solar Abundance Determination From Ultraviolet Emission Lines. Solar Phys., vol. 1, 1967, p. 229.
49. POTTASCH, S. R.: On the Relative Abundances in the Solar Corona as Determined From the Ultraviolet Spectrum. Astrophys. J., vol. 150, 1967, p. 361.
50. POTTASCH, S. R.: The Lower Solar Corona: Interpretation of the Ultraviolet Spectrum. Astrophys. J., vol. 137, 1963, p. 945.
51. ATHAY, R. G.: On the Relative Abundances in the Solar Corona as Deter-
52. DAEHLER, M.: The Solar Disk Spectrum Near 6708 Å. Astrophys. J., vol. 150, 1967, p. 667.

53. Peach, J. V.: The Solar Lithium Abundance. Astron. J., vol. 72, 1968, p. 822.
54. Grevesse, N.: The Abundance of Lead in the Sun. Astrophys. J., vol. 149, 1967, p. 37.
55. Ross, J. E.; Aller, L. H.; and Mohler, O. C.: The Abundance of Lead in the Sun. Proc. Roy. Astron. Soc., vol. 59, 1968, p. 1.
56. Ross, J. E.; and Aller, L. H.: Solar Abundance of Chromium. Astron. J., vol. 72, 1967, p. 825.
57. Lambert, D. L.: Abundance of Helium in the Sun. Nature, vol. 215, 1967, p. 43.
58. Lambert, D. L.; and Warner, B.: The Abundances of the Elements in the Solar Photosphere. II. Sodium, Aluminum, Phosphorus, Sulphur and Potassium. Monthly Notices Roy. Astron. Soc., vol. 138, 1968, p. 181.
59. Lambert, D. L.; and Warner, B.: The Abundances of the Elements in the Solar Photosphere. III. Silicon. Monthly Notices Roy. Astron. Soc., vol. 138, 1968, p. 213.
60. Warner, B.: The Abundances of the Elements in the Solar Photosphere. IV. The Iron Group. Monthly Notices Roy. Astron. Soc., vol. 138, 1968, p. 229.
61. Biswas, S.; and Fichtel, C. E.: Nuclear Composition and Rigidity Spectra of Solar Cosmic Rays. Astrophys. J., vol. 139, 1964, p. 941.
62. Mugglestone, D.; and O'Mara, B. J.: Saturation Effects in Stellar Atmospheric Absorption Lines. Monthly Notices Roy. Astron. Soc., vol. 129, 1965, p. 41.
63. Watts, R. N., Jr.: OSO 4 Ultraviolet Solar Observations. Sky and Telescope, vol. 34, 1967, p. 362.
64. Lemaire, P.; and Blamont, J. E.: Stigmatic Balloon Spectra of the Solar Mg II Doublet. Astrophys. J. Letters, vol. 150, 1967, p. 129.
65. Bonnett, R. M.; Blamont, J. E.; and Gildwarg, P.: Limb Darkening Observations From 1800 to 2800 Angstroms. Astrophys. J., vol. 148, 1967, p. 115.
66. Sandlin, G. D.; and Widing, K. G.: Energy Distribution in the Solar Ultraviolet Continuum between 1550 and 2100 Angstroms. Astrophys. J., vol. 149, 1967, p. 129.
67. Porter, J. R.; Tilford, S. G.; and Widing, K. G.: Carbon Monoxide in the Solar Ultraviolet Spectrum. Astrophys. J., vol. 147, 1967, p. 172.
68. Appenzeller, I.; and Schroeter, E. H.: Center-to-Limb Variations of the Intensity and the Wavelength of Several Fraunhofer Lines Along the Sun's Polar and Equatorial Diameter. Astrophys. J., vol. 147, 1967, p. 1100.
69. Zirker, J. B.: The Solar H and K Lines of Ionized Calcium. Solar Phys., vol. 3, 1968, p. 164.
70. Burton, W. M.; Ridgeley, A.; and Wilson, R.: The Ultraviolet Emission Spectrum of the Solar Chromosphere and Corona. Monthly Notices Roy. Astron. Soc., vol. 135, 1967, p. 207.
71. Elton, R. C.: Intercombination Line Oscillator Strengths in the Helium Isoelectronic Sequence. Astrophys. J., vol. 148, 1967, p. 573.
72. Lambert, D. L.; and Swings, J. P.: Forbidden Carbon I Lines in the Solar Spectrum. Solar Phys., vol. 2, 1967, p. 34.
73. Houtgast, J.: The High-Dispersion Continuous Solar Spectrum and Balmer-Jump. Solar Phys., vol. 3, 1968, p. 47.
74. Labs, D.: Die Intensitaet des Kontinuierlichen Spektrums der Sonnenmitte im Wellenlaengenbereich $3300 \leq \lambda \leq 6900$ Å. Z. Astrophys., vol. 44, 1957, p. 37.
75. Howard, R.: Velocity Fields in the Solar Atmosphere. Solar Phys., vol. 2, 1967, p. 3.

76. Roddier, F.: Observation of the Solar Line Oscillations With an Atomic-Beam Spectrophotometer. Astrophys. J., vol. 147, 1967, p. 1113.
77. Janssens, T. J.; Rogers, E. H.; and Vrabec, D.: Sixty-two Hour (Continuous) Solar Movie for the Study of Supergranules. Astron. J., vol. 72, 1967, p. 806.
78. Evans, J. W.: Solar Granules in the Ultraviolet and Yellow. Astron. J., vol. 72, 1967, p. 795.
79. Vassiljeva, G. Y.: Photoelectric Photometry of Solar Granulation in Several Regions of the Continuum. Solar Phys., vol. 1, 1966, p. 16.
80. Bumba, V.: Magnetic Fields in Small and Young Sunspots. Solar Phys., vol. 1, 1967, p. 371.
81. Sheeley, N. R., Jr.: Observations of Small-Scale Solar Magnetic Fields. Solar Phys., vol. 1, 1967, p. 171.
82. Sheeley, N. R., Jr.: Measurements of Solar Magnetic Fields. Astrophys. J., vol. 144, 1966, p. 723.
83. Zwaan, C.: Small Scale Solar Magnetic Fields and Invisible Sunspots. Solar Phys., vol. 1, 1967, p. 478.
84. Hale, G. E.; and Nicholson, S. B.: Magnetic Observations of Sunspots 1917–1929. Carnegie Inst. Publ. No. 498, 1938.
85. Beckers, J. M.; and Schroeter, E. H.: (To be published.)
86. Kuperus, Max; and Athay, R. Grant: On the Origin of Spicules in the Chromosphere-Corona Transition Region. Solar Phys., vol. 1, 1967, p. 361.
87. Kawaguchi, Ichiro: On the Dome Formation in the Corona Around a Prominence Observed at the Total Eclipse of 15 February 1961. Solar Phys., vol. 1, 1967, p. 420.
88. Eddy, John A.; and Malville, J. McKim: Observations of the Emission Lines of Fe XIII during the Solar Eclipse of 30 May 1965. Astrophys. J., vol. 150, 1967, p. 289.
89. Eddy, John A.; Firor, John W.; and Lee, Robert H.: Near Infrared Measurements of Coronal Polarization in Line and Continuum. Astron. J., vol. 72, 1967, p. 793.
90. Conway, John G.; Morris, William F.; and Andrews, C. Frederick: Airborne Spectrograph Observations of the Solar Eclipse of November 12, 1966. Astrophys. J., vol. 150, 1967, p. 299.
91. Annual Report of the Director, Mt. Wilson and Palomar Observatories, 1963–1964. Carnegie Inst., Washington Year Book, 1963.
92. Münch, G.; Neugebauer, G.; and McCammon, D.: Infrared Coronal Lines. II. Observations of (Si X) 1.43 and (Mg VIII) 3.03. Astrophys. J., vol. 149, 1967, p. 681.
93. Kaufmann, Pierre; Matsuura, Oscar T.; and Marques dos Santos, P.: Experimental Results From Measurements Performed During the 12 November 1966 Total Solar Eclipse With a 4.28-cm Radio Polarimeter. Icarus, vol. 7, 1967, p. 380.
94. Letfus, V.; Tlamicha, A.; and Valuicek, B.: Occultation of a Noise Storm Source During the Partial Solar Eclipse of May 20, 1966. Solar Phys., vol. 1, 1967, p. 474.
95. Takakura, Tatsuo: Theory of Solar Bursts. Solar Phys., vol. 1, 1967, p. 304.
96. Ramaty, R.; and Lingenfelter, R. E.: The Influence of the Ionized Medium on Synchrotron Emission Spectra in the Solar Corona. J. Geophys. Res., vol. 72, 1967, p. 879.
97. Razin, V. A.: Paper presented at Gorkii State University, 1957.

98. WARWICK, JAMES W.: Solar Radio Bursts of Type V Interpreted as Type III in Superheated Coronal Streamers. Astrophys. J., vol. 150, 1967, p. 1081.
99. YOH, PHILIP; AND JAMES, JESSE C.: Short-Duration, Narrow-Band Solar Bursts at 38 Mc/s. Astrophys. J., vol. 149, 1967, p. 441.
100. ATHAY, R. GRANT: Theoretical Line Intensities. V. Solar UV Emission Lines of Heavy Elements. Astrophys. J., vol. 145, 1966, p. 784.
101. DUPREE, ANDREA K.; AND GOLDBERG, LEO: Solar Abundance Determination From Ultraviolet Emission Lines. Solar Phys., vol. 1, 1967, p. 229.
102. NEUPERT, WERNER M.: The Solar Corona Above Active Regions: A Comparison of Extreme Ultraviolet Line Emission With Radio Emission. Solar Phys., vol. 2, 1967, p. 294.
103. BURGESS, A.; AND SEATON, M. J.: The Ionization Equilibrium for Iron in the Solar Corona. Monthly Notices Roy. Astron. Soc., vol. 127, 1964, p. 355.
104. PARKER, EUGENE: Dynamical Theory of the Solar Wind. Space Sci. Rev., vol. 4, 1965, p. 666.
105. WEBER, E. J.; AND DAVIS, L., JR.: The Angular Momentum of the Solar Wind. Astrophys. J., vol. 148, 1967, p. 217.
106. JAMES, JESSE C.: Radar Studies of the Sun at 38 Mc/s. Astrophys. J., vol. 146, 1966, p. 356.
107. BRANDT, JOHN C.: Radar Studies and the Extent of Coronal Heating. Astrophys. J., vol. 149, 1967, p. 447.
108. BRANDT, JOHN C.: Interplanetary Gas. XIII. Gross Plasma Velocities From the Orientation of Ionic Comet Tails. Astrophys. J., vol. 147, 1967, p. 201.
109. WILCOX, JOHN M.; AND NESS, NORMAN F.: Solar Source of the Interplanetary Sector Structure. Solar Phys., vol. 1, 1967, p. 437.
110. MODISETTE, J.: Solar Wind Induced Torque on the Sun. J. Geophys. Res., vol. 72, 1967, p. 1521.
111. BRANDT, JOHN C.: Solar Wind and Solar Rotation. Astron. J., vol. 72, 1967, p. 787.
112. BRANDT, JOHN C.: On the Extent of Effective Corotation. Astrophys. J., vol. 148, 1967, p. 905.
113. FERRARO, V. C. A.; AND BHATIA, V. B.: Corotation and Solar Wind in the Solar Corona and Interplanetary Medium. Astrophys. J., vol. 147, 1967, p. 220.
114. PARKER, E. N.: Interplanetary Dynamic Processes. Interscience (New York), 1963.
115. BLIZARD, J. B.: A Long Range Solar Flare Prediction Technique. Trans. Am. Geophys. Union, vol. 46, no. 3, 1965, p. 533.
116. BLIZARD, J. B.: Prediction of Solar Flares Months in Advance. Astron. J., vol. 70, 1965, p. 667.
117. HEAD, R. M.: Solar Proton Event Centers of the Chromosphere. COSPAR Proceedings 5, North-Holland Publ. Co. (Amsterdam), 1966.
118. JOSE, P. D.: Sun's Motion and Sunspots. Astron. J., vol. 70, 1965, pp. 3, 193.
119. TRELLIS, M.: Solar Tides of Planetary Origin. Comptes Rend., vol. 262, nos. 3–5, 1966.
120. WOOD, R. M.; AND WOOD, K. D.: Solar Motion and Sunspot Comparison. Nature, vol. 208, no. 5006, 1965.
121. BIGG, E. R.: Influence of the Planet Mercury on Sunspots. Astron. J., vol. 72, 1967, p. 463.
122. SHEELEY, N. R., JR.: The Average Profile of the Solar K-line During the Sunspot Cycle. Astrophys. J., vol. 147, 1967, p. 1106.
123. BUMBA, V.; AND RUZICKOVA-TOPOLOVA, B.: Variability of the Integrated Solar K Line Emission. Solar Phys., vol. 1, 1967, p. 216.

124. WEEKS, L. H.: Lyman-Alpha Emission From the Sun Near Solar Minimum Astrophys. J., vol. 147, 1967, p. 1203.
125. GNEVYSHEV, M. N.: On the 11-Year Cycle of Solar Activity. Solar Phys., vol. 1, 1967, p. 107.
126. FORBUSH, S. E.: A Variation, With a Period of Two Solar Cycles, in the Cosmic-Ray Diurnal Anisotropy. J. Geophys. Res., vol. 72, 1967, p. 4937.
127. GODOLI, G.; AND MAZZUCONI, F.: The Sun's Polar Surges and Magnetic Fields. Astrophys. J., vol. 147, 1967, p. 1131.
128. YUN, H. S.: Model Sunspots. Astron. J., vol. 72, 1967, p. 838.
129. DEINZER, W.: On the Magneto-Hydrostatic Theory of Sunspots. Astrophys. J., vol. 141, 1965, p. 548.
130. CHITRE, S. M.; AND SHAVIV, G.: A Model of the Sunspot Umbra. Solar Phys., vol. 2, 1967, p. 150.
131. RAYROLE, J.: Contribution a l'Étude de le Structure du Champ Magnetique dans les Taches Solaires. Ann. d'Ap., vol. 30, 1967, p. 257.
132. TREANOR, P. J.: The Spatial Analysis of Magnetic Fields in Sunspots. Monthly Notices Roy. Astron. Soc., vol. 12, 1960, p. 412.
133. ADAM, M. G.: The Pattern of Magnetic Fields in Sunspots: An Observational Determination. Monthly Notices Roy. Astron. Soc., vol. 126, 1963, p. 135.
134. ADAM, M. G.: Line Contours in Sunspot Regions. Monthly Notices Roy. Astron. Soc., vol. 136, 1967, p. 71.
135. BRAY, R. J.; AND LOUGHHEAD, R. E.: Pitman Press, Bath, England, 1964.
136. KJELDSETH MOE, OLAV: A Generalized Theory for Line Formation in a Homogeneous Magnetic Field. Preprint 1968.
137. BUMBA, V.: Radial Motions in Small and Young Sunspots. Bull. Astron. Inst. Czechoslovakia, vol. 18, 1967, p. 238.
138. MALTBY, P.; AND ERICKSON, G.: The Evershed Effect as a Wave Phenomenon. Solar Phys., vol. 2, 1967, p. 249.
139. ERICKSON, G.; AND MALTBY, P.: The Effect of Progressive Sound Waves on the Profiles of Stellar Spectral Lines. Astrophys. J., vol. 148, 1967, p. 833.
140. MUSMAN, S.: Alfven Waves in Sunspots. Astrophys. J., vol. 149, 1967, p. 201.
141. SCHROETER, E. H.: Atti del Convequo sulle Macclise Solari, G. Barbera, ed., Firenze, 1964.
142. ALTSCHULER, M. D.: Electrical Conductivity Gradients in Sunspots. Solar Phys., vol. 1, 1967, p. 377.
143. RUST, DAVID M.: Magnetic Fields in Quiescent Solar Prominences. I. Observations. Astrophys. J., vol. 150, 1967, p. 313.
144. ZIRIN, HAROLD: The Solar Atmosphere. Blaisdell Publ. Co., Waltham, Mass., ch. 11, 1966.
145. DE JAGER, C.: Structure and Dynamics of the Solar Atmosphere. Handb. Physik., vol. 52, Springer (Berlin), 1959.
146. KUPERUS, MAX; AND TANDBERG-HANSSEN, EINAR: The Nature of Quiescent Solar Prominences. Solar Phys., vol. 2, 1967, p. 39.
147. FURTH, H. P.; KILLEEN, J.; AND ROSENBLUTH, M. N.: Finite Resistivity Instabilities in a Sheet Pinch. Phys. Fluids, vol. 6, 1963, p. 459.
148. KIPPENHAHN, R.; AND SCHLÜTER, A.: Eine Theorie der solaren Filamente. Z. Astrophys., vol. 43, 1957, p. 36.
149. THOMPSON, WILLIAM I., III; AND BILLINGS, DONALD E.: Observations Bearing on the Kippenhahn-Schlüter Quiescent Prominence Model. Astrophys. J., vol. 149, 1967, p. 269.
150. BRUZEK, A.: On Arch-Filament Systems in Spot Groups. Solar Phys., vol. 2, 1967, p. 451.

151. Bruzek, A.: On the Association Between Loop Prominences and Flares. Astrophys. J., vol. 140, 1964, p. 746.
152. Jefferies, J. T.; and Orrall, F. Q.: Loop Prominences and Coronal Condensations. I. Non-Thermal Velocities Within Loop Prominences. Astrophys. J., vol. 141, 1965, p. 505.
153. Jefferies, J. T.; and Orrall, F. Q.: Loop Prominences and Coronal Condensations. II. The Source of Mass and Energy and a Model of the Loop Prominence Mechanism. Astrophys. J., vol. 141, 1965, p. 519.
154. Jefferies, J. T.; and Orrall, F. Q.: Loop Prominences and Coronal Condensations. III. The Abundances of Iron and Calcium. Astrophys. J., vol. 145, 1966, p. 231.
155. Olson, Carl A.; and Lykoudis, Paul S.: Solar Loop Prominences: A Theoretical Model. Astrophys. J., vol. 150, 1967, p. 303.
156. Sawyer, C. B.: Correcting Solar Flare Data. Astrophys. J., vol. 147, 1967, p. 1135.
157. Sawyer, C. B.: Apparent Area as a Basis for Solar Flare Importance. Astrophys. J., vol. 147, 1967, p. 193.
158. Sawyer, Constance B.: A Daily Index of Solar Flare Activity. J. Geophys. Res., vol. 72, 1967, p. 385.
159. Křivský, L.; and Knoška, Š.: Time-Latitude Occurrence of Flares in Two Activity Cycles. Bull. Astron. Inst. Czechoslovakia, vol. 18, 1967, p. 325.
160. Zirin, Harold; and Acton, Loren W.: Spectrographic Observations of the Flare of July 20, 1961. Astrophys. J., vol. 148, 1967, p. 501.
161. Tandberg-Hanssen, Einar: Comments on a Flare of September 20, 1966. Solar Phys., vol. 2, 1967, p. 98.
162. Ohman, Y.; Stiber, J.; and Kussofsky, U.: Observations of a Flare Spray at the Solar Limb on July 11, 1966. Solar Phys., vol. 1, 1967, p. 60.
163. Gurtovenko, E. A.: A Peculiar Sodium "Flare" on the Sun. Solar Phys., vol. 1, 1967, p. 389.
164. Janssens, Thomas J.; and Rogers, Ernest H.: Solar Flare Movies in 24 Different Wavelengths About H-alpha. Astron. J., vol. 72, 1967, p. 805.
165. Smith, Sara F.; and Ramsey, Harry E.: Flare Positions Relative to Photospheric Magnetic Fields. Solar Phys., vol. 2, 1967, p. 158.
166. McKenna, Susan M. P.: East Limb Passage of an Active Solar Region, July 7–10, 1959. Astrophys. J., vol. 150, 1967, p. 1087.
167. Zirin, Harold; and Werner, Susan: Detailed Analysis of Flares, Magnetic Fields and Activity in the Sunspot Group of September 13–26, 1963. Solar Phys., vol. 1, 1967, p. 66.
168. de Jager, C.: The Hard Solar X-Ray Burst of 18 September 1963. Solar Phys., vol. 2, 1967, p. 327.
169. Fokker, A. D.: Homology of Solar Flare-Associated Radio Events. Solar Phys., vol. 2, 1967, p. 316.
170. Banos, G.: L'éruption d'importance 2 du 4 octobre 1965. Solar Phys., vol. 1, 1967, p. 397.
171. Antalová, A.: The Photospheric Situation Connected With the Development of Flares Accompanied by the Type IV Radio Bursts. Bull. Astron. Inst. Czechoslovakia, vol. 18, 1967, p. 61.
172. Kleczek, J.; and Olmr, J.: Type IV Bursts and Associated Active Regions. Bull. Astrom. Inst. Czechoslovakia, vol. 18, 1967, p. 68.
173. Warwick, Constance S.: Longitude Distribution of Proton Flares. Astrophys. J., vol. 141, 1965, p. 500.

174. WILCOX, JOHN M.; AND SCHATTEN, KENNETH: Longitude Distribution of Proton Flares as a Function of Recurrence Period. Astrophys. J., vol. 147, 1967, p. 364.

175. HYDER, CHARLES L.: A Phenomenological Model for Disparitions Brusques Followed by Flarelike Chromospheric Brightenings: I. Solar Phys., vol. 2, 1967, p. 49.

176. HYDER, CHARLES L.: A Phenomenological Model for Disparitions Brusques Followed by Flarelike Chromospheric Brightenings: II. Solar Phys., vol. 2, 1967, p. 267.

177. ŠVESTKA, Z.; AND FRITZOVÁ-ŠVESTKOVÁ, L.: Electron Density in Flares: I. Solar Phys., vol. 2, 1967, p. 75.

178. FRITZOVÁ-ŠVESTKOVÁ, L.; AND ŠVESTKÁ, Z.: Electron Density in Flares: II. Solar Phys., vol. 2, 1967, p. 87.

179. GREIG, J. R.; LIM, C. P.; MOO-YOUNG, G. A.; PALUMBO, G.; AND GRIEM, H. R.: Measurements of the Stark Broadening of Two Neutral Helium Lines in a Plasma. (To be published.)

180. KEPPLE, P.; AND GRIEM, H. R.: Improved Stark Profile Calculations for the Hydrogen Lines Hα, Hβ, Hγ, and Hδ. Phys. Rev., vol. 173, 1968, p. 371.

181. LIN, R. P.; AND ANDERSON, K. A.: Electrons >40 keV and Protons >500 keV of Solar Origin. Solar Phys., vol. 1, 1967, p. 446.

182. KAHLER, S. W.; PRIMBSCH, J. H.; AND ANDERSON, K. A.: Energetic Protons From the Solar Flare of March 24, 1966. Solar Phys., vol. 2, 1967, p. 179.

183. BOSTROM, C. O.; KOHL, J. W.; AND WILLIAMS, D. J.: The February 5, 1965, Solar Proton Event. J. Geophys. Res., vol. 72, 1967, p. 4487.

184. BAIRD, G. A.; BELL, G. G.; DUGGAL, S. P.; AND POMERANTZ, M. A.: Neutron Monitor Observations of High Energy Solar Particles During the New Cycle. Solar Phys., vol. 2, 1967, p. 491.

185. GOEDEKE, A. D.; MASLEY, A. J.; AND ADAMS, G. W.: Riometer Observations in the Polar Caps of Solar Cosmic Ray Events During the IQSY. Solar Phys., vol. 1, 1967, p. 285.

186. KRIMIGIS, S. M.: Interplanetary Diffusion Model for the Time Behavior of Intensity in the Solar Cosmic Ray Event. J. Geophys. Res., vol. 70, 1965, p. 2943.

187. MALVILLE, J. MCKIM; ALLER, H. D.; AND JENSEN, C. J.: Spike Bursts During the Type IV Event of February 5, 1965. Astrophys. J., vol. 147, 1967, p. 711.

188. BOISCHOT, A.; AND CLAVELIER, B.: Razin Effect in the Solar Corona and Determination of Magnetic Field at One Solar Radius. Astrophys. J. Letters, vol. 1, 1967, p. 7.

189. RAMATY, R.; AND LINGENFELTER, R. E.: The Influence of the Ionized Medium on Synchrotron Emission Spectra in the Solar Corona. J. Geophys. Res., vol. 72, 1967, p. 879.

190. CASTELLI, J. P.; AARONS, JULES; AND MICHAEL, G. A.: Flux-Density Measurements of Radio Bursts of Proton-Producing Flares and Non-Proton Flares. J. Geophys. Res., vol. 72, 1967, p. 5491.

191. CASTELLI, J. P.; AND MICHAEL, G. A.: The Sagamore Hill Solar Radio Observatory and the Event of August 28, 1966. Solar Phys., vol. 1, 1967, p. 125.

192. PETSCHEK, H. E.: Magnetic Field Annihilation. AAS–NASA Symposium on the Physics of Solar Flares, Oct. 1963, NASA SP–50.

193. GREEN, R. M.; AND SWEET, P. A.: Note on the Dissipation of Magnetic Fields at Neutral Lines. Astrophys. J., vol. 147, 1967, p. 1153.

194. PETSCHEK, H. E.; AND THORNE, R. M.: The Existence of Intermediate Waves in Neutral Sheets. Astrophys. J., vol. 147, 1967, p. 1157.

195. ALFVÉN, H.; AND CARLQUIST, P.: Currents in the Solar Atmosphere and a Theory of Solar Flares. Solar Phys., vol. 1, 1967, p. 220.

196. PNEUMAN, G. W.: Solar Flares as Resulting From the Temporary Interruption of Energy Flow to the Corona: A Case of Hydromagnetic Resonance. Solar Phys., vol. 2, 1967, p. 462.

197. APPARAO, M. V. K.; DANIEL, R. R.; VIJAYALAKSHMI, B.; AND BHATT, V. L.: Evidence for the Possible Emission of High-Energy Neutrons From the Sun. J. Geophys. Res., vol. 71, 1966, p. 1781.

198. HOLT, S. S.: Satellite Protons as a Test of Solar Neutron Observations. J. Geophys. Res., vol. 72, 1967, p. 3507.

199. WEBBER, W. R.; AND ORMES, J. F.: An Upper Limit on the Quiet Time Solar Neutron Flux at Energies >60 MeV. J. Geophys. Res., vol. 72, 1967, p. 3387.

200. HESS, W. N.; AND KAIFER, R. C.: The OSO–1 Solar Neutron Experiment. Solar Phys., vol. 2, 1967, p. 202.

201. DANIEL, R. R.; JOSEPH, G.; LAVAKARE, P. J.; AND SUNDERRAJAN, R.: High-Energy Neutrons From the Sun. Nature, vol. 213, 1967, p. 21.

202. UNDERWOOD, J. H.; AND MUNEY, W. S.: A Glancing Incidence Solar Telescope for the Soft X-Ray Region. Solar Phys., vol. 1, 1967, p. 129.

203. REIDY, W. P.; VAIANA, G. S.; ZEHNPFENNIG, T.; AND GIACCONI, R.: Study of X-Ray Images of the Sun at Solar Minimum. Astrophys. J., vol. 151, 1968, p. 333.

204. BROADFOOT, LYLE: Coronal Fine Structure in X-Ray Emission. Astrophys. J., vol. 149, 1967, p. 675.

205. LANDINI, M.; RUSSO, D.; AND TAGLIAFERRI, G. L.: Solar X-Ray Flux Measured by the 1964–01–D Solar Radiation Satellite During the IQSY. Planetary Space Sci., vol. 15, 1967, p. 231.

206. VAN GILS, J. N.; AND DE GRAAFF, W.: Absolute Intensities in the Solar X-Ray Spectrum Near Minimum Activity. Solar Phys., vol. 2, 1967, p. 290.

207. EDWARDS, PAUL J.; AND MCCRACKEN, K. G.: Upper Limits to the Hard X-Ray Flux From the Quiet Sun and Jupiter. J. Geophys. Res., vol. 72, 1967, p. 1809.

208. BOWLES, J. A.; CULHANE, J. L.; SANFORD, P. W.; SHAW, M. L.; COOKE, B. A.; AND POUNDS, K. A.: A Measurement of the Solar X-Ray Flux in the Wavelength Below 5 Å. Planetary Space Sci., vol. 15, 1967, p. 931.

209. PETERSON, LAURENCE E.; HUDSON, HUGH S.; AND SCHWARTZ, DANIEL A.: Preliminary Results of the University of California X-Ray Experiment on the OSO–III. Reprint UCSD–SP–67–10, Nov. 1967.

210. GREGORY, BRUCE N.; AND KREPLIN, ROBERT W.: Observations of Solar X-Ray Activity Below 20 Angstroms. J. Geophys. Res., vol. 72, 1967, p. 4815.

211. TESKE, R. G.: Observations of Solar Soft X-Rays From OSO–III; First Results. Astron. J., vol. 72, 1967, p. 832.

212. FAZIO, G. G.; AND HAFNER, E. M.: The OSO–I High-Energy Gamma Ray Experiment. J. Geophys. Res., vol. 72, 1967, p. 2452.

213. FRITZ, G.; KREPLIN, R. W.; MEEKINS, J. F.; UNZICKER, A. E.; AND FRIEDMAN, H.: Solar X-Ray Spectrum From 1.9 to 25 Å. Astrophys. J., vol. 148, 1967, p. L133.

214. WALKER, A. B. C., JR.; AND RUGGE, H. R.: Variation in the Solar X-Ray Line Spectrum. Astron. J., vol. 72, 1967, p. 835.

215. POUNDS, K. A.; AND EVANS, K.: The X-Ray Emission Spectrum of a Solar Active Region. Paper presented at the meeting of Commission 44 of the IAU (Prague), 1967.

216. VENABLES, F. H.: Solar X-Rays in the Wavelength Band 44–60 Å Observed by the NRL Satellite 1965–16D and Atmospheric Optical Densities Deduced From These Observations. Planetary Space Sci., vol. 15, 1968, p. 681.

217. LANDINI, M.: Determination of the Solar X-Ray Spectrum by Using the Atmospheric Extinction. Solar Phys., vol. 2, 1967, p. 106.

218. NEUPERT, W. M.; GATES, W.; SWARTZ, M.; AND YOUNG, R.: Observation of the Solar Flare X-Ray Emission Line Spectrum of Iron From 1.3 to 20 Å. Astrophys. J., vol. 149, 1967, p. L79.

219. FELDMAN, U.; AND COHEN, L.: An Iron Spark Line List in the 8–18 Å Range and Its Comparison With Flare Spectra. Astrophys. J., vol. 151, 1968, p. L55.

220. ARNOLDY, R. L.; KANE, S. R.; AND WINCKLER, J. R.: A Study of Energetic Solar Flare X-Rays. Solar Phys., vol. 2, 1967, p. 171.

221. VALNICEK, B.: The X-Ray Emission of Expanding Flares. Bull. Astron. Inst. Czechoslovakia, vol. 18, 1967, p. 249.

222. DE JAGER, C.: Note on Hard Solar X-Ray Bursts. Solar Phys., vol. 2, 1967, p. 347.

223. DE JAGER, C.: The Hard Solar X-Ray Burst of 18 September 1963. Solar Phys., vol. 2, 1967, p. 327.

224. VAN ALLEN, J. A.: The Solar X-Ray Flare of July 7, 1966. J. Geophys. Res., vol. 72, 1967, p. 5903.

225. VAN ALLEN, J. A.: Soft X-Ray Emission by the Sun Since 1 July 1966. Astron. J., vol. 72, 1967, p. 833.

226. STROKE, G. W.: Hand. Physik. Vol. XXIX, Springer (Berlin, Heidelberg, New York), 1967.

227. FRANKS, A.: NPL Diffraction Gratings for X-rays. Paper presented at the Second Internatl. Conf. on VUV and X-ray Spectroscopy, Univ. of Maryland, 1968.

228. MATHER, J. W.: Formation of a High-Density Deuterium Plasma Focus. Phys. Fluids, vol. 8, 1965, p. 366.

229. PEACOCK, N. J.; AND SPEER, R. J.: Emission Spectra of Highly Stripped Ions in a keV Temperature Laboratory Plasma. Paper presented at the Second Internatl. Conf. on VUV and X-ray Spectroscopy, Univ. of Maryland, 1968.

230. BURGESS, D. D.; FAWCETT, B. C.; AND PEACOCK, N. J.: Vacuum Ultra-Violet Emission Spectra From Laser-Produced Plasmas. Proc. Phys. Soc. (London), vol. 92, 1967, p. 805.

231. CONRADS, H. P. F.; AND OERTEL, G. K.: Laboratory Observation of a Visible Emission Line of Highly Ionized Argon at 4412 Å. Astrophys. J., vol. 153, 1968. (To be published.)

232. LIE, T. N.; AND ELTON, R. C.: X-ray Spectra and Diagnostics of a Vacuum Spark Focus. Paper presented at the Second Internatl. Conf. on VUV and X-ray Spectroscopy, Univ. of Maryland, 1968.

233. COWAN, R. D.: Classification of Observed $3p^6 3d–3p^5 3d4s$ Lines of Fe VIII, Mn VII and Cr VI. Astrophys. J. Letters, vol. 147, 1967, p. 377.

234. FELDMAN, U.; AND FRAENKEL, B. S.: Unclassified $3p^6 3d–3p^5 d4s$ Transition Lines of Fe VIII, Mn VII, and Cr VI. Astrophys. J., vol. 145, 1966, p. 959.

235. DEUTSCHMANN, W. A.; AND HOUSE, L. L.: Additional Resonance Lines of Highly Ionized Sulfur, Chlorine, Argon, and Potassium. Astrophys. J., vol. 149, 1967, p. 451.

236. FELDMAN, U.; AND COHEN, L.: Newly Identified Lines in the Ne I Isoelectronic Sequences. Astrophys. J., vol. 149, 1967, p. 265.

237. COHEN, L.; FELDMAN, U.; SWARTZ, M.; AND UNDERWOOD, J. H.: X-ray Spectra of Highly Stripped Atoms Produced in a Vacuum Spark. Paper presented at the Second Internatl. Conf. on VUV and X-ray Spectroscopy, Univ. of Maryland, 1968.

238. KELLY, R.: Atomic Emission Lines Below 2000 Angstroms Hydrogen Through Argon. NRL Rept. 6648, 1968.

239. BENGSTON, R. D.: The Measurement of Transition Probabilities and Stark Widths for C I, F I, Ne I, Cl I, Cl II, Br I, and Br II. Dissertation, Univ. of Maryland, 1968. Univ. of Maryland Tech. Note BN–559, 1968.

240. MILLER, M.: Thermally Insensitive Detection of Transition Probabilities for Ci, O I, Ne I, Al I, Si I, Si II, P I, P II, S I, S II, and Cl I. Paper presented at the Univ. of Maryland, 1968.

241. HOUSE, L. L.: Some Intermediate Coupling Transition Probabilities in Ca XV and Fe XIII. Astrophys. J., vol. 149, 1967, p. 211.

242. KASTNER, S. O.: Oscillator Strengths for Resonance Lines of Some Silicon and Sulfur Ions. Solar Phys., vol. 2, 1967, p. 196.

243. BASHKIN, S.: Optical Spectroscopy With Van de Graaff Accelerators. Nucl. Instr. Methods, vol. 28, 1964, p. 88.

244. CHUPP, E. L.; DOTCHIN, L. W.; AND PEGG, D. J.: Radiative Mean Life Measurements of Some Atomic Hydrogen Excited States Using Beam-Foil Excitation. (To be published.)

245. SMITH, T. S.: Two-Photon Processes in the Solar X-ray Spectrum. Paper presented at the Second Internatl. Conf. on VUV and X-Ray Spectroscopy, Univ. of Maryland, 1968.

246. ELTON, R. C.; PALUMBO, L. J.; AND GRIEM, H. R.: Observation of Two-Photon Continuum Emission From Neon IX. Phys. Rev. Letters, vol. 20, 1968, p. 783.

247. SHAPIRO, J.; AND BREIT, G.: Metastability of $2s$ States of Hydrogenic Atoms. Phys. Rev., vol. 113, 1959, p. 179.

248. RUGGE, H. R.; AND WALKER, A. B. C., JR.: Solar X-ray Line Emission in the 8A to 25A Region. Paper presented at the Second Internatl. Conf. on VUV and X-Ray Spectroscopy, Univ. of Maryland, 1968.

249. BELY, O.: Theoretical Excitation Rate Coefficients in O VII. Paper presented at the Second Internatl. Conf. on VUV and X-ray Spectroscopy, Univ. of Maryland, 1968.

250. BELY, O.; AND BELY, F.: The Excitation of Fe XVII by Electron Impacts. Solar Phys., vol. 2, 1967, p. 285.

251. BOLAND, B. C.; JONES, T. J. L.; AND MCWHIRTER, R. W. P.: Experimental Measurements of the Excitation Coefficients for Some Vacuum Ultraviolet Lines of Nitrogen V. Paper presented at the Second Internatl. Conf. on VUV and X-ray Spectroscopy, Univ. of Maryland, 1968.

252. KUNZE, H. J.: Measurement of Collisional Excitation Rate Coefficients for Lithium-like O VI Ions. Paper presented at the Second Internatl. Conf. on VUV and X-ray Spectroscopy, Univ. of Maryland, 1968.

253. KUNZE, H. J.; GABRIEL, A. H.; AND GRIEM, H. R.: Measurement of Collisional Rate Coefficients for Helium-like Carbon Ions in a Plasma. Phys. Rev., vol. 165, 1968, p. 267.

254. BURKE, P. J.; TAIT, J. H.; AND LEWIS, B. A.: Excitation of N V by Electron Impact. Proc. Phys. Soc. (London), vol. 39, 1967, p. 209.

255. BELY, O.: Excitation of Lithium-Like Ions by Electron Impacts. Proc. Phys. Soc. (London), vol. 88, 1966, p. 587.
256. HINNOV, E.: Excitation and Ionization Rates of Neon Ions in a Stellerator Discharge. J. Opt. Soc. Am., vol. 56, 1966, p. 1179.
257. HINNOV, E.: Revision of the Temperature Dependence of the Ionization Rates of Neon Ions. J. Opt. Soc. Am., vol. 57, 1967, p. 1392.
258. MICKEY, D. L.: Ionization Rates of Ions in $2s^q\ 2p^r$ Configurations. Paper presented at the Second Internatl. Conf. on VUV and X-ray Spectroscopy, Univ. of Maryland, 1968.
259. LOTZ, W.: Electron Impact Ionization Cross Sections and Ionization Rate Coefficients for Atoms and Ions. Astrophys. J. Suppl., vol. 14, 1967, p. 207.
260. BURGESS, A.: Dielectronic Recombination and the Temperature of the Solar Corona. Astrophys. J., vol. 139, 1964, p. 776.
261. ALLEN, J. W.; AND DUPREE, A. K.: Calculation of Ionization Equilibria for Oxygen, Neon, Silicon, and Iron. Harvard Univ. Sci. Rept. no. 24, 1967.
262. VAN RENSBERGEN, W.: The Influence of Doubly Excited Levels on the Ionization Formula for the Solar Corona. Solar Phys., vol. 1, 1967, p. 354.
263. GOLDBERG, L.; AND DUPREE, A. K.: Population of Atomic Levels by Dielectronic Recombination. Nature, vol. 215, 1967, p. 41.
264. SCHMELTEKOPF, A. L.; FEHSENFELD, F. C.; AND FERGUSON, E. E.: Laboratory Measurement of the Rate Constant for $H^- + H \rightarrow H_2 + e$. Astrophys. J. Letters, vol. 148, 1967, p. L156.
265. GRIEM, H. R.: Plasma Spectroscopy. McGraw-Hill Book Co., Inc. (New York), 1964.
266. JALUFKA, N. W.; OERTEL, G. K.; AND OFELT, G. S.: Measurements of Stark Broadening of Some Singly Ionized Argon Lines. Phys. Rev. Letters, vol. 16, 1966, p. 1073.
267. BENGTSON, R. D.: The Measurement of Transition Probabilities and Stark Widths in C I, F I, Ne I, Cl I, Cl II, Br I, Br II. Dissertation, Univ. of Maryland, 1968. (To be published.)
268. BENGTSON, R. D.: Measurements of Stark Broadening of Some Isolated Neutral Chlorine Lines. Bull. Am. Phys. Soc., vol. II, no. 13, 1968, p. 614.
269. COOPER, J.; AND OERTEL, G. K.: Electron Impact Broadening of Isolated Lines of Neutral Atoms in a Plasma I. Phys. Rev. (In press.)
270. OERTEL, G. K.: Debye Shielding in Stark Broadening of Isolated Helium I Lines. Proceedings of the 8th Internatl. Conf. on Phenomena in Ionized Gases (Vienna), 1967, p. 279.
271. GRIEM, H. R.: Semiempirical Formulas for the Electron-Impact Widths and Shifts of Isolated Ion Lines in Plasmas. Phys. Rev., vol. 165, 1968, p. 258.
272. COOPER, J.; AND OERTEL, G. K.: Stark Broadening of Isolated Ion Lines in a Plasma. Phys. Rev. Letters, vol. 18, 1967, p. 985.
273. BRECHOT-SAHAL, S.: On Electron Impact Broadening of Positive Ion Lines. Phys. Rev. Letters, vol. 24A, 1967, p. 476.
274. DAVIS, J.; AND ROBERTS, D. E.: The Influence of Elastic Collisions on the Broadening of Ion Lines. Proc. Phys. Soc. (London), vol. 2, 1968, p. 48.
275. O'MARA, B. J.: The Solar Abundance of Light Elements. Paper presented at the Univ. of California, Los Angeles, 1967.
276. KUSCH, H. J.; AND MEINHOLD, G.: Druckverbreiterung von Titanlinien durch Neutrale Argonatome. Z. Astrophys., vol. 66, 1967, p. 364.

U.S. GOVERNMENT PRINTING OFFICE: 1969 O—333–240